Sonderheft 25

der Österreichischen Zeitschrift für Vermessungswesen

Proceedings of the International Symposium Figure of the Earth and Refraction

Vienna, March 14th—17th, 1967

By Order of the Austrian Geodetic Commission
published by
Karl LEDERSTEGER

Under the Joint Sponsorship of
GIMRADA, AFCRL and Geodetic
Institute, Uppsala University

Herausgeber: Österreichische Kommission für die Internationale Erdmessung
Verleger: Österreichischer Verein für Vermessungswesen, Wien VIII,
Friedrich-Schmidt-Platz 3

Vienna 1967

Sonderheft 25

der Österreichischen Zeitschrift für Vermessungswesen

Proceedings

of the International Symposium

Figure of the Earth and Refraction

Vienna, March 14th—17th 1967

By Order of the Austrian Geodetic Commission
published by
Karl LEDERSTEGER

Under the Joint Sponsorship of
GIMRADA, AFCRL and Geodetic
Institute, Uppsala University

Herausgeber: Österreichische Kommission für die Internationale Erdmessung
Verleger: Österrechischer Verein für Vermessungswesen, Wien VIII,
Friedrich-Schmidt-Platz 3

Vienna 1967

Druck: Rudolf M. Rohrer, Baden bei Wien

In memoriam

of the late

Dr. J. J. de Graaff-Hunter

who always followed the work on both topics
of this symposium with great interest, and has
contributed with own investigations of everlasting
value. When he passed away, 3rd February 1967,
he was still Honorary President of SSG 16

Preface

The idea for the Vienna Symposium of March of this year, the Proceedings of which are presented herewith to the professional world, dates back almost three years. It has been proposed by the Secretary General of the IAG Dr. J. J. Levallois at the Prague Conference in October 1964, and the original notion was that of a meeting where the problem of the reference body for all branches of geodesy and the question of the normal spheroid of the earth should thoroughly be discussed. As this idea was enthusiastically welcome by Dr. E. Tengström, the President of Section V (Physical Geodesy), I was able to invite the scientists assembled in Prague on behalf of the Autrian Geodetic Commission to come to Vienna in autumn 1965. Realization of this plan, however, was delayed again and again by various events, till at last owing to the energy of Mr. Tengström it assumed the form of IAG-Conferences on "The Normal Spheroid and the Figure of the Earth" (SSG 16), and on "Recent Research on Atmospheric Refraction for Geodetic Purposes" (SSG 23). Thanks to generous pecuniary help by the Federal Ministry of Constructions and Technique and to the financial assistance of the IAG, credit for which goes to Secretary General Levallois, the Austrian Geodetic Commission finally was able to invite specialists to come to Vienna in March 1967. Though many prominent scientists unfortunately had to decline their participation because of obligations during the University term, I nevertheless dare say that the Symposium "Figure of the Earth and Refraction", as I have shortly named the meeting, has met great interest which last not least is stated by the fact that besides the Secretary General three presidents and two secretaries of different sections were present. I feel free to assert that the Symposium was a complete success not only with regard to our science but also from a social point of view. The friendly words of thanks expressed by so many participants on their departure confirmed me of the fact that everybody had a really nice time owing to the unique atmosphere of the town, to the considerate attendance by the Organization Committee, and last but not least to the wonderful program managed by my trustworthy colleague Prof. Dr. F. Hauer. Highlights of the social events were the reception in the Marble-Hall of the Governmental Building given by the Federal Minister Dr. V. Kotzina, and the reception in the Heraldic Rooms of the Town Hall by the Mayor of Vienna Mr. B. Marek. An evening in Deutsch-Wagram, and a final trip to the Wachau combined with an inspection of the Danube-Power Plant "Ybbs-Persenbeug" provided opportunity for closer personal contacts.

Following an international scientific custom, I thought about publication of the Proceedings already months before the Symposium. My application for financial support directed to the Geodesy, Intelligence and Mapping Research and Development Agency (GIMRADA), U. S. Army, by way of the European Research Institute was kindly granted thanks to the efforts of Prof. Dr. A. Bjerhammar and Mr. B. Bodnar. Similarly successful were the efforts of Mr. Tengström to secure a subsidy for the Proceedings from the Air Force Cambridge Research Laboratories (AFCRL), for which in the first place I have to thank Mr. Owen W. Williams. Being in the possession of both these generous grants, I thought the printing secured. However, the very rich scientific harvest, being pleasing in itself, taught me the better. My colleague Dr. Tengström fully appreciated this difficult situation and contributed a considerable amount out of the funds of his Institute, which example I followed with a similar amount. Finally, the Federal Board of Education guaranteed the printing by donating a considerable sum, which the Austrian Geodetic Commission is very grateful for.

To many the combination of the figure of the earth und refraction in the topic of a special symposium may seem somewhat constructed. But in the age of artificial satellites this is by no means the case. We need only think about the classic non-hypothetical solution of the problem of the earth figure by means of Bruns polyhedron, which solution then seemed almost

impossible just because of the refraction. But we also may think about the possibility to determine strictly geocentric coordinates of points of the earth surface provided by artificial satellites by which the problem of a uniform, physically well-founded surface of reference again gains increased significance. The solution of the boundary value problem of geodesy, be it for the geoid or be it in the meaning of Molodenskij for the surface of the earth, only then is fully satisfying if the elements, i. e. the gravity anomalies, are pure effects of the mass anomalies in the earth body. This again shows the necessity of a harmonious connexion of geometry and physics, whereby finally geodesy may become what it ought to be: an important, even fundamental discipline of the comprehensive geophysics.

I dare say that the Vienna Symposium showed a pleasing tendency in that direction. The results now can thoroughly be studied in the publication at hand. The struggle of the spirit and the pros and contras of the opinions were vividly expressed in the interesting discussions of the short reports. But unfortunately only a very few of the participants have given their contributions in the discussion in writing so that the publication of the discussions had to be renounced. However, a comprehensive representation of the progress of the meeting by the President of the Section could be put at the end of the Proceedings, for which we express our thanks to Mr. Tengström.

On account of the abundance of contributions, and because of lack of time not every author could read his paper; these papers are ranged here in their proper place. Some authors also were hindered to come to Vienna in the very last minute. Partly, their contributions only now can be taken notice of by the orther participants. Finally, some have preferred to withdraw their report, obviously in order to present it to the General Assembly in Lucerne

The Austrian Geodetic Commission would have been glad to be able to submit the Proceedings already in Lucerne. But because of the great extent of material, and last not least because of vacations this intention proved to be impossible. But the delay is not serious and after Lucerne, with regard to the increased possibilities of comparison, the study of the collection at hand, so I hope, will even be more productive.

Last not least I wish to express my sincere thanks to my colleague Prof. Dr. H. Rohrer for his valuable assistance in the edition of the Proceedings.

Vienna, October 1967

Karl Ledersteger

Symposium Report

by *F. Hauer*

The Austrian Geodetic Commission (ÖKIE) and Section V (Physical Geodesy) of the International Association of Geodesy held a Symposium in Vienna from March 13 to March 17, 1967. The first part of the meeting dealt with problems concerning the "Figure of the Earth" while the subject of the second meeting was "Recent Research on Atmospherical Refraction for Geodetic Purposes."

It was my responsibility to plan and organize the Symposium so that the participants would have suitable accommodations and would enjoy their stay in Vienna. Thanks to the assistance of the staff of the Institute of General Geodesy of the Technical University, we were ready to welcome the almost 100 scientists who came to Vienna from eighteen countries, among them North and South America and Australia, to take part in this Symposium. A part of our Institute served as the reception area and acted as a meeting place and information center.

For the evening of March 13 an informal welcome in the Vienna Rathauskeller was arranged to give our guests a glimpse of genuine "Viennese atmosphere" before the hard work of the Symposium itself began. The opening of the Symposium was held on Tuesday, March 14, in the Festive Hall of the Technical University in Vienna, and its President Magnificenz Dr. R. Stix welcomed the honoured guests. Among those present were Sektionschef Dr. H. Schipper who represented the Federal Minister for Construction and Technology, Dr. Vinzenz Kotzina, Ministerialrat Dr. W. Hafner representing the Federal Minister of Education; and Dr. h. c. Dr. E. Schmid, President of the Austrian Academy of Science. Addresses were given by Prof. Dr. J. J. Levallois, General Secretary of the IAG, Paris; Lect. Dr. E. Tengström, President of Section V of IAG and SSG 16 and 23, Uppsala; and Prof. Dr. K. Ledersteger, President of the ÖKIE, Vienna. At the end of this impressive ceremony the Symposium was officially declared as opened by Dr. Schipper.

After the opening, the participants who had come for the first meeting retreated into Lecture Hall XI of the Technical University and the lectures and discussions began. The organization of the meeting "Figure of the Earth" was under the supervision of Prof. Dr. Ledersteger. After the conclusion of the first meeting, the chairmanship and the lecture hall was handed over to the President of Section V of IAG, Dr. E. Tengström, who was in charge of the second meeting "Recent Research on Atmospherical Refraction for Geodetic Purposes."

While the lectures and discussions were going on, the relatively small group of ladies were kept busy with activities expecially organized for them. The ladies program included a sight seeing bus tour of Vienna and visits to St. Stephans Cathedral, the Vienna Spring Fair, the Belvedere Palace and Museum, and other points of interest in Vienna. We hope that the rich pastries in the Viennese "Kaffeehaus", which was also part of the program, did not do too much damage to the "Figure of the Ladies."

But the men also had chances to take their minds off their work, for the conference was intersperced with several social activities. On the evening of March 14, the delegation leaders from all of the participating countries were invited to a reception given by Federal Minister Dr. Kotzina in the Marble Hall of the governmental building. On the evening of March 16, Bruno Marek, Mayor of Vienna, gave a reception for all of the participants of the Symposium in the Heraldic Rooms of the Town Hall. The impressive surroundings and delicious food were enjoyed by all.

As is generally true of meetings of this kind, time was too short for the enormous scope of the problems being handled, and to the regret of many, the Symposium ended on the afternoon of Friday, March 17, with a summary presented by the chairman and a last word of farewell and thanks by the President of the ÖKIE, Dr. Ledersteger. However, a few hours later everyone met again in Marchfelderhof in Deutsch Wagram for a delicious Viennese-type dinner. There, over a glass of "heurigen"

wine many of the problems which had been discussed during the week were brought up again but perhaps were not taken quite as seriously. On Saturday, a small group of participants still remaining in Vienna made a day long bus tour through the Wachau.

Program of the Symposium
Figure of the Earth and Refraction

arranged by the Austrian Commission of International Geodesy and by Section V (Physical Geodesy) of the International Association of Geodesy.

Place of the conference: Technical University, Karlsplatz 13, Vienna 4.

Monday, March 13, 1967

from 19h — Informal welcoming at the "Rathauskeller".

Tuesday, March 14

from 8h — Registration and reception of informational material and invitations at the Reception Office located in the Seminar Room of the Institute of General Geodesy, 2nd floor, main staircase.

10h — Opening of the meeting by Dr. Vinzenz Kotzina, Federal Minister of Constructions and Technique; at the Festive Hall of the Technical University.
Addresses will be given by:
Magn. Prof. Dr. R. Stix, Rector of the Technical University Vienna
Prof. Dr. J. J. Levallois, Paris, Secretary General of the IAG
Dr. E. Tengström, Uppsala, President of Section V of IAG and President of SSG 16 and 23
Prof. Dr. K. Ledersteger, President of the Austrian Geodetic Commission

14h–17h30 — First Working Session "Figure of the Earth",
Chairman Prof. Dr. U. Uotila, Columbus, Ohio

18h — Reception given by Dr. Vinzenz Kotzina, Federal Minister of Constructions and Technique; at the Marble Hall of the Governmental Building (on special invitation)

Wednesday, March 15

9h–12h: — Second Working Session "Figure of the Earth",
Chairman Prof. Dr. H. Moritz

14h–17h30: — Third Working Session "Figure of the Earth",
Chairman Dr. M. Burša, Secretary of Section V

Thursday, March 16

9h–12h: — First Working Session "Refraction", Chairman Prof. L. Asplund, President of Section I of IAG

13h30–17h — Second Working Session "Refraction",
Chairman Brig. E. W. Denison, President of SSG 19

18h30: — Reception given by Bruno Marek, Mayor of the Federal Capital Vienna; at the Heraldic Rooms of the Town Hall

Friday, March 17

9h–13h: — Third Working Session "Refraction",
Chairman Prof. P. L. Baetsle

14h–17h20: — Fourth Working Session "Refraction",
Chairman Dr. E. Tengström

17h20–17h40: — Summary by Dr. E. Tengström; Vote of thanks by Prof. Ledersteger

19h: — Departure to an evening at the "Heurigen"

Saturday, March 18

Day-long tour to the Wachau with lunch in Dürnstein.

Ladies Program:
a) Visit of the Vienna Spring Fair
b) Visit at the Belvedere
c) Visit of a Viennese Coffee-House

List of Participants

Ackerl F.	Wien 19, Peter Jordanstr. 82
Angus-Leppan P.V.	University of N. S. W. Kensington, New South Wales, Australia
Asplund L.	Fack, Vällingby 1, Schweden
Baarda W.	Onderafd. d. Geod., Kanaalweg 4, Delft, Holland
Baetsle P. L.	149 Boulvard Brand Whitlock, Bruxelles 4, Belgique
Barvir A.	Wien 4, Techn. Hochschule — Karlsplatz 13
Bell J. F.	Elmwood Avenue, Feltham, Middlesex, England
Biro Peter	Budapest 11, Müegyetem rkp. 3, Ungarn
Bocchio Franco	Universita di Trieste, Via dell'Universita 7, Triest
Bodnar B. J.	Gimrada, Research Institute, Fort Belvoir, Virginia, USA
Böhm Josef	Praha 1, Husova 5
Bragard L.	Namur, 5 Rue Ernotte, Belgique
Bretterbauer K.	Wien 8, Friedrich Schmidtplatz 3
Bruins G. J.	Delft, Kanaalweg 4, Niederlande
Bursa Milan	Politických veznu 12, Praha 1, CSSR
Chán Bohumil	Praha 4, Bocni II., CSSR
Cubranić Nikola	Zagreb, Drziceva 71a
Culley Frank L.	Dept. of Geod., Army Map Service, 6500 Brooks Lane, Washington, D. C. 20315, USA
Denison E. W.	Elmwood Avenue, Feltham, Middlesex, England
Draheim H.	D-75 Karlsruhe, Englerstr. 7, Deutschland
Dufour H. M.	2 Avenue Pasteur, 94 Saint-Mande, France
Eidherr F.	Wien 16, Landsteinerg. 5
Embacher W.	Wien 4, Karlsplatz 13, TH
Eördögh W.	Wien 1, Ebendorfer Str. 4
Fischer I.	6500 Brookslane, Washington, DC. 20315, USA
Fischer W.	ETH Zürich
Gale L. A.	1953 Bromley Rd., Ottawa 13., Canada
Gerke K.	Braunschweig TH., Pockelsstr. 4, Deutschland
Glennie E. A.	Seaton House, Shrublands Road, Berkhamsted Herts, England
Härmälä S.	Hämeentie 31, Helsinki 50, Finnland
Hafner W.	Bundesministerium für Unterricht, Wien 1, Minoritenplatz 5
Hauer F.	TH Wien 4, Karlsplatz 13
Heinrich G.	TH Wien 4, Karlsplatz 13
Herbsthofer W.	Wien 8, Krotenthaller G. 3
Hirsch O.	D-1 Berlin 13, Heilmannring 24b
Hofbauer P.	2340 Mödling, J. Thomasstr. 14/III/7
Homorodi L.	Budapest XI., Müegyetem rkp. 3, Ungarn
Hradilek L.	Albertov 6, Praha 2, CSSR
Inzinger R.	1238 Mauer, Jaschkag. 22
Jeske H.	D-2 Hamburg 13., Von-Melle-Park 6, Deutschland
Jobst H.	Wien 12, Schwenkgasse 10/17
Kaspar Jan	Praha 4 — Sporilov
Killian K.	Wien 14, Hadikg. 40
Klak Stjepan	Zagreb Radicevo, Setaliste 7, Jugoslavija
Kling R.	Wien 4, Gußhausstr. 26/10

Kobold F.	TH 8006 Zürich, Schweiz
Köhler G.	Wien 4, Karlsplatz 13
Korschinek E.	TH Wien 4, Karlsplatz 13
Kotzina V.	Stubenring, Regierungsgebäude — Wien
Kresser W.	TH Wien 4, Karlsplatz 13
Kruspe G.	D-2 Hamburg 13., Von-Melle-Platz 6, Deutschland
Krynski St.	Instytut Geodezji, ul. Jasna 2/4, Warszawa, Polen
Kukkamäki T. J.	Hämsentie 31, Helsinki 50, Finnland
Lambeck K.	University of Oxford, 62 Banbury Rd., Oxford, England
Lang M.	Wien 12, Schönbrunner Str. 238
Ledersteger K.	TH Wien 4, Karlsplatz 13
Lego K.	Wien 13, Montecuccolipl. 12/5
Lehr C.	60 Garden Street, Cambridge, Mass. 02138, USA
Levallois I. I.	19 rue Auber, Paris, France
Lichte H.	TH Karlsruhe, Englerstr. 7, Deutschland
Lippold H. R.	Rockvelle, Maryland, USA
Löschner F.	Wien 19, Vegagasse 7
Losert W.	Wien 8, Friedrich-Schmidt-Pl. 3
Mälzer H.	TH Karlsruhe, Englerstr. 7, Deutschland
Manzoni G.	Universita'di Trieste, Italia
Markowits Wm.	Marquette University, Milwaukee, Wisconsin 53233, USA
Meissl P.	TH Wien 4, Karlsplatz 13
Meixner E.	Wien 1, Fichtegasse 2a
Mierlo J.	Onderafd. der Geodesie, Kanaalweg 4, Delft, Holland
Mikesi A.	3390 Melk a/D., Schrattenbruck 19, Österreich
Mitter J.	Wien 8, Friedrich-Schmidt-Platz 3
Mittermayer E.	Berlin 20, Lynarstr. 17, Deutschland
Morelli C.	Osservatorio Geofisico Trieste, Italia
Moritz H.	D-1 Berlin 12, Bleibtreustr. 19
Mueller I.	164 West 19th Ave, Columbus, Ohio, 43210, USA
Munck J. C.	Onde afd. der Geodesie, Kanaalweg 4, Delft, Holland
Nagy D.	Dominion Observatory, Ottawa 3, Canada
Nagy St.	Wen 2, Schüttelstr. 11
Neumaier K.	THi Wien 4, Karlsplatz 13
Otepka G.	Wien 7, Seideng. 39/7
Ottersböck F.	TH Wien 4, Karlsplatz 13
Orbán A.	MTA Sopron, Lackner Kristó, U. 1, Ungarn
Owens J. C.	Section 4402.03, ESSA, U. S. Dept. of Commerce Boulder, Colorado 80302, USA
Palfinger G.	TH Wien 4, Karlsplatz 13
Pelikan M.	Husova 5, Praha 1, CSSR
Pelzer H.	D-33 Braunschweig, Pockelstr. 4, Deutschland
Peters K.	TH Wien 4, Karlsplatz 13
Petković V.	Zagreb, Svearova 5, Jugoslavija
Pick M.	Praha 4 - Sporilov, CSSR
Poder K.	Nörre Farimagsgade 1, Köbenhaun K, Danmark
Pola I.	Praha 4 — Sporilov, CSSR
Ramsayer K.	TH Stuttgart, D-7 Stuttgart 1, Postfach 560, Deutschland
Reibhorn V.	2340 Mödling, Managehag. 18
Rinner K.	TH Graz, Österreich
Rohrer J.	TH Wien 4, Karlsplatz 13
Sanchez R. N.	Ayacucho 482, Tucuma'n, Argentina
Schmid H.	Wien 19, Hofstätteng. 7—9
Senftl E.	Wien 14, Penzingerstr. 108

Slavoy D. E.	22 Orel Court, San Francisco, USA
Sommer L.	Wien 8, Bundesamt
Sona A.	Casella postale 3986 — Milano, Italia
Spickernagel H.	Montanistische Hochschule — A-8700 Leoben
Stange L.	Potsdam, Telegrafenberg, DDR
Steinhauser F.	Wien 19, Hohe Warte 38
Stickler A.	Wien 8, Krottenthaler G. 3
Stix R.	TH Wien 4, Karlsplatz 13
Stolitzka G.	Wien 13, Hietzinger Hauptstr. 149
Stulla-Götz J.	Wien 18, Gentzg. 3
Szabó Bela	AFCRL/CRJ, L. G. Hanscom F, Bedford, Mass., USA
Szadeczky G.	Sopron, Madach Gasse 5, Ungarn
Szkalnitzky P.	Wien 3, Löwengasse 35/38a
Szmielew B.	ul. Jasna 2/4, Warszawa, Polen
Tatár J.	Budapest XI, Eötvös Inst., Homonna U. 1, Ungarn
Tarcy-Hornoch A.	Sopron, Ungarn
Tavenner M. S.	AFCRL/CRJG, L. G. Hanscom Field, Mass., USA
Tengström E.	Hällby, Uppsala, Sweden
Thompson M. C.	ESSA/ITSA Boulder, Colo., USA
Ulbrich K.	Wien 8., Friedrich-Schmidt-Platz 3
Uotila U. A.	164. W. Nineteenth Avenue, Columbus, Ohio 43210
Veis G.	Athens, 147 Greece, National Technical University
Vyskocil V.	Praha 4 — Sporilov, CSSR
Waldhäusl P.	TH Wien 4., Karlsplatz 3
Williams Owen	AFCRL/CRJ, L. G. Hanscom Field, Bedford, Mass., USA
Wunderlich W.	TH Wien 4., Karlsplatz 13
Wunderlin N.	ETH Zürich, Schweiz

Address of His magnificence, Prof. Dr. R. Stix

Meine Herren Vertreter der beiden Ministerien,
meine Damen und Herren!

Es ist wohl ein seltenes Ereignis, daß ein internationales Symposium in den Räumen unserer Hochschule abgehalten wird. Dies ist umso erfreulicher, weil es nicht nur die große Bedeutung der technischen Wissenschaften für die moderne Kultur unterstreicht, sondern auch das Ansehen unserer hohen Schule hebt. Ich habe daher mit Freuden zugestimmt, die Eröffnung dieses Symposiums im Festsaal abzuhalten, als die Österreichische Kommission für die Internationale Erdmessung, die ja am Istitut für Höhere Geodäsie ihren Sitz hat, mit diesem Gedanken an mich herantrat. Leider ist der Herr Minister für Bauten und Technik, dem die Kommission untersteht, im letzten Augenblick verhindert, persönlich zu erscheinen, was natürlich die hohe Bedeutung dieses Symposiums und das Bestreben unserer Regierung, die Wissenschaft in unserem Lande nach besten Kräften zu fördern, besonders unterstrichen hätte. Ich freue mich ganz besonders, an erster Stelle den Vertreter des Herrn Ministers Dr. Kotzina, Herrn Sektions-Chef Dr. Schipper begrüßen zu können sowie den Vetreter des Unterrichtsministeriums, Herrn Ministerialrat Dr. Hafner. Ferner begrüße ich namentlich den Herrn Präsidenten der Österreichischen Akademie der Wissenschaften, Herrn Univ.-Prof. Dr. DDr. h. c. E. Schmid, den Herrn Generalsekretär der Internationalen Assoziation für Geodäsie, Dr. J. J. Levallois, Paris, den Präsidenten der Sektion V (Physikalische Geodäsie) der IAG, Herrn Dozent Dr. E. Tengström, Uppsala, die zahlreichen prominenten Gäste aus dem Ausland, die teilweise mit ihren Damen erschienen sind, die Mitglieder der Österreichischen Kommission für die Internationale Erdmessung, sowie viele Angehörige und Freunde unserer Hochschule.

Ich wünsche dem Symposium einen vollen Erfolg und würde mich freuen, anläßlich der Empfänge im Regierungsgebäude und im Rathaus einige der hier anwesenden Kapazitäten etwas näher kennen zu lernen!

Address of the General Secretary of IAG, J. J. Levallois, Paris

Mes chers collègues,

Ce m'est un agréable devoir de prendre la parole devant vous pour la séance d'ouverture de ce Symposium et, comme Secrétaire de notre Association, de présenter à nos collégues Autrichiens l'expression de notre amitié.

Je désirerai d'abord, avant de le leur dire plus longuement, m'adresser à Monsieur le Ministre qui a bien voulu accorder son haut patronage à cette manifestation et honorer la séance inaugurale de sa présence.

Nous savons tous combien est précieux le temps de ceux sur qui reposent la lourde charge de la marche et de la direction des affaires de l'Etat, et nous n'en ressentons qué plus vivement l'honneur de la présence et de la participation d'une si haute personnalité.

Qu'il me soit permis de lui adresser en votre nom et en celui de notre Association Internationale de Géodésie, l'expression de nos respects, de nos remerciements et de notre profonde gratitude.

Je m'adresserai alors à Monsieur le Recteur qui a accueilli l'organisation du Symposium auquel nous allons assister.

Nous avons pu déjà apprécier il y a quelques instants la belle tenue et la charmante amabilité de la réception, mais sur un plan supérieur nous comprenons mieux quel rôle une école aussi renommée et aussi bien équipée que la Technische Hochschule de Vienne peut jouer dans le développement technique et intellectuel d'un pays. Nous nous réjouissons de faire plus ample connaissance avec ces éminents collègues dont nous avions souvent entendu parler, dont les prédécesseurs ont eux aussi illustré notre Science et nous remercions Monsieur le Recteur de l'intérêt qu'en nous donnant l'hospitalité, il montre une fois de plus pour la Géodésie.

Qu'il veuille bien agréer notre reconnaissance déférente.

Liebe Kollegen!

Zum erstenmal habe ich die Ehre, ein Symposium in deutscher Sprache zu eröffnen. Daran bin ich ganz unschuldig; Sie müßten hierfür Herrn Kollegen Prof. Ledersteger verantwortlich machen. Dieses kann ich leicht erklären: als ich ihm nämlich anläßlich dieses Symposiums einmal deutsch geschrieben hatte, hat er mir versichert, daß er sich darüber sehr gefreut habe. Lieber Kollege Ledersteger, bei der Vorbereitung der Tagung haben Sie wohl kaum Gelegenheit gehabt zu lachen. Ich möchte Sie aber dieser Möglichkeit nicht berauben; denn heute werden Sie mich nicht lesen, sondern hören!

Liebe Kollegen! Wir freuen uns sehr, hier wieder einmal beisammen zu sein, vertraute Gesichter zu sehen und lieben Freunden die Hände drücken zu können. Leider aber werden wir einige alte Gesichter nie mehr wiedersehen. Felix Vening-Meinesz und James de Graff-Hunter sind kürzlich gestorben. Sie alle kennen die großen Erfolge und Fortschritte, welche die Geodäsie ihnen zu danken hat. Oft hatten wir die Ehre und das Vergnügen, mit ihnen zu sprechen und zu diskutieren. Ihr Tod ist für uns alle ein großer Kummer. In Anbetracht der Zuneigung, die wir für sie empfanden, sei dieses Symposium ihrer Erinnerung gewidmet! Tatsächlich werden wir in den kommmenden Tagen oft Gelegenheit haben, von ihren Arbeiten und Ergebnissen zu sprechen. Ist das nicht die beste Art, ihrer zu gedenken?

Meine lieben Kollegen, wir haben uns hier für ein Symposium versammelt und es wäre daher an der Zeit, an die Arbeit zu denken. Aber in der schönen österreichischen Hauptstadt Wien, die voll von historischen und künstlerischen Erinnerungen ist, an der schönen blauen — Verzeihung — gelben Donau wird uns dies nicht so leicht fallen wie es sollte. Doch haben wir neue Fragen zu studieren, neue Ergebnisse kennen zu lernen und neue Flächen zu betrachten.

Lieber Ledersteger, es wäre leicht, jetzt meinen schlechten Scherz, den Sie wohl schon tausendmal gehört haben, zu wiederholen: in der Geodäsie soll man viele Flächen betrachten, das Ellipsoid, das Sphäroid, das Geoid und die Lederstegeroide... Seien Sie bitte nicht böse! Dieser Scherz ist nur der humoristische Widerschein und der Beweis des Interesses und der Hochachtung, welche Ihre schönen und schwierigen Arbeiten gefunden haben, und es wäre besser, Ihnen im Namen allen unserer Kollegen, die aus vielen Ländern hierher kamen, zu sagen, daß wir Ihnen für ihre Bemühun-

gen dankbar sind, und daß wir nicht nur zur Arbeit nach Wien kommen, sondern auch, um mit den österreichischen Geodäten besser bekannt zu werden und diese glänzende Wiener Schule der Geodäsie näher kennen zu lernen.

Ich bin sicher, der allgemeinen Meinung Ausdruck geben zu können, wenn ich der Österreichischen Geodätischen Kommission und ihrem verehrten Präsidenten sehr herzlich für die Organisation dieses Symposiums danke, dem ein voller Erfolg beschieden sein möge!

Lieber Freund! Vor wenigen Tagen hatten Sie mir gedrahtet, eine Fünf-Minuten-Ansprache für die Eröffnung dieses Symposiums vorzubereiten. Ich hatte mit „einverstanden" geantwortet, aber ich fürchte, es war nicht mit Invardraht, denn ich glaube, daß ich die Zeit überschritten habe. Verzeihen Sie, aber es war nur, um das Vergnügen zu haben, es wiederholen zu dürfen und zwar diesesmal ohne Hilfe meines Wörterbuches: «A tous un très grand merci»!

Address given by the President of Section V and President of SSG 16 and 23, Dr. E. Tengström

Your Excellency, Dear Colleagues, Ladies und Gentlemen,

We are together this time to discuss two different kinds of problems of utmost importance for Geodetic Science.

The first type of problems belongs to the work of Special Study Group No. 16 of Sec. V. One of them deals with the determination of the Figure of the Earth and its Gravitational Potential, but carried out in such a manner, that the deviations from an *accepted physical* model of the Earth may be used for an immediate interpretation of the real physical properties of the Earth's interior. The inverse problem of potential theory has an infinite number of solutions. But there exist a lot of restrictions, defined by our present geophysical knowledge, which make it possible to use the unique solution of the geodetic boundary value problem — which I think is attainable with different, formally defined models, or without using a model at all — for constructing geophysically plausible and detailed pictures of the Earth's interior.

The easiest and best starting-point would naturally be to use a model, which has clearly defined physical properties. The deviations from such a model, reflected in the solution of the Geodetic Boundary Value Problem as an external distribution of the s. c. disturbing potential, will then more easily be utilized to formulate explanations of these deviations in correct physical terms.

I admit, that the Pizetti-Somigliana ellipsoidal model is mathematically as good as any other by solving the external problem, if the model can be properly correlated to the gravity-measurements and geometrical measurements along the Earth's Surface, but the *deviations* from most of these models have no physical meaning. If the Earth was covered by oceans, I am sure, that Stokes' Solution gives the correct "size, shape" and external gravitational field of the real Earth, referred to the geocentric coordinate-system. However, introducing the topography, we have no longer an equipotential surface for the boundary-values, and it is not clear, that the conventional boundary values are, in fact, sufficient for a proper solution, if the topography and its mass-distribution is very irregular. For the maximum slopes of 1/10, we might perhaps be satisfied, either with the integral equation of Molodenskij or with some reduction-principle, which may be appropriate. For an Earth with very steep topographical contours and irregular topographical masses, the model, used for computing the deviations, is no longer so easy to define. Fortunately, the irregularities in the shape of the surface of the Earth and in its subsurface density distribution are usually more or less local, and therefore perhaps make our normal heights, surface gravity, and geometrical measurements sufficient for obtaining a result, which at least satisfies the accuracy of Stokes everywhere.

The introduction of models with reasonable correct physical properties, has been suggested by many scientists, who are trying to help geophysicists to understand the meaning of the geodetic result, when looked upon from the geophysical point of view.

Dr. *John O'Keefe*, whom we had expected to be among us to day, presenting his opinion to us, sent a telegram from London, that he had to return home because of death in his family. We are very sorry because of his personal loss, and naturally also extremly unhappy, that he could not join us and

explain his opinion. O'Keefe has suggested, that we keep the actual moment of inertia around the rotation-axis fixed for the physical model, and that we compute the flattening of this model so that the resulting figure – with the present value of the speed of rotation – will be in complete hydrostatical equilibrium.

Professor *Karl Ledersteger*, who has been working during some years on possible solutions of equilibrium and non-equilibrium figures, defined by the constants of Stokes, that is, normal spheroids in Helmert's Sense, will here present a possibility of defining a suitable model from a special type of regularization, involving horizontal displacements of matter.

This kind of questions will be dealt with during the first session on "Figure of the Earth", this afternoon. During the same session, Mrs. Irene Fischer is going to treat a question, which has close connection to the above-mentioned ones, namely, "the deviations of the actual Earth (Geoid) from an equilibrium figure".

I sincerely hope, that we might be able to come to a clearer understanding of the aim of such studies, not at all being meant to neglect the importance of the work, having been done with the Somigliana-ellipsoid up till now, but carried out for the purpose of better physical understanding of the s. c. disturbing potential, coming out from most solutions of the Boundary Value Problem of Physical Geodesy – at the same time reflecting the possibilities of getting an easy way of delivering a geodetic contribution to the inverse problem of potential theory in Geophysics.

The first session on Wednesday will mainly debate more direct questions of the solution of the Geodetic Boundary Value problem, and will contain some very interesting new investigations.

The last session on "Figure of the Earth", Wednesday afternoon, will deal with special questions, also belonging to the workingarea of SSG 16.

I hope, that the schedules will give us many opportunities to discussions, which could help us still more to understand the essential questions – and give us their answers – with the help of clear information from various experts in presented fields of investigation.

This symposium, which – in fact – was meant merely as a combination (for many reasons) of two working sessions, one for SSG 16 of Sec. V with the title "The Normal Spheroid and the Figure of the Earth", and one for SSG 23 of Sec. I "On recent research on atmospherical refraction for geodetic purposes" will be of great help, when mapping the activity of these study groups during the years since Berkeley 1963. As regards SSG 16 many working-sessions at different places (Paris and Prague 1964, Uppsala 1965, Prague 1966) have been reported. All this work and its results may give us a better background for the discussions in Lucerne, where we are obliged to contribute with carefully contemplated recommendations for future work.

The four meetings on refraction will deal with atmospherical influences on both dinstance-measurements *and* direction-measurements in Geodesy, and using both optical waves und radio waves. I think, that these problems are essential for the sections I, II, III, and to some extent also to Sec. V of IAG, but SSG 23 belongs formally to Sec. I. It is a pleasure to be able to tell you, that the president of Sec. I will give you an introduction of the problem and its importance for Geodesy at the beginning of the first session on refraction, Thursday morning.

The aim for combining the discussions on geodetic refraction, and for including these discussions in one meeting, dealing with different components of the gradient vector of refraction index, is clear. I am not in favour of splitting up the refraction problem into various groups of investigations, defined by different applications, but I'll try to convince people to deal with the whole question as one item. The theory of refraction, and all practical possibilities of determining grad n, are then applicable to any type of geodetic work, which needs information about the influence of the n-distribution in the atmosphere on our measurements.

This point of view will be explained also in Prof. *Moritz*' contribution "Applications of the conformal theory of refraction", which will be presented at the end of the last session on refraction, Friday afternoon.

Our Symposium in Vienna can, of course, not solve all the problems, included in the titles of its working-sessions. But, I am sure, it will give us some new starting-points in our continued work to clear up these essential questions for the benefit of Geodetic Science.

As president of SSG 16 and SSG 23, I like to express my sincere hope, that you will return home with new ideas, which may positively influence your future work. I also hope, that you will feel

strongly, again, that the system of special study groups – typical for the activity of IAG – is still a good system, and that it functions efficiently to day, as it has always done in our association.

I am glad, that professor Ledersteger and his collegues – I am especially thinking of professor Hauer – have been able to organize these meetings in such a nice way. And to have been in Vienna in spring in the famous atmosphere of Austrian friendship and hospitality is also a memory to take home as a gift.

I also like to express – on behalf of my special study groups 1:23 and 5:16. and on behalf of Sec.:s I and V – my sincere gratitude for what the Austrian Commission of International Geodesy, the Austrian Government, the General Secretary of IAG, the GIMRADA and AFCRL, and UNESCO through IUGG, have done to make this symposium possible.

I am feeling extremely sad, that we can not at this time profit on the help from Dr. de Graff-Hunter, who always followed our working meetings with great interest und valuable advice. Dr. de Graff-Hunter died 4 February in Australia, shortly after having finished an important paper dealing with the regularization of the Earth's topography for the purpose of an easy calculation of the disturbing potential. He was also initiator to the solution of various problems of refraction, and I think he was one of the first, who suggested the use of dispersion measurements for deriving actual refraction values. I suggest, that we send his wife a greeting from this symposium where we express our deep sorrow of the loss of a great scientist and an inspiring friend. I also suggest, that the printed results of this symposium will be dedicated to his wife to celebrate part of his important work.

I am sure, that the enthusiasm and a clear interpretation of essential problems, which was typical for him, will also caracterize this meeting, in which he would have liked to participate, and the preparations of which he followed with great interest.

Spring is the time of extensive changes in the nature around us. It is a period of violent evolution and the play of strong forces of growth. Let us be inspired of this demonstration of the nature itself and try to insert a little more of spring-feelings into our scientific discussions. Do not be afraid of telling us your opinion, if you have a clear one. Your contribution may help us to solve our problems in a better way. This was always Graff-Hunters encouragement to young scientists.

Everything must be renewed but of course without destroying the important and true fundaments of the past.

Adress of the President of ÖKIE, Prof. Dr. K. Ledersteger

Herr Sektions-Chef, Magnifizenzen, Meine Damen und Herren!

In wenigen Minuten werden Sie, hochverehrter Herr Sektions-Chef, in Vertretung des Herrn Bundesministers für Bauten und Technik, dem die Österreichische Kommission für die Internationale Erdmessung untersteht, unser Symposium feierlich eröffnen. Der Herr Bundesminister, der leider im letzten Augenblick verhindert war, persönlich zu erscheinen, hat dennoch durch seine Bereitwilligkeit, selbst das Symposium zu eröffnen, das hohe Interesse unserer Regierung am Fortschritt der Wissenschaften, der auch unser Land einer schöneren und innerlich reicheren Zukunft entgegenführen soll, bekundet, wofür wir ihm zu tiefsten Damke verpflichtet sind.

Aber auch Ihnen, Magnifizenz, sind wir zu großem Danke verpflichtet, dafür, daß Sie den Festsaal unserer Hochschule freundlicherweise für die heutige Eröffnungsfeier zur Verfügung gestellt haben!

Unser Symposium, das ich kurz als der Erdfigur und der Refraktion gewidmet bezeichnen will, wurde bereits im Herbst 1964 vom Generalsekretär der Internationalen Assoziation für Geodäsie, Herrn Levallois, anläßlich einer ähnlichen Tagung in Prag geplant und vom Präsidenten der Sektion Physikalische Geodäsie, Herrn Kollegen Tengström, lebhaft begrüßt. Er war es auch, der diesen Gedanken nie einschlafen ließ und, was die Frage der Erdfigur betrifft, in erster Linie an eine gründliche Diskussion des Problems des besten Bezugskörpers für die gesamte Geodäsie dachte. Da Herr Tengström gleichzeitig den beiden Spezial-Studiengruppen 16 und 23 präsidiert, lag der Gedanke eines Symposiums „Erdfigur und Refraktion" nahe. Diese Verbindung ist aber auch deshalb nicht abwegig, weil die Refraktion beim Aufbau des Brunsschen Polyeders mit Hilfe der künstlichen Satelliten eine wichtige Rolle spielt, während andererseits die Bahnstörungen der Satelliten die

Kenntnis der wichtigsten Massefunktionen der Erde vermitteln, eine Kenntnis, die für die Wahl des Bezugskörpers von ausschlaggebender Bedeutung ist.

Die Wichtigkeit unserer Tagung wird auch dadurch unterstrichen, daß nicht nur Herr Levallois, sondern auch der Präsident der Sektion I, Herr Kollege Dr. Asplund, Stockholm, erschienen ist, während heute nachmittags noch der Präsident der Sektion III, Herr Prof. Dr. Markowitz, eintrifft. Überdies ist die Sektion V nicht nur durch ihren Präsidenten, sondern auch durch beide Sekretäre Frau Fischer und Herrn Burša, vertreten.

Ich habe nur mit wenigen Worten nicht nur die gesamte Situation gekennzeichnet, sondern auch kurz den Aufgabenkreis des Symposiums charakterisiert, zumal ja mein Freund Tengström darüber schon wesentlich ausführlicher in seiner Präsidialansprache die wichtigsten Mitteilungen gemacht hat. Ich habe Herrn Tengström übrigens gebeten, diese Präsidialansprache bereits bei der Eröffnung zu halten, teils um damit nachmittags Zeit für die Vorträge und Diskussionen zu gewinnen, nicht zuletzt aber auch deshalb, damit sich die Damen vom Ernst unserer Arbeit überzeugen können, und uns dann abends, wenn wir müde und abgekämpft von den Sitzungen kommen, umso lieber und herzlicher betreuen.

Auf die finanziellen Probleme dieser Tagung will ich in dieser feierlichen Stunde nicht tiefer eingehen. Ich halte es aber für meine Pflicht, allen jenen Stellen herzlichst zu danken, welche das Symposium und die geplante Veröffentlichung der "Proceedings" ermöglicht haben. In erster Linie dankt die Österreichische Kommission für die Internationale Erdmessung dem HerrnVizekanzler und dem Herrn Bundesminister für Bauten und Technik für eine großzügige Sonderdotation, die es uns ermöglicht hat, auch ein geselliges Beiprogramm zu gestalten und unseren Gästen die Kongreßstadt Wien von der schönsten Seite zu zeigen. Die Höhepunkte dieses Programms werden aber der Empfang im Marmorsaale des Regierungsgebäudes, den der Herr Minister heute abends für einen Teil der Gäste gibt, sowie der allgemeine Empfang durch den Herrn Bürgermeister im Rathaus sein, der am Donnerstag abends stattfindet. Zu danken habe ich aber auch Herrn Levallois für den Beitrag der Internationalen Assoziation für Geodäsie, Herrn Bodnar als Repräsentanten von GIMRADA, dem European Research Office und Mr. Williams als Repräsentanten der US Air Force. Alle diese Unterstützungen werden, so hoffe ich zuversichtlich, zumindest den Großteil der Druckkosten der Proceedings decken, die als Sonderheft der Österreichischen Zeitschrift für Vermessungswesen erscheinen sollen. Schließlich habe ich auch der Union für Geodäsie und Geophysik zu danken, die es über Bitte von Herrn Tengström ermöglicht hat, einer Reihe von Gästen, die sich aktiv an der Arbeit des Symposiums beteiligen, über ihre Devisenschwierigkeiten hinwegzuhelfen.

Schon die Vorbereitung unserer Tagung hat mannigfache Probleme gezeitigt, die unser schon mehrfach bewährter Organisationsleiter, Kollege Hauer, wieder, wie ich hoffen möchte, zur vollsten Zufriedenheit gemeistert hat. Die Aufgabe war und ist noch schwierig, aber auch sehr beneidenswert. Schwierig ist die Aufgabe, weil sie viel Opfer an Zeit und Mühe erfordert, beneidenswert aber deshalb, weil es Kollegen Hauer damit leicht fällt, sich in die Herzen der Damen einzuschmuggeln! Jedenfalls bitte ich alle Teinehmer und Gäste, sich in allen an sie herantretenden Fragen vertrauensvoll an die Rezeption zu wenden.

Ich bin überzeugt, daß unsere wissenschaftliche Arbeit gut vorangehen und auch Früchte zeitigen wird, wiewohl leider einige besonders wichtige Referenten durch verschiedene Umstände verhindert waren, zu uns zu kommen. Die Geodäsie als weltweite Wissenschaft hat durch die modernen Verkehrsmittel und besonders durch die künstlichen Satelliten viel an Bedeutung gewonnen und verlangt eine immer engere internationale Zusammenarbeit. Wohl ist unser Symposium in erster Linie streng theoretischen Fragen gewidmet. Aber es ist eine alte Erfahrungstatsache, daß die Lösung rein theoretischer Probleme schon morgen eine oft ungeahnte praktische Bedeutung gewinnen kann. Überdies liegt Wien im Schnittpunkt zweier Welten, so daß unsere ernste, friedliche und freundschaftliche Arbeit auch einen hohen moralischen Gewinn zeitigen kann.

Damit dürfte das Wesentlichste gesagt sein und ich möchte abschließend Sie, hochverehrter Herr Sektions-Chef bitten, nach der musikalischen Einlage einige Worte an uns zu richten und damit die Tagung zu eröffnen!

Address of Sektions-Chef Dr. Hans Schipper

Meine Damen und Herren!

Nachdem im vorigen Frühjahr in der Wiener Hofburg der neunte Kongreß des Committee on Space Research (Cospar) seinen glanzvollen Verlauf nahm, hat der Herr Minister gerne der Bitte stattgegeben, heute eine zwar kleinere, aber nicht minder wichtige Tagung zu eröffnen, welche die Österreichische Kommission für die Internationale Erdmessung zusammen mit der Sektion Physikalische Geodäsie der Internationalen Assoziation für Geodäsie veranstaltet. Leider ist der Herr Minister verhindert, persönlich zu erscheinen, und hat mich daher beauftragt, an seiner Stelle dieses Symposium zu eröffnen. Selbstverständlich wünsche ich Ihrer Tagung einen vollen wissenschaftlichen Erfolg, aber ebenso, daß diese Versammlung namhafter Gelehrter aus der ganzen Welt ihr Scherflein zur Völkerverständigung beiträgt, welche die Welt heute mehr denn je nötig hat.

Die Bundeshauptstadt Wien öffnet ihre Pforten jederzeit gerne für internationale Veranstaltungen, um so, entsprechend ihrer geographischen Lage zwischen Ost und West, ihre Tradition als Mittler zwischen den verschiedenen Weltanschauungen erfolgreich fortzusetzen, wozu uns unsere Neutralität nicht nur berechtigt, sondern sogar verpflichtet. Darüber hinaus aber wünsche ich Ihnen einen recht angenehmen Aufenthalt in Wien und hoffe zuversichtlich, daß Ihre Zufriedenheit unserem Fremdenverkehr förderlich sein wird. Vielleicht findet der eine oder andere von Ihnen später Gelegenheit, rein privat unser schönes Land zu besuchen und sich, unbeschwert von der Wissenschaft, dem Studium einer traditionsreichen Kultur zu widmen, was Ihre Damen bereits in dieser Woche versuchen können.

Hoffentlich hat der Herr Minister heute abends Gelegenheit, die prominentesten Vertreter unter Ihnen im Regierungsgebäude begrüßen zu können.

In diesem Sinne hoffe ich, daß Sie nach arbeitsreichen Tagen schöne Abendstunden verbringen werden, und erkläre hiermit das Symposium für eröffnet!

First Conference (SSG 16)

The Normal Spheroid and the Figure of the Earth

Part I:

The Normal Spheroid and the Regularization of the Earth's Crust

Equilibrium Figure of the Earth and the Scientific Reference Surface*)

by *John A. O'Keefe*, Greenbelt, Maryland

In his very exhaustive treatment, K. Ledersteger (1966) has demonstrated once more the fact that the hydrostatic equilibrium value of the flattening of the earth is determined to within a few tenths in its reciprocal by the earth's moment of inertial. This proposition is one which has gradually emerged with increasing certainty from researches going back over several centuries. Ledersteger has also made it clear that the satellite observations of the earth are irreconcilable with the hypothesis that the earth is, actually in hydrostatic equilibrium. In fact, as my colleague, S. W. Henriksen (1960), pointed out, we can determine the hydrostatic value of the flattening of the earth by combining satellite observations with those of the lunisolar precession. Ledersteger (1960) made a very similar calculation, which he did not take very seriously. The values obtained by Henriksen (1/299.8) and Ledersteger (1/299.54) fall quite close to the more rigorous determination by H. Jeffreys (1963) of 1/298.67.

It is clear that we should not attempt to use these values for the calculation of triangulation on the surface of the earth. They differ rather widely from the best-fitting ellipsoid, whose flattening is now well established as 1/298.25 or, with quite sufficient accuracy, 1/298.3 as employed by I. Fischer (1961). The use of the ellipsoid of fluid equilibrium for ordinary geodetic triangulation will lead to heights of the geoid above the ellipsoid sufficient to cause inconvenient discrepancies between various methods of reducing the geoid to the ellipsoid.

On the other hand, it is my contention that it is our duty as geodesists to make it clear to other geophysicists that it is this flattening of 1/299.67 which should be used as the reference figure whenever anything of a *geophysical* nature is to be deduced from the results of geodetic work. The reason is that there is a significant difference between the actual state of the earth and the state of hydrostatic equilibrium, which must be attributable to stress differences in the interior in one way or another. The stress differences which are implied by the disagreement between the hydrostatic and the best-fitting value of the flattening of the earth are of approximately the same kind as those implied by higher harmonics in the earth's gravitational field. They are numerically larger. It is therefore logical to seek the same explanation for these discrepancies as for the others. One could put the proposition in this form: The spectrum of harmonics which arises because of non-hydrostatic distortions of the earth's density distribution include among others the second degree zonal harmonic. To exclude this harmonic in discussions of the mechanics of the earth's interior requires some special justification.

A number of authors, including Hulley (1963); Girdler (1963); Runcorn (1964); Wang (1965), and several others have interpreted the harmonics of the earth's gravitational field from charts red trefero the best-fitting ellipsoid. The significance of these results is immediately open to question

*) This paper was presented later because of the absence of the author.

since they have omitted the most significant feature of the anomalous gravitational field of the earth.

It was pointed out (Kaula and O'Keefe, 1963) that if one is prepared to regard the discrepancy of the second zonal harmonic as the result of a lag in the adjustment of the earth to its changed velocity of rotation, then there is a physical reason for referring gravitational anomalies to the best-fitting ellipsoid. However, it has been shown by numerical calculations by MacDonald (1963) that the implied value of the viscosity of the earth is about 10^{26} poises. That is, if the earth is less viscous than this then the actual figure of the earth will keep step with the changes in its velocity of rotation. Hence, we might say that those authors who employed anomalies or geoid heights referred to best-fitting figure were implicity assuming this value of the viscosity. Even this attempt to rationalize the situation becomes ineffectual, however, when we find that some of these authors are discussing problems of mantle-wide convection. Such convection becomes meanigless if the viscosity is of the order of 10^{26} poises because the turn-over time exceeds the generally accepted age of the earth. It is to be feared that at least some of the authors simply fell into the trap which we unwittingly prepared for them and equated the irregularities of the gravitational field with those required to produce the discrepancies from the best-fitting ellipsoid.

I don't think that we geodesists are being unduly vain in saying that our discipline is among tho most difficult for the outsider. Its ancient traditions, its antique language, the formidable precision which is required just to find the basis from which these discrepancies can be calculated — all create a barrier to the full understanding of our subject by outsiders. It is not reasonable, as I see it, to say, in effect, that if you were a good geodesist, you would not misuse our data.

It seems to me that it is our duty to warn possible users of geodetic data of the pitfalls which lie in their path. It is our duty to warn anyone who might use a diagram of gravity anomalies based on the best-fitting ellipsoid that these anomalies represent only a part of the actual discrepancies from a hydrostatic ellipsoid. This applies in particular to the suggestions brought forward by our host, Dr. Ledersteger, to the effect that we should take as a reference ellipsoid the figure of rotation which the earth would have if it rotated in fluid equilibrium in such a way that the hydrostatic second harmonic became the one which we actually now observe, i. e., with an angular velocity of

$$\omega^2 = 5.368273 \times 10^{-7}\,\mathrm{sec}^{-2}.$$

We should warn anyone using these data that they will require a special explanation for the exclusion of the second-zonal harmonic from their calculations.

I think it would be even better if we could avoid permanently the drawing of world-wide geoidal maps or gravity-anomaly maps which are referred to the best-fitting ellipsoid. These maps, which are so likely to be seized upon the geophysicists, should always be referred, in my opinion, to the flattening of the ellipsoid of fluid equilibrium. I would suggest that the flattening that we take for that should be the flattening calculated so carefully by Jeffreys (1963), namely 1/299.67.

In the United States, some medicines are plainly marked "For External Use Only." Let us mark all data coming from the best-fitting ellipsoid as "For Internal Use Only" in our profession.

References:

Ledersteger, K. (1966), Multiparametric-theory of spheroidal equilibrium figures and the normal spheroids of earth an Moon, European Research Office, Contract Number 91-591-EUC-3779, Final Technical Report, June 1966, pp. i—vii, 1—244.

Henriksen, S. W. (1960), The hydrostatic flattening of the earth, Annals of the IGY, Vol. 12, Part 1, pp. 197—198.

Ledersteger, K. (1960), Dynamischc, statische und geometrische Abplattung. Bayerische Akademie der Wissenschaften, Mathematisch-Naturwissenschaftliche Klasse, Sitzungsberichte 1940, 213—226.

Jeffreys, H. (1963), On the hydrostatic theory of the figure of the earth, *Geophysical Journal, 8,* 196—202.

Fischer, I. (1961), The present extent of the astrogeodetic goid and the geodetic world datum derived from it, Bulletin Géodésique, Nouvelle Seric, *61,* 245—250.

Hulley, J. L. C. (1963), Correlation between gravity anomalies, transcurrent faults, and pole positions, *Nature, 198,* 466—467.

Girdler, R. W. (1963), Rift valleys, continental drift, and convection in the earth's mantle, *Nature, 198*, 1037–1039.

Runcorn, S. K. (1964), Satellite gravity measurements and a laminar viscous flow model of the earth's mantle, Journal Geophys. Res., *69*, 4389–4394.

Wang, Chi-yuen (1965), Some geophysical implications from gravity and heat flow data, Journal Geophys. Res., *70*, 5629–5634.

Kaula, W. M. and J. A. O'Keefe, (1963), Stress differences and the reference ellipsoid, *Science, 142*, 382.

MacDonald, G. J. F. (1963), The deep structure of the continents, *Rev. of Geophys., 1*, 587–665

The Equilibrium Figure of the Earth and the Normal Spheroid

by *K. Ledersteger*, Vienna

In the following a short summary of my Final Report: "Multi-parametric Theory of Spheroidal Equilibrium Figures and the Normal Spheroids of Earth and Moon", June 1966, may be given, concerning the normal spheroid of the earth, which is no equilibrium figure, but the best reference body of geodesy. We start with the homogeneous MacLaurin ellipsoids or the so called zero-parametric equilibrium figures. Each ellipsoid is for a certain rotational velocity such an equilibrium figure. Of course we restrict ourselves immediately to spheroidal figures, since the flattening of the earth $e = 1:298{,}25$ is a quantity of second order. But a second-order approximation does not suffice, for the earth is by far not homogeneous and the undulations of the geoid or the height anomalies after Molodensky are quantities of fourth order. Therefore we must begin with the equipotential spheroids of Helmert, which are based on the development

$$U_4 = \frac{k^2 E}{r}\left[1 - J_2\left(\frac{a}{r}\right)^2 P_2 - J_4\left(\frac{a}{r}\right)^4 P_4 + \frac{\omega^2 a^3}{3 k^2 E}\left(\frac{r}{a}\right)^3 (1 - P_2)\right] \tag{1}$$

and on the formula for the theoretical gravity

$$\gamma = \gamma_o\left(1 + \beta \sin^2 \varphi - \frac{1}{4}\beta_4 \sin^2 2\varphi\right). \tag{2}$$

In the Helmert-system, as I may call it, we have eight equations which combine 13 quantities, i. e. besides the mass E of the earth

a) the geometrical quantities: equatorial axis a, flattening e and the first form-parameter f_4;

b) the constants of the gravity formula: the gravity γ_0 at the equator, the gravitational flattening β and the quantity β_4 of fourth order;

c) the mass-quantities: the mean density ρ_m, the static flattening $J_2 = (C - A) : E a^2$, where C and A are the polar and the equatorial moment of inertia, and the mass-function J_4 of fourth order;

d) three further physical quantities: the rotational velocity ω, the potential value W_o of the surface or of any external equipotential and the ratio $\bar{\varepsilon} = \omega^2 a^3 / k^2 E$.

Therefore five quantities must be given for a unique solution, totally independent of equilibrium, especially (E, ω, a, J_2, J_4). For the axis of the geoid we take the best value of Mrs. Fischer: $a = 6378.165$ km. But since the normal figure of the earth should be of the same volume as the real earth-body, we have to enlarge this axis by 234 m, the mean continental height following from the new Delft development: $a = 6\,378399$ m. The flattening follows from the satellite value of $J_2 = 108271 \cdot 10^{-8}$ to $e = 1:298{,}25$. The quantity k^2E can be determined either from the third law of Kepler $k^2 E = n^2 a^3$ or from the gravity γ_o as purely terrestrial determination:

$$k^2 E = (\gamma_o a^2 + \omega^2 a^3) : \left(1 + \frac{3}{2} J_2 - \frac{15}{8} J_4\right). \tag{3}$$

From Kaula's value

$$k^2 E = (398606{,}24 \pm 5{,}06) \cdot 10^{15}\ \mathrm{cm^3\,sec^{-2}} \tag{4}$$

we find $E = 5976{,}106 \cdot 10^{24}\, g$, if we use $k^2 = 66{,}7 \cdot 10^{-9}\, g^{-1}\, \mathrm{cm}^3\, \mathrm{sec}^{-2}$. The rotational velocity ω is known very well: $\omega^2 = 5{,}317496 \cdot 10^{-9}\ \mathrm{sec}^{-2}$. With the static flattening J_2 we get the mass-moment $K_2 = J_2\, a^2 = 44048{,}95 \cdot 10^{10}\ \mathrm{cm}^2$ and the difference of the moments of inertia: $K_2\, E = (C - A) = 263{,}241 \cdot 10^{40}\, g\ \mathrm{cm}^2$. Together with the dynamical flattening or mechanical ellipticity $H = 327300 \cdot 10^{-8} = 1 : 305{,}53$ we find the principal moment of inertia $C = 80428{,}1 \cdot 10^{40}\, g\ \mathrm{cm}^2$.

At first we have to test whether it is possible to define the normal spheroid as a one -parametric equilibrium figure with the continuous density law

$$\rho = \rho_{max}\left[1 - \nu\left(\frac{x}{a}\right)^2\right]^2. \tag{5}$$

For these figures we have a ninth equation

$$J_4 = -\frac{4}{5}e^2 + \frac{6}{7}e\bar{\varepsilon} - \frac{5}{14}\bar{\varepsilon}^2, \tag{6}$$

so that four quantities are sufficient for a unique determination, e. g. (E, ω, a, J_2). Now a linear series of such figures exists, which have in common both the moments of inertia besides the data E, ω and a, and we have to test whether the three figures (E, ω, a, J_2), (E, ω, a, C) and (E, ω, a, H) coincide or not. Some years ago I found with somewhat other initial data as given above for these three figures following solutions:

	J_2	H	C	$(C - A)$	e^{-1}
with C :	$107327 \cdot 10^{-8}$;	$324267 \cdot 10^{-8}$;	$\underline{80473 \cdot 10^{40}}$;	$260{,}95 \cdot 10^{40}$;	299,70
with J_2 :	$\underline{108310}$;	326065 ;	80762 . ;	$\underline{263{,}34}$;	298,25
with H :	108960 ;	$\underline{327236}$;	80955 ;	264,91 ;	297,38 .

These solutions must coincide, if the normal spheroid of the earth would be a one-parametric equilibrium figure. But this of course is not the case. In fact we have to distinguish some different parts in the earth's interior. The greatest density discontinuity occurs at the separating surface of shell (mantle) and core with about $3-4$ units in a depth of 2900 km. Computing the two-parametric equilibrium figure or the Wiechert-model (E, ω, a, a_c, J_2) with $a_c = a - 2900$ km, consisting of a homogeneous mantle and a homogeneous core we find $C = 80663 \cdot 10^{40}$. The density discontinuity is 8,25. Of course the equilibrium figure of the earth must lie between this Wiechert-model and the one-parametric figure (E, ω, a, J_2), which means $80663 \leqq C \leqq 80762$ or $C \sim 80720 \cdot 10^{40}\ \mathrm{g\,cm}^2$. Therefore the last figure has a C-value relatively too great by about $42 \cdot 10^{40}$, while the figure searched for has a C-value absolutely too great by about $247 \cdot 10^{40}\ \mathrm{g\ cm}^2$, compare Report, p. 115. A six-parametric model (homogeneous ocean, heterogeneous mantle and heterogeneous core) as well as an eight-parametric model (homogeneous ocean, homogeneous crust, heterogeneous mantle and heterogeneous core) confirm the result.

If we, on the other hand, start with the figure (E, ω, a, C) and compute the corresponding Wiechert-model (E, ω, a, a_c, C), we find (Report p. 204):

one-par. fig. :	$e^{-1} = 299{,}75$;	$J_2 = 107195 \cdot 10^{-8}$;	$J_4 = -328{,}5 \cdot 10^{-8}$
Wiech.-mod.:	299,25	107550	$-291{,}9$,

therefore always a too small static flattening. The deviation is about $(108270 - 107270) = 1000 \cdot 10^{-8}$, and we may conclude: no equilibrium figure exists, which has in common with the real earth the mass, the rotational velocity, the axis and both the moments of inertia.

However, it is known that the angular velocity of the earth slightly decreases which causes a lengthening of the day by about 1^s in 120000 years. In three or four milliards of years the day increased from about $8-12^h$ to 24 hours. Therefore we compute the one-parametric figure (E, a, J_2, C) which in fact has a somewhat greater angular velocity corresponding to a day shorter by $7^m 11^s$ (Report, pp. 205/6). But since the earth surely is not one-parametric we search for a better solution with the greater $C' = (80428 + 42) = 80470 \cdot 10^{40}$ and find an ω', corresponding to a day shorter by $6^m 10{,}5^s$ (Report p. 206). Besides this solution $(E, a, J_2, C') = (E, \omega', a, J_2)$, again two more one-parametric figures exist:

	J_2	H	C	$(C-A)$	e^{-1}
(E, ω', a, C):	$108130 \cdot 10^{-8}$;	$326875 \cdot 10^{-8}$;	$80428 \cdot 10^{40}$;	$262{,}90 \cdot 10^{40}$;	297,15
(E, ω', a, J_2):	108271	327129	80470	263,24	296,96
(E, ω', a, H):	108366	327300	80498	263,47	296,84

The deviations are much smaller, because we are nearer by the unique solution.

A further discussion yields the rotational velocity $\omega^2 = 5{,}368273 \cdot 10^{-9}\ \mathrm{sec}^{-2}$, corresponding to a day shorter by $6^m48{,}5^s$, or a further approximation to the unique solution, and finally an eight-parametric model with $J_4 = -315{,}5 \cdot 10^{-8}$ Report, p. 211). Thus we have found the equilibrium figure of the earth with a surface-flattening of about 1:297. Of course it is only an accident that this figure almost coincides with the International Ellipsoid. It has the same density law as the real earth after regularization of the crust, naturally abstracting from the ocean. The lengthening of the day usually is explained by the tidal friction. But only if the earth would be totally rigid, the computed 408^s would represent the tidal effect. If the earth were an ideal fluid, it still would be in hydrostatic equilibrium despite decreasing angular velocity. The effect of the tidal friction would consist only in a slight diminution of the flattening connected with a slight increase of the moment of inertia C. But since the earth is plastic, the total tidal effect of possibly 74000 seconds in 4 milliards of years must be multiplied by a fraction n, which is zero in case of a fluid body and 1 for complete rigidity.

The ocean, representing the geoid, therefore has the flattening 1:298,25, while the ocean bottom has the greater flattening of about 1:297,3. Thus we find the normal spheroid, if we combine the equilibrium figure with the present angular velocity or the normal spheroid has, besides the ocean, the same mass-configuration as the equilibrium figure. With other words: the normal spheroid results as a solution of the Helmert-system with the data (E, ω, a, J_2) of the real earth but with the mass-function J_4 of the equilibrium figure. Given are:

$$E = 5976{,}106 \cdot 10^{24} g\,; \quad \omega^2 = 5{,}317496 \cdot 10^{-9}\,\mathrm{sec}^{-2}\,;$$
$$a = 6{,}378399 \cdot 10^8\,\mathrm{cm}\,; \quad J_2 = 108271 \cdot 10^{-8}\,; \quad J_4 = -315{,}5 \cdot 10^{-8}, \tag{7}$$

wherefrom results:

$$\bar{\varepsilon} = 346175 \cdot 10^{-8}\,; \quad e = 1:298{,}28 = 335260 \cdot 10^{-8}\,; \quad f_4 = -348 \cdot 10^{-8}\,;$$
$$h_{max} = \frac{a}{4} f_4 = -5{,}546\,\mathrm{m}\,; \quad \gamma_o = 977{,}9704\,\mathrm{gal}\,; \quad \beta = 530461 \cdot 10^{-8}\,; \tag{7a}$$
$$\beta_4 = 3383 \cdot 10^{-8}\,; \quad W_o = 62635{,}3 \cdot 10^7\,\mathrm{cm}^2\,\mathrm{sec}^{-2}\,; \quad \rho_m = 5{,}5164\,.$$

This figure is an equilibrium configuration, disregarding the ocean, but it has a smaller angular velocity as the corresponding equilibrium figure. The advantage consists in the fact that the configuration is clearly defined. Therefore this normal spheroid represents the best reference body of geodesy: all deviations, gravity anomalies and undulations of the geoid are caused by the mass-irregularities in the earth's crust and have a correct physical meaning.

Of course the gravity formula better is refered to the surface of the ocean (geoid). Appropriately we reduce γ_0 with the Prey-gradient 0,2224 mgal/m belonging to a water-plate of density 1,028 to the geoid: $\gamma_0 = 978{,}0204$ gal. If we wished to enlarge γ_0 by further 12 mgals, we had either to diminish the axis by 39 m or to put $E = 5976{,}179 \cdot 10^{24}$ g. Probably this small difference is caused by the uncertainty of $k^2 E$. In that way we get the formula for the theoretical gravity

$$\gamma = 978{,}0\,\frac{20}{32}\,(1 + 0{,}0053046 \sin^2\varphi - 0{,}0000085 \sin^2 2\varphi)\,. \tag{8}$$

The Mass-Functions and the Equipotential Ellipsoid

by *K. Ledersteger*, Vienna

We compare the potential expansion of the real earth, restricted to zonal terms

$$V = \frac{k^2 E}{r}\left[1 - \sum_{n=2}^{\infty} J_n \left(\frac{a}{r}\right)^n P_n(\cos\vartheta)\right] \tag{1}$$

with the analogoues expansion of the normal spheroid

$$U = \frac{k^2 E}{r}\left[1 - \sum_{n=2}^{\infty} J_n^* \left(\frac{a}{r}\right)^n P_n(\cos\vartheta)\right] \tag{2}$$

wherein all odd mass-functions vanish, while the even mass-functions decrease so rapidly that we are allowed to restrict the expansion to

$$U_4 = \frac{k^2 E}{r}\left[1 - J_2^* \left(\frac{a}{r}\right)^2 P_2 - J_4^* \left(\frac{a}{r}\right)^4 P_4\right] \tag{2a}$$

Thus the remainder function $T = (V - U)$ results in the form

$$T = -\frac{k^2 E}{r}\left[\sum_{n=2}^{\infty} J_n \left(\frac{a}{r}\right)^n P_n - J_2^* \left(\frac{a}{r}\right)^2 P_2 - J_4^* \left(\frac{a}{r}\right)^4 P_4\right] \tag{3}$$

There the mass-functions may be related to the level surface with the equatorial radius $a = 6378{,}16$ km Their influence decreases with growing elevation; e.g. already in a height of 1000 km $(a/r)^2 = 0{,}7473$ and $(a/r)^4 \sim 0{,}5585$.

If we neglect the flattening according to the Stokes' approximation, i. e. if we substitute a by the mean spherical radius R, we get

$$V_r = \frac{k^2 E}{R}\left[\left(\frac{R}{r}\right) - \sum_{n=2}^{\infty} J_n \left(\frac{R}{r}\right)^{n+1} P_n(\cos\vartheta)\right] \tag{4}$$

and

$$T_r = -\frac{k^2 E}{R}\left[\sum_{n=2}^{\infty} (J_n - J_n^*)\left(\frac{R}{r}\right)^{n+1} P_n(\cos\vartheta)\right] \tag{5}$$

If e. g. h means the hight of an artificial satellite $(r = R + h)$, the errors of the mass-functions deduced therefrom enter the potential function V_R magnified by

$$\left(1 + \frac{h}{R}\right)^{n+1}$$

The expression 5) for the remainder function of course has to be extended by the longitudinal terms neglected in 1). If the normal spheroid has in common with the real earth both the moments of inertia C and $A^* = (A + B)/2$, then the difference $(J_2 - J_2^*)$ vanishes exactly. Further, if only the coordinate axes coincide with the principal axes of inertia of the terrestrial body, the products of inertia

$$\int \xi\eta \, dm = \int \eta\zeta \, dm = \int \zeta\xi \, dm = 0 \tag{6}$$

vanish together with the three related spherical harmonics of 2nd order so that the sectorial function

$$C_{2,2} = -(B - A) : 4\,ER^2 \tag{7}$$

remains, which is responsible for the so-called ellipticity of the terrestrial equator.

For the normal spheroid being of equal volume with the real earth and representing no equilibrium figure but an equilibrium configuration, we obtained in [1, p. 211] on basis of the initial data

$$E = 5976{,}106 \cdot 10^{24}\, g; \quad \omega^2 = 5{,}317496 \cdot 10^{-9}\,\mathrm{sec}^{-2}; \tag{8}$$

$$a^* = 6{,}378390 \cdot 10^8\,\mathrm{cm}; \quad J_2^* = 108271 \cdot 10^{-8}; \quad J_4^* = -315{,}5 \cdot 10^{-8}$$

by means of Helmert's equation system

$$\bar{\varepsilon}^* = 346175{,}4 \cdot 10^{-8}; \quad e^* = 335260{,}4 \cdot 10^{-8} = 1 : 298{,}28;$$

$$f_4^* = -347{,}8 \cdot 10^{-8}; \quad h^*_{max} = \frac{a^*}{4} f = -5{,}546\,\mathrm{m}; \quad \gamma_o^* = 977{,}9704\,\mathrm{gal};$$

$$\beta^* = 530460{,}7 \cdot 10^{-8}; \quad \beta_4^* = 3382{,}9 \cdot 10^{-8}; \quad W_o = 62635{,}315 \cdot 10^7\,\mathrm{cm}^2\,\mathrm{sec}^{-2}$$

$$\rho_m = 5{,}5164 \tag{8a}$$

In the assumed value of the axis the average height of the continents of 225 m according to Prey's development of the heights and depths of the earth has been considered. Thus for the transition to the geoid ($a = 6378{,}165$ km) γ_0 has to be reduced by means of Prey's gradient of 0,2224 mgal/m, corresponding to a plate of water of density 1,028. Hence, $\gamma_0 = 978{,}0204$ gal which value might be too small by about 12 mgal. This small discrepancy is due to the empirical inaccuracy of the significant quantity $k^2 E$.

The following analysis is based on Kozai's [2] values for the mass-functions J_3 to J_6 as derived from artificial satellites

$$\begin{aligned} J_3 &= -225 \cdot 10^{-8}; \quad J_5 = -21 \cdot 10^{-8} \\ J_4 &= -165 \cdot 10^{-8}; \quad J_6 = +65 \cdot 10^{-8} \end{aligned} \tag{9}$$

First with $R = 6371{,}2$ km the potential value $k^2 E/R = 62563{,}8 \cdot 10^7\,\mathrm{cm}^2\,\mathrm{sec}^{-2}$ results. Then with $\gamma = k^2 E/r^2$ the theorem of Bruns according to 5) gives the contributions in undulation of the individual terms

$$\Delta N_{r,n} = (\Delta T_n/\gamma)_r = -R\,(J_n - J_n^*)\left(\frac{R}{r}\right)^{n-1} P_n. \tag{10}$$

For J_4 the difference $(J_4 - J_4^*) = (-165 + 316) = +151 \cdot 10^{-8}$ results, hence at the surface ($r = R$)

$$\Delta T_4 = -0{,}0945 \cdot 10^7\, P_4\,\mathrm{cm}^2\,\mathrm{sec}^{-2}; \quad \Delta N_4 = -9{,}62\, P_4\,\mathrm{m}$$

and in a height of $h = 1000$ km analogous

$$\Delta T_4 = -0{,}0456 \cdot 10^7\, P_4\,\mathrm{cm}^2\,\mathrm{sec}^{-2}; \quad \Delta N_4 = -6{,}21\, P_4\,\mathrm{m}.$$

For an exact approximation of fourth order we proceed from the normal spheroid 8) and find from the data $(E, \omega, W_0, C - A, J_4)$ in successive approximation

$$a = 6378\,386{,}41\,\mathrm{m}; \quad e = 335354{,}7 \cdot 10^{-8} = 1 : 298{,}19. \tag{11}$$

This level surface of the same potential value, though being of equal volume with the normal spheroid shows depressions at the pole and at the equator characterized by $(c - c^*) = -9{,}59$ m and $(a - a^*) = -3{,}59$ m. In contrast to that we have now $f_4 = +312 \cdot 10^{-8}$ and thus $h_{max} = +4{,}975$ m. At the same time the difference ot the radii-vectors of the corresponding ellipsoids at the latitude of 45^0 is $(s - s^*) = -6{,}58$ m so that the new spheroid in that latitude is 3,94 m above the normal spheroid. If we compare these results with the above approximation $\Delta N_4 = -9{,}62\, P_4$ m, we obtain for the pole, for the equator and for $\varphi = 45^0$ one after the other $-9{,}62$ m, $-3{,}61$ m and $+3{,}91$ m, and we can see that the deviations are only 3 cm. Thus the quality of the approximation 10) has been proved in a purely empirical way.

For the mass-function J_3 equation 5) gives $\Delta T_3 = +0{,}1595 \cdot 10^7 \left(\frac{R}{r}\right)^4 P_3\,\mathrm{cm}^2\,\mathrm{sec}^{-2}$ and 10): $\Delta N_3 = +16{,}25 \left(\frac{R}{r}\right)^2 P_3$ m. Hence for $r = R$ we get at both the poles of the surface the undulations

$\pm 16{,}25$ m, which result is well known under the misleading slogan of the "pearshaped earth". Now we extend the analysis to all four of the above mass-functions, whereat we only have to consider that for the normal spheroid J_3^* and J_5^* vanish, while $J_6^* = +1$ unit of the eight decimal place. Thus we get at the surface expressed in meters:

$$\Delta N = +16{,}25\, P_3 - 9{,}62\, P_4 + 1{,}34\, P_5 - 4{,}08\, P_6 \tag{12}$$

and analogously for the heights $h = 1000$ km and for $r = 2R$, $3R$ and $4R$

$$\begin{aligned}
\Delta N &= +12{,}140\, P_3 - 6{,}212\, P_4 + 0{,}748\, P_5 - 1{,}968\, P_6 \\
\Delta N &= +\ 4{,}062\, P_3 - 1{,}202\, P_4 + 0{,}084\, P_5 - 0{,}128\, P_6 \\
\Delta N &= +\ 1{,}806\, P_3 - 0{,}356\, P_4 + 0{,}017\, P_5 - 0{,}017\, P_6 \\
\Delta N &= +\ 1{,}015\, P_3 - 0{,}150\, P_4 + 0{,}005\, P_5 - 0{,}004\, P_6
\end{aligned}$$

The following small table results:

h_{km}	$+90^0$	$+45^0$	0^0	-45^0	-90^0
$r = R$	+ 3,89	+ 1,15	— 2,33	+ 7,89	— 31,29
$r = R + 1000$	+ 4,71	+ 0,39	— 1,71	+ 5,24	— 21,07
$r = 2R$	+ 2,82	— 0,24	— 0,41	+ 1,26	— 5,48
$r = 3R$	+ 1,45	— 0,18	— 0,13	+ 0,47	— 2,20
$r = 4R$	+ 0,87	— 0,12	— 0,06	+ 0,24	— 1,17

The undulations undoubtedly have to decrease with increasing elevation for any possible perturbing potential, and have to vanish sufficiently in a particular height. This applies to each of the four terms separatly. Because of the restriction to the four zonal spherical harmonics $J_3 - J_6$ the above results permit no convincing conclusion as to the magnitude of the undulations and their decrease with height. For both the mass-functions J_3 and J_5 alone we would get the undulations $\pm 17{,}59$ m for both the poles; these values diminish to $\pm 1{,}02$ m for $r = 4R$, while at the equator always $N = 0$. On the other hand, in case of rotational and equatorial symmetry ($J_3 = J_5 = 0$) at both the poles $\Delta N = -13{,}70$ m and at the equator $-2{,}33$ m, which values diminish to $-0{,}15$ m and $-0{,}06$ m for $r = 4R$. The above table, however, discloses a contradiction which can clearly be recognized by the incipient increase of the undulation above the northern pole and the impossible change of sign for $\varphi = +45^0$. The reason for this contradiction lies in the incommensurability of the mass-functions J_3 and $(J_4 - J_4^*)$, as can be proved by restriction to the first two terms of 12).

In order to study this problem in more detail we reason as follows. The mass-function $J_3 = -255 \cdot 10^{-8}$ offers no foothold. An asymmetry between the northern and the southern hemisphere, effecting a deviation of ± 16 m in the polar radii, is within the empirical magnitude of the undulations. However, it is very dubious that the ratio of the mass-function $J_4 = -165 \cdot 10^{-8}$ and $J_4^* = -315{,}5 \cdot 10^{-8}$ should be almost 1:2. We go back to the normal spheroid 8) and find for its mass-moment of fourth order $K_4^* = J_4^* E a^4 = -31{,}2077 \cdot 10^{56}$ g cm^4. The homogeneous water cover may have the density 1,028 and a depth of 2601 m at the equator. The equilibrium figure of the earth shows further that the ocean bottom has the somewhat greater flattening of about $e' = 1 : 297{,}3 = 336360 \cdot 10^{-8}$. Hence we find for the volumes of the total earth V and of the solid earth V', further for the mass of the ocean O and for the mass E' of the solid earth

$$\begin{gathered}
V = 1083{,}336 \cdot 10^{24}\ \text{cm}^3\ ; \quad V' = 1082{,}000 \cdot 10^{24}\ \text{cm}^3\ ; \quad O = 1{,}374 \cdot 10^{24}\ g \\
E' = 5974{,}732 \cdot 10^{24}\ g\,.
\end{gathered} \tag{13}$$

The proportion of the mass-moment K_4 due to the ocean becomes

$$\Delta K_4 = -\frac{12}{35}\, 1{,}028\, [(e^2 - e^3)\, V a^4 - (e'^2 - e'^3)\, V' a'^4] = +0{,}0260 \cdot 10^{56}\, g\ \text{cm}^4, \tag{14}$$

so that for the solid earth with the equatorial radius $a' = 6375{,}789$ km holds

$$K_4 = -31{,}2077 - 0{,}0260 = -31{,}2337 \cdot 10^{56}\, g\ \text{cm}^4. \tag{14a}$$

In analogy we get for a homogeneous crust of density 2,80 and a magnitude of 33 km ($a'' = 6345{,}390$ km)

$$V'' = 1066{,}611 \cdot 10^{24}\ \mathrm{cm}^3\ ; \quad Cr = 43{,}088 \cdot 10^{24}\ g\ ; \quad E'' = 5931{,}644 \cdot 10^{24}\ g$$

and for the remaining earth down to the surface of the mantle

$$K_4 = -31{,}2337 + 0{,}7862 = -30{,}4475 \cdot 10^{56}\ g\ \mathrm{cm}^4 = J''_4\, E''a''^4,$$

hence

$$J''_4 = -316{,}6 \cdot 10^{-8}, \tag{15}$$

but referred to the surface of the normal spheroid:

$$J''_4 = -310{,}1 \cdot 10^{-8} \tag{15a}$$

The removal of the ocean and of the whole crust results only in a variation of $\Delta J_4 = +5{,}4 \cdot 10^{-8}$. We conclude that the mass-irregularities in the crust can have only an almost vanishing effect.

Putting

$$\bar{\varepsilon} = x\,e + \ldots\ ; \quad f_4 = -\varkappa e^2\ ; \quad J_4 = -\xi e^2 \tag{16}$$

we get for the normal spheroid $x = 1{,}03256$, $\varkappa = +0{,}30943$, $\xi = +0{,}28070$, while the observed value $J_4 = -165 \cdot 10^{-8}$ leads to $\xi = +0{,}14680$ which in turns gives by means of the equation generally valid

$$-\varkappa + 4{,}374\,\xi = 3{,}5 - 2{,}5\,x \tag{17}$$

the values $\varkappa = -0{,}27635$ or $f_4 = +310 \cdot 10^{-8}$. In the $(x,\varkappa)$-diagram [1, p. 66] the new figure thus lies far below the normal spheroid and even far below the external equipotential of the same data (E, ω, a, J_2) of the corresponding MacLaurin ellipsoid ($J_4 = -251{,}3 \cdot 10^{-8}$; $f_4 = -67{,}1 \cdot 10^{-8}$). Series of figures with the data (E, ω, a, J_2) are not strictly vertical as with J_4 also e and thus x vary slightly. It may be demonstrated by means of two characteristic examples that the homogeneous ellipsoid or one of its equipotentials never can be part of a physically sound series of equipotential spheroids. It may be noted that in general we have not equilibrium figures in mind, even if these equipotential spheroids coincide with the surfaces of mass-configurations.

At first we turn our attention to the series of external equipotentials of so-called one-parametric mass-configurations which are characterized either by the continuous density law

$$\rho = \rho_c \left[1 - \nu \left(\frac{x}{a}\right)^2\right]^2 \tag{18}$$

or by the property that at their surface the variation of the form parameter f_4 in outer space is $a df_4/da = A = 0$. The curve $A = 0$ represents a parabola with its vertex in the point $(x = 2/5, \varkappa = -1/4)$; ρ_c stands for the density at the center of gravity. For $\nu = 0$ the ellipsoid of MacLaurin results, and for $0 \leqq \nu < 1$ the series of one-parametric equilibrium figures up to the one-parametric spheroid of greatest mass-concentration for which ν is just below unit. Below the ellipsoid, i. e. within the region of positive form-parameters, ν becomes negative, which means that the density increases continuously from the center of gravity to the surface, a physically absurd case. The constancy of J_2 and thus of the mass-moment K_2 is responsible for the fact that we have to deal with external equipotentials of figures of the series (ω, K_2) with constant principal moment of inertia C. Hence, beyond the ellipsoid the mass-concentration is compensated by an expansion of the figures (increasing equatorial radius of the surface $a' \leqq a$), while below the ellipsoid the equatorial radius a' decreases with simultaneous condensation toward the surface. Thus our series starts with a one-parametric equilibrium figure ($a' = a$, $J_4 = -332{,}4 \cdot 10^{-8}$). Descending in the series at first the external equipotentials of one-parametric equilibrium figures follow down to the MacLaurin-ellipsoid ($a' = 5811{,}99$ km, $e' = 326539 \cdot 10^{-8}$) with $J_4 = -251{,}2 \cdot 10^{-8}$. The parabola $F = |J_4| : J_2^2 = 1{,}8080$ passes through the vertex of the parabola $A = 0$, from which follows $J_4 = -212 \cdot 10^{-8}$ for the external level surface. The pertinent figure itself is characterized by the data: $a' = 4773{,}93$ km, $e' = 362853 \cdot 10^{-8}$, $J'_2 = 193277 \cdot 10^{-8}$, $J'_4 = -677{,}1 \cdot 10^{-8}$. Beyond the vertex of the parabola, i. e. for $x < 0{,}4$, F decreases only slightly ($x = 1/5$, $F = 1{,}7857$) and then increases again to 1,8 for $x = 0$. For $x < 0{,}05$, however, the flattening e' increases so rapidly that Helmert's equation system soon becomes inapplicable.

As a seco nd example we consider the binary-shell models. Because of

$$3J_2 = 2e - \bar{\varepsilon} - 2e^2 + 2e\bar{\varepsilon} - \frac{5}{4}J_4$$

$$f_4 = \frac{7}{2}e^2 - \frac{5}{2}e\bar{\varepsilon} + \frac{35}{8}J_4 \tag{19}$$

to every f_4 a particular pair of values e and J_4 belongs, since with the given data (E,ω,a,J_2) $\bar{\varepsilon} = \omega^2 a^3/k^2 E$ also is determined. Because of the constancy of J_2, e can vary only within very narrow limits. With x and $\varkappa$ always a definite point of the $(x,\varkappa)$-diagram is determined, which generally within a certain region an infinite number of two-layer models belong to, whose surfaces are equipotentials save that equilibrium follows therefrom. If we choose e. g. a partial mass $E_1 = E - E_2$ for a "mantle-figure", then we have [1, p. 114/5] except for quantities of 6^{th} or 5^{th} order, in

$$J_2 = \frac{1}{5}(2e - e^2)(E_1 : E) + \frac{1}{5}(2e_c - e_c^2)(a_c : a)^2 (E_2 : E)$$

$$J_4 = -\frac{12}{35}(e^2 - e^3)(E_1 : E) - \frac{12}{35}(e_c^2 - e_c^3)(a_c : a)^4 (E_2 : E) \tag{20}$$

two equations with both the unknowns a_c and e_c, i. e. axis and flattening of the core.

Our series starts with the model $a_c = 0$, or more general, with $e_c = 0$ as a homogeneous sphere irrespective of its radius contributes nothing to the mass-functions. Together with 19) the equations

$$5J_2 = (2e - e^2)(E_1 : E)\,; \quad -\frac{35}{12}J_4 = (e^2 - e^3)(E_1 : E) \tag{21}$$

furnish a rigorously unique solution for the four unknowns e, J_4, E_1 and f_4, i. e. the Wiechert-model with the core's radius being equal to zero which lies in the straight line $(\varkappa + 35\,\xi/8) = 1{,}5$:

$$e = 335263{,}4 \,.\, 10^{-8}\,; \quad J_4 = -310{,}7 \,.\, 10^{-8}\,; \quad E_1 : E = 0{,}8087\,;$$
$$f_4 = -326{,}7 \,.\, 10^{-8}\,: \quad \varkappa = +0{,}2907\,. \tag{21a}$$

Every lower point (J_2, J_4) or every $(x,\varkappa)$ with smaller $|J_4|$ and $\varkappa$ represents an infinite number of binary-shell models. For the determination of these models we transform equations 20). Putting for short $(E_1 : E) = z$ and $(a_c : a)^2 = y$ we find

$$[5J_2 - (2e - e^2)z] = (2e_c - e_c^2)\,y\,(1 - z)$$
$$-\left[\frac{35}{12}J_4 + (e^2 - e^3)z\right] = (e_c^2 - e_c^3)\,y^2\,(1 - z)\,. \tag{20a}$$

Now $(2e_c - e_c^2)^2 \sim 4(e_c^2 - e_c^3)$. Thus, if we square the first equation and subtract the second one multiplied by $4(1 - z)$, we get

$$[5J_2 - (2e - e^2)z]^2 + \left[\frac{35}{3}J_4 + 4(e^2 - e^3)z\right](1 - z) = 0$$

or

$$z\left[10J_2(2e - e^2) - 4(e^2 - e^3) + \frac{35}{3}J_4\right] - \left[(5J_2)^2 + \frac{35}{3}J_4\right] = 0 \tag{22}$$

For all these solutions

$$(2e_c - e_c^2)(a_c : a)^2 = [5J_2 - (2e - e^2)z] : (1 - z) \tag{20b}$$

E_1 or the density of the mantle are nearly constant. We recognize easily that the case $z = 1$ or $E_1 = E$, $E_2 = 0$ is impossible; otherwise we would deal with a homogeneous body whose surface is an equipotential. Thus the body itself had to be an equilibrium figure contrary to the well-known fact that in the vicinity of the sphere the MacLaurin-ellipsoids are the only possible homogeneous equilibrium figures. In fact, beginning with the value 21a): $z = 0{,}8087$ and proceeding downwards z decreases

continuously till in the parabola $F = 15/7$ or for $J_4 = -251{,}2 \cdot 10^{-8}$ the value $z = 0$ is reached. In the whole region $-310{,}7 \cdot 10^{-8} \leqq J_4 \leqq -251{,}2 \cdot 10^{-8}$ to every point a Wiechert-model or a two-parametric equilibrium figure belongs inclusively the already fictitious boundary solution of the external equipotential of a MacLaurin-ellipsoid: $a_c = 5811{,}988$ km, $e_c = 326538{,}5 \cdot 10^{-8}$ which results from ($z = 0$)

$$(2e_c - e_c^2)(a_c : a)^2 = 5J_2\,; \quad \omega^2 a_c^3/k^2 E = \frac{4}{5}e_c + \frac{22}{35}e_c^2\,. \tag{23}$$

The last equation may be considered an equilibrium condition. All possible binary-shell models lie, as always, between the limits $e_c = e$ or $a_{c,\,min}$ and $e_{c,\,min}$ or $a_{c,\,max}$, the latter boundary solution being defined by equal polar axes $(c_c = c) : a(1-e) = a_c(1-e_c)$.

If we fictitiously continue the series downwards, then negative z-values will result. i.e. the density of the mantle becomes negative and the mass of the core is greater than E. However, the absolute limit soon is reached. There applies:

$$z \to \infty\,; \quad (2e_c - e_c^2)(a_c : a)^2 \to (2e - e^2)\,. \tag{20c}$$

At the same time the factor z in 22) vanishes:

$$-\frac{35}{3}J_4 = 10J_2(2e - e^2) - 4(e^2 - e^3)\,, \tag{24}$$

leading together with 19) to $e = 335309{,}6 \cdot 10-8$, $J_4 = -237{,}1 \cdot 10^{-8}$ and $f_4 = -4{,}2 \cdot 10^{-8}$. But the solution $a_c \to a$ and $e_c \to e$ represents the equipotential ellipsoid corresponding to the given data (E, ω, a, J_2) for which equations 19) for $f_4 = 0$ render directly $e = 335310{,}2 \cdot 10^{-8}$ and $J_4 = -236{,}2 \cdot 10^{-8}$. Thus the physical absurdity of the equipotential ellipsoid is revealed especially clearly. Besides, this figure is no exact ellipsoid at all, but certainly has higher form parameters. In the same fourth-order approximation this figure also represents the external equipotential of a small one-parametric mass-configuration with $F = 2{,}01466$, thus likewise belonging to the fictious region.

Hence, this first solution is, strictly speaking, no equipotential ellipsoid at all, which should represent a mass-configuration whose surface coincides with the equipotential ellipsoid desired. But this is easily accomplished by mass-displacements in homogeneous confocal ellipsoidal shells which leave the external potential unaltered. The second solution stands in an interesting analogy to the equipotential ellipsoid of W. D. Lambert [3]; the homogeneous ellipsoid has too great a mass ($E_2 = 7732{,}4 \cdot 10^{24}$ g) which is reduced by a fictitious areal coating of great negative density. A fourth solution represents the theory of Pizzetti and Somigliana. It is based on the following, mathematically sound fact. Given be a physically possible mass-configuration and a pertinent external equipotential. Then the given equipotential and the total external potential remain unaltered in case the total mass will be distributed homogeneously within the equipotential while all deviations from homogeneity can be mastered by an areal coating of partly positive, partly negative density with the mass-sum zero. But if, vice versa, the equipotential is arbitrarily prescribed then generally a fictitious solution results. As a fifth solution we finally get in fourth-order approximation the so-called third normal form of Helmert for which per definitionem $f_4 = 0$. Thus with (E, ω, a, e) or (E, ω, a, J_2) the second equation 19) gives directly J_4 as before. If in this case we want to obtain a physically sound solution we have to neglect together with f_4 all remaining fourth-order quantities, which means a retreat to the second-order approximation in which all equipotential spheroids are ellipsoids; the second-order approximation, however, does not suffice for the problem of the figure of the earth as is well-known.

Hence, all these equipotential ellipsoids regardless whether they are exact ellipsoids or mere fourth-order approximations, are of fictitious nature. But in [1, p. 163] we succeeded in showing independently of the character of the mass-configuration that for the x-value of the earth ($x \sim 1{,}032$) an equipotential ellipsoid still is conceivable in eight-order approximation which, however, is erroneous already in the fourth-order quantities. For if we put (compare 16)

$$\bar{\varepsilon} = xe + \ldots, J_2 = \frac{1}{3}(2 - x)e\,, \quad J_4 = -\xi e^2\,, \quad J_6 = +\eta e^3\,,$$
$$J_8 = -\zeta e^4\,; \quad f_4 = -\varkappa e^2\,, \quad f_6 = -\lambda e^3\,, \quad f_8 = -\mu e^4 \ldots\,, \tag{25}$$

then applies generally (compare 17)

$$-\varkappa+\frac{35}{8}\xi=\frac{7}{2}-\frac{5}{2}x$$

$$B=\left(-\lambda+\frac{231}{80}\eta\right)=(3{,}3-2{,}75\,x)+\varkappa\,(1{,}2-0{,}5\,x)\,; \tag{26}$$

$$C=\left(-\mu+\frac{1287}{896}\xi\right)=\frac{1}{56}(143-130\,x)+\frac{\varkappa}{56}(64-40\,x)+$$

$$+\frac{\lambda}{56}(64-20\,x)+\frac{4}{35}\varkappa^2$$

The straight line $\xi=0=F$ intersects the x-axis at point $x=1{,}4$ herewith defining the absolute upper limit. The curves $B=$const are the equilateral hyperbolas

$$(x-2{,}4)(\varkappa+5{,}5)=-(2B+6{,}6)\,, \tag{27}$$

wherefrom $x=1{,}2$ results for the curve $B=0$ and as intersection with the x-axis. Since the curves $B<0$ follow in the direction of increasing x-values and since for the latter $\lambda>231\,\eta/80$ must be positive together with η, equipotential ellipsoids in sixth-order approximation are possible only for $x=1{,}2$. Further conclusions follow analogously. For $\varkappa=\lambda=0$ and the curve $C=0$ we obtain the intersection point $x=1{,}1$, and equipotential ellipsoids in eight-order approximation are possible only in the region $x<1{,}1$. Continuing this mode of reasoning we learn easily that the exact equipotential ellipsoid coincides with the MacLaurin-ellipsoid.

Thus we arrived at the result that the equipotential ellipsoid pertinent to the empirical data (E,ω,a,J_2) of the real earth can only be thought of as approximation and only for a fictitious mass-configuration. The arbitrary assumption $f_4=0$ also leads to a different mass-function $J_4=-236{,}2\,.\,10^{-8}$ and to a theoretical gravity formula which must not be designated as "normal". Neither the gravity anomalies derived therefrom nor the resulting geoid undulations have any clear physical meaning. Of course, the splitting into a theoretical field and the pertinent corrections is an arbitrary act within certain limits. But it is certainly desirable to proceed from a model physically possible, which has both the principal moments of inertia in common with the real earth so that the mass-function J_2 is identical while the mass-function J_4 deviates only slightly from its true value. Then the gravity anomalies and the undulations are the clear effects of the mass-anomalies.

The curve defined by the data (E,ω,a,J_2) of the $(x,\varkappa)$-diagram almost coincides with a vertical line $x=$const. Both the boundary cases discussed: continuous density law and binary-shell model, have shown that below the parabola $F=15/7$ only fictitious mass-configurations result extended for the continuous density law down to $J_4=-209{,}5\,.\,10^{-8}$ and for the binary-shell model to the equipotential ellipsoid $J_4=-236{,}2\,.\,10^{-8}$. The "empirical" value $J_4=-165\,.\,10^{-8}$ is not reached at all. Beyond that it becomes obvious that the normal spheroid as well as the corresponding equipotential spheroid of the real earth-body must lie between both the boundary cases of the one-parametric equlilibrium figure with the continuous density law 18) and the binary-shell model with depth of the core 2900 km. The first one renders $J_4=-332{,}4\,.\,10^{-8}$, while for the binary-shell models J_4 lies between the limits $-310{,}7\,.\,10^{-8}\leqq J_4\leqq-288{,}8\,.\,10^{-8}$. These values, of course, suffer a small variation as they have been calculated in [1, p. 182] with somewhat different initial data. One could rightfully object the definition of the upper limit by the one-parametric equilibrium figure as we have to abstract totally from the equilibrium. In fact we could proceed from the binary-shell model to the N-shell model whereby with the transition to the limit $N\to\infty$ any continuous density law may be approximated. In that general case the limit possibly is $|J_4|>332{,}4\,.\,10^{-8}$.

With all these arguments the value $J_4=-165\,.\,10^{-8}$ appears at least very problematic. Equally problematic also is the empirical result that the higher even mass-functions are approximately of the same order of magnitude. In contrast to that the general expansion of the equipotential spheroids to eight-order [1, pp. 87–97] gives:

$$J_4=-\frac{4}{5}e^2+\frac{4}{7}e\,\bar{\varepsilon}+\frac{8}{35}f_4\,;$$

$$J_6 = \frac{8}{7}e^3 - \frac{20}{21}e^2\bar{\varepsilon} - \frac{96}{231}ef_4 - \frac{80}{231}f_6 + \frac{40}{231}\bar{\varepsilon}f_4\,; \tag{28}$$

$$J_8 = \frac{1}{1287}\Big(-2288\,e^4 + 1024\,e^2 f_4 + 1024\,ef_6 + 896 f_8 - \frac{512}{5}f_4{}^2 + 2080\,e^3\bar{\varepsilon} - 640\,\bar{\varepsilon}\,ef_4 - 320\,\bar{\varepsilon}f_6\Big).$$

True, there the mass-functions and the form-parameters can not be separated uniquely; they are correlated by the equations 26). Thus we evaluate these formulas for the data 8a) for e and $\bar{\varepsilon}$ of the fictitious equipotential ellipsoid ($f_4 = f_6 = f_8 = 0$) and find:

$$J_4 = -236{,}0\,.\,10^{-8}\,; \quad J_6 = +0{,}6\,.\,10^{-8}\,; \quad J_8 = -0{,}002\,.\,10^{-8}, \tag{29}$$

i. e. $J_4 = -393 J_6$ and $J_6 = -286\ J_8$! Hence, the absolute values of the mass-functions decrease approximately with the powers of the flattening. For the normal spheroid 8), when f_6 is neglected which enters only with one third of its value, we get $J_6 = +0{,}88\,.\,10^{-8}$, thus $J_4 = -396\ J_6$. The empirical value 9) would result for $f_6 = -185{,}2\,.\,10^{-8}$ or for $\lambda = +49{,}1$ which is extremely improbable.

Finally we combine the empirical values $J_4 = -165\,.\,10^{-8}$ and $J_6 = +65\,.\,10^{-8}$. We find from 19) and 28)

$$e = 335354{,}8\,.\,10^{-8}\,; \quad f_4 = +312{,}033\,.\,10^{-8}\,; \quad f_6 = -186{,}664\,.\,10^{-8}, \tag{30}$$

hence

$$\lambda = +49{,}5\,(!)\,,$$

which is nearly the same impossible result. Neither J_4 nor J_6 are authentic: $|J_4|$ is only about one half of the plausible value and J_6 is much too great; it exceeds the correct value by about the 70-fold quantity.

In any case, we are permitted to state that the theory of the general equipotential spheroids represents a very effective mean for the critical discussion of the mass-functions hitherto derived from artificial satellites. Above we have found lower limits for the fictitious solutions namely for the equipotential ellipsoid ($J_4 = -236{,}2\,.\,10^{-8}$) on the one hand, and for the continuous density law 18) ($J_4 = -209{,}5\,.\,10^{-8}$) bound to the condition $A = 0$ on the other. Here, however, the question arises whether it is possible at all to find mass-configurations, being physically sound or not, for the spheroids which lie in the curve defined by $(E, \omega, a.J_2)$ below the solution mentioned above: $-209{,}5\,.\,10^{-8} \leqq J_4 \leqq 0$.

Literature:

1. K. Ledersteger: "Multi-parametric Theory of Spheroidal Equilibrium Figures and the Normal Spheroids of Earth and Moon", Vienna 1966
2. J. Kozai, Report, Satellite-Symposium Athens, April 1965
3. W. C. Lambert: "The Gravity Field of an Ellipsoid of Revolution as a Level Surface", Ann. Acad. Scient. Fennicae, Helsinki 1961.

The Horizontal Isostasy

by *K. Ledersteger*, Vienna

According to the new Delft-expansion of the heights and depths of the earth in spherical harmonics up to the 32nd order inclusively, the average depth of the lithosphere is $L_0 = -2367$ m, that of the hydrosphere $H_0 = -2601$ m and therefore the average height of the continents for the whole surface of the earth + 234 m. If we postulate for the normal spheroid equality of volume with the real earth-body we get $a = (6378{,}165 + 0{,}234) = 6378{,}399$ km. When using the flattening 1:298,28 the volume

of the earth-body results to $V = 1083{,}341 \cdot 10^{24}$ cm^3 and the volume of the "solid earth" to $V' = 1082{,}016 \cdot 10^{24}$ cm^3, hence the mass of the ocean waters ($\rho_w = 1{,}028$) to $\rho_w (V - V') = 1{,}362 \cdot 10^{24}$ g. Since the mass of the earth is $E = 5976{,}106 \cdot 10^{24}$ g, that of the solid earth is $E' = 5974{,}744 \cdot 10^{24}$ g and the mean density $\rho_m = 5{,}5218$. The crust consists of the sial-stratum (granite) of density 2,67 and the basalt-like sima of density 2,87. In addition we shall neglect the flattening, and therefore we substitute the mean lithosphere by the sphere of equal volume with the radius $R = 6368{,}665$ km. The Mohorovicić-surface, running in variable depth, represents the separating surface between crust and mantle, and which after regularization lies in a depth of about 33 km of the normal spheroid. If we hold the assumption for the density of the mantle at its surface to be $\rho_{Mo} = 3{,}32$, a density discontinuity of 0,45 occurs there. Finally we suppose the separating surface of sial and sima, the so-called Conrad-discontinuity, to be in a depth of 20 km and to represent a density discontinuity of 0,20. With the normal spheroid the surface of the ocean is 234 m above the geoid, and the ocean-bottom, the idealized lithosphere, lies in a depth of 2367 m. This latter surface we designate as the upper reference level, and, contrary to the usual definition, we consider as topography all deviations of the real earth-crust from the normal spheroid.

In the following calculation of the mass-differences with respect to the normal spheroid, the convergency of the spherical radii must be considered. The comparison column of the normal spheroid with a cross-section of 1 m^2 in the assumed basis contains the mass:

$$1{,}028 \int_0^{2601} (1 + z/R)^2 \, dz \doteq 1{,}028 \int_0^{2601} (1 + 2\,z/R) \, dz = 1{,}028 \cdot 2601 \, (1 + 2{,}601/R) = 2674{,}920 \text{ t/m}^2 . \qquad (1)$$

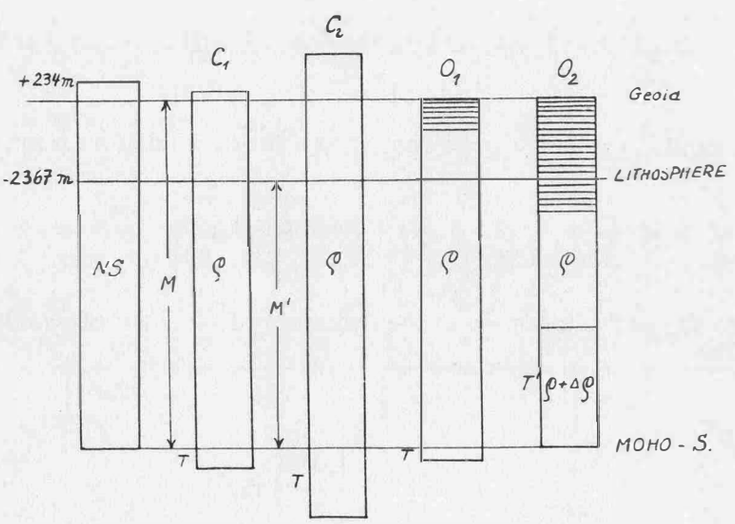

Fig. 1

On the continents we have to distinguish two cases according to the elevation above sea level being $h \leqq 234$ m. In the first case the mass difference (Fig. 1) with $\rho = 2{,}67$ results to

$$\Delta q_1 = (\rho - 1{,}028) \int_0^{2367 + h} (1 + 2\,z/R) \, dz - 1{,}028 \int_{2367 +}^{2601} (1 + 2\,z/R) \, dz =$$

$$= (\rho - 1{,}028)(2367 + h)\left(1 + \frac{2{,}367 + h_{\text{km}}}{R}\right) - 1{,}028\,(234 - h)\left(1 + \frac{4{,}968 + h_{\text{km}}}{R}\right).$$

For the second case ($h > 234$ m) we find in analogy:

$$\Delta q_2 = (\rho - 1{,}028)\, 2601 \left(1 + \frac{2{,}601}{R}\right) + (h - 234)\left(1 + \frac{4{,}968 + h_{\text{km}}}{R}\right),$$

and it can easily be proved that both expressions not only agree for $h = 234$ m, but are altogether identical. In fact, it would not at all be necessary to distinguish these two cases, but it seems better so with respect to the following pressure equations. By collecting the terms independent of h the continental final value results:

$$q_c = A + h\left(1 + \frac{4{,}734 + h}{R}\right) \tag{2}$$

with

$$A = 2367{,}880\,\rho - 2674{,}920\,. \tag{2a}$$

In the oceanic case t stands for the ocean-depth thought of as being positive. Here we need not even consider both cases $t \lesseqgtr 2367$ m separately since the distinction refers only to the sign of the difference $(2367 - t)$. We find

$$\Delta q_o = -1{,}028\,.\,234\left(1 + \frac{4{,}734 + 0{,}234}{R}\right) + (\rho - 1{,}028)\,(2367 - t)\left(1 + \frac{2{,}367 - t_{\mathrm{km}}}{R}\right).$$

The terms independent of t are identical with A so that

$$\Delta q_o = A - (\rho - 1{,}028)\,t\left(1 + \frac{4{,}734 - t_{\mathrm{km}}}{R}\right). \tag{3}$$

If, according to Vening-Meinesz [1] the ocean water is condensed to crust density but under neglection of the convergency of the plumblines, we obtain the defintion of a new litosphere

$$\bar{L} = \left(L - \frac{1{,}028}{\rho} H\right). \tag{4}$$

On the continent $H = O$ and $\bar{L} = L = h$, and on the ocean $L = H = -t$ so that because of

$$\rho\bar{L} = \rho\, h \text{ and } \rho\bar{L} = -(\rho - 1{,}028)\,t \tag{5}$$

both the formulas 2) and 3) formally can be combined if the ocean depth t is introduced as a negative height $(t = -h)$:

$$\Delta q = A + \bar{L}\left(1 + \frac{4{,}734 + h_{\mathrm{km}}}{R}\right), \tag{6}$$

without detriment to the neglection done in the definition of $\bar{L}$. The mean value of $\bar{L}$ is:

$$\bar{L}_o = \left(L_o - \frac{1{,}028}{\rho} H_o\right) = \left(-2367 + \frac{1{,}028}{\rho} 2601\right) \tag{7}$$

$$\bar{L}_o = \left(1 - \frac{1{,}028}{\rho}\right) h_o\,. \tag{7a}$$

With the sial-density 2,67 results $\bar{L}_o = -1365{,}566$ m and $h_o = -2220{,}500$ m, further $A = 3647{,}320\ t/\mathrm{m}^2$ and thus for $\bar{L}_o$

$$q_o = (3647{,}320 - 3647{,}500) = -0{,}180\ t/_{\mathrm{m}^2}\,. \tag{8}$$

It is obvious that the small difference is caused only by the approximations in the preceding formulas and that therefore the topographical mass-differences Δq vanish when summarized over the whole earth. In fact, because of 6) and 7a)

$$\Delta q_o = 2367{,}880\,\rho - 2674{,}920 + 1{,}0003947\,\rho\left(-2367 + \frac{2673{,}828}{\rho}\right) = -0{,}054\,\rho - 0{,}037 \sim 0 \tag{9a}$$

and we see that $\Delta q_o = 0$ must always hold almost independently of ρ. Hence the sial-density mus be given.

The column of the real earth corresponding to the value $\bar{L}_o$ is "equivalent" to a column of the normal spheroid provided both contain equal masses. According to 3) and because of $(\rho - 1{,}028) =$

1,642 from

$$q_o = 3647{,}320 + 1{,}642\, h_o\left(1 + \frac{4{,}734 + h_o}{R}\right) = 0 \tag{9b}$$

results easily $h_o = -2220{,}390$ m. Due to the consideration of the convergency of the radii the absolute value is somewhat smaller than the approximation $h_o = 2220{,}500$ m resulting from 7a). Namely, because of its larger cross-section the water stratum of the depth 234 m, removed from above the geoid, has to supplement to crust-density at the basis a water stratum of the slightly greater depth of 146,610 m.

In the hitherto non-isostatic case the removal of the topography or the regularization by mass-displacements in direction from the continents to the oceans, runs principally in a horizontal way and in the level of the mean lithosphere. But since the real earth-body, too, is close to a hydrostatic equilibrium configuration, the continental excess pressure on the one hand, and the pressure deficit of the deep oceans on the other hand require negative, resp. positive compensating masses as resulting e. g. from Airy's hypothesis of floating equilibrium. According to this pyhothesis the continental shells with their "roots" immerse the deeper into the ultra-sima below the idealized Moho-surface the greater their magnitude, while below the deeper oceans ultra-sima ascends into the "anti-root" of the crust. The basis of the mightiest sial-shell may be considered to represent the compensating surface of pressure. In the continental case and for oceans of depth $t < 2220$ m the density discontinuity $\Delta\rho$ at the surface of the mantle characterizes the negative compensating masses, for oceans of depth $t > 2220$ m the positive ones. If $T > 0$ stands for the magnitude of the root and $T < 0$ for that of the anti-root, the topographic mass-differences Δq_t are combined with the isostatic mass-differences

$$\Delta q_i = -\Delta\rho \int_{-(M'+T)}^{-M'} (1 + 2\,z/R)\,dz = -\Delta\rho\,.\,T\left(1 - \frac{2\,M' + T}{R}\right), \tag{10}$$

with $M' = (M - 2{,}367)$ km being the depth of the idealized Moho-surface below our level of reference.

Because of the opposite sign of the compensation in every vertical column the sum of topography and isostatic compensation $\Delta q = (\Delta q_t + \Delta q_i)$ is considerably smaller in its absolute value than the purely topographical mass-difference Δq_t, but does not vanish. However, for the conservation of the total mass the sum of the isostatic compensating masses over the whole earth as well as the sum of the topographic mass-differences must vanish. We may interpret this fact in that way that parts of the ultra-simatic masses of quantity 10) are displaced in the roots and reappear as additional (positive) masses in the anti-roots. Then the regularization produces a horizontal flux of ultra-simatic masses in opposite direction, i. e. from the oceans to the continents. Hence, we only have to deal with horizontal mass-displacements, namely with those of topographic masses along the mean lithosphere and those ol ultra-simatic masses along the mean Moho-surface in opposite direction. The usual, vertical interpretation according to the floating equilibrium is not much more evident. For it is not true that the root of a mountain is that deeply immersed in the ultra-sima that the weight of the displaced ultra-sima equals the total weight of column. On the contrary, the vertical column rests upon the idealized surface of the mantle, as in the normal spheroid, and only the positive topographic masses produce an excess pressure which is compensated by the displacement of parts of the ultra-sima in the root. Because of the downward gravity increase not all of the topographic mass is needed for replacing the density deficit in the root. Thus the purely "local" isostasy, i. e. only a vertical displacement of masses, is insufficient. Mass-compensation and pressure-compensation in a vertical way only are not compatible, and again the vertical mass-displacements are accompanied by horizontal displacements in direction from the continents to the oceans. Actually, for greater ocean depths the mass-surplusses in the anti-root would have to be used for replacing the mass-deficit of the oceans of a depth less than 2220 m which, however, reduces the pressure and reestablishment of equilibrium requires additional masses. True, the integrals of Δq_t, Δq_i and Δq vanish when extended over the whole surface. But the sum of the negative (positive) compensating masses is smaller than the sum of the positive (negative) topographic masses.

The magnitudes of roots and anti-roots are determined by rigorous pressure equations. To that purpose we use for every column the gravity g_o in the mean lithosphere as comparative value, and thus have to determine the gravity in the centers of Bouguer-plates of the densities 1,028, $(\rho - 1{,}028)$ and

ρ in various combinations. These centers have the heights f with respect to the reference level and the free-air reduction is $2g_o f/R$. The reduction for the plate of density ϑ and thickness d reads in Helmert's form: $3\vartheta\ g_o/2\rho_m R$.

We investigate the first continental case $h < 234$ m. The pressure equatiou reads obviously

$$-1{,}028\,(234-h)\,g_1+(\rho-1{,}028)\,(2367+h)\,g_2=\Delta\rho\,T g_3\,.$$

The center of the missing water layer lies by $f_1 = 2367 + (234 + h)/2$ above the reference level, and Prey's reduction gives with sufficient approximation ($\rho/\rho_m \sim 1/2$)

$$g_1 = g_o\left(1-\frac{2{,}367+0{,}468-h_{km}}{2R}\right).$$

The center of the positive topography is by $f_2 = (2367 + h)/2$ above the reference level and the effect of this plate ($d = 2f_2$) of density ρ vanishes in its center, so that

$$g_2 = g_o\left(1-\frac{2{,}367+h_{\mathrm{km}}}{4R}\right).$$

For the center of the root $f_3 = M' + T/2$. In consideration of other neglections we need not worry about the density difference of sial and sima; for sial $\rho/\rho_m = 0{,}4835$ and for sima 0,5198 so that we are permitted to use the mean value 0,5. Thus

$$g_3 = g_o\left(1+\frac{(2M'+T)_{\mathrm{km}}}{4R}\right)$$

and the pressure equation reads:

$$-(1{,}028)\,(234-h)\left(1-\frac{2{,}835-h}{2R}\right)(\rho-1{,}028)\,(2367+h)\,.$$

$$\cdot\left(1-\frac{2{,}367+h}{4R}\right)=\Delta\rho\,T\left(1+\frac{2M'+T}{4R}\right). \tag{11}$$

For the second continental case ($h > 234$ m) results in analogy:

$$(\rho-1{,}028)\,2601\left(1-\frac{2{,}601}{4R}\right)+\rho\,(h-234)\left(1-\frac{4{,}968+h}{4R}\right)=\Delta\rho\,T\left(1+\frac{2M'+T}{4R}\right). \tag{12}$$

Both equations 11) and 12) coincide for $h = 234$ m, as it should be. Yet they are not identical. On the contrary, the difference 11) − 12) = + 3 . 1,028 $(234-h)^2/4R$, and the maximum amount for $h = 0$ is 0,0066 t/m^2. Neglecting this small difference, 12) may be considered the general pressure equation of the continental case. We transcribe it into the form:

$$\rho\,h\left(1-\frac{4{,}734+h}{4R}\right)+(2366{,}780\,\rho-2673{,}555)=T\left(1+\frac{2M'+T}{4R}\right). \tag{13}$$

Now we turn our attention to the oceanic pressure equation, and start with the case $t < 2367$ m. Again using $\rho = \rho_m/2 = 2{,}761$ in the correction terms, we find:

$$-1{,}028\,.\,234\left(1-\frac{4{,}968}{R}+\frac{3}{2}\,\frac{2{,}367-t}{R}+\frac{3}{2}\,\frac{1{,}028}{2{,}761}\,\frac{t}{R}\right)+(\rho-1{,}028)\,.$$

$$.\,(2367-t)\left(1-\frac{2{,}367-t}{4R}\right)=\Delta\rho\,T\left(1+\frac{2M'+T}{4R}\right). \tag{14}$$

Simple transformation gives

$$-(1{,}028)\,t\left(1-\frac{4{,}734-t}{4R}\right)+(2366{,}780\,\rho-2673{,}548)+226{,}481\,\frac{t}{R}=\Delta\rho\,T\left(1+\frac{2M'+T}{4R}\right). \tag{14a}$$

If we bring the first continental pressure equation 11) into the analogous form

$$\rho h\left(1-\frac{4{,}734+h}{4R}\right)+(2366{,}780\,\rho-2673{,}548)-360{,}828\,\frac{h}{R}+$$

$$+1{,}028\,h\,\frac{3h}{4R}=\Delta\rho T\left(1+\frac{2M'+T}{4R}\right), \tag{11a}$$

both the last equations are identical for $h=t=0$, as it should be. If we further suppress in 11a) the sum of the two last terms, since their maximum value for $h=234$ m only amounts to 0,020 t/m^2, and similarly the last term of the left-hand member of 14a), which for $t=2220$ m only amounts to 0,079 t/m^2, then 14a) also agrees sufficiently with 13) when, according to 5), the fictitious lithosphere $\bar{L}$ is introduced and t is substituted by $-h$:

$$\rho\bar{L}\left(1-\frac{4{,}734+h}{4R}\right)+(2366{,}780\,\rho-2673{,}552)=\Delta\rho T\left(1+\frac{2M'+T}{4R}\right). \tag{15}$$

In this equation the continental and the first oceanic case are comprised namely for all $h>-2220$ m. For equation 14a) is exactly valid only as long as a root exists, but which vanishes for a particular h_o. With $\rho=2{,}67$ we find h_0 from

$$2{,}67\,\bar{L}_o\left(1-\frac{4{,}734+h_o}{4R}\right)+3645{,}751=0\,, \tag{16}$$

which together with 7a) gives $\bar{L}_0=-1365{,}585$ m and $h_o=-2220{,}530$ m. These values are almost identical with those of 7). An exact identity is impossible, because previoulsy $\bar{L}_o$ was derived from the assumption of an approximate mass-equality under neglection of the convergency of the spherical radii, but now from the requirement of pressure-equality. The transfer of the water-masses from above the geoid to the lithosphere produces an increase in pressure which can only be compensated by a diminution of mass, i. e. by a greater ocean depth. Correspondingly the ocean depths of the equivalent columns must turn out differently. Above we found from 9b) with exact mass-equality $h_o=-2220{,}390$ m, from 7) with approximate mass-equality $h_o=-2220{,}500$ m, and now with pressure equality $h_o=-2220{,}530$ m. Apart from this, the fact that $\bar{L}_o$ is connected with $T=0$ proves that the isostatic mass as well as the topographic mass vanish when summed up over the whole earth, as already has been stated above. In that way the simultaneous conservation of mass and pressure is obtained, a result hitherto impossible in the isostatic models with local and even with regional isostasy.

As a consequence of the new definition of the topography not the column $h=0$, but the normal spheroid itself or the equivalent column $\bar{L}_o$ serves as a comparative column. Hence, for the ocean depth of $2221\leqq t\leqq 2367$ m the roots are already substituted by anti-roots with homogeneously distributed additional mass of density $\Delta\rho$. The gravity value g_o of the lithosphere contains the effect of such a plate of magnitude T' in form of the positive quantity $3\,\Delta\rho T' g_o$: $2\rho_m R$, while the effect vanishes at the center of the anti-root by reasons of symmetry. Thus the value

$$T'.\,0{,}27165\,\Delta\rho\,\frac{T'}{R}\,g_o \tag{17}$$

is to be subtracted. But since the maximum mass at the lithosphere which is to be compensated, amounts only

$$(\rho-1{,}028)(2367-2221)=240\,t/m^2\,,$$

the magnitude of the anti-root is approximately $T'=240/\Delta\rho$, i. e. for $\Delta\rho=0{,}5$ only 480 m so that 17) renders 0,0049 t/m^2 which value obviously may be neglected.

In the second oceanic case ($t>2367$ m) the following applies:

$$-1{,}028\,.\,234\left(1-\frac{4{,}968}{R}+\frac{3}{2}\,\frac{1{,}028}{2{,}761}\,\frac{2{,}367}{R}\right)-(\rho-1{,}028)(t-2367)\,.$$

$$\cdot\left(1+\frac{t-2{,}367}{R}-\frac{3}{4}\,\frac{1{,}028}{2{,}761}\,\frac{t-2{,}367}{R}\right)=-\Delta\rho T'\left(1+\frac{2M'-T'}{4R}-\frac{3}{4}\,\frac{\Delta\rho}{2{,}761}\,\frac{T'}{R}\right). \tag{18}$$

For $t = 2367$ m both the equations 14) and 18) agree; their left-hand and right-hand members are equal, if in 14) the neglected term 17) is considered. But despite continous transition both the expressions 14a) and

$$-(\rho - 1{,}028)\, t\left(1 - \frac{4{,}734 - t}{4R}\right) + (2366{,}366\,\rho - 2673{,}039) + \tag{18a}$$

$$\frac{t}{R}(2889{,}499\,\rho - 2970{,}405 - 0{,}75\,\rho\, t + 0{,}771\, t) = -\Delta\rho\, T'\left(1 + \frac{2M' - T'}{4R} - \frac{3}{4}\,\frac{\Delta\rho}{2{,}761}\,\frac{T'}{R}\right)$$

are not identical. Strictly spoken, we have to distinguish four cases, namely the continental case ($h > 0$), the first oceanic case with a root ($0 < t < 2221$ m) and an anti-root ($2221 < t < 2367$ m); and finally the second oceanic case ($t > 2367$ m). The third case needs not to be separately dealt with because of its trifling deviation.

At first we may analyse the case of the root ($h > -2220{,}5$ m) uniformly. If we substract the pressure equation 15) reduced to zero from the total mass equation, i. e. from the sum of 6) and 10), we get

$$\Delta q = \bar{L}\,\frac{5}{4}\,\frac{4{,}734 + h}{R}\,(1{,}100\,\rho - 1{,}368) + \frac{5}{4}\,\Delta\rho\, T\,\frac{2M' + T}{R}. \tag{19}$$

Expressing $\bar{L}$ and T in km and introducing, for the purpose of eliminating $\Delta\rho\, T$ and T, the first approximation of 15) which means a slight loss in accuracy

$$\Delta\rho\, T = \rho\bar{L} + (2{,}36678\,\rho - 2{,}67355) = \rho\bar{L} + B, \tag{15a}$$

we obtain

$$\Delta q = \frac{5000}{4R}\,[\rho\bar{L}\,(2M + h + 2B/\Delta\rho) + (\rho\bar{L})^2/\Delta\rho + (C + 2M'B + B^2/\Delta\rho)], \tag{20}$$

where M is the mean depth of the Moho-surface, $M' = (M - 2{,}367)$ the mean thickness of the solid crust and C is an abbreviation for

$$C = \frac{4R}{5000}\,(1{,}100\,\rho - 1{,}368) = 5{,}6044\,\rho - 6{,}9699. \tag{20a}$$

The third term of 20) represents the mass-increment of the column for $h = \bar{L} = 0$ with respect to the normal spheroid. With the assumption of $\rho = 2{,}67$, $\Delta\rho = 0{,}5$ and $M' = 30{,}6$ km this increment results from 20) to $\Delta q = 50{,}579$ t/m^2, while the more rigorous calculation with 19) and 15) gives: $\Delta q = 50{,}434$ t/m^2. The error of the approximation thus amounts to 0,145 t/m^2 or 0,29 %.

But now we have to distinguish the continental and the first oceanic case. In the continental case $h = \bar{L}$ and 20) proceeds to

$$\Delta q = \frac{5000}{4R}\,[\rho L\,(2M + 2B/\Delta\rho) + \rho\bar{L}^2\,(1 + \rho/\Delta\rho) + (C + 2M'B + B^2/\Delta\rho)], \tag{21a}$$

while in the oceanic case according to the second equation 5) with $h = -t$ and $\rho = 2{,}67$ holds: $h = 1{,}626066\ \bar{L}$; hence 20) reads

$$\Delta q = \frac{5000}{4R}\,[\rho\bar{L}\,(2M + 2B/\Delta\rho) + \rho\bar{L}^2\,(1{,}626066 + \rho/\Delta\rho) + (C + 2M'B + B^2/\Delta\rho)]. \tag{21b}$$

Thus we have to deal with two parabolas $\Delta q = F(\bar{L})$, which merge continuously with a common tangent at point $\bar{L} = 0$.

In the second oceanic case we have to subtract the pressure-equation 18a), reduced to zero, from the mass-equation. At first we transform the pressure-equation with $T' = -T$ to

$$\rho\bar{L}\left(1 - \frac{4{,}734 + h}{4R}\right) + (2366{,}366\,\rho - 2673{,}039) - \frac{h}{R}\,(4744{,}557 + \tag{18b}$$

$$+ 1{,}2315\,h) - \Delta\rho T\left(1 + \frac{2M' + T}{4R} + 0{,}27165\,\Delta\rho\,\frac{T}{R}\right) = 0.$$

There we have substituted $-t$ by h and have introduced $\rho = 2{,}67$ into the small correction terms. In analogy to 21b) we find the mass difference by subtraction of equation 18b) from the sum of 6) and 10) when using the first approximation of 18b)

$$\Delta q = \frac{5000}{4R}\left[\rho\bar{L}\left(2M + 2B'/\Delta\rho + 0{,}43464\,B' + \frac{3{,}79565}{\rho - 1{,}028}\right) + \rho\bar{L}^2\left(\frac{\rho}{\rho - 1{,}028} + \right.\right. \tag{22}$$

$$\left.\left. + \frac{\rho}{\Delta\rho} + 0{,}21732\,\rho + \frac{0{,}98520\,\rho}{(\rho - 1{,}028)^2}\right) + (C' + 2\,M'\,B' + B'^2/\Delta\rho + 0{,}21732\,B'^2)\right]$$

with: $B' = 2{,}36637\,\rho - 2{,}67304\,;\quad C' = \frac{4R}{5000}(1{,}514\,\rho - 1{,}881) = 7{,}71373\,\rho - 9{,}58357.$ (22a)

The oceanic parabola of the first case with anti-root, not expressively shown here, merges of course with 22) for $h = -2{,}367$ km; this also applies to 21b) and 22). When neglecting the very small difference $(B' - B)$, we get $\delta(\Delta q) = 0{,}085\ t/\mathrm{m}^2$ which almost entirely is caused by the neglections committed in the derivation of 21b).

ρ, $\Delta\rho$ and M may be considered the free parameters of the problem. The mean sial-density $\rho = 2{,}67$ is the most secure value. That is why ρ stands only in the principal terms of the preceding developments, while for the numerical calculation of the additional terms the value 2,67 or even the mean crust-density $\rho_m/2 = 2{,}7609$ was used, as with the gravity values and in 17). In fact, for the regularization the horizontal mass-flux of the topography should be calculated with the sial-density, while for the counter-running flux of the isostatic compensation the density difference $\Delta\rho$ between mantle and sima, being about $\Delta\rho \sim (3{,}32 - 2{,}87)$ should be used almost exclusively. Only above the Conrad-discontinuity, i. e. in very great ocean depths the density difference mantle — sial is in question, too. But the Conrad-discontinuity is not at all strongly marked over the whole earth. Further, for the most interesting case of maximum depth of the ocean, the anti-root rises far into the sial so that we better use the mean density of crust in this case: $\Delta\rho \sim (3{,}32 - 2{,}76)$.

The mass-difference is a minimum at the vertex of the second oceanic parabola, for which by differentiation of 22) under consideration of 5) easily the ocean depth t results:

$$t_v = \frac{M + 1{,}68357 + 3{,}64516/\Delta\rho}{1{,}73344 + 1{,}642/\Delta\rho}\ \mathrm{km}\,. \tag{23}$$

By computing the pertinent magnitude T'_v of the anti-root from the principal terms of 18b)

$$T'_v = +\,1{,}642\,t_v - 3{,}645216\,, \tag{18c}$$

we finally obtain the remaining magnitude of the crust $C_v = (M - t_v - T'_v)$. The quantities t_v, T'_v and C_v may be tabulated for several equidistant values for the mean depth of the Moho-surface and for the density discontinuity $\Delta\rho$:

M	29	31	33	35	37	km
0,4	6,82	7,16	7,50	7,84	8,19	t_v
	18,87	20,28	21,68	23,09	24,50	
	3,32	3,57	3,82	4,07	4,32	
0,5	7,57	7,97	8,37	8,76	9,16	
	17,56	18,87	20,18	21,49	22,80	T'_v
	3,87	4,16	4,45	4,74	5,04	
0,6	8,22	8,67	9,12	9,57	10,01	
	16,43	17,65	18,88	20,10	21,33	
	4,35	4,68	5,00	5,33	5,66	C_v
0,7	8,80	9,29	9,78	10,27	10,76	
	15,43	16,58	17,73	18,88	20,03	
	4,77	5,13	5,49	5,85	6,21	

Simultaneously, of course, t_ν defines the maximum ocean depth, since with the ocean depth increasing further the mass-deficit with respect to the normal spheroid can in no way decrease. But now the crust does not vanish altogether for the maximum ocean depth, while in the usual definition of the topography t_{max} at the vertex of the oceanic parabola was connected with $C_\nu = 0$. Now it becomes obvious that the remaining crust magnitude C_ν increases with increasing M and $\Delta\rho$.

The greatest ocean depth known has been measured to 10,8 km in the Philippine Graben. With maximum t equation 23) renders

$$M - 17{,}03758 = 14{,}08844/\Delta\rho \tag{24}$$

and we find the following pairs of values:

$M = 33$ km :	$\Delta\rho = 0{,}883$	$M = 39$ km ;	$\Delta\rho = 0{,}642$
35	0,784	41	0,588
37	0,706	43	0,543 .

Hence, we had either to adopt a greater depth of the Moho-surface in contrast to the seismic finding or a greater density discontinuity, i. e. a greater surface density of the mantle. But actually we have to consider that the density of the crust is not at all constant and that therefore the assumption of $\Delta\rho$ as well as the calculation of the magnitude of roots and anti-roots are doubtful. Besides, the isostasy must not be overcharged; already the above computation of the gravity values and of the pressure equation shows that our formulas can only be used for columns of considerable cross-section. Furthermore, just for maximum ocean depth the anti-root extends almost equally into sima and sial so that we better use the mean $\Delta\rho = 0{,}55$. But for the plausible model $M = 33$ km and $\Delta\rho = 0{,}55$ the maximum ocean depth results to 8,75 km and the remaining magnitude of the crust to 4,72 km, and we may consider these results to be very satisfactory.

Finally the location of the center of gravity may be analyzed. In the non-isostatic case we find the displacement of the center caused by the topography from the first-order terms of the harmonical expansion of the lithosphere and the hydrosphere. According to 4)

$$\bar{L} = L - 0{,}38502\,H\,; \quad q = 2{,}67\,\bar{L}. \tag{25}$$

Proceeding from the Delft-expansion we have

$L_{1,0} = +1157$ m ;	$H_{1,0} = +1026$ m ;	$\bar{L}_{1,0} = +762$ m ;	$q_{1,0} = 2103{,}1\ t/m^2$
$L^{(c)}_{1,1} = +1029$	$H^{(c)}_{1,1} = +911$	$\bar{L}^{(c)}_{1,1} = +678$	$q^{(c)}_{1,1} = 1810{,}9$
$L^{(s)}_{1,1} = +693$	$H^{(s)}_{1,1} = +560$	$\bar{L}^{(s)}_{1,1} = +477$	$q^{(s)}_{1,1} = 1274{,}6$

and

$$q_1(\varphi,\lambda) = q_{1,0}\sin\varphi + q^{(c)}_{1,1}\cos\varphi\cos\lambda + q^{(s)}_{1,1}\cos\varphi\sin\lambda\,. \tag{26}$$

The displacement is directed to the maximum of q_1:

$$s = \frac{1}{\rho_m}\,q_{1,\,max} = \frac{4\pi}{3E}R^3 q_{1,\,max} = \frac{1}{\rho_m}\sqrt{q_{1,0}^2 + q^{(c)2}_{1,1} + q^{(s)2}_{1,1}}\,, \tag{27}$$

hence

$$s = 553{,}08\text{ m}\,. \tag{27a}$$

The entire topography is interpreted as areal coating onto the mean lithospere (radius R) with the constant part A of 6) being neglected as it obviously creates no displacement of the center of gravity. The direction of the translative vector is:

$$\begin{gathered} tg\,\varphi_\nu = q_{1,0} \;:\; \sqrt{q^{(c)2}_{1,1} + q^{(s)2}_{1,1}} = 0{,}9497\,; \quad \varphi_\nu = 43^0\,31'\,; \\ tg\,\lambda_\nu = q^{(s)}_{1,1} : q^{(c)}_{1,1} = 0{,}7039;\ \lambda_\nu = 35^0\,09'\,. \end{gathered} \tag{28}$$

The vector approximately points to the center of the Black Sea.

However, it would be more correct to condense the continental and the oceanic topography onto the sphere of radius $(R + 2{,}367 + h/2)$, which means an increase, respectively decrease of surface $(h \lesseqgtr 0)$ at the ratio $[1 + (4{,}734 + h)/R]$ so that in both cases $\rho\bar{L}$ represents the surface density of the topography. The compensating masses 10) must be condensed onto the center of the root, resp. the anti-root, i. e. onto the sphere of radius $[R - M' + T/2)]$, thus causing an surface change at the ratio of $[R - -(2M' + T)/R]$. Hence, $\Delta\rho$ always means the areal density of the compensation and we recognize by 15) and 18a) that the areal density of the compensation is less than the areal density of the topography. 15) and 18a) can be combined in good approximation to

$$\Delta\rho T = \rho\bar{L}\left(1 - \frac{2M + T + h}{4R}\right) + 3645{,}454\left(1 - \frac{2M - 4{,}734 + T}{4R}\right), \tag{29}$$

where the second term, being almost constant, may be neglected. Thus, in the isostatic case the displacement of the center of gravity results to:

$$s_i = \frac{4\pi}{3E}\left[\rho\bar{L}_{1,\,max}\left(R + \frac{4{,}734 + h}{2}\right)^3 - \left(R - \frac{2M' + T}{2}\right)^3 \cdot \left(1 - \frac{2M + T + h}{4R}\right)\right],$$

hence

$$s_i = s\left[\left(1 + \frac{3}{2}\,\frac{4{,}734 + h}{R}\right) - \left(1 - \frac{3}{2}\,\frac{2M - 4{,}734 + T}{4R}\right) \cdot \left(1 - \frac{2M + T + h}{4R}\right)\right]$$

or finally

$$s_i = \frac{7}{4}\,\frac{2M + T + h}{R}\,s\,. \tag{30}$$

For the model $M = 33$ km and $\Delta\rho = 0{,}55$, and with 27a) and the mean values $h = -2{,}367$ km and $T = -0{,}240/0{,}55 = -0{,}436$ km we get

$$s_i = 9{,}604\,\text{m}\,. \tag{30a}$$

It is obvious that with the pressure compensation always a greater displacement of the center of gravity results than with the mass compensation. For the pressure reduction created by the vertical build-up of the continents must be compensated again by a horizontal flux of masses. But in fact, of course, a displacement of the center of gravity is not possible at all. Its apparent existence therefore can only be understood by the imperfection of the isostatic concept, i. e. according to Vening-Meinesz by the fact that the variation of the potential caused by the mass-transport creates deformations of the surfaces of equal density in greater depths of the plastic earth, too. Actually always a displacement of the center of gravity must occur with the isostatic mass-transports if we consider the earth below the compensating surface of pressure, i. e. below the basis of the mightiest montain root, falsely as being rigid.

Literature:

1. Vening-Meinesz, F. A.: "The Indirect Isostatic or Bowie Reduction and the Equilibrium Figure of the Earth", Bull. géod., N. S. Nr. 1, Paris 1946
2. Ledersteger, K.: „Die prinzipiellen Mängel des isostatischen Konzeptes", Schweiz. Zeitschrift für Vermessung, Kulturtechnik und Photogrammetrie, Winterthur 1963
3. Ledersteger, K.: „Das Problem der Regularisierung der Erdkruste und die Isostasie", Gerlands Beiträge zur Geophysik, Leipzig 1965

New Conception of the "Equilibrium-condition" of One-parametric Spheroid and the Normal Spheroid of the Earth

by *Z. Zątbek*, Warszawa

Two fundamental statements of new Ledersteger's theory [1] concerning spheroidal equilibrium figures, i. e. the rigorous unequivocalness of density-law of these figures and the principle of destratification, have been mathematically demonstrated [2] by development of the Wavre's theory on

stratification of inhomogeneous figures of equilibrium. On the contrary, the promulgated hypothesis of "equilibrium-condition" of one-parametric spheroid in form of equation $\frac{df_4}{da} = 0$ has not been strictly proved leaving this problem still opened. Nevertheless, two formerly mentioned statements provide the possibility of further researches in the matter of equilibrium condition.

In classical theory of equilibrium figures the possibility of examination of inhomogeneous figures was given by the well known Clairaut's differential equation relating the flattening-function of inner level surfaces with the density-function. The formulae of density-law had to be so chosen as to facilitate the integration of this linear differential equation of second order. In this way the Clairaut's theory solved the problem with assumption of a definite density-law and omission of small quantities of flattening of second order.

A similar role is actually played by the principle of destrafication. Superiority of this method consists in the fact that by carrying on destrafication of any examined figure with a definite density-law until a suitable inner level surface has been attained, one can determine the flattening of this figure with a fair degree of accuracy while taking into consideration the potential theory of outer space.

Nevertheless, when using this method for computation of any one-parametric figure of equilibrium with accuracy to the square of flattening, yet the equilibrium condition of this figure must be known besides the equations system of level spheroid of fourth order. 13 parameters appear in Helmert's theory of level spheroid, viz.: besides the mass M three geometric elements — equatorial semi-axis a, geometric flattening α and parameter f_4; three elements of theoretical acceleration — equatorial acceleration γ_o, gravity flattening β and coefficient β_4; three mass-functions — mean density ρ_m, static flattening J_2 and mass-function δ or J_4; moreover three physical quantities — rotation velocity ω, relation of centrifugal force to gravity at equator $\varepsilon = \omega^2 a/\gamma_o$ or parameter $\bar{\varepsilon} = \omega^2 a^3/\varkappa M$ and the value of potential U which for a normal earth's spheroid must be equal to the geoid potential W_o.

8 equations made up by Helmert to relate those 13 quantities are presented by Ledersteger as follows:

1) $$\alpha + \beta = \frac{5}{2}\bar{\varepsilon} - \alpha^2 - 3\alpha\bar{\varepsilon} + \frac{15}{4}\bar{\varepsilon}^2 - \frac{5}{4}J_4$$

2) $$\gamma_o = \frac{\varkappa M}{a^2}\left(1 + \alpha - \frac{3}{2}\bar{\varepsilon} - \alpha^2 + \alpha\bar{\varepsilon} - \frac{5}{2}J_4\right)$$

3) $$J_2 = \frac{K_2}{a^2} = \frac{1}{3}\left(2\alpha - \bar{\varepsilon} - 2\alpha^2 + 2\alpha\bar{\varepsilon} - \frac{5}{4}J_4\right)$$

4) $$U = \frac{\varkappa M}{a}\left(1 + \frac{1}{3}\alpha + \frac{1}{3}\bar{\varepsilon} - \frac{1}{3}\alpha^2 + \frac{1}{3}\alpha\bar{\varepsilon} - \frac{7}{12}J_4\right) \qquad (1)$$

5) $$\beta_4 = -11\alpha^2 + 10\alpha\bar{\varepsilon} - \frac{105}{8}J_4$$

6) $$\varepsilon = \frac{\omega^2 a}{\gamma_o} \quad or \quad \bar{\varepsilon} = \frac{\omega^2 a^3}{\varkappa M} = \varepsilon\left(1 + \alpha - \frac{3}{2}\varepsilon\right)$$

7) $$f_4 = \frac{7}{2}\alpha^2 - \frac{5}{2}\alpha\bar{\varepsilon} + \frac{35}{8}J_4$$

8) $$\rho_m = \frac{3M}{4\pi}\,\frac{1}{a^3(1-\alpha)}$$

Mass-function J_4 is associated with Helmert's δ by equation

$$J_4 = -\frac{8}{35}\delta. \qquad (1a)$$

The difference between radii-vectors of spheroid and co-axial ellipsoid of revolution is defined by means of Darwin's form-parameter f_4

$$(l - s) = \frac{a}{4} f_4 \sin^2 2\varphi\,; \quad h_{max} = \frac{a}{4} f_4\,. \tag{1b}$$

where h_{max} presents the greatest height of spheroid above the ellipsoid of revolution and which appears at 45^0 of latitude.

The searched equilibrium condition of one-parametric spheroid leads in any case to elimination of one unknown from every equation of system (1). Therefore a new equation appears in a general form

$$\delta = u_1 \alpha^2 + u_2 \alpha \bar{\varepsilon} + u_3 \bar{\varepsilon}^2\,, \tag{2}$$

which characterizes the one-parametric figures of equilibrium and, in this sense, can be called "equilibrium condition" of one-parametric spheroid. The unknown values of coefficients u_1, u_2 and u_3 of this equation can be determined on the basis of known elements α, $\bar{\varepsilon}$ and δ for three one-parametric equilibrium figures. To this aim the use of two boundary figures seems to be most purposely, that is of the homogeneous MacLaurin's ellipsoid and of the spheroid of greatest mass-concentration the density of which on the free surface satisfies the Poincaré's barrier

$$\omega^2 = 2\pi k \rho_{\min}\,. \tag{3}$$

The third necessary equilibrium figure can be the one-parametric spheroid of the earth for which we have at least four empirically defined elements γ_o, ω, a and J_2.

Considering in equation system (1) the equilibrium-condition of a homogeneous ellipsoid

$$\frac{\omega^2}{2\pi k \rho} = \frac{8}{15}\alpha - \frac{4}{35}\alpha^2 \tag{4}$$

and assuming $f_4 = 0$, we obtain

$$\bar{\varepsilon} \approx \frac{4}{5}\alpha\,; \quad \delta = \frac{3}{2}\alpha^2 \tag{5}$$

and thus equation (2) for this figure takes the shape

$$\frac{3}{2} = u_1 + \frac{4}{5} u_2 + \frac{16}{25} u_3\,. \tag{6}$$

Applying the method of destrafication instead, flattening-functions of inner level surfaces of the earth's spheroid and of the spheroid of greatest mass-concentration can be examined providing thus the foundation for computation of the mass-function δ of these figures.

Adopting for density-function a general expression

$$\rho = \rho_{max} f\left(\frac{x}{a}\right), \tag{7}$$

where ρ_{max} stands for density in the mass centre and x for the equatorial radius of inner level surface, and denoting by α_x the flattening of this surface, we start from the expression of mass-moment of fourth order of an homogeneous ellipsoid approaching the square of flattening

$$K_4 M = -\frac{16}{35}\pi \rho a^7 \alpha^2$$

and finally we get the necessary formulae for an inhomogeneous figure:

$$K_4 M = -\frac{16}{35}\pi \int_o^a \rho \frac{d}{dx}(x^7 \alpha_x^2)\,dx = -\frac{16}{5}\pi \rho_{max} \int_o^a \left(\alpha_x^2 + \frac{2}{7}\alpha_x x \frac{d\alpha}{dx}\right) f\left(\frac{x}{a}\right) x^6\,dx$$

$$J_4 = \frac{K_4}{a^4} = -\frac{12}{5}\frac{\rho_{max}}{\rho_m}\frac{1}{a^7}\int_o^a \left(\alpha_x^2 + \frac{2}{7}\alpha_x x \frac{d\alpha}{dx}\right) f\left(\frac{x}{a}\right) x^6\,dx\,. \tag{8}$$

Therefore we see that the knowledge of equilibrium condition, lacking in the system of equations (1), is necessary for computation of one-parametric spheroidal equilibrium-figure of the earth and of the spheroid of greatest mass-concentration as well as for examining the flattening-function α_x of these figures by means of the method of destrafication. On the other hand the obtained parameters α, $\bar{\varepsilon}$ and δ of these figures allow to determine the coefficients of "equilibrium-condition" (2) we are looking for. The problem can be solved by the method of successive approximations when the density-law of one-parametric equilibrium figures is known. Density-law itself can be defined by examining the mass-distribution known from seismic observations. Yet this law should be theoretically confirmed.

This new conception of determination of "equilibrium-condition" and of the normal earth's spheroid by making use of some elements of Ledersteger's theory has practically been realized and the formulae necessary for respective computations presented in a more widely treated publication [3]. Here we restrain ourselves to give essentials of computation only and final results.

Taking the modified Lévy's formula

$$\rho = \rho_{max}\left[1 - \nu\left(\frac{x}{a}\right)^{\lambda}\right]^{\mu} \tag{9}$$

as basis of investigation of density-law of the one-parametric spheroid, Ledersteger has demonstrated [4] that when considering various physical possibilities represented by exponents λ and μ the solution

$$\rho = \rho_{max}\left[1 - \nu\left(\frac{x}{a}\right)^{2}\right]^{2} \tag{10}$$

yields the best approximation of the earth's density independently of equilibrium. In consequence this formula has been adopted as the most probable for one-parametric figures of equilibrium and used to determination of "equilibrium-condition" (2).

In order to obtain the first approximations of coefficients characterizing equation (2), besides MacLaurin's ellipsoid the one-parametric earth's spheroid defined by Ledersteger has been considered. Computation of the latter was completed by obtaining the value of function J_4 from formula (8) and using the given values α_x. On the basis of known functions respective integrals were calculated by applying the Simpson's method of approximate integration. The obtained values are: $J_4 = -275 \cdot 10^{-8}$ and $\delta = 1203 \cdot 10^{-8}$. In view of deficiency of respective data, the spheroid of greatest mass-concentration has been replaced in the first approximation by the mass-point spheroid for which we have $J_2 = J_4 = 0$ and $\bar{\varepsilon} \approx 2\alpha$. After having determined with these data the first approximation of coefficients u_1, u_2 and u_3 of the "equilibrium-condition" (2) and completed in this way the Helmert's equations system (1), computations have been started to infer the first approximation of one-parametric spheroidal equilibrium figure of the earth as well as approximation of the spheroid of greatest mass-concentration.

The same elements which determine the normal spheroid of the earth as equilibrium figure must also refer to the earth regularized in such a manner as to form an equilibrium figure. It is generally admitted that the disturbances of hydrostatic equilibrium occur exclusively in the earth's crust isostatically equilibrated. Therefore, the first stage of regularization of the earth must be performed in accordance with the theory of isostasy. The equatorial acceleration γ_o accords with this theory. The effect of regularization upon the principal moment of inertia $\Delta_{is} C$ and upon the statical flattening $\Delta_{is} J_2$ has also been examined. Taking into consideration the theory of Airy-Heiskanen and Prey's development for the height of lithosphere and deepness of hydrosphere, the values $\Delta_{is} C = 0{,}0604 \cdot 10^{40}$ g cm^2 and $\Delta_{is} J_2 = 37 \cdot 10^{-8}$ have been obtained. The effect of terms of zero degree of Prey's development has been omitted. The earth regularized in this way would possess a homogeneous all over the world extending ocean 2456 m deep and protruding to 225 m above the geoid as well as a homogeneous rocky layer 17,8 m thick. Since the inertia moment C becomes increased, it can be reduced to its former value by condensing the water mass of world ocean in the manner as to make its upper surface coincide with the spheroid surface corresponding to the geoid and by concentrating gradually masses in the crust, which thus becomes one-parametric. It has been calculated that the static flattening is but slightly affected by $\Delta' J_2 = -0{,}1 \cdot 10^{-8}$ owing to this operation.

Finally the following values determining the earth's spheroid have been adopted:

$$\gamma_o = 978{,}037 \text{ gal}; \quad \omega^2 = 5{,}317496 \cdot 10^{-9} \text{ sec}^{-2}; \quad a = 6378155 \text{ m}; \quad J_2 = 108305 \cdot 10^{-8}. \tag{11}$$

In consequence of the error of Potsdam system γ_0 value has been adopted 12 mgal less than in the international formula in accordance with Fischer's 1961 determination [5]. J_2 has been defined as mean value derived from observations of artificial satellites carried out by King-Hele, Cook and Rees in 1963 [6], Kozai in 1963 and 1964 [7] [8], with correction due to regularization of the earth.

After introduction of data (11), Helmert's equations system completed by the first approximation of equation (2) has been solved. Quantities characterizing the density-law (10) have also been calculated. Then, applying the principle of destrafication, flattening of inner level surfaces of this figure spaced in deepness at ten 0,1 a. intervals have been computed. Hence, by using the formula (8), values

$$J_4 = -276 \cdot 10^{-8}; \quad \delta = 1208 \cdot 10^{-8} \tag{11a}$$

have been obtained.

Considering these values and data (11), second approximation of the earth's spheroid by means of Helmert's equations has been determined and the following obtained:

$$M = 5976{,}072 \cdot 10^{24}\, g; \quad \alpha = 335313 \cdot 10^{-8}; \quad \bar{\varepsilon} = 346139 \cdot 10^{-8} \tag{11b}$$

As boundary figure necessary to determination of the coefficients of "equilibrium-condition" (2) the spheroid of greatest mass-concentration of the series of the figures (belonging to one-parametric earth spheroid) with constant mass, revolution velocity and equator radius (M, ω, a), has been adopted. Characteristic data of this spheroid are

$$M = 5976{,}072 \cdot 10^{24}\, g; \quad \omega^2 = 5{,}317496 \cdot 10^{-9}\,\mathrm{sec}^{-2}; \quad a = 6378155\ \mathrm{m};$$
$$\bar{\varepsilon} = \frac{\omega^2 a^3}{\varkappa M} = 346139 \cdot 10^{-8}; \quad \rho_{min} = \frac{\omega^2}{2\pi\varkappa} = 0{,}01269. \tag{12}$$

After this figure with first approximation of "equilibrium-condition" (2) has been computed and the flattening-functions of inner level surfaces examined, the following values were obtained by means of formula (8)

$$J_4 = -48 \cdot 10^{-8}; \quad \delta = 209 \cdot 10^{-8}. \tag{12a}$$

These data enable us to obtain the second approximation of flattening for spheroid (12)

$$\alpha = 235964 \cdot 10^{-8} \tag{12b}$$

The elements of one-parametric earth's spheroid (11a) and (11b) as well as of the spheroid of greatest mass-concentration (12a) and (12b), inferred by the aid of destrafication principle, yield the second approximation of coefficients of equilibrium-condition (2). Subsequently, the latter equation for three figures of equilibrium can be written in the following form:

for Mac Laurin's ellipsoid $\quad \frac{3}{2} = u_1 + \frac{4}{5}u_2 + \frac{16}{25}u_3,$

for normal earth's spheroid $\quad 1208 = 1124{,}3\,u_1 + 1160{,}6\,u_2 + 1198{,}1\,u_3,$

for spheroid of greatest mass-concentration $\quad 209 = 556{,}8\,u_1 + 816{,}8\,u_2 + 1198{,}1\,u_3.$

Solving the system of these three equations we obtain

$$u_1 = 3{,}242; \quad u_2 = -2{,}446; \quad u_3 = 0{,}335,$$

while we get as second approximation for "equilibrium-condition" of one-parametric spheroid

$$\delta = 3{,}242\,\alpha^2 - 2{,}446\,\alpha\bar{\varepsilon} + 0{,}335\,\bar{\varepsilon}^2$$
$$J_4 = -\frac{8}{35}\delta = -0{,}741\,\alpha^2 + 0{,}559\,\alpha\bar{\varepsilon} - 0{,}077\,\bar{\varepsilon}^2 \tag{13}$$

Including this condition the third equation of Helmert's system (1) takes the form

$$3J_2 = 2\alpha - \bar{\varepsilon} - 1{,}074\,\alpha^2 - 1{,}301\,\alpha\bar{\varepsilon} + 0{,}096\,\bar{\varepsilon}^2 \tag{14}$$

Similarily by means of (13) the unknown J_4 can be eliminated from the remaining equations of system (1).

Applying the principle of destrafication and considering the second approximation of "equilibrium-condition", computation of the flattening of inner level surfaces of the normal earth's spheroid and of the spheroid of greatest mass-concentration has been repeated. This provided the foundation to the

renewed calculation of functions J_4 of these figures. The obtained results are presented in the Table 1.

Table 1

$\frac{x}{a}$	Normal spheroid of the earth			Spheroid of greatest mass-concentration		
	ρ	α_x	$x\frac{d\alpha}{dx}$	ρ	α_x	$\frac{d\alpha}{dx}$
1	2,6179	335313 10^{-8}	2977 10^{-6}	0,0127	235964 . 10^{-8}	3860 . 10^{-6}
0,9	3,7807	307984	2249	1,0153	202294	2614
0,8	5,0017	285201	1654	3,2701	176213	1861
0,7	6,2208	266456	1182	6,3243	155422	1292
0,6	7,3848	251237	818	9,7789	139091	860
0,5	8,4476	239088	537	13,2876	126543	543
0,4	9,3703	229640	329	16,5577	117152	320
0,3	10,1210	222578	179	19,3496	110375	169
0,2	10,6749	217696	77	21,4769	105804	71
0,1	11,0144	214825	19	22,8065	103170	17
0	11,1287	213874	0	23,2586	102309	0
J_4		$-276 . 10^{-8}$			$-48 . 10^{-8}$	
δ		$1208 . 10^{-8}$			$209 . 10^{-8}$	

Identity of J_4 values for the normal earth's spheroid and the spheroid of greatest mass-concentration with J_4 as obtained in first approximation (11a) and (12a) shows that the approximation for equilibrium-condition (13) is final and computation by the method of successive approximations came to an end.

The inferred "equilibrium-condition" (13) of one-parametric spheroid is connected with the density-law (10). Yet, since formula (10) is not strictly proved, the flattening-function of inner level surfaces and mass-function J_4 of normal earth's spheroid have been examined for other power exponents of modified Lévy's law (9), namely for ($\lambda = 2$, $\mu = 3$) ($\lambda = 2$, $\mu = 1$) and ($\lambda = 4$, $\mu = 2$). Although Ledersteger expels the possibility of existence of Roche's distribution ($\lambda = 2$, $\mu = 1$), this case has also been examined in order to get the most just representation of the effect of density variation upon the quantities being examined.

The obtained results are given in the Table 2.

Table 2 Normal spheroid of the earth

$\frac{x}{a}$	$\lambda = 2$, $\mu = 3$		$\lambda = 2$, $\mu = 1$		$\lambda = 4$, $\mu = 2$	
	ρ	$\alpha_x . 10^8$	ρ	$\alpha_x . 10^8$	ρ	$\alpha_x . 10^8$
1	2,7192	335312	2,2431	335315	1,8919	335317
0,9	3,7845	307461	3,7978	309690	3,7290	311798
0,8	4,9464	283984	5,1889	288979	5,4256	294563
0,7	6,1507	264455	6,4163	272444	6,7763	282700
0,6	7,3405	248440	7,4801	259347	7,7376	275011
0,5	8,4596	235557	8,3802	249093	8,3524	270372
0,4	9,4556	225470	9,1167	241225	8,7006	267836
0,3	10,2821	217895	9,6895	235411	8,8681	266634
0,2	10,9011	212647	10,0986	231407	8,9308	266194
0,1	11,2841	209552	10,3441	229068	8,9453	266085
0	11,4138	208529	10,4259	228298	8,9462	266079
J_4	$-277 . 10^{-8}$		$-273 . 10^{-8}$		$-270 . 10^{-8}$	

We notice the relatively insignificant variation of mass-function J_4. Strictly speaking, the most digressing result for ($\lambda = 4$, $\mu = 2$) cannot be taken into consideration because of striking deviation of this density distribution from the ideas generally admitted. The best approximation of the earth density distribution presents the one-parametric earth's spheroid with density-law (10) as shown by Ledersteger. Since the internal earth's constitution is not one-parametric, the formula (10) cannot strictly be referred to every one-parametric equilibrium figure and hence supposition can be made that this formula approximates only the density distribution proper to equilibrium figures. Therefore, equation (13) derived by means of distribution formula (10) can also be considered as approximating only the "equilibrium-condition" of one-parametric spheroid. Nevertheless, taking into consideration the results presented in Table 2 one can estimate that the error of approximation of function J_4 does not excel 1%. In the point of view of geodesy such an approximation is amply sufficient.

Ledersteger's hypothesis defining "equilibrium-condition" in the form of equation $\frac{df_4}{d\lambda} = 0$ is not confirmed by "equilibrium-condition" (13) deduced on the basis of destrafication principle. Using equation (13) it is easy to show that on the free surface of inhomogeneous equilibrium figure the above mentioned derivative is less than zero and vanishes in the case of homogeneous ellipsoid only. Equation (13) provides the possibility for a definitive explanation of this problem so essential in the Ledersteger's theory of spheroidal equilibrium figures.

Coming to an end we present all elements of the normal earth's spheroid which result from solution of the system of Helmert's equations (1) with "equilibrium-condition" (13) added and starting data (11) considered:

$$M = 5976{,}072 \cdot 10^{24}\, g\,; \quad a = 6{,}378155 \cdot 10^{8}\,\text{cm}\,; \quad \alpha = 335313 \cdot 10^{-8}$$

$$f_4 = -174 \cdot 10^{-8}\,; \quad h_{max} = \frac{a}{4} f_4 = -278\,\text{cm}\,; \quad \alpha^{-1} = 298{,}23$$

$$\gamma_o = 978{,}037\,\text{gal}\,; \quad \beta = 530262 \cdot 10^{-8}\,; \quad \beta_4 = 2863 \cdot 10^{-8}$$

$$\omega^2 = 5{,}317496 \cdot 10^{-9}\,\text{sec}^{-2}\,; \quad \varepsilon = 346774 \cdot 10^{-8}\,; \quad \bar{\varepsilon} = 346139 \cdot 10^{-8}$$

$$J_2 = 108305 \cdot 10^{-8}\,; \quad K_2 = 44059{,}4 \cdot 10^{10}\,\text{cm}^2\,; \quad \delta = 1208 \cdot 10^{-8}$$

$$\rho_m = 5{,}51697\,; \quad W_o = 626372{,}4 \cdot 10^{6}\,\text{cm}^2\,\text{sec}^{-2}; \quad J_4 = -276 \cdot 10^{-8}$$

$$C - A = K_2 M = 263{,}302 \cdot 10^{40}\, g\,\text{cm}^2\,. \tag{15}$$

When comparing the theoretically inferred mass-function J_4 with its values empirically obtained by observation of artificial satellites, one can affirm a general accordance of determinations. Yet a noticeable divergence among empirical determinations of J_4 speaks in favour of theoretical result.

Values (15) enable us to form a formula for theoretical gravity on the surface of normal spheroid of the earth

$$\gamma = 978{,}037\,(1 + 0{,}0053026\,\sin^2\varphi - 0{,}0000072\,\sin^2 2\varphi)\,\text{gal} \tag{16}$$

First we have to confirm the truth of Helmert's formula (1901), except for γ_0 value. A pleasing accordance is shown by coefficient $-\frac{1}{4}\beta_4$ with its theoretical value as obtained by Wiechert and Darwin. Comparison of the formula of normal gravity with data empirically obtained in 1962 by Uotila [9] appears also to be favourable.

Literature

1. Ledersteger K.: Die Neubegründung der Theorie der sphäroidischen Gleichgewichtsfiguren und das Normalsphäroid der Erde. Österr. Zeitschrift für Vermessungswesen, Sonderheft 24, Wien 1964.
2. Ledersteger, K.: Zur Begründung einer Theorie der hydrostatischen Gleichgewichtsfiguren auf dem Außenraumpotential. Sitzungsberichte der Bayer. Akad. d. Wiss., Math.-Nat. Kl., München 1962.

3. Zabek, Z.: Critical analysis of Ledersteger's theory of spheroidal equilibrium figures and a new conception of spheroidal equilibrium figure of the earth. "Geodezja i Kartografia" XV, No 2, Warsaw 1966. (In Polish).
4. Ledersteger, K.: Zur Frage des Dichtegesetzes der einparametrigen heterogenen Gleichgewichtsfiguren, Schweiz. Z. f. V. K. u. Ph., Winterthur 1960.
5. Fischer, I.: The present extent of astro-geodetic geoid. Bull. Géodés., No 61, 1961.
6. King-Hele, D. G., Cook, G. E., Rees, J. M.: Determination of the even harmonics in the Earth's gravitational potential. The Geophys. Jour. of RAS, 1963, 7.
7. Kozai, Y.: Numerical results from orbits, SAO Special report 1963, No 101.
8. Kozai, Y.: New determination of zonal harmonics coefficients in the earth gravitational potential, COSPAR, Florence, 1964.
9. Uotila, U. A.: Harmonic analysis of world-wide gravity material. Publ. Isos. Inst. IAG, No 39, Helsinki, 1962.

Critical Remarks Concerning the Preceding Article

by *K. Ledersteger*, Vienna

As Mr. Zabek was prevented from attending the Symposium, and as the preceding article arrived only shortly prior to the Symposium, I was unable to report on it at once. Quite naturally I feel obliged to present it subsequently, but also I feel entitled to give my critical point of view, the more so as Mr. Ząbek has already published his article in more extensive form in Polish [1].

We proceed at best from Helmert's fourth-order equipotential spheroid of revolution, which is uniquely determined, as is well known, if four suitably chosen data are given besides the terrestrial mass E. In second-order approximation $\bar{\varepsilon} = \omega^2 a^3/k^2 E = xe$ and $3J_2 = (2-x)e$, and in fourth-order approximation the first form parameter $f_4 = -\varkappa e^2$ and the mass function $J_4 = -\xi e^2$. If e. g. (E, a, e) are kept fixed, then the rotational velocity ω is determined by x and every point of the $(x,\varkappa)$-diagram [2, Figure on p. 66] represents a solution of the Helmert-system. However, if only E is given, every point of the diagram represents ∞^2 equipotential spheroids of Helmert. If an equipotential spheroid $S(a,e,f_4,f_6,\ldots)$ shall be free surface of an equilibrium figure, then in addition the equilibrium condition must be known in some form, e. g. $\omega = \omega(E,S)$. Because, every mass configuration which is representing a possible equilibrium figure, and which we therefore denote in short an equilibrium configuration, becomes an equilibrium figure only for a particular rotational velocity. The details become most clear, if we proceed from the elements of Stokes (E,ω,S). From $(E,\omega,a,e,f_4=0)$ we get for the ellipsoids an infinite number Helmert equipotential spheroids in the x-axis ($\varkappa=0$), the so-called equipotential ellipsoids, but we obtain exact homogeneous MacLaurin-ellipsoids only if in addition the equilibrium condition

$$\bar{\varepsilon} = \frac{4}{5}e + \frac{22}{35}e^2 \tag{1}$$

is given, while all other solutions can never represent equilibrium figures but can only be approximately thought of as equipotential spheroids having a physically impossible mass configuration. We also designate the MacLaurin-ellipsoids as "zero-parametric" equilibrium figures, because they have no form parameter at all. They can already be uniquely determined in second-order approximation. In the $(x,\varkappa)$-diagram the MacLaurin-ellipsoids are represented by the point $E(x=\frac{4}{5},\ \varkappa=0)$.

A strictly one-parametric surface never can be free surface of an equilibrium figure. Thus, if we speak of "one-parametric" equilibrium figures we understand such equilibrium figures which are uniquely determined already in fourth-order approximation. Hence, the knowledge of the first form parameter should be sufficient, i. e. these figures are uniquely determined by (E,ω,a,e,f_4) or as Helmert equipotential spheroids, wherein ω or x cannot be chosen arbitrarily but represents the equilibrium condition. In our diagram they are represented by a curve originating at point E, i. e. there are ∞^3 one-

parametric equilibrium figures. Accordingly they must have a density law with three constants. The first density constant, the mean density ϱ_m, is given by the mass E and the volume. Thus, if in the definition of the figure we want to substitute the surface $S(a,e,f_4)$ by the density law, the equatorial axis can easily be introduced instead of ϱ_m. Moreover, as in an equilibrium figure the density can never decrease toward the interior, for both the other density constants the surface density ϱ_{min} and the maximum density ϱ_{max} at the center of gravity may serve, which means that the density law must be continuous. Therefore we may state the density law conveniently in the form

$$\varrho = \varrho_{max}\, f\left(\frac{r}{a}\right) \tag{2}$$

where the continuous function f contains a suitably chosen constant ν instead of ϱ_{min}. r stands for the running equatorial radius of the internal level surfaces: $0 \leqq r \leqq a$. The detection of this unique density law could not be accomplished in a sufficient way as long as it could merely be orientated on the homogeneous ellipsoids and on the density distribution in the earth known only vaguely. This problem can be solved successfully only if the curve of the one-parametric equilibrium figures is known. In this curve, beginning with the homogeneous ellipsoids, the mass concentration must increase continuously till in the ∞^2 boundary figures, the one-parametric spheroids of greatest mass concentration, the surface density reaches a minimum value.

The region of all equilibrium figures on the right-hand side is bounded by the parabola $F = |J_4| : J_2^2 = 15/7$ between the points E and N which represents the external equipotentials of the MacLaurin ellipsoids and which terminates in point N in the absolute spheroids of greatest mass concentration or in the ∞^2 equipotentials of the mass point ($x = 2$, $\varkappa = 3/2$). Besides, the level surfaces of the ellipsoids can be interpreted as two-parametric boundary solutions, i. e. as Wiechert-models with the mantle-density zero. Thus, it is rather plausible that the left-hand boundary line of the region of equilibrium figures also is defined in an analogously simple way, i. e. by the one-parametric equilibrium figures directly succeeding the ellipsoids. Now it can easily be proved that the form parameter $f_4 \leqq 0$ can only increase in its absolute value when rising above the surface of an equilibrium figure: $df_4/da \leqq 0$. But since the form parameter itself vanishes only for the homogeneous ellipsoids, it is obvious to identify the desired left-hand boundary line with the parabola $A = a\, df_4/d\, a = 0$ between the points E and $M(x = 1{,}458, \varkappa = 3/2)$. This hypothesis at once is confirmed by the following facts:

a) Point M represents boundary figures since there the mass function J_6 vanishes which otherwise always is positive.

b) The form parameter f_6 vanishes in E as well as in M, so that it seems obvious to conclude that $f_6 = 0$ in the whole curve of $A = 0$. But then f_6 together with f_4 is negative in the whole region of equilibrium figures.

Should there be a density law which satisfies the homogeneous ellipsoids exactly, giving plausible values for the mean density and for the surface density of the earth, and which above all permits to recognize the figures in point M uniquely as one-parametric spheroids of greatest mass-concentration, then not only the density law but also the hypothetical proposition $A = 0$ seems to be verified. After various trials the law

$$\varrho = \varrho_{max}\left[1 - \nu\left(\frac{r}{a}\right)^2\right]^2 \tag{3}$$

seemed to satisfy all conditions mentioned quite well. For the ellipsoids $n = \varrho_{max}/\varrho_m = 1$ and $\nu = 0$, and for the earth with $\varrho_m = 5{,}5168$ we found the surface density to be 2,618 and the maximum density to be 11,127, which result is almost coinciding with that one of Helmert obtained by a totally different statement for the density law, while for a boundary figure in point M with the rotational velocity of the earth the corresponding results were: $n = 4{,}179$, $\nu = 0{,}970$ and the surface density $\varrho_{min} = \varrho_{max}(1 - \nu)^2 = 23{,}031\ (0{,}03)^2 = 0{,}020$. Besides, in point M the constants n and ν are almost unchangea, and $n\,(1 - \nu)^2 \sim 0{,}0035$.

Poincaré stated, as is well known, the following limit for the rotational velocity:

$$\omega^2 < 2\pi k^2 \varrho_m . \tag{4}$$

According to Lichtenstein [3] it can be shown that pressure prevails in the whole fluid, if the more rigorous inequality

$$\omega^2 < 2\pi k^2 \rho_{min} \tag{5}$$

holds true. Besides, Poincaré's barrier for spheroidal figures can easily be narrowed. For it is

$$\Omega = \omega^2/2\pi k^2 \rho_m = \frac{2}{3}\bar{\varepsilon}(1-e) \sim \frac{2}{3}\bar{\varepsilon} \ll 1 . \tag{4a}$$

There $\bar{\varepsilon}$ between the points E and M lies within the limits $\frac{4}{5}e \leqq \bar{\varepsilon} \leqq 1{,}4583e$, i. e.

$$\frac{8}{15}e \leqq \Omega \leqq 0{,}9722\,e . \tag{6}$$

Further, with $\rho_{min} = n\rho_m (1-\nu)^2$ follows easily

$$\Omega' = \omega^2/2\pi k^2 \rho_{min} = \Omega/n(1-\nu)^2$$

or

$$\frac{8}{15}\frac{e}{n(1-\nu)^2} \leqq \Omega' \leqq \frac{0{,}9722\,e}{n(1-\nu)^2} . \tag{7}$$

In our examples was $n(1-\nu)^2 \sim 0{,}0035$, thus $\Omega' \sim 277{,}8\,e$ or $\Omega < 0{,}66$. Anyway, there must be $\Omega' < 1$, i. e. $e \leqq n(1-\nu)^2$. For the rotational velocity of the earth follows from the equation $\omega^2 = 2\pi k^2 \rho_{min}$ at once $\rho_{min} = 0{,}0127$. It is certain that this limit never can be reached in the one-parametric spheroids of greatest mass-concentration.

The fact that the density law (3) primarily is based on the spheroids of greatest mass concentration is of special significance. This is most clearly shown e. g. by the statement of Legendre's density function [2, p. 47]:

$$\rho = \frac{1}{r} G \sin mx . \tag{8}$$

Thus, for $x = r/a = 0$ results:

$$\rho_{max} = mG \lim_{r=0} \frac{\sin mx}{mx} = mG \tag{9a}$$

and for $x = 1$

$$\rho_{min} = G \sin m = \rho_{max} \frac{\sin m}{m} . \tag{9b}$$

For the homogeneous ellipsoids $\rho_{min} = \rho_{max}$, i. e. $\frac{\sin m}{m} = 1$ or $m = O$. Generally, according to (2)

$$\rho = \rho_{max} f(x) = mG \frac{\sin mx}{mx}, \text{ hence } f(x) = \frac{\sin mx}{mx} \tag{10}$$

and in analogy to the equations (10.9) in [2, pp. 75–76]:

$$A = \frac{1-e}{1-\bar{e}_2} = \frac{\rho_{max}}{\rho_m} 3\int_0^1 f(x)\,x^2\,dx = 3n\int_0^1 \frac{\sin mx}{mx}\,x^2\,dx$$

$$B = \left(\frac{a_h}{a}\right)^2 \cdot \frac{1-e}{1-e_h} = \frac{\rho_{max}}{\rho_m} 5\int_0^1 f(x)\,x^4\,dx = 5n\int_0^1 \frac{\sin mx}{mx}\,x^4\,dx . \tag{11}$$

With the new variable $y = mx$ we get:

$$A = \frac{3n}{m^3}\int_0^m \sin y \,.\, y\,dy = \frac{3n}{m^3}(\sin y - y\cos y)\Big|_0^m$$

$$B = \frac{5n}{m^5}\int_0^m \sin y \,.\, y^3\,dy = \frac{5n}{m^5}[(3y^2 - 6)\sin y - (y^3 - 6y)\cos y]\Big|_0^m \tag{11a}$$

or

$$A = \frac{n}{m^5}(3\,m^2 \sin m - 3\,m^3 \cos m)$$

$$B = \frac{n}{m^5}(15\,m^2 \sin m - 30 \sin m - 5\,m^3 \cos m + 30\,m \cos m)\,. \tag{11b}$$

Hence, we find for the one-parametric normal spheroid:

$$m = 2{,}513711 = 518490{,}14'' = 144^0\,01'\,30{,}14'';$$

$$n = 2{,}02168\,; \quad \rho_m = 5{,}5168\,; \quad \rho_{max} = 11{,}153\,; \quad \rho_{min} = 2{,}597, \tag{12}$$

i. e. almost the same results as in [2, p. 76] with the density law (3). However, for the one-parametric spheroid of greatest mass concentration used in [2, p. 77] results:

$$m = 3{,}24601 \quad \text{or} \quad 185^0 58'57{,}6''$$

and thus because of

$$\rho_m = 5{,}5113\,, \quad \rho_{max} = 19{,}558\,, \quad \rho_{min} = -0{,}628\,,$$

i. e. already an impossible solution. Actually, m must be smaller than π, and we could fix the limit at most by $\rho_{min} = \omega^2/2\,\pi\,k^2 = 0{,}0127$. Putting $m = \pi - \tau$ we find according to (9):

$$\sin m = \tau\,; \quad \cos m = -1\,; \quad \rho_{min} = 0{,}0127 = G\,; \quad \rho_{max} = 0{,}0127\,(\pi - \tau) : \tau\,, \tag{13}$$

which together with the first equation (11b) leads to

$$\tau = 0{,}0381/\pi\,\rho_m\,. \tag{14}$$

With $\rho_m = 5{,}5113$ e. g. we get $\tau = 0{,}00220050$ or $m = 3{,}13939215 = 179^0 52'26{,}1''$.

Similar statements apply to the original law of Lévy with $\lambda = \mu = 2$. This means that in (3) the right-hand member does not represent the density in the level surface, but the mean density of the mass enclosed within that equipotential. Then the individual density according to (7,10a) in [2, p. 48] is, when we again put $r/a = x$:

$$\rho = \rho_{max}\left(1 - \frac{10}{3}\nu x^2 + \frac{7}{3}\nu^2 x^4\right). \tag{3a}$$

Both the constants ρ_{max} and ν result from the equations

$$\frac{1-e}{1-\bar{e}_2} = n(1 - 2\nu + \nu^2)$$

$$\left(\frac{a_h}{a}\right)^2 \frac{1-e}{1-e_h} = n\left(1 - \frac{50}{21}\nu + \frac{35}{27}\nu^2\right). \tag{15}$$

For the one-parametric normal spneroid we find $n = 1{,}981957$, $\nu = 0{,}289744$, $\rho_{max} = 10{,}934$, $\rho_{min} = 2{,}516$, i. e. again almost the same density distribution as according to (3). (3a) however gives in point M already a greater negative surface density ($\rho_{min} = -1{,}323$, $\rho_{max} = 20{,}513$), wherefore statement (3) was favoured.

If we consider the hypothesis $A = 0$ as sufficiently secured for the one-parametric equilibrium figures, we obtain a determining equation for J_4:

$$J_4 = -\frac{4}{5}e^2 + \frac{6}{7}e\bar{\varepsilon} - \frac{5}{14}\bar{\varepsilon}^2, \tag{16}$$

which may stand for an equilibrium condition. Thus we find for the one-parametric normal spheroid of the earth $J_4 = -332 \cdot 10^{-8}$ [2, p. 85], and that completely independent of the knowledge of the density law. On the other hand, the pertinent Wiechert-model with the depth of the core of 2900 km can be computed in fourth order approximation, and we get $J_4 = -295 \cdot 10^{-8}$ [2, p. 115]. But then it is clear that the J_4-value of the real equilibrium figure of the earth must lie approximately in the middle of both values, because the density discontinuity at the core's surface amounts with the Wiechert-model to about 8 units, with the equilibrium figure of the earth to about 4 units, and vanishes with the one-parametric model. Actually, in [2, p. 111] we found $J_4 = -315 \cdot 10^{-8}$ in remarkable agreement with the equilibrium value computed by Kopal and James [4] on basis of a plausible density distribution. If, vice versa, we proceed from the Wiechert-model and from Kopal's J_4 for the equilibrium figure of the earth, then it seems very probable that independently of the hypothesis $A = 0$ for the one-parametric model of the normal spheroid must sesult: $|J_4| > 315 \cdot 10^{-8}$. As a matter of fact, at the transition to the continuous density law mass has to flow from the core to the mantle above to permit the density discontinuity to vanish; however, this is counteracted by a further mass concentration in the mantle.

With J_2 and $\bar{\varepsilon}$ kept fixed, Helmert's system furnishes for an external equipotential or for the free surface of a mass configuration independently of the equilibrium:

$$|J_4| = \frac{4}{5}(3J_2 + \bar{\varepsilon}) - 1{,}6(e + e\bar{\varepsilon} - e^2) \tag{17}$$

and we see that the absolute value of J_4 decreases with increasing e: $\Delta|J_4| \doteq -1{,}6\Delta e$. An increase of e by only $30 \cdot 10^{-8}$, i. e. by a quantity of sixth order, already causes a decrease of the absolute value of J_4 by $48 \cdot 10^{-8}$. This is shown especially clearly by the dual-layer models belonging to the data:

$$\begin{gathered} E = 5976{,}318 \cdot 10^{24}\, g\,; \quad \omega^2 = 5{,}317496 \cdot 10^{-9}, \quad a = 6378{,}290\,\text{km}\,; \\ a_k = a - 2900\,\text{km}\,; \quad J_2 = 108310 \cdot 10^{-8}\,; \quad \bar{\varepsilon} = 346146{,}9 \cdot 10^{-8} \end{gathered} \tag{18}$$

which were computed in [2, pp. 182–183] – neglecting the form parameter f_4 in computing the mass-functions –:

e	e_c			
$335308{,}0 \cdot 10^{-8}$;	0	$\rho_M = 4{,}834$;	$\rho_C = 10{,}942$;	$J_4 = -310{,}7 \cdot 10^{-8}$
335317,4	$233235{,}4 \cdot 10^{-8}$;	4,187	12,377	−295,6
335317,8	243039,9	4,173	12,454	−294,9
335321,6	335321,6	4,016	13,270	−288,8

Naturally, this is connected with the variation of the density law: the greater the density of the mantle, the greater $|J_4|$. All these figures, but one, are not equilibrium figures; for the Wiechert-model we find $e = 335317{,}7 \cdot 10^{-8}$, $J_4 = -295{,}15 \cdot 10^{-8}$.

For the models with continuous density law we must search for the equilibrium solution somewhere between the limits $A = 0$ and $F = 15/7$ without further clue and without any hypothesis:

		corresponds to
$A = 0$: $e = 335294{,}2 \cdot 10^{-8}$;	$J_4 = -332{,}5 \cdot 10^{-8}$	
335304,9	−315,5	the normal spheroid
335317,7	−295,2	the Wiechert-model
335329,7	−276,0	Ząbek's solution
$F = 15/7$: 335345,1	−251,4	the equipotential of the homogen. ellipsoid

In the third solution e. g., the increase of the mass of the mantle connected with the vanishing of the

density discontinuity $\Delta\rho = 8{,}25$ should just be compensated by the concentration in the mantle; the like applies to the second solution corresponding to the normal spheroid with a small density discontinuity (about 3,5) and with an already heterogeneous mantle.

Mr. Ząbek proceeds from the idea of controlling the hypothesis $A = 0$ and the density law (3) by a direct computation of the mass function J_4 accordingly to his equations (3.12) [1]. He finds, in contrast to the above value in the parabola $A = 0$, the absolute value $|J_4| = 276 \cdot 10^{-8}$ which is smaller by $56{,}5 \cdot 10^{-8}$ or by 17 %. The integration, of course, requires besides the density law the knowledge of the flattening function, but which can only be derived for the rigorous continuous density law of the one-parametric equilibrium figures according to the principle of peeling. If we thus consider the exposed discrepancy as proof for the incorrectness of the density law (3), we also are ignorant of the corresponding flattening function, and beyond that Ząbek's result itself becomes illusory. This fact in general states the difficulty of the infinite variety of models (E, ω, a, J_2) which all have different continuous density laws with unknown flattening functions.

The mass functions J_{2i} of the dual-layer models can rigorously be computed from the density law. This certainly also applies to multi-layer (N)-models. But with the transition $N \to \infty$ the generalization of the formulas for the homogeneous ellipsoid can produce progressive percentual errors with increasing i. Both the constants ρ_{max} and ν of the density law (3), however, were only derived from the generalization (10.2 and 3) [2, p. 73] for the mass E and the moment of inertia C, whereat only the factors $(1 - e_x)$ occur in the integrand, which, because of their very limited variability may be represented by a weighted mean and put in front of the integral sign. There, the more rigorous expressions of Ząbek $(3.2 - 5)$ [1] are superfluous. The generalized integral for J_2 merely served the purpose of showing that the average value $\bar{e}_4$ may be identified with the flattening e_h of the homogeneous initial ellipsoid of the corresponding one-parametric series of figures $(\omega, K_2) = (\omega, C)$. In that way the determining equations (10.16) [2, p. 78] for the one-parametric normal spheroid in second order approximation originated, which we now write in the form:

$$\begin{aligned} 0{,}9998\,\rho_m &= \rho_{max}\left(1 - \frac{6}{5}\nu + \frac{3}{7}\nu^2\right) \\ 0{,}8304\,\rho_m &= \rho_{max}\left(1 - \frac{10}{7}\nu + \frac{5}{9}\nu^2\right). \end{aligned} \tag{19}$$

But already Ząbek's integral (3.6) for J_2 leads to contradictions. For the expression (3.8a) he finds the value $3205 \cdot 10^{-6}$ in contrast to $e_h = 3266 \cdot 10^{-6}$, i. e. a value too small by 1,9 % or, expressed in a better way, by $5{,}4e^2$ which in turn causes the integral for J_2 to furnish the value $J_2 = 106290 \cdot 10^{-8}$ which is too small by $2020 \cdot 10^{-8} = 1{,}8e^2$. Hence, it is not to be wondered at that the integral (3.12) for J_4 shows an error of $56{,}5 \cdot 10^{-8}$ or $14{,}7e^3$, i. e. a quantity of fifth order. As compared with equation (19) the integrals for J_2 and J_4 have rapidly decreasing weights. Therefore, they must not be used with equal weights for the determination of the unknowns ρ_{max} and ν. This can clearly be recognized by writing the last integral in the form:

$$|J_4|\,\rho_m = \mu \cdot 10^{-8}\,\rho_m = \alpha \cdot 10^{-8}\,\rho_{max}\left(1 - \frac{14}{9}\nu + \frac{7}{11}\nu^2\right). \tag{20}$$

Besides, we have for the one-parametric normal spheroid: $\nu = 0{,}514990$; $n = \rho_{max} : \rho_m = 2{,}017176$; $e = 335313 \cdot 10^{-8}$ and with the already fictitious assumption $e_x = \text{const} = e : \alpha \cdot 10^{-8} = \frac{12}{35}(e^2 - e^3) = 384{,}2 \cdot 10^{-8}$, $\alpha n = 775.10^{-8}$ and $|J_4| = 285.10^{-8}$ which value is already greater than Ząbek's result.

Thus, with regard to the deviation in J_2 the discrepancy in J_4 gives no permission to abandon the density law (3) and the hypothesis $A = 0$. On the contrary, the discussion in [2, § 10] has proved sufficiently that the figures with continuous density law lie in the parabola $A = 0$ and that in point M with $J_6 = 0$ they have their absolute boundary. By no means, however, must the hypothesis $A = 0$ be abandoned, while at the same time maintaining the density law (3) which primarily is based on the boundary figures in point M. Just that is Ząbek's procedure, who defines the one-parametric

spheroids of greatest mass concentration only by $\Omega' = 1$, without being able to state a characteristic property which is independent of the density law. This comes up to the fact that from every point of the parabola $A = 0$ one goes downward in the corresponding vertical $x = \text{const}$ till reaching the smaller absolute value of J_4 desired. Since further in M: $\Omega' \sim 0{,}66$, the x-value of Ząbek's spheroids of greatest mass-concentration is somewhat greater, namely $x \sim 1{,}4669$, and they are located in the point ($x = 1{,}467$, $\varkappa = 0{,}542$), i. e. right in the middle of the region of Wiechert-models. From the general equation

$$-\varkappa + \frac{35}{8}\xi = \frac{7}{2} - \frac{5}{2}x \tag{21}$$

we find $\xi = 0{,}0857$, and further with $J_6 = +\eta e^3$ and $f_6 = -\lambda e^3$:

$$B = (-\lambda + 2{,}8875\,\eta) = 3{,}9504 - 3{,}0210\,x = -0{,}4812\,. \tag{22}$$

In the (x,λ)-diagram for $\varkappa = 0{,}542$ – vide Figure in [2, p. 156] – the straight line $\eta = 0$ thus intersects the vertical $x = 1{,}4669$ in the point $\lambda = +0{,}4812$, while according to the procedure in [2, pp. 150–152] $\lambda_{min} = 0{,}598$ results. Thus λ and η are positive and Ząbek's spheroids of greatest mass concentration are not to be considered as boundary figures.

Besides, the following arguments can be stated against Ząbek's equilibrium condition for the one-parametric figures:

1) While it is very probable that the most simple equilibrium figures, after the ellipsoids of MacLaurin, represent the left-hand boundary of the region of all equilibrium figures in the $(x,\varkappa)$-diagram, now their curve runs entirely within the region of the Wiechert-models. The parabola $A = 0$, exclusively of point E, would lie completely outside the region of equilibrium figures.

2) The equilibrium figures with a heterogeneous part, e. g. the three-parametric figures with homogeneous core and heterogeneous mantle, or vice versa, would be restricted to the incredible narrow region $15/7 \leqq F \leqq 2{,}75$.

3) Evaluating the integral for J_4, especially of a heterogeneous figure, the form parameter f_4 must not be neglected [5].

Finally, if we were forced to abandon the hypothesis $A = 0$ the question of the density law of one-parametric epuilibrium figures again is totally open.

Literature:

1. Ząbek, Z.: "Krytyczna analiza teorii Lederstegera sferoidalnych figur równowagi i nowa koncepcja sferoidalnej figury równowagi Ziemi", Geodezja i Kartografia Rocznik XV (1966) nr 2
2. Ledersteger, K.: "Multi-parametric Theory of Spheroidal Equilibrium Figures and the Normal Spheroids of Earth and Moon", Final Report, Vienna 1966
3. Lichtenstein, L.: „Gleichgewichtsfiguren rotierender Flüssigkeiten", Berlin 1933
4. Kopal, Z. and James, R.: Technical Summary Report No. 193, Math. Res. Center, US Army, Univ. of Wisconsin, 1960
5. Darwin, G. H.: "The theory of the Earth carried to the second order of small quantities", Monthly Not. Roy. Astr. Soc., London 1900, pp. 82–124.

Part II:

The Figure of the Earth and the External Gravity Field

Deviations of the Geoid from an Equilibrium Figure

by *Irene Fischer*, Washington, D. C.

The theoretical equilibrium figure of a fluid rotating body serves as a model for the earth when studying geophysical features and speculating about the forces producing these features. Since the choice of a model is essentially arbitrary, suggested by the focus of the study, the question is not that of being correct or incorrect, but rather that of being useful or not. Up to the time of the Vanguard satellite it was assumed that the earth was essentially in equilibrium and that its deviations from an equilibrium figure were small. Under this assumption the actual flattening of the earth would not be much different from a hydrostatic value. A model of the earth with the flattening and fitting other observable facts would then insure that unobserved facts could be predicted with only small errors. The Vanguard satellite changed this trend of thought.

The hydrostatic theory of the earth implied a flattening within a small range of values around 1/297, but the actual value derived from satellite observations was well outside that range. O'KEEFE [1], MARCHANT and HERTZ of the U. S. Army Map Service, were the first ones to compute this new value at 1/298.3. HENRIKSEN [2] computed the corresponding hydrostatic flattening at around 1/300, and O'KEEFE [3] interpreted the discrepancy as the failure of the hydrostatic theory concerning the equilibrium state of the earth.

The discussion now turned to the choice of a useful model to suit the changed circumstances. LEDERSTEGER [4] points out that no theoretical equilibrium figure satisfies all observed quantities and he proceeds to compute various models with slightly larger than actual angular velocity. The underlying philosophy refers to the lengthening of a day by at least one second on the last hundred thousand years and tentatively puts this model at an early date in the history of the earth. We are warned, however, not to take such speculation too literally, since the equatorial radius had been held fixed in the computations. Values derived for the flattening stay consistently around 1/296. O'KEEFE [5], by contrast, insists that the proper equilibrium figure for geophysical reference should have a flattening of around 1/300, corresponding to the present dynamical flattening. He refers to the lengthening of the day also, quoting MUNK and MAC DONALD's [6] interpretation of the observed greater actual bulge as a lag in the adjustment to a decelerating earth in the last ten million years. Thus Ledersteger's and O'Keefe's suggested reference models belong to opposite ends of a geological time interval.

The present paper offers a chart of detailed astrogeodetic geoid features referred to the flattening of 1/299.67 as computed by JEFFREYS [7], to see what geophysicists can infer from it.

An equilibrium figure representing the same mass as the earth in a different distribution should have the same volume as a best fitting ellipsoid, for which the geoid deviations above and below should even out by definition. If a and f are the parameters of the latter and f_H is the hydrostatic flattening, then the corresponding change in a for the condition of equal volume is

$$\frac{\Delta a}{a} = \frac{1}{3} \cdot \frac{\Delta f}{1 - f_H}$$

For the FISCHER [8] ellipsoid with parameters $f = 1/298.3$ and $a = 6378166$ m the change in a for $f_H = 1/299.67$ is a decrease by 32.7 m.

Figure 1 shows the astrogeodetic geoid — as much as we known of it at this time — on the Mercury Datum [8], with a tentative extension across Greenland by stellar triangulation. Figure 2 is referenced to the corresponding equilibrium figure with parameters $f = 1/299.67$ and $a = 6378133.3$ m.

It has been shown that only a homogeneous fluid can assume an ellipsoidal shape, otherwise there will be a slight depression in the middle latitudes. DE SITTER [9] gives the amount of this depression as $-\ a.k.\sin^2 2\varphi$ where k is estimated around $.5(10^{-6})$ independent of the mass distribution. While this amount reaches only 3.2 meters at most, it gives a slight systematic increase to the geoidal heights, and has therefore been included in Figure 2.

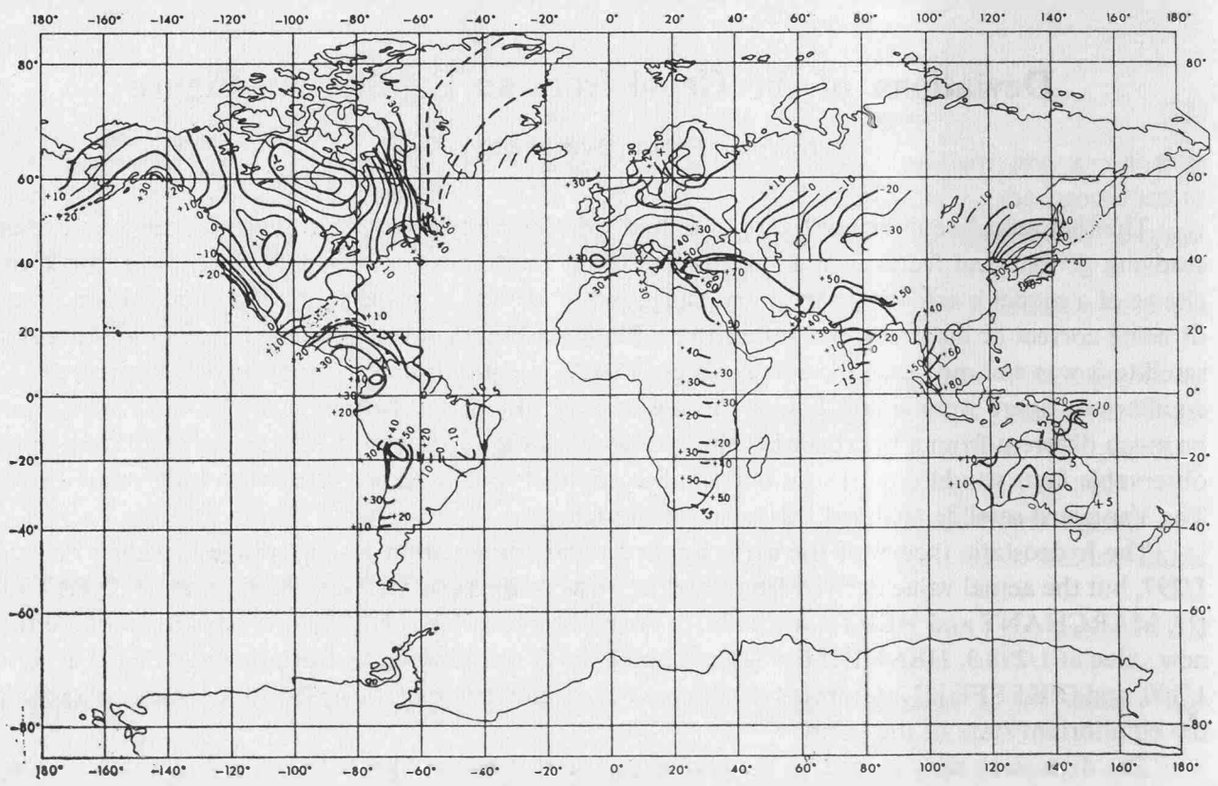

FIGURE 1. GEOID CONTOURS ON MERCURY DATUM, IN METERS.

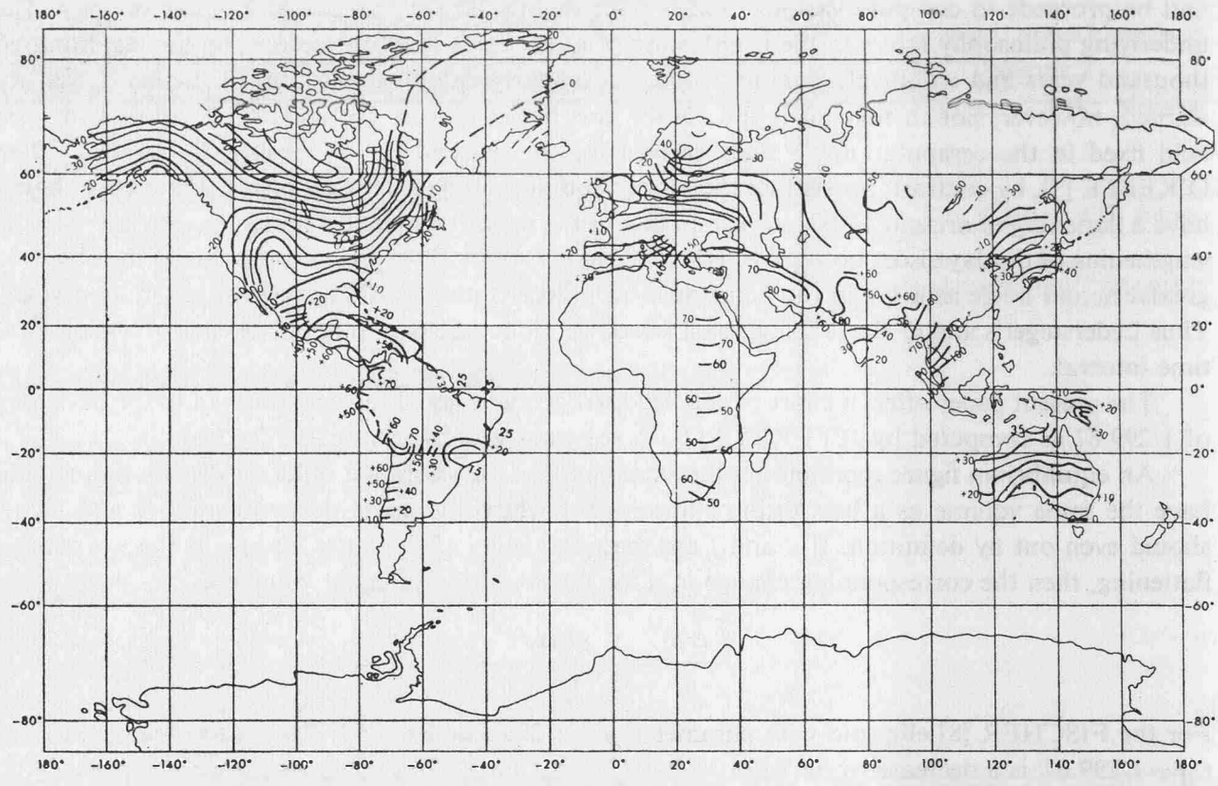

FIGURE 2. GEOID CONTOURS REFERRED TO f=1/299.67, a=6378133.3 + (K)m, IN METERS.

As expected, some geoid features stand out more strongly from the hydrostatic reference figure (Figure 2) than from one with the actual flattening (Figure 1). Some features are pronounced enough to appear clearly in both figures, such as the Pleistocene depression around the Hudson Bay. The shallower Fennoscandian depression is clearer in Figure 2. Various geoid features are strongly correlated with the topography, following tertiary mountain ranges. Note the high along the Eurasian montain range, with the bridge-like Himalaya flanked by the Innerasian and Indian depressions; the high in Bolivia and Colombia; and the concentric feature around the Caribbean. Areas of volcanic and seismic activity seem to be correlated with geoidal extremes. There is the build-up in Japan and Southeast Asia towards the activity zone in West Pacific, the high in the active Turkish area, the buildup towards volcanic Iceland, the maxima in Central America and on the southern shore of Alaska and on the Aleutians, and probably more such features upon closer scrutiny.

References

[1] Harvard Announcement Card No. 1408, June 24, 1958.
[2] Henriksen, S. W., Annals of IGY, Vol. 11, 1959.
[3] O'Keefe, J. A. et al, Geophys. Monogr. No. 4, AGU 1959, p. 50.
[4] Ledersteger, K., Zeitschr. f. Verm., 90. Jahrg., H. 11, Nov. 1965.
[5] O'Keefe, J. A. and W. M. Kaula, Science, Vol. 142, No. 3590, Oct. 1963, p. 382; also O'Keefe, J. A., Letter to the Symposium on the Determination of the Figure of the Earth in Prague 1964, Studia Geophysica et Geodaetica, 2, 9, 1965, p. 214.
[6] Munk, W. H. and G. J. F. MacDonald, J. Geophys. Res., Vol. 65, No. 7, July 1960.
[7] Jeffreys, H. Geophys. J., RAS, Vol. 8, No. 2, Dec. 1963, p. 202.
[8] Fischer, I., Bull. Geod., No. 61, Sept. 1961, p. 249.
[9] De Sitter, W., Bull. Astr. Inst. Netherlds., Vol. II, No. 55, May 1924, p. 97.

Addendum:

After presentation of her paper "Deviations of the Geoid from an Equilibrium Figure" Mrs. Fischer added following supplementation:

This paper was written as a follow-up to the Prague Symposium on the Figure of the Earth, in 1964. A letter by John A. O'Keefe was read there, proposing that a reference figure with a flattening near 1/300 be used for geophysical purposes (see Studia Geophysica et Geodaetica, 1965, 2, p. 214). All I intended to do at today's meeting was to contribute a one-minute paper showing a geoid chart on such a reference figure — and then listen to a lively discussion between O'Keefe and Ledersteger. But now that O'Keefe suddenly had to cancel his trip, I will try to present his point of view.

The discrepancy between the actual and the theoretical flattening, as derived from satellite analyses, should give some insight into geophysical forces that keep the earth from being in perfect hydrostatic equilibrium. The exaggeration of the geoid features when referred to a fluid equilibrium figure linked to the present rate of rotation should show more clearly where the earth has failed to attain equilibrium; and then the geophysicists should come up with theories of explanations. One such is the deceleration of the earth's rotation; and the earth's failure to catch up represents itself in the systematically negative geoid heights in the high latitudes. Known areas of seismic and volcanic activities would also show up in exaggerated geoid heights.

I am sure that O'Keefe does not propose to use this theoretical flattening for geodetic purposes. Figure 1 shows a geodetic world datum currently used by NASA in its Mercury, Gemini, and Apollo programs. The question whether these or some other parameters would be a good choice for a geodetic reference figure has been brought up already at the General Assembly in Berkeley, in 1963. While discussing that the International Ellipsoid may be obsolete, the Association of Geodesy could not make up its mind about a replacement at that time and left it to the astronomers, scheduled to meet in Hamburg a year later, to make up its mind for it. You will recall that a small working group with Cook as chairman was appointed to make proposals to the IAU committee on fundamental astronomical constants. The IAU was careful to point out that the values adopted at Hamburg (J_2 equivalent to $f = 1/298.25$ and $a = 6378160 \pm 80$ m) were not meant to prejudice a decision by the IAG.

The president of the IAG, Bomford, has recently sent out a circular urging that such a decision be made at Luzern next fall.

Now, O'Keefe would surely enter this discussion with proposing the actually observed flattening of 1/298.3 or thereabout for the purely geodetic purpose of representing the current state of affairs. The flattening of 1/299.67 is proposed for a specific purpose, namely to assist geophysicists in their study of the interior forces, finding or refuting correlations with convection currents or heat flow etc.

The 234 m of topographic layer above the geoid, which Ledersteger added to the major axis for the condition of equal volume with the real earth would seem to affect the computation of the axis for my Figure 2. But, as Ledersteger points out, one would have to reduce the deviations on that height level down again through these 234 m for a representation on the geoid level and such reduction for astrogeodetic deflections would be insignificant. Thus the topographic layer cancels out for practical purposes and the equal volume condition between the ellipsoids of Figures 1 and 2 still holds. Besides, a change in the major axis of Figure 2 would result in a blanket correction of all geoidal heights and thus leave the relative size of the features unchanged.

On the Solvability of Molodensky's Integral Equation

by *Miloš Pick*, Prague

The determination of the shape of the Earth from gravity data is usually reduced to the computation of the disturbing potential, expressed as a potential of a single layer, located on the surface of the first approximation. That is such a surface whose heights above the reference-ellipsoid are equal to the normal heights. An integral equation has been developed by Molodensky and has been solved by extending it in a potential series according to a small parameter. However, this solution is limited to the case, when not only the slopes of the terrain but also the slope of any line connecting the fixed and not too distant varying point respect to the vertical are to be less than 45^0.

The object of this contribution is to modify Molodensky's integral equation and to solve it also for the case when the prescribed conditions are not fulfilled.

It is apparent that these conditions need not be fulfilled in the immediate sourroundings of the fixed point only. Therefore let us take out from the surface of the first approximation such areas in which the slope conditions are not fulfilled. Let the intersections of the surface and cones be the boundaries of these areas, where the cones are rotational with the top in the gravity centre of the Earth.

We shall now deform the surface of the first approximation inside the area, in which the prescribed conditions are not fulfilled, as follows:

a) The deformed surface will again be the Liappunoff's surface,
b) the original and deformed surface will have a common tangential plane at the boundary,
c) the deformed surface will fulfil the prescribed slope-conditions,
d) let the prescribed direct proportion exist between the tangens of slopes of the original and deformed surface in the central point.

There exist infinitely many functions deforming the surface according to the given conditions. One of them, for example, is

$$\overline{H} - H = \frac{k-1}{a^2}\left(a - \frac{r_o^2}{a}\right)^2 . (H - Q) . \tag{1}$$

There are three constants in this equations: k, a, Q.
Let us write Molodensky's integral equation

$$2\pi\chi\cos^2\alpha_o = \Delta g + \frac{3}{2} R \int_\omega \frac{\chi}{r}\, d\omega + R^2 \int_\omega \frac{\chi . \Delta H}{r^3}\, d\omega . \tag{2}$$

We are able to put for any point

$$\chi = \bar{\chi} + \delta\chi, \quad \bar{r} \sim [r_o^2 + \bar{\Delta H}^2]^{\frac{1}{2}}$$

and to write analogously to the Eq. (2).

$$2\pi\bar{\chi}\cos^2\bar{\alpha}_o = \bar{\Delta g} + \frac{3}{2}R\int_{\omega}^{\cdot}\frac{\bar{\chi}}{\bar{r}}d\omega + R^2\int_{\omega}^{\cdot}\frac{\bar{\chi}\,.\,\bar{\Delta H}}{\bar{r}^3}\delta\omega\,, \tag{3}$$

where

$$\tan^2\bar{\alpha}_o = \left(\frac{\partial\bar{H}}{\partial x}\right)^2 + \left(\frac{\partial\bar{H}}{\partial y}\right), \quad \Delta g = \Delta g + (\bar{H} - H)\,.\,\frac{\partial\Delta g}{\partial H}\,.$$

Eq. (3) refers to the deformed surface and it can be solved using Molodensky's method. The prescribed accuracy in the vertical gradient of the anomaly is fairly small, only ± 100 Eötvös (± 0,01 mgl/m) that is why the vertical gradient of the anomaly may be derived using e. g. Numerow's equation

$$\frac{\partial\Delta g}{\partial\bar{H}} \sim \frac{1}{2\pi}\int\frac{\Delta g - \Delta g_o}{r_o^3}d\sigma\,.$$

Then we compute the correction

$$\delta g = -2\pi\chi\delta c - \left\{\left(\frac{\partial g}{\partial H} - \frac{\partial\gamma}{\partial H}\right)(H - Q) + \frac{\partial g}{\partial H}\,.\,\frac{T_o}{\gamma}\right\}\,.\,\frac{\bar{H} - H}{H - Q} + \tag{4}$$

$$+ \frac{3}{2}R\int_{\varepsilon}^{\cdot}\bar{\chi}\left(\frac{1}{r} - \frac{1}{\bar{r}}\right)d\omega + R^2\int_{\varepsilon}^{\cdot}\bar{\chi}\left(\frac{\Delta H}{r^3} - \frac{\bar{\Delta H}}{\bar{r}^3}\right)d\omega\,,$$

where

$$\delta c = \cos^2\alpha_o - \cos^2\bar{\alpha}_o\,.$$

Finally we are able to compute the value $\delta\chi$ from the following Eq.

$$2\pi\delta\chi\cos^2\alpha_o = \delta g + \frac{3}{2}R\int_{\varepsilon}^{\cdot}\frac{\delta\chi}{r}d\omega + R^2\int_{\varepsilon}^{\cdot}\frac{\delta\chi\,.\,\Delta H}{r^3}d\omega\,. \tag{5}$$

The area of integration ε will usually be small, as a rule $a < 1$ km. Of course, it will be necessary to use electronic computors for solving Eqs. (3)—(5).

References

1. Molodensky, M. S., Jeremejev, V. F., Jurkina. M.I.: Metody izučenija vnĕšnĕgo gravitacionnogo polja i figury Zemli. Trudy CNIIGAIK, 131, M. 1960.

Lineare Lösungen des Problems vom Molodenskij

by *H. Moritz*, Berlin

Since this paper will be published as Publ. No. 51 of the International Isostatic Institute, Helsinki, in English: "Linear Solutions of the Geodetic Boundary Value Problem" the author prefers to give only a short Abstract:

The linear (first-order) solutions of Molodensky's problem are derived in an elementary way, without using integral equations. The point of departure is the "gradient solution", which is obtained from geometric intuition. The other solutions follow by mathematical transformations of the gradient solution. A relation to the terrain correction and the effect of first-order corrections on the deflections of the vertical are investigated.

About a System of Integral Equations for the Determination of the Earth Shape Regionally only by Means of Gravity Measures.

by *L. Bragard*, Namur

Summary.

Applying the divergence theorem, a system of two Fredholm's equations admitting a unique solution, is obtained, which is equivalent to an analogous system previously found up. That system gives the distance between the points of the central part of an area of the topographical earth surface and the correspondent points of a reference area only in function of gravity values upon these areas and the one of an external level reference surface.

For the ocean areas, the system is reduced to one Fredholm's equation, admitting a unique solution.

So it is possible to obtain the earth shape by succesive regional determinations, without having to conserve the same external surface from one to another region.

1. Let us consider the topographical earth surface S_t, an external level surface S_e und the bulk e comprised inside the corresponding areas σ_e, σ_t of the surface S_e, S_t and the lateral boundary of which is such as the gravity vector $\vec{g}$ is tangent at each of its points (Fig. 1)

Applying the divergence theorem, we have, V being the earth potential, and the positive normal being bend outward

$$V_e \iint_{\sigma_e} g_e' \, d\sigma_e - \iint_{\sigma_t} V_t' \, g_t' \cos\alpha' \, d\sigma_t = -2\omega^2 \iiint_e V' \, d\tau - \iiint_e \Sigma \left(\frac{\partial V}{\partial x}\right)'^2 d\tau \qquad (1)$$

where α is the angle of the direction of g_t with the normal to the topographical surface.

Applying besides the particular case of Green's theorem

$$\iint_S \frac{dV}{dn} \, dS = \iiint_T \Delta_2 V \, d\tau$$

to the same bulk, we shall have

$$\boxed{\iint_{\sigma_t} g_t' \cos\alpha' \, d\sigma_t - \iint_{\sigma_e} g_e' \, d\sigma_e = 2\omega^2 e}$$

hence

$$-V_t \iint_{S_e} g_e' \, d\sigma_e + V_t \iint_{\sigma_t} g_t' \cos\alpha' \, d\sigma_t = 2\omega^2 V_t e \qquad (3)$$

2. The equations (1) and (3) added up member to menber give us

$$(V_e - V_t) \iint_{\sigma_e} g_e' \, d\sigma_e + \iint_{\sigma_t} (V_t - V_t') g_t' \cos\alpha' \, d\sigma_t = 2\omega^2 \iiint_e (V_t - V') \, d\tau - \iiint_e g'^2 \, d\tau$$

or again

$$(V_e - V_t)\left[\iint_{\sigma_e} g_e' \, d\sigma_e - \iint_{\sigma_t} g'_t \cos\alpha' \, d\sigma_t\right] + \iint_{\sigma_t} (V_e - V') g_t' \cos\alpha' \, d\sigma_t = \qquad (4)$$

$$= 2\omega^2 \iiint_e (V_t - V') \, d\tau - \iiint_e g'^2 \, d\tau$$

upon the condition expressed by the relation (2).

As we can write *in first approximation*

$$V_t - V_e = N_1 g_t \cos\alpha$$

N_1 being the distance between the surfaces σ_e and σ_t along the normal to S_t at P_t (Fig 2), the equation (4) finally will become

$$N_1 g_t \cos\alpha \left[\iint_{\sigma_e} g'_e \, d\sigma_e - \iint_{\sigma_t} g'_t \cos\alpha' \, d\sigma_t\right] + \iint_{\sigma_t} N'_1 g'^2_t \cos^2\alpha' \, d\sigma_t = \\ = 2\omega^2 \iiint_e (V' - V_t) \, d\tau + \iiint_e g'^2 \, d\tau \tag{5}$$

in which we can put

$$V' - V_t = -g_m . h$$

g_m being the mean gravity computed along the normal h to σ_t, comprised between that and an inter mediate level surface σ' (Fig. 3)

The integral equation (5) is equivalent to a similar equation previously given out [1] and calling in the underlying mass considered from σ_t until the origin of the coordinate system choosed inside the earth

3. Let us now consider an area σ_r of the level reference surface S_r corresponding to σ_e and bounding a bulk e' the lateral boundary of which is such as the gravity vector $\vec{\gamma}$ (proceeding from the reference mass, the potential of which is U), is tangent at each of its points (Fig. 4).

We shall obtain likewise the integral equation

$$(U_e - U_r)\left[\iint_{\sigma_r} \gamma_r' \, d\sigma_r - \iint_{\sigma_e} \gamma_e' \cos\beta' \, d\sigma_e\right] + \iint_{\sigma_e} (U_e' - U_r)\gamma_e' \cos\beta' \, d\sigma_e = \\ = 2\omega^2 \iiint_{e'} (U_e - U') \, d\tau - \iiint_{e'} \gamma'^2 \, d\tau \tag{6}$$

owing to the condition

$$\iint_{\sigma_r} \gamma_r' \, d\sigma_r - \iint_{\sigma_e} \gamma_e' \cos\beta' \, d\sigma_e = 2\omega^2 e' \tag{2'}$$

β being the angle of the direction of γ_e with the normal to σ_e at P_e. We shall have again *in first approximation*

$$U_e - U_r = -(N_1 + N_2)\gamma_r \cos D$$

where γ_r is the reference gravity at the point P_r corresponding to P_e and D is the vertical deflection at the point P_r as the normal to σ_t at P_t (Fig. 2).

4. The equation (6) becomes thus

$$(N_1 + N_2)\gamma_r \cos D \left[\iint_{\sigma_r} \gamma_r' \, d\sigma_r - \iint_{\sigma_e} \gamma_e' \cos\beta' \, d\sigma_e\right] + \iint_{\sigma_e} (N_1 + N_2)' \gamma_r' \gamma_e' \cos D' \cos\beta' \, d\sigma_e \\ = -2\omega^2 \iiint_{e'} (U_e - U') \, d\tau + \iiint_{e'} \gamma'^2 \, d\tau \tag{7}$$

We can put in the equation (7)

$$U_e - U' = -h \cdot \gamma_m$$

γ_m being the mean gravity computed along the normal h to σ_e comprised between that and an intermediate level surface σ' (Fig. 5).

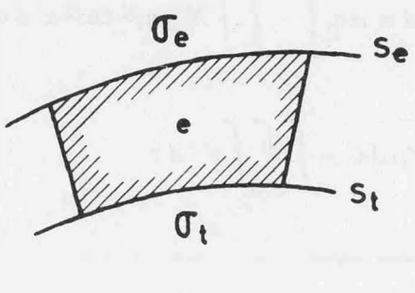

Fig. 1

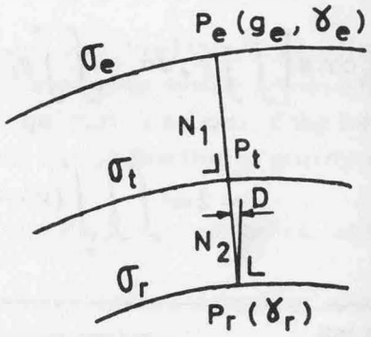

Fig. 2

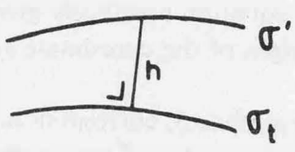

Fig. 3

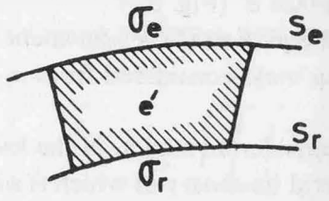

Fig. 4

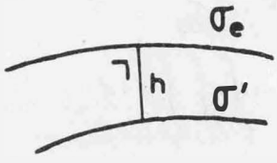

Fig. 5

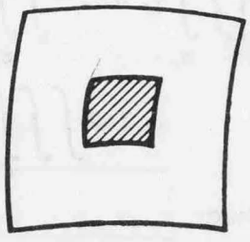

Fig. 6

The integral equation (7) is equivalent to a similar equation previously given out [1] and calling in the underlying mass considered from σ_r until the origin of the choosed coordinate system.

5. Solving the Fredholm's equations (5) and (7) each of which admit a unique solution, it willl be possible to get N_1 (and hence D) and $(N_1 + N_2)\cos D$, whence finally N_2 distance between σ_t and the referential σ_r.

Using the same process to successive shares ot the topographical earth surface so as to cover it entirely, we shall be able to determine its shape.

That method for determining regionally the earth shape offers the double advantage to need know the gravity values only relating to the considered region of the topographical earth surface and to be able to change the external level surface S_e from one to another region. It is, indeed, necessary to use whenever as intermediate such an external surface, if we will avoid to call in the knowledge of the densities comprised between σ_t and σ_r.

6. For an *ocean area* σ_o, we have $\cos \alpha = 1$ and the equation (1) is simplified. Taking into account the equation (2) and the relation

$$V_o = C^{te},$$

it is written finally

$$N_1 g_0 \iint_{\sigma_e} g_e' \, d\sigma_e = 2\omega^2 \iiint_e (V' - V_0) \, d\tau + \iiint_e g'^2 \, d\tau \tag{8}$$

g_o being the corresponding gravity.

7. It would be possible also to use the gravity gradients. Indeed, if we apply the particular cases of Green's formula

$$\iint_S \left[V \frac{d^2 V}{dn^2} - \left(\frac{dV}{dn} \right)^2 \right] dS = \iiint_T \left(V \Delta_2 \frac{dV}{dn} - \frac{dV}{dn} \Delta_2 V \right) d\tau$$

$$\iint_S \frac{d^2 V}{dn^2} \, dS = \iiint_T \Delta_2 \frac{dV}{dn} \, d\tau$$

to the bulk e previously considered, we obtain the equations

$$V_e \iint_{\sigma_e} \left(\frac{dg}{dn} \right)_e' d\sigma_e - \iint_{\sigma_t} V_t' \left(\frac{dg}{dn} \right)_t' \cos\alpha' \, d\sigma_t - \iint_{\sigma_e} g_e'^2 \, d\sigma_e + \iint_{\sigma_t} g_t'^2 \cos^2\alpha' \, d\sigma_t =$$

$$= -2\omega^2 \iiint_e \left(\frac{dV}{dn} \right)' d\tau \tag{9}$$

$$\iint_{\sigma_e} \left(\frac{dg}{dn} \right)_e' d\sigma_e = \iint_{\sigma_t} \left(\frac{dg}{dn} \right)_t' \cos\alpha' \, d\sigma_t \tag{10}$$

Subtracting member to member from the equation (9) the equation (10), after having multiplied its two members by V_t, we get the equation

$$\iint_{\sigma_t} (V_e - V_t') \left(\frac{dg}{dn} \right)_t' \cos\alpha' \, d\sigma_t - \iint_{\sigma_e} g_e'^2 \, d\sigma_e + \iint_{\sigma_t} g_t'^2 \cos^2\alpha' \, d\sigma_t = -2\omega^2 \iiint_e \left(\frac{dV}{dn} \right)' d\tau$$

which becomes for an *ocean area* σ_o

$$N_1 g_o \iint_{\sigma_o} \left(\frac{dg}{dn} \right)_o' d\sigma_o + \iint_{\sigma_e} g_e'^2 \, d\sigma_e - \iint_{\sigma_o} g_o'^2 \, d\sigma_o = -2\omega^2 \iiint_e \left(\frac{dV}{dn} \right)' d\tau$$

8. The surfaces σ will be practically curved squares of large sides. To obtain values of N_1 and $(N_1 + N_2)$ relating to a given area, which are sufficiently representative, it will be convenient to compute only those which are concerning the central square the surface of which is about the ninth of the curved square (Fig. 6).

9. If instead of the bulks e, e' we took the bulks $E = \Sigma e$, $E' = \Sigma e'$, we should obtain instead of the equations (5) and (7), the equations

$$\left\{ N_1 g_t \cos\alpha \left[\int\int_{S_e} g_e' \, dS_e - \int\int_{S_t} g_t' \cos\alpha' \, dS_t \right] + \int\int_{S_t} N_1' \, g_t'^2 \cos^2\alpha' \, dS_t \right.$$
$$\left. = 2\omega^2 \int\int\int_E (V' - V_t) \, d\tau + \int\int\int_E g'^2 \, d\tau \right.$$

$$\left\{ (N_1 + N_2)\gamma_r \cos D \left[\int\int_{S_r} \gamma_r' \, dS_r - \int\int_{S_e} \gamma_e' \cos\beta' \, dS_e \right] + \int\int_{S_e} (N_1 + N_2)' \gamma_r' \gamma_e'' \cos D' \cos\beta' \, dS_e \right.$$
$$\left. = -2\omega^2 \int\int\int_{E'} (U_e - U') \, d\tau + \int\int\int_{E'} \gamma'^2 \, d\tau \right.$$

The latter are equivalent to two equations previously given out [2], owing to the additional conditions of mass and volume equality of the bulks bounded by the surfaces S_t and S_r. But they need know the gravity values all over the topographical earth surface to determine its shape even regionally.

References

[1] Bragard, L. Methods to determine the shape of the topographical earth surface by successive regional determinations of this in function of regional gravity measurements or in function of these and regional vertical gravity gradient measurements, Uppsala, Geodetic Institute Series (on printing).

[2] Bragard, L. Method to determine the shape of the topographical earth surface by means of gravity measurements on that surface by solving two integral equations, Studia Geophysica at Geodetica, Prague, t. 9, fasc. 2, 1965, 110–111.

Analytical Integration of the Orbital Perturbations Caused by Gravity-Anomalies

by *K. Arnold*, Potsdam

Summary

In former publications a solution was presented fot the computation of pertubations of satellite orbits caused by mean values of gravity anomalies of $10^0 \times 10^0$, $15^0 \times 15^0$ or $20^0 \times 20^0$ surface elements. Thereby the perturbations result from numerical integrations. Because of the very great number of necessary integration steps, the computation expense is considerable.

Therefore a way is shown for the analytical integration of orbital perturbations of terrestrial gravity anomalies. The disturbance potential corresponding with the mean gravity anomaly of one surface element is described as a series of spherical harmonics. By simple substitutions it is possible, to transform this expression in the same form, which G. V. Groves or W. M. Kaula have found in their perturbation theory for the potential described by spherical harmonics.

It is advantageous that in this way the existing computer programs for the computation of perturbations from spherical harmonics can be applied.

Note: This summary was presented by Dr.-Ing. habil. L. Stange. The complete paper will be published in „Gerlands Beiträge zur Geophysik".

On the Determination of the Earth's Ellipsoid on the Basis of Satellite Observations

by *M. Burša*, Prague

The problem of determination of the Earth's ellipsoid parameters on the basis of satellite observations has been solved theoretically by Albrecht Euler of about 200 years before the era of the artificial satellites [1]. Euler's theory concernes especially the determination of the form of the meridian ellipse on the basis of zenith distances measurements of the Moon at its transit through the meridian, from the stations spaced at the meridian being investigated.

Actually, at the time of artificial satellites, the situation is much more advantageous as at Euler's times from the point of view of accuracy of the parameters being determined, than the artificial bodies are nearer to the Earth. At the beginning the situation had been considered very optimistic, but later it had been necessary to correct this optimism. According to Izotov [2] it appeared that the equations being used for determining the ellipsoid parameters correspond formally to the classic ones, only the information source is another, namely, the origin of the absolute terms.

Here we would like to point out a further fact being not respected before which also underlines the pessimistic point of view: using the values of the orbital elements calculated from observations at satellite stations not covering (homogeneously) the whole Earth's surface, we cannot obtain the *exactly geocentric orbit*. That is why the obtained ellipsoid parameters cannot be also exactly geocentric being only of a local significance in general. Therefore we will not obtain the Earth's ellipsoid replacing the Earth body as a whole.

The absolute term in the equation for the quasi-geoid height ζ which can be used for the determination of the ellipsoid's parameters by $\Sigma\zeta^2 = \min$ has the approximate form [3]

$$\zeta_o = (X^2 + Y^2 + Z^2)^{1/2} - a_o\left[1 - \frac{1}{2}e_o^2\left(1 - \frac{X^2 + Y^2}{X^2 + Y^2 + Z^2}\right) - e_o^4(\ldots)\right] - H_q, \tag{1}$$

where

a_o, e_o^2 — accepted approximate parameters of the reference ellipsoid,

X, Y, Z — coordinates of respective satellite station (M) on the Earth's surface, whereby

$$\begin{aligned} X &\doteq x - \triangle' \cos\delta' \cos(\alpha' - S), \\ Y &\doteq y - \triangle' \cos\delta' \sin(\alpha' - S), \\ Z &\doteq z - \triangle' \sin\delta'; \end{aligned} \tag{2}$$

H_q — normal height of the satellite station in question,

x, y, z — geocentric satellite coordinates (the x axis is parallel to the plane of the Greenwich astronomic meridian, the z axis coincides with the rotation Earth's axis), whereby

$$\begin{aligned} x &= \triangle\,[\cos u \cos(\Omega - S) - \sin u \sin(\Omega - S)\cos i], \\ y &= \triangle\,[\cos u \sin(\Omega - S) + \sin u \cos(\Omega - S)\cos i], \\ z &= \triangle \sin u \sin i; \end{aligned}$$

$\triangle'$ — topocentric satellite distance,

α', δ' — topocentric equatorial satellite coordinates (right ascension, declination),

S — Greenwich sidereal time for the observed position Sp,

Ω — right ascension of the ascending node,

i — inclination of the orbital plane,

u — argument of declination.

The coordinates of satellite stations can be determined on the basis of satellite observations more conveniently than by eqs. (2) e. g., from equations of orbital planes of numerous satellites [4]

$$\begin{aligned} &[X + \triangle' \cos\delta' \cos(\alpha' - S)] \sin(\Omega - S) \sin i - [Y + \triangle' \cos\delta' \sin(\alpha' - S)] \cdot \\ &\cdot \cos(\Omega - S) \sin i + (Z + \triangle' \sin\delta') \cos i = 0. \end{aligned} \tag{4}$$

In this case it is sufficient to know only two orbital elements, namely Ω, i.

In any case we determine the satellite orbital elements on the basis of topocentric observations and if they ought to have an *exactly geocentric character*, we had *to know the geocentric position of all used stations in advance.* At present we do not know the geocentric coordinates — their determination is actually the basic task of geodesy, which involves also the problem of determination of the general Earth's ellipsoid.

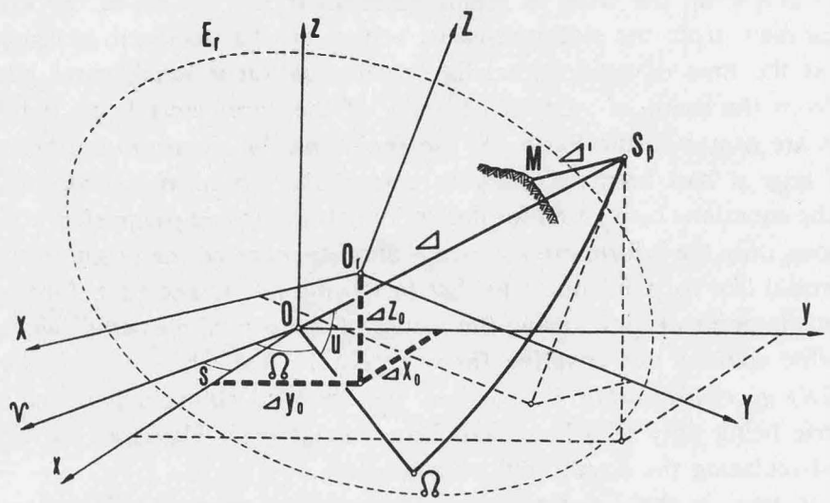

For the present we dispose only of the coordinates in reference systems differing from the geocentric ones in general by the following quantities

$$\begin{aligned} \delta X &= \triangle x_o + \omega Y - \psi Z, \\ \delta Y &= \triangle y_o - \omega X + \varepsilon Z \ , \\ \delta Z &= \triangle z_o + \psi X - \varepsilon Y \ , \end{aligned} \tag{5}$$

where $\triangle x_o$, $\triangle y_o$, $\triangle z_o$ are coordinates of the centre 0_r (see fig. 1) of the reference ellipsoid E_r in relation to the Earth's mass centre 0 and ε, ψ, ω small angles defining the directions of the reference system axes X, Y, Z in relation to the geocentric ones x, y, z.

The fact that the quantities δX, δY, δZ are not known, creates errors in the calculated elements Ω, i etc. namely $\delta\Omega$, δi etc., being functions of the same arguments $\triangle x_o$, $\triangle y_o$, $\triangle z_o$ ε, ψ, ω.

As an example we have analysed a case [4, 5], where the orbital elements are determined from one position x, y, z and the velocity components $\frac{dx}{dt} = \dot{x}, \frac{dy}{dt} = \dot{y}, \frac{dz}{dt} = \dot{z}$. For the distorsion of the rectascension of the ascending node we obtained, if the components $\dot{x}, \dot{y}, \dot{z}$ are errorless

$$\begin{aligned} \delta\Omega = -\{ &\triangle x_o \dot{z} \sin(\Omega - S) - \triangle y_o \dot{z} \cos(\Omega - S) + \triangle z_o [\dot{y} \cos(\Omega - S) - \\ &- \dot{x} \sin(\Omega - S)] - \varepsilon (Z \dot{z} \cos(\Omega - S) - Y [\dot{x} \sin(\Omega - S) - \dot{y} \cos(\Omega - S)]) - \\ &- \psi (Z \dot{z} \sin(\Omega - S) + X [\dot{x} \sin(\Omega - S) - \dot{y} \cos(\Omega - S)]) + \\ &+ \omega \dot{z} [X \cos(\Omega - S) + Y \sin(\Omega - S)]\} [(x\dot{y} - y\dot{x})^2 + \\ &+ (z\dot{x} - x\dot{z})^2 + (y\dot{z} - z\dot{y})^2]^{-1} \operatorname{cosec} i, \end{aligned} \tag{6}$$

and for the distorsion of the inclination

$$\delta i = \{ \triangle x_o [\dot{z} \cos(\Omega - S) \cos i - \dot{y} \sin i] + \triangle y_o [\dot{x} \sin i +$$
$$+ \dot{z} \sin(\Omega - S) \cos i] - \triangle z_o [x \cos(\Omega - S) + y \sin(\Omega - S)] \cos i +$$
$$+ \varepsilon (Z [\dot{x} \sin i + \dot{z} \sin(\Omega - S) \cos i] + Y [x \cos(\Omega - S) +$$
$$+ \dot{y} \sin(\Omega - S)] \cos i) - \psi (X [\dot{x} \cos(\Omega - S) - \dot{y} \sin(\Omega - S)] \cos i - \quad (7)$$
$$- Z [\dot{y} \sin i - \dot{z} \cos(\Omega - S) \cos i]) - \omega (Y [\dot{y} \sin i -$$
$$- \dot{z} \cos(\Omega - S) \cos i] + X [\dot{x} \sin i + \dot{z} \sin(\Omega - S) \cos i]) \} .$$
$$. [(x\dot{y} - y\dot{x})^2 + (z\dot{x} - x\dot{z})^2 + (y\dot{z} - z\dot{y})^2]^{-1} .$$

Analogically we obtained distorsions of other elements [5]. Distorsion of each element (N) can be expressed in general by the formula

$$\delta N = a_N \triangle x_o + b_N \triangle y_o + c_N \triangle z_o + d_N \varepsilon + e_N \psi + f_N \omega , \quad (8)$$

where $a_N, \ldots, f_N$ are coefficients namely, functions of approximate (quasi-geocentric) coordinates of satellite as well as of velocity components, orbital elements and time.

Given example is rather schematic but it sufficiently illustrates the fact that the determination of exactly geocentric elements of satellite orbits requires the knowledge of the geodetic fundamental parameters $\triangle x_o$, $\triangle y_o$, $\triangle z_o$, ε, ψ, ω of those reference systems in which the position of the satellite stations is expressed. Actually these parameters are not known with sufficient accuracy and if neglected, the orbital elements should involve distorsions independent on the observation errors. Partially these distorsions are of a systematic character being dependent on the concrete distribution of satellite stations.

Because of distorsions δN of the orbital elements N the determined position of the satellite should be also distorsed, namely by the errors δx, δy, δz being the total differentials of functions (3). These values influence then the quantities (2) and later also (1).

By this reason the situation concerning the determination of the general Earth's ellipsoid on the basis of satellite observations would be very unsatisfactory, if it would not exist the real possibility that the satellite stations could cover the whole Earth's surface, including islands etc. This fact should weaken essentially the distorsions δN as well as their influence on ζ_o. Out of this — from the point of view of the solution of the given problem — an absolute advantage of the satellites is the well known possibility to determine the polar flattening of the Earth's ellipsoid on the basis of perturbation of Ω or of argument of perigee with high accuracy.

References

[1] Euler, I. A.: Versuch die Figur der Erden durch Beobachtungen des Monds zu bestimmen. Abh. d. Churfürst.-baier. Ak. d. Wiss., Bd. 5, (1768), 198.

[2] Izotov, A. A.: On the Determination of the Shape and Dimensions of the Earth from Observations of Artificial Satellites. Studia geoph. et geod., 9 (1965), 201.

[3] Burša, M.: Theorie der Bestimmung der Dimensionen des mittleren Erdellipsoids und der geodätischen Ausgangsdaten aus Beobachtungen künstlicher Erdsatelliten. Nachr. aus d. Kart.- u. Vermessungsw., Reihe III., Nr. 17, Frankfurt a. M. 1965. (Transl. from Studia geoph. et geod., 5 (1961), 312.)

[4] Burša, M.: Теория определения положения центра референц-эллип-соида по наблюдениям искусственных спутников Земли. Studia geoph. et geod., 9 (1965), 225.

[5] Burša, M.: К определению элементов орбиты спутника по положению и скорости. Studia geoph. et geod., 10 (1966), 401.

[6] Burša, M.: On the Determination of the Geocentric Orbital Elements from Quasi-Simultaneous Direction Observations to Satellites. Studia geoph. et geod., 11 (1967), No 2.

A New Parameter for Ellipsoidal Calculus

by *G. J. Bruins*, Delft

To describe the meridianplane of an ellipsoid of revolution different parameters and quantities are used. So Jordan ([1] page 35 and next) uses a, b, α, e, e' m, n, φ, ψ, γ, W, V, w, v, M and N. The meaning of these symbols is well known. Jordan gives also a great number of formulae to describe their interrelations, but it is not easy to see the general line of these interrelationships and to reproduce them instantly.

Therefore we will now introduce another parameter δ and show that most quantities, indicated above, can be expressed as very simple trigonometric functions of δ.

The new parameter δ is defined as half of the angle between P on the ellipse and the two foci of the ellipse A and B. (see figure 1). The bisectrix of this angle is normal to the ellipse and intersects the equatorial plane under an angle φ . φ is the geographic latitude.
The sine-rule in ΔACP and ΔBCP gives:

$$\frac{AP}{\sin\varphi} = \frac{AC}{\sin\delta} \quad \text{and} \quad \frac{BP}{\sin\varphi} = \frac{BC}{\sin\delta}$$

or

$$\frac{\sin\varphi}{\sin\delta} = \frac{AP}{AC} = \frac{BP}{BC} = \frac{AP+BP}{AC+BC} = \frac{2a}{2c} = \frac{a}{\sqrt{a^2-b^2}} = \frac{1}{e}$$

or

$$\boxed{\sin\delta = e\sin\varphi} \qquad (1)$$

and if $\varphi = 90^0$

$$\boxed{\sin\delta_o = e} \qquad (1a)$$

The formula for the second principal radius of curvature N (= PD in figure 1) can also be derived from this figure in the following way.

$$AD^2 = AP^2 + N^2 - 2AP\,.\,N\cos\delta$$

$$BD^2 = BP^2 + N^2 - 2BP\,.\,N\cos\delta$$

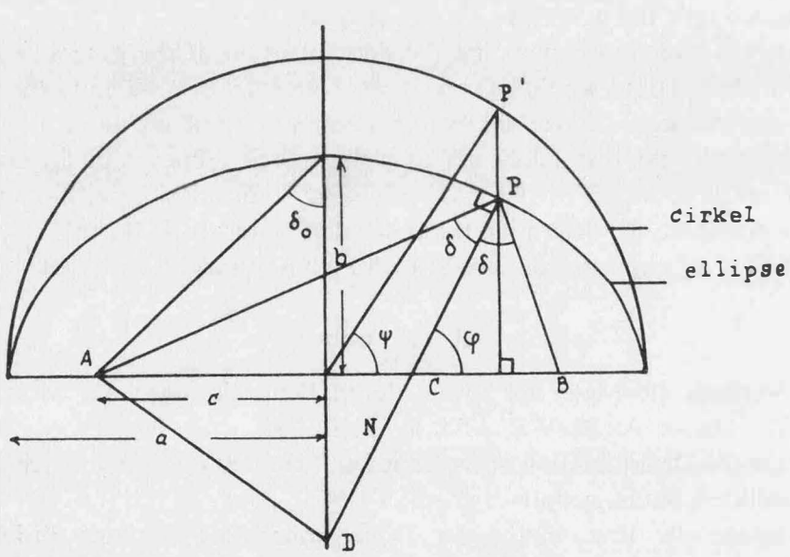

Subtracting these two formulae, we get:

$$0 = (AP - BP)\{(AP + BP) - 2N\cos\delta\}$$

As

$$AP - BP \neq 0 \qquad \text{except for } \delta = \delta_o$$

and

$$AP + BP = 2a$$

we get:

$$\boxed{N = \frac{a}{\cos \delta}} \tag{2}$$

and with (1):

$$N = \frac{a}{\sqrt{1 - e^2 \sin^2 \varphi}} = \frac{a}{W}$$

the well-known expression for N. (Jordan).

It is also easy to introduce the reduced latitude ψ.
From figure 1 follows:

$$N \cos \varphi = a \cos \psi$$

and with (2):

$$\boxed{\cos \varphi = \cos \psi \cos \delta} \tag{3}$$

Squaring (3) we get with (1):

$$\frac{1}{1 + \tan^2 \varphi} = \frac{1}{1 + \tan^2 \psi} \cdot (1 - e^2 \sin^2 \varphi)$$

and after some mathematical manipulations:

$$\frac{\tan \psi}{\tan \varphi} = \sqrt{1 - e^2} = \cos \delta_o \tag{4}$$

also a well-known expression given by Jordan.

It is easy now to express all the formulae that appear in Jordan et. al. [1] as functions of δ and δ_o :

$$e = \frac{\sqrt{a^2 - b^2}}{a} = \sin \delta_o$$

$$e' = \frac{\sqrt{a^2 - b^2}}{b} = \tan \delta_o$$

$$\frac{b}{a} = \cos \delta_o$$

$$\sqrt{1 - e^2} = \cos \delta_o$$

$$\sqrt{1 + e'^2} = \frac{1}{\cos \delta_o}$$

$$\alpha = \frac{a - b}{a} = 1 - \cos \delta_o$$

$$n = \frac{a - b}{a + b} = \frac{1 - \cos \delta_o}{1 + \cos \delta_o} = \tan^2 {}^1/_2 \delta_o$$

$$m = \frac{a^2 - b^2}{a^2 + b^2} = \frac{1 - \cos^2 \delta_o}{1 + \cos^2 \delta_o}$$

In the following formulae, according to Jordan [1]:

φ stands for the geographic latitude
ψ stands for the reduced latitude
γ stands for the geocentric latitude

$$\sin\varphi = \frac{\sin\delta}{\sin\delta_o} \qquad \frac{\tan\varphi}{\tan\psi} = \frac{1}{\cos\delta_o} = \frac{a}{b} \qquad W = \sqrt{1 - e^2\sin^2\varphi} = \cos\delta$$

$$\sin\psi = \frac{\tan\delta}{\tan\delta_o} \qquad \frac{\tan\gamma}{\tan\varphi} = \cos^2\delta_o = \frac{b^2}{a^2} \qquad V = \sqrt{1 + e'^2\cos^2\varphi} = \frac{\cos\delta}{\cos\delta_o}$$

$$\frac{\sin\varphi}{\sin\psi} = \frac{\cos\delta}{\cos\delta_o} \qquad \frac{\tan\gamma}{\tan\psi} = \cos\delta_o = \frac{b}{a} \qquad w = \sqrt{1 - e^2\cos^2\psi} = \frac{\cos\delta_o}{\cos\delta}$$

$$\frac{\cos\varphi}{\cos\psi} = \cos\delta \qquad v = \sqrt{1 + e'^2\sin^2\psi} = \frac{1}{\cos\delta}$$

We also get simple formulae for the principal radii of normal curvatures M and N:

$$m = a\frac{\cos^2\delta_o}{\cos\delta} \qquad M_{pole} = N_{pole} = \frac{a}{\cos\delta_o}$$

$$N = a\frac{1}{\cos\delta} \qquad M_{equator} = a\cos^2\delta_o$$

$$\frac{N}{M} = \frac{\cos^2\delta}{\cos^2\delta_o} \qquad N_{equator} = a$$

$$\sqrt{N\,M} = a\frac{\cos\delta_o}{\cos^2\delta}$$

Hence we see that all quantities of the ellipsoid can be expressed in simple trigonometric functions of δ and δ_o, the latter being the parameter of the special ellipsoid with eccentricity $e = \sin\delta_o$ and focal distance $c = \sqrt{a^2 - b^2}$.

With these formulae it is not only easy to see the relations between the different quantities themselves but also between their differentials.

It seems worthwhile to introduce this parameter in [1] especially in Chapters XII, XIII and XIV (zweite Hälfte) in order to investigate wheter the many deductions can be given in a more simple form. This will be done in a following paper.

Literature:

[1] Jordan, Eggert, Kneissl: Handbuch der Vermessungskunde, Band IV, erste und zweite Hälfte, 10. Ausgabe (1958, 1959).

Some Remarks about Ellipsoidal Coordinate Systems

by *G. J. Bruins*, Delft

Summary

In problems concerning the figure of the earth different coordinate-systems and parameters are used, lineair and curvilinear, orthogonal as well as oblique, isometric and non-isometric.

In this paper some properties of the coordinates and parameters used by Hirvonen [1] and Molodenski [2] are compared.

par 1.

In geodesy, in two- as well as in three-dimensional space, in most problems the metric cartesian coordinate system (x, y, z) is adopted to locate a point in the plane or in space.

However also curvilinear coordinates may be introduced.

For example we may have the coordinate transformations.

a) spherical coordinates (r, φ, λ)

$$x = r\cos\varphi\cos\lambda\,, \quad y = r\cos\varphi\sin\lambda\,, \quad z = r\sin\varphi$$

With varying values of the parameter r a family of spheres is associated. On each sphere $r =$ $=$ constant a point is defined by the latitude φ and longitude λ.

b) ellipsoidal coordinates according to Hirvonen [1] page 4 $(\alpha, \beta\,\lambda)$

$$x = c\,\mathrm{cosec}\,\alpha\cos\beta\cos\lambda\,, \quad y = c\,\mathrm{cosec}\,\alpha\cos\beta\sin\lambda\,, \quad z = c\cot\alpha\sin\beta$$

(c is a constant)

c) ellipsoidal coordinates according to Molodenski [2] page 39 (u, β, λ)

$$x = c\cosh u\cos\beta\cos\lambda\,, \quad y = c\cosh u\cos\beta\sin\lambda\,, \quad z = c\sinh u\sin\beta$$

(c is a constant)

In the following the latter two systems will be compared, especially the differences between the parameters α and u.

Therefore we may consider a meridian section, thus eliminating λ in the equations.

System 1: $$x = c\,\mathrm{cosec}\,\alpha\cos\beta\,, \quad z = c\cot\alpha\sin\beta \tag{1}$$

System 2: $$x = c\cosh u\cos\beta\,, \quad z = c\sinh u\sin\beta \tag{2}$$

In both systems c is a constant. If in system 1, α is constant we may write:

$$c\,\mathrm{cosec}\,\alpha = a\,, \quad c\cot\alpha = b \tag{3}$$

and so: $$x = a\cos\beta\,, \quad y = b\sin\beta \tag{4}$$

which are the well-known parameter formulae of an ellipse, in which β is the reduced latitude. The focal distance is:

$$\sqrt{a^2 - b^2} = c\sqrt{\mathrm{cosec}^2\alpha - \cot^2\alpha} = c \qquad \text{(indepentend of } \alpha\text{!)} \tag{5}$$

If, on the other hand $\beta =$ constant we may write:

$$c\cos\beta = a'\,, \quad c\sin\beta = b' \tag{6}$$

and so: $$x = a'\,\mathrm{cosec}\,\alpha = a'\sec(90 - \alpha)\,, \quad y = b'\cot\alpha = b'\tan(90 - \alpha) \tag{7}$$

which are the well-known parameter formulae of a hyperbola. The focal distance is:

$$\sqrt{a'^2 + b'^2} = c\sqrt{\cos^2\beta + \sin^2\beta} = c \qquad \text{(independent of } \beta\text{!)} \tag{8}$$

From (5) and (8) we find: $$a^2 - b^2 = a'^2 + b'^2 = c^2 \tag{9}$$

Consequently system 1 defines a family of confocal ellipses – one for each value of α – and a family of confocal hyperbolas – one for each value of β.
The same conclusion holds for system 2 if we put:

$$c\cosh u = a\,, \quad c\sinh u = b \tag{10}$$

If c is the same constant in both systems 1 and 2, we also see that a and b are the same in both systems, because:

$$\mathrm{cosec}^2\alpha - \cot^2\alpha = 1 = \cosh^2 u - \sinh^2 u$$

Or in other words:

if we take: $$\mathrm{cosec}\,\alpha = \cosh u \tag{11}$$

then we also have: $$\cot\alpha = \sinh u \tag{11a}$$

This relation between α and u can be transformed into another form:
From (11) and (11a) we get:

$$\cos\alpha = \tanh u$$

or

$$\frac{1 - \tan^2 {}^1\!/_2\,\alpha}{1 + \tan^2 {}^1\!/_2\,\alpha} = \frac{e^u - e^{-u}}{e^u - e^{-u}} = \frac{1 - e^{-2u}}{1 + e^{-2u}}$$

or $$\tan^2 {}^1/_2\alpha = e^{-u}, \quad \cot {}^1/_2\alpha = e^{u}, \quad u = {}^{e}ln \cot {}^1/_2\alpha \tag{12}$$

par 2.

Until now we saw the agreement between the systems 1 and 2. We now want to see whether there are any differences. In both systems the parameter curves (α, β) and (u, β) constitute a system of ellipses and hyperbolas.

To find additional conditions we consider the derivatives (as Hirvonen has already done for system 1):

System 1:
$$\frac{\partial x}{\partial \alpha} = -c\frac{\cos\alpha}{\sin^2\alpha}\cos\beta\ ; \quad \frac{\partial x}{\partial \beta} = -c\frac{\sin\beta}{\sin\alpha}$$
$$\frac{\partial z}{\partial \alpha} = -c\frac{\sin\beta}{\sin^2\alpha}\ ; \quad \frac{\partial z}{\partial \beta} = +c\frac{\cos\alpha}{\sin\alpha}\cos\beta$$

System 2:
$$\frac{\partial x}{\partial u} = +c\ \sinh u\cos\beta\ ; \quad \frac{\partial x}{\partial \beta} = -c\cosh u\sin\beta$$
$$\frac{\partial z}{\partial u} = +c\ \cosh u\sin\beta\ ; \quad \frac{\partial z}{\partial \beta} = +c\sinh u\cos\beta$$

For both systems the condition of orthogonality holds:

$$\frac{\partial x}{\partial \alpha}\frac{\partial x}{\partial \beta} + \frac{\partial z}{\partial \alpha}\frac{\partial z}{\partial \beta} = 0 \tag{13}$$

However the condition for isometry holds only for the system 2 (Canchy and Riemann equations):

$$\frac{\partial x}{\partial u} = \frac{\partial z}{\partial \beta} \quad \text{and} \quad \frac{\partial x}{\partial \beta} = -\frac{\partial z}{\partial u} \tag{14}$$

This means that in system 2, x and z are conjugate harmonic functions of u and β and that they may be written in analytic form:

$$x + iz = f(u + i\beta)$$

To find this function we substitute (2):

$$\begin{aligned} x + iz &= c\,(\cosh u\cos\beta + i\sinh u\sin\beta) \\ &= c\,(\cosh u\cosh i\beta + \sinh u\sinh i\beta) \\ &= c\,.\cosh(u + i\beta) \end{aligned} \tag{15}$$

Because u and β are an isometric system all properties of conformal transformations are valid for this transformation. So the fundamental quantities of the first order are:

$$E = G = \left(\frac{\partial x}{\partial u}\right)^2 + \left(\frac{\partial z}{\partial u}\right)^2 = \left|\frac{\partial(x+iz)}{\partial(u+i\beta)}\right|^2 = c^2\left|\sinh^2(u+i\beta)\right|$$

or:
$$\begin{aligned} E &= c^2(\sinh^2 u\cos^2\beta + \cosh^2 u\sin^2\beta) \\ &= c^2(\cosh^2 u - \cos^2\beta) \end{aligned}$$

With (6) and (10) we get:

$$E = a^2 - a'^2 \tag{16}$$

An arbitrary point P is defined by the parameters u and β, or, if we like, by the semi major axis of the ellipse $a = c\cosh u$ (10) and the semi axis of the hyperbola $a' = c\cos\beta$. (6).

From elementary mathematics it is known that:

$$AP + BP = 2a$$
$$AP - BP = 2a',$$

where A and B are the focal points.

So we get: $$E = AP \,.\, BP \tag{17}$$

In the same way other applications can be made with the isometric system (u, β) but also in the metric system (a, a'), e. g. the computation of the lane-width of a Decca-system.

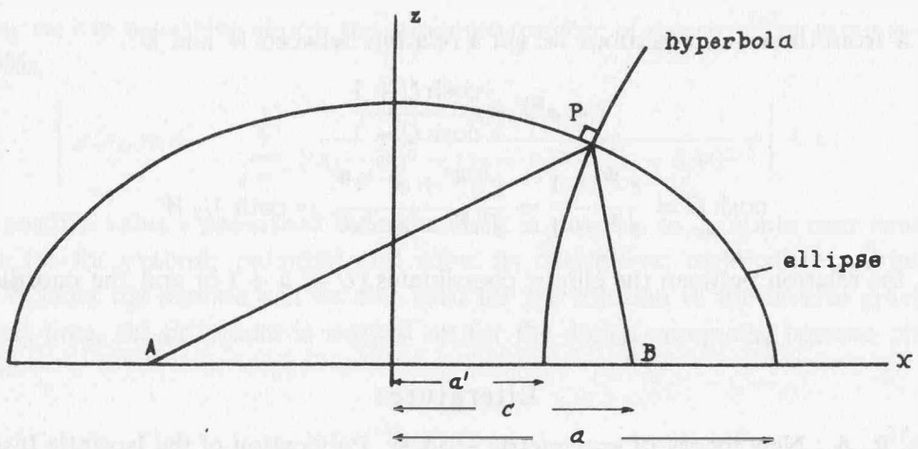

Fig. 1

par 3.

In the theory of conformal transformations often the following transformation is used:

$$W = {}^{e}ln \frac{X + c}{X - c} \tag{18}$$

wherein: $W = w + iv$ and $X = x + iz$

and c is the focal distance (see figure 1)

From the theory of complex functions it is known that:

$${}^{e}ln(a + ib) = {}^{e}ln|a + ib| + i \text{ argument } (a + ib)$$

with $|a + ib| = \text{modulus of } (a + ib) = \sqrt{a^2 + b^2}$

Applying this to W we get:

$$w + iv = {}^{e}ln\left|\frac{X + c}{X - c}\right| + i \arg\left(\frac{X + c}{X - c}\right)$$

as: $|X + c| = PB\,, \quad |X - c| = PA$

and: $$\text{argument} \frac{X + c}{X - c} = < APB \qquad \text{(figure 1)}$$

so: $$w = {}^{e}ln \frac{PB}{PA} \tag{19}$$

and: $$v = < APB = 2\delta \tag{20}$$ [1]

From this we see that the curves $w =$ constant are circles of Apollonius because $\frac{PB}{PA} =$ constant and the curves $v =$ constant are circles of Steiner through the points A and B. This system is useful in geodesy e. g. in demonstrating map projections.

Combining the transformation (18) with the transformations (2) or (15) we find a relation between the system (w, v) and the system (u, β).

---

[1] $\delta = {}^1/_2 v$ is also a very useful parameter to describe the inter-relationships between the different quantities of the meridianplane of an ellipsoid of revolution. These interrelationships are described by the author in a separate paper, also published in these proceedings.

Suppose $U = u + i\beta$

Then (15) $X = c \cosh U$ (15)

and $W = {}^{e}ln \dfrac{X + c}{X - c}$ (18)

Eliminating X from these two equations we get a relation between W and U:

$$e^{W} = \frac{\cosh U + 1}{\cosh U - 1}$$

or $$\cosh U = \frac{e^{W} + 1}{e^{W} - 1} = \frac{e^{1/2 W} + e^{-1/2 W}}{e^{1/2 W} - e^{-1/2 W}} = \coth {}^{1}/_{2}\, W \qquad (21)$$

which gives the relation between the elliptic coordinates ($U = u + i\,\beta$) and the coordinates ($W = w + iv$).

Literature:

[1] Hirvonen, R. A.: New theory of gravimetric geodesy. Publication of the Isostatic Institute nr. 32, Helsinki 1960.

[2] Molodenski, M. S., Eremeev V. F., Yurkina M. J.: Methods for study of the external gravitational field and figure of the earth.
Moscow 1960. Israel Program of Scientific Translations, Jerusalem 1962.

Mass-Sources of the Gravitation Anomalies

by *Ivan Pola*, Prague

It is possible to substitute the mass of the Earth by the mass-points, in such a way that the gravitation effect equals the observed values of gravity, corrected by the centrifugal acceleration.

Let us denote these values $g(x_i, y_i, z_i)$, where x_i, y_i, z_i are the coordinates of the observed points on the Earth surface. It is not necessary to introduce any other reductions or to interpolate the gravity values.

The procedure of computation of the position and the magnitude of the almost minimum number of mass-points consists of two nonlinear operators; one of them serves for determining the magnitude and the location of the sources, the other one is for the determining of z-coordinates of the computed sources.

The form of the first operator in general three-dimensional case on the Earth surface is

$$M_j = \sup_{\substack{(u_j, v_j) \leftarrow D \\ h_j \leftarrow (\max z_i + h_\varepsilon, H) \\ O_j}} \min_{(x_i, y_i) \leftarrow O_j} \left\{ \frac{g_j(x_i, y_i, z_i)}{(h_j - z_i)} [(x_i - u_j)^2 + (y_i + v_j)^2 + (z_i - h_j)^2]^{3/2} \right\},$$

where $g_j(x_i, y_i, z_i)$ is the gravitation anomaly in the point $(x_i, y_{,i}, z_i)$, x_i, y_i, z_i being the coordinates of the observation points on the Earth's surface, u_j, v_j, h_j being the coordinates of the computed mass-point M_j, $M_j = f \,.\, m_j$, f is the gravitation constant and m_j is the mass of mass point M_j. O_j is the suitable vicinity of the point (u_j, v_j) in the plane (x, y); let us apply the operator in all points (x_i, y_i) from this vicinity. D is the two-dimensional interval, which includes all the observation-points, h_ε is the minimum possible distance of the sources M_j from the Earth's surface.

The second operator can be written in the form

$$\overline{h_j} = \max_{(x_i, y_i) \leftarrow O_j} \left\{ \left[1{,}1547 \frac{M_j}{g_j(x_i, y_i, z_i)} \cos(4{,}1888 + \alpha_i/3) \right]^{1/2} + z_i \right\},$$

where $\bar{h}_j$ is the corrected coordinate h_j of the source M_j, $\bar{g}_j$ is the difference between the gravitation anomaly g_j and the vertical gravitation effect of the source M_j in all the observed points,

$$\cos \alpha_i = 2{,}5981 \frac{M_j}{\bar{g}_j (x_i, y_i, z_i)} [(u_j - x_i)^2 + (v_j - y_i)^2] .$$

In such a way we can determine almost the minimum number of mass-sources using two operators, so that it holds

$$\left| g(x_i, y_i, z_i) - \sum_{j=0}^{s} \frac{M_j (h_j - z_i)}{[(x_i - u_j)^2 + (y_i - v_j)^2 + (z_i - h_j)^2]^{3/2}} \right| < \varepsilon ,$$

for a small positive value ε prescribed beforehand. It is possible to compute next values from the mass-sources (as for example potential and some its derivatives, regional or residual values of gravity a. s. o.) and the method can be also used for the solution of the inverse gravity-problem. At the present time, the procedure is worked up for the digital computer, because otherwise it is not realizable.

A Contribution to the Determination of Gravity by a Transformation Method*)

by *Jan Kašpar*, Prague

Introduction

The paper presents several possibilities provided by transformation methods in solving problems which are related to the determination of the figure of the Earth in a limited region. It thus follows up papers of Marussi and Hotine (see [2], [5]).

The basic idea of the solution is in ascribing known points of a "model" surface, — approximating the Earth's surface in a "model" —, to corresponding points of an image surface, which is an approximation of the real Earth's surface. The „model" surface is immersed into the "model" space related to a reference body, — or reference surface —. The image surface is then in space corresponding to the real Earth.

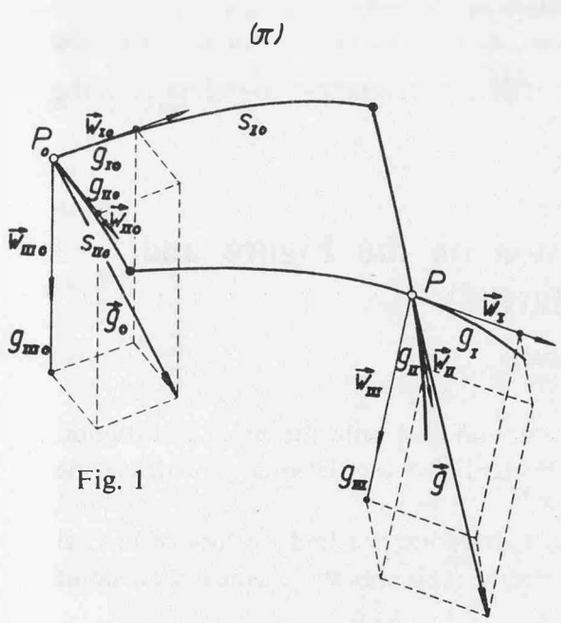

Fig. 1

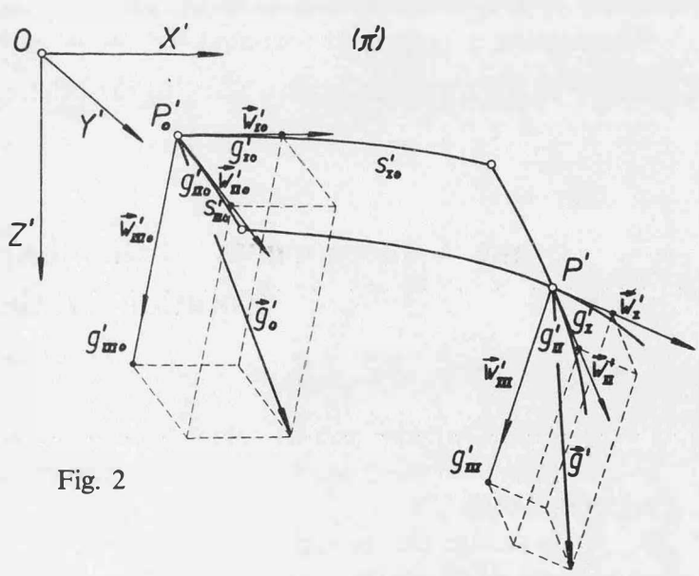

Fig. 2

*) The paper was already published in "Studia Geophysica et Geodetica", No. 2, Prague 1966

If vectors of a known "model" gravity $\vec{g}$ in points P of the original ("model") surface (π) are related to vectors $\vec{g'}$ of real gravity in corresponding points P' of the image surface (π'), not only the shape, orientation and dimensions of the surface approximating the Earth's surface can be determined, but also the transformation of one surface into the other (see Fig. 1, 2). The quantities defining the gravity vector relation may also be determined, so that it is possible to interpolate gravity acceleration over the image surface.

These quantities may be determined by measurements of astronomical longitudes and latitudes, by gravity measurements and by measurements of spacial distances and relative co-ordinate differences in an arbitrary co-ordinate system.

This paper links up with paper [1] and [7], in which equations of general transformation of one surface into another, as well as equations of the image surface, have been deduced. Arcs of measurement along the basic lines of principal curvature of the original surface were selected as parameters. The suitability of the choice of parameters as well as the invariability of the expressions occuring in the power expansion series is discussed. The achieved results will be mentioned as necessary, and some of the deduction sequences will also be given.

The paper also presents, in short, an expansion of the position function of a point on the original surface, as well as the image surface. This result is used in determining the expansion of extreme values of scale (linear magnification, extention ratio) and of its directions, with respect to the lines of principal curvature, as well as for expanding the gravity vector on the image surface. The process of application of these results in determining the image surface, which approximates to the Earth's surface in a limited region, is also mentioned. Closed equations of correction for measured astronomical latitude and longitude are given. The corrected geographic co-ordinates are related to the gravity vector on the image surface. The equation of correction of the absolute value of the gravity vector is mentioned, as well as the equation for the spacial distance of two points on the image surface and the equation for corresponding zenith distance.

In these equations the known quantities are co-ordinates — parameters — of the original points on the "model" surface and invariants determining the shape of this surface and the "model" gravity vektor $\vec{g}$ on this surface. The unknowns are invariants determining the shape, transformation and the gravity vector on the image surface. The equations also contain expressions which determine the orientation of this surface in a co-ordinate system related to the Earth's axis and the Greenwich meridian.

After linearization of the equations of deviations, it is possible with the use of the minimum condition $\left\{l^v, n\right\}\left\{\begin{matrix} Q_e^{-1} \\ n, n \end{matrix}\right\}\left\{n^v, l\right\} = \text{min.}$ (see [6]), to determine the unknown quantities and thus the orientation, shape and magnitude of the image surface, as well as the co-ordination of the gravity vector, $\vec{g'}$, which in turn leads to the determination of the geographic co-ordinates in the corresponding point of the image.

Some Consequences of the Expansion on the Figure and Rotation of the Earth*)

by *L. Egyed*, Budapest

The Earth's figure and its rotation show a close connection and only the mass distribution and the angular momentum, i. e. the mechanical energy — potential + inertial energy — determine the level surface.

If no change can be supposed in the structure of the Earth's interior and no loss of inertial energy occurs, the shape of the Earth can be regarded as steady. This was the classical view point in geodesy.

*) This paper was presented by Dr.- Ing. habil. P. Biró.

There are, however, very important observed variations, e. g. the slowing down of the Earth's rotation etc. which in more detailed investigations must be considered.

In this article it is suggested that nearly all the known changes observed on the Earth figure and structure can be reduced to the expansion of the Earth.

If a Dirac cosmology is valid — Dirac, 1938 — and the existence of high-pressure phases in the sense of Ramsey — Ramsey, 1949 — can be accepted, than an expansion of the Earth amounting to a yearly radius increase of 0,65 ± 0,15 mm/year can be theoretically derived.

It is surprising that the same rate of expansion can be obtained from the distribution of continental and oceanic areas, from the retreat of water covered areas during geological ages — Egyed, 1956 a, b —, as well as palaeomagnetic data do not contradict to the rate indicated above. Moreover, it is very easy to show that the recent slowing down of the Earth is consistent with the above value.

According to the law of the conservation of angular momentum the formula $\omega J = \text{const}$ should be considered as valid for the Earth, if the well known outer effects are eliminated, where J is the momentum of inertiae and ω the angular velocity of the Earth.

From this formula

$$\frac{1}{J}\frac{dJ}{dt} = -\frac{1}{\omega}\frac{d\omega}{dt}$$

But for a shorter time — which in the case of the Earth also may amount to some hundred million years —

$$\frac{1}{J}\frac{dJ}{dt} = \frac{2}{R}\frac{dR}{dt} = \frac{2\alpha}{R}$$

where dR is the radius increase and R the radius of the Earth. Hence the yearly radius increase

$$\alpha = \frac{1}{2} R \frac{1}{\omega} \cdot \frac{d\omega}{dt} .$$

According to the newest data $\frac{dw}{dt} = -4{,}81 \cdot 10^{-22}$ radian $\text{sec}^{-2} = 1{,}44 \cdot 10^{-14}$ rad sec^{-1}/ /year; $\omega = 7{,}29 \cdot 10^{-5}\ \text{sec}^{-1}$, $R = 6{,}37 \cdot 10^{8}$ [Munk and MacDonald, 1960].

This results in $\alpha = 0{,}63$ mm/year, a value in excellent agreement with that obtained theoretically as well as from geological-geophysical observations. This result says that, at least at the present, no effect of tidal forces is involved into the slowing down of the Earth. If this is right this can be extrapolated for the future of the Earth too: the slowing down effect can be only the result of the expansion.

It was K. Ledersteger who tried to compare some extreme values of the Earth in the case of a contracting Earth. In the case of an expanding Earth it is possible to give an upper limit — i. e. the value without energy loss — for the minimum value of angular velocity.

The greatest volume and greatest momentum of inertiae can be obtained if the effect of gravity does not exist more. This is the end result of the extrapolation of the Dirac cosmology. Then the Earth becomes a homogeneous body with a density of that of the basic-ultra-basic rocks. As a reliable value for it $\rho = 3{,}2$ can be chosen. This corresponds however to a radius of $7{,}64 \cdot 10^{8}$ cm. The momentum of inertiae at this end-phase will be $13{,}95 \cdot 10^{44}$. The application of the law on the constancy of angular momentum results in the formula

$$T_\infty = \frac{J_\infty}{J_o} T_o = 41{,}85 \text{ hours}$$

for the greatest length of the day.

There are some hints that in the very past the slowing down of the Earth was affected also by tidal forces.

One can show, that in the case of a Dirac-cosmology the distance of planets from the Sun was proportional to a time parameter t corresponding to the age of the Solar-system, while that of the length of the year — τ — proportional to the square of this time-parameter:

$$r = k\,t$$

$$\tau = \mu t^2$$

This formula enable us to calculate for the geological past the numbers of rotations of the Earth during an actual year i. e. during the time span corresponding to a whole orbit around the Sun. As the most probable value of the radius increase amounts to 0,65 ± 0,15 mm/year, using this value, the following table was calculated for $t = 4{,}5$ to $t = \infty$ and for the time interval of the last 400 million years.

Table 1. Number of rotations as a function of Δt and t_o

Δt 10^8 years \ t_o 10^9 years	4,5	5	6	8	10	12	
0	365	365	365	365	365	365	365
50	361	362	363	365	365	366	369
100	356	358	361	364	365	367	373
150	352	354	358	363	365	368	377
200	347	350	356	362	365	368	381
250	342	346	353	361	365	369	385
300	337	342	350	360	365	369	389
350	332	338	347	358	365	370	393
400	327	334	344	357	365	371	398

According to this table the numbers of Earth's rotation have surpassed the recent value only if the correct value of time parameter higher was than about $1{,}1 \cdot 10^{10}$ years.

On the other side Wells — 1963 — made the suggestion that the Devonian corals show that the number of rotations in this period amounted to 400 in an actual year, which at a radius increase of 0,65 ± 0,15 mm/year, can be fulfiled at $t = \infty$ only. If Wells is correct and $t \neq \infty$, the contradiction can be solved only by supposing that the rest of the slowing-down effect was due to tidal friction which must have been more effective in the past, as the planets and so the Earth too, were much closer to the Sun.

Concerning the change in ellipticity one can derive [Egyed, 1965] by using the generalized Clairant-equation the following formula:

$$\frac{d\varepsilon}{\varepsilon} = \frac{2Q}{\omega} \cdot \frac{d\omega}{dt} + \frac{Q}{t} + \left(5Q + \frac{3\rho_o}{\rho\varkappa} - 2\right)\frac{\alpha}{a}$$

where the meaning of the letters:

$\varepsilon = 3{,}3535 + 0{,}0003 \cdot 10^{-3}$, ellipticity
$\omega = 7{,}29 \cdot 10^{-5}\ \mathrm{sec}^{-1}$, angular velocity
$\alpha = 6{,}5 \pm 1{,}5 \cdot 10^{-2}$ cm/year, yearly radius increase
$a = 6{,}378 \cdot 10^8$ cm, the greater axis of the Earth's spheroid
$\rho_o = 2{,}85\ g\ \mathrm{cm}^{-3}$, density of the Earth at the surface
$\rho\varkappa = 5{,}52\ g\ \mathrm{cm}^{-3}$, average density of the Earth

$$Q = \frac{\mathrm{m}}{2\varepsilon} = 0{,}513$$

$$\mathrm{m} = \frac{\omega^2, r_1{}^3}{fM}, \quad r_1 \text{ being the mean radius of the Earth.}$$

The computed value for the relative yearly change in ellipticity will be

$$\frac{d\varepsilon}{\varepsilon} = +\,1{,}26 \cdot 10^{-10}$$

This is a positive number which can be interpreted, that recently the expansion manifesting himself in the change of gravity and that of the centrifugal force results in an increase of the ellipticity.

According to Bullard – 1948 –, the ellipticity of an Earth in hydrostatic equilibrium amounts to $3{,}3632 \pm 0{,}006 \cdot 10^{-3}$ i. e. it surpasses the actual value of the ellipticity. If this value can be regarded as real, then the discrepancy between the two ellipticity values may be regarded as a delay recovering hydrostatic equilibrium in a solid Earth at a steady increasing ellipticity. Taking the value of Bullard as correct, the actual value of $d\varepsilon/\varepsilon$ amounts to $2{,}9 \pm 0{,}3 \cdot 10^{-3}$ which corresponds to a delay of about $2{,}3 \cdot 10^{7}$ year in recovery, and shows towards a viscosity of $8 \cdot 10^{26}$ poise for the interior of the Earth.

In any case an effect of the increasing ellipticity is reflected in the discovery of Krause – 1965 – that there exists a belt of equatorial shear zone for the recent as well as for the past.

The greatest tensional effects in the upper mantle and crust arise in the case of an expanding Earth along the equator. The increasing ellipticity increases also the tensional forces in a non-linear way and the shear faults would act as the release of strain energy. An iteration is insured exactly by the non linear stresses. According to Krause a second shear zone corresponding to a past equator can be traced along the ocean bottom.

References

Bullard, E. C.: Mon. Not. Roy. Astr. Soc. Geophys. Suppl. 5, p. 186, 1948
Dirac, P. A. M.: Proc. Roy. Soc. A. 165, pp. 199–208, 1938
Egyed, L.: Nature 173, p. 534, 1956a
Egyed, L.: Acta Geol. Acad. Sci. Hung. 4, pp. 43–83, 1956b
Egyed, L.: Nature 207, pp. 846–847, 1945
Krause, D. C.: The World Rift System, Ottawa, pp. 400–443, 1965
Munk, W. H. and MacDonald, C. J. F.: The Rotation of the Earth, Cambridge, 1960
Wells, J. W.: Nature 197, pp. 948–950, 1963

The Asymmetric Structure of the Earth and its Secular Processes*)

by *G. Barta*, Budapest

It is known that in the direction of Australia the intensity of the geomagnetic field is by 30% greater than in the opposite Atlantic areas. From the strong deformation of the magnetic field the conclusion can be drawn that the whole Earth's body is asymmetrically built up. If we approximate to the magnetic field by a dipole, so the dipole lies about 300 or 400 km for from the geometrical centre in the direction of Australia.

Supposed, that the magnetic dipole corresponds to the Earth's inner core, then the core is excentric in that direction. It is remarkable that the equatorial major axis obtained from observations of satellites coincides with the direction of excentricity of the magnetic dipole with an accuracy of 1^0. Consideration of this striking accordance not as an incidental one has far-reaching consequences. [2]

Owing to the secular magnetic variation is namely the magnetic dipole moving to West by $0{,}2^0$ in a year, therefore we may assume that the equatorial major axe is wandering to West.

This assumption is supported by the fact, that the positions of the equatorial major axis calculated by different authors with classic geodetic methods based on long series of observations, are generally lagging to East behind the positions of the major axis, which resulted from observations of satellites [2, 6].

If the secular magnetic variation has some kind of connection with a motion of the Earth's core, i. e. with displacements of masses, so must the observable partial periods of the secular

---

*) This paper was presented by Dr.-Ing. habil. P. Biró.

magnetic variation manifest themselves in phenomena, which are connected with the density distribution, respectively with the moment of inertia of the Earth.

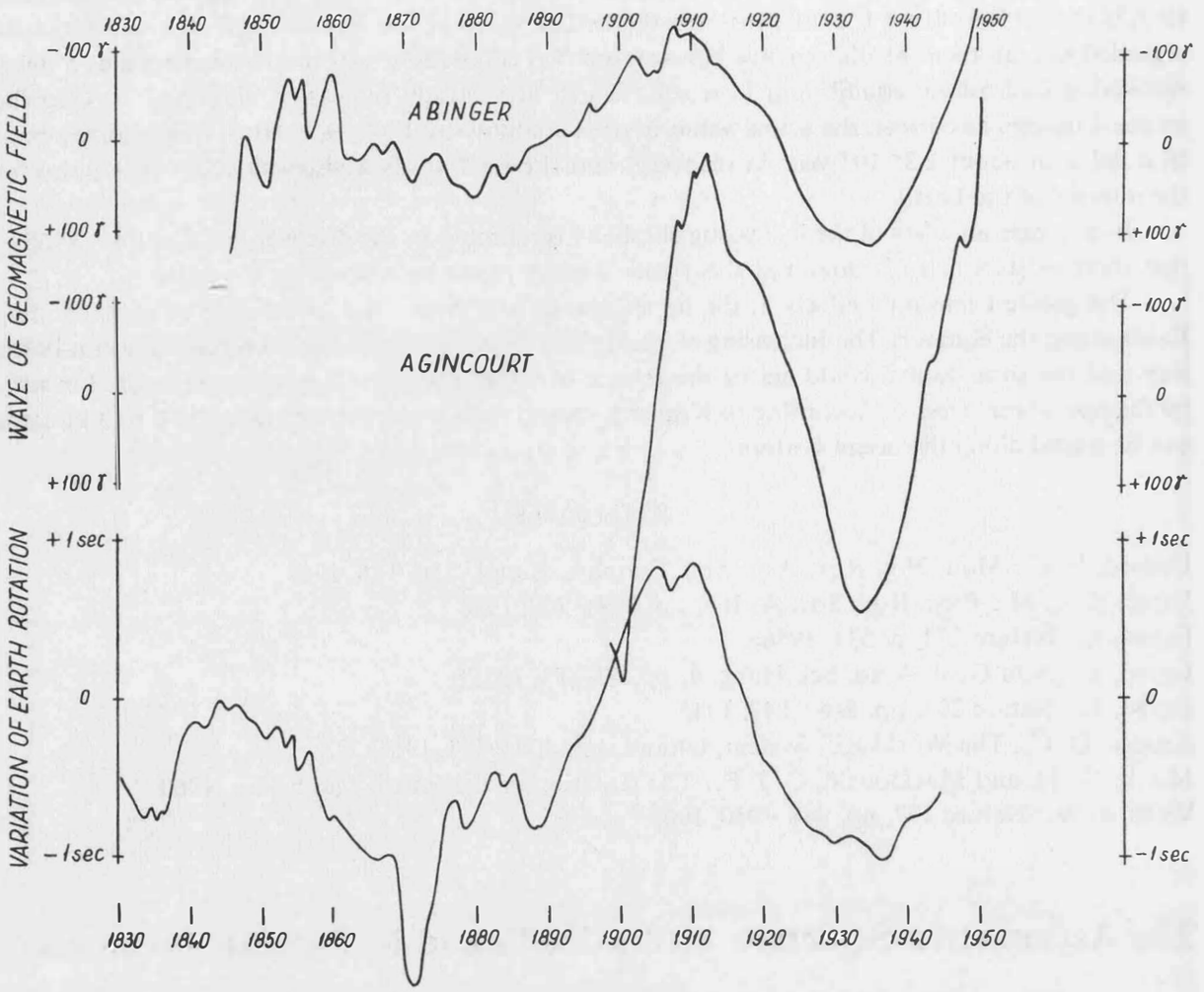

Fig. 1. Variation with 50 years period in the secular variation of the magnetic field and in the variation of the Earth's rotatory speed [1, 2].

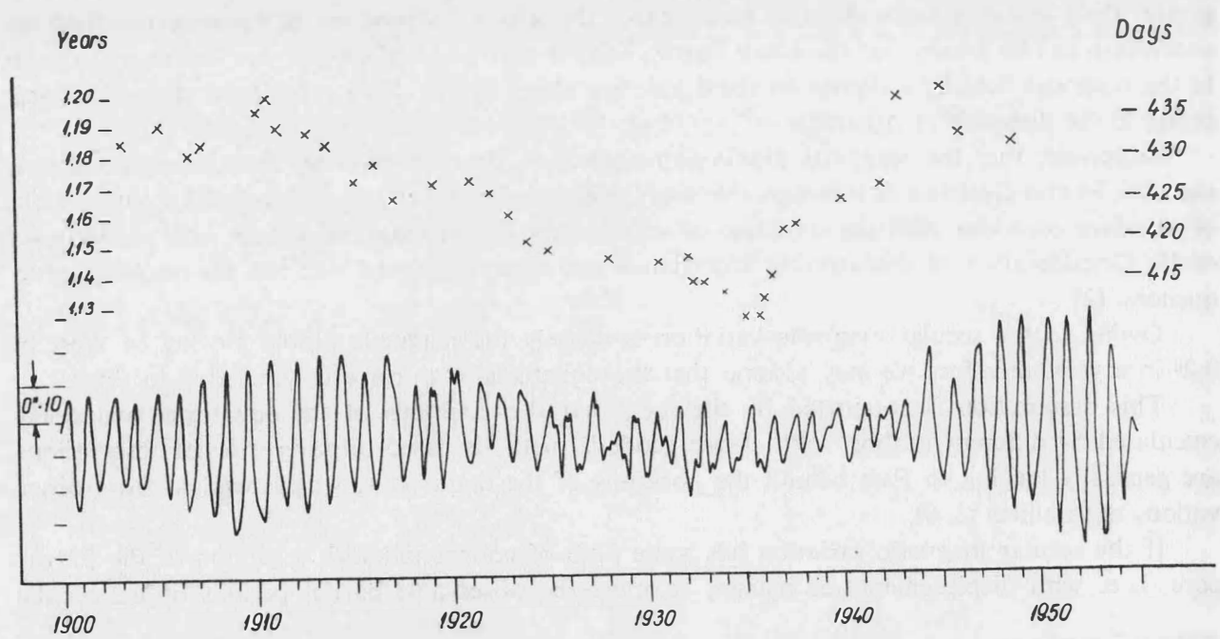

Fig. 2. Variation of the Chandler-period according to Melchior. Below: Variation of the polar altitude after elimination of the seasonal variation [3, 5].

In series of secular variations at most of the magnetic observatories is demonstrable an oscillation with a period of about 50 years [1]. The greatest positive departure of the direction of the variation from the adjusted variation arose in 1935, and the greatest negative one in 1910, and in 1960, respectively. Same extreme time data appear also in the amplitude and period of the polar altitude, in the oscillation of the Earth's rotational velocity, and in the variation of sea level at several marigraph stations.

It appears as a certain power effect concerning the whole Earth had been maximal. This effect gave rise to the increase of the amplitude and period of variation of polar altitude [3, 5]. In 1935 this effect caused by increase of the westward drift the maximal deviation from the uniform trend of the secular magnetic variation and caused by its braking force the maximum deviation from the uniform rotation of the Earth, which appeared in chronometry.

It is interesting to compare those results with the frequence of earthquakes. If about 1910 the Earth was touched by a certain power effect, what caused certain changes in the Earth's body, then these changes ought to bring about strains in the Earth's crust. According to F. Mosetti's investigations in the frequence of earthquakes is observable a maximum in 1910, and a minimum in 1935 [4]. The earthquake activity in the last ten years suggests again to a maximal earthquake frequency. Examination of the earthquake frequencies corroborates therefore our previous considerations.

Gravimetric, electromagnetic, and seismological measurements discover more and more further asymmetries in the Earth's structure, as the domain of researches is penetrating down to greater depths. From investigations of the last decade we know unambiguously, that the Mohorovicic layer, the low-velocity layer, and probably even the Gutenberg-Wiechert layer are lying higher underneath the oceans, then under the continents. The above summary considerations emphasize the asymmetric material structure of the total Earth, as they are resting on results of magnetic measurements, which are related to the total Earth. In this way they are drawing our attention to the recognition, that the asymmetric structure can cause important phenomena.

Naturally, a centric homogeneous model of Earth, being in hydrostatic equilibrium is a very useful approximation, but results of the measurements are compelling us to take in account physical reality beyond mathematical abstraction.

References:

1. Barta, G.: Longitudinal and transversal effect of the secular variation of the geomagnetic field, Geofizikai Közelmények, Vol. VII. N. 1., Budapest, 1958.
2. Barta, G.: The secular variation in the geomagnetic field and other geophysical phenomena Annales Universitatis Scientiarum Budapestinensis de Rolando Eötvös Nominatae, Sectio Geologica, Tomus VII., Budapest, 1964.
3. Gutenberg, B.: Physics of the Earth's interior Academic Press New York and London, 1959.
4. Mosetti, F.: Sull'esistenza di un ritmo con periodo di 45 anni in talune fluttuazioni geofisiche, Boll. die Geof. Teor. et Appl. Vol. V. N. 18, 1963.
5. Munk – MacDonald, G. J. F.: The rotation of the Earth, Cambridge University Press, 1960.
6. Tuman, V. S.: The satellite geoid may have a westward drift, Nature, Vol. 210. N. 5038., 1966.

Part III:

Gravity Anomalies, Deviations of the Vertical, Observations (Methods and Results)

Aerial Gravimetry for Direct Observation of the External Gravity Field

by *Bela Szabo*, Bedford, Mass. U. S. A.

I

The knowledge of the earth's external gravity field is an essential requirement for precise determination of gravity dependent earth parameters and for the successful utilization of gravity data in physical geodesy. Over accessible land areas terrestrial gravimetry provides the measurements with adequate accuracy, however, this method is economically feasible only over well developed areas. In inaccessible land areas and over the oceans, which constitute more than two-thirds of the earth's surface, new methods and instruments are required for the accomplishment of gravity measurements.

Theoretically, there are two possible to obtain the global external gravity field of the earth: First, by direct surface and aerial gravity surveys filling in the gaps existing over unsurveyed areas; and second, by utilization of the external gravity field described by spherical harmonic coefficients derived from satellite tracking data. Studies conducted on this subject indicate that harmonic coefficients, derived from satellite data are both unreliable and inadequate to satisfy the requirements of scientific geodesy and navigation without the support of direct global measurements. The combination of the two methods would be the best approach for a reliable solution of all problems dependent on the gravity field of the earth. The minimum requirement for direct measurements would be a global coverage in form of mean anomalies for $5^0 \times 5^0$ blocks with $\pm$ 5 to $\pm$ 10 mgal accuracy. The mean values can be derived most economically from two or three east-west aerial profiles across each block.

II

In 1958 AFCRL conducted the first experiments of aerial gravimetry with a modified LaCoste and Romberg sea gravimeter in a KC-135 aircraft. Later, the Askania-Graf sea gravimeter was also included in the tests. These early experiments proved that aerial gravimetry is feasible and satisfactory accuracies can be achieved provided navigation errors can be reduced below certain limits. Additional test flights and experiments have been carried out by AFCRL in 1960 and 1962. The feasibility of aerial gravimetry was confirmed by these experiments and it was also concluded that a great number of problems must be resolved before an operational airborne gravity measuring system could be achieved. Fairchild (FLAGS) Corporation flew a triangle at 12,000 ft. using a LaCoste and Romberg instrument and a B-57 aircraft in 1961. This test also indicated the feasibility of aerial gravimetry. In January 1965 AFCRL was provided with a KC-135 aircraft and the means required for the intensification of research and tests in aerial gravimetry. The goals of the new effort were: the selection and designation of the components of a complete airborne gravity measuring system which would satisfy minimum requirements; the derivation of data reduction methods

including computer programs, and to resolve the downward continuation problem of gravity for the purpose of obtaining useful ground or sea level values from high altitude aerial profiles.

Gravity measurements obtained by airborne sensors, like any other moving gravity measuring technique, are affected by the Eötvös effect. This is composed from the vertical components of the Coriolis and centripetal accelerations resulting from the motion of the aircraft. This effect, which is several thousand milligal, can be computed from the aircraft's navigation data. If the navigation data are not accurate enough the Eötvös correction will be in error. The critical navigation data are ground speed (velocity error) for east-west flights and azimuth for north-south flights.

One knot (one nautical mile/hour) error in the ground speed for east flights at 400 knots produces errors in the Eötvös correction ranging from 10.8 mgals at the equator to 4.6 mgals at latitude of 80°. For west flights the same velocity error will affect the Eötvös correction by 4.2 mgals at the equator and by 2.0 mgals at latitude 80°.

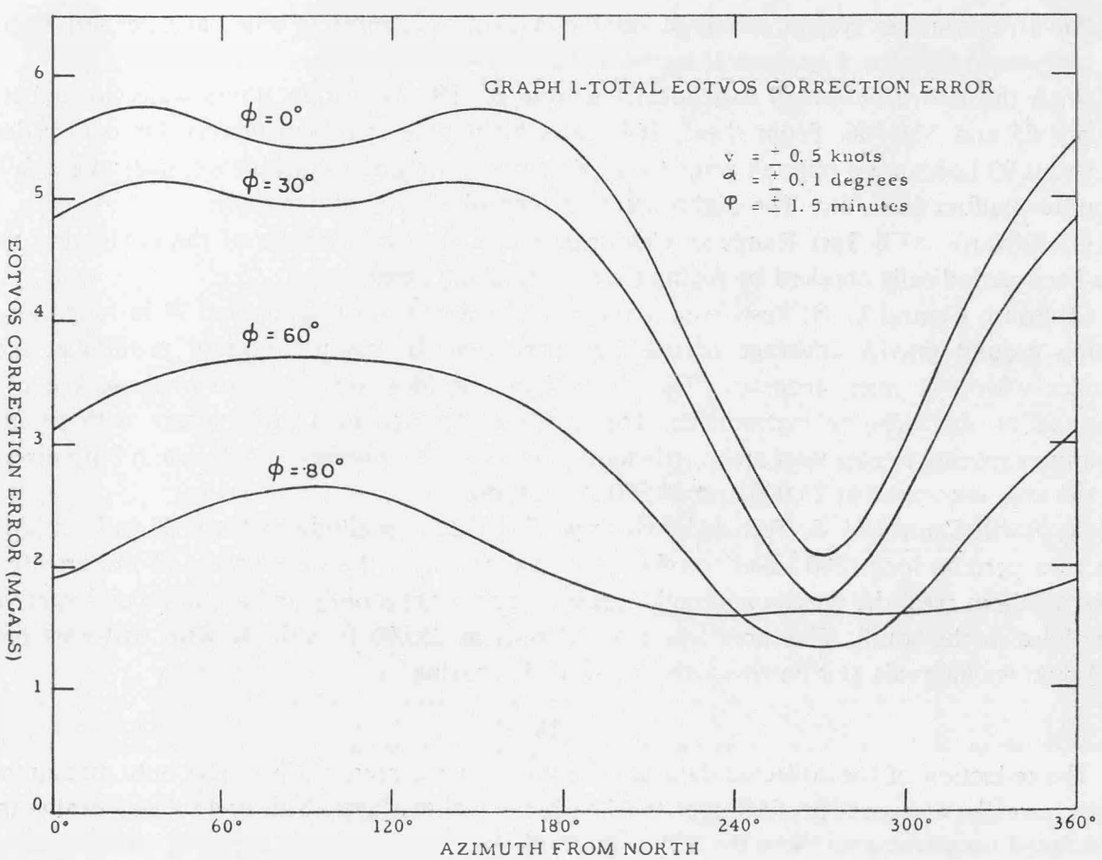

Fig. 1

The effects of azimuth errors are linear functions of aircraft velocity. An error of 0.1 degree in azimuth for north-south flights at 400 knots will result in Eötvös correction errors from 5.2 mgals (at the equator) to 0.9 mgals. (lat 80°).

Geographic latitude and earth radius errors contribute to the Eötvös correction errors but the combined effect is less than one mgal under current conditions. Figure No. 1 shows the errors in the Eötvös correction at various latitudes and azimuths assuming that: (a) the ground speed is accurate to ± 0.5 knots; (b) the azimuth error is ± 0.1 degree; and (c) the latitude error is ± 1.5 minutes of arc.

In addition to the Eötvös correction error, errors in the verticallity of the stabilized platform, vertical accelerations of the aircraft, and errors in the elevation (flight altitude) of the aircraft are the major error sources in aerial gravimetry. Any one of these errors could exceed the allowed maximum for the combined total error under certain conditions, therefore, the greatest care is necessary in the selection of instruments, operation and data reduction to achieve acceptable results.

III

The KC-135 aircraft equipped with an APN-99 doppler radar navigation system was gradually instrumented and modified to include the following gravity sensors and auxiliary instruments.

1. LaCoste and Romberg modified sea gravity meter with new solid state electronics, mounted on an ART-57 stable platform.
2. Askania-Graf modified sea gravity meter with new solid state electronics, mounted on an ART-25 platform.
3. Worden-quartz digital aerial gravity meter by Texas Instruments, Inc., mounted on an ART-57 platform.
4. APR-5 airborne profile recorder with spotting camera.
5. Photo panel to record data from aircraft navigation system.
6. Analog-to-digital converter and magnetic tape recorder for recording gravimeter, APR-5 and navigation data.
7. MD-1 astrotracker for improved heading.
8. An accelerometer system mounted on the ART-57 platform of the LaCoste and Romberg instrument, to record horizontal accelerations.

With the above described instruments a total of 450 measuring hours were flown between January 65 and May 66. From these, 364 hours flight time were satisfactory for data reduction and about 90 hours were rejected prior to the data reduction due to turbulence, instrument failures, autopilot malfunctions, etc. The flights were accomplished over three areas:

(1) Edwards AFB Test Range in California where the performance of the navigation system have been periodically checked by flights over the tracking range.

(2) South Central U. S. Test Area covering an area of 6^0 in latitude and 7^0 in longitude. The existing ground gravity coverage of the area permitted the computation of profiles at aircraft altitudes with $\pm$ 1 mgal accuracy. These "uplifted" profiles were used to evaluate the profiles measured by the airborne instruments. The area was covered in a grid pattern with profiles of 30 minutes spacing in east-west and north-south directions. All profiles were flown in both directions and the area is covered at 25,000 and 30,000 ft. altitudes.

(3) North Central U. S. Test Area which is 17^0 long in longitude and it is 3^0 wide in latitude. This area permits long (800 miles) profiles and in contrast to the smoothness of the gravity field in the southern area, the gravity anomalies are changing more rapidly and attain much larger values than those in the south. This area was covered only at 25,000 ft. altitude with east-west profiles at 30 minutes intervals and north-south lines with 1^0 spacing.

IV

The reduction of the collected data is in progress at the present time. The only measurements reduced are the east-west profiles over the South Central test area. The preliminary evaluation of the reduced measurements show the following results:

1. *Mean Anomalies for* $5^0 \times 5^0$ *Blocks.* The error of the mean anomaly of an area is composed from the representation error of the number of profiles available for the computation of the mean value and from the measurement errors. Since the statistical representation error for one central profile in a $5^0 \times 5^0$ square is 13.4 mgals, a minimum of two profiles symmetrically located inside the blocks are required to meet the desired 5 to 10 mgal accuracy. Four pairs of symmetrically located profiles were found within the $5^0 \times 5^0$ block of the South Central test area. Three pairs were observed with the LaCoste and Romberg gravimeter and include one east and one west line each. The fourth pair was observed with both the LaCoste and Romberg and the Askania-Graf instruments. (The Askania gravimeter can measure, at the present time, only in west direction because of its short range for airborne use).

One mean anomaly value was computed from each profile pair selected to represent the mean anomaly of the block. The mean was also computed from all available ground survey data and utilized as standard. From ground data the "uplifted" profiles, corresponding to the aerial profiles, were derived and from each corresponding pair the mean value of the block was computed (control profile pairs). From the comparison of these values the actual representation error, the actual total error and the measurement error was obtained for each observed pair. The figures are shown

Table 1. Values from Symmetrical Pairs (mgals)

(1) Gravity Meter	$L-R$	$L-R$	$L-R$	$L-R$	$A-G$
(2) Fligthline Pair	$35^{\circ}.5\,E/39^{\circ}.5\,W$	$38^{\circ}.5\,E/36^{\circ}.5\,W$	$37^{\circ}\,E/38^{\circ}\,W$	$39^{\circ}\,W/36^{\circ}.5\,W$	$39^{\circ}\,W/36^{\circ}.5\,W$
(3) Mean Anomaly $5^0 \times 5^0$ Square (Standard)			-5.7		
(4) Mean Anomaly (Control Profile Pair)	-1.2	-5.6	-5.1	-7.8	-7.8
(5) Actual Representation Error (4) $-$ (3)	$+4.5$	$+0.1$	$+0.6$	-2.1	-2.1
(6) Mean Anomaly (Observed Profile Pair)	$+8.2$	-10.7	-0.6	-10.1	-7.8
(7) Actual Total Error (3) $-$ (6)	-13.9	$+5.0$	-5.1	$+4.3$	$+2.1$
(8) Measurement Error (4) $-$ (6)	-9.4	$+4.1$	-4.5	$+2.2$	0
(9) Mean of $L-R$ Actul Total Errors			7.1		
(10) Statistical Representation Error			± 6.4		
(11) Total Error for $5^0 \times 5^0$ Square			± 11.0		± 6.4

in Table 1. It can be seen that the mean of the LaCoste and Romberg actual total errors for this particular block is 7.1 mgal, and 2.1 mgal is the actual total error of the mean value derived from one pair of *west* profiles measured by the Askania sensor.

The representation error termed as "actual" is valid only for this particular block and it is relatively small due to the smoothness of the gravity field in this area. If we use the statistical representation error determined from a statistical analysis of all existing gravity data, then for a $5^0 \times 5^0$ block, represented by two symmetrical profiles, the representation error will be $\pm$ 6.4 mgal. Combining this with the standard measurement errors the total standard error for an average $5^0 \times 5^0$ block is obtained. (Line 11 of Table 1).

The measurement errors were also derived from all available profiles in the test area. For the LaCoste and Romberg gravimeter 55 east-west pair combinations were available (one east and one west line in each pair). For the Askania gravimeter 36 pairs of west profiles were used. The differences between the measured and the "uplifted" consrol profiles were used for the computation of the standard errors which are $\pm$ 7.4 mgal for the LaCoste and Romberg and $\pm$ 4.2 mgal for the Askania Graf gravimeter. Combining these standard errors with the statistical representation

errors for two symmetrical profiles we obtain ± 9.8 mgals standard total error for the LaCoste and Romberg and ± 7.7 mgals for the Askania instrument.

The Worden airborne gravimeter showed large systematic and random discrepancies with respect to the control data and to the values measured by the other two instruments. The average discrepancey was about 50 mgals. The electronics and the sensor of this system require additional studies before final conclusions can be made.

2. *Mean Anomalies for $1^0 \times 1^0$ Blocks.* A preliminary study was made to determine the obtainable accuracy for $1^0 \times 1^0$ squares. The mean values for 25 $1^0 \times 1^0$ blocks were computed from two symmetrical east-west profiles across each block. In the South Central Test area the representation error for two such profiles is practically zero and the statistical representation error is only ± 0.6 mgal. An average standard error of ± 29.7 mgals was obtained for the LaCoste and Romberg and ± 9.7 mgals for the Askania gravimeter.

V

From the preliminary reduction and analysis of the measurements in the South Central test area it can be seen that the Askania-Graf instrument performed better than the LaCoste and Romberg. However, it must be noted that the LaCoste and Romberg results are derived from both east and west profiles, the Askania results contain only west profiles. The effect of the same ground speed error is larger in east direction, therefore, the comparison cannot be considered as final conclusion. It is true, however, that profile to profile comparisons under identical flight conditions are still in the favour of the Askania instrument. Both instruments are acceptable for global surveys provided navigation errors are reduced.

The errors from present aircraft navigation are excessive where cartographic corrections obtained from existing map coverage and aerial photography would not be possible. Estimates for cartographically corrected navigation accuracies achieved during test flight are:

ground speed	± 1.1 to 1.5 knots
azimuth	± 0.2 to 0.4 degrees
position	± 0.3 to 0.5 nautical miles

For global surveys requiring about ± 8 mgal accuracy for $5^0 \times 5^0$ mean anomalies the desired navigation accuracies would be:

ground speed	± 0.5 knots
azimuth	± 0.1 degree
latitude	± 1.5 minutes of arc

The random stabilization error of the ART-57 platform is ± 3.5 minutes of arc according to simulation tests. To obtain more accurate gravity data it is required that the stable platform be aligned with respect to the local vertical or the apparent vertical to an accuracy of 1 (one) minute of arc. The apparent vertical is the direction of the resultant between gravity, Coriolis and other constant effects, therefore, post flight corrections to the local vertical can be computed.

The present computer program for data reduction is not final. The vertical acceleration problems and spectral analyses of gravity data are being studied to establish optimum filtering method, Theoretical studies on the downward continuation of gravity have been made at Ohio State University and the results are published. The application of these studies for the observed material will be done at AFCRL after the final filtering method is determined.

The instrumentation research to improve airborne gravity sensors and related instruments is continuing. To resolve the critical navigation problems and for the improvement of gravity sensor stability, various inertial guidance system components are under investigation for possible use in aerial gravimetry. As a result, a pendulus integrating gyro accelerometer was laboratory tested and converted into a gravity sensor. This sensor is prepared for flight testing which will start in August 67.

The ART-57 platform is inadequate to support accelerometer type of gravity sensors, in addition the use of separate stable platforms for two or three different instruments introduces a variable in the comparison of the results. As a solution an airborne platform is being developed for AFCRL capable of supporting two or three sensors. The platform design and quality of components will

provide stabilization with respect to the local vertical within 3 to 10 seconds of arc in the presence of horizontals acceleration up to 100 gals.

Bell Aerosystems Company developed a shipboard gravity measuring system with an accelerometer sensor. The system was developed under contract to NAVOCEANO. The first tests have been completed very satisfactorily and additional tests are scheduled by USC&GS. The Air Force is considering testing this system in an aircraft when the shipboard tests are completed.

Some Remarks on the Accuracy of Interpolation of Gravity Anomalies.*)

by *Vincenc Vyskočil*, Prague

The interpolated value of gravity anomaly can be determined from the Lagrange formula of interpolation

$$g_{int} = \sum_{i=0}^{n} g_i q_i , \qquad \left(\sum_{i=0}^{n} q_i = 1 \right) \tag{1}$$

in which g_i indicates the values of anomalies in observation points and q_i are the Lagrange's coefficients. The error $m(g_{int})$ of interpolated value g_{int} is a resultant of several partial errors.

The first partial error $m(\mathrm{I})$ expressing the effect of mean square errors $m(g_i)$ of "observed" values g_i can be determined from the formula

$$\mathrm{m}^2(\mathrm{I}) = \mathrm{m}^2(g_i) \sum_{i=0}^{n} q_i^2 . \tag{2}$$

The Lagrange's coefficients $q_i(x)$ for the function of one variable $g(x)$ can be easily computed. For the function of two variables $g(x,y)$ the coefficients $q_{i,j}(x,y)$ are practically derived only for squared or oblong net of observation points.

The magnitude of the error $m(\mathrm{I})$ is dependent on the value

$$A = \sqrt{\left(\sum_{i=0}^{n} q_i^2 \right)}$$

I have computed the values $A(x)$ for equidistant observation points and different degrees n of interpolation polynomials. The values $A(x) \leqq 1$, if the number of equidistant observation points on both sides of the point $P(x)$ is the same. Since the number of observation points on both sides is different, the values $A(x)$ can be greater than 1. In this case the stability of interpolation is not guaranteed. A relatively small error in a distant observation point can cause a great error $m(\mathrm{I})$ in the interpolated value g_{int}.

When using an unsuitable method of interpolation, the accuracy of interpolated values g_{int} can be essentially diminished. Therefore it is necessary to find a criterion for applicability of interpolation formulae. The condition

$$A \leqq 1 \quad \text{or} \quad |\mathrm{m}(\mathrm{I})| \leqq |\mathrm{m}(g_i)| \tag{3}$$

can be considered as such a criterion. The condition (3) is always fulfilled in the case of linear interpolation and of the plane interpolation in a triangle or a tetragon. Using interpolation polynomials of higher degree ($n > 2$) this condition is fulfilled only by a certain distribution of observation points.

---

*) Abstract. The paper will be published in "Travaux Géophys. Acad. Tchécosl. Sci., Geofysikální sborník 1967, Academia Praha".

The second partial error $m(\mathrm{II})$ can be regarded as an error of the method of interpolation. Since the exact form of function g in unknown it cannot be computed theoretically. Two effects can be distinguished in this error. One of them $m(\mathrm{II}_1)$ represents practically the remainder term in interpolation formula and its values diminish increasing the degree n of interpolation polynomial. The other $m(\mathrm{II}_2)$ includes the effect of local irregularities (disturbances) of function g. Its value can be diminished only when decreasing the distances among the observations points.

When the condition (3) of stability is fulfilled the validity of relation

$$\mathrm{m}^2(\mathrm{I}) + \mathrm{m}^2(\mathrm{II}_1) \leqq \mathrm{m}^2(g_i)$$

can be reached.

The third partial error $m(\mathrm{III})$ is caused by mean square errors in the coordinates x, y of the point P and the observation points.

The values of gravity anomalies are often dependent on the altitude h. Let us assume that we are to interpolate a function $g(x, y, h)$ on the surface $h(x, y)$ expressing the shape of terrain. The Lagrange's coefficients are invariant only with respect to the linear substitution of arguments x and y. When interpolating the function $g(x, y, h)$ as a function of two variables (values of arguments x, y are taken from the maps and the altitudes h are not considered), the deformation of interpolation process can occur. It depends on the magnitude of the partial error $m(\mathrm{IV})$ caused by neglecting the altitudes h, if such an interpolation is possible at all.

I tried to show that methods of interpolation using polynomials of higher degrees do not guarantee more accurate results by themselves. It is always necessary to consider the stability of interpolation process. The error $m(g_{int})$ is regarded as a resultant of four partial errors.

On the Accuracy of the Deviations of the Vertical Interpolated by Gravimetric Methods

by Dr. *P. Biró*, Budapest

It is known, that the mean square error (m. s. e.) of the *absolute* deviation of the vertical, calculated by the formula of Vening-Meinesz resp. that of Molodensky will be hardly less than $\pm 1''$ even in Middle-Europe. But the influence of the far unsurveyed areas changes very slowly, and therefore one can interpolate the *relative* deviations of the vertical more accurately using the mentioned formulae only for a certain district.

If we have some astrogeodetic points with ξ', η' known relative deviation of the vertical inside of an area with the radius r and we calculate the so-called *gravimetric* deflections of the vertical in the same points taking in account the anomalies of zones up to the radius R, we can expreses the difference of the two deflections of the vertical as a linear function of the co-ordinates. For example in point A

$$\begin{aligned} \xi_A^r - \xi_A^{gr} &= a\varphi_A + b\lambda_A + c \\ \eta_A^r - \eta_A^{gr} &= a'\varphi_A + b'\lambda_A + c' \end{aligned} \qquad (1)$$

Having more astropoints than three, the coefficients can be calculated. Then we can determine the relative deviation of the vertical in an arbitrary point P. We have to determine only the gravimetric deviation of the vertical (ξ^{gr}, η^{gr}) in the same point, and we get

$$\begin{aligned} \xi_P^{int} &= \xi_P^{gr} + a\varphi_P + b\lambda_P + c \\ \eta_P^{int} &= \eta_P^{gr} + a'\varphi_P + b'\lambda_P + c' \end{aligned} \qquad (2)$$

If our point P is in the middle of n astrogeodetic points lying symmetrically to each other

$$\xi_P^{int} = \xi_P^{gr} + \frac{1}{n}\sum_{i=1}^{n}(\xi^r - \xi^{gr})_i$$

$$\eta_P^{int} = \eta_P^{gr} + \frac{1}{n}\sum_{i=1}^{n}\eta^r - \eta^{gr})_i \tag{3}$$

We will check the accuracy of these components of the *interpolated* deviation of the vertical. The m. s. e. of the North-South component is

$$m^2_{\xi int} = \frac{1}{n} m^2_{\xi r} + \frac{n+1}{n} m^2_{\xi gr} + \delta^2 \tag{4}$$

(using the formula of the propagation of errors), where δ is the error of the linear interpolation (the sum of the neglected terms). We can get a similar formula for the East-West component, too.

We will estimate the value of the terms in formula (4).

In *the first term* $m_{\xi r}$ means the m. s. e. of the components of the relative deviation of the vertical which depends on the m. s. e. of the astronomical positioning, being less than $\pm 0{,}1''$ in latitude and $\pm 0{,}2''$ in longitude. It can be written

$$|m_{\xi r}| \sim |m_\varphi| < 0{,}1''$$

$$|m_{\eta r}| \sim |m_\lambda \cos_\varphi| < 0{,}2''$$

We can assume with safety

$$|m_{\xi r}| \sim |m_{\eta r}| < 0{,}2'' \tag{5}$$

In the *second term* of formula (4) $m_{\xi gr}$ means the m. s. e. of the component of the *gravimetric* deviation of the vertical. This later can be determined by the well known formulae of Vening-Meinesz or Molodensky by the summation of the effects of surface elements. Using for the practical calculation for example the grid-net of Jeremejev, the m. s. e. of the components of the gravimetric deviation of the vertical can be expressed as the quadratic sum of the m. s. e. of a central circle and the same of three zones (each zone consisting of more circular rings with the same effect) as follows:

$$m^2_{\xi gr} = m^2_{\xi_o} + m^2_{\xi_1} + m^2_{\xi_2} + m^2_{\xi_3} \tag{6}$$

where the zones are the followings:

central circle	r_o	= 5 km
zone 1	5 km	– 100 km
2	100 km	– 300 km
3	300 km	– 1000 km

The effect of each zone can be expressed as a sum of the effect of surface elements, being the product of a constant and Δg the mean anomaly multiplicated by a trigonometric function of the azimuth of the surface elements i. e.

$$\xi_z^{gr} = a \sum_{i=1}^{n}\sum_{k=1}^{m} \Delta g_{ik} \cos \alpha_k$$

$$\eta_z^{gr} = a' \sum_{i=1}^{n}\sum_{k=1}^{m} \Delta g_{ik} \sin \alpha_k \tag{7}$$

The m. s. e. of the effect of each zone can be expressed as a function of the m. s. e. of the gravity anomalies.

$$
\begin{aligned}
&m_{\xi_o} = \pm 0{,}15'' \quad r_o \\
&m_{\xi_o} = \pm 0{,}50'' \quad \text{for} \quad r_o = 5\,\text{km} \\
&m_{\xi_1} = \pm 0{,}040''\, m_{\Delta g_1} \\
&m_{\xi_2} = \pm 0{,}015''\, m_{\Delta g_2} \\
&m_{\xi_3} = \pm 0{,}014''\, m_{\Delta g_3}
\end{aligned} \tag{8}
$$

If we have a more detailed gravimetric net in the neighbourhood of the point and a higher accuracy is to be achieved, we can carry out a more detailed evaluation in the central and 1st zone taking the following values:

$r_o = 1{,}1$ km		$m_{\xi_o} = \pm 0{,}16''$
zone 1′	1,1 – 7,3 km	$m_{\xi_{1'}} = \pm 0{,}032''\, m_{\Delta g_{1'}}$
1″	7,3 – 100 km	$m_{\xi_{1''}} = \pm 0{,}038''\, m_{\Delta g_{1''}}$
2	100 – 300 km	$m_{\xi_2} = \pm 0{,}015''\, m_{\Delta g_2}$
3	300 – 1000 km	$m_{\xi_3} = \pm 0{,}014''\, m_{\Delta g_3}$

The unknown m. s. e. of the gravity anomalies can be usually replaced by the *error of interpolation* of the gravity anomalies – in the case of a detailed gravity net – or by the *error of representation* in the case of a thin net, which both can be determined on test areas.

The general experience is that the mentioned two errors are function of the square root of the density s of gravimetric points. For the free-air anomalies we can find the following values for different terrains in the literature:

	$m_{\Delta g}$	
	in flat and hilly areas	in mountains of medium heigth
USSR	$\pm 1{,}08\sqrt{s}$	
GDR	$\pm 1{,}0\sqrt{s}$	$\pm 4{,}5\sqrt{s}$
India	(average) $\pm 1{,}1\sqrt{s}$	

All the values have been got with a *linear* interpolation of the free-air anomalies. Considering the possibility of a hypsographic interpolation, the coefficients can be less (For example in GDR in mountains only $\pm 1{,}15\sqrt{s}$).

We too have carried out some numeric investigations in test-areas, and have got the following results in Hungary.

in flat areas $\Delta h < 2$ m	$m_{\Delta g} = \pm 0{,}6\sqrt{s}$
in hilly areas of 200 – 300 m height	$\pm 2{,}8\sqrt{s}$ $(\pm 1{,}6 \cdot s)$
in mountains of 200 – 750 m height	$\pm 8{,}0\sqrt{s}$

On the base of these values we are able to estimate the m. s. e. of the components of the *gravimetric* deviation of the vertical. (Some numeric results are in the first part of table II.)

Turning back to the problem of the accuracy of the *interpolated* deviation of the vertical we have further to investigate the *3rd term* of equ. (4). It is the error of the linear interpolation of the deviation of the vertical.

According to Molodensky

$$|\delta''| \leqslant \frac{0{,}16''}{q^2 - 1} \overline{\Delta g}\,; \tag{10}$$

where $q = R/r$, the ratio of the radius of the area with known astrogeodetic points to the radius of the gravimetrically surveyed area, while $\overline{\Delta g}$ is the mean anomaly round the circle with a radius R.

From equ. (10) one can determine the R radius of that area from where gravimetric data are needed if we want to interpolate the deviation of the vertical inside of an area with the radius r.

$$R \geqslant r \sqrt{\frac{0{,}16''}{\delta} \overline{\Delta g}}$$

Let we take an error of interpolation $\delta = 0{,}16''$;

$$R \geqslant r \sqrt{\overline{\Delta g}}$$

Some values of R, r and $\overline{\Delta g}$ are the following.

Table I.

$\overline{\Delta g}$ mgal	R/r	$r = 20$	30	40	60	100 km
		R km				
30	5,5	110	160	220	330	550
40	6,3	130	190	250	380	630
50	7,1	140	210	280	430	710
60	7,7	150	230	310	460	770
70	8,4	170	250	330	500	840

Table II

	$m\,\xi_o$	$m\,\xi_{1'}$	$m\,\xi_{1''}$	$m\,\xi_2$	$m\,\xi_3$	$m\,\xi_{gr}$	$m\,\xi_r$	δ	$m\,\xi_{int}$
Flat land	$\pm 0{,}160''$	$\pm 0{,}030''$	$\pm 0{,}080''$	$\pm 0{,}150''$	$\pm 0{,}140''$	$\pm 0{,}28''$	$\pm 0{,}20''$	$\pm 0{,}16''$	$\pm 0{,}36''$
Hilly land 200 — 300 m	0,160	0,130	0,410	0,150	0,140	0,50	0,20	0,16	0,59
Mountains 300 — 800 m	0,160	0,360	1,120	0,150	0,140	1,20	0,20	0,16	1,36

As it appears, in Middle-Europe, where we have sure more astrogeodetic points inside of a circle with a radius $r = 100$ km, it is enough to have gravimetric data from an area of some hundred or a thousand kilometers.

In conclusion we have the following results. If we estimate the accuracy of the *interpolated* components of the deviation of the vertical on the base of the mean distance of the gravimetric points, we can wait for the following accuracy in a point in Middle-Europe, supposing a detailed gravity net in the vicinity of the point (5—6 measured points in the central circle of $r_o = 1{,}1$ km and an average density of 2 km) up to 7,5 km, a gravity net with a density of $s = 15$ km in the zone 7,5 — 100 km, and having Arnold's and some satellite data in the zones 100 — 1000 km. (See table II.)

Summary

The mean square error of the components of the deviation of the vertical interpolated by gravimetric methods has been investigated and expressed as a function of the error of interpolation of the free-air anomalies. Later has been determined in test areas of different kind of terrains. In result the errors of interpolation are in

flat land ($\triangle h < 2$ m)	$\pm 0{,}6 \sqrt{s}$ mgal
hilly land (200 – 300 m)	$\pm 2{,}8 \sqrt{s}$ mgal
mountains (300 – 800 m)	$\pm 8{,}0 \sqrt{s}$ mgal

where s is the mean distance of gravimetric points.

Taking these results in account the mean square error of the interpolated components of the deviation of the vertical has been calculated for a point in Middle-Europe surrounded by a detailed ($s \sim 2$ km) gravity net up to 7,5 km, a normal density of gravimetric points ($s \sim 15$ km) between 7,5–100 km, and in the far zones up to 1000 km having Arnold's and some satellite data. The calculations have shown, that the mean square error of the interpolated component of the deviation of the vertical is in

flat land	$\pm 0{,}3''$
hilly land (200 – 300 m)	$\pm 0{,}5''$
mountains (300 – 800 m)	$\pm 1{,}2''$

including the error of the components of the astrogeodetic (relative) deviation of the vertical and the error of the linear interpolation.

Determination of Scale in Spatial Direction Networks

by *K. Rinner*, Graz

1. Introduction

Procedures for determining the scale in spatial direction networks are actually of practical importance and are also used for the determination of the PAGEOS world network.

Spatially oriented directions between observation points can be calculated from photogrammetric astronomical direction observations to satellites and simultaneous time measurements. They constitute a spatial direction network connecting points on the earth's surface. The calculation and adjustment of a spatial direction network determines shape and space position of the polyhedron formed by the observation points; the scale of the polyhedron is, however, unknown (Fig. 1).

On account of the geometric similarity of the model constituted by the space directions, measurement of the lenght of one side of the direction network would be sufficient for the scale determination. For known geodetic principles, however, it is desirable to measure the lengths of several sides thus improving and controlling the scale determination.

The sides of a spatial direction network are running through the terrestrial body as straight-lined distances between two points on the earth's surface. Therefore, their lenght cannot be measured directly; it has to be derived with the aid of a spatial base network in which the side to be determined is a diagonal.

On continents this base network may be a spatial geodetic network of the 1st order sufficiently reinforced by additional measurements (distances, zenith distances and astronomic measurements). Sides running below the surface of the sea must be determined with the aid of network containing space points (satellite positions). Secor, Laser and Doppler measuring devices can be used to form such networks.

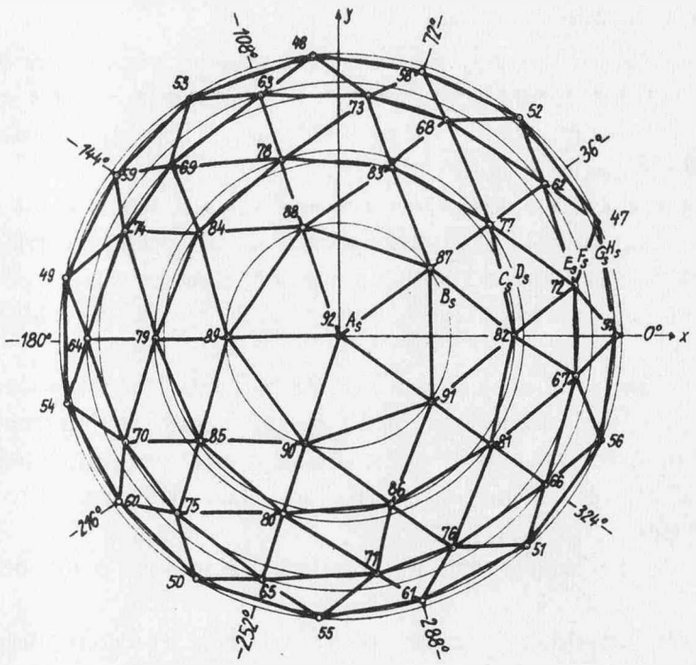

Fig. 1

A systematic investigation of procedures for determining the scale in direction networks was carried out by the author in [1]. The following report deals with the scale determination, acutally of practical importance, with the aid of a spatial polygonal traverse and by means of a prodecure suited for the application of Secor.

2. *The spatial polygonal traverse*

A space polygon may be oriented or non-oriented. In the former case, the oriented directions of the polygon sides are known and we have got the spatial analog to the two dimensional oriented travers.

For the non-oriented polygonal traverse we have got the projections of the spatial polygon angles into the equatorial plane and the declination angles of the polygon sides. The projection of the traverse into the equatorial plane corresponds therefore to a non-oriented plane polygonal traverse. The spatial traverse is derived therefrom by means of the declination angle of the polygon sides.

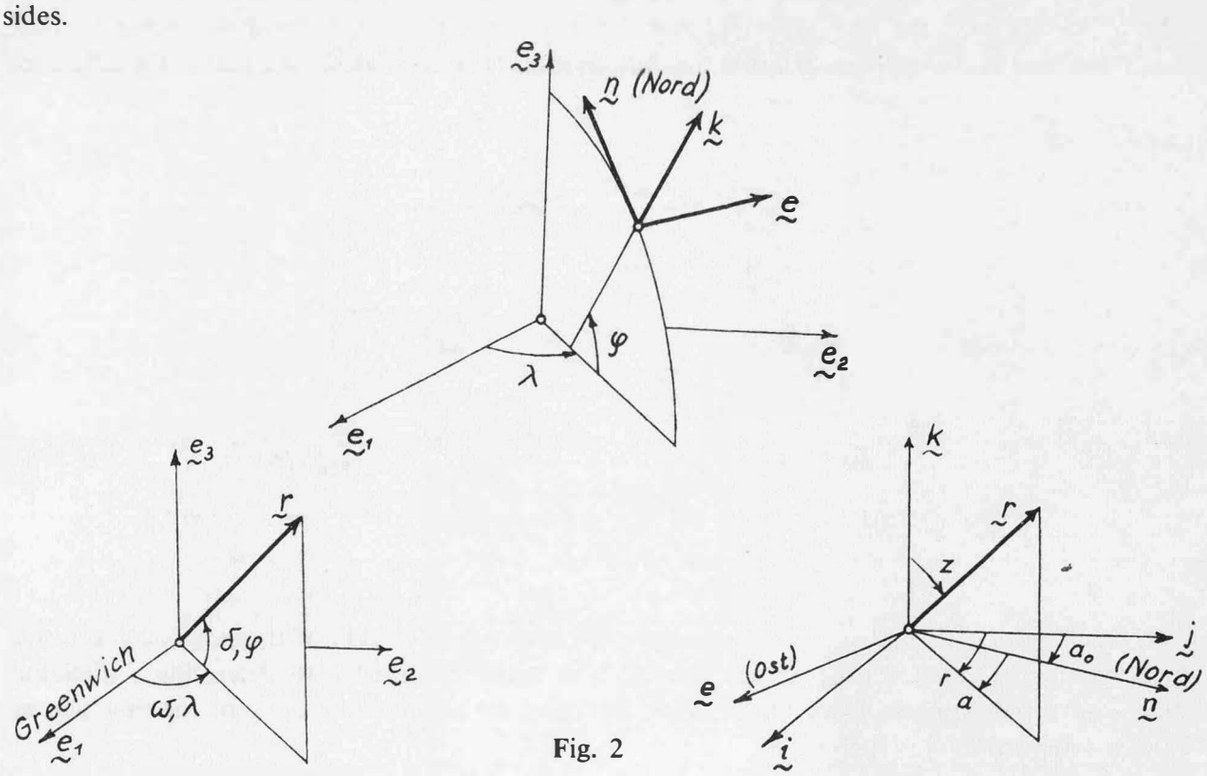

Fig. 2

2.1. *The oriented spatial polygonal traverse*

The directions of all polygon sides in space can be oriented by determining astronomically the longitude λ, latitude φ, and azimuth a in every second point of a space polygon. In this case, the latter is formed by simply joining the oriented sides. It corresponds to a two-dimensional compass traverse measured by jumps (Fig. 2).

For determining an oriented traverse every other polygon point must be a Laplace point, and geodetic direction and zenith distance measurements need be carried out in these points only. However, the traverse contains no control and there is no possibility of controlling and improving the always uncertain refraction. This is only possible by making additional measurements in the omitted (jumped) points.

In the case of an additional observation of horizontal directions and zenith distances in one of the jumped points the spatial angle of the polygon sides starting from this point can be derived both from these observations and from the oriented directions on the neighboring points. Equating the two expressions gives a conditional equation which may be used to determine a value for the refraction coefficient.

Every further astronomical quantity observed in a jumped points provides another conditional equation.

Altogether four conditional equations are available by determining all astronomical data in such a point so that three successive points of the polygon are Laplace points. They are the equations (3b, c) derived in the Annex for each of the two polygon sides.

They can be used to determine an improved value of the refraction coefficient for each side and to improve the observed astronomic and geodetic data.

The derivation of the formulas as well as linear forms therefore are contained in the Annex. It should be pointed out that Eq. (6a) contains no longitudinal term and, therefore, also exists if the astronomical longitude was not determined.

The adjustment of a system of such equations leads to optimum values for the coordinates of the polygon points from which the base can be determined as diagonal.

It is also possible to introduce parameters λ, φ or α_o of the orientation matrices which are not observed as unknowns into the adjustment and to determine them at the same time.

2.2. *The non-oriented spatial polygonal traverse*

We obtain a non-oriented space polygon by observing the latitude φ_i, the azimuths a_{ij} in each polygon point as well as the directions and zenith distances of the polygon sides. In this case, relations for determining the declination δ_{ij} and the hour angle $t_{ij} = \omega_{ij} - \lambda_i$ of the polygon sides follow from Eq. (2), Annex (Fig. 3). Since the difference of the hour angles t_{ij} is equal to the difference

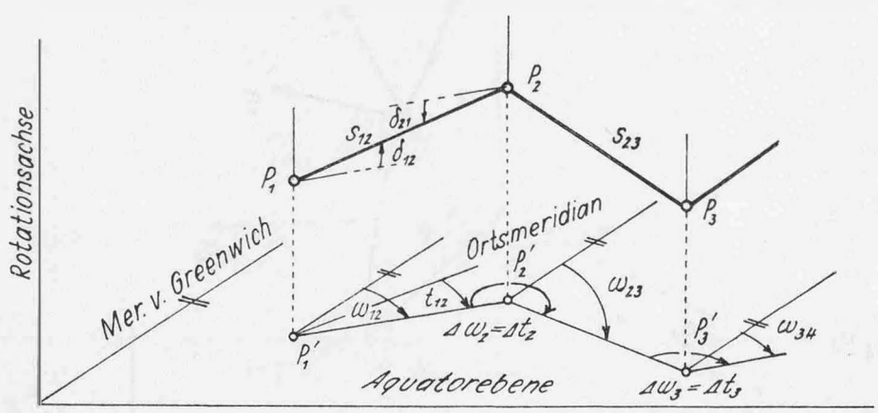

Fig. 3

of the time angles ω_{ij} counted from Greenwich, the angles $\Delta\omega_{ij} = \Delta t_{ij}$ of the polygonal traverse projected into the equatorial plane are known. It is therefore possible to determine a direction angle ω_{ij} of a polygon side from the observed data and an assumed direction of the first side as for the two-dimensional polygon.

$$\omega_{ij} = \omega_{12} + \sum_{\rho=1}^{n} \Delta t_\rho \pm n \tag{1}$$

This equation is supplemented by the condition given in Eq. (3c), Annex:

$$\delta_{ij} + \delta_{ji} = 0 \tag{2}$$

If the polygon contains two-non-consecutive Laplace points, m and n, Eq. (1) delivers a condition for the intermediate observed data.

$$\omega_{m,m-1} = \omega_{n,n+1} + \sum_{\rho=n}^{m} \Delta t_\rho \pm (m-n)\pi \tag{3}$$

We can eliminate the influence of refraction for each side with the aid of Eq. (2). The linear form (6a) derived in the Annex can be used therefore. An approximate elimination is provided by the following system:

$$z_{ij} = z'_{ij} + \frac{1}{A_{ij}} \cos\delta_{ij}(\delta'_{ij} + \delta'_{ji}) \tag{4a}$$

$$A_{ij} = -\sin z'_{ij}(\sin\varphi_i + \sin\varphi_j) + \cos z'_{ij}(\cos\varphi_i + \cos\varphi_j)$$

Often it will be sufficient to use the simplified relations

$$\delta_{ij} = \frac{1}{2}(\delta'_{ij} - \delta'_{ji}), \quad \delta_{ji} = -\delta_{ij} \tag{4b}$$

(in Eqs. (4a, b), z' are observed zenith distances and δ' are values calculated with z').

2.3. *The observed data*

Geodetic observed data for three-dimensional networks and the space polygon are horizontal directions r, zenith distances z and lenghts s of the network sides. (r, z) determines the bundle of directions for every network point. In addition we use the coordinates (φ, λ) of the plumb line obtained by astronomic measurements and the direction of the meridian determined by the orientation constand a_o of the horizontal directions. The procedures of astronomy and of the observation of horizontal directions are well tried and need not be discussed.

The distance observation must be made by light waves to obtain an accuracy of some mm/km. Longer distances (over 20 km) should be determined in sections to reduce the influence of refraction and permit additional controls. Local direction and distance networks with known transfer properties can be provided for calculating the total distances.

In microwave observations we must endeavour to eliminate the influence of reflections. This may be done by additional eccentric measurements or multiple controlled subdividing. The latter is recommended for better elemination of the refraction influence. An average accuracy of only $\pm$ 5 mm/km for network sides may be expected from microwave measurements.

The most difficult task is the determination of good zenith distances for long network sides. Favorable conditions prevail in the mountains where we can expect an accuracy of $\pm$ 2″. Observation from platforms about 20 m high in the flat country should be provided.

If this were not possible zenith distances may be derived from the difference in leveling heights if the difference of the geoid undulations is known. This is always the case when the vertical direction has been determined in the distance end points P_i, P_j.

In the region of network sides 1.0 we can assume spherical potential surfaces. Besides it is permissible to assume that the orthometric height difference ΔH_{ij} can be determined by leveling and gravity observation in the flat country. From the known vertical directions in P_i, P_j we know the angle ϑ_{ij} formed by the verticals

$$\cos\vartheta_{ij} = \sin\varphi_i \sin\varphi_j + \cos\varphi_i \cos\varphi_j \cos(\lambda_j - \lambda_i), \tag{5}$$

The true zenith distances Z_{ij} and Z_{ji} can be calculated from the height difference ΔH_{ij} and the

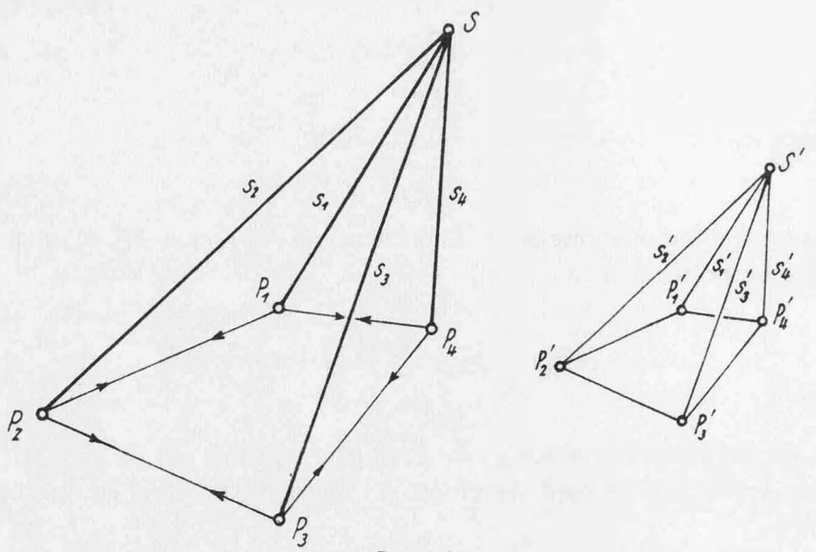

Fig. 4

measured side s_{ij}. From *Fig. 4* we take the following relations:

$$\Delta H_{ij} \cos \frac{\vartheta_{ij}}{2} = s_{ij} \cos\left(z_{ij} - \frac{\vartheta_{ij}}{2}\right) \tag{6a}$$

Hence follows for the true zenith distance not affected by refraction:

$$\tan \frac{z_{ij}}{2} = \frac{s_{ij}}{s_{ij} + \Delta H_{ij}} \tan \frac{\vartheta_{ij}}{2} \pm \sqrt{\frac{s_{ij} - \Delta H_{ij}}{s_{ij} + \Delta H_{ij}} + \left(\frac{s_{ij}}{s_{ij} + \Delta H_{ij}} \tan \frac{\vartheta_{ij}}{2}\right)^2} \tag{6b}$$

In this equation, only the positive root makes sense for the flat country.

With the aid of the known vertical directions in P_i, P_j it is also possible to free the observed zenith distances Z_{ij}, Z_{ji} from the refraction influence if the assumption of a symmetrical (circular) path curve is permissible. *Fig. 5* shows a projection onto a plane, parallel to the two verticals, in

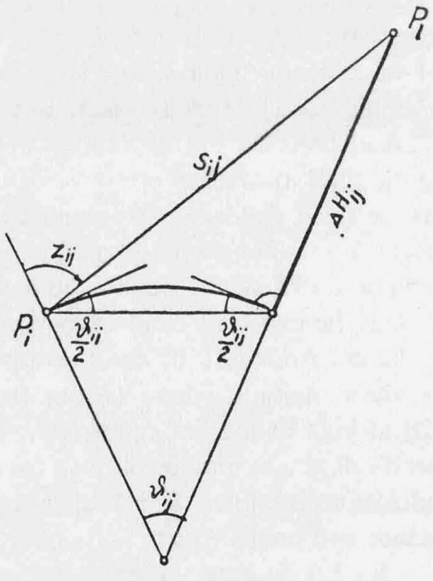

Fig. 5

which the zenith distances Z_{ij}, Z_{ji} and the angle ϑ_{ij} between the verticals appear because of the small distance of the vertivals accurate to terms of higher order. We take therefrom the following equation existing between the observed zenith distances z', the refraction amounts δz, the true zenith distances z and ϑ.

$$\delta z_{ij} + \delta z_{ji} = \vartheta_{ij} + \pi - (z'_{ij} + z'_{ji}) \tag{7a}$$

For a symmetrical path curve, i. e. if $\delta z_{ij} = \delta z_{ji}$ it follows because of $z = z' + \delta z$:

$$z_{ij} = \frac{1}{2}(\pi + \vartheta_{ij} + z'_{ij} - z'_{ji}) \tag{7b}$$

$$z_{ji} = \frac{1}{2}(\pi + \vartheta_{ij} - z'_{ij} + z'_{ji})$$

If the vertical directions of the end points are unknown the refraction coefficient

$$k = \frac{R}{r} = \frac{R}{s}(\delta z_{ij} + \delta z_{ji}) \tag{8a}$$

R radius of curvature, r radius

must be introduced as an unknown and be determined in the course of the calculation. k can be determined for a certain area, for every station, or — if the network has sufficient redundancy in determination — for each side. From the known coefficient k follows according to Eq. (8a) for a symmetrical path curve the refraction angle:

$$\delta z = \frac{s}{2R} k \tag{8b}$$

Errors in the determination of δz effect for flat bearings $\left(z \doteq \frac{\pi}{2}\right)$ direction errors:

$$d\delta = \frac{\sin\varphi}{\cos\delta}\delta z, \qquad d\omega = \frac{\cos\varphi \sin t}{\cos\delta}\delta z \tag{8c}$$

The influence is particularly high for large δ, i. e. near the poles

2.4. *Calculation of the space polygon*

From the available observed data we determine, uncontradictedly, sides s_{ij} and directions r_{ij}. With them we can determine the base length.

$$\underset{\sim}{b} = \underset{\sim}{x}_n - \underset{\sim}{x}_1 = \sum s_{ij} \underset{\sim}{r}_{ij} \tag{9}$$

$$b = |\underset{\sim}{b}| = \sqrt{(\underset{\sim}{x}_n - \underset{\sim}{x}_1)^2}$$

For the adjustment we form the differential formula:

$$db = \frac{\underset{\sim}{x}_n - \underset{\sim}{x}_1}{b} \cdot (d\underset{\sim}{x}_n - d\underset{\sim}{x}_1) = \sum (\underset{\sim}{r}^T_{1n}\, \underset{\sim}{r}_{ij}\, ds_{ij} + s_{ij}\, \underset{\sim}{r}^T_{1n}\, d\underset{\sim}{r}_{ij}) \tag{10a}$$

In it we represent the directional variation $d\underset{\sim}{r}_{ij}$ as a function of the observed quantities which we combine to a vector:

$$d\underset{\sim}{r}_{ij} = \underset{\sim}{f}_{ij}\, d\underset{\sim}{p}_{ij}$$

$$d\underset{\sim}{p}^T_{ij} = (z, r, \lambda, \varphi, a)_{ij}$$

If $\underset{\sim}{Q}_p$ denotes the weighting matrix of $d\underset{\sim}{p}$ it follows, according to know rules, for the base error:

$$Q_{bb} = \sum (\underset{\sim}{r}^T_{in} \underset{\sim}{r}_{ij})^2 Q_{ss} + s^2_{ij} (\underset{\sim}{r}^T_{ij} \underset{\sim}{f}_{ij})^T Q_p (\underset{\sim}{r}^T_{ij} f_{ij}) \tag{10b}$$

$$m_b = m_o \sqrt{Q_{bb}}$$

A strict numerical adjustment should be carried out by the more expensive, but clearer procedure of adjustment by variation of parameters. The value of a strict adjustment is, however, as for the plane polygonal traverse, problematic because of the low redundancy in determination since the gain in accuracy attainable stands in no reasonable relation to the necessary expenditure in calculation.

For this reason, an approximation method is indicated that fulfills all revlevant conditions. We assume that all directions and zenith distances have been observed, the first and every further fifth point are Laplace points, in the other points of the polygon φ and a are assumed to be observed.

Here, the procedure is described by individual calculation steps (Fig. 3):

1. The orientation matrices $\underset{\sim}{R}_{\lambda\varphi}$, $\underset{\sim}{R}_{\varphi}$ are formed by means of the astronomic data and all local directions $r'(z, a)$ are transformed to the equatorial system in directions $\underset{\sim}{r}(\delta, \omega)$ and $\underset{\sim}{r}(\delta, t)$. Preliminary direction coordinates are known as a result of the operation to be carried out according to Eqs. (1) and (2), Annex.

   (δ), (ω) in Laplace points
   (δ), (t) in points with observed (φ, a)

2. We correct the two (δ)-values obtained for each traverse side according to point 1, with the aid of Eq. (4b):
   This procedure corresponds to an approximate correction for refraction assuming a circular path curve.
3. The refraction angles determined according to point 1

$$\Delta t_i = t_{ik} - t_{ij} = \omega_{ik} - \omega_{ij} \tag{11}$$

   of the polygon projected in the equatorial plane are corrected, as for the plane polygon, by means of the conditions, Eq. (1). Thus, we obtain uncontradicted direction coordinates ω for each polygon side.
4. With the values (δ, ω) obtained according to points 2,3 we calculate corrected directions $\underset{\sim}{r}_{ij}$ of the polygon sides and enter Eq. (9) with them.

For an error estimation we form according to Eq. (9):

$$\begin{aligned}(X_n - X_1) &= \Delta X = \sum s \cos\delta \cos\omega \\ (Y_n - Y_1) &= \Delta Y = \sum s \cos\delta \sin\omega \\ (Z_n - Z_1) &= \Delta Z = \sum s \sin\delta\end{aligned} \tag{12a}$$

If we denote the direction coordinates of the base by b_1, b_2, b_3 i. e.

$$\frac{1}{b}\,(\underset{\sim}{x}_n - \underset{\sim}{x}_1)^T = (b_1, b_2, b_3)$$

it follows from Eq. (12a) and the first Eq. (10a):

$$Q_{bb} = b_1^2 Q_{xx} + b_2^2 Q_{yy} + b_3^2 Q_{zz} + 2\,(b_1 b_2 Q_{xy} + b_2 b_3 Q_{yz} + b_3 b_1 Q_{xz}) \tag{12b}$$

The weight coefficients Q_{ik} can be expressed, according to known rules, by $Q_{\delta\delta}, Q_{\omega\omega}, Q_{\delta\omega}$ and the uncorrelated Q_{ss}. The following holds for the quadratic coefficients:

$$\begin{aligned}Q_{xx} = \sum \{&(\cos\delta\cos\omega)^2 Q_{ss} + (s\sin\delta\cos\omega)^2 Q_{\delta\delta} + (s\cos\delta\sin\omega)^2\, Q_{\omega\omega} + \\ &+ 2\,(s^2 \sin\delta\cos\delta\sin\omega\cos\omega)\, Q_{\delta\omega}\}\end{aligned} \tag{12c}$$

$$\begin{aligned}Q_{yy} = \sum \{&(\cos\delta\sin\omega)^2\, Q_{ss} + (s\sin\delta\sin\omega)^2 \quad Q_{\delta\delta} + (s\cos\delta\cos\omega)^2\, Q_{\omega\omega} - \\ &- 2\,(s^2 \sin\delta\cos\delta\sin\omega\cos\omega)\, Q_{\delta\omega}\}\end{aligned}$$

$$Q_{zz} = \sum \{\sin^2\delta\, Q_{ss} + (s\cos\delta)^2\, Q_{\delta\delta}\}$$

Similar expressions are found for the mixed coefficients Q_{xy}, Q_{yz}, Q_{xz}. We are not going to write them down; we just point to the remarkably simple sum

$$Q_{xx} + Q_{yy} + Q_{zz} = \sum (Q_{ss} + s^2\, Q_{\delta\delta} + s^2 \cos^2\delta\, Q_{\omega\omega}) \tag{13}$$

The latter determines the point error of the end point and gives an upper bound for the accuracy of the base length. The observed data should be introduced in Eqs. (12) (13) but in most cases it will be sufficient to use estimated weights of the direction coordinates (δ, ω).

The two first Eqs. (12) describe the projection of the space polygon into the equatorial plane, the last Eq. (12) the projection into planes normal thereto. This concept facilitates the estimation of errors.

For a schematic polygon with equal side errors and equal errors in δ, ω it follows from Eq. (13):

$$Q_{bb} \leqslant n Q_{ss} + n s Q_{\delta\delta}{}^2 \, (1 + \sum \cos^2 \delta)$$

$0 \leqslant \cos\delta \leqslant 1$ holds for a north-south traverse, $\cos\delta = 1$ for an east-west traverse.

An estimation of errors for a traverse 2,500 km long with sides 20 km long and measurement errors

$$m_s = \pm (2\,\text{cm} + 2 \,.\, 10^6) s\,, \quad m_z = \pm 3''$$

shows that a relative side accuracy of $\pm$ 1.5 mm/km can be attained.

3. *Scale determination by Secor*

3.1. *The basic idea*

The scale of a direction network may be also derived from four distances s_i ($i = 1$ to 4) which are measured from an arbitrary point S to arbitrary four network points $P_i (i = 1 \ldots 4)$. If P'_i denote the points corresponding to P_i in the network model, the model point S' can be determined from three side ratios (Fig. 6).

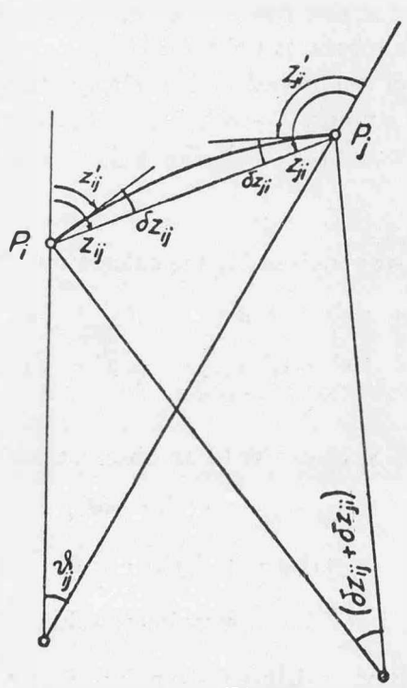

Fig. 6

$$\mu_{ij} = \frac{s_i}{s_j} = \frac{s'_i}{s'_j} \tag{1}$$

Each ratio determines an Apollonian sphere as the locus for S' whose center M'_{ij} lies on the line $\overline{P'_i P_j} = \overline{s_{ij}}$ at a distance of

$$m'_{ij} = \frac{\mu_{ij}{}^2}{\mu_{ij}{}^2 - 1} s'_{ij} \tag{2a}$$

from P_i, and has the radius:

$$r'_{ij} = \frac{\mu_{ij}}{\mu_{ij}{}^2 - 1} s'_{ij} \tag{2b}$$

The point S' corresponding to the measuring point S is fixed as point of intersection of three Apollonian spheres or by space section from the three centers M'_{ij} with the distances r'_{ij}. When S' has been determined the scale factor follows as ratio of corresponding sides:

$$\lambda = \frac{s_i}{s_j'} \tag{3}$$

The problem has an infinite number of solutions if the three Apollonian spheres form a bundle as in this case each point of the common intersecting circle may be regarded as a solution. This is, for instance, the case if the four points P_i form a square and S lies above the center. In this case, the Apollonian spheres degenerate to the symmetry planes of the sides s_{ij} and intersect in the normal to the plane of the points P_i passing through the center of the square. The common line of intersection corresponds to the intersecting circle of the degenerate Apollonian sphere. Analogous conditions exist if a larger number of points P form a regular polygon and the point S lies above their point of intersection.

Besides these critical loci providing an infinite number of solutions there are others for which the solution is unique but uncertain. They follow from a discussion of the differential formulas for the problem. For the analytic representation of the problem it is convenient to start from the relation

$$s_i^2 = \lambda^2 (\underset{\sim}{y'} - \underset{\sim}{x'}_i)^2 = (\underset{\sim}{y} - \underset{\sim}{x}_i)^2 \tag{4}$$

Then, $\underset{\sim}{x}_i$, $\underset{\sim}{y}_i$ denote the position vectors of the points P'_i, S in the model, and $\underset{\sim}{x}_i$, $\underset{\sim}{y}_i$ the corresponding vectors in nature. Four distances s_i give rise to four equations (4) in which the three coordinates x, y, z of S and the scale factor λ appear as unknowns.

In the practical application of the procedure it is always possible to carry out $n > 1$ quadruples of four measurements s_{ij} each to n points S_j (with Secor). In such a case we have got an adjustment problem since a system of $4n$ equations with $(3n + 1)$ unknowns, i. e. with $(n - 1)$ excessive observations, is given.

3.2. *Calculation and adjustment*

Differential formulas of (4) are required for the calculation. It follows:

$$d s_i = a_i d\lambda + \alpha_i \, dx' + \beta_i dy' + \gamma_i dz' \tag{5a}$$

$$a_i = \frac{s_i}{\lambda}, \quad \alpha_i = \lambda \frac{x' - x_i'}{s_i}, \quad \beta_i = \lambda \frac{y' - y'_i}{s_i}, \quad \gamma_i = \lambda \frac{z - z'_i}{s_i}$$

Each side s_{ij} measured from P_i to S_j gives rise to an observational equation:

$$\begin{gathered} s_{ij} + v_{ij} = \lambda (s'_{ij}) + d s_{ij} \\ (s'_{ij}) = \sqrt{[(\underset{\sim}{y'_j}) - \underset{\sim}{x'_i}]^2} \\ (\underset{\sim}{y'_j}) = \text{approximate value} \end{gathered} \tag{5b}$$

The system of observational equations existing for n points S_j and four points P_i can be represented by the equation

$$\underset{\sim}{v} = \underset{\sim}{A}\,\underset{\sim}{x} + \underset{\sim}{l} \tag{6a}$$

In it

$$\underset{\sim}{x}^T = (d\lambda, d\underset{\sim}{y}_1, d\underset{\sim}{y}_2, \ldots d\underset{\sim}{y'}_n)$$

denotes the vector of the $(3n + 1)$ unknowns. The coefficient matrix $\underset{\sim}{A}$, with the auxiliary quantities

$$\underset{\sim}{k}^T_j = (a_{1j}, a_{2j}, a_{3j}, a_{4j})$$

$$\underset{\sim}{K_j} = \begin{pmatrix} \alpha_{1j} & \beta_{1j} & \gamma^1 j \\ \alpha_{2j} & \beta_{2j} & \gamma_{2j} \\ \alpha_{3j} & \beta_{3j} & \gamma_{3j} \\ \alpha_{4j} & \beta_{4j} & \gamma_{4j} \end{pmatrix} \tag{6b}$$

assumes the simple form:

$$\underset{\sim}{A} = \begin{pmatrix} \underset{\sim}{k_1} & \underset{\sim}{K_1} & 0 \cdots\cdots & 0 \\ \underset{\sim}{k_2} & 0 & \underset{\sim}{K^2} \cdots\cdots & 0 \\ \vdots & \vdots & \vdots & \vdots \\ \underset{\sim}{k_n} & 0 & 0 & \underset{\sim}{K_n} \end{pmatrix} \tag{6c}$$

The vector of the absolute quantities is given by

$$\underset{\sim}{l}^T = (\lambda) \quad \underset{\sim}{(s')}^T - \underset{\sim}{s}^T \tag{6d}$$

(λ) , $\underset{\sim}{(s')}$ from approximate values

Since the variations of the coordinates $\underset{\sim}{d_y}$ are not required it is convenient to eliminate them so that, after elimination, λ is left as the only unknown of the normal equation system.

An investigation carried out in [1] on optimum and critical configurations leads to the following result:

a. The procedure fails if the points P and S lie on a sphere. This is always the case if the points Pi are located on a circle.
b. If the points of the terrestrial figure lie in the corners of a regular polygon and the $(n + 1)$ in the center of the circumscribed circle, the relative accuracy of the scale factor will be independent of the number n. Therefore, a terrestrial figure formed by the corners of an equilateral triangle and its center of gravity makes expect a good result for the scale determination.

3.3. *Numerical studies*

The procedure described might be used to carry out the scale determination of a direction network with the aid of the known Secor measuring device. A high accuracy can be expected because a very great number of distance quadruples can be measured to four points P_i of the network by means of Secor.

Numerical studies were carried out on a seriex of models to gain an insight into the accuracy with different arrangements of the terrestrial point groups and of the space points S_j. They were chosen so that they corresponded to the conditions prevailing in the PAGEOS world network.

The root of the weight coefficient of the scale factor was calculated for each assumption. The error of the observed distances was assumed to be constant. The calculation was made dimensionless with an arbitrary unit E. The scale error is determined by the following relation:

$$m_\lambda = \frac{1}{E} m_s \sqrt{Q_{\lambda\lambda}}$$

where m_s denotes the distance error and E the unit of the model. The conditions of the PAGEOS world network follow approximately if E is chosen with 500 km. Herewith and for $m_s = \pm 5\ m$ it follows:

$$m_\lambda = \pm 10^{-5} \sqrt{Q_{\lambda\lambda}}.$$

This means that the tabulated values of the numerical studies correspond, in this case, to units of the 5th decimal of the scale error. Now we are going to report on the investigations carried out and the results obtained.

First study

It has been shown in section 2.2 that for theoretical deliberations favorable results will be obtained by a configuration in which three of the terrestrial points form an equilateral triangle and the fourth point lies in the center of gravity of the latter. This assumption constituted the basis for the first study. The radius of the circumscribed circle was assumed with $4E$, the height of the points S with $3E$ (Fig. 7a–d).

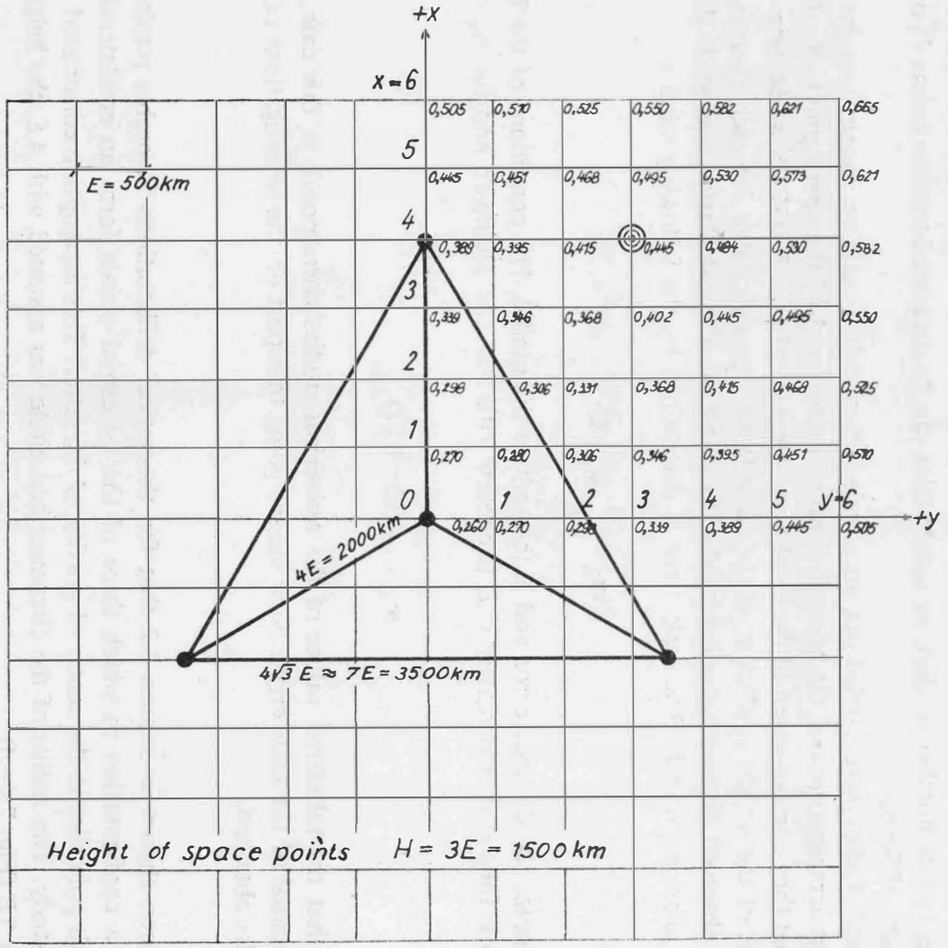

1 Space point Fig. 7a

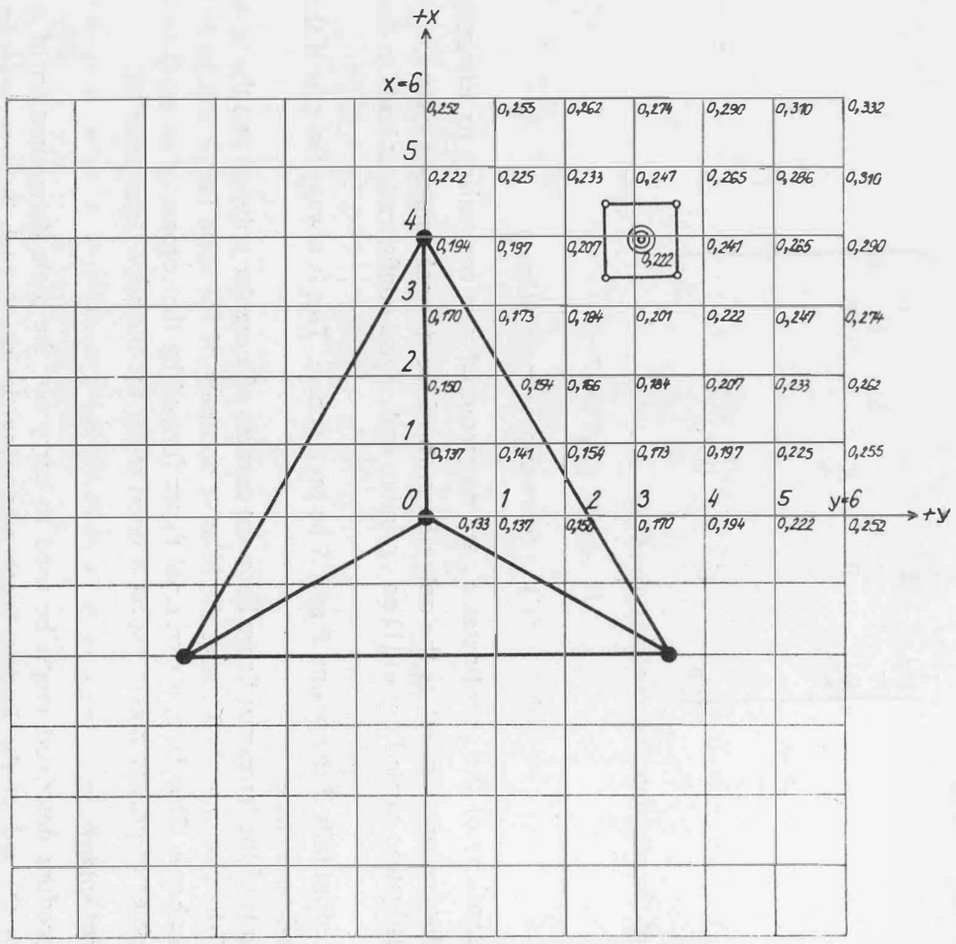

4 Space points Fig. 7b

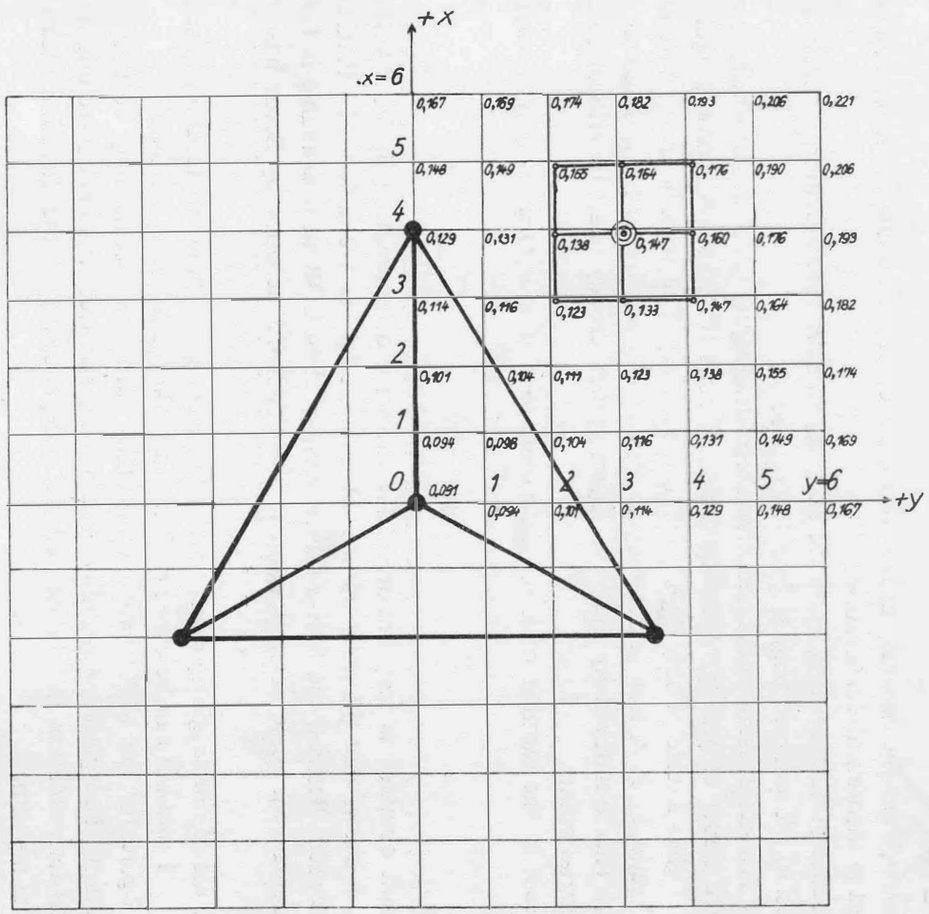

9 Space points

Fig. 7c

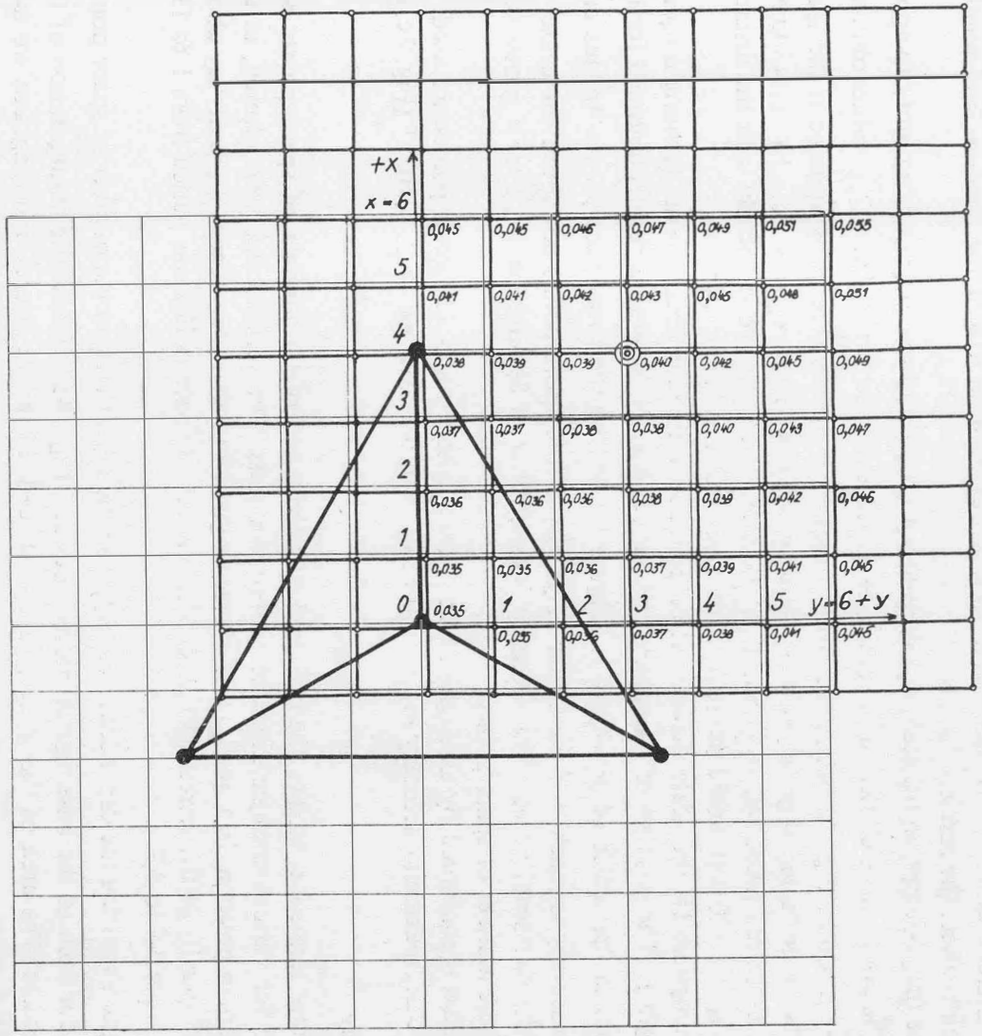

121 Space points

Fig. 7d

Four different assumptions were made to find out to what extend the position and number of space points affect the result.

For the first assumption the scale was derived with the aid of one single space point of varying position. The points were chosen in the nodes of a lattice of mesh with. The $\sqrt{Q_{\lambda\lambda}}$ valuesobtained were written down in Fig. 7a beside the lattice points. An optimum result is attained if he space point lies above the center of gravity of the base figure. A scale error $m_\lambda = \pm 2{,}6 \cdot 10^{-6}$ isobtained with the assumptions made ($m_s = \pm 5m$, $E = 500$ km). The error grows linearly with thedistance error; for $m_s = \pm 20m$ it would amount to the fourfold, i. e. about 10^{-5}.

In assumption 1b the scale determination is made with four space points forminga square of side length E. The position of the square was varied. Fig. 7b shows the results obtained for the $\sqrt{Q_{\lambda\lambda}}$ values in the center of gravity of the figure formed by the four space points. Inthis case maximum accuracy is reached if the center of gravity of the space points lies above the center of gravity of the terrestrial points. The accuracy is twice that of assumption 1a, i. e. it grows with the root of the number of space points.

This result is confirmed by assumptions 1c and 1d where 9 and 121 space points are used. In the former case, maximum accuracy $m_\lambda = \pm 0{,}9 \cdot 10^{-6}$ in the latter $m_\lambda = \pm 0{,}310^{-6}$ (Fig. 7c, d).

Second study

In further numerical studies the influence of height and of the number of space points was investigated for various configurations of terrestrial points. The space points were chosen, in the known optimum position, in a quadrangle of side length $2E$ so that their center of gravity ay above the center of gravity of the terrestrial figure. The number of space points was varied from 1 to 196, the heights from $5E$ to $8E$.

A diagram showing the dependence of $\sqrt{Q_{\lambda\lambda}}$ on the height and on the number of space points was drawn for each of the base figures chosen. Besides, Figs. 8a–f show the configuration of the terrestrial points. The area of the space points is shaded. From the figures and diagrams we take the following results:

a. In all assumptions the accuracy grows with the root of the number of space points as has been presumed in theoretical deliberations.
b. The influence of different heights on the accuracy of scale determination is small. In any case, the lowest of the assumed heights gives the best result.
c. The most favorable result is obtained with a terrestrial figure the points of which lie in the corners and in the center of gravity of an equilateral triangle (Fig. 8a). A rhombic figure of diagonal ratio 1 : 3 gives a scale of only slightly reduced accuracy. The same holds for a rhombic figure of diagonal ratio 1 : 2. A loss in accuracy of about 40% was found for a diagonal ratio of 2 : 3 (Fig. 8c). This is noteworthy since this figure comes already near the critical configuration of the terrestrial points.
d. An increase in the number of terrestrial points to 6 (Fig. e, f) gives only a small increase in accuracy.

3.4. *Result*

The result obtained is very important for the scale determination in the PAGEOS network by SECOR. It shows that the great number of rhombic figures available in the PAGEOS network may well be used. Besides, the four-distance version of SECOR now available is fully sufficient.

In particular, the scale determination in the PAGEOS network by Secor has the following advantages:

a. With the use of one single figure and a distance error of $\pm$ 20 m, an accuracy in scale determination of $\pm$ 1 mm/km can be expected if at least 200 space points are used.
b. Various figures of the world network including such over oceans may be used for the scale determination. This gives a possibility of improving the accuracy and controlling the procedure.
c. The scale determination can be carried out independently of the direction measurement and repeated at any time.

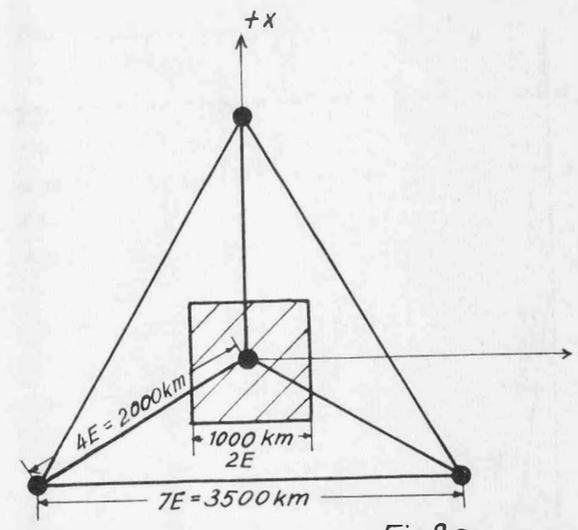

Fig.8a

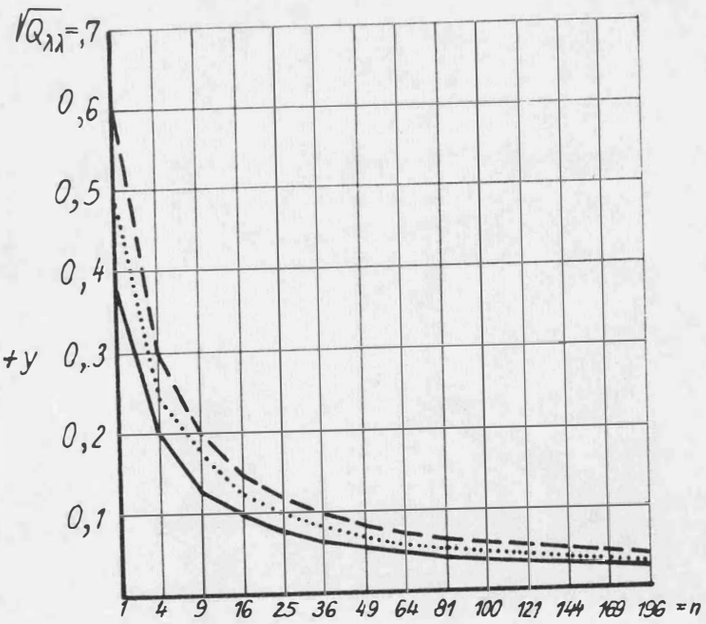

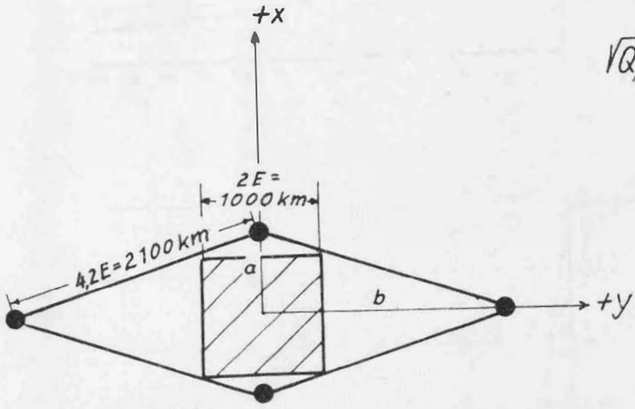

a = 1,3E = 650km
b = 4 E =2000 km
a : b = 1 : 3

Fig.8b

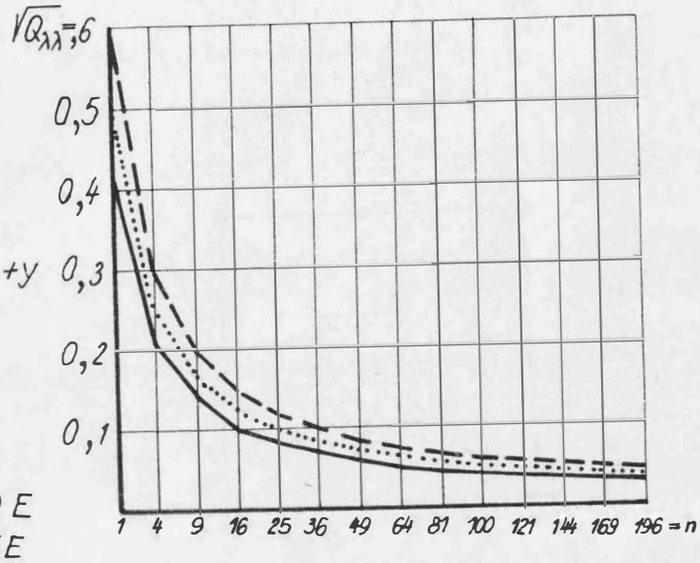

——— h = 5,0 E
..... h = 6,5E
— — — h = 8,0E

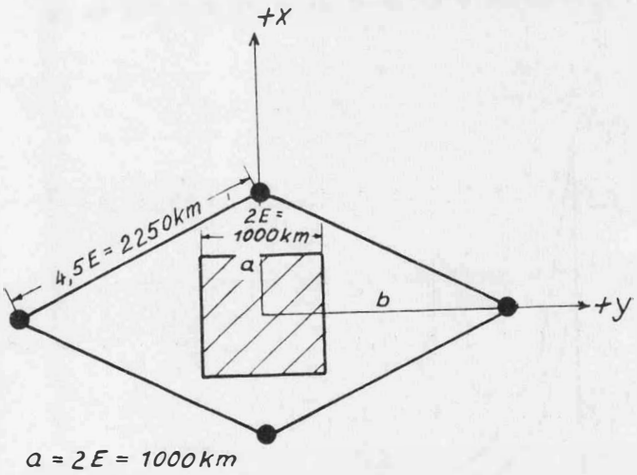

a = 2E = 1000km
b = 4E = 2000km
a : b = 1 : 2

Fig.8c

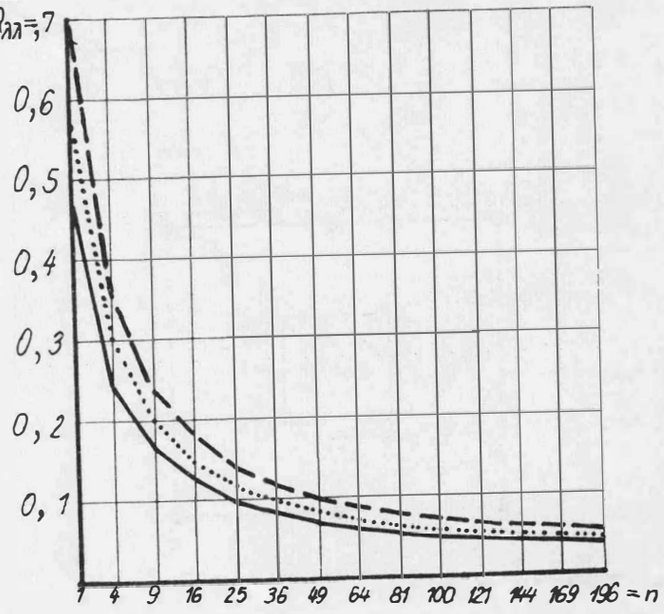

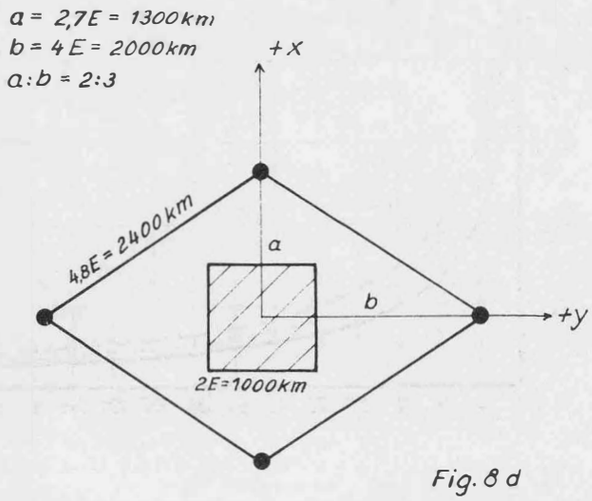

Fig. 8 d

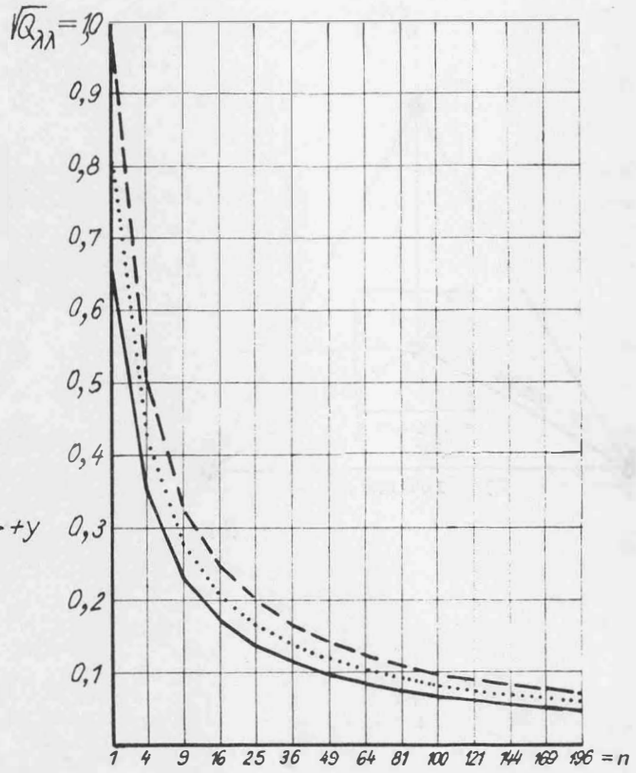

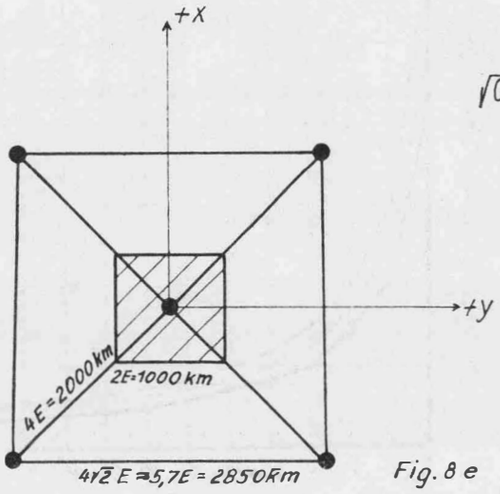

Fig. 8 e

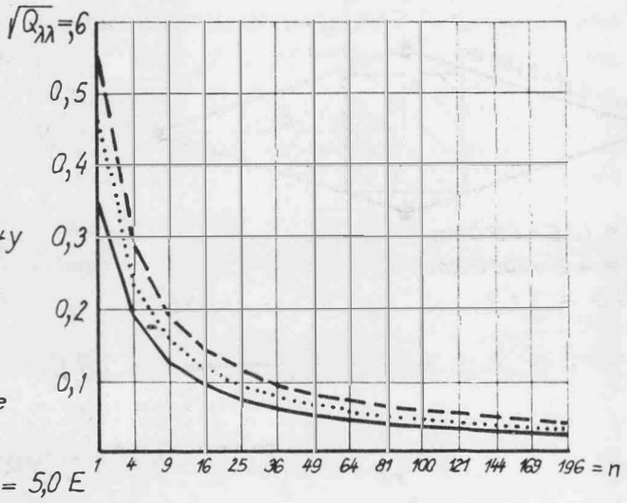

——— h = 5,0 E
..... h = 6,5 E
— — — h = 8,0 E

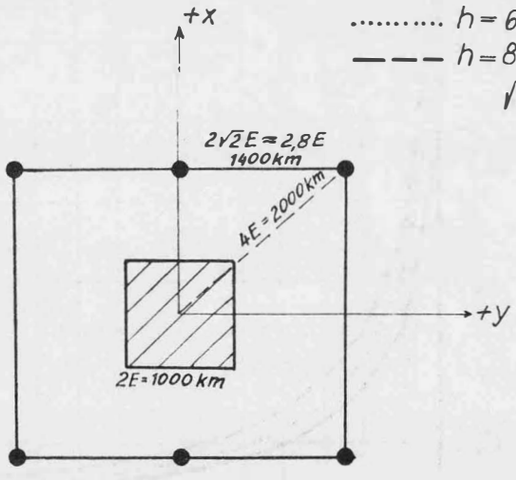

Fig. 8 f

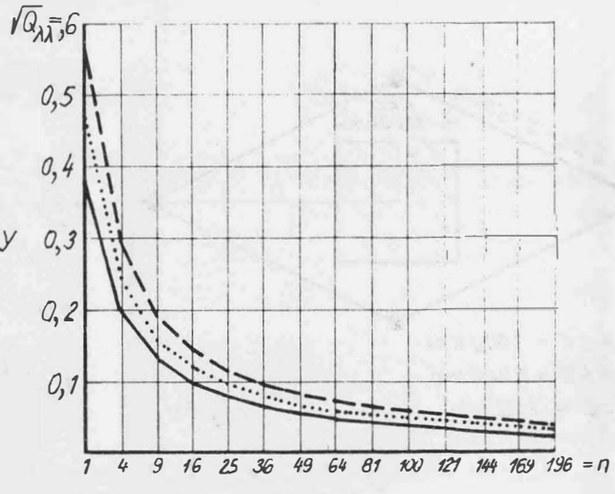

Summary

The scale determination in spatial direction networks is an actual problem of geometric satellite geodesy. The present paper reports on two practicable methods. They are the spatial polygonal traverse measured along the earth's surface on continents, and the use of Secor that is also possible over water surfaces. The former method requires a great expenditure of observations and is restricted to continents. The accuracy attainable was found to be $\pm$ 1 mm/km. The latter method may be used in any number of quadrangles of a direction network. Its accuracy can be increased over $\pm$ 1 mm/km by repeating the observations. Further suggestions for the scale determination with other configurations and with other measuring devices (Laser and Doppler) have been made in [1].

The present paper originates from a research project sponsored by Gimrada, USA, under contract no. 91—591—EUC—4006.

Literature:

1. *Rinner, K.:* Annual Technical Report, Contract Number 91—591—EUC—4006.

Conditional Equations in Three-Dimensional Polygon

1. *General form*

The horizontal directions r_{ij} and r_{ji}, the zenith distances Z_{ij}, Z_{ji} and the side s_{ij} are assumed to have been observed between two Laplace points P_i and P_j. a_{ol} denotes the orientation constants with which the horizontal directions r_{lj} are transformed to azimuths a_{lj}, $\underset{\sim}{R}^{l}{}_{\varphi\lambda}$ be the orientation matrix that can be calculated from the astronomic data $(\varphi, \lambda)_l$ in the Laplace point P_l. The local directions

$$\underset{\sim}{r}_{ij}(z, r) = \begin{pmatrix} \sin z_{ij} \sin (r_{ij} - a_{oi}) \\ \sin z_{ij} \cos (r_{ij} - a_{oi}) \\ \cos z_{ij} \end{pmatrix} \tag{1a}$$

can be transformed with the aid of the matrix

$$\underset{\sim}{R}^{l}{}_{\varphi\lambda} = \begin{pmatrix} -\sin\lambda_l & -\sin\varphi_l \cos\lambda_l & \cos\varphi_l \cos\lambda_l \\ \cos\lambda_l & -\sin\varphi_l \sin\lambda_l & \cos\varphi_l \sin\lambda_l \\ 0 & \cos\varphi_l & \sin\varphi_l \end{pmatrix} \tag{1b}$$

to the equatorial system through Greenwich.

$$\underset{\sim}{r}_{ij}(\delta, \omega) = \begin{pmatrix} \cos\delta_{ij} \cos\omega_{ij} \\ \cos\delta_{ij} \sin\omega_{ij} \\ \sin\delta_{ij} \end{pmatrix} = \begin{pmatrix} u_{ij} \\ v_{ij} \\ w_{ij} \end{pmatrix} \tag{1c}$$

The transformation equation has the form:

$$\underset{\sim}{r}_{ij}(\delta, \omega) = \underset{\sim}{R}^{i}{}_{\varphi\lambda}\, \underset{\sim}{r}_{ij}(z, r - a_o) \tag{2}$$

Since the directions oriented in the equatorial system are available for each Laplace point, the following vector equation exists between two Laplace points $P_i P_j$:

$$\underset{\sim}{r}_{ij} = -\underset{\sim}{r}_{ji} \tag{3a}$$

Hence the scalar equations:

$$\begin{aligned} w_{ij} + w_{ji} &= 0 \\ u_{ji} v_{ij} - u_{ij} v_{ji} &= 0 \end{aligned} \tag{3b}$$

They are equivalent to two conditions for the direction coordinates δ, ω

$$\begin{aligned} \delta_{ij} + \delta_{ji} &= 0 \\ \omega_{ji} - \omega_{ij} + \pi &= 0 \end{aligned} \tag{3c}$$

This gives differential formulas with the following coefficient schedule:

	$d\lambda$	$d\varphi$	da	dz
du	A'	B'	C'	D'
dv	A''	B''	C''	D''
dw	0	B'''	C'''	D'''

(4a)

$$A' = -\cos\lambda\sin z\sin a + \sin\varphi\sin\lambda\sin z\cos a - \cos\varphi\sin\lambda\cos z$$
$$B' = -\cos\varphi\cos\lambda\sin z\cos a - \sin\varphi\cos\lambda\cos z$$
$$C' = -\sin\lambda\sin z\cos a + \sin\varphi\cos\lambda\sin z\sin a$$
$$D' = -\sin\lambda\cos z\sin a - \sin\varphi\cos\lambda\cos z\cos a - \cos\varphi\cos\lambda\sin z$$

$$A'' = -\sin\lambda\sin z\sin a - \sin\varphi\cos\lambda\sin z\cos a + \cos\varphi\cos\lambda\cos z$$
$$B'' = -\cos\varphi\sin\lambda\sin z\cos a - \sin\varphi\sin\lambda\cos z$$
$$C'' = \cos\lambda\sin z\cos a + \sin\varphi\sin\lambda\sin z\sin a \qquad (4b)$$
$$D'' = -\cos\lambda\cos z\sin a - \sin\varphi\sin\lambda\cos z\cos a - \cos\varphi\sin\lambda\sin z$$

$$B''' = -\sin\varphi\sin z\cos a + \cos\varphi\cos z$$
$$C''' = -\cos\varphi\sin z\sin a$$
$$D''' = \cos\varphi\cos z\cos a - \sin\varphi\sin z$$

2. *Linear forms for the equations*

From the first equation (3b) follows system (5a) in which we have designated the observed values by strokes:

$$dw_{ij} + dw_{ji} + W^I{}_{ij} = 0 \qquad (5a)$$
$$W^I{}_{ij} = \sin\delta'_{ij} + \sin\delta'_{ji}$$

We introduce Eqs. (4a) (4b) and replace the differentials of the observed quantities φ, λ and r by corrections v. Since the zenith distances z are distorted by a systematic portion of refraction we introduce for each side a refraction coefficient k. (this corresponds to the assumption of a circular refraction curve) and replace the differentials of the zenith distances by the following expressions:

$$dz_{ij} = v_{zij} + \alpha_{ij}k_{ij} \qquad \alpha_{ij} = \frac{s_{ij}}{2R} \qquad (5b)$$
$$dz_{ji} = v_{zij} + \alpha_{ij}k_{ij}$$

R = mean radius of curvature

As a result we obtain the equation:

$$b'_{ij}v_{\varphi_i} + b'_{ji}v_{\varphi_i} + c'_{ij}v_{\alpha ij} + c'_{ji}v_{\alpha ji} + d'_{ij}v_{zij} + d'_{ji}v_{zji} + \alpha_{ij}(d'_{ij} + d'_{ji})k_{ij} + W^I{}_{ij} = 0 \qquad (6a)$$

The following system holds for the coefficients:

$$b'_{ij} = B'''_{ij} \qquad b'_{ji} = B'''_{ji}$$
$$c'_{ij} = C'''_{ij} \qquad c'_{ji} = C'''_{ji} \qquad (6b)$$
$$d'_{ij} = D'''_{ij} \qquad d'_{ji} = D'''_{ji}$$
$$W^I{}_{ij} = \sin\delta'_{ij} + \sin\delta'_{ji}$$

From the second equation (3b) we obtain the differential relation:

$$v_{ij}du_{ji} + u_{ji}dv_{ij} - v_{ji}du_{ij} - u_{ij}dv_{ji} + W^{II}{}_{ij} = 0 \qquad (7a)$$

After some transformations we obtain the equation:

$$-\sin\omega'_{ij}(du_{ij}+du_{ji})+\cos\omega'_{ij}(dv_{ij}+dv_{ji})+\cos\delta_{ij}(\omega'_{ij}-\omega_{ji}+\pi)=0 \tag{7b}$$

Introducing the relations according to Eqs. (4a, b) we obtain the linear form for the second Laplace condition.

$$\begin{aligned}&a''_{ij}v_{\lambda i}+a''_{ji}v_{\lambda j}+b''_{ij}v_{\varphi i}+b''_{ji}v_{\varphi j}+v'_{ij}c''_{ij}v_{aij}+c''_{ji}v_{aji}+\\&+d''_{ij}v_{zij}+d''_{ij}v_{zji}+\alpha_{ij}(d''_{ij}+d''_{ji})k_{ij}+W^{II}_{ij}=0\end{aligned} \tag{8a}$$

The following system holds for the coefficients:

$$\begin{aligned}a''_{ij}&=-\sin\omega'_{ij}A'_{ij}+\cos\omega'_{ij}A''_{ij}\\a''_{ji}&=-\sin\omega'_{ij}A'_{ji}+\cos\omega'_{ij}A''_{ji}\\b''_{ij}&=-\sin\omega'_{ij}B'_{ij}+\cos\omega'_{ij}B''_{ij}\\b''_{ji}&=-\sin\omega'_{ij}B'_{ji}+\cos\omega'_{ij}B''_{ji}\\c''_{ij}&=-\sin\omega'_{ij}C'_{ij}+\cos\omega'_{ij}C''_{ij}\\c''_{ji}&=-\sin\omega'_{ij}C'_{ji}+\cos\omega'_{ij}C''_{ji}\\d''_{ij}&=-\sin\omega'_{ij}D'_{ij}+\cos\omega'_{ij}D''_{ij}\\d''_{ji}&=-\sin\omega'_{ij}D'_{ji}+\cos\omega'_{ij}D''_{ji}\\W''_{ij}&=+\cos\delta'_{ij}(\omega'_{ij}-\omega'_{ji}+\pi)\end{aligned} \tag{8b}$$

The two equations (6a) and (8a) are the linear forms for Laplace's equations between two space points. They contain corrections for all observed quantities and the refraction coefficient as the only unknown.

Elimination of the latter leaves one equation containing only correction quantities.

If astronomic quantities φ or λ were not observed the corrections V_φ, V_λ must be replaced by differentials $d\varphi$, $d\lambda$ and the latter be introduced as unknowns.

$$d\varphi, d\lambda \text{ instead of } v_\varphi, v_\lambda \tag{9a}$$

If the azimuth a_{ij} was not observed the orientation constant a_{oi} of the horizontal directions will be unknown and we must introduce

$$v_{aij}=v_{rij}+da_{oi} \tag{9b}$$

into the Eqs. (6a) and (8a).

Studies of Gravity in Space According to Bjerhammar

by *Bo-Gunnar Reit*

Abstract

An investigation is made of the possibilities to use Bjerhammar's new gravity reduction method for a study of the gravity in space.

For this purpose Bjerhammar's theory is applied to two test models. The basic integral equation of the theory is solved by different approaches and the results are compared. Although the test models were of ill-behaved nature, with mass focused between the topographical and the reference surface the results from the applications are in very good agreement with the theoretical values both at the topographical surface and in space. Hence Bjerhammar's theory can be successfully applied to gravity problems in space.

Introduction

In 1849 Stokes published his famous solution of the gravimetric boundary value problem. The solution refers to an approximately ellipsoidal equipotential surface the so-called *geoid*. Applied

on the gravity field of the earth all external masses had to be reduced inside the geoid. Rudzky and Heiskanen among others developed reduction methods for this purpose. The methods however, were not entilrely satisfactory because densities had to be guessed or estimated. In 1945 Molodensky presented a quite new solution of the boundary value problem. However, also his solution had some drawbacks. All integrations were carried out at the unknown physical surface. Furthermore the convergence of the solution for terrain inclination above 45^0 is questioned. Later on new methods have been developed by among others Bjerhammar [4] and Hirvonen [8]. In Bjerhammar's new theory the problem is revised in the following way:

"A finite number of gravity data (gravity anomalies) is given for a nonspherical surface, and it is required to find such a solution that the boundary values for the gravity data (gravity anomalies) are satisfied in all given points. (External boundary value problems for finite number of points.)" (See [4].)

The gravity anomaly

The normal way of tackling the gravimetric problem is to separate the gravity field of the earth in a regular and an irregular part. This can be done by introducing a reference sphere with the same rotation as the earth. Then the irregularities in the potential can be described by

$$T = W - U \tag{1}$$

where

W = potential of the earth
U = potential of the reference sphere (theoretical potential)
T = disturbance potential

By taking the normal derivative of T we obtain

$$\frac{\partial T}{\partial n} = \frac{\partial W}{\partial n} = \frac{\partial U}{\partial n} = -(g - \gamma) \tag{2}$$

where

g = gravity at a surface point of the earth
γ = theoretical gravity at the same point
$g - \gamma$ = gravity disturbance
n = normal of the reference sphere

Here only g can be determined since we don't know the actual height above the reference sphere.

From measurements it is possible to obtain an estimate of the height by

$$Z_o = \frac{W_o - W}{\gamma_o}$$

where

Z_o = theoretical height
W_o = potential at a point of the sphere
γ_o = theoretical gravity at the sphere

(For higher accuracy a correction is needed.)

By the aid of the theoretical height we define the gravity anomaly as

$$\Delta g = g - \gamma_{Z_o} \tag{4}$$

It can be shown [4] that the anomaly defined in this way satisfies the boundary condition

$$\frac{\partial T}{\partial n} - \frac{T}{\gamma_o} \cdot \frac{\partial T}{\partial n} = -\Delta g \qquad \text{(Brun's formula)} \tag{5}$$

Gravity reduction

From the usual approximation of the boundary condition

$$\Delta g_j = -\frac{\partial T}{\partial r_j} - \frac{2T}{r_j} \tag{6}$$

and the generalized Stokes' formula

$$T_j = \frac{1}{4\pi r_j} \iint_{Sn} \Delta g^* \sum_{n=2}^{\infty} \frac{2n+1}{n-1} \left(\frac{r_o}{r_j}\right) P_n(\cos\omega_{ij})\, dS \tag{7}$$

Bjerhammar [3] derived the integral equation for gravity reduction

$$\Delta g_j = \frac{1}{4\pi r_j^2} \iint_{S} \Delta g^* \left(\frac{1}{r} - 3t\cos\omega_{ij} - \frac{2(t^2 - t\cos\omega_{ij})}{r^3} - 1\right) dS \tag{8}$$

where

r_o = radius of the reference sphere
r_j = distance between the origin and the actual point P_j at the physical surface or in space
T = disturbance potential
Δg_j = gravity anomaly at P_j
Δg^* = "gravity anomalies" at the reference sphere
ω_{ij} = geocentric angle between actual and moving points
$P_n(\cos\omega_{ij})$ = Legendre polynomial
S = surface of the reference sphere
t = r_o/r_j
r = r_{ij}/r_j
r_{ij} = distance between the moving point on the reference sphere and the actual point P_j

It should be noted that Δg^* has no direct physical meaning if there exist masses between the reference sphere and the physical surface.

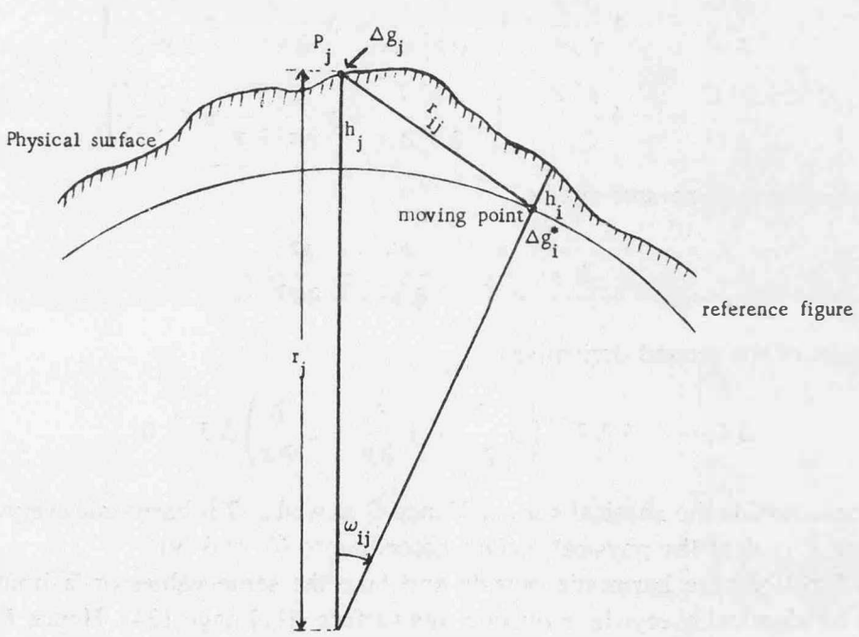

fig. 1.

By omitting the two terms of lowest order in (8), the following integral equation is obtained

$$\Delta g_j = \frac{r_j^2 - r_o^2}{4\pi r_j} \iint \frac{\Delta g^*}{r_{ij}^3}\, dS \tag{9}$$

In this equation Δg^* is an unknown function at the reference sphere and Δg a function, known in discrete points at the physical surface.

Once we have a solution Δg^* to (9) we can make the following statement.

If T is harmonic and condition (6) is fulfilled at the physical surface the following relation is valid for T in space

$$-\frac{\partial T}{\partial r_j}-\frac{2T}{r_j}=\frac{r_j^2-r_o^2}{4\pi r_j}\int\int\frac{\Delta g^*}{r_{ij}^3}dS \tag{10}$$

(Here of course the notations refer to a point P_j in space.)

In order to prove this statement we introduce the following notations

$$G=-r_j\frac{\partial T}{\partial r_j}-2T$$

or with

$$r_j^2=x^2+y^2+z^2$$

$$G=-2T-\left(x\frac{\partial T}{\partial x}+y\frac{\partial T}{\partial y}+z\frac{\partial T}{\partial z}\right)$$

and

$$F=\frac{r_j^2-r_o^2}{4\pi r_o}\int\int\frac{r_o\,\Delta g^*}{r_{ij}^3}dS$$

F is harmonic outside the reference sphere and equal to $r_o\Delta g^*$ at the sphere (see [11] page 262).

G and its first derivatives are continuous. By differentiating G twice with respect to x, y and z we obtain

$$\frac{\partial^2 G}{\partial x^2}=-4\frac{\partial^2 T}{\partial x^2}-\left(x\frac{\partial^3 T}{\partial x^3}+y\frac{\partial^3 T}{\partial x^2\partial y}+z\frac{\partial^3 T}{\partial x^2\partial z}\right)$$

$$\frac{\partial^2 G}{\partial y^2}=-4\frac{\partial^2 T}{\partial y^2}-\left(x\frac{\partial^3 T}{\partial y^2\partial x}+y\frac{\partial^3 T}{\partial y^3}+z\frac{\partial^3 T}{\partial y^2\partial z}\right)$$

$$\frac{\partial^2 G}{\partial z^2}=-4\frac{\partial^2 T}{\partial z^2}-\left(x\frac{\partial^3 T}{\partial z^2\partial x}+y\frac{\partial^3 T}{\partial z^2\partial y}+z\frac{\partial^3 T}{\partial z^3}\right)$$

After introducing the operator symbol

$$\Delta=\frac{\partial^2}{\partial x^2}+\frac{\partial^2}{\partial y^2}+\frac{\partial^2}{\partial z^2}$$

we get for the sum of the second derivatives

$$\Delta G=-4\Delta T-\left(x\frac{\partial}{\partial x}+y\frac{\partial}{\partial y}+z\frac{\partial}{\partial z}\right)\Delta T\equiv 0$$

since T is harmonic outside the physical surface Hence G as well as T is harmonic everywhere in space.

Furthermore $F\equiv G$ at the physical surface according to (6) and (9).

But if two functions are harmonic outside and take the same values on a bounding surface, then they must be identical everywhere outside this surface ([11] page 134). Hence $F\equiv G$ in space and (10) is valid.

Let us study a very simple model. The model is a homogeneous sphere of radius r_o with a disturbing point mass m at the center of the sphere.

Here it is natural to define Δg as the attraction caused by the point mass m. Then (6) must be replaced $\Delta g=-\dfrac{\partial T}{\partial r}$.

If the sphere is taken as reference surface we have

$$\Delta g^*=\frac{Gm}{r_o^2}$$

where

G = gravitational constant = $6.66 \cdot 10^{-8}$ in c. g. s. units. The continuation of Δg^* in space is then

$$\Delta g_j = \frac{r_j^2 - r_o^2}{4\pi r_j} \int\int \frac{G m}{r_o^2 r_{ij}^3} dS$$

or

$$\Delta g_j = G m \frac{r_j^2 - r_o^2}{4\pi r_j} \int_o^{2\pi} \int_o^{\pi} \frac{\sin\omega}{(r_j^2 + r_o^2 - 2 r_o r_j \cos\omega)^{3/2}} d\omega\, d\lambda$$

After evaluation of the integral we obtain

$$-\frac{\partial T}{\partial r_j} = \Delta g_j = G m \frac{r_j^2 - r_o^2}{2 r_i^2 {}_o r} \left(\frac{1}{r_j - r_o} - \frac{1}{r_j + r_o} \right)$$

or

$$\Delta g_j = \frac{Gm}{r_j^2}$$

which we recognize as Newton's law of gravitation.

In the generel problem (6) must be fulfilled. At the physical surface the gravity anomaly had to be defined as the difference between g and γ taken at different heights for reasons mentioned before (4). In space we obtain the gravity disturbance as the difference between g and γ taken at the same point. Then the disturbance in space can be computed by the formula

$$g - \gamma = -\frac{\partial T}{\partial r_j} = \frac{2T}{r_j} + \frac{r_j^2 - r_o^2}{4\pi r_j} \int\int \frac{\Delta g^*}{r_{ij}^3} dS \tag{11}$$

The vertical deflection

The vertical deflection is defined in the following way

$$\xi = \frac{1}{\gamma_j} \cdot \frac{\partial T_j}{\partial x} \qquad \text{(North-South)}$$

$$\eta = \frac{1}{\gamma_j} \cdot \frac{\partial T_j}{\partial y} \qquad \text{(East-West)}$$

Here

$$\frac{\partial T}{\partial x} = \frac{1}{r_j} \frac{\partial T}{\partial \omega}_{\alpha = 0}$$

$$\frac{\partial T}{\partial y} = \frac{1}{r_j} \cdot \frac{\partial T}{\partial \omega}_{\alpha = \frac{\pi}{2}}$$

α = azimuth

Before the derivatives of T_j are determined we rewrite (7) in the more suitable form

$$T_j = \frac{1}{4\pi r_j} \int\int \Delta g^* \left(\frac{2}{r} - 3r + 1 - 5t\cos\omega_{ij} - 3t\cos\omega_{ij} 1n \frac{1 - t\cos\omega_{ij} + r}{2} \right) dS \tag{12}$$

By the aid of these expressions Bjerhammar derived the following formulas for the vertical deflection which can be used when the unknown function Δg^* has been determined.

$$\xi_j = \frac{1}{4\pi \gamma_j r_j^2} \int\int \Delta g^*\, t \sin\omega \cos\alpha\, k'\, dS \tag{13}$$

$$n_j = \frac{1}{4\pi\gamma_j r_j^2} \int\int \Delta g^* \, t \sin\omega \sin\alpha \, k' \, dS \tag{14}$$

(Generalized Vening Meinesz formulae)

where

$$k' = \frac{2}{r^3} - 8 + \frac{3(r+1)^2}{r^2\Phi} 3 \, ln \, \Phi \tag{15}$$

$$2\Phi = \frac{(r+1)^2 - t^2}{2}$$

In order to test the theories of Bjerhammar, several applications have been made, all of which have been quite successful [4], [6]. Until now, however no applications have been made to theoretical models with disturbance masses focused between the reference sphere and the physical surface. Such models cause very large oscillations in the reduced gravity anomaly field Δg^* and might be difficult to handle numerically [4].

Also the possibilities to continue the anomaly field in space have been left uninvestigated in the preceeding applications.

In this paper we have solved equation (9) for two models of the type mentioned above. As a check of our solutions the vertical deflection is computed at different points in *space* and at the *physical surface* by the aid of formula (13) and compared with the corresponding true values obtained from Newton's law of gravitation.

Since gravity measurements can only be made in a finit number of discrete points at the surface of the earth, it will never be possible to obtain a strict mathematical solution of eq. (9). Nevertheless it is allways possible to obtain a "solution" Δg^* that satisfies eq. (9) in all given points.

In this way the "final solution" is immediately obtained.

For practical applications it will often be suitable to start with a "preliminary solution" according to the method of least squares. This means that a low order solution is computed with consideral degrees of freedom ("supernumerary equations"). Then the sum of the squares of the residual gravity anomalies at the measured points is minimized. Cf. Bjerhammar 1964 p. 25 eq. 33. Here the "preliminary solution" represents the case when the residuals are neglected. However, the residuals cannot be considered as stochastic variables and therefore the preliminary solution is only a part of the final one. In order to obtain the final solution we add corresponding corrections for the residuals.

In order to obtain a preliminary solution of eq. (9) two different techniques have been used.

1. *Zero order approximation method* [4]

By substracting and adding Δg^* to the numerator of the right member of (9) we obtain

$$\Delta g_j = \frac{r_j^2 - r_o^2}{4\pi r_j} \int\int \frac{\Delta g^* - \Delta g^*_j + \Delta g^*_j}{r_{ij}^3} dS \tag{16}$$

Since Δg^*_j is constant with respect to the integration

$$\frac{r_j^2 - r_o^2}{4\pi r_j} \int\int \frac{\Delta g^*_j}{r_{ij}^3} dS = \left(\frac{r_o}{r_j}\right)^2 \Delta g^*_j \approx \Delta g^*_j \tag{17}$$

Hence

$$\Delta g^*_j = \Delta g_j + \frac{r_j^2 - r_o^2}{4\pi r_j} \int\int \frac{\Delta g^*_j - \Delta g^*}{r_{ij}^3} dS \tag{18}$$

with the first iterative solution

$$\Delta g^*_j = \Delta g_j + \frac{r_j^2 - r_o^2}{4\pi r_j} \int\int \frac{\Delta g_j - \Delta g}{r_{ij}^3} dS \tag{19}$$

or

$$\Delta g^*_j = 2\Delta g_j - \frac{r_j^2 - r_o^2}{4\pi r_j} \int\int \frac{\Delta g}{r_{ij}^3} dS \tag{20}$$

By the aid of formula (20) we can generate a Δg^*-field which can be used for determination of other quantities, for instance the vertical deflection.

Vertical deflections for this solution are given in tables 3–6.

The accuracy of the solution, however, is comparatively low but could be increased by the following procedure.

The Δg^*-field should satisfy (9). Therefore an estimate of the error in our solution is

$$\delta \Delta g_j = \Delta g_j - \frac{r_j^2 - r_o^2}{4\pi r_j} \int\int \frac{\Delta g^*}{r_{ij}^3} dS \tag{21}$$

To this residual-field $\delta \Delta g$ we could apply the zero order approximation

$$\delta \Delta g^*{}_j g_j = 2\delta \Delta g_j - \frac{r_j^2 - r_o^2}{4\pi r_j} \int\int \frac{\delta \Delta g}{r_{ij}^3} dS \tag{22}$$

From the new solution $\Delta g^* + \delta \Delta g^*$ a new residual-field can be determined and so on. The procedure can be repeated as long as the residual-field is decreasing in magnitude.

It should be noted that the method is time-consuming since every determination of a point in the Δg^*-field necessitates the evaluation of two integrals at each stage in the procedure according to (21) and (20) or (22).

2. *Height-parameter solution* [4]

We approximate Δg^* by a polynomial in h in the following way

$$\Delta g^* = \Delta g + c_1 h + c_2 h^2 + \ldots + c_{m-1} h^{m-1} + c_m h^m \tag{23}$$

where

Δg = anomaly at the physical surface
h = height above the reference sphere
c_i = unknown constants

For the determination of the polynomial coefficients c_i we use the fact that Δg^* should satisfy (9). Of course it is normally impossible to satisfy (9) in every point. Instead we pick out n ($n \geq m$) discret points which gives us the following linear equation system

$$\left\{\begin{array}{l} a_{11} c_1 + a_{12} c_2 + \ldots + a_{1m} c_m = \Delta G_1 \\ a_{21} c_1 + a_{22} c_2 + \ldots + a_{2m} c_m = \Delta G_2 \\ \cdot \\ \cdot \\ \cdot \\ a_{n1} c_1 + a_{n2} c_2 + \ldots + a_{nm} c_m = \Delta G_m \end{array}\right. \tag{24}$$

where

$$a_{jk} = \frac{r_j^2 - r_o^2}{4\pi r_j} \int\int \frac{h^k}{r_{ij}^3} dS \tag{25}$$

$$\Delta G_j = \Delta g_j - \frac{r_j^2 - r_o^2}{4\pi r_j} \int\int \frac{\Delta g}{r_{ij}^3} dS \tag{26}$$

Here a_{jk} and ΔG_j are determined by numerical integration.

If the rank of the system is equal to m equation (9) is satisfied in all our discret points and a final solution is obtained. It has been found convinient, however, to have the rank greater than m and solve the system according to the method of least squares [1]. Then (9) is satisfied in none of the discrete points but instead we have a much better fit to the Δg-field in general.

Descriptions of the models

Two test models have been used. In both cases the reference sphere is replaced by a plane

in order to simplify the computations. As a consequence of this the boundary condition, which is used to generate the given Δg values, is changed to

$$\Delta g = -\frac{\partial T}{\partial n} \tag{27}$$

Both models have the same topographical shape. A cone of height 4.1 km and radius at the base 24.6 km, which is placed on the reference plane. The difference in the models lies in the distribution of the disturbing masses.

Model No. 1: Two point masses are located on the axis of the cone. One (m_1) 4 km below and the other (m_2) 2 km above the plane. The vertical components of attraction of the point masses at the vertex are 148.154 and 95.295 mgal respectively. The masses are then $m_1 \approx 145.798 \,.\, 10^{13}$ kg and $m_2 \approx 6.334 \,.\, 10^{13}$ kg. (Yeremeyev's model)

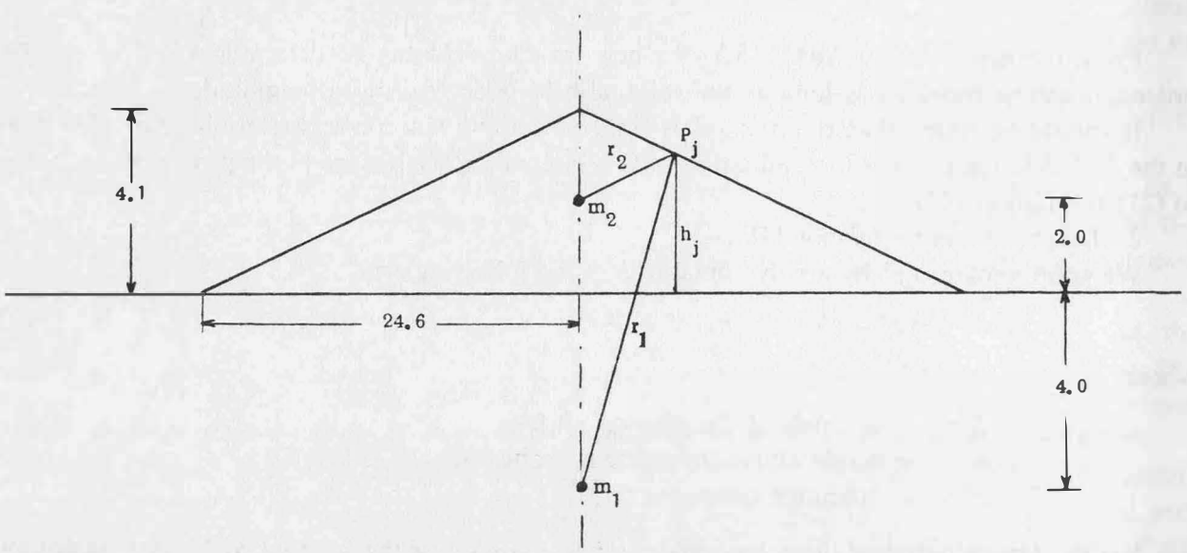

Fig. 2.

The gravity anomalies are considered to be given at the surface of the cone and in the plane beyond the cone, and are computed by the formula

$$\Delta g = -\frac{\partial T}{\partial n} = Gm_1 \frac{\cos(n, r_1)}{r_1^2} + Gm_2 \frac{\cos(n, r_2)}{r_2^2} \tag{28}$$

The true vertical deflection ξ_j at the point P_j on the surface or in space is obtained as the ratio between the horizontal component of the gravity anomaly at P_j and the theoretical gravity γ_j. Hence

$$\xi_j = \frac{G}{\gamma_j}\left(m_1 \frac{\sin(n, r_1)}{r_1^2} + m^2 \frac{\sin(n, r_2)}{r_2^2}\right) \tag{29}$$

where r_1 and r_2 are the distances from P_j to m_1 and m_2.

The values of the true vertical deflection at the surface of the cone and in space is given in Table 1.

Model No. 2: A rod of infinitesimal thickness and of 6 km lenght is placed along the cone axis from a point A 4 km beneath the plane to a point B 2 km above. (Because of the symmetry of the model only a cut along the axis is studied.).

The density is a linear function of the relative position on the rod. By introducing a coordinate system according to fig. 3 the density function can be written

$$\sigma(z) = c \,.\, (z - z_B) \qquad\qquad z_B \leq z \leq z_A \tag{30}$$

where c is a suitable constant. In c. g. s. units the constant is $c = 0.5 \,.\, 10^7$. Then the total mass of the rod is $90 \,.\, 10^{13}$ kg and the corresponding attraction at the vertex of the cone 202.856 mgal.

TABLE 1

Model 1

True vertical deflection at the physical surface and in space.

L	h	ξ_o	$\xi_{5\,KM}$	$\xi_{10\,KM}$	$\xi_{15\,KM}$	$\xi_{20\,KM}$	$\xi_{25\,KM}$
0.0	4.1	0".00000	0".00000	0".00000	0".00000	0".00000	0".00000
0.6	4.0	8.20522	3.52527	0.54880	0.20274	0.09778	0.05465
1.2	3.9	14.16207	6.42513	1.08522	0.40342	0.19497	0.10907
1.8	3.8	16.82767	8.47921	1.59789	0.60006	0.29100	0.16306
2.4	3.7	17.69961	9.81754	2.07725	0.79080	0.38530	0.21640
3.0	3.6	17.99966	10.66106	2.51602	0.97392	0.47735	0.26888
3.6	3.5	18.15612	11.17868	2.90936	1.14796	0.56666	0.32031
4.2	3.4	18.22592	11.47052	3.25469	1.31168	0.65278	0.37051
4.8	3.3	18.17447	11.59253	3.55139	1.46408	0.73531	0.41930
5.4	3.2	17.97281	11.57907	3.80036	1.60445	0.81392	0.46653
6.0	3.1	17.61678	11.45536	4.00367	1.73230	0.88830	0.51206
6.6	3.0	17.12232	11.24284	4.16418	1.84740	0.95824	0.55575
7.2	2.9	16.51642	10.96080	4.28528	1.94973	1.02355	0.59752
7.8	2.8	15.82968	10.62657	4.37061	2.03944	1.08412	0.63726
8.4	2.7	15.09139	10.25543	4.42394	2.11685	1.13989	0.67490
9.0	2.6	14.32698	9.86036	4.44899	2.18243	1.19082	0.71039
9.6	2.5	13.55703	9.45214	4.44939	2.23673	1.23696	0.74370
10.2	2.4	12.79732	9.03940	4.42853	2.28038	1.27836	0.77479
10.8	2.3	12.05926	8.62888	4.38962	2.31409	1.31513	0.80366
11.4	2.2	11.35067	8.22568	4.33555	2.33856	1.34739	0.83032
12.0	2.1	10.67646	7.83353	4.26898	2.35454	1.37532	0.85478
12.6	2.0	10.03934	7.45504	4.19226	2.36278	1.39908	0.87708
13.2	1.9	9.44039	7.09193	4.10747	2.36401	1.41888	0.89726
13.8	1.8	8.87949	6.74521	4.01647	2.35893	1.43491	0.91537
14.4	1.7	8.35571	6.41539	3.92082	2.34822	1.44739	0.93147
15.0	1.6	7.86759	6.10254	3.82191	2.33252	1.45655	0.94562
15.6	1.5	7.41333	5.80644	3.72089	2.31246	1.46261	0.95790
16.2	1.4	6.99096	5.52668	3.61876	2.28857	1.46578	0.96838
16.8	1.3	6.59841	5.26269	3.51635	2.26141	1.46628	0.97714
17.4	1.2	6.23363	5.01381	3.41433	2.23143	1.46434	0.98426
18.0	1.1	5.89463	4.77930	3.31327	2.19909	1.46015	0.98982
18.6	1.0	5.57947	4.55842	3.21364	2.16477	1.45391	0.99392
19.2	0.9	5.28633	4.35042	3.11578	2.12885	1.44583	0.99663
19.8	0.8	5.01351	4.15454	3.01999	2.09165	1.43606	0.99803
20.4	0.7	4.75942	3.97005	2.92649	2.05346	1.42480	0.99822
21.0	0.6	4.52259	3.79624	2.83544	2.01453	1.41221	0.99727
21.6	0.5	4.30165	3.63245	2.74696	1.97509	1.39842	0.99526
22.2	0.4	4.09535	3.47802	2.66112	1.93535	1.38360	0.99226
22.8	0.3	3.90255	3.33237	2.57796	1.89548	1.36786	0.98836
23.4	0.2	3.72218	3.19491	2.49750	1.85563	1.35133	0.98363
24.0	0.1	3.55329	3.06512	2.41973	1.81595	1.33413	0.97812
24.6	0.0	3.39500	2.94250	2.34464	1.77654	1.31636	0.97192

ξ_o = vertical deflection at the physical surface.
ξ_5 km = vertical deflection 5 km above the reference surface.

L = distance from the cone axis (km).
h = height of the model above the reference surface (km).

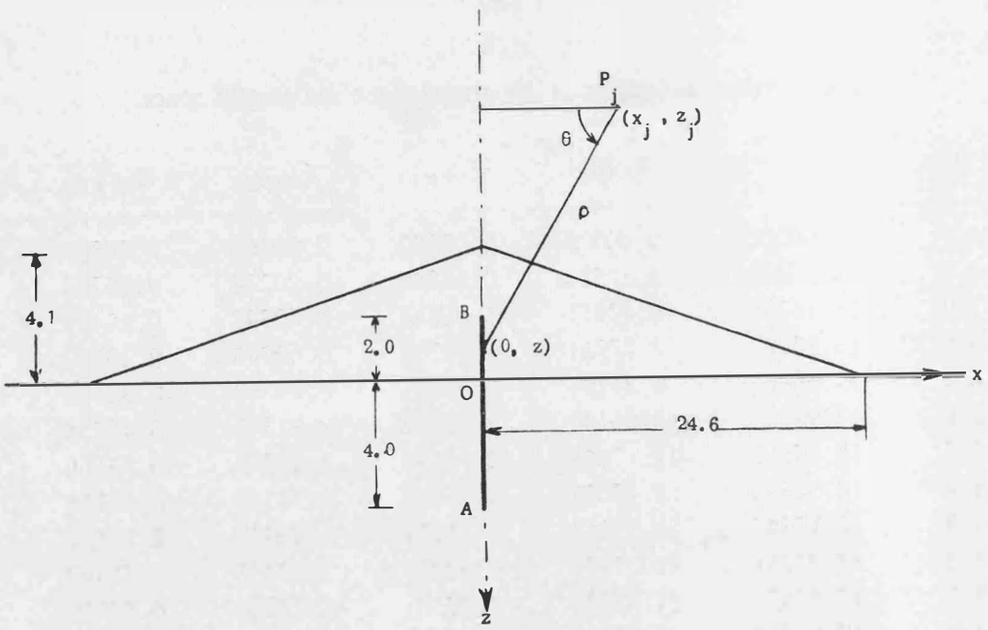

Fig. 3

At a point P_j with coordinates (x_j, z_j) the disturbance potential is

$$T = G \int_{z_1}^{z_A} \frac{\sigma(z)}{\rho} \, dz \tag{31}$$

where

ρ = distance from P_j to the element of integration.

Hence we have

$$\frac{\partial T}{\partial x_j} = -G \int_{z_B}^{z_B} \frac{\sigma(z) \cos\theta}{\rho^2} \, dz \tag{32}$$

$$\frac{\partial T}{\partial z_j} = G \int_{z_B}^{z_A} \frac{\sigma(z) \sin\theta}{\rho^2} \, dz \tag{33}$$

By the transformation $z - z_j = x_j tg\theta$ we get

$$\frac{\partial T}{\partial x_j} = -G \int_{z_B}^{z_A} \sigma \cos\theta \, d\theta \qquad \frac{\partial T}{\partial z_j} = G \int_{z_B}^{z_A} \sigma \sin\theta \, d\theta$$

After evaluation of the integrals we have

$$\frac{\partial T}{\partial x_j} = -\frac{G.c}{x_j} \left\{ (z_j - z_B)(\sin\theta_A - \sin\theta_B) + x_j(\cos\theta_B - \cos\theta_A) \right\}$$

$$\frac{\partial T}{\partial z_j} = \frac{G.c}{x_j} \left\{ \left(z_j - z_B \right)(\cos\theta_B - \cos\theta_A) - x_j(\sin\theta_A - \sin\theta_B) + \right.$$

$$\left. + x_j ln \left[tg \left(\frac{\pi}{4} + \frac{\theta_A}{2} \right) : tg \left(\frac{\pi}{4} + \frac{\theta_B}{2} \right) \right] \right\}$$

TABLE 2

Model 2

True vertical deflection at the physical surface and in space.

L	h	ξ_o	$\xi_{5\ KM}$	$\xi_{10\ KM}$	$\xi_{15\ KM}$	$\xi_{20\ KM}$	$\xi_{25\ KM}$
0.0	4.1	0".00000	0".00000	0".00000	0".00000	0".00000	0".00000
0.6	4.0	5.69800	3.05344	0.48054	0.16094	0.07291	0.03910
1.2	3.9	11.01071	5.77049	0.94861	0.31995	0.14531	0.07801
1.8	3.8	15.06323	7.93467	1.39270	0.47517	0.21671	0.11658
2.4	3.7	17.63322	9.48270	1.80305	0.62487	0.28662	0.15461
3.0	3.6	18.92577	10.46217	2.17222	0.76749	0.35461	0.19196
3.6	3.5	19.26798	10.97262	2.49528	0.90170	0.42025	0.22846
4.2	3.4	18.96135	11.12380	2.76981	1.02642	0.48318	0.26397
4.8	3.3	18.24184	11.01479	2.99563	1.14083	0.54307	0.29836
5.4	3.2	17.28128	10.72675	3.17434	1.24438	0.59965	0.33150
6.0	3.1	16.19947	10.32245	3.30892	1.33675	0.65270	0.36328
6.6	3.0	15.07702	9.84866	3.40326	1.41788	0.70206	0.39361
7.2	2.9	13.96609	9.33915	3.46175	1.48792	0.74760	0.42242
7.8	2.8	12.89879	8.81767	3.48896	1.54716	0.78927	0.44965
8.4	2.7	11.89339	8.30041	3.48944	1.59607	0.82704	0.47524
9.0	2.6	10.95885	7.79804	3.46747	1.63520	0.86094	0.49916
9.6	2.5	10.09808	7.31724	3.42701	1.66521	0.89102	0.52139
10.2	2.4	9.31012	6.86183	3.37165	1.68680	0.91739	0.54193
10.8	2.3	8.59176	6.43368	3.30451	1.70068	0.94016	0.56078
11.4	2.2	7.93850	6.03330	3.22834	1.70758	0.95948	0.57796
12.0	2.1	7.34529	5.66030	3.14546	1.70825	0.97551	0.59349
12.6	2.0	6.80692	5.31371	3.05787	1.70336	0.98843	0.60742
13.2	1.9	6.31827	4.99225	2.96719	1.69359	0.99842	0.61978
13.8	1.8	5.87453	4.69439	2.87480	1.67958	1.00568	0.63063
14.4	1.7	5.47121	4.41857	2.78180	1.66190	1.01040	0.64001
15.0	1.6	5.10422	4.16320	2.68908	1.64109	1.01278	0.64800
15.6	1.5	4.76983	3.92673	2.59734	1.61766	1.01300	0.65465
16.2	1.4	4.46471	3.70767	2.50715	1.59203	1.01125	0.66003
16.8	1.3	4.18585	3.50463	2.41893	1.56463	1.00772	0.66421
17.4	1.2	3.93060	3.31630	2.33299	1.53580	1.00258	0.66725
18.0	1.1	3.69657	3.14147	2.24956	1.50586	0.99600	0.66924
18.6	1.0	3.48163	2.97902	2.16880	1.47510	0.98812	0.67022
19.2	0.9	3.28390	2.82794	2.09082	1.44376	0.97910	0.67028
19.8	0.8	3.10171	2.68728	2.01565	1.41205	0.96908	0.66947
20.4	0.7	2.93355	2.55619	1.94331	1.38017	0.95818	0.66787
21.0	0.6	2.77810	2.43389	1.87379	1.34826	0.94652	0.66553
21.6	0.5	2.63417	2.31967	1.80706	1.31648	0.93420	0.66251
22.2	0.4	2.50070	2.21287	1.74304	1.28492	0.92135	0.65888
22.8	0.3	2.37674	2.11291	1.68168	1.25370	0.90803	0.65468
23.4	0.2	2.26146	2.01926	1.62290	1.22289	0.89434	0.64998
24.0	0.1	2.15407	1.93141	1.56661	1.19257	0.88034	0.64481
24.6	0.0	2.05392	1.84893	1.51272	1.16277	0.86612	0.63923

ξ_o = vertical deflection at the physical surface.

$\xi_{5\ km}$ = vertical deflection 5 km above the reference surface.

L = distance from the cone axis (km).

h = height of the model above the reference surface (km).

By introducing the height as $h_j = -z_j$ we obtain

$$\sin\theta_A = \frac{h_j+4}{\sqrt{(h_j+4)^2+x_j^2}} \qquad \cos\theta_A = \frac{x_j}{\sqrt{(h_j+4)^2+x_j^2}}$$

$$\sin\theta_B = \frac{h_j-2}{\sqrt{(h_j-2)^2+x_j^2}} \qquad \cos\theta_B = \frac{x_j}{\sqrt{(h_j-2)^2+x_j^2}}$$

which finally gives

$$\frac{\partial T}{\partial x_j} = 333\left\{\frac{h_j-2}{x_j}\left(\frac{h_j+4}{\sqrt{(h_j+4)^2+x_j^2}} - \frac{h_j-2}{\sqrt{(h_j-2)^2+x_j^2}}\right) + \right.$$

$$\left. + \frac{x_j}{\sqrt{(h_j-2)^2+x_j^2}} - \frac{x_j}{\sqrt{(h_j+4)^2+x_j^2}}\right\} mgal \tag{34}$$

$$\frac{\partial T}{\partial z_j} = 333\left\{\ln\frac{\sqrt{(h_j+4)^2+x_j^2}+h_j+4}{\sqrt{(h_j-2)^2+x_j^2}+h_j-2} - \frac{6}{\sqrt{(h_j+4)^2+x_j^2}}\right\} mgal \tag{35}$$

From these expressions it is possible to obtain the given gravity anomalies at the surface and the true vertical deflection in space and at the surface since

$$\Delta g_j = -\frac{\partial T}{\partial n} = \frac{\partial T}{\partial z_j} \tag{36}$$

$$\xi_j = -\frac{1}{\gamma_j}\frac{\partial T}{\partial x_j} \qquad \text{radians} \tag{37}$$

Table 2 gives the true vertical deflection at the surface of the cone and in space for model No. 2. For the numerical application three different types of integrals have to be evaluated

1) $$\frac{r_j^2 - r_o^2}{4\pi r_j}\int\int \frac{\Delta g}{r_{ij}^3}\,dS$$

2) $$\frac{r_j^2 - r_o^2}{4\pi r_j}\int\int \frac{h^k}{r_{ij}^3}\,dS$$

3) $$\frac{1}{4\pi\gamma_j r_j^2}\int\int t\,\Delta g^* \sin\omega\cos\alpha\, k'\, dS$$

Before the numerical integration was carried out the integrals were rewritten in the following way (l and α are polar coordinates)

1) $$\frac{h_j}{\pi}\int_0^{100}\int_0^{\pi}\frac{\Delta g}{r_{ij}^3}\,l\,d\alpha\,dl \qquad \text{(lengths in km)} \tag{38}$$

2) $$\frac{h_j}{\pi}\int_0^{26.4}\int_0^{\pi}\frac{h^k}{r_{ij}^3}\,l\,d\alpha\,dl \qquad \text{(lengths in km)} \tag{39}$$

3) $$\frac{1}{2\pi\gamma_j r_j^3}\int_0^{100}\int_0^{\pi}\Delta\ ^*\,l^2\,k'\cos\alpha\,d\alpha\,dl \qquad \text{(lengths in km)} \tag{40}$$

where

r_{ij} = distance between the element of integration and the actual point P_j (km)

h_j = height above the plane (km)

$$k' = \frac{2}{r^3} - 8 + \frac{3(1+r)}{r2\Phi} - 3ln\Phi$$

$$2\Phi = \frac{(1+r)^2 - t^2}{2}$$

$r = r_{ij}/(6370 + h_j)$

$t = 6370/(6370 + h_j)$

α = azimuth (The vertex of the cone as North-Pole)

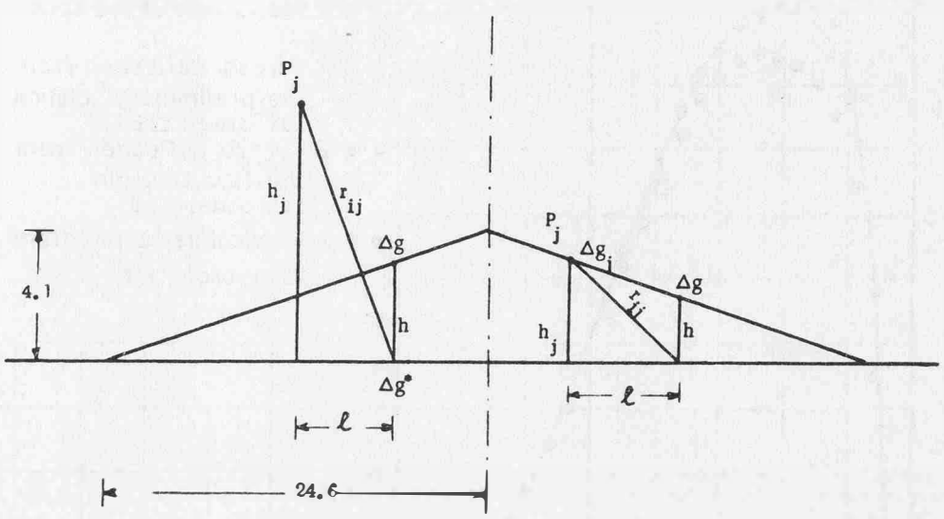

Fig. 4.

The left side of the fig. 4 shows the princip of integration for a point P_j in space the right side for a point at the physical surface.

Application of the zero order approximation method to model No. 1

By formula (20) Δg^* was computed in 100 equidistant points, 0—24.6 km from the cone axis. Simultaneously residuals were determined in the corresponding points at the surface of the cone by the simple formula

$$\delta \Delta g_j = \Delta g^*_j - \Delta g_j \tag{41}$$

Beyond the cone Δg^* was taken equal to Δg.

From the preliminary solution the vertical deflection was computed by formula (13) in 41 points along the cone slope and at different levels in space. For the determination of the influence of the residuals on the vertical deflection it was considered to be sufficient to apply the classical formula of Vening Meinesz to the residuals. The final solution was obtained by adding the result from this application to the result from the preliminary solution.

The results from the computations are presented in the following tables and diagrams. Table 3.*) and 5. give the vertical deflection from the preliminary and final solutions respectively. In Table 4. and 6. the corresponding errors are given. The last row in Table 4. and 6. represents the "standard error" s (no statistical parameter) at the actual level defined as

$$s^2 = \sum_{i=1}^{41} \frac{\varepsilon_i^2}{41} \tag{42}$$

*) This paper is only part of the complete text published Stockholm 1966.

THE MODEL OF YEREMEYEV-MOLODENSKY SOLVED ACCORDING TO BJERHAMMAR

1st order fit is made in two steps.
10th order fit is made in one step.

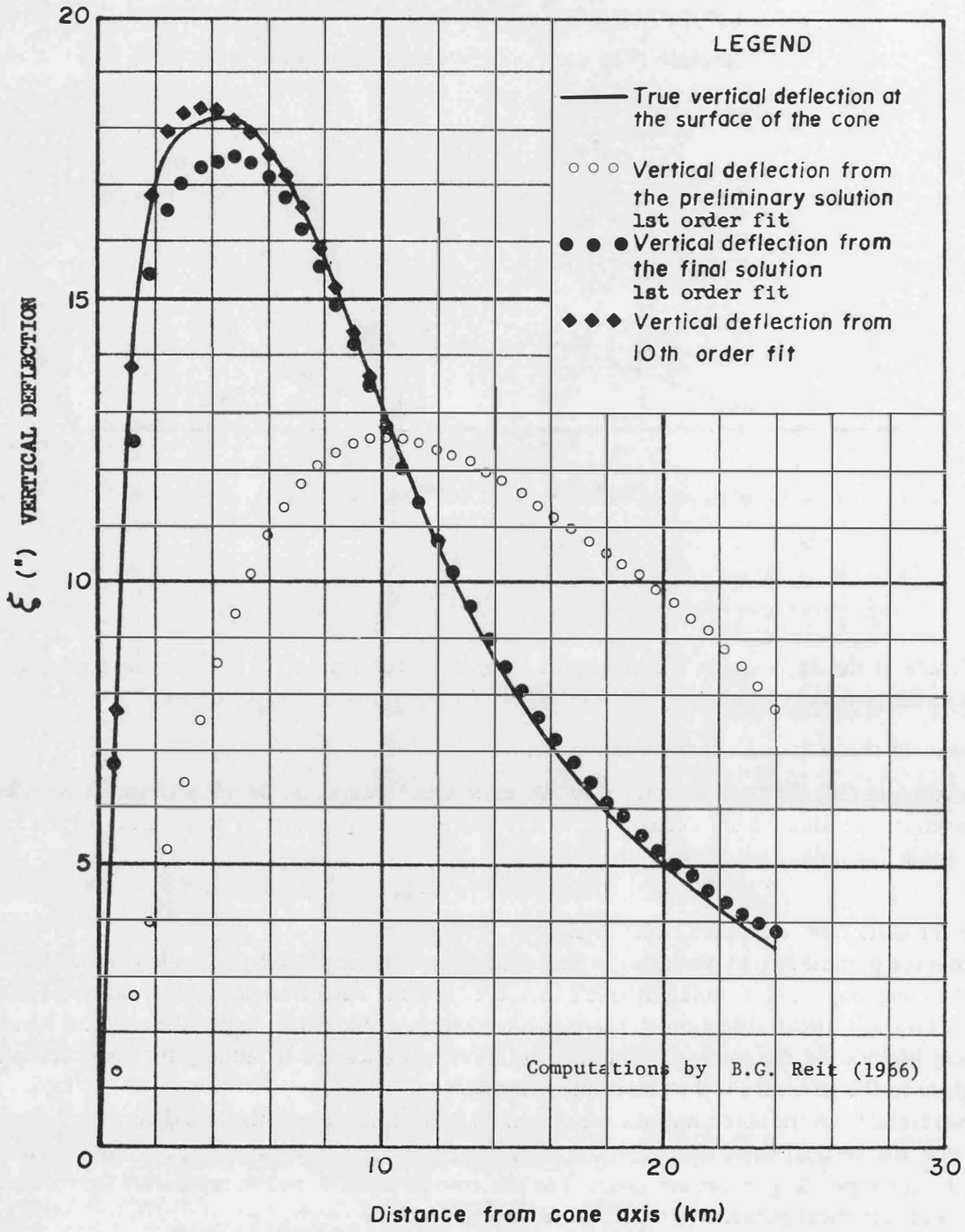

THE MODEL OF YEREMEYEV-MOLODENSKY SOLVED ACCORDING TO BJERHAMMAR

20^{th} order fit

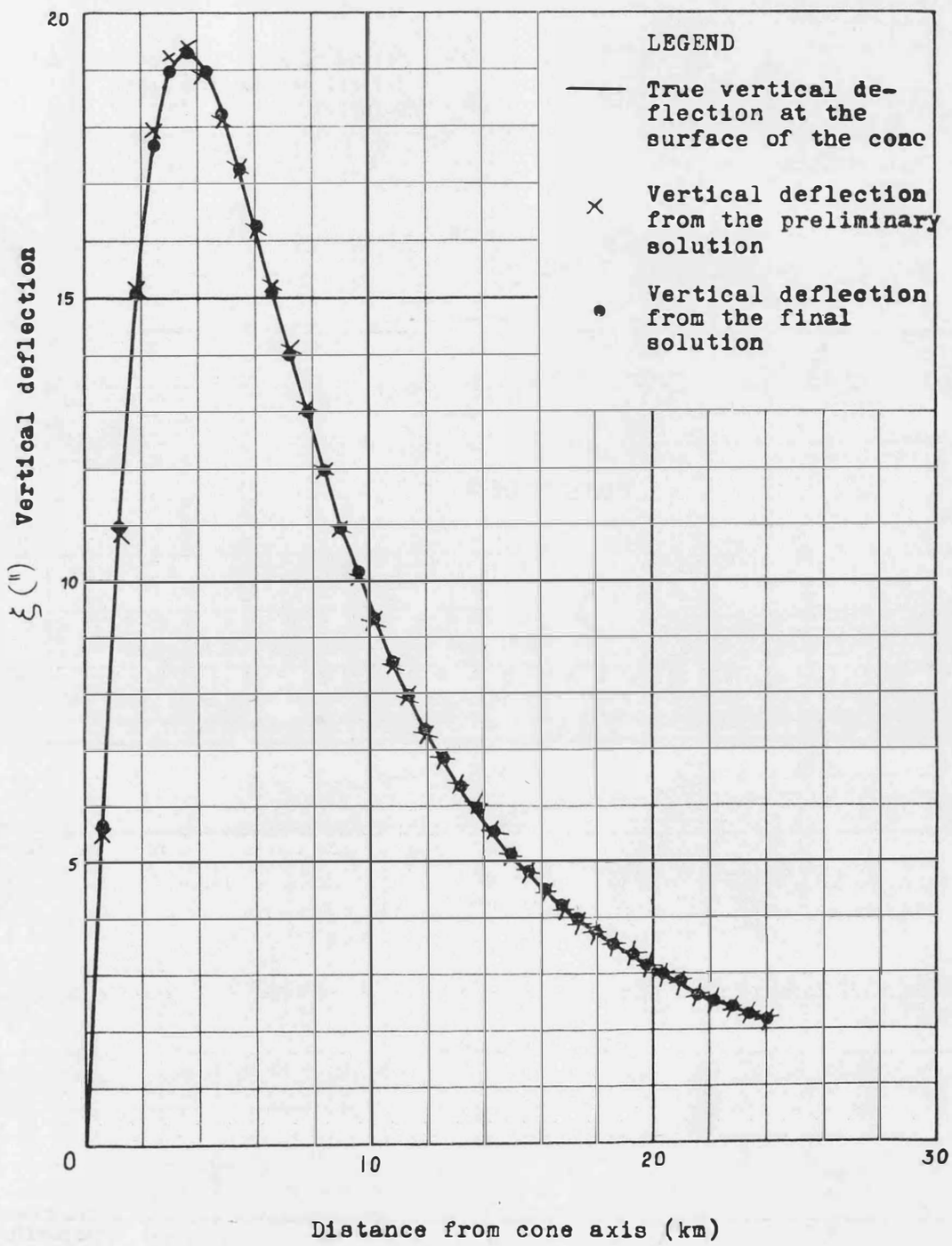

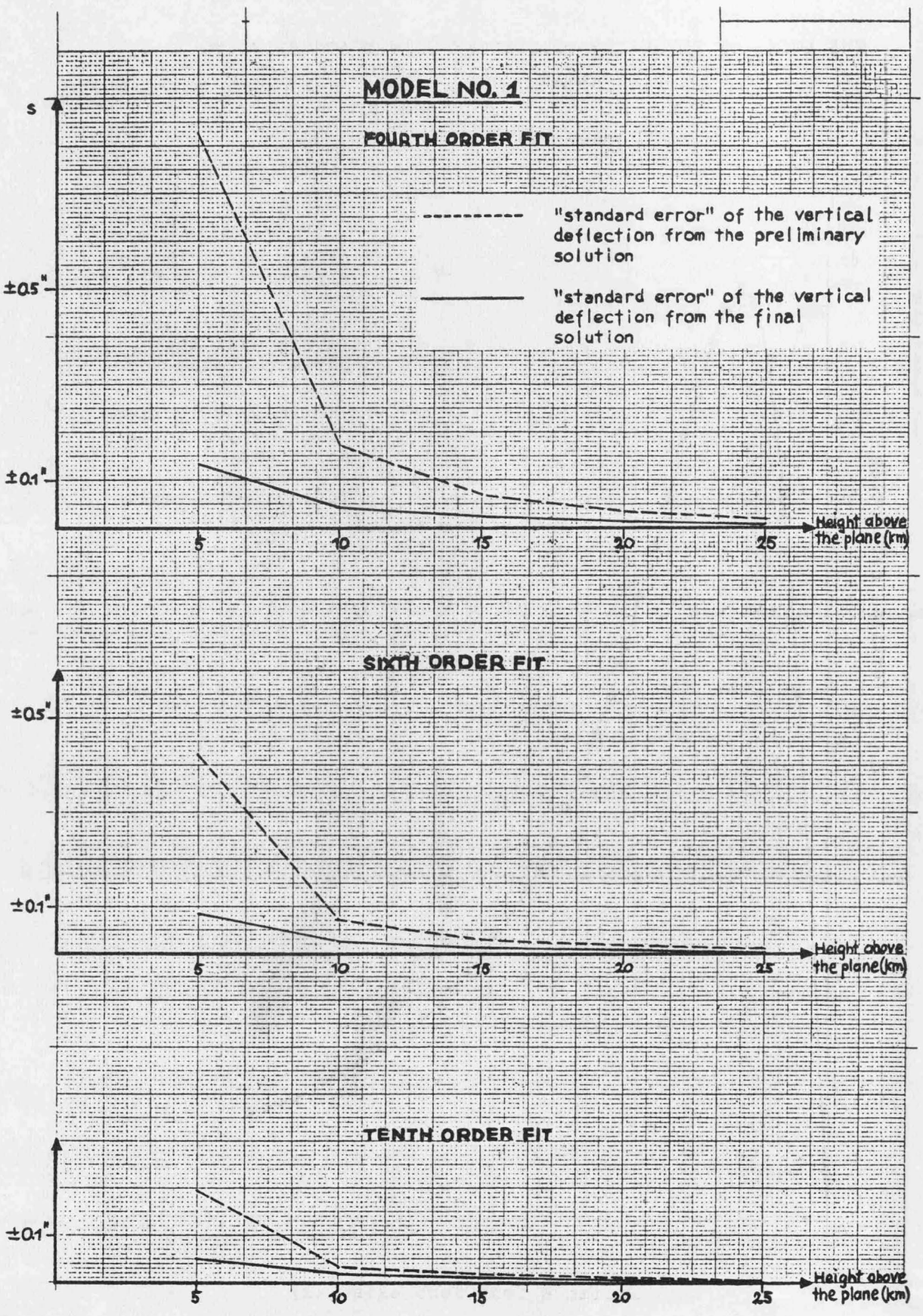
MODEL NO. 1
FOURTH ORDER FIT
s
±0.5"
±0.1"
"standard error" of the vertical deflection from the preliminary solution
"standard error" of the vertical deflection from the final solution
5
10
15
20
25
Height above the plane (km)
SIXTH ORDER FIT
±0.5"
±0.1"
5
10
15
20
25
Height above the plane (km)
TENTH ORDER FIT
±0.1"
5
10
15
20
25
Height above the plane (km)

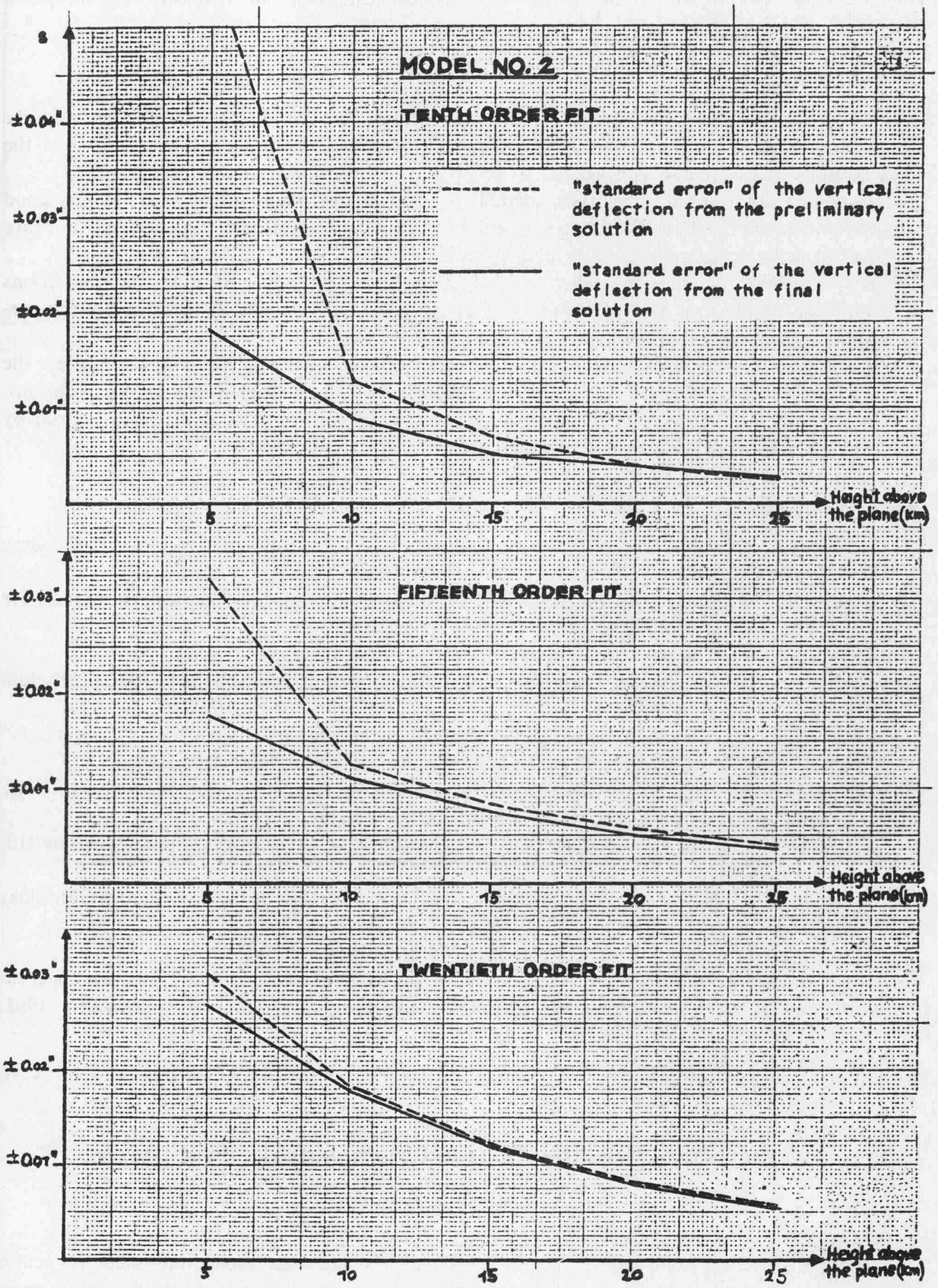
MODEL NO. 2
TENTH ORDER FIT
"standard error" of the vertical deflection from the preliminary solution
"standard error" of the vertical deflection from the final solution
±0.04"
±0.03"
±0.02"
±0.01"
5
10
15
20
25
Height above the plane(km)
FIFTEENTH ORDER FIT
±0.03"
±0.02"
±0.01"
Height above the plane(km)
TWENTIETH ORDER FIT
±0.03"
±0.02"
±0.01"
Height above the plane(km)

where

ε_i = error in the computed vertical deflection

(In the summation the number in the first row has been excluded. This row was only computed as a check of the programming.)

Conclusions:

1:0 For ill-behaved theoretical models, with mass focused between the reference sphere and the physical surface, low order fits give preliminary solutions where a considerable part of the original gravity anomaly is neglected.

2:0 In the final solutions all the gravity anomaly is taken care of. These solutions are in very good agreement with the theoretical values. Normally, preliminary solutions of high accuracy improve the final solution to the limit of rounding errors.

3:0 In space the errors diminish when the height increases. At higher altitudes the corrections employed do not improve the final results. However, at such heights the accuracy of the preliminary solution will probably be sufficient.

4:0 In solutions of very high order rounding errors from the numerical processes will affect the solution. These errors can to some extent be avoided by using multiple-precision computations.

5:0 In the present study no other limitations of accuracy have been found than those given by the boundary value and the rounding off-errors.

References

1) *Bjerhammar, A.:* A Generalized Matrix Algebra, Royal Institute of Technology, Geodesy Division, Stockholm 1958.

2) *Bjerhammar, A.:* Solution of the Resolvent Equation by the Aid of Spherical Harmonics for a Nonspherical Surface, 12. Assembly IUGG Helsinki 1960.

3) *Bjerhammar, A.:* Gravity Reduction to a Spherical Surface, Stockholm 1962.

4) *Bjerhammar, A.:* Gravimetric Geodesy Tree of Density Estimates through Analysis of Discrete Gravity Data. Fort Belvoir 1963.

5) *Bjerhammar, A.:* A Solution of the Gravimetric Boundary Value Problem for a "Continuous" Gravity Field. Royal Institute of Technology, Geodesy Division, Stockholm 1965.

6) *Förstner, W.:* Investigation of Bjerhammar's New Gravity Reduction Method. Royal Institute of Technology, Geodesy Division, Stockholm 1964.

7) *Heiskanen, W. A. and Vening Meinesz, F. A.:* The Earth and its Gravity Field. McGraw-Hill Book Co. Inc., New York.1958.

8) *Hirvonen, R. A.:* New Theory of the Gravimetric Geodesy. Publ. of the Isostatic Inst. Helsinki 1960.

9) *Lanczos, C.:* Applied Analysis. Prentice-Hall Mathematics Series, 1961.

10) *Molodensky, M. S.; Eremeev, V. F.; Yurkina, M. I.:* Methods for a Study of the External Gravitational Field and Figure of the Earth. Israel Progr. for Sc. Transl. Jerusalem 1962. (Russian book: Moskva 1960.)

11) *Mac Millan, W. D.:* The Theory of the Potential. Dover Publ., Inc., New York.

About Some Results in the Czechoslovak Test Area

by *Miloš Pick, Ivan Pola,* Prague

In the High Fatras mountains a new Czechoslovak test area has been established. Its centre is Laplace's point Križná. In the nearest surroundings of this point a complementary gravity survey has been carried out (see Tab. 1):

For a 50 km square in this test area gravimetric deflections of the vertical and the heights of the quasigeoid have been computed using Molodensky's method.

Tab. 1

Distance from the initial point	Number of points	Accuracy	
		in the gravity	in the height
0			
0,25 km	20	± 0,07 mgl	± 0,08 m
3,5 km	62	± 0,05 mgl	± 0,10 m
	1 point / 5 km²	better than ± 0,5 mgl	better than ± 0,3 m

Let us divide the area of integration into two parts: the inner area to the 50 kms from the fixed point and the distant zones. The determination of the influence of the distant zones is not difficult. The effect of the inner area was established in zero, first and second approxiamations

$$\zeta = \frac{1}{2\pi\gamma}\int\frac{1}{r_o}(\Delta g + G_1 + G_2)\,d\sigma\,,$$

$$\xi'' = -\frac{\rho''}{2\pi\gamma}\int\frac{1}{r_o^2}\Delta g\cos A\,d\sigma - \frac{\rho''}{2\pi\gamma}\int\frac{1}{r_o^2}G_1\cos A\,d\sigma - \frac{\rho''}{\gamma}\Delta g\frac{\partial H}{R\,\partial\varphi} -$$

$$- \frac{\rho''}{2\pi\gamma}\int\frac{1}{r_o^2}G_2\cos A\,d\sigma + \frac{3\rho''}{4\pi\gamma}\int\frac{\Delta H^2\,.\,\Delta g}{r_o^4}\cos A\,d\sigma - \frac{\rho''}{\gamma}G_1\frac{\partial H}{R\,\partial\varphi}\,,$$

$\eta'' =$ analogously.

The magnitude of Molodensky's functions G_1, G_2 is evident from the maps. We can also see that the used method converges very well.

The results were compared with 6 astro-geodetic deflections of the vertical, and after transforming to the common system, the deviations in Tab. 2 were found.

Tab. 2

Point	$\eta_A - \eta_G$	$\xi_A - \xi_G$
1	− 0,18″	− 0,95″
2	+ 0,02″	+ 0,45″
3	+ 0,92″	− 0,75″
4	− 1,18″	+ 0,55″
5	+ 0,92″	+ 0,65″
6	− 0,48″	+ 0,05″

It has been shown that the procedure used in the High Fatras as well as the program prepared for the electronic computer is applicable for high mountain territory and that the results are representative and reproducible with a sufficient accuracy. This procedure will be used in the West Alps test area as well.

The Extension of the Gravity Field in South Australia*)

by *R. S. Mather*, Kensington N. S. W., Australia

Summary:

A uniform geodetic gravity network has been compiled from all gravity data available over the state of South Australia. Mean free air anomalies for $^1/_2{}^0 \times {}^1/_2{}^0$, $1^0 \times 1^0$ and $2^0 \times 2^0$ squares are computed in all regions where gravity data are available. The sample is analysed for the mean free air anomaly which best represents each area. The errors of representation computed are in general agreement with Hirvonen's values. The extension of this field to unsurveyed areas is attempted using a least squares fit of a two-dimensional trigonometrical series, which is periodic in character. The accuracy of the values so obtained is studied.

Introduction

Gravity surveys have been in progress in South Australia for over 20 years (Thyer, 1963). The overall control has been provided by the Authority of the Commonwealth of Australia, the Bureau of Mineral Resources, Geology and Geophysics (B. M. R.) (Dooley et al, 1961: Dooley, 1965). Subsidiary gravity surveys have been carried out by the South Australian Department of Mines, and by various petroleum exploration companies. These surveys, some of which are quite extensive, are often based on arbitrary datums for both height and gravity and considerable time was spent unifying the surveys onto the national datum (Mather, 1966b). This national datum, established by the Isogal Regional Gravity Survey, was based on the value of 979,979.0 mgal at the National Gravity Base Station at Melbourne.

All available gravity readings in the region bounded by the parallels 26^0 S and 40^0 S and the meridians 128^0 E and 142^0 E were considered in compiling the sample. The area is reasonably flat with a mean elevation of 120 meters, the maximum and minimum $1^0 \times 1^0$ square mean elevations being 565 meters and $-$ 275 meters respectively. (The regions beyond the continental shelf area were not considered). The Western half of the state is part of the pre-Cambrian granitic shield, extending further westward and is semi-desert in character. The rock formations are essentially sedimentary, being generally cainozoic with some proterozoic formations in the hilly regions.

The Sample

The representation of the mean anomaly of a square by the mean value of all the observed gravity readings has generally been considered to be unacceptable (e. g. Jeffreys, 1941) as any tendency for the sample to be unevenly distributed in a square could lead to misconceptions as regards the accuracy of the mean anomaly obtained. A more representative sample is obtained by subdividing each square into equi-areal sections, representing the gravity field in each section by a single anomaly and computing the areal mean from these representative anomalies. In the present analysis, the basic square unit considered was the $^1/_2{}^0 \times {}^1/_2{}^0$ square. $0.1^0 \times 0.1^0$ squares were chosen as the basic sub-divisional unit within the $^1/_2{}^0 \times {}^1/_2{}^0$ square as these would be less than 3 times the basic spacing of gravity stations for normal computations of deflections of the vertical (Rice, 1952, 289); (Mather, 1966a, 10).

In computing the geoid-spheroid spearation using Stokes' integral and the deflections (ξ & η) of the vertical using the Vening Meinesz formulae, not only is it necessary to compute the $^1/_2{}^0 \times {}^1/_2{}^0$ square mean anomalies, but it is equally important to assess the accuracy of the quantity computed. This is dependant on the sample variance (σ^2), the sample size (n) and the distribution of readings over the square. As a result, only about 10 per cent of the available gravity data could be included in the sample. In addition, limited geodetic gravity surveys were also carried out using the South Australian Institute of Technology's Worden Geodesist gravimeter (Mather, 1966b). The elevations established on this survey by barometric means had a standard error of the order of $\pm$ 3 metres and the resulting error in the $^1/_2{}^0 \times {}^1/_2{}^0$ mean free air anomaly would be $\pm$ 0.2 mgal if there were no sources of systematic error in the final heights.

---

*) Presented by Prof. Angus-Leppan.

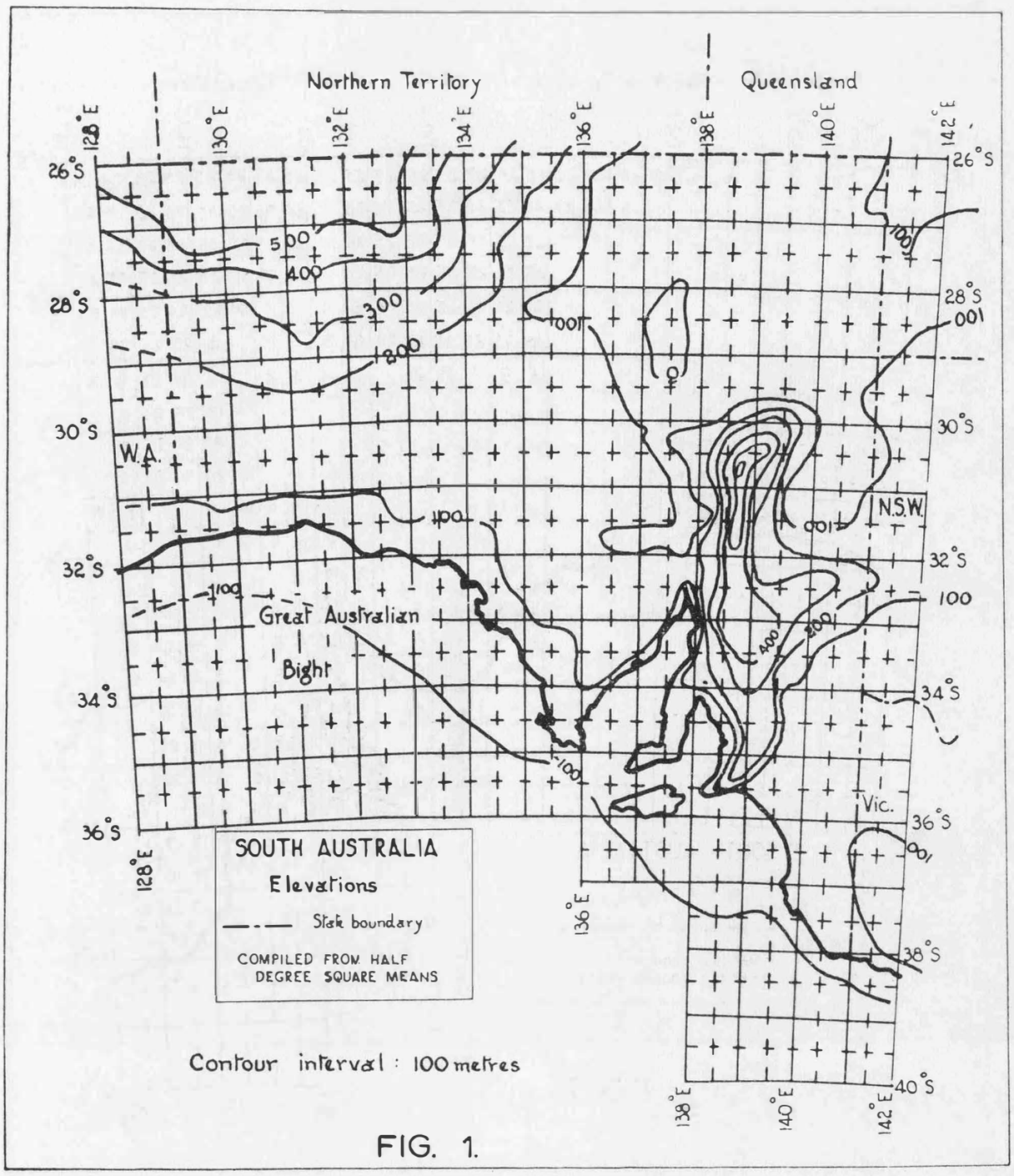

FIG. 1.

In this manner, readings were chosen to represent the corners of $0.1^0 \times 0.1^0$ squares. When readings did not quite fall on square corners, representation was adopted instead of interpolation (Moritz, 1966, 167). Approximately 4000 stations were incorporated in the analysis, the majority being concentrated along the northern and eastern borders of the state (see fig. 2). The area is essentially a region of negative free air anomalies (see fig. 3), the field being extremely variable in the north-west. (see fig. 4).

Correlation of Mean Free Air Anomalies and Mean Square Elevations

The regional free air anomaly can be represented (Uotila, 1960) over limited extents, by the expression

$$\Delta g_f \doteqdot C + 0.1118\,h \tag{1}$$

where

h = elevation of gravity station in meters

Δg_f = free air anomaly in mgal

C = a constant over the region.

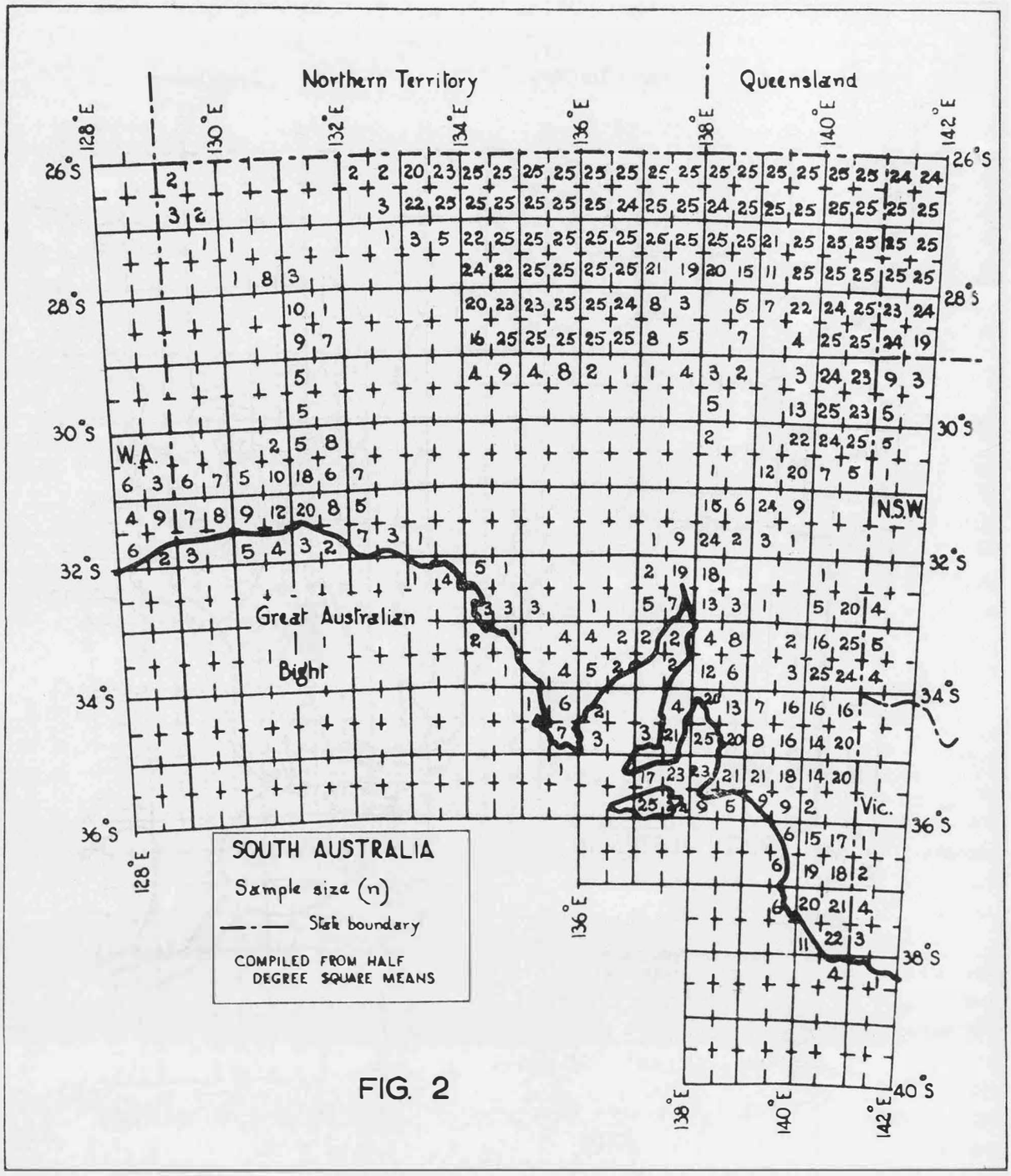

FIG. 2

Longitude (degrees *E*)

Latitude (Degrees *S*)	128	132	136	142
26		− 64 (415)	− 49 (262)	− 14 (58)
30		− 26 (86)	− 21 (39)	− 19 (175)
34			22 (− 70)	2 (9)
38				

TABLE 1

Evaluation of C in mgal. Mean elevations (in parantheses) in meters.

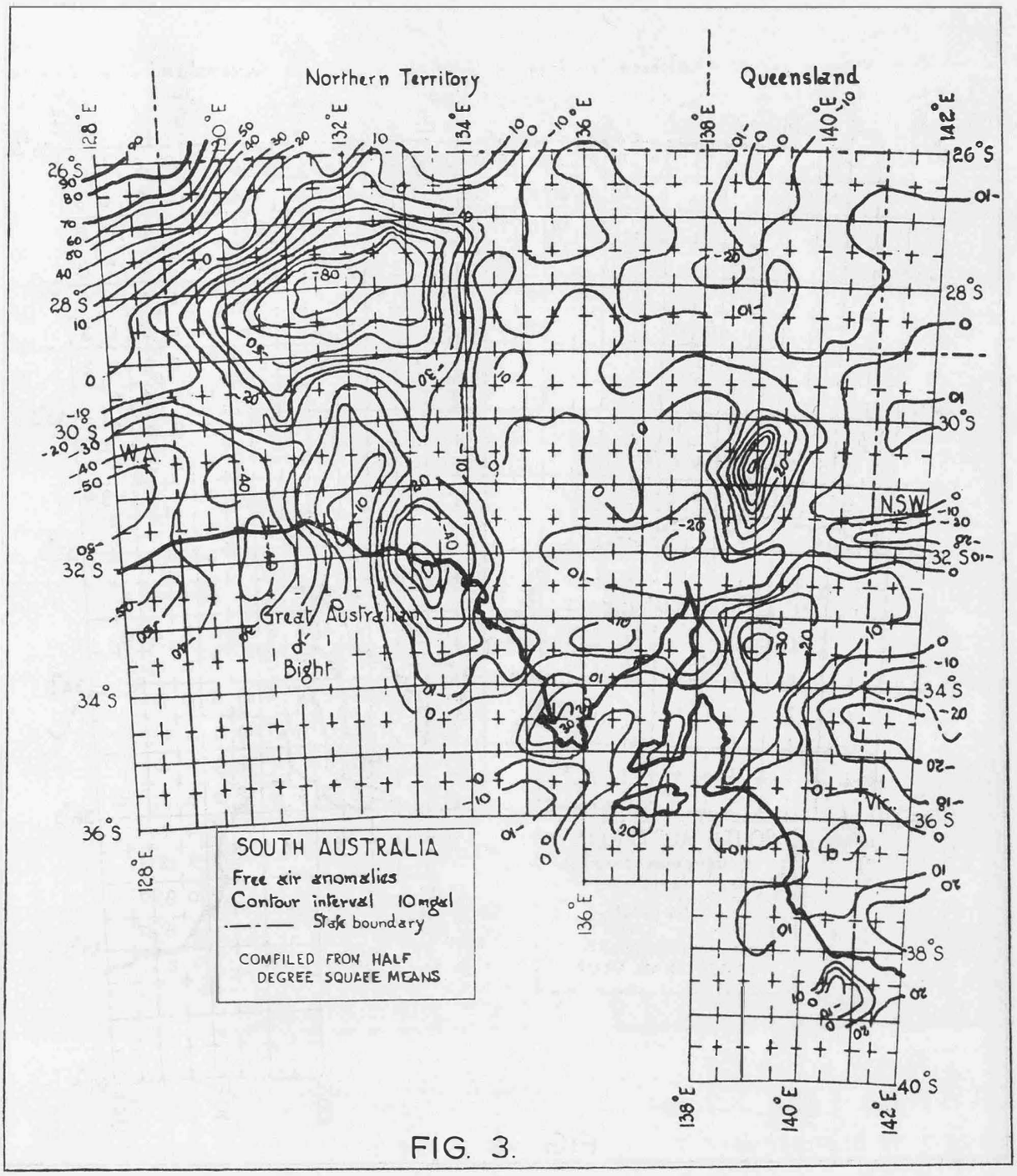

FIG. 3.

This expression implies that the Bouguer anomalies are more regional than positional in character. While this expression cannot represent limited extents with any degree of accuracy, the evaluation of a constant for larger areas is of relevance in establishing values for regional mean free air anomalies to be used in low order harmonic analysis of gravity material.

A least squares analysis of the data in 9 sub-divisional areas, using $^1/_2{}^0 \times {}^1/_2{}^0$ means gave values for C as shown in Table 1. The regional character of C is emphasised when these values are compared with the overall mean value of -20 mgal over the entire area, corresponding to a regional mean elevation of 130 meters.

This relation was not used to evaluate square means as the variation of gravity with height over any limited area in the sample considered was found, in most cases, to be small, compared to the variations with position, independent of height, as represented by Bouguer anomalies.

The Spread of a Sample

The criterion already defined for the spread of a sample is the "Error of Representation" (E_s) (Hirvonen, 1956), given by

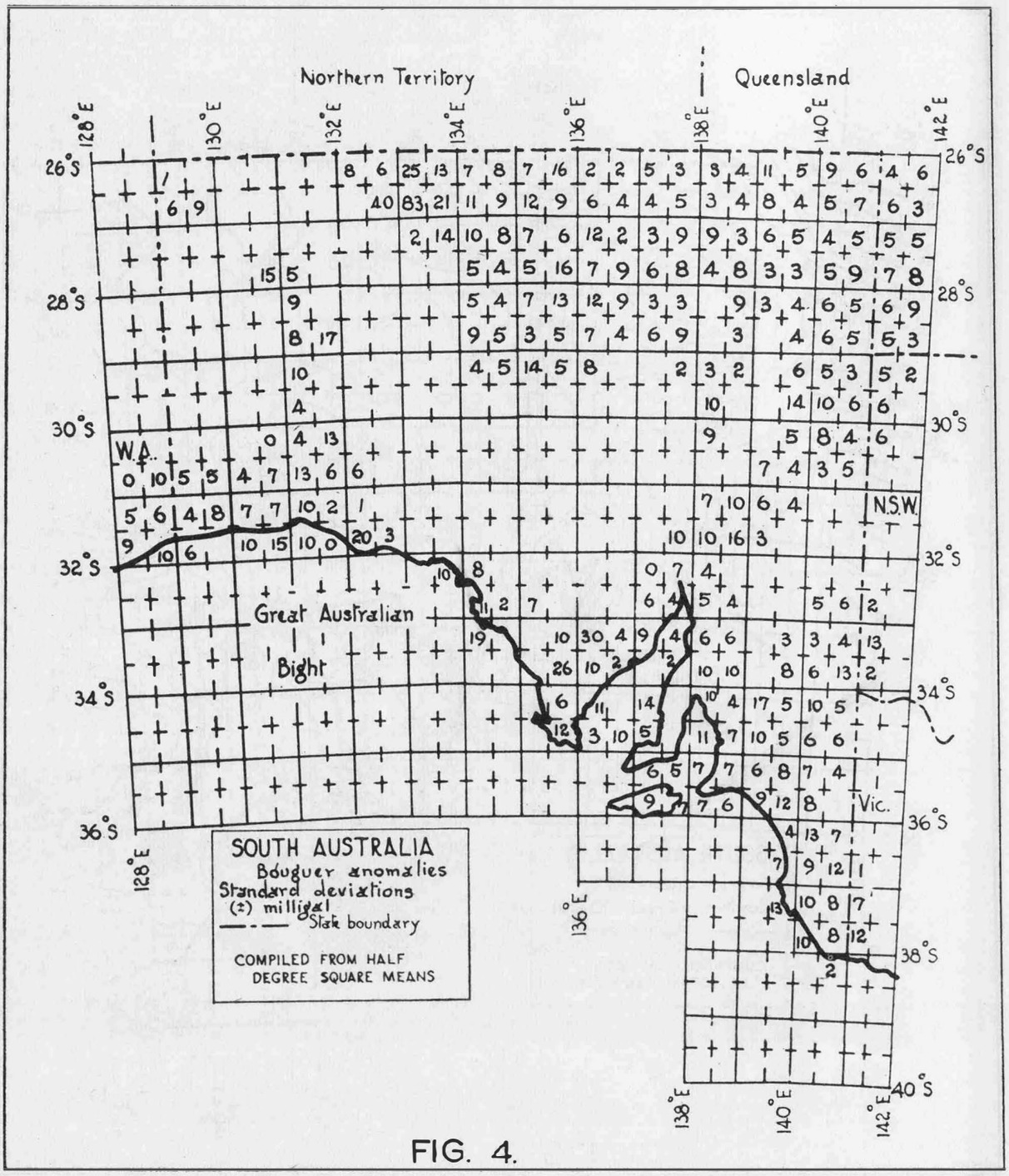

FIG. 4.

$$t E_s^2 = \sum_{i=1}^{t} \sum_{j=1}^{n} \frac{(\triangle g_{ij} - \triangle g_{Mi})^2}{n} \qquad (2)$$

where

Δg_M = mean anomaly for a square
Δg = observed anomaly
n = no. of stations in a square
t = no. of squares considered

As $n < 25$ for $1/2^0 \times 1/2^0$ squares, the denominator used for calculations was $(n - 1)$ instead of n (Spiegel, 1961, 70). The analysis of a high proportion of the South Australian sample shows good agreement with Hirvonen's values except, possibly, in the case of $1/2^0 \times 1/2^0$ square means. This is due to the highly variable field in the North West corner of the state where the free air anomalies approach -100 mgal and the standard deviation of free air anomalies in a single square could be as large as $\pm$ 80 mgal for a $1/2^0 \times 1/2^0$ square.

The E_s values in Table 2 represent values obtained from the analysis of free air anomalies, and, in view of the nature of the topography, would apply, with relatively small variations, to both Bouguer and Isostatic anomalies. Thus, while the variation of gravity is similar to that of the European gravity field over large extents (Hirvonen, 1956), it can be slightly greater over limited ones.

The extension of the gravity field to unsurveyed areas

The extension of gravity fields from limited gravity data to obtain a continuous field has already been investigated by Jeffreys (1941), Kaula (1959), Uotila (1962) and Moritz (1966). The methods of extension used are fully described by the first two investigators and the last. Jeffreys had much less data available to him than Kaula and sets out his method of computation exhaustively. He worked on a 10^0 square unit, assuming one value to represent each square and allowing for height correlation. A series of observation equations were then fitted for each parallel and harmonic coefficients were evaluated to the 4th order. Kaula, on the other hand, used Markov theory to interpolate 1^0 square means from available values. 10^0 square means were then evaluated using autocorrelation analysis. Thereafter, a set of low order harmonics (to the 8th degree) was fitted by the simple orthogonal method using fully normalised coefficients (Kaula, 1959, 89). Uotila used harmonic analysis by least squares.

The application of spherical harmonics is obviously unsuited for field extension over limited extents and Moritz has used covariance analysis for this purpose. However, both Markovian predictions and covariance analysis, when used under economically feasible conditions, tend to give overly smoothened fields (Kaula, 1965, 4) and such field extensions, under adverse conditions, give results which are hardly better than direct representation.

Square sice	Sample Size (n)										Total Sample		Hirvonen's Value
	A		B		C		D		E				
	E_s	t	E_s	t	E_s	t	E_s	t	E_s	t	E_s	t	E_s
$1/2^0 \times 1/2^0$	± 11	60	± 11	61	± 11	13	± 9	15	± 10	62	± 10.1	211	± 9.0
$1^0 \times 1^0$	± 12	21	± 16	26	± 13	10	± 13	7	± 9	12	± 13.5	76	± 12.7
$2^0 \times 2^0$	± 21	13	± 15	15	± 14	6	± 14	2	± 11	2	± 17.7	28	± 17.6

TABLE 2

The Error of Representation E_s (mgal)

Key to Classes

Square sice	A	B	C	D	E
$1/2^0 \times 1/2^0$	$0 < n \leq 5$	$5 < n \leq 10$	$10 < n \leq 15$	$15 < n \leq 20$	$n > 20$
$1^0 \times 1^0$	$0 < n \leq 10$	$10 < n \leq 30$	$30 < n \leq 50$	$50 < n \leq 75$	$n > 75$
$2^0 \times 2^0$	$0 < n \leq 50$	$50 < n \leq 100$	$100 < n \leq 200$	$200 < n \leq 300$	$n > 300$

In the analysis of the South Australian sample, the field extension was performed in two distinct stages using a two-dimensional trigonometrical series. The first stage was the extension of the gravity anomaly field in a limited $u^0 \times u^0$ area in which each single anomaly value represents $a\ v^0 \times v^0$ square. (The total number of readings possible in the area (N) is given by $N = u^2/v^2$). The anomalies used should only have variations dependent on position. Thus Bouguer anomalies were used. If free air anomalies are used, a three-dimensional series should be used with the height variable introduced into the series.

The second stage was the extension of $w^0 \times w^0$ square means over a large area to unsurveyed squares.

In the analysis, it was sought to evaluate the coefficients A_i, $i = 1,n$ of a series of the form $\sum_{=1}^{n} A_i f_i(\Phi, \lambda)$ which could be used to predict anomalies using the relation

$$E\{\Delta g(\Phi, \lambda)\} = \sum_{i=1}^{n} A_i f_i(\Phi, \lambda) \tag{3}$$

where $E\{\Delta g(\Phi, \lambda)\}$ is the predicted gravity anomaly at the point whose latitude is Φ and longitude λ.

The $A_i (i = l,n)$ are determined by setting up observation equations and minimising the sum of the squares of the weighted residuals

$$\sum_{j=1}^{m} w_j r_j^2 = \sum_{j=1}^{m} w_j \left[\Delta g_j - \sum_{i=1}^{n} A_i f_i(\Phi_j, \lambda_j)\right]^2 = \text{minimum} \tag{4}$$

where $w_j (j = l,m)$ are the weight coefficients, which, in the first case, would be equal to unity.

The required set of equations for solution are

$$\sum_{j=1}^{m} w_j \left[\Delta g_j - \sum_{i=1}^{n} A_i f_i(\Phi_j, \lambda_j)\right] f_k(\Phi_j, \lambda_j) = 0, \; k = l, n \tag{5}$$

These equations, in matrix notation, will be of the form

$$F.A = G, \tag{6}$$

where

$$F = \begin{pmatrix} f_{11} & f_{12} & f_{13} \cdots & f_{1n} \\ \cdot & & & \cdot \\ \cdot & & & \cdot \\ \cdot & & & \cdot \\ f_{m1} & f_{m2} & f_{m3} \cdots & f_{mn} \end{pmatrix} \quad A = \begin{pmatrix} A_1 \\ A_2 \\ \cdot \\ \cdot \\ \cdot \\ A_n \end{pmatrix} \quad G = \begin{pmatrix} \Delta g_1 \\ \Delta g_2 \\ \cdot \\ \cdot \\ \cdot \\ \Delta g_m \end{pmatrix}$$

and

$$f_{ij} = f_j(\Phi_i, \lambda_i)$$

The matrix of residuals (R) is given by

$$R = FA - G \tag{7}$$

For a least squares solution

$$1/2 \, R^T W R = \text{minimum} \tag{8}$$

where W is the matrix of weight coefficients, given by

$$W = \begin{pmatrix} w_{11} & 0 & 0 & 0 \ldots\ldots 0 \\ 0 & w_{22} & 0 & 0 \ldots\ldots 0 \\ 0 & 0 & w_{33} & 0 \ldots\ldots 0 \\ . & 0 & 0 & 0 \ldots\ldots w_{mm} \end{pmatrix}$$

Substituting for R from (7) in (8), after expansion and differentiation partially with reference to A, (8) reduces to

$$F^T W F A - F^T W G = 0 \tag{9}$$

the solution of which is

$$A = (F^T W F)^{-1} F^T W G \tag{10}$$

The extension of gravity fields in $2^0 \times 2^0$ *areas*

The choice of a suitable trigonometrical series hardly depends on the available computer storage but, paradoxically, on the available gravity field. The field extensions obtained from limited amounts of data using functions with a high degree of resolution are generally unreliable. The

computations in the case of the South Australian data were carried out on a C. D. C. 3200 computer and from the point of view of convenience in handling data, u was chosen as equal to two degrees. v, as explained earlier was chosen to be 0.1^0. A number of series were experimented with and a general series which gave adequate results was

$$E\{\Delta g(\Phi,\lambda)\} = \sum_{i=0}^{a} A_i \cos[\pi(\Phi-\Phi_o)i] + \sum_{i=(a+1)}^{2a} A_i \sin[\pi(\Phi-\Phi_o)(i-a)] + \sum_{i=(2a+1)}^{3a} A_i \cos[\pi(\lambda-\lambda_o)(i-2a)] + \sum_{i=(3a+1)}^{4a} A_i \sin[\pi(\lambda-\lambda_o)(i-3a)] \quad (11)$$

where Φ_o, λ_o are the co-ordinates of the SW corner of the $2^0 \times 2^0$ area, and Φ, λ are the geographical co-ordinates of the $0.1^0 \times 0.1^0$ square corner which is represented by the gravity anomaly $\Delta g(\Phi, \lambda)$.

Repeated application to varying sets of data showed that the minimum conditions for a non-trivial solution are:

(*i*) at least 5 readings should be available in every constituent $^1/_2{}^0 \times {}^1/_2{}^0$ square.

(*ii*) at least 1 reading should be available in every row and column of the 20×20 array.

While lesser data have provided seemingly acceptable solutions, the results are subject to fortuitous circumstances. Thus 80 well distributed observations can give estimates of the balance 320 values, i. e., a 1 to 5 extension.

The value of a in equation (11) governs the degree of resolution of the function and while the maximum value is controlled by the available storage, the actual value used would be influenced by the amount of gravity data available. In a pilot investigation, it was found that decreasing the ratio $a : u/v$ below $^1/_2$, while requiring much more computer time, did not materially improve the accuracy of extensions. Reasonable adequate representation was obtained by setting $a : u/v = {}^1/_3$ in the case of well surveyed fields. In regions with inadequate data, better results were obtained by reducing a in equation (11) in the range of values $7 \geq a \geq 0$ progressively as m in equation (5) reduces through the range $80 \geq m \geq 1$, the extreme case being one of direct representation.

These conclusions were used to predict values of gravity anomalies to represent unsurveyed areas, using Bouguer anomalies. The Bouguer anomaly so predicted was then corrected for the height term (Heiskanen and Vening Meinesz, 1958, 153) using the estimated elevation of the 0.1^0 square corner. An attempt was made to check the accuracy of field extension by studying comparisons between predicted values in areas satisfying conditions (*i*) and (*ii*) for non-trivial solutions, with gravity data which was available subsequent to the computations. 154 comparisons were made in 6 different $2^0 \times 2^0$ areas and the differences (Predicted-Observed) were found to be normally distributed with a standard deviation of $\pm$ 7.2 mgal.

In fitting the two-dimensional series defined in equation (11) to a field with a variable number (n) of gravity stations in it, the error of prediction (e_p), given by

$$e_p = E\{\Delta g(\Phi, x)\} - \Delta g(\Phi, \lambda) \quad (12)$$

was found to increase with n for a fixed value of a. Table 3 sets out values of $M\{e_p\}$ for $a = 7$, where $M\{e_p\}$ is the mean error of prediction.

Thus, if the available computer storage limits the maximum possible value of a, it is necessary to "normalise" predicted values prior to use, due to the magnitude of prediction errors in well represented fields. This can be effected either manually using a graphical extension technique or by the use of Markov theory (Bartlett, 1960, 24 et seq), as the accuracy of the predicted value obtained is dependent not only on the error of prediction e_p at adjacent stations but also on the average gravity anomaly gradient (G), where

$$|G| = \left| \frac{d\,\Delta\, g}{dl} \right| \tag{13}$$

where $d\Delta g$ is the change in gravity anomaly over a distance dl.

$1/2^0 \times 1/2^0$ squares		$2^0 \times 2^0$ squares	
Sample size (n)	$M\{e_p\}$ (*mgal*)	Sample size (n)	$M\{e_p\}$ (*mgal*)
$0 < n \leq 5$	± 4.4	$0 < n \leq 20$	± 1.8
$5 < n \leq 10$	± 6.0	$20 < n \leq 50$	± 2.3
$10 < n \leq 15$	± 6.4	$50 < n \leq 100$	± 4.7
$15 < n \leq 20$	± 7.3	$100 < n \leq 200$	± 6.7
$20 < n \leq 25$	± 6.5	$200 < n \leq 300$	± 8.3
		$300 < n \leq 400$	± 8.3
Total sample	± 6.5	Total sample	± 8.3

TABLE 3

Classification of Errors of Prediction

Following a procedure similar to that adopted by Kaula (1959, 9) let the couplet c_{iu} be given by

$$c_{iu} = \begin{pmatrix} e_{p_i} \\ G_u \end{pmatrix} \tag{14}$$

The expected error or prediction ($E\{e_{p_i}\}$) is given by

$$E\left\{e_{p_i}\right\} = \frac{c_i\, p_{jv}^{iu}\,(\Delta\, 1)}{p_{jv}^{u}\,(\Delta\, 1)} \tag{15}$$

where $p_{jv}^{iu}(\Delta\ 1)$ is the probability of the couplet c_{iu} occurring a distance $\Delta 1$ away from couplet c_{jv}; and suppression of an index denotes summation with respect to that index. The mean value of $|G|$ was 8.9 mgal/50 km, with maximum, modal and minimum values of 48 6 and 0 respectively.

The mean comparison error (e_c), $M\{e_c\}$, given by

$$[M\{e_c\}]^2 = \frac{1}{n} \sum_{i=1}^{n} [E\,\Delta\, g\,(\Phi, \lambda) - E\{e_{p_i}\} - \Delta\, g_i\,(\Phi, \lambda)]^2 \tag{16}$$

was $\pm$ 3.2 mgal for the 154 comparisons.

Field extensions under the above conditions can be expected to have an estimated error of $\pm$ 3 mgal, which is of an accuracy comparable with representation of a single tenth degree square by a single reading (Hirvonen, 1956, 2). Relaxation of criteria at (*i*) to 3 stations within each of the constituent $1/2^0 \times 1/2^0$ squares and maintaining those at (*ii*) gave estimated comparison errors of $\pm$ 8 mgal, which, on normalisation reduced to $\pm$ 6 mgal.

If these minimum conditions are not satisfied, the error of field extension becomes much larger and, unless a in equation (11) is reduced proportionately, the functional representation becomes erratic. This, in effect, reduces the resolution of the trigonometrical series, which, in the limit, becomes a case of direct representation.

The extension of the field to $1/2^0 \times 1/2^0$ *square means over a* $14^0 \times 14^0$ *area*

A field extension, similar to the above, can be performed from the $1/2^0 \times 1/2^0$ square means obtained from the gravity data available to evaluate estimates of the $1/2^0 \times 1/2^0$ means of areas in which no readings occur. The field extensions are made from data not of equal weight (w) as

(*i*) the number (n) of readings used to evaluate the mean

(*ii*) the standard deviation (σ) of each sample vary from square to square.

While n is dependent on the available gravity field, σ is a function of the variability of the latter, which is not dependent on topography alone.

The weight coefficient

$$w = f(n, 1/\sigma^2)$$

In the evaluation of $f(n, 1/\sigma^2)$, it should be borne in mind that the final weight coefficient must reflect the distribution of the sample within the area represented (i. e., a high sample density in a restricted area may give a value for σ which is not a true representation of the variability of the gravity field within the square considered). Further, the expression should reduce to

$$w = 1/E_s^2 \tag{17}$$

when $n = 1$ and $\sigma = 0$

and

$$w \to \frac{N}{\sigma^2} \tag{18}$$

where N is the maximum number of readings possible, as $n \to N$.

In general, the weight coefficient should be inversely proportional to the variance of the sample mean. However, in squares where the sample covers only a small fraction of the total area, the use of σ^2/n tends to over-estimate the weight coefficient. An expression for the latter, which satisfies not only the limiting conditions, but also the general requirements is

$$w = \frac{n}{\sigma^2}\left\{1 + \frac{(N-n)^2 e_s^2}{(N-1)^2 \sigma^2}\right\}^{-1} \tag{19}$$

as

$$\frac{1}{w} = \frac{1}{n}\left\{\sigma^2 + \left[\frac{N-n}{N-1}\right]^2 e_s^2\right\} \tag{20}$$

The individual weight coefficients for each $1/2^0 \times 1/2^0$ square were incorporated in Equation (5), which was expressed in the form set out in Equation (11) prior to solution. In this manner the field was extended to the unsurveyed areas.

The use of the weight coefficients in the analysis of a given field with considerable local variation was found to give rise to a smoothened field, when compared with a similar extension, but with the weight coefficients set at unity for all values. The values of $E\{\Delta g(\Phi, \lambda)\}$ so obtained in the weighted solution were normalised as explained earlier, using Equations (12) to (15) and the final extended value accepted was

$$\Delta g\,(\Phi, \lambda) = E\{\Delta g\,(\Phi, \lambda) - E\{e_p\,(\Phi, \lambda)\} \tag{21}$$

The assumption that the Bouguer anomalies used in the extension were free from height correlation is justifiable as the maximum mean $1/2^0 \times 1/2^0$ square elevation in the region considered was 803 meters.

The extended free air anomaly means were then obtained by allowing for the mean Bouguer reduction, using the mean square elevation. These extended values were used to supplement the observed values in compiling Figure (3).

The accuracy of the field extension

The accuracy of the field extension can be checked in one of two ways. Firstly, the extended values can be compared with actual values. An alternative method would be the comparison of the extended values as obtained from field extensions carried out by more than a single acceptable method.

Let the predictions be required in certain positions of a $m \times n$ array of Δg where certain values of Δg are available. Three distinct cases of prediction of the anomaly $\Delta g(i, u)$ are possible

(*i*) *Interpolation:*

In this case, the readings $\Delta g(h, u)$, $\Delta g(j, u)$, $\Delta g(i, t)$ and $\Delta g(i, v)$ are available; $h < i < j$; $t < u < v$.

(*ii*) *Interpolation/extrapolation:*

The circumstance in which *only one* of h, j, t, v is zero, on adopting the convention that $\Delta g(0, u) = \Delta g(i, 0) =$ no reading available.

(*iii*) *Extrapolation:*

At least one each of (h, j) and (t, v) is zero.

A preliminary study showed that the reliability of the predictions were strongly affected by the variability of the gravity field and all predictions were normalised in terms of the average gravity gradient in the area using the relation

$$N\{C\} = \frac{E\{C\}}{E\{G\}} M\{G\} \tag{22}$$

where
$N\{C\}$ = the normalised prediction
$E\{C\}$ = the predicted value
$E\{G\}$ = the predicted gravity anomaly gradient
$M\{G\}$ = the mean gravity anomaly gradient.

The normalised predictions so obtained were classified according to

a) the minimum interval (I_i) $(j - h)$ or $(v - t)$, as the case may be for interpolations and interpolation/extrapolations.
b) the minimum interval (I_E) $|i - h(\text{or } j)|$ or $|u - v \text{ (or } t)|$ in the case of extrapolation.

In all, four methods of prediction were used:

a) graphical
b) Markov theory
c) trigonometrical series with weighting
d) trigonometrical series without weighting.

If the standard deviations of the comparisons between method (c) and the others were σ_{c_i} $(i = 1, 3)$, the reliability limits were set to the values of $I_{i(E)}$ accepted on the basis that

$$\left(\sigma_{c_i} - \sigma_{c_{i+1}}\right) \not> K \,.\, M\{G\} \tag{23}$$
$$i = 1,3 \text{ (if } i > 3, \text{ then } i = 1)$$

where K is a comparison factor.

For interpolations, in cases where $I_i \leq 6$, good agreement was obtained between the σ_{c_i} for each of the different methods of extension. For $I_i > 6$, however, the comparison between the values for σ_{c_i} was erratic (K was generally greater than 0.2).

	Standard deviations of discrepancies in field extension (± *mgal*) (Numbers in brackets represent sample size)					
$I_{i(E)}$	1	2	3	4	5	6
Interpolation	2 (15)	5 (22)	5 (22)	5 (45)	5 (61)	6 (71)
Interpolation/ Extrapolation	6 (2)	5 (7)	11 (20)	18 (37)	10 (41)	9 (44)
Extrapolation	10 (29)	12 (46)	14 (56)	15 (61)	15 (63)	— — —

TABLE 4

Field Extension discrepancies for $^1/_2{}^0 \times {}^1/_2{}^0$ *square means; Case (i) / Case (iii)*

In case (*ii*), no comparison of $\sigma_{c_i} - \sigma_{c_{i+1}}$ could be considered acceptable unless the comparison factor was increased to $K = 0.4$.

In case (*iii*) too, the value 0.4 was adopted for K.

The results in Table 4 summarise the accuracy of comparisons in one instance, after discarding those whose I_i values are large enough to make the resulting extensions unreliable, by the standards defined in expression (23), with $K = 0.4$.

While the samples are too small for definite conclusions to be drawn, it would appear that, as a general rule, the weighting of extensions according to

Interpolations: Interpolations/Extrapolations: Extrapolations:

$$= \frac{1}{1^2} : \frac{1}{2^2} : \frac{1}{3^2} = 1 : 0.25 : 0.11$$

is indicated.

The factors to be considered in estimating the error of the predicted value are

a) the nature of the extension, i. e., interpolation, interpolation/extrapolation or extrapolation,

b) the interval from the most reliable value,

c) the accuracy of this value.

If the error of representation of the nearest basic square mean is e_{ref} and the estimated error in the extension is e_{ext}, the estimated error of prediction ($E\{e_p\}$) is given by

$$[E\{e_p\}]^2 = e_{ref}^2 + e_{ext}^2 \tag{24}$$

The value for e_{ref} is obtained from Equation (20)

Conclusion

The extension of gravity fields using mathematical functions, unless carried out under carefully controlled conditions, could produce results of questionable accuracy. The use of the two dimensional trigonometrical series described in Equation (11) is quite satisfactory for limited extents, provided that the degree of resolution of the function is adequately reduced when a paucity of data occurs. In the case where field extension is effected using area means which could be of differing reliability, the extension should be performed after adequate weighting. The accuracy of the values so predicted is dependent on whether the extension performed was an interpolation, interpolation/extrapolation or an extrapolation. Field extensions over intervals more than 6 positions from the nearest available value (i. e., $I_{i,E} > 6$) were found to be unreliable. For $I_{i,E} \leq 6$, the ratios of the accuracies of interpolation: interpolation/extrapolation: extrapolation = 1 : 2 : 3.

Within this range, the error of the predicted value would not be materially larger than the error of representation of the nearest value used in the extension.

Acknowledgments

The major portion of this work was carried out while the author was attached to the South Australian Institute of Technology, which made funds available for purchase of computer time.

All gravity information was made available by courtesy of the Director, South Australian Department of Mines, Adelaide, Australia, Delhi Petroleum Company and other prospection companies. Their co-operation is gratefully acknowledged.

References

1. *Bartlett, M. S.:* "An Introduction to Stochastic Processes", Cambridge University Press, 1960.
2. *Dooley, J. C.:* "National Report of Gravity in Australia January, 1962 — June, 1965", B. M. R. Rec 1965/62, 1965.
3. *Dooley, J. C., McCarthy, E., Keating, W. D., Maddern, C. A. and Williams, L. W.:* "Pendulum Measurements of Gravity in Australia 1950—1951", B. M. R. Bull. 46, 1961.
4. *Heiskanen, W. A. and Vening Meinesz, F. A.:* "The Earth and its Gravity Field", McGraw Hill, 1958.
5. *Hirvonen, R. A.:* "On the Precision of the Gravimetric Determination of the Geoid", Trans. A. G. U., 37, 1—8, 1956.

6. *Jeffreys, H.:* "Determination of the Earth's Gravitational Field", M. N. R. A. S. Geoph. Sup., 5, 1, 1–22, 1941.
7. *Kaula, W. M.:* "Statistical and Harmonic Analysis of Gravity", Army Map Service Tech. Rep. 24, 1959.
8. *Kaula, W. M.:* "Comparison and Combination of Satellite with other Results for Geodetic Parameters", Inst. Geoph. and Plan. Phys., U. C. L. A. Pub. 431, 1965.
9. *Mather, R. S.:* "The Geodetic Uses of Gravity", 9th Survey Congress, Perth, Australia, 1966a
10. *Mather, R. S.:* "The Establishment of Geodetic Gravity Networks in South Australia", Uniciv. Rep. R 17, 1966b.
11. *Moritz, H.:* "Accuracy of Mean Gravity Anomalies Obtained from Point and Profile Measurements", Bull. Geod., 80, 157–169, 1966.
12. *Rice, D. A.:* "Deflections of the Vertical from Gravity Anomalies", Bull. Geod., 25, 285–312, 1952.
13. *Speigel, M. R.:* "Statistics", Schaum, 1961.
14. *Thyer, R. F.:* "Geophysical Exploration – Australia", Geophysics, 28(2), 273–305, 1963.
15. *Uotila, U. A.:* "Investigations of the Gravity Field and Shape of the Earth", Ann. Acad. Scient. Fenn. Ser A III, Geologica, 55, 1960.
16. *Uotila, U. A.:* "Harmonic Analysis of World Wide Gravity Material", Ann. Acad. Scient. Fenn., Ser A III, Geologica, 67, 1962.

The Course of the Plump-Line at the Transit through the Physical Earth-Surface, and the Determination of its Curvature by Local Gravimetry

by *W. Embacher*, Vienna

This investigation is part of the research program of the Institute of Geodesy and Spherical Astronomy (Director Prof. Dr. Karl Ledersteger).

In order to understand the theoretical course of the horizontal gradient we make use of a formula for the infinite rectangular prism as stated by K. Mader. That prism may extend in the x-direction from $-\infty$ to $+\infty$, in the y-direction from y_1 to $+\infty$ and in the z-direction from z_1 to z_2. Thus:

$$\frac{1}{k2\sigma} V_{yz} = ln \frac{y_1^2 + z_2^2}{y_1^2 + z_1^2}. \tag{1}$$

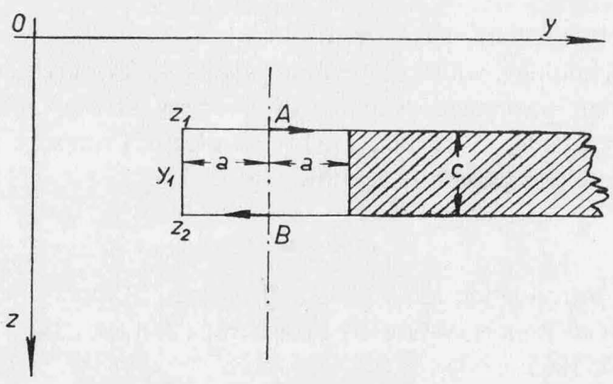

Figure 1

Though the formula only applies to the external potential, the horizontal gradient can be calculated for any point of the plate, e. g. also for the straight line AB, if we bear in mind that the effect of the prism extending in the x-direction from $-\infty$ to $+\infty$ and being 2a wide in the y-direction, is compensated in the straight line AB by reasons of symmetry. Thus, one only needs to compute

the effect of the hatched remainder prism. When choosing point A as reference point z_1 is zero, and the horizontal gradient has a definite value. However, when taking point B as reference point, then z_2 is zero and the horizontal gradient is of the same quantity but of opposite sign.

A small sloped region of terrain can well be approximated by a stair-model consisting of a number of infinitely extended quadrilateral plates.

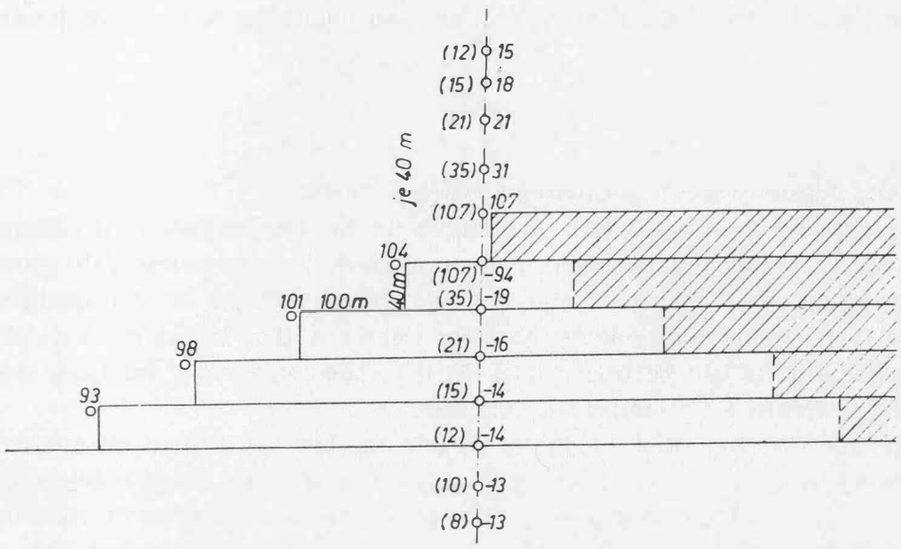

Figure 2

By means of this model the theoretical course of the horizontal gradient below and above the plates may now be analyzed. The steps may have a lenght of 100 m and a height of 40 m. For the five plates, one put upon the other as described above, the horizontal gradientes have been computed for reference points in the vertical of point I according to the formula mentioned before. We see that the horizontal gradient inside and outside the model is pointing in direction differing by 180^0.

Numerous models also have been computed according to the formulas of Helmert and Prey. The following characteristic properties of the gradients became obvious:

The horizontal as well as the vertical gradients not only depend on the slope but also on the cross section of the terrain.

The horizontal gradients always have opposite signs and are of equal absolute value. The external horizontal gradient always is directed towards the slope.

H. Bodemüller determined numerous external vertical gradients by observations on towers. The agreement of the theoretical models stated above with those pratical measurements is obvious. At the bottom of valleys the negative anomalous gradient reduces the free-air gradient, while the positive anomalous gradient on top of the slope increases the free-air gradient. The gravity differences Δg measured with a gravimeter in the line of maximum slope of the terrain can be represented by the gradients as follows (n be the height difference of the measuring points and $s = n \operatorname{cotg} \delta$ be their horizontal distance, when δ means the inclination of the terrain).

$$\begin{aligned} \Delta g &= -n V_a + s H_a \\ \Delta g &= -n V_i + s H_i \,. \end{aligned} \tag{2}$$

We are justified to assume that the density within the proximity of station P_o is constant. If we then form the gravity differences between P_o and the points P_i around P_o in possibly equidistant azimuths α, the equations (2) take the form

$$\begin{aligned} \Delta g + n V_a - s (H_a)_x \cos\alpha - s (H_a)_y \sin\alpha &= 0 \\ \Delta g + n V_i - s (H_i)_x \cos\alpha - s (H_i)_y \sin\alpha &= 0 \end{aligned} \tag{3}$$

Hence:

$$\Delta g + n\left(\frac{V_a + V_i}{2}\right) - s\left(\frac{H_a + H_i}{2}\right)_x \cos\alpha - s\left(\frac{H_a + H_i}{2}\right)_y \sin\alpha = 0. \tag{4}$$

Both the unknown $^1/_2(V_a + V_i)$ and $^1/_2(H_a + H_i)$ with respect to the origin P_o are obtained from two measured differences or, in case of over determination, by an adjustment.

If V_a is measured, equation (2) directly gives H_a, and from the adjusted means of the gradients we obtain the internal gradients V_i ond H_i, and finally the formulas of Bruns

$$\begin{aligned} V_i - V_a &= -4\pi k^2 \sigma \cos^2\delta \\ H_i - H_a &= -4\pi k^2 \sigma \cos\delta \sin\delta \end{aligned} \tag{5}$$

furnish the ground density twice, thus offering a welcome check.

In a previous paper: "A Comparison of Methods for the Determination of Ground Density" (Ö. Z. f. V. vol. 49, no. 4) I have stated an error equation for the determination of the ground density. The determining equation for that error equation is identical with the second equation of (3). It could be shown that by neglecting one or the other unknown the existing methods of Nettleton, Steiner, Parasnis and Jung can be traced back to the above statement. All these methods also presume an average density for a limited working area.

For further considerations it is significant to find the law, or at least an approximation to that law, according to which the horizontal gradients decrease along the plumbline starting from the density discontinuity at the transit through the physical surface of the earth. Here the synthetic investigation of Helmert about the effect of given masses on the level surface near the ground showed the way.

Again we proceed from the formula for the infinitely extended quadrilateral rectangular prism (1). It may extend in the x-direction from $-\infty$ to $+\infty$, in the y-direction from y_1 to $+\infty$, and in the z-direction from z_1 to z_2.
Thus

$$\frac{1}{k^2\sigma} V_{yz} = ln \frac{y_1^2 + z_2^2}{y_1^2 + z_1^2}. \tag{1}$$

where σ stands for the density, and V_{yz} for the horizontal gradient in point 0. For simplification we choose $y_1 = 0$ and put $z_1 = z$, $z_2 = z + c$. Thus we get

$$\frac{1}{k^2\sigma} V_{yz} = ln \frac{z^2 + 2cz + c^2}{z^2}, \tag{1a}$$

which because of $c \ll z$ transforms to

$$\frac{1}{k^2\sigma} V_{yz} = ln\left(1 + \frac{2c}{z}\right) \sim \frac{2c}{z}. \tag{1b}$$

The gradients along a plumb-line were computed for some models according to Helmert and Prey. Now, as a trial calculation, for each of these models c has been determined according to the above formula (1 b), and then the other gradients were calculated back. Their values are given in Fig. 2 in parentheses. The fair agreement proves that the approximate formula for the gradient

$$G = \frac{2c}{z} \tag{6}$$

is feasible. This means that for the determination of gradients any model can be approximated by an infinite plane of thickness c.

Formula (1) from which the approximation (6) has been derived only holds for the external potential, yet the computed models show that the horizontal gradients of outer and inner space behave like reflected images, i. e. approximation (6) also is feasible for the calculation of the internal horizontal gradient.

We get the curvature picture of a curve by representing the curvature k in function of the arc length z.

For the circle $k = k_o = \text{const}$, which together with

$$d z = R\, d \tau \tag{7}$$

leads to

$$d \tau = k_o\, d z$$

and

$$\Delta \tau = k_o \int_o^z d z = k_o z = \frac{z}{R} \tag{8}$$

If we assume the plumb-line to be a wide circle (which is certainly the case with the normal curvature) we have for an elevation above sea H:

$$z = H,\ \Delta \tau'' = \frac{H}{R} \rho'' = \frac{G H}{g} \rho'' . \tag{9}$$

Now the curve shall be analyzed whose curvatore is

$$\frac{1}{R} = \frac{2 c}{g . z} . \tag{10}$$

The curvature picture can be seen in Figure 3.

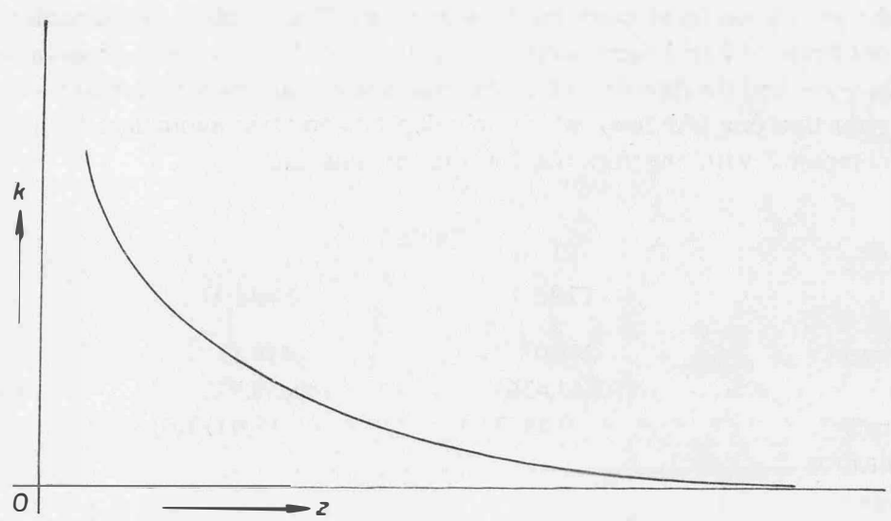

Figure 3

We find

$$\Delta \tau = \frac{2 c}{g} \int \frac{dz}{z} = \frac{2 c}{g}\, ln\, z + C . \tag{11}$$

The limits of the definite integral result from the reflected height of the center of the gravimeter of 0,5 m on the one hand, and by the assumption on the other that at z_o the curvature vanishes practically; e. g. $G_{z_o} = 0{,}010$ mgal/m. If c is not much less than z, the term c^2/z^2 must not be neglected. For determining c use is made of equation (1 a). The mean density σ is assumed to be $\sigma = 2$; thus $k^2\, \sigma = 133{,}4 \,.\, 10^{-9}$. Denoting $V_{yz}/k^2\, \sigma$ with A, the equation

$$\frac{1}{k^2\, \sigma} V_{yz} = ln \left(\frac{z^2 + 2\, c\, z + c^2}{z^2} \right)$$

proceeds to

$$ln \left(\frac{c^2}{2500} + \frac{c}{25} + 1 \right) = A$$

and

$$\frac{c^2}{2500} + \frac{c}{25} + 1 = e^A .$$

Further:

$$\log\left(\frac{c^2}{2500} + \frac{c}{25} + 1\right) = A \log e = A \,.\, 0{,}43429 . \tag{12}$$

z may be reckoned positively downwards. Hence, in the quadratic equation the negative solution must be considered since the internal gradient also has negative sign. The same negative root should be used for computing the external gradient since there z becomes negative.

We obtain z_o from:

$$0{,}01 = \frac{2\,c}{z_o}\,; \quad z_o = 200\,c\,. \tag{6a}$$

For $\Delta\tau''$ we get:

$$\Delta\tau'' = \frac{2\,c\,\rho''}{g}\,ln\,\frac{z_o}{0{,}5}. \tag{11a}$$

With the measuring results of the gravimeter test field „Buschberg" (mean latitude 48°40′) the plumb-line curvature has been computed for 3 fields assuming the curvature laws mentioned above. The results are listed in Table 1. The first line gives the fields' height above sea level, while the second one states the gravity values as measured by gravimeter. The intensity and direction of the internal horizontal gradients of line 3 were computed on basis of the gravimeter observations. The fourth line gives the value and the direction of the internal horizontal gradients found vectorially by means of Bessel's reduction (see fifth line), which only depends on mass anomalies. Line 6 shows the normal $\Delta\rho''$ computed with the formula for the circular arc.

Table 1

	Field I	Field II	Field 34
1. H in meters	398,05	419,13	437,13
2. g mgal	980863,436	980858,972	980854,687
3. G' intensity 10^{-3} mgal/m (direction)	7,4 (123°)	15,0 (130°)	28,5 (114°)
4. G intensity 10^{-3} mgal/m (direction)	7,9 (129°)	15,6 (132°)	29,0 (116°)
5. G normal intensity 10^{-3} mgal/m (direction)	0,813 (0°)	0,813 (0°)	0,813 (90°)
6. $\Delta\overline{\varphi}''$ (direction of the osculating plane)	0.″068 (180°)	0.″071 (180°)	0.″074 (180°)
7. z_o in meters	203,0	206,2	211,5
8. c in cm	101,5	103,1	111,5
9. $\Delta\tau''$ (direction of the osculating plane)	0.″451 (129°)	0.″460 (132°)	0.″467 (116°)
10. $(\Delta\varphi')''$	− 0.″358	− 0.″378	− 0.″278
$(\Delta\lambda')''\cos\varphi$	+ 0.″348	+ 0.″336	+ 0.″420

Assuming a curvature law corresponding to the quadrilateral hyperbola, according to formula (6a), the depth z_o has been computed for that place where the curvature vanishes practically. z_o is tabulated in line 7.

The thickness c of the compensating plate, which with density 2 (about the density of the upper ground layers at „Buschberg") corresponds to the course of the horizontal gradient along the plumb line, can be found in line 8. It was calculated by means of formula (12).

Line 9 states the curvature computed by the approximate formula (11a) and wich is created by the effect of mass anomalies, line 10 gives the components of the total reduction $(\Delta\varphi')''$ and $(\Delta\lambda')'' \cos\varphi$, i. e. the reduction of the observed latitude and longitude.

For an estimate of the rotation of the osculating plane the radius of curvature and its direction was calculated for points of the plumb lines of the principal points of the fields I, II and 34:

Table 2

	Field I Length km (direction)	Field II Length km (direction)	Field 34 Length km (direction)
Surface point	124.000 (123°)	62.500 (130°)	33.800 (114)
10 m lower	1,530.000 (26° 48′)	1,530.000 (63° 05′)	755.000 (82° 25′)
50 m lower	1,280.000 (4° 21′)	1,360.000 (9° 15′)	1,330.000 (20° 42′)
100 m lower	1,240.000 (2° 04)	1,280.000 (4° 21′)	1,290.000 (9° 56′)
200 m lower (about half the heigth)	1,220.000 (1° 04′)	1,240.000 (2°)	1,240.000 (4°)
on the geoid	1,200.000 (0° 30′)	1,200.000 (0° 30′)	1,220.000 (1° 47′)

Hence, the plumb line curvature and the rotation of the osculating plane can be calculated from local gravimeter measurements without consideration of the topography.

Geodetic Interpretation of the Results

Resumé, already presented at COSPAR.

by *George Veis*, Cambridge, Mass. and Athens

The results obtained for the geodetic parameters adopted for the Standard Earth provide all information needed to establish a universal geodetic datum.

The spherical harmonics, the 14 zonals (Kozai, 1964) and the 50 tesseral (Gaposchkin, 1966), a total of 128 coefficients derived from the satellite-tracking data, describe the generalized gravitational field of the earth. From this field, a map of the generalized geoid can be derived as well as a map of the generalized gravity anomalies. As reference for the geoid and the gravity anomalies, an ellipsoid of revolution of a = 6,378,165 m and f = 1/298.25 has been used.

Furthermore, the solution gives precise rectangular coordinates of 12 points. The system to which the coordinates refer is as close as possible to a geocentric terrestrial system, i. e., the z axis is oriented in the direction of mean pole 1900−1905, and the x axis in the direction of the meridian of the mean observation.

As in all reference systems defined on a theoretical basis but applied in an experimental numerical way, this one — as defined by the coordinates of twelve physical points on the surface of the earth — has an uncertainty associated with it. This uncertainty is estimated to about 10 m for the origin (or geocentricity), 0″.2 for the directions of the axes, and a few parts per million for the scale. Actually, the scale depends on the adopted value for $GM = 3.986032 \times 10^{20}$ cm^3 sec^{-2}. The

internal accuracy of the coordinates of each station, i. e., the accuracy of the relative positions in the above reference system, is between ± 10 and ± 15 m.

Thus, the absolute coordinates of the twelve Baker-Nunn camera stations are given to an accuracy of 15 to 20 m or approximately 3 ppm.

Since all twelve stations are connected to major geodetic datums, and their coordinates in those datums are known, a simple comparison of the datum geodetic coordinates with the terrestrial coordinates will yield the datum shifts as well as the deflection of the vertical for those datums (Veis, 1965). When the absolute deflection of the vertical for the different datums has been derived, all geodetic coordinates can be converted to this new universal geodetic datum or, in other words, to terrestrial coordinates. In addition, local geoids determined geometrically from astrogeodetic leveling can be properly oriented and will provide the details of the geoid that satellite dynamic methods cannot provide.

Once a system for geodetic parameters has been established and the coordinates of tracking stations are given in this system, it is then possible to use the so-called navigation method for the determination of new stations. This method consists in the determination of the orbit of a satellite, in which are used observations from the known stations. Then, since the geocentric position of the satellite can be established for any given time, observations from an unknown station, at known times, can be used to determine the position of this station in the same reference system.

This method has been tested by determining the position of each Baker-Nunn camera station separately from a completely new set of observations, and using as geodetic parameters (both dynamic and geometric) the values given by the Standard Earth. From this analysis, we conclude that a tracking station capable of making observations of an average accuracy of ± 2″ in position and ± 1 msec in time can be tied to the Smithsonian reference system with an accuracy of ± 15 m if 500 observations (on a satellite like Midas 4) can be secured from this station in a period of time that the Baker-Nunn camera network monitors this satellite. It would therefore appear that the navigation principle can now be used quite efficiently.

References

Gaposchkin, E., A dynamical solution for the tesseral harmonics of the geopotential, and station coordinates using Baker-Nunn Data. COSPAR Proceedings (1966).

Kozai, Y., New determination of zonal harmonics coefficients of the earth's gravitational potential. Smithsonian Astrophysical Observatory Special Rep. No. 165, 38 p., 1964.

Veis, G., The deflection of the vertical of major geodetic datums. Space Research V, D. King-Hele, P. Muller, and G. Righini, eds., North-Holland, 849–875, 1965.

Ideas and Propositions on Marine Geodesy.

by *Karl Killian*, Vienna

In marine geodesy – that branch of science we up to now know only by name and which is just at the beginning but certainly will develop – the problem is to establish fix points on the sea bottom, and to measure their mutual position in space and with respect to fix points on the continents.

The fix point for the sea (= *marine fix point*), displayed in Figure 1, is likely to represent a feasible proposition. It consists of a triple-reflector system for ultra-sound (1), of a tube (2), and of a steel case (3) which carries four arms (4) fitted with pointed anchoring plates (5).

The center of gravity of the whole system lies in the lower part of the steel case (3). Thus, a marine fix point lowered from a ship will maintain its axis of symmetry in a vertical position while submerging. This is further promoted by fins (6). Ocean currents are small as compared with the sinking velocity of the device, especially in greater depths. Underneath the case has a dome-shaped center-piece. This serves only for the reduction of the resistance-coefficient when sinking.

Currents created by moderate wind and by the tides have a total velocity on the open sea of less than 0,2 m/sec. Currents produced by wind reach down only to 100—200 m. The Gulf Stream, the Kuro-Schio and the Agulhas Stream have surface currents of 1 to 2 m/sec. In a depth of 1000 m their velocity also is negligible.

Hence, the points of the anchoring plates will penetrate the sea bottom approximately in vertical direction with considerable cinetic energy. The dropping of a marine fix point is done after preceding surveys by echo-sounding profiles in possibly horizontal regions of the ocean bottom. According to the nature of the ocean bottom (methods exist for digging up samples for geological analyses) and to the future deep-sea depositions to be expected one will select size (length of the tube about 5 to 15 m) and weight of the whole device. Eventually the anchoring could be checked by a television system.

The determination of the spatial position of the anchored marine fix points is done by means of "*marine stations*". By "marine station" we understand a ship which at "calm" sea is kept fixed in a vertical through the center of the triple-reflector as accurate as possible. As previous solutions of the problem to maintain a ship in a fixed position the methods of laying deep-sea cables and the project "*Mohole*" (drilling at the sea bottom in a depth of 3600 m) can be claimed. The following solution will suit the present conditions better.

At the marine station (1) (Figure 2) a *gyro-stabilized platform* (2) is necessary. For the stabilization we assume about one minute of arc in amplitude and one minute for the period of oscillation. On the platform an *ultra-sound transmitter* (3) is fitted. It transmits vertically (accurate to about 1′) onto the triple-reflector (5). The reflected ultra-sound waves reach the four *receivers* (4) arranged symmetrically with respect to the transmitter. Both the plotted receivers (4) and the two receivers not plotted are hooked up in a bridge circuit. If equal energies are recorded in any two opposite receivers the marine station is in correct position. If this is not the case, *automatic pilot systems of the vessel* should be set to work. Consequently, the marine station is continuously shifted about a fixed point.

As an ultra-sound transmitter perhaps the shaft-emitter described in [12] will be suitable. The manoeuvring of the marine station certainly can be done to a few meters by *Voith-Schneider propellers* [11] or by *Escher Wyss-adjustable propellers* [4]. The ocean depth corresponding to the marine station and eventually also the tide lift can be measured.

For locating a marine fix point and for navigation the fix point should be able to transmit on call, and furthermore, the triple-reflector must be cleanseable of depositions before measurements. The source of energy necessary for transmitting is stored in the case (3), being either *fuel cells* [1], [3] or *high-pressure air tanks.* Water could also be used by letting it flow in through a small nozzle fitted to the upper part of the tube thus driving a small *pelton turbine.* In great depth, of course, preceding pressure reduction is necessary. In smaller depths the *cleansing of the triple-reflector* can be accomplished by a jet of compressed air. For greater depths the following device will be useful. Figure 3 gives the top view. When not in operation the reflector (dashed circle) is covered by a plate (1). This plate is mounted on guide rails (2) fitted to the reflector. To the right-hand and the left-hand edges of the plate cables (3), (4) are fastened which run over pulleys (5), (6) and carry the weights (7), (8). Parts of the weights can be burst off by small explosive charges thus effecting the opening and closing of the reflector. The plate has a ridge-roofed top whose ridge is parallel to the guide rails. The marine depositions slip off the roof; hence, they cannot increase the weight of the movable parts. Marine fix points having become inoperable after years, can be reactivated by means of *submersed robots.* Today submersed robots are in a state of development that one thinks about restoring the treasures of the "Titanic" from 4600 m below sea-level. Much simpler is the following way: the marine fixpoints are not used till their energy is exhausted but before that happens a new fix point is dropped in a distance of about 50—100 m. Above both fix points marine stations are set up, and their distance and mutual azimuths are measured.

The main problem is the tying-in of the marine stations by means of stellar triangulation into a net of continental stations determined by stellar triangulation.

At first a global *stellar triangulation net* may be mentioned, recently proposed by the author: this net comprises *31 stations* located on the continents or on islands. The net extends round the whole equator like a belt. All 31 stations are positioned *in very favourable latitudes* ($\pm$ 18^0 to $\pm$ 28^0)

concerning the clouding of the sky. The zenith distances occurring in observations are less than 60^0. As a high target an *equator satellite* is necessary, orbiting the earth in a distance of 7000 km possibly in a circle. Its orbital period with respect to a terrestrial point amounts to about 5,2 hours. We presuppose an active satellite, flashing on call. The electric energy created in the satellite by conversion of solar energy is too small for frequent flashing (e. g. project ANNA), and the illumination of the satellite by Laser-pulses is not yet solved sufficiently. However, a thermo-nuclear reactor is in a promising state of development for creating electric energy in the satellite.

It may be pointed out that without entering into the mechanics of the satellite orbit *a smoothing of the computed positions of the target* is possible. Thus the positions of the terrestrial stations can be improved. Progressively with every orbit the positions of the stations and the satellite paths can be determined more and more accurate. It may further be mentioned that *no time measurement* occurs in this method of stellar triangulation, that *not the right ascensions* of the stars but only their *differences* enter the calculations, and that for the establishment of this net only a *rather small number of stars*, as compared to the whole sky, are necessary whose coordinates and proper motions will be determined the more accurately. The error-theoretical analyses and numerical calculations of this net were done by P. Meissl, who will report on this topic separately.

Stellar triangulation of stations outside that belt mentioned above will be accomplished by satellites with inclined orbits and by rockets. The necessary elevations are less than 3000 km.

If the positions of marine stations are to be determined by stellar triangulation, their displacements amounting to a few meters can be considered negligible as the stations are oscillating about a fixed point. However, when using even a small astrograph ($f = 1$ m), which needs only a few seconds of tracking for photographing the stars, a great problem arises; the above-mentioned oscillation of the gyro-stabilized platform is a hundred times too great. But the use of *star sensors* [10] developed during the last years (they were developed from photo-electric tracking devices e. g. [5], [8], [9], [13]) promises a solution of our problems, and this opinion is even more true as the further development of star sensors is of decisive importance for the progress of astrophysics (photography outside the atmosphere). The required accuracy of the stabilization by star sensors is stated to be 0,1″.

Another way is to *cut down on exposure times* for the star photographs. This can be accomplished by special emulsions and developing methods, and by photomultipliers. The use of short-focus cameras also permit short-time exposures; for they have wide picture angles thus catching brighter stars within their regions. As the satellites are flashing only on command, flashes and exposures can sufficiently be synchronized. We not only have to deal with inaccuracies due to the short focal lenght and to scintillation, but also elimination of refraction effects states a serious problem: the angles between the bright stars and the flashes are too wide.

A further possibility to determine the position of the marine stations with respect to the fixed ones is the measurement of distances to the high targets of stellar triangulation. There the oscillations of the marine station affect the distances only as small quantities of second order. For instance, at different times stellar triangulation observations are executed to three high targets (two targets are represented by different positions of one satellite, the third target is another satellite). Simultaneously with this observations the distances to the targets are measured from a marine station. Thus the position of the marine station can be calculated with respect to the existing net of stellar triangulations, provided the scale of the net is known. For the determination of the scale the measurement of the distance between any two points of the net (e. g. the distance between an arbitrary station and a high target) is sufficient theoretically.

Electro-magnetic *cm*- and *dm*-waves suffer from spatial and temporal variations of refraction and velocity in the ionosphere which are difficult to be compensated for. The precision of distance measurements by these waves as stated in literature are contradictory. With Laser, however, an excellent measuring accuracy has already been obtained (some decimeters).

If in a particular region an *especially dense net of marine fix points* has to be established, the interpolation of the net will not be done by stellar triangulation. One will rather make use of trilateration of the marine stations or of photogrammetric methods. The marine stations floating above the marine fix points are illuminated. Then photogrammetric pictures are taken at night from air crafts, stratosphere-balloons or rockets. Of course, only those marine stations have to be

set up which are in the picture area of the photograph. In the present case a very valuable condition results for the analytical aero-triangulation: all points have to lie on a continuous slightly curved surface. The effect of refraction is smaller for pictures taken downward from above than it is for those taken upwards from below. The procedure may also serve for the survey of densely clouded areas.

If the marine stations form triangles with side-lenght of only a few kilometers, their *position fixing* can be done solely by *ultra-sound.*

Example 1: The ocean dephts of the marine fix points P, Q, R may be known. From three unknown positions F_1, F_2, F_3 of a vessel turn by turn the three spatial distances to the three fix points are measured simultaneously. As the ocean depths are known the horizontal distandes can be calculated (Pythagoras). Figure 4 gives a top-view representation. Wanted are the sides of the triangle P, Q, R. A different paper of the author will deal with this geometrical problem (dangerous loci).

Example 2: The ocean depths of the three marine fix points P, Q, R may not be known. In that case two vessels A, B are necessary. From both vessels the spatial distances to P, Q, R are measured simultaneously while at the same time the distance AB is recorded electronically. The triangles ABP, ABQ and ABR thus known have a common horizontal side $\overline{AB}$. We assume the triangles to be rotated about that side into the horizontal plane, thus causing the points P, Q, R to move in vertical planes p, q, r (in Figure 5 this rotation is plotted only for point P, its unknown ocean depth being t). The measured distances determine uniquely the positions of those three planes. Both vessels move on, and the above measurements are executed from two more positions A', B' and A'', B''. Thus we have three given systems with three parallel rays each. These systems of rays have to be adjusted in such a way that any three corresponding lines intersect in one point. The solution of this problem leads to a quadratic equation. A dangerous locus occurs if the connecting lines between both the vessels are parallel to each other in at least two cases. Then two of the systems of rays are congruent. The most favourable intersections occur in case the connecting lines between two corresponding positions of the vessels suspend angles of 120^0.

The distance measurements stated in the above examples are executed in sloped directions. The refractions and variations in velocity encountered thereby are very large but hardly investigated yet, and depend on temperature, pressure and on the saline proportion as well as an plankton [7]. It may be mentioned that the temperature rapidly decreasing with depth, and the increasing pressure are responsible for the deep-sea sound channel (900 to 1300 m). In this channel detonations are perceivable even in a distance of 10.000 km. Trilaterations in the sound channel gave an accuracy of $0{,}3 \cdot 10^{-4}$ [2], [6].

The soaring world population requires the opening of new sources of nutrition, energy and raw materials.

Apart from some underwater mining near the coast, we have only random samples of the gigantic riches of the sea bottom (sea-weed, phosphates, natural oil, iron ore, magnesia, manganese, nickel). Now man is about to take possession of them.

Beyond that, a *very significant problem of geodesy* could be solved: if points of the surface of the ocean as well as points on the continents are determined by stellar triangulation the mutual spatial position of all points is uniquely defined. The points of the calm surface of the sea are *natural points of the geoid* which can be *determined by stellar triangulation in a non-hypothetical way.* In addition, the points are distributed on a surface twice the area of the continents where the geoid cannot be found without hypotheses and dogmas.

If the problem should arise to determine *points of the geoid without marking them by marine fix points,* the procedure described in Figure 6 might be useful. The method has the purpose to stabilize the marine station MS so that during the observations it can only perform the oscillations described at the beginning. The escort vessels 1, 2, 3 are anchored by means of the anchoring weights $\bar{1}, \bar{2}, \bar{3}$. (4) represents a hollow aluminium buoy. The latter is carrying the triple-reflector and is connected with the anchoring weights by thin steel-cables. After completion of the survey the hawzers are hoisted, the buoy emerges, and the whole system can be set up again in a desired position. Perhaps the escort vessels could be substituted by buoys, and the whole work done by a single ship.

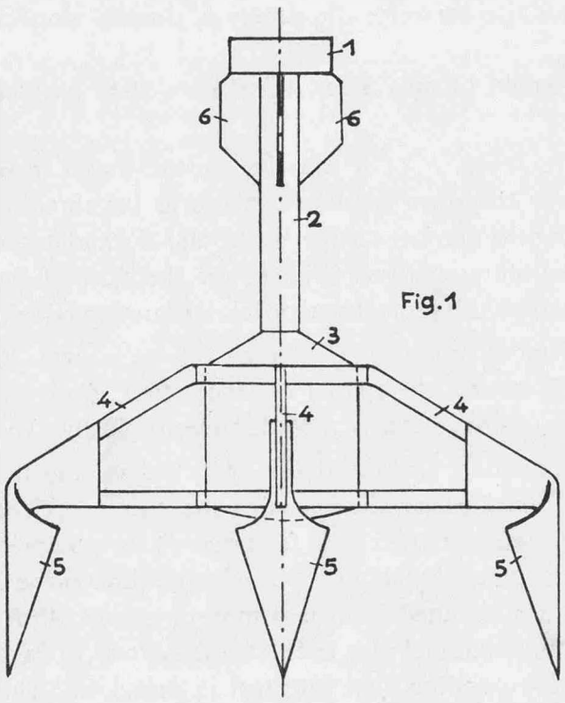

Fig.1

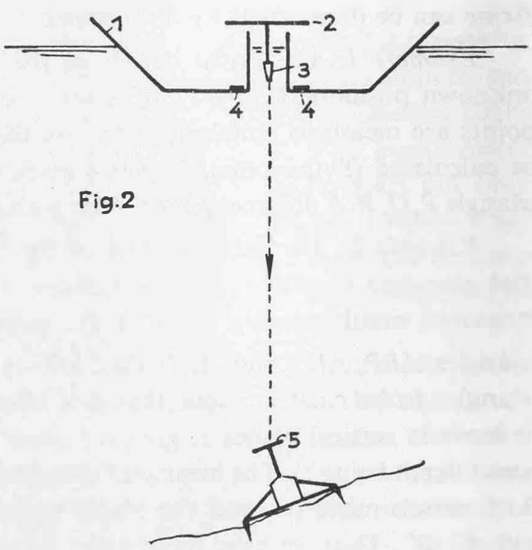

Fig.2

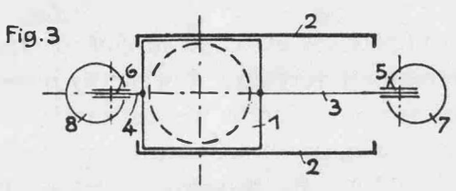

Fig.3

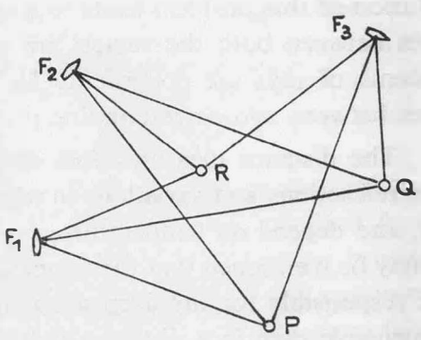

Fig.4

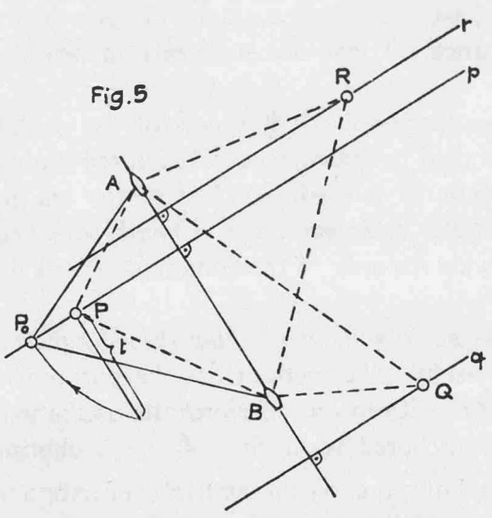

Fig.5

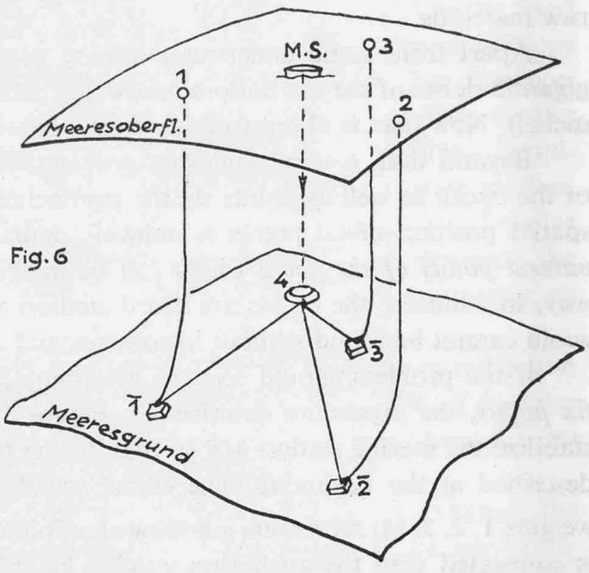

Fig.6

The survey is performed only when the sea is "calm". If in addition it is done in a distance of more than 100 km off coast the tidal lift is insignificant (less than 1 m).

The author conceived the above ideas and propositions as part of an American research contract (Prof. Dr. K. Rinner, Technical University Graz.).

Literature:

1. *Bode, H.:* Stand der Entwicklung von Brennstoffzellen, Erdöl und Kohle, 19 (1966), no. 9
2. *Bryan, G. M., Truchan and Ewing:* Long-Range SOFAR Studies in the South Atlantic Ocean, Journal of the Acoustical Society of America, Vol. 35, no. 3.
3. *Douglas:* Aus der Entwicklung der Brennstoffzellen, Arch. Energ.-Wirtschaft, 14 (1960), no. 11.
4. *Escher-Wyss:* Verstellpropeller, Prospectus 1964.
5. *Kovit, B.:* Astro-Compass Brings Space Navigation Closer, Space Aeronautics, June 1959.
6. *Piip, A. T.:* Fine Structure and Stability of the Sound Channel in the Ocean, Journal of the Acoustical Society of America, Vol. 36, no. 10.
7. *Pohlman, R.:* Die neuesten Ergebnisse der Ultraschall-Forschung in Anwendung und Ausblick auf die moderne Technik, und
   Ahrens, E.: Schall und Ultraschall in der Unterwasser-Nachrichtentechnik, Arbeitsgemeinschaft für Forschung des Landes Nordrhein-Westfalen, no. 101.
8. *Rabben, H. H.:* Einfache lichtelektrische Nachführvorrichtungen für astronomische Fernrohre, Elektronische Rundschau (1956), Vol. 10, no. 7.
9. *Simon and Suhrmann:* Der lichtelektrische Effekt und seine Anwendungen, pp. 594–595.
10. *Sprengel, U.:* Lageregelung und Stabilisierung von Raumfahrzeugen, Luftfahrttechnik-Raumfahrttechnik 13 (1967), no. 1.
11. *Voith-Schneider* Schiffsantrieb, Voith-Schneider Propeller, and other publications of the Voith-factories St. Pölten and Heidenheim.
12. *Wille, P.:* Ein strömungsgünstiges Richtmikrofon für Wasserschall als Analogon des dielektrischen Stielstrahlers, Acustica, Vol. 17 (1966).
13. *Zeiss, C.:* Photoelektrisches Sonnenleitrohr mit Verstärker, Prospectus and description in AsPlan 56–012–d.

Second Conference (SSG 23)

Recent Research on Atmospherical Refraktion for Geodetic Purposes

Part I

Problems of Atmospherical Refractive Iudex and its Influence upon Electro-optical Distance Measurements

A. Refraction Effect on Optical Distance-Measurements

Introduction and Opening by Prof. L. Asplund, President of Section I

Ladies and Gentlemen,

It is a great pleasure to me to be present here today and a great honour to open now this symposium on geodetic refraction.

Refraction or the refractive power of the atmosphere has always created problems to geodesists. The difficulties in determining its influence upon geodetic measurements are in many cases the main limiting factor of the accuracy obtainable by geodetic methods.

This fact was very much stressed when the electromagnetic distance measurement methods began to open new possibilities in geodetic technique. In the early discussions of the practical aspects of the three-dimensional geodesy, refraction in vertical angle measurements was predominant. For such reasons Section I decided at the Helsinki General Assembly 1960 to propose a Special Study Group on refraction, and following this proposal the Association formed the SSG I : 23.

Fortunately, Dr. Tengström, who by that time had started promising research on determining vertical refraction by dispersion methods, agreed to lead this SSG.

Since 1960, the question of refraction has become still more important due to the increasing accuracy of geodetic instruments, for instance for distance measurements. The development of satellite methods also has opened a new field for study of the influence of refraction.

As far as EDM is concerned, a review of the research on refraction problems, was given at the EDM symposium at Oxford in 1965. On that occasion we had the privilege to have amongst us experts on physics, meteorology, and radio-meteorology. They certainly could not present any ready-made solutions to our geodetic problems, but they helped in elucidating the full complexity

and all difficulties of determining the momentary effect of refraction along a path as used in geodesy, due to the large changes with time and space.

Approaches to solve the refraction problem have hitherto followed three different lines or combinations of these lines.

The first line is the averaging of a large number of measurements, systematically distributed in time with the view to obtaining such a spread of refraction influence, that the average can be succesfully reduced by some normal refraction formula.

The second line is the collecting of as much information on meteorological data along the path as possible and to make these observations as representative as possible. This method is very difficult in practice, but maybe in future information obtained by radio-meteorological means might be useful.

The third line is the direct determination of the total effect of refraction along the path at the observation moment, an approach used for instance in the dispersion measurement technique.

Maybe this symposium will show new possiblities. The papers, which will be presented to us these two days, will review the latest developments of the various attempts to master the refraction problem in geodesy. I am confident, that very much new and promising results will be reported and I am sure the discussions will be fruitful and that many new ideas for future development will be born.

Report from SSG 19 to SSG 23 on Matters of Common Interest Connected with Refraction

by *E. W. Denison, Feltham, England*

1. This is a report fromSSG 19 to SSG 23, since the overlap of interests of the two groups is obvious. This review is therefore intended to draw the attention of members of SSG 23 to work which has been reported to SSG 19. In many instances members belong to both groups, and therefore this report is not aimed at them. Indeed, those of them who are about to present papers at this conference need not worry that their papers will be forestalled here.

2. The most recent comprehensive account of research into Electromagnetic Distance Measurement is the printed record of the symposium held by SSG 19 at Oxford in September 1965. The full record of this symposium has now been printed and is available. (This is in accordance with Resolution Nr. 4 of the Final Plenary Session of that symposium.) There is no need to teach this conference the value of interchanging different aspects of scientific knowledge. Perhaps one example may be recalled. There may be some people at this conference who do not remember that the whole war-time theory of servomechanisms fell straight out of the theory of feed-back amplifiers, — one recalls the many applications of the Nyquist Diagram. By the use of feed-back techniques, the rapid progress of Radar came about, because the development of servomechanisms allowed the Radar sets to follow the tiniest of signals. Geodesy may directly benefit from this, perhaps by equipment intended to lock-follow stars or satellites. Geodesists are likely to owe an even greater debt in future to the electronic scientists, because the total effort in money and manpower which is going into electronic research is so colossal. This exchange of knowledge is therefore the justification for putting before one group a summary of some of the papers which were presented to another group.

3. Many of the subjects discussed at Oxford will not be mentioned here, such as descriptions of new equipment, zero errors of instruments, reflection problems, results of trilateration and triangulation tests, etc. Quite a lot which is directly connected with refraction remains. Relevant papers were: —

4. "Some Aspects of the Meteorology and Refractive Index of the Air near the Earth's Surface", by G. D. Robinson, of the Meteorological Office, Bracknell, Berkshire, UK.

Mr. Robinson pointed out that there is no satisfactory theoretical treatment of the temperature and humidity distribution near the ground. Dimensional methods and empirical results have been

combined. For instance, in the UK, measurements of refractive index over a 16 metre path over grass at two heights have given variations

	Height 5 cm	50 cm
Light	5 N units	1 N unit
Cm. waves	25 N units	6 N units.

In general, the higher the measurement above the ground, the more constant the result. At night things are better than by day, because the total heat transfer is less. Even so, if the wind falls to less than 1 metre/sec., considerable inhomogeneities may develop. The conclusions are not comforting. All that the surveyor can do is to choose the best conditions, i. e. times when the flux of heat and water vapour is least. This happens at morning or evening, when skies are overcast, and with a wind of at least a few metres/sec. Measurements of temperature, etc. should be taken at least ten feet above the ground. Even after taking every precaution, results can be bad near discontinuities such as coastlines. In fact, meteorologists think that surveyors are extremely lucky to get results as good as they appear to be. In the discussion on the paper, Professor Marussi said that geodesists relied on statistics, and expected the average of many results to be good.

5. "The Caithness Base Investigation", by Major M. R. Richards, the Ordnance Survey of Great Britain.

Large numbers of Tellurometer measurements were made on an accurately measured base, with meteorological readings taken at both ends of the line, on towers near the ends, and on towers near the actual line of the radio rays at intermediate points. There were so many readings that the full analysis of the results has not yet been done (though Mr. Poder may add something during this conference). In general, the results suggested that it is best to take the meteorological readings well clear of the ground, while keeping the E. D. M. instruments low down in order to reduce the effect of reflections. This agrees, of course, with the previous paper by Mr. Robinson.

6. "Some Results of Microwave Refraction Measurements over Snow and Ice Fields", by K. Nottarp, Institut für Angewandte Geodäsie, Frankfurt am Main.

Measurements over snow and ice fields struck two difficulties. On some occasions high refraction gradients reflected the wave upwards, just as though the earth had an extra surface a few feet above the ground, while at other times a cold dense layer of air refracted the wave down into the snow. The cure to both troubles was to elevate the (MRA 2) aerials at both stations.

As a contrast, the author made some measurements in the Libyan desert, where meteorological conditions were so regular that errors were easily kept within 2 N units. This shows that there are reasonable areas of the world, where the natural pessimism of meteorologists working in the UK is not justified.

7. "The Meteorological Conditions of Electromagnetic Wave Propagation above the Sea", by K. Brocks and H. Jeske, Meteorological Institute of the University of Hamburg.

Mr Jeske is the joint author of a paper due to be presented at this conference on a related subject. However, the earlier paper may contain some extra information of value to anyone who is measuring distance or angles over the sea.

8. "On the Path Curvature of Electromagnetic Waves", by J. Saastamoinen, Division of Applied Physics, National Research Council, Ottawa, Canada.

This paper describes the effect of the curvature of radio waves, and of light, as a function of temperature, pressure, and humidity, giving numerous mathematical relations. It suggests that if meteorological soundings (radio sondes) are available while E. D. M. measurement is going on, then appropriate corrections to the measured lengths should be made. In the discussion on this paper, Mr Robinson gave a warning about "do-it-yourself" radio sondes. These instruments are tricky, and they tend to smooth out irregularities.

9. „Multiple Wavelength Optical Distance Measurements", by J. C. Owens and P. L. Bender. "The Use of Atmospheric Dispersion for the Refractive Index Correction of Optical Distance Measurements", by M. C. Thompson and L. E. Wood.

These two papers are considered together. Joint authors of each of them will be presenting similar papers at this conference. However, they are of such importance that it is impossible to avoid mentioning them. The use of dual-wave optical measurements does seem to hold out a real

prospect of finding the average refractive index just where it is wanted most. No doubt Mr. Owens and Mr. Thompson will bring us up-to-date.

10. "The Accuracy of a 50 km Over-Sea Geodimeter Distance and a Study of Temperature Correction by Means of a Temperature Gradient Formula", by E. Bergstrand, Geographical Survey Office of Sweden.

SSG 23 may be particularly interested in this account of Geodimeter measurements over 50 km of the Baltic Sea. During the measurements, there should have been 5 metres clearance for the sight line to the reflector target, but the warm summer sea caused much negative deviation. During one whole month the target was seen after sunset over the horizon only once. At other times the reflector was visible before sunset, and then sank below the horizon. By making use of the dip of the horizon, temperature differences were computed, and the average temperature over the line was estimated to $\pm$ 0.3^0 C.

11. "Distance Measurement by Means of a Modulated Light Beam yet Independent of the Speed of Light", by K. D. Froome and R. H. Bradsell, National Physical Laboratory, Teddington UK.

This paper describes a new kind of instrument, the "Mekometer". In it the basic frequency standards are cavity resonators, constructed out of Invar, and filled with dry air which is allowed to acquire atmospheric pressure and temperature. The radio frequency is used to produce polarization modulation, via a crystal of ammonium dihydrogen phosphate (ADP), of a light beam. The light passes through a folded path to the distant reflector, and then returns through the same crystal, where it is reinforced or diminished in accordance with the phase change of the radio frequency. The resulting measurement gives the distance as a multiple of the physical dimensions of the invar cavity resonators, and should therefore be independent of the speed of light. The instrument can hardly be of much use to Geodesists, because its maximum range is about 2 km. However, the idea may be of interest to SSG 23.

12. "Range and Accuracy of the EOS Electro-Optical Telemeter", by H. Richter and H. Wendt, VEB Carl Zeiss, Jena.

This instrument is similar in principle to the Geodimeter, except that the modulation is produced by the ultrasonic oscillation of a crystal, — which acts as a grating, — instead of a Kerr cell. The light transmission of a grating is better, and therefore greater range is claimed.

13. That concludes the brief account of those papers which should be of interest to SSG 23. It is by no means complete. For example, Mr Culley's paper on SECOR has not been included, but he is due to speak at this conference. At the concluding session of the Oxford Symposium, one of the resolutions contained "the lack of sufficient information about refractive index along the path of electromagnetic distance measurements is the most serious of the remaining sources of error". Perhaps SSG 23 will be able to help? It will certainly be interesting to learn how much farther the dual wave length techniques have been taken during the last few months.

Recent Progress in Optical Distance Measurement: Lasers and Atmospheric Dispersion

by *James C. Owens*, Boulder, Colorado

Abstract

The development of lasers, new electro-optic light modulation methods, and improved electronic techniques have made possible significant improvements in the range and accuracy of optical distance measurements. Accuracies as high as a few parts in ten million appear feasible through the use of the dispersion method, in which simultaneous measurements of optical path length at two widely separated wavelengths are used to determine the average refractive index over the path. The design of a new instrument based on this method, and initial test results, are presented.

Introduction

The application of lasers and modern electronic techniques has resulted in significant improvements within the last few years in the measurement of long distances. Both a thorough general re-

ference on electromagnetic distance measurement (1) and an excellent survey of the applications of lasers to geodetic, geophysical, and astronomical problems (2) have recently become available. It now appears that a method has been developed which will permit rapid and convenient measurement through the normal, uncontrolled atmosphere of paths several tens of kilometers long to an accuracy better than one part per million.

The most convenient technique for making geodetic distance measurements involves the measurement of the transit time of electromagnetic waves over the path, multiplication of this transit time by the propagation velocity of the radiation in vacuum, and application of an appropriate correction for the refractive index of the atmosphere along the path. Because pulse techniques do not provide the requisite precision at present and direct optical interferometry is precluded by atmospheric turbulence, the transit time is normally found through measurements of the phase of a radio-frequency or microwave signal. This signal may be either propagated directly as an unmodulated wave, in which case the refractive index correction involves the low-frequency phase refractive index of air, or used to modulate a light beam, in which case the correction requires the use of the group refractive index for the optical carrier wavelength.

The modern optical method was first developed by Bergstrand (3), whose instrument utilized amplitude modulation of the light at 8,3 MHz and a photomultiplier tube for demodulation. Subsequent development has been sufficiently successful that although their maximum range is typically less than half of that achievable with microwave methods, the Geodimeter and related instruments are now routinely used in a large fraction of firstorder surveys. Under good conditions, when sufficiently accurate meteorological information along the path can be obtained, these instruments are capable of an accuracy of about one part per million over paths of a few kilometers or, at night, a few tens of kilometers. Replacement of the conventional tungsten or arc lamp by a gas laser, however, and utilization of recently developed UHF and microwave modulation methods (4, 5) and of modern phase measurement techniques can result in significant improvements in range and precision. By replacing the light source with a helium-neon laser, replacing the Kerr cell with a KH_2PO_4 modulator, and using an improved photomultiplier tube, the operating range of an otherwise conventional Geodimeter has been doubled (6).

The principal limitation to the accuracy of both microwave and optical measurements is the uncertainty in the average refractive index over the path due to inhomogeneity and turbulence in the lower atmosphere. At present, the average refractive index is usually estimated from measurements of pressure, temperature, and humidity made at one or more points along the path. Higher accuracy in the point measurements could be achieved by using optical or microwave cavity refractometers instead of meteorological sensors, but the fundamental problem of averaging over the path would still remain. Very good results can be obtained under favorable circumstances, that is, when the path is horizontal and at a constant distance above the ground, meteorological conditions are relatively uniform along the path and slowly varying in time, several sets of sensors are used, and averaging times are sufficiently long. An example of the precision attainable is given by a set of microwave measurements over a 17.1 km path along the coast of Florida using refractive index measurement at both end points (7), for which the standard deviation of the mean was found to be less than 1×10^{-6} for averaging times longer than 12 hours. Under unfavorable circumstances, however, as in measuring the distance between mountain peaks where meteorological conditions are less uniform and sensors can be placed only at the ends of the path, accuracies much less than one part per million would normally be expected. Microwave measurements over a 25.9 km path in Hawaii between the peak of Mt. Haleakala and sea level, corrected using refractivity measurements at the end points, have shown (8) that a 1 hour averaging time results in a standard deviation in path length of 9×10^{-6}, while increasing the averaging time to 8 hours decreases the standard deviation only to 7×10^{-6}. Moreover, even if meteorological conditions and path geometry permit the correct spatial average of refractive index to be found by this technique, drifts and rapid fluctuations in transit time due to atmospheric turbulence provide a background noise which can, under unfavorable conditions, severely limit the precision of existing instruments and can even preclude their use.

Although these limitations apply to both optical and microwave systems, the much smaller effect of water vapor in the optical region should permit the corrections to be made with somewhat

higher accuracy for optical than for microwave measurements. Nevertheless, even using optical techniques, rapid measurements or measurements of the highest accuracy will require a direct measurement of the average refractive index over the path rather than an approximation obtained by sampling.

Use of Athmospheric Dispersion

A direct optical method of determining the desired average was proposed by Prilepin in 1957 (9), although the technical feasibility of the method was unclear (10). The same idea has recently been put forward independently (11) along with suggestions for its experimental realization (12, 13). The method is based on the fact that the refractive index n of the lower atmosphere is dispersive in the visible spectral region, and hence two light signals traversing the same path but having different wavelengths will travel at slightly different velocities. Because $(n\text{-}1)$ at a given wavelength is proportional to air density for dry air, the difference in refractive index and hence the difference in transit time for the two signals will be proportional to the average air density over the path. A measurement of the difference in transit times, therefore, can be used to give the average density over the path. From this quantity the average refractive index for either wavelength may be calculated, providing the desired correction.

If L is the geometrical path length between light source and reflector, we may write the one-way optical path as $L + S$, where S is the additional contribution due to the atmosphere. We define the group refractive index by

$$n^G = c/U$$

where c is the speed of light in vacuum and U is the group velocity. Then S is given by

$$S = \int_0^L (n^G - 1)\, dx.$$

If the red 6328 Å helium-neon laser line is chosen for one wavelength and the blue 3660 Å mercury line for the other, the extra optical paths S_B and S_R for the blue and red light, respectively, will differ by about 10% (14). Because the refractivity of air increases sharply as the wavelength is reduced, in order to have large dispersion it is desirable to choose the shorter wavelength in the violet or near ultraviolet spectral regions. The ratio $A = S_R/(S_B - S_R)$, which is known to be essentially independent of air density (15) and only weakly dependent on atmospheric composition (16) (the largest effect being due to water vapor), can be determined satisfactorily for most purposes from published dispersion formulas for dry air. Since an error of 8 mb in the average partial pressure of water vapor (corresponding to a relative humidity of about 50% at 15° C.) leads to an error of 1×10^{-6} in the ultimate length determination, it will be necessary to have an estimate of the average humidity over the path under conditions of high absolute humidity or for highest accuracy, but this is the only meteorological measurement required. Hence an accurately measured value of $\Delta S = S_B - S_R$ can be used to find the desired correction S_R to approximately the same fractional accuracy. For a 15 km path, ΔS is about 40 cm and must be measured to 1.3 mm (one part in 300) to give L to 1×10^{-6}.

The New Instrument

A block diagram of the dual wavelength, microwave modulation frequency instrument under development at the ESSA Institute for Telecommunication Sciences and Aeronomy in Boulder, Colorado, is shown in Figure 1. The basic principles of the instrument are quite straightforward and are known to anyone familiar with conventional optical measurements of the velocity of light. For light of either wavelength passing out and back through the modulator, the intensity at the appropriate detector, averaged over a time long in comparison with the modulation period, will be a maximum if the round-trip transit time is an integral multiple of the modulation period. Hence observation of this intensity permits measurement of the transit time in terms of the modulation period. Measurements at different modulation frequencies permit the resolution of path length ambiguity.

Two separate light sources are simultaneously used, a helium-neon gas laser and a high pressure mercury arc lamp filtered to emit a narrow spectral band centered at 3669 Å, because at present there is no satisfactory laser which operates in the 3500—4000 Å range. The light from the two sources is collimated and superimposed, passed through a KDP electro-optic light modulator (17) operating at a frequency of 3 GHz, and transmitted by an 8″ Cassegrainian telescope. The light

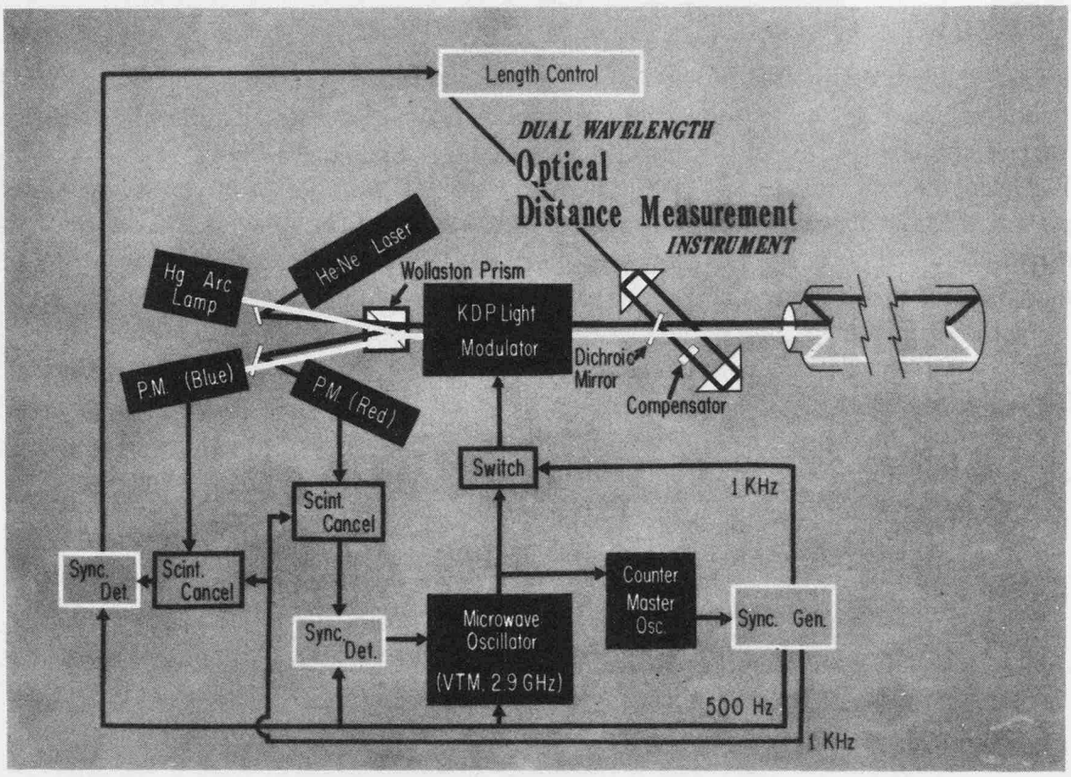

Fig. 1 Block diagram of the instrument

traverses the path to be measured and is returned by an 8″ cat's-eye retroreflector, passes through the modulator a second time, and is detected by one of a pair of photomultiplier tubes. Because the polarization, rather than the amplitude, of the light is modulated, a Wollaston prism may be used instead of a beamsplitter to separate the outgoing and returning beams. This prism also polarizes the light, combines the beams for transmission and separates them upon reception, and separates the modulated from the unmodulated component of the returning light. Thus one prism replaces an array of beamsplitters, polarizers, and dichroic mirrors. The use of a high modulation frequency provides the required precision with simpler methods of phase measurement than are possible with modulation frequencies of a few tens of megahertz, and thus tends to reduce certain systematic errors. This instrument, having a modulation wavelength of 10 cm, will measure the one-way distance to a precision of 1.5 mm if the modulation phase can be determined to 10^0.

The arrangement for measuring the difference in optical path ΔS is very simple. The blue light is transmitted directly from the modulator to the telescope, but the red light is diverted by a dichroic mirror and two prism reflectors around an adjustable supplementary path. A polarization compensator corrects for the effects of the prisms. By adjusting the position of one of the reflectors to give simultaneous intensity minima for both colors, the optical paths for red and blue are made equal (aside from an integral number of modulation wavelengths) and the difference in atmospheric optical path may be read out simply in terms of the distance the prism is moved from a reference position.

In order to track the fluctuations in optical path caused by changes in refractive index, a servo-control circuit locks the microwave modulation frequency to the optical path length in such a way that the path always remains an integral number of modulation wavelengths. This is done by modulating the frequency of the microwave oscillator by a small amount at 500 Hz, causing the re-

turning light signal to be amplitude modulated at 500 Hz unless the transit time is an integral number of modulation half-periods. The output of the photomultiplier detecting the red light is synchronously demodulated at 500 Hz, thus generating an error signal if the average refractive index over the path changes and hence the transit time no longer satisfies the half-integral condition. This error signal is applied to the microwave oscillator and shifts its frequency until the error is minimized. The necessary averaging over the frequency fluctuations is then performed by a counter which continuously monitors the microwave frequency. A second servo loop controlling the length of the "line stretcher" for red light tracks the changes in dispersion. These servo systems make the instrument self-balancing, a convenience when the optical path length is systematically changing, as at sunrise and sunset.

Finally, the effects of scintillation are largely cancelled by automatic normalizing circuits between the photomultipliers and the synchronous detectors. Rather than using beamsplitters to pick off reference signals, the microwave power is applied to the modulator in 100-μsec pulses with a pulse repetition rate of 1 kHz. The light intensity leaking through the modulator between signal pulses is monitored and used to control the gain of the normalizing amplifiers. In this way, optimum amplification can be maintained in the servo system without overloading during periods of high light intensity.

Results of Field Testing

The instrument was tested during August, 1966, using a 1.6 km path across Lake Hefner, near Oklahoma City. Although this path was too short and too uniform to illustrate clearly the advantages of the dispersion technique over conventional methods, it was chosen because meteorological data from a network of stations around and at the center of the lake and also a continuous record of microwave distance over the same path were available for comparison at this site. The final measurements were made during a 4-day period of nearly continuous operation at the end of the month. From one-minute samples of this data, the corrected distance was calculated using the two-wavelength method at 177 times.

The precision of the instrument in detecting optical path length changes for either wavelength was found to be about 3×10^{-8} with an averaging time of 10 seconds. This was checked by actually

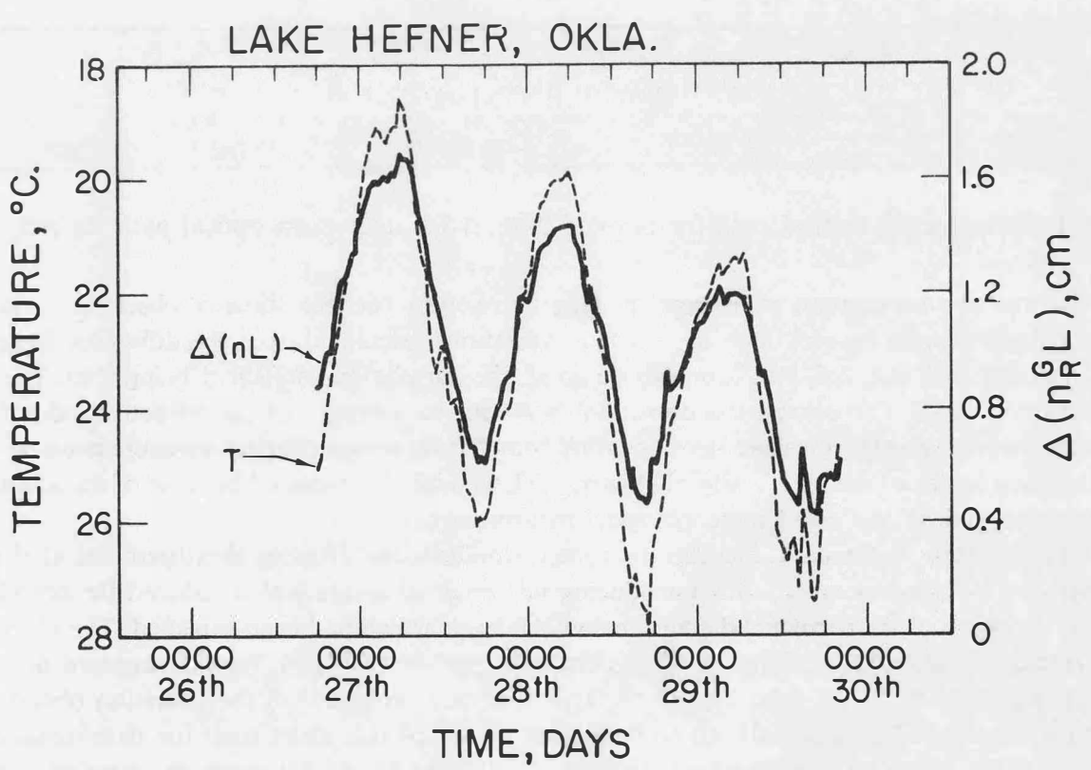

Fig. 2. Change in optical path for red light ($n_R^G L$), and temperature at midpoint of path versus time.

moving the retroreflector in small increments; a motion of about 50 μm could be detected. It is believed that the remaining limitation to precision is primarily due to instrumental noise and to amplitude scintillation of the light.

The temporal variation of optical path length for red light, $\Delta\ (n_R^G L)$, along with measurements of temperature made every half hour at the midpoint of the path, are shown in Figure 2. The diurnal variation of these quantities is very evident. The passage of a weather front late on August 29 caused the irregularity which can be seen in both curves. As expected, the variations in reciprocal temperature and in optical path length are highly but not perfectly correlated; the correlation coefficient is 0.915. A slightly higher correlation, 0.923, was found by including pressure variations and comparing the fluctuations in air density and optical path. The standard deviation of optical path length, which would have been the standard deviation of a one-wavelength distance measurement at this time and location if no meteorological information were used for correction and there were no other sources of error, was 2.2×10^{-6}.

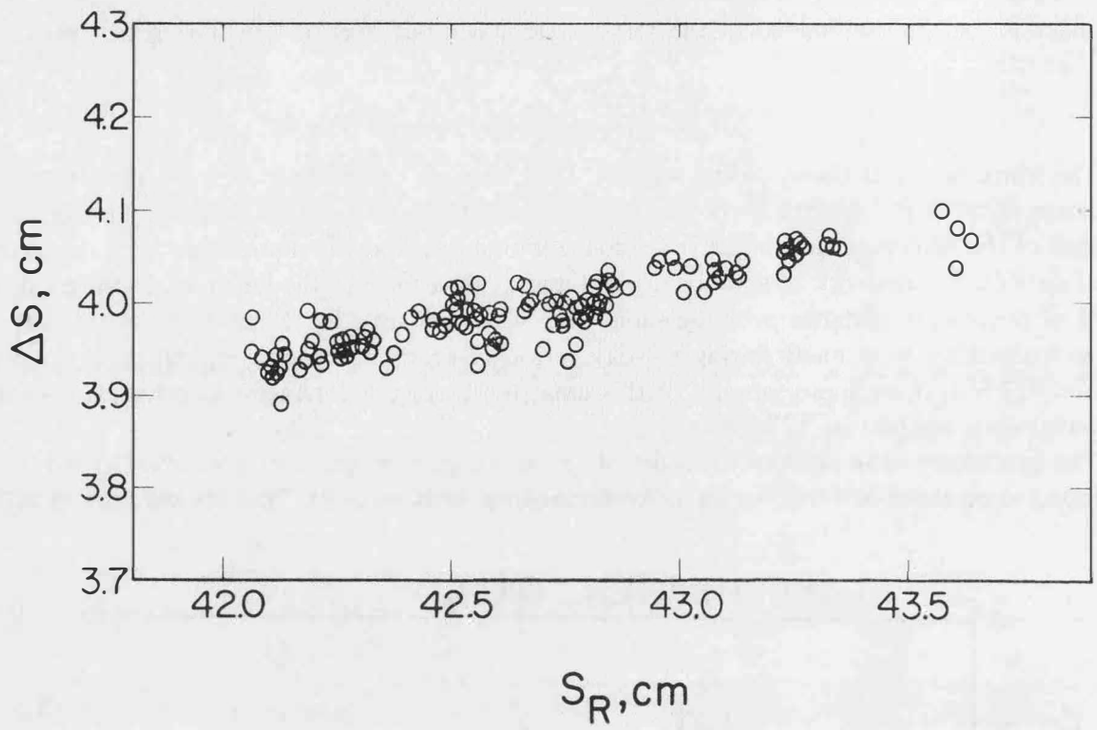

Fig. 3. Difference in optical path for red and blue, ΔS, versus extra optical path for red, S_R.

For the two-wavelength measurements, the correlation between directly observed variations in optical path length for red light, S_R, and the variations calculated from the difference in optical paths for blue and red, ΔS, was found to be good, the correlation coefficient being 0.89. The data are shown in Fig. 3. The correlation coefficient between the average optical refractive index found from the two-wavelength measurement and that found from meteorological measurements at both ends and the center of the path is slightly lower, 0.83, as might be expected because of the additional error introduced by the point meteorological measurements.

Unfortunately, technical difficulties prevented simultaneous distance measurements at the two wavelengths from being made, thus introducing instrumental errors which reduced the correlation and the precision of the corrected distance below the levels which had been expected. The 177 values of corrected distance found from the data, which are shown in Fig. 4, have a standard deviation of 1.55 mm, slightly better than 1×10^{-6}. This is somewhat less than the precision obtained by using meteorological data from both ends and the center of this short path for determination of the correction, which gave a standard deviation of 0.75×10^{-6}. Although the precision of the dispersion-corrected measurements is lower, it is better than had been expected for sequential measurements over such a short path and is highly encouraging, for we expect that the precision

of the dispersion correction relative to the meteorological correction will increase with longer, less uniform paths and simultaneous measurements.

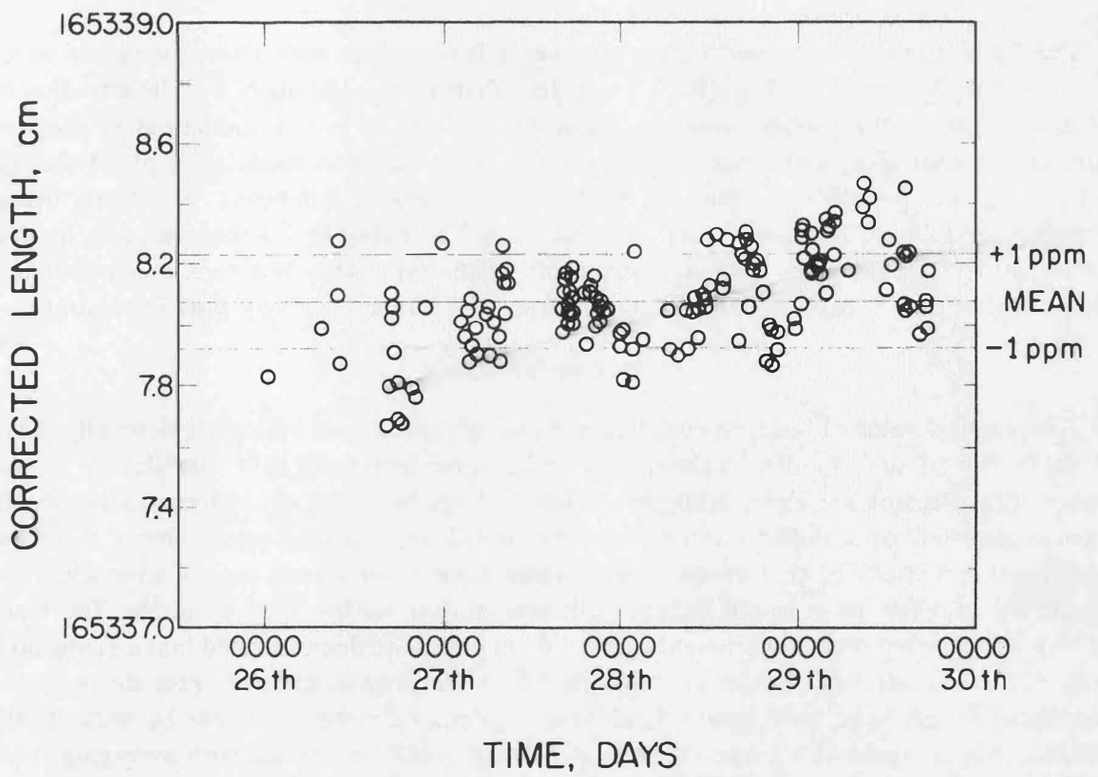

Fig. 4. Distance measurements made during a 4-day period using the dispersion method of refractive index correction.

For comparison, measurements of microwave distance were made over the same path during the same 4-day period using a new instrument (18) operating at 9.6 GHz, and corrected using the same 3-point meteorological data used with the optical measurements. The standard deviations of both uncorrected and corrected microwave measurements, which were 10.5×10^{-6} and 1.6×10^{-6}, respectively, are larger than the corresponding optical results. Finally, measurements taken over a parallel path during the 4 days with a commercial microwave instrument, corrected using meteorological data from both ends of the path, had a standard deviation of about 4×10^{-6}.

Averaging can, of course, give a mean value determined to higher precision than the individual data points. A conventional autocorrelation analysis showed that the standard error of the mean for the entire 4 days of optical measurements was a few parts in 10^7, which is comparable to previously reported microwave results. Although the standard error of the mean might decrease more rapidly with increasing averaging time if the data were continuous, the desirability of a sufficiently accurate measurement of the line integral of refractive index over the path which does not rely on long averaging times is clear.

The absolute accuracy of the corrected length measurements cannot be ascertained from these data. The most direct and accurate calibration could be made by taking measurements through a long (1 km or more) pipe which could be evacuated. If the position of the effective modulation point (the "zero error") and the modulation frequency were known with sufficient accuracy, measurements through such a pipe at various air densities could be used to determine the absolute accuracy of the correction method, within, the small remaining uncertainty due to variations in air composition. The same calibration could be made using data taken under a wide variety of meteorological conditions over a fixed outdoor path, but a much longer time would be required and the calibration would probably be less precise due to additional noise and extrapolation errors. The primary source of systematic error with the present instrument is the uncertainty in the effective wavelength of the light emitted by the mercury arc lamp, which gives rise to an error in the corrected distance of 3×10^{-7}/Å. The use of a narrower optical filter or of a laser instead of the arc lamp would correct

this problem. Part of the possible systematic error at Lake Hefner may also be due to the sequential measurements for red and blue; it is expected that an improved optical system, now being built, which permits simultaneous measurements will give a marked improvement in the precision of the corrected length measurements.

The fluctuations in path length observed over a few minutes with 10-sec averaging were typically less than 0.15 mm, or 1×10^{-7}, much less than one modulation wavelength. For homogeneous turbulence the root-mean-square value of modulation phase fluctuation is proportional to the square root of L, and hence we estimate that fluctuations in modulation phase during such short periods will probably be small for paths of a few tens of kilometers. Therefore, the use of microwave modulation frequencies on light beams will probably be feasible for quite long atmospheric paths, especially when used in instruments of the type described here which include servo systems having time constants short enough to track the larger, relatively slow fluctuations.

Conclusions

The practical value of lasers as convenient, monochromatic, and optically efficient light sources, and the utility of such modern techniques as microwave-frequency light modulation in geodetic distance measurement are clear. Although it has not yet been actually demonstrated, the use of the two-wavelength optical dispersion method is expected to permit the measurement under average atmospheric conditions of true geometrical distance over paths several tens of kilometers long to an accuracy of a few parts in ten million with averaging times less than a minute. The results of field tests of a developmental instrument over a 1.6 km path have demonstrated that a precision better than 1×10^{-7} in detecting changes in optical path for either wavelength and a precision of 1×10^{-6} in corrected length have been attained, although systematic errors may still be present. We are optimistic that an absolute accuracy of at least 1×10^{-6} will be attained with averaging times less than a minute.

Acknowledgments

The assistance of K. B. Earnshaw, who has been largely responsible for building and testing the instrument, and of the members of the Radio Meteorology Section, especially B. R. Bean, R. E. McGavin, and R. O. Gilmer, who provided and analyzed the meteorological and microwave measurements at Lake Hefner, are gratefully acknowledged. Discussions with P. L. Bender of the Joint Institute for Laboratory Astrophysics during the entire course of the work have been particularly helpful.

This work was partially supported by the Research Institute of GIMRADA, Ft. Belvoir, Virginia, and by the Advanced Research Projects Agency of the Department of Defense.

References

1. Jordan/Eggert/Kneissl, *Handbuch der Vermessungskunde, Band VI: Die Entfernungsmessung mit Elektro-Magnetischen Wellen und ihre Geodätische Anwendung*, K. Rinner and F. Benz, Eds. (J. B. Metzlersche Verlagsbuchhandlung, Stuttgart, 1966).
2. P. L. Bender, "Laser measurements of long distances", Proc. IEEE *55*, 1039–1045 (1967).
3. E. Bergstrand, "A determination of the velocity of light", Arkiv Fysik *2*, 119–151 (1950).
4. K. D. Froome and R. H. Bradsell, "Distance measurement by means of a light ray modulated at a microwave frequency", J. Sci. Instr. *38*, 458–462 (1961).
5. I. P. Kaminow, "Microwave modulation of the electro-optic effect in KH_2PO_4", Phys. Rev. Letters *6*, 528–530 (1961).
6. S. E. Smarthers, G. B. Lesley, R. Tomlinson, and H. S. Boyne, "Preliminary measurements with a laser geodimeter", to be published.
7. M. C. Thompson, Jr., "The effects of propagation on measurements of distance, angle-of-arrival, and Doppler effect in ground-to-ground systems", presented at XV General Assembly of URSI, Munich, Sept. 1966; to be published in Progress in Radio Science 1963–1966.
8. M. C. Thompson, Jr., H. B. Janes, and F. E. Freethey, "Atmospheric limitations on electronic distance-measuring equipment", J. Geophys. Res. *65*, 389–393 (1960).

9. M. T. Prilepin, "Light-modulating method for determining the average index of refraction of air along a line", Trudi Tsentral'nogo Nauchno-Issledovatel'skogo Instituta Geodezii, Aeros'emki i Kartografii, No. 114, pp. 127–130 (1957).
10. E. Bergstrand, "The geodimeter system: a short discussion of its principal function and future development", J. Geophys. Res. *65*, 404–409 (1960).
11. P. L. Bender and J. C. Owens, "Correction of optical distance measurements for the fluctuating atmospheric index of refraction", J. Geophys. Res. *70*, 2461–2562 (1965).
12. M. C. Thompson, Jr. and L. E. Wood, "The use of atmospheric dispersion for refraction correction of optical distance measurements," to be published in Proceedings of International Association of Geodesy Symposium on Electromagnetic Distance Measurement, Oxford, England, Sept. 1965.
13. J. C. Owens and K. B. Earnshaw, "Long-distance optical strainmeters for fault zone instrumentation", Proceedings of ESSA Symposium on Earthquake Prediction, United States Government Printing Office, 1966, pp. 85–92.
14. B. Edlen, "The refractive index of air", Metrologia *2*, 71–80 (1966).
15. K. E. Erickson, "Investigation of the invariance of atmospheric dispersion with a long-path refractometer", J. Opt. Soc. Am. *52*, 777–780 (1962).
16. J. C. Owens, "Optical refractive index of air: dependence on pressure, temperature, and composition", Appl. Opt. *6*,5 1–59 (1967).
17. I. P. Kaminow and E. H. Turner, "Electrooptic light modulators, Appl. Opt. *5*, 1612–1628 (1966).
18. R. O. Gilmer and D. M. Waters, "A solid-state system for measurement of integrated refractive index", Tech. Rept. IER-40/ITSA-40 (U. S. Government Printing Office, 1967) (to be published).

A Radio-Optical Dispersion Technique for Higher-Order Correction of Optical Distance Measurements*)

by *M. C. Thompson, Jr.*, Boulder, Colorado

A potentially serious error in electromagnetic distance measurements is the method of the estimation of the refractive index of the atmosphere. Current practice is to determine index values at each path terminal and to use the average to represent the entire path.

One approach for reducing this source of error exploits the atmospheric dispersion of certain regions of the spectrum. The use of this technique has been described previously in several papers [Tikhov, 1954; Prilepin, 1957; Bergstrand, 1960; Sullivan and Richardson, 1965; Bender and Owens, 1965; Thompson and Wood, 1965; Fowler, Castellano, and Hofmann, 1966]. Atmospheric dispersion over tropospheric paths has been measured in the cm-mm wavelength region by Sullivan and Richardson [1965], in the visible spectrum by Thompson and Wood [1965], and for the interval between cm and visible wavelengths by Thompson and Waters [1967]. The values obtained by Thompson and Wood were compared with expected values based on Edlén's formula [Edlén, 1953] and local measurements of atmospheric temperature and pressure. The mean values differed by about 2×10^{-8} with an estimated precision of 2×10^{-7}.

In dry air, measurement of the dispersion at two visible wavelengths gives sufficient information to estimate the spatial average of air density from which the desired index average can be obtained (see references in preceding paragraph). The accuracy of this estimate is determined by the accuracies of the measured dispersion and of the laboratory determined coefficients, and is also limited because the actual ray paths are generally not straight lines.

A potential source of error in this approach which, under certain atmospheric conditions, can be as large as or greater than those noted above, results from neglecting the presence of water vapor in the air. The value of this error calculated from Barrell [1951] is shown in Table I for sa-

*) A more complete paper giving the detailed analysis is currently being prepared for publication.

turated atmospheres at temperatures from 0 to 40° C (and 760 mm Hg total air pressure) [Thompson and Wood, 1965]. The importance of this error is, of course, influenced by the problem requirement and by the degree to which the spatial average of water vapor can be estimated from other supplementary atmospheric data.

By introducing a third wavelength in the microwave region, it should be possible to reduce significantly the uncertainty caused by water vapor. A system that measures range with a 5790 Å signal and dispersions between this wavelength and two signals at 4048 Å and 3 cm has been analyzed. The results indicate that to obtain an accuracy of 1 ppm in the corrected distance measurement requires an accuracy of better than 0.05 ppm in the 5790 Å to 4048 Å dispersion, and better than 40 ppm in the 5790 Å to 3 cm dispersion.

Although a complete three-wavelength system providing direct measurements of the two dispersions has not been operated, the elements of such a system have been used separately. The variability of the microwave-optical dispersion has been calculated from independent, but simultaneous, measurements of microwave and optical phase variations over a common 25-km path [Thompson and Waters, 1967]. Instrumentation developed by Thompson and Wood of the Institute for Telecommunications Sciences and Aeronomy is being used currently to record variations of the dispersion between 3.2-cm and 6328 Å signals over a 65-km path in Hawaii; the dispersion across the visible spectrum has been measured using several different techniques [Thompson and Wood, 1965; Fowler, Castellano, and Hofmann, 1966; and Earnshaw and Owens, 1967].

Based on this experience, noise levels of about 0.5 and 0.05 part per million or better seem to be feasible within a pass-band of 0 to 1 Hz over periods of about 1 hour for these respective radio-optical and optical-optical dispersions. The corresponding error in the refraction correction is about 1 part per million set principally by the uncertainty in the optical-optical dispersion measurement. As improvements are made in the necessary instrumentation for measuring the dispersion in the optical region, the overall errors should approach the limit from propagation effects.

The latter limit is probably the result of inexact estimation of the temperature along the path. Calculations were made for a case where one terminal is 3 km higher than the other, assuming a linear decrease of temperature with height from 40° C to 10° C, and linear variation of relative humidity from 50% at the lower end to 100% at the upper end. Taking the path temperature as the average of the terminal temperatures, an error of about 1 in 10^8 is introduced in the estimate of the refractive index correction for the optical distance measurement. This is about an order of magnitude better than one would expect from the two optical wavelength technique, even if the average relative humidity along the path were known to within a few percent [Thompson and Wood, 1965]. Thus the use of the third measurement in the microwave region appears to give significant improvement in accuracy for humid paths.

Effect of neglecting water vapor in *saturated atmosphere* at temperature, T, using 5790 Å for the distance measurement and 5790 Å and 4048 Å for the dispersion.

$T - {}^0C$	$\overline{N_t} - \overline{N_{calc}}$
0	0.77 N-unit
10	1.49
20	2.74
30	4.81
40	8.09

Table I

Abstract

A three-wavelength technique for refraction correction has been analyzed. Apparently by using 3 cm, 5790 Å and 4048 Å signals, the optical range measurement can be corrected for propagation effects to a few parts in 10^8 even in humid atmospheres. The present instrumentation, however, limits this accuracy to about 1 part in 10^6.

References

Barrell, H., The dispersion of air between 2500 Å and 6500 Å, *J. Opt. Soc. Am., 41*, 295–299, 1951.

Bender, P. and *J. C. Owens*, Correction of optical distance measurements for the fluctuating atmospheric index of refraction, *J. Geo. Res., 70*, 2461–2462, 1965.

Bergstrand, Erik, The Geodimeter system: A short discussion of its principal function and future development, *J. Geo. Res., 65*, No. 2, 404–409, Feb. 1960.

Edlén, B., The dispersion of standard air, *J. Opt. Soc. Am., 43*, 339–344, 1953.

Earnshaw, K. B. and *J. C. Owens*, Private communication, 1967.

Fowler, R. A., V. Castellano, and *R. Hofmann*, Geodetic laser survey system (GLASS) – An application to earthquake prediction (a paper presented at the 1966 Annual Meeting of the Am. Geophys. Union, Washington, D. C.).

Prilepin, M. T., Light-modulating method for determining average index of refraction of air along a line, *Tr. Tsentr. Nauchn.-Issled. Inst. Geod. Aeros. Kartog., 114*, 127–130, 1957.

Sullivan, J. F., and *H. Richardson*, Final report on the integral refractometer, The Mitre Corp., Report MTP-19, Dec. 1965.

Thompson, M. C., Jr., and *Donald M. Waters*, Radio-optical dispersion observed over a 25-km tropospheric path (to be published by IEEE, May 1967) 1967.

Thompson, M. C., Jr., and *Lockett E. Wood*, The use of atmospheric dispersion for refractive correction of optical distance measurements (a paper presented at the Int. Assn. of Geod. Symp. on Electromag. Distance Measure., Oxford, England, Sept. 1965).

Tikhov, G. A., Principal works of astrophysics and atmospheric science, Vols. I and II, 1954.

Satellite Ranging with a Laser and the Correction for Atmospheric Refraction*

by *C. G. Lehr, L. A. Maestre, P. H. Anderson*

Smithsonian Astrophysical Observatory, Cambridge, Mass.

1. *Introduction*

Laser systems[1–3] are useful in satellite geodesy because they can measure distances of the order of megameters with a precision of about one meter. Furthermore, the complexity and cost of such systems are moderate. The laser systems now in service in Europa and in North America use pulsed ruby lasers. At the present time, this type appears to have certain advantages over continuous-wave or other types of pulsed lasers. These advantages are the following:

1. The ruby laser generates the peak powers of tens or hundreds of megawatts necessary in measuring distances whose lengths are in megameters.
2. The ruby laser emits its radiation in pulse durations of tens of nanoseconds. These short pulses facilitate precise range measurements.
3. The ruby laser emits its radiation with a high degree of coherence; consequently, its energy can be focused to within a beamwidth of several minutes of arc. This value corresponds to the accuracy within which a typical satellite can be located by visual tracking or by prediction from computed orbits.
4. The ruby laser emits its radiation at a wavelength of 694.3 nm, where the retroreflectors on satellites currently in orbit are effective and wher ephotomultipiers, although not at their peak efficiency, are still more efficient than the other types of detectors that must be used at longer wavelengths.

The accuracy of the laser-range measurements depends on how well the two-way travel-time of the pulse can be measured and how well the correction for the atmosphere can be applied. The

*) This work was supported in part by Grant No. NsG 87–60 from the National Aeronautics and Space Administration.

error in the travel time measurement are not easily calculated from the characteristics of the system. The major difficulty arises in the determination of exact points on the leading edges of the transmitted and received pulses. It is between such points that the travel time of the laser pulse is measured. Small random instabilities occur in the shapes of these pulses and in the electrical circuits of the time-interval counter. The round-off error in the counter's last digit also introduces an error into the measurement.

The object of this report is an experimental determination of the error in the travel-time measurement. The experiment involves statisticalaveraging: consequently, it determines the *minimum* error that might be expected when the present system is used. The result shows what corrections for atmospheric effects will improve the accuracy of the range measurements and what corrections will be ineffective because they are dominated by system errors.

2. *The Laser System*

The present laser system was designed and built by the General Electric Company. It was designed for an initial experiment following the launch of the first satellite that carried a retro-reflector. Consequently, it does not utilize fully the very latest technology. However, it has operated continually since June 1965, and has made well over a thousand precise range measurements, some of which have already been used, along with Baker-Nunn camera measurements, in orbit calculations.

Figure 1 shows the laser on the naval gun mount that is used in tracking the satellite. Two observers acquire the satellite by cranking in predicted values of azimuth and elevation for the start of a given pass. When the satellite comes within the fields of view of their telescopes, they begin to track it visually. They continue tracking it to within one or two minutes of arc until it can no longer be seen. The characteristics of the laser are given in Table 1.

Table 1. Characteristics of the laser

Pulse duration	40—60 nsec
Power output	8 Mw
Beamwidth	1 mrad
Diameter of transmitted beam	10 cm
Wavelength	694 nm

The receiver is a modified 1.5-m searchlight. It has a Cassegrain configuration. The searchlight's paraboloid is the primary mirror. The secondary mirror produces a beam of parallel rays that strike the interference filter in front of the phototube at normal incidence. Table 2 summarizes the characteristics of the receiver. Figure 2 shows the receiver (with a cover that is in place for the tests that will be described below, but that is removed in actual operation). Visual tracking is accomplished by an observer who varies the velocities of the azimuth- and elevation-drive motors with a single control.

Table 2. Characteristics of the photoelectric receiver

Effective aperture	0.5 m (approximately)
Bandwidth	7 nm
Beamwidth	$1/3 - 1/2^0$
Quantum efficiency	3%

Table 3. Satellites with retroreflectors

Name	International designation	Inclination (degrees)	Apogee (*Mm*)	Perigee (*Mm*)
BE-B	1964-64*A*	80	1.1	0.9
BE-C	1965-32*A*	41	1.1	0.9
GEOS	1965-89*A*	59	2.3	1.1
DIC	1967-11*A*	40	1.4	0.6
DID	1967-14*A*	39	1.9	0.6

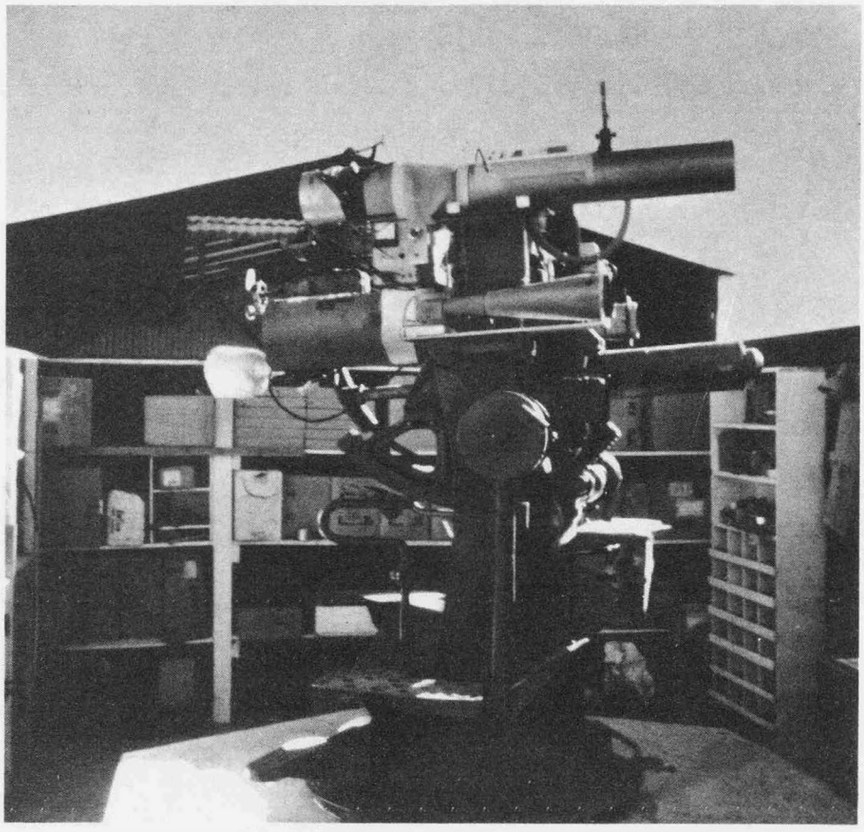

Fig. 1. The laser and tracking mount

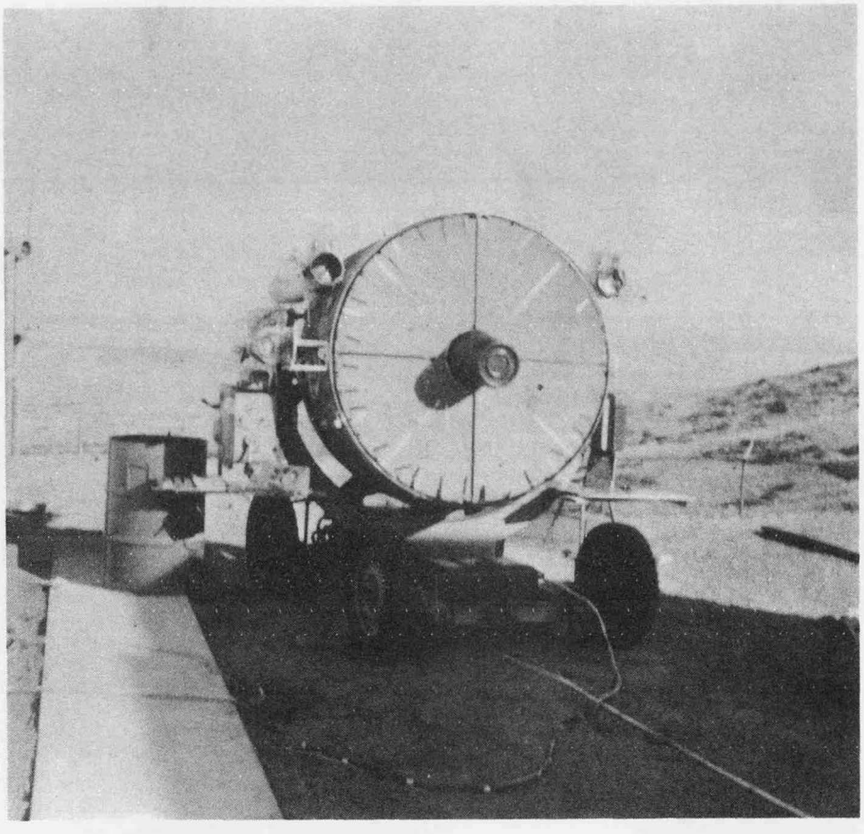

Fig. 2. The receiver with aperture covered for the experiment

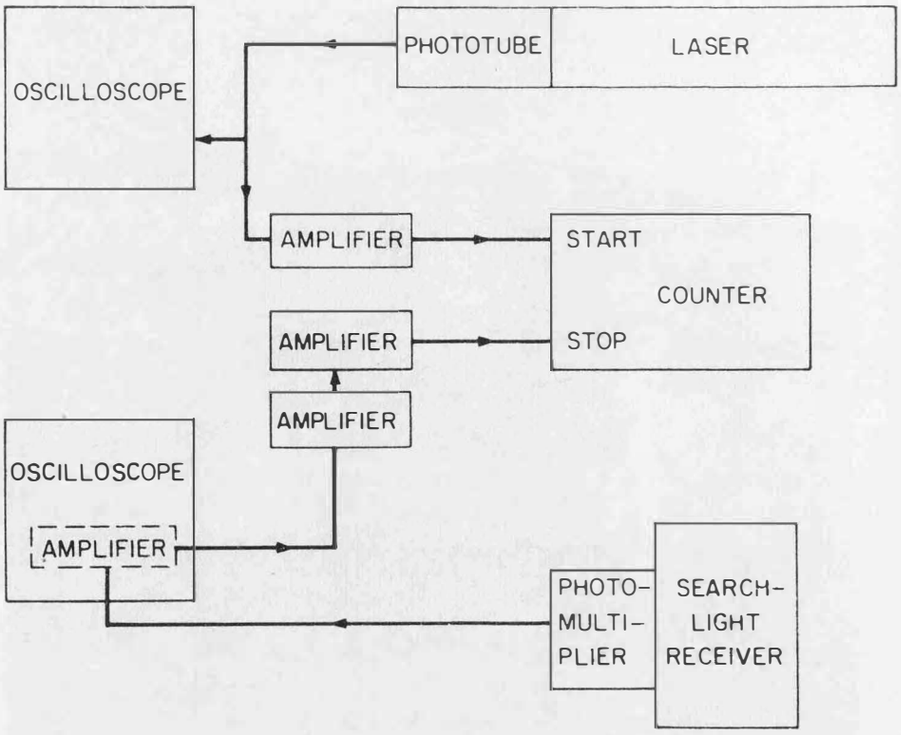

Fig. 3. Block diagram of laser-ranging system

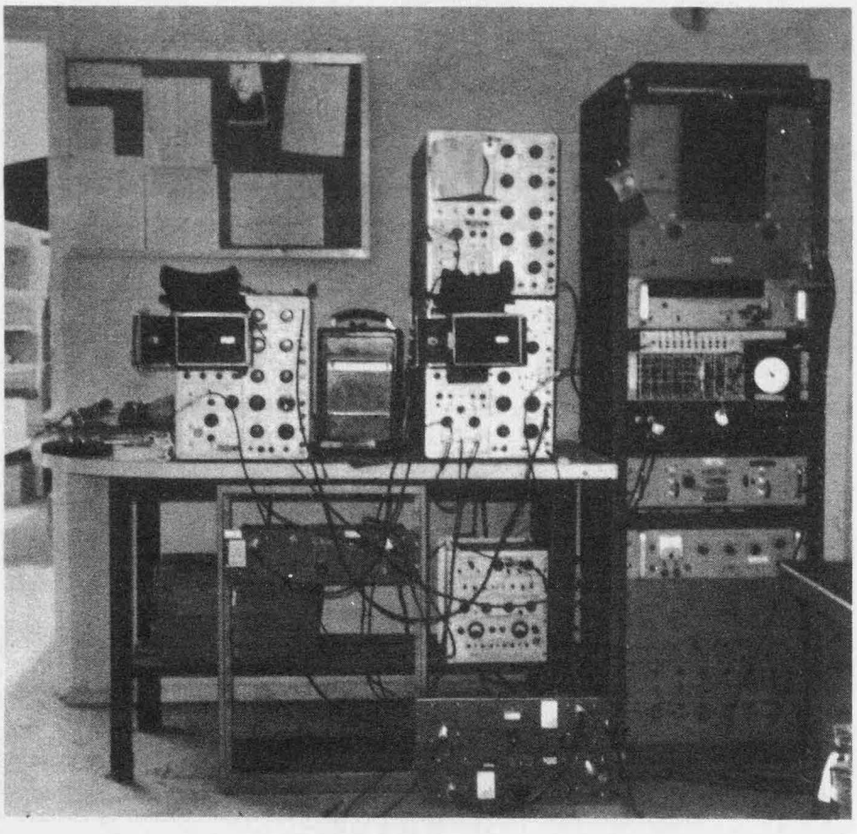

Fig. 4. The oscilloscopes, time-interval counter, and associated equipment

The laser system can range only on those satellites that carry retroreflectors. These retroreflectors return the reflected laser energy to the photoreceiver with sufficient concentration to make its detection possible. The five satellites with retroreflectors currently in orbit are given in Table 3.

The laser system is located at the Smithsonian astrophysical observing station, Organ Pass, New Mexico, U. S. A. The laser, the receiver, and the Baker-Nunn camera are within about 20 m of each other.

The operation of the laser system is governed by the station clock. This clock fires the laser every 30 seconds at epochs that are known to within 100 μsec. The clock also provides an accurate 1-MHz synchronizing signal for measuring the travel time of the laser pulse to the satellite and back. The timing is done by an electronic time-interval counter, the last displayed digit of which represents 10 nsec. The received laser pulses are presented on oscilloscopes. The amplitude of the signal is obtained from their displays. Figure 3 is a block diagram of the system. Figure 4 is a photograph of the time-interval counter, oscilloscopes, and associated equipment.

3. *The Accuracy of the Range Measurements*

Preliminary estimates of the accuracy of the laser-range measurements were obtained in two ways. The first involved the use of the range measurements along with the measurements of right ascension and declination from the Baker-Nunn cameras in the determination of satellite orbits. These computations gave a value of 34 m for the standard deviation of 29 range measurements on GEOS for the period 20 December 1965 to 5 February 1966. This standard deviation shows to what extent the data from the laser system are consistent with those of the network of cameras. The value of 34 m most likely comes mainly from the errors in the Baker-Nunn observations and from their imperfect geographical distribution. The errors in the laser system should be smaller. A second estimate of the error in the range measurements is a value between 1.5 and 4 m. The lower figure corresponds to the 10 nsec represented by the last digit of the time-interval counter. The higher figure corresponds to 30 nsec, one-half the transmitted pulse lenght (or the greatest error that might be expected in timing the reception of the laser signal). This second estimate is probably also a high one because the counter is triggered on the pulse's leading edge and because variations in the counter's last digit (for a fixed range) probably do not occur randomly, but contain infor-

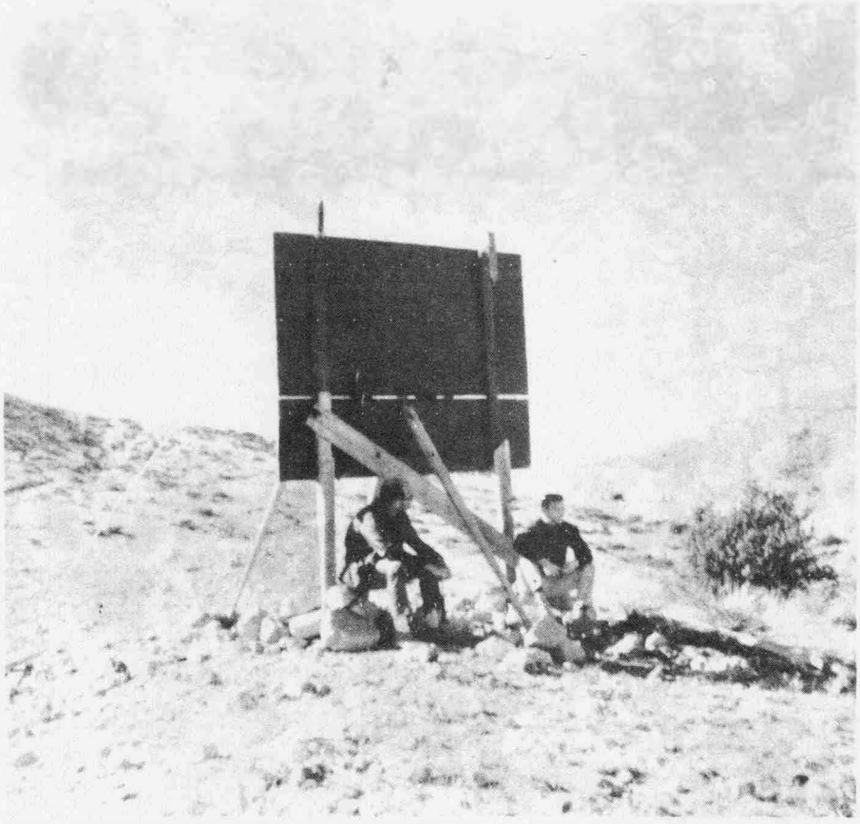

Fig. 5. The target

mation that can be used to approximate an additional digit. In order to evaluate these effects for the present system, the following experiment was performed.

Laser-range measurements were made on a fixed target 0.81 km from the laser system. This target is shown in Figure 5. The receiver was moved along the 10-m tape, which extended toward the target. Measured points on the tape were used to position the receiver. The target was painted black, the searchlight was covered, and a neutral density filter was placed over the photomultiplier to reduce the returned signals to values comparable to those received from satellite ranging. The cover of the searchlight had a number of small holes drilled in it. Most of these holes were taped

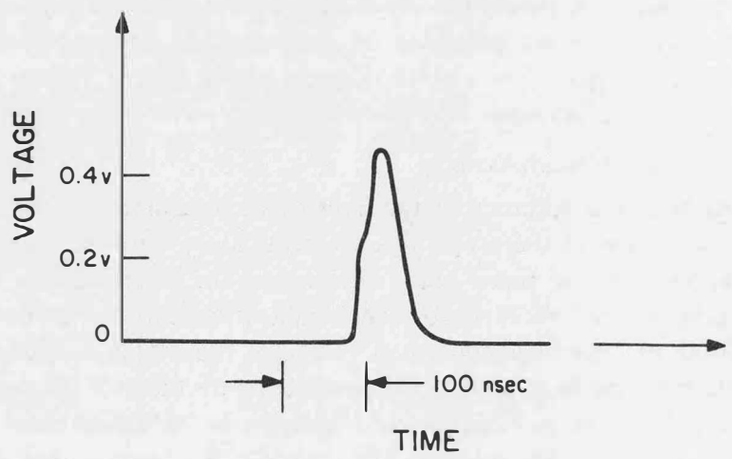

Fig. 6. A returned signal with a nonlinear leading edge.

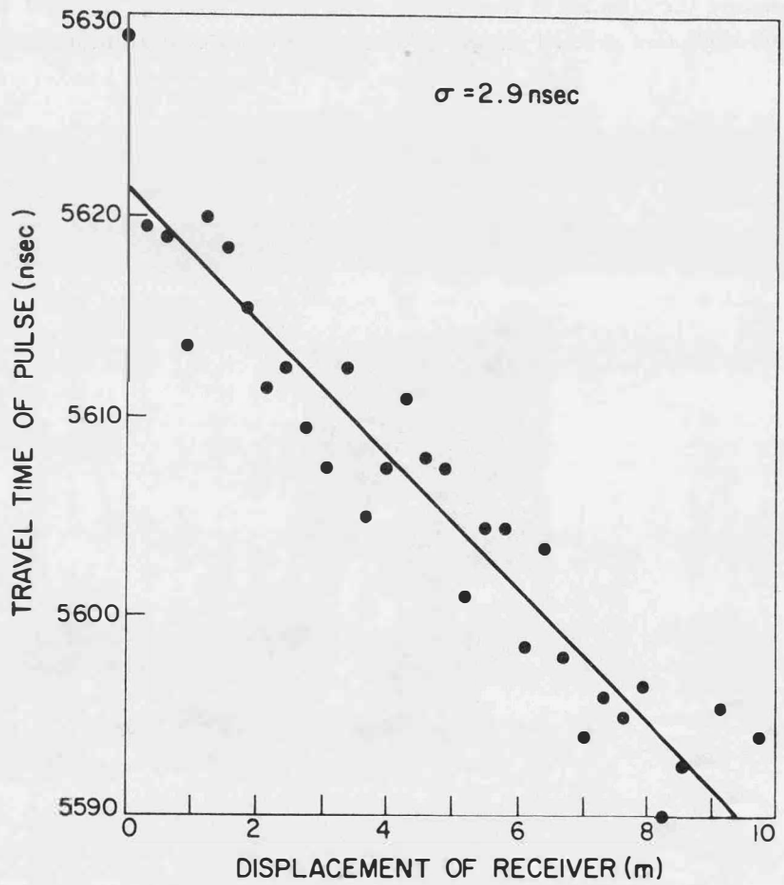

Fig. 7. Travel time of laser pulse versus displacement of receiver.

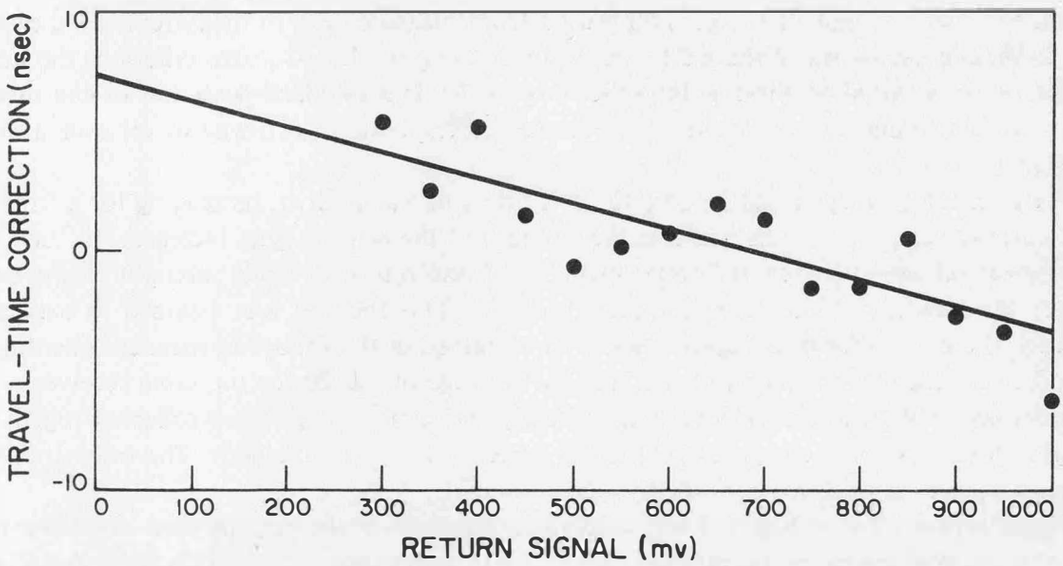

Fig. 8. Variation of travel time of laser pulse with strength of received signal.

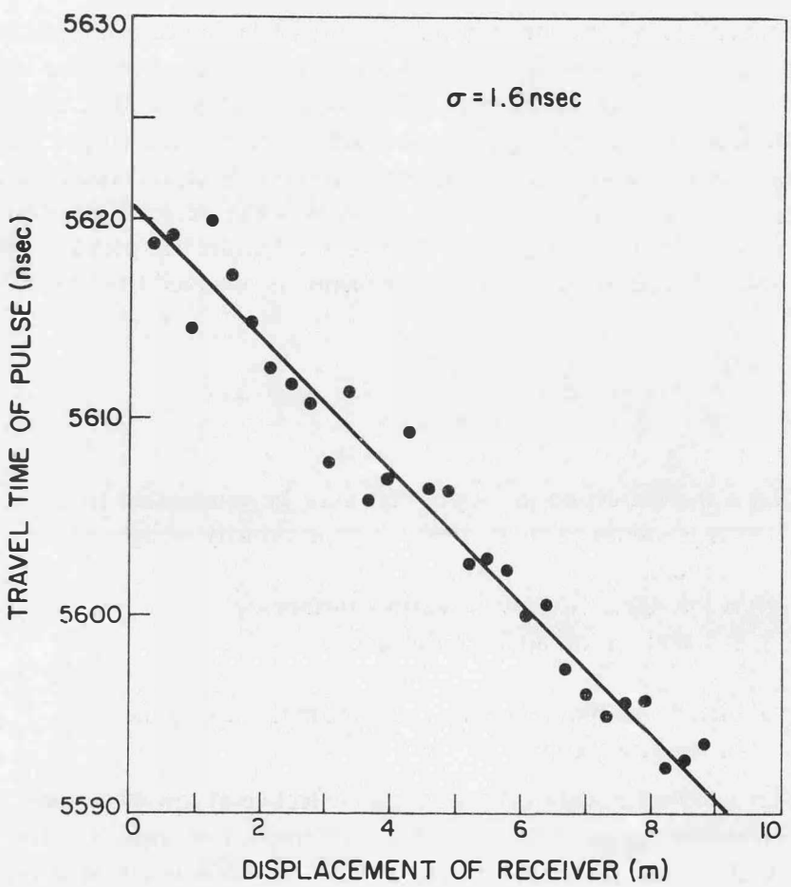

Fig. 9. Travel time of laser pulse versus displacement of receiver.

up. A few of the others were successively taped and untaped to minimize variations in the returned signal as the experiment proceeded. The leading edges of most returned signals were linear. A few, like the one in Figure 6, were a bit jagged.

The experiment consisted of a series of range measurements made with the receiver at a number of equally spaced points along the measuring tape. At each point, 20 time-interval measurements

were made. The last digit of the counter varied from measurement to measurement; the average of all 20 measurements was obtained for each point. Using the least-squares criterion, the best line of slope c^{-1} was fitted to these points. (See Figure 7.) The standard deviation of the measured points was then found to be 2.9 nsec, a value that corresponds to two-way travel over a distance of 0.44 m.

If a threshold voltage exists for stopping the time-interval counter, its reading for a fixed-range and fixed-pulse shape should decrease as the strength of the return signal increases. In such a case an empirical relation between the time interval and the returned signal strength might be used to lower the standard deviation of the measurements. This relation was assumed to exist and to be linear. The curve shown in Figure 8 was then obtained in the following manner. The difference between each time-interval measurement and the average of the 20 for the same receiver position were obtained. Differences corresponding to nearly the same voltage were collected together and averaged (regardless of the receiver position at which they were obtained). The best straight line (in a least-squares sense) was then fitted to these data.

The linear function of Figure 8 was used to correct each of the original time-interval measurements and again a best-fitting curve with slope c^{-1} was determined. The result is plotted in Figure 9. For this case the standard deviation is 1.6 nsec and the corresponding value for the measured distance is 0.24 m.

4. *Consideration of the Atmospheric Correction*

The earth's atmosphere affects the transmission of the laser beam in two ways. It decreases the velocity of propagation, and it bends the beam toward the earth. The bending introduces a geometrical effect, whose effect on the measured range is negligible. The change in the velocity of propagation introduces a small but significant refraction error in the range measurements.

In the correction for refraction, the atmosphere is commonly considered to have an exponential variation with height above the earth. Then the correction can be made of the refractivity at the earth's surface is known. Its value is proportional to the barometric pressure and inversely proportional to the absolute temperature. The range correction is obtained from the following equation:

$$\Delta R = \int_P Nds = \frac{N_s}{138.5 \sin \beta_o} \tag{1}$$

where

ΔR is the correction in meters that must be substracted from range values calculated by using the velocity of light in vacuum,

N_s is the refractivity at the earth's surface,

β_o is the elevation angle of the satellite,

and

P includes all points within the atmosphere along the path of the laser beam.

The retroreflectors on satellites now in orbit become ineffective at low elevations. With our system, no returns below elevation angles of 16^0 have been observed. Consequently, the use of $N_s = 292$ (for standard temperature and pressure) in eq. (1) shows that ΔR is 2.1 m at zenith and 7.7 m at minimum elevation.

The variation of this correction with changes in local weather may now be considered. Assume that N_s is proportional to p/T, where p is the local barometric pressure, and T is the local absolute temperature. Assume that corrections less than 0.24 m are not significant because, as shown above, they are dominated by errors in the system. Then the temperature and pressure variations should be considered in making range corrections when the standard deviation in the temperature is greater than

$$\Delta T = 273 \times \frac{0.24}{7.7} = 8.5^0 C$$

or the standard deviation in the pressure is greater than

$$p = 760 \times \frac{0.24}{7.7} = 24 \text{ Torr}$$

5. *References*

1. *Plotkin, H. H.:* "Tracking of Beacon-Explorer satellites with laser beams," COSPAR Information Bulletin No. 29, Regular Issue, pp. 18—21, December 1965.
2. *Bivas, R., and Moreal-Courtois, N.:* "Détermination de l'orbite du satellite GEOS-A au moyen d'un télémètre à laser à partir d'un station," C. R. Acad. Sci. Paris, Vol. 262, pp. 935—937, April 18, 1966.
3. *Anderson, P. H., Lehr, C. G., Maestre, L. A., and Snyder, G. L.:* "Laser experiments for determining satellite orbits," IEEE Journal of Quantum Electronics, Vol. QE-2, No. 8, pp. 215—219, August 1966.

The Effect of the Atmosphere on Precise Satellite Ranges Obtained by a Laser

by *K. Bretterbauer*, Vienna

A) Introduction

Recently a method has been developed which will help to establish a uniform world triangulation net of a precision never known before. This method concerns electro-optical distance measurements to artificial satellites. American and French scientists have reported on first results [1], [2], [3]. The range is obtained by measurement of the time a Laser pulse needs to travel from the ground station to the satellite and back. The resolution power of the time interval counter stated in [3] was $\pm$ 10 nanosec, which corresponds to an error of $\pm$ 1,5 m in the distance. We are justified to assume that the technique will be further improved and that finally a resolution of a few tenth of a meter will be feasible. Perhaps a combination of the pulse method with a phase measuring technique would serve this purpose. In such a system the pulse component could provide the coarse distance needed for the phase measuring technique.

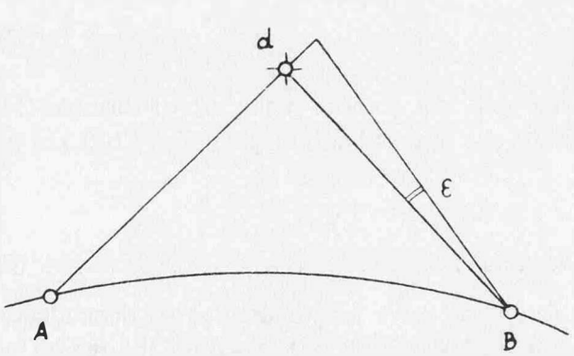

Fig. 1

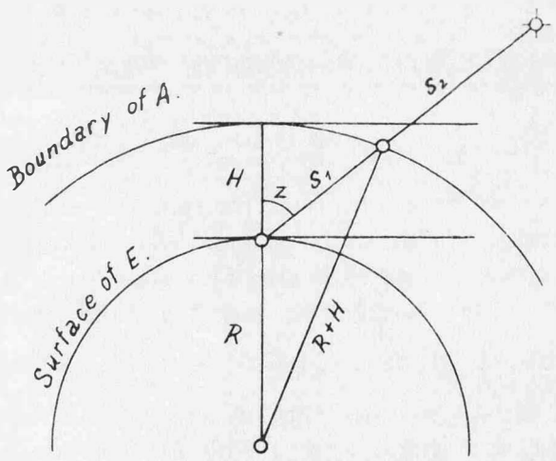

Fig. 2

The intensity of the Laser not only renders possible the direct measurement of ranges, but also is capable of illuminating a satellite fitted with retro-reflectors so that it can be photographed against the star background. Thus, a passive satellite becomes an active one. If the satellite is photo graphed by several stations, synchronism of the observation is guaranteed. With the photography obtained by longfocus astrographs, as is proposed by the Austrian scientist K. Killian [4], a final accuracy of 0,1″ in the determination of the satellite with respect to the star background seems

possible. For a satellite in a distance of 1000 km this amounts to a linear displacement of ± 0,5 m which is just the order of magnitude we have named desirable above. Hence, direction and range measurements can perfect each other in an ideal way, as can be seen from Figure 1. A ranging error of station A corresponds to a directional error of station B. Thus, one station can check the other.

In ranging geodetic satellites we are confronted with facts never encountered before in conventional electro-magnetic distance measurements: the beam of light passes the entire terrestrial atmosphere. Despite this fact, the effect of the atmosphere is surprisingly small. However, in order to maintain the accuracy of the ranging as stated above, it is necessary to study the constitution of the atmosphere.

The refractive index is defined as the ratio of the velocity of light in vacuo (c) to that one in air (v):

$$n = \frac{c}{v} = 1 + N \,.\, 10^{-6}; \qquad v = \frac{c}{1 + N} = c\,(1 - N)\,. \tag{1}$$

The distance between ground station and satellite consists of two parts, namely s_1 = path in the atmosphere and s_2 = path in free space. Thus (vide Figure 2):

$$s = s_1 + s_2 = \frac{t}{2}\left(\frac{v s_1 + c s_2}{s_1 + s_2}\right) = \frac{t}{2}\,\frac{c(1-\bar{N})s_1 + c s_2}{s_1 + s_2} = c\,\frac{t}{2}\left(1 - \frac{N s_1}{s}\right) = s' + \Delta s$$

where

$$s' = c\,\frac{t}{2} \quad \text{and} \quad \Delta s = - N s_1\,. \tag{2}$$

Since N is a function of the density of air, we understand N to be the integral mean along the path s_1, hence

$$N = \frac{1}{s_1}\int_0^{s_1} N(s)\,ds \tag{3}$$

Equation (2) shows that the atmospheric correction is independent of the distance of the satellite, but only a function of the height of the atmosphere and of the zenith distance of the satellite.

s_1 is obtained by the rigorous equation:

$$s_1 = - R\cos z + \sqrt{R^2\cos^2 z + 2RH + H^2}, \quad R = 6378 \text{ km} \tag{4}$$

As $H \ll R$, we may expand (4) into a binomial series. After some neglections we arrive at

$$s_1 = \frac{H}{\cos z}, \tag{5}$$

i. e. we have substituted the spherical earth by a plane one. All authors make use of formula (5), and justifiably so as even for H = 50 km and $z = 60^0$ the approximation gives s_1 = 100 km as compared with 98,85 km of equation (4).

The connection between N and the density of air ρ is defined by [5]:

$$n - 1 = N = k\,\rho\,. \tag{6}$$

k is nearly constant in air, and depends only slightly on the wave length used. This dependency on wave length is responsible for the variation of N from 290 to 298 . 10^{-6} within the region of the visible spectrum. The dependency of the refractive index on wave length is well known [6]. Thus, with λ = 6941 Å, i. e. the wave length of the Laser used by the Smithonian Institution [3]. $N_o = 291\,.\,10^{-6}$ for normal conditions ($t = 0^0 C$, p = 760 Torr). The surface value of N is accessible to observation via pressure and temperature of the ambient air according to the formula

$$N_s = \frac{N_o}{1 + \frac{t}{273}} \cdot \frac{p}{760} \tag{7}$$

The effect of water vapor is negligible.

B) The Atmospheric Reduction on Basis of Hypothetical Atmospheres

When advancing hypothetical theories on the structure of the atmosphere we have to consider a few physical laws. First, to heavy gases in aerostatic equilibrium the equation applies:

$$d\,U = -\frac{d\,p}{\rho} \tag{8}$$

U = potential, p = pressure, ρ = density.
Equation (8) states that the equipotentials are surfaces of equal pressure and of equal density. Further:

$$d\,U = -\,g\,d\,h \tag{9}$$

h = altitude, g = gravity. Finally there is the law of Gay-Lussac:

$$p = p_o\left(1 + \frac{t}{273}\right) \tag{10}$$

Together with the boundary conditions $t = t_o$, $p = 1$ for $h = 0$, and $p = 0$ for $h = H$ (H = height of entire atmosphere), the above equations provide the correlation between any two of the four variables t, p, ρ and h.

The first and simplest theory was stated by Cassini in 1662. Though physically absurd the atmospheric model is capable of representing all refraction phenomena surprisingly accurate. Cassini assumed density and gravity to be constant. From (8) and (9) follows at once after introduction of the usual units of measure:

$$p = \frac{\vartheta_L}{l_o\,\vartheta_{Hg}}(H - h) = 0{,}12514\,(H - h) \tag{11}$$

H and h in km, $\vartheta_L = 0{,}001293$ density of dry air at $0^0\,C$ and 760 Torr, with respect to water, $\vartheta_{Hg} = 13{,}596$ density of mercury, $l_o = 7{,}6\,.\,10^{-4}$ km length of the mercury column at normal pressure.

For $h = 0$, $p = 1$ the height of the atmosphere results to

$$H = 7{,}991 \text{ km}\,. \tag{12}$$

The temperature gradient also is constant and equal to $-\,34^0$ per km as results from (10), i. e. a multiple of the adiabatic gradient. Since in Cassini's homogeneous atmosphere the density is constant, the same holds for N which can be verified by introducing the pressure and temperature gradients into equ. (7). The atmospheric reduction of the path length then results from the formulas (2), (5) and (12). Table 1 gives the reduction for various values of pressure, temperature and zenith distance.

	$z = 0^0$			$z = 30^0$			$z = 60^0$		
$t =$	0^0	$+\,10^0$	$+\,20^0$	0^0	$+\,10^0$	$+\,20^0$	0^0	$+\,10^0$	$+\,20^0$
$p = 760$	2,33	2,27	2,21	2,69	2,61	2,55	4,66	4,53	4,42
740	2,25	2,18	2,13	2,60	2,52	2,46	4,50	4,37	4,26
720	2,17	2,11	2,06	2,50	2,44	2,37	4,33	4,22	4,12

Table 1
All values in meters

The values deviate only slightly from those of other authors. Immediately we shall use this simple law to test the effect of an error in N on the reduction:

$$\Delta s = -\,s_1\,\overline{N}\,;\quad d\,\Delta s = -\,s_1\,d\,\overline{N}\,;$$

for $d\overline{N} = \pm\,1\,.\,10^{-6}$ we get $\mathrm{d}\Delta s = \mp\,8$ mm for $z = 0^0$, and $\mp\,16$ mm for $z = 60^0$.

The next step in approximating the true atmosphere was done by Tobias Mayer (1760) [5]. He prescribed a linear decrease of density with increasing altitude:

$$\rho = 1 - \frac{h}{H}. \tag{13}$$

Again we get from (8) and (9) together with the boundary conditions:

$$p = 1 - \frac{\vartheta_L}{l_o \vartheta_{Hg}} \left(h - \frac{h^2}{2H} \right).$$

The height of the total atmosphere is $H = 15.982$ km. The temperature gradient again is constant and equal to $-17{,}1^0 C$ per km. Thus, the function $N = N(h)$ also is linear

$$N = N_s \left(1 - \frac{h}{H} \right) = N_s (1 - 0{,}0626\, h), \; h \text{ in km}.$$

Hence, the mean value becomes $\bar{N} = N_s/2$ and the reduction of the path length $\Delta s = -\bar{N} s_1$ renders exactly the same values as the model of Cassini (vide Table 1).

Contrary to the above hypotheses which give too great a lapse rate of temperature, Newton suggested a model atmosphere with constant temperature ($t = 0$). For the density distribution and thus for the refractive index an exponential law follows:

$$N = N_s\, e^{-\frac{R}{7{,}991} \frac{h}{(R+h)}}, \quad R = 6378 \text{ km},$$

We may write accurately enough

$$N = N_s\, e^{-0{,}125\, h}, \quad h \text{ in km}. \tag{14}$$

There the refractive index theoretically vanishes only at infinity. Hence, the integration should be extended up to the satellite itself. However, the e-term diminishes very rapidly after a few tens of kilometers so that

$$\bar{N} = \frac{N_s}{H} \int_o^H e^{-0{,}125\, h}\, dh = -\frac{N_s}{0{,}125\, H},$$

and

$$\Delta s = -\frac{N_s}{0{,}125 \cos z}$$

which formula again leads to the values of Table 1.

Formula (14) formally agrees with that one derived by G. Veis [7], only that Veis uses the numerical parameter $-0{,}1385$. As shown above, it is superfluous to adopt an exponential law for the lapse rate of N as such a law in practice gives the same values as the simple assumption of Cassini.

The preceding theories are contradictory to the observed facts concerning the temperature decrease with increasing height. In the case of the linear law the gradient was too great, in the case of the exponential law it was zero. The truce is somewhere in between. The idea is obvious to try a connexion of a linear and an exponential density law. We make the statement:

$$N = N_s \left(1 - \frac{h}{H} \right) e^{-\frac{h}{H}}. \tag{15}$$

For $h = 0$, $N = N_s$, and for $h = H$, $N = 0$. Since the real variable of equ. (15) is the ratio h/H, the integral mean proves to be independent of the assumed height of the atmosphere. Actually the integral gives:

$$\bar{N} = \frac{N_s}{H} \int_o^H \left(1 - \frac{h}{H} \right) . e^{-\frac{h}{H}} dh = \frac{N_s}{e}, \; e = 2{,}7183 \tag{16}$$

But in order to be able to calculate the correction in path length we have to dispose of H. Here we use no theoretical assumption, but suppose we had succeeded in obtaining the atmospheric

conditions in a particular height, for instance by a weather aircraft. With N_s, h and N_h known, we get at once H from equ. (15) and thus the correction of the path length

$$\Delta s = \frac{N_s}{e} \frac{H}{\cos z} . \tag{17}$$

In the following example we make use of the ICAO-Standard Atmosphere [8] which is defined in that way: surface values $p = 760$ Torr, $t = 15^0 C$, gradient $\Delta t/\Delta h = -6{,}5^0 C$ per km, and constant temperature of $-56{,}5^0 C$ from 11 km on. This gives: $N_s = 276 \cdot 10^{-6}$, $N_{11\,\mathrm{km}} = 73{,}5 \cdot 10^{-6}$, $\frac{h}{H} = 0{,}542$, $H = 20{,}3$ km and $\bar{N} = \frac{276}{e} = 101{,}6 \cdot 10^{-6}$. Table 2 states the path correction thus obtained. For collation purposes we also give the corresponding values of the homogeneous atmosphere.

Table 2, all values in meters.

$z =$	0^0	30^0	60^0	
$\Delta s =$	$-2{,}06$	$-2{,}38$	$-4{,}13$	ICAO-Standard Atmosphere
$\Delta s =$	$-2{,}21$	$-2{,}55$	$-4{,}42$	homogeneous atmosphere

C) Model Atmospheres on a Statistical Basis

We have arrived at model atmospheres which are not based on theoretical considerations but on statistics of the results of radio-sonde ascents. Besides the ICAO-Standard Atmosphere already mentioned, several other model atmospheres are in use, e. g. the CRPL Exponential Reference Atmosphere [9] which is defined by:

$$N = N_s e^{-c_e h}, \; c_e = \log\mathrm{nat} \frac{N_s}{N_s - \Delta N}, \; \Delta N = 7{,}32\, e^{0{,}005\,577\, N_s}. \tag{18}$$

Being formally identical with Newton's hypothetical atmosphere, it offers the advantage of having a variable parameter which can be adapted to prevailing conditions.

Purely empirical atmospheres also exist, being based on average results of numerous sounding balloon ascents [10]. Table 3 gives the average values of the atmosphere in temperate latitudes for summer and for winter.

Table see next page.

We can recognize clearly the well-known fact that the density of air in the troposphere is greater in winter than it is in summer. In the stratosphere, however, the density in winter is smaller than it is in summer.

For the reduction of electro-magnetic distance measurements often parabolically stratified atmospheres are used [9]. The general law of their refractivity reads:

$$N = N_s + a\,h + b\,h^2 \tag{19}$$

The parameters of equ. (19) usually are determined by way of a least square adjustment. But most of these atmospheres are defined only for the region $0 < h < 10$ km, which makes them useless for our purpose. If we want to derive the parameters of such a parabolic law, we have to dispose of H, and to determine the coefficients in such a way that N vanishes at the boundary of the atmosphere. The integral mean is:

$$\bar{N} = N_s + \frac{a}{2} H + \frac{b}{3} H^2 . \tag{20}$$

As an example the parameters have been derived for both the atmospheres of Table 3, but without an adjustment. We obtained the following formulas:

$$\begin{aligned} &\text{Summer:} \quad N = 277 - 18{,}68\,h + 0{,}294\,h^2 ; \quad \bar{N} = 60 \cdot 10^{-6} ; \quad H = 40\,\mathrm{km} \\ &\text{Winter:} \quad N = 290 - 19{,}75\,h + 0{,}313\,h^2 ; \quad \bar{N} = 62 \cdot 10^{-6} ; \quad H = 40\,\mathrm{km} \end{aligned} \tag{21}$$

Table 3

Summer					Winter					
h km		t^0 C	p_{mm}	$N \cdot 10^{-6}$	h_{km}		t^0 C	p_{mm}	$N \cdot 10^{-6}$	
0	+	14,8	762,6	277	0	+	1,7	763,4	290	
1	+	11,8	677,2	249	1	—	0,6	674,1	259	
2	+	6,3	600,3	225	2	—	4,2	594,4	231	
3	+	1,0	530,8	203	3	—	9,1	523,0	207	
4	—	4,3	468,2	182	4	—	15,3	458,9	187	
5	—	9,9	411,9	164	5	—	22,2	401,3	167	
6	—	16,3	361,3	147	6	—	29,3	349,6	150	
7	—	23,3	315,8	132	7	—	36,6	303,3	134	Troposphere
8	—	30,8	275,0	118	8	—	43,6	261,9	119	
9	—	38,3	238,4	106	9	—	49,6	225,4	106	
10	—	44,9	205,8	94	10	—	54,3	193,2	92	
11	—	50,1	177,0	83	11	—	56,8	165,2	80	
12	—	52,9	151,8	72	12	—	57,2	141,1	68	
13	—	52,8	130,1	62	13	—	56,3	120,6	58	
14	—	52,4	111,6	53	14	—	56,5	103,0	50	
15	—	52,0	95,7	45	15	—	57,1	88,0	43	
16	—	51,6	82,0	39	16	—	57,3	75,2	37	
17	—	51,1	70,3	33	17	—	57,6	64,2	31	
18	—	50,2	60,3	28	18	—	57,6	54,9	26	
19	—	49,6	51,7	24	19	—	57,6	46,9	23	
20	—	49,0	44,4	21	20	—	57,6	40,1	20	Stratosphere
25		—	20,6	10	25		—	18,3	9	
30		—	9,6	4	30		—	8,4	4	
35		—	4,5	2	35		—	3,8	2	
40		—	2,1	1	40		—	1,8	1	

The resulting atmospheric corrections of the path lengths (for $z = 0$) are listed below. For collation purposes we also state the corresponding values for the homogeneous atmosphere as well as those obtained by a graphic integration:

	Summer	Winter
Parabolic density law:	$\Delta s = -2{,}40$ m	$-2{,}48$ m
Homogeneous atmosphere:	$\Delta s = -2{,}22$	$-2{,}32$
Graphical integration:	$\Delta s = -2{,}33$	$-2{,}35$

Table 4

Hitherto we have tacitly assumed that the ray path is a straight line. But in fact it represents a spatial curve with negligible torsion and continuously decreasing curvature, provided the density also decreases continuously. We may presume that the entire curve runs in a vertical plane. Then its curvature can easily by stated and we shall estimate the error caused by neglection of the curvature. The curvature is [9, p. 548]:

$$x = \frac{1}{r} = -\frac{dN}{dh} \sin z \tag{22}$$

For obtaining dN/dh we use the parabolic law, and get from (19):

$$x = \frac{1}{r} = -(a + 2\,b\,h) \sin z\,.$$

Hence, the integral mean along the total path is:

$$\bar{x} = \frac{1}{\bar{r}} = -(a + b\,H)\sin z\,.$$

According to (21) the approximate values for the parameters are $a = -20\,.\,10^{-6}$ and $b = +0{,}3\,.\,10^{-6}$. Thus for $z = 60^0$ $\bar{x} = \frac{1}{\bar{r}} = (20 - 0{,}3\,.\,40)10^{-6}\,.\,0{,}866 = 7\,.\,10^{-6}$, and $\bar{r} = 1{,}4\,.\,10^5$ km. The difference between an arc and the corresponding chord is

$$d\,s = \frac{s^3}{24\,\bar{r}^2},$$

and with $s = \frac{H}{\cos z} = 80$ km, and $\bar{r} = 1{,}4\,.\,10^5$ km we get the effect of curvature on path length:

$$ds = 1{,}1\,.\,10^{-6}\text{ km} = 1\text{ mm}.$$

Hence, the path curvature may be neglected in any case.

D) Conclusions

The actual constitution of the atmosphere certainly will deviate more or less from the above model conceptions. The deviations are caused primarily by temperature anomalies, the so-called inversions. At night always surface inversions build up, because of radiation, especially in winter. At higher levels especially strong and extensive inversions, so-called free inversions, are frequently observed. Inversions are responsible for an even more rapid decrease of the refractive index. Of course, the results of radio sonde ascents will always be made use of, as far as available. Perhaps even special ascents should be arranged for the satellite observation. In order to test their value, the results of some radio ascents have been analysed according to different points of view. A detailed discussion in this paper would lead us too far. However, in any case the mean refractive index could be determined with sufficient accuracy by one of the model atmospheres discussed above. The correct determination of the surface value of N is much more significant. This is in analogy with the astronomical refraction. True, there is a fundamental difference between both these atmospheric phenomena: in case of angular measurements to celestial objects the curvature of the ray path near the observation station is of prime interest, and the effect of anomalies decreases with increasing distance. In distance measurements, however, all sections of the ray path are equally significant. Yet we have to bear in mind that only the lower parts of the atmosphere are subject to anomalies, and that the higher levels behave very regularly. Besides, any anomaly affects $\bar{N}$ only at the ratio of its linear extension, to the total magnitude of the atmosphere. With the height of the effective atmosphere being about 40 km, an anomaly even of $10\,.\,10^{-6}$ in N affects the mean value only by $0{,}5\,.\,10^{-6}$, provided the extension of the anomaly is 2 km.

There might be one more possibility of improving the determination of N_s by means of vertical angle measurements, as has already been proposed before [12], [13]. The knowledge of accurate geographical coordinates of the Laser-station provided, we could measure zenith distances of stars in nearest vicinity of the satellite. From the difference between computed and observed zenith distances, we can derive the refractive index:

$$z_{\text{comp.}} - z_{\text{obs.}} = r = \frac{N_s}{\sin 1''}\tan z,\; N_s = r \sin 1''\,\operatorname{cotg} z\,.$$

Finally a word on the velocity of light in vacuo. The American scientists use the value $c = 299\,792{,}8$ km/sec, the value of the IUGG is 299 792,5 km/sec, while Karolus [11] states 299 792,1 km/sec. Even if we assume we were in possession of a definite value with a standard deviation of only $\pm$ 0,2 km/sec as Karolus affirms for his value, this uncertainty would create an error in a distance of 1000 km of $\pm$ 0,67 m, which is a multiple of the uncertainty of the atmospheric reduction.

Summarizing, we may say that we are able to master the problem of the atmospheric reductions in satellite ranging even for the highest demands on accuracy. Since the same applies to the photographic position fixing of satellites with respect to the system of stars, the combination of both methods at last represents a geodetic procedure which is sufficiently free of the unfavourable

effects of the atmosphere. The border line of accuracy is drawn by the present state of instrumental techniques and of researches concerning the determination of the velocity of light.

References

[1] "The Two-Way Transmission of a Ruby-Laser Beam Between Earth and a Retroreflecting Satellite." Proceedings of the IEEE, Vol. 54, No 3, March 1966, pp. 426–427.

[2] *Bivas, R.:* "Telemetrie des Satellites Artificiels par Laser." Paper presented at the Oxford Symposium on EDM, 1965.

[3] *Anderson, P. H., C. G. Lehr, and L. Maestre:* "Use of a Laser for Satellite-Range Measurements", SAO Special Report No. 190 R, Smithonian Institution, 1965.
Lehr, C. G., L. A. Maestre, and P. H. Anderson: "Measurements of Satellite Range with a Ruby Laser". SAO Special Report No. 211, 1966.
Lehr, C. G.: "Satellite Tracking with a Laser" SAO Special Report No. 215, 1966.

[4] *Killian, K.:* „Über Verfahren zur Stellartriangulation", Österreichische Zeitschrift für Vermessungswesen, Vol. 51, No. 1, Febr. 1963, pp. 3–14.

[5] *Bemporad, A.:* Refraktion und Extinktion", Enzyklopädie der mathematischen Wissenschaften, Vol. VI/2, pp. 287–314.

[6] *Edlen, B.:* "The Refractive Index of Air", Metrologia, Vol. 2, No. 2, pp. 71–80, 1966.

[7] *Veis, G.:* "Geodetic Uses of Artificial Satellites", Smithonian Contributions to Astrophysics, Vol. 3, pp. 95–161.

[8] *Meyer, H. K.:* "The Troposphere", NATO Conference Series, Vol. 3.

[9] *Jordan-Eggert-Kneissl:* Handbuch der Vermessungskunde, Vol. VI, § 38, p. 224.

[10] *Humphreys, W. J.:* "Physics of the Air", Third Edition, Dover 1964.

[11] *Karolus, A.:* „Neue Ergebnisse der Lichtgeschwindigkeitsmessungen...", V. Internationaler Kurs für geodätische Streckenmessung, Zürich 1965.

[12] *Saastamoinen, J.:* "Some Experimental Results on the NASM 4-B Geodimeter", The Canadian Surveyor, Vol. XVII, March 1963.

[13] *Bretterbauer, K.:* „Über den Brechungsindex der Luft" Zeitschrift für Vermessungswesen, Vol. 91, No. 2, Febr. 1966.

B. Refraction Effect on Distance Measurements, Using Radio Wave Propagation

Atmospheric Corrections to Tellurometer Measurements

by *Knud Poder*, Copenhagen

The subject of this paper are the corrections applied to Microwave Distance Measuring (MDM) equipment used for measuring distances (in the troposphere) between stations in ordinary geodetic networks (i. e. stations with distances up to 100 km).

As the troposphere is a non-dispersive medium (except for some discrete frequencies where strong molecular or atomic energy absorption occurs), the dual frequency method, which is very promising both for light-waves in the troposphere and microwaves in the ionosphere, cannot be used.

It should be added, that a dual frequency technique or rather a multifrequency technique is used for this type of measurement for a quite different reason. There will in general be more than one "propagation path" due to the wide beam transmitted and received, and it is possible to separate the information from the "reflection" path(s) from the "direct" path if several carrier frequencies are used in turn. MDM equipment with shorter wavelengths than mostly used to day may be useful for reducing these multipath effects both by narrow beamwidths and more diffuse reflection.

After all these pessimistic remarks, we should note that the well-proven geodetic technique of reiterated measurements for "randomizing" errors is possible in a much higher degree than with optical methods, because MDM can be executed in almost any weather and is not restricted to a special weather situation, which gives sufficient visibility.

The problem therefore is limited to

1. Establishment of a model of the atmosphere by means of which the reduction formulae may be found.
2. A method for determining the parameters of the atmosphere model.
3. Estimate of errors, number of measurements for randomizing errors, design of network types, which can be brought to agree with accuracy specifications.

1. *Atmosphere Model and Reduction Fomulae.*

1.1. *Fundamental Assumptions and Formulae.*

1.1.1. The instrument indicates the transit time θ multiplied with some constant (mostly a multiple of a modulation frequency, which is assumed to be known with sufficient accuracy). If more than one propagation path is possible, we assume that it has been possible to detect the direct one.

1.1.2. The concept of propagation paths and rays in general is permitted, when

1) the radius of curvature of the surface of equal phase must be larger than the local wavelength and
2) the variation of the refractive index with height, dn/dH, must satisfy

$$\frac{dn}{dH}\frac{\lambda}{2\pi}\cos z \ll 1, \tag{1.1}$$

where z is the zenith distance of the ray (APPLETON, 1946).

1.1.3. The transit time may be expressed by

$$\theta = \int_S d\theta = \int_S \frac{ds}{c} = \frac{1}{c_v}\int_S n\,ds\,, \tag{1.2}$$

where

ds is an element of the propagation path,
c is the velocity of the waves at the path element ds,
c_v is the vacuum velocity of electromagnetic waves,
n is the refractive index at ds. $cn = c_v$
The integral is evaluated along the propagation path of the length S, which gives a minimum of θ.

Reference is made to MORITZ, 1961, who solves the problem in a very elegant way by integration along the straight line (station chord) between the two terminals of the line.

1.1.4. The atmosphere is assumed horizontally stratified. This means that the refractive index can be expressed as

$$n = n_o + H\frac{dn}{dH}, \tag{1.3}$$

where H is the height over zero level. This model of the atmosphere has two parameters only. Objections against this simple approximation will be discussed later Sec. 1.6.

1.1.5. The refractive index is given by the formula of ESSEN and FROOME.

$$(n-1)10^{-6} = 103\,.\,49\,P/T - 17\,.\,23\,e/T + 495822\,e/T^2, \tag{1.4}$$

where

P is the total air pressure in mm Hg
T is the air temperature in K^0
e is the partial pressure of water vapuor, in mm Hg

With

$$M = (n - n_s)\,.\,10^6 \tag{1.5}$$

$$n_s = 1.000\,308\,6 \tag{1.6}$$

$$T_o = 313^0\,K, \tag{1.7}$$

the formula can be simplified to

$$M = 103\,.\,49\,P/T + 4\,.\,904\,10^5\,e/T - 308\,.\,6 \tag{1.8}$$

where the error is

$$17\,.\,23\,(T_o - T)e/T^2,$$

which never exceeds 0.15 inside the range of validity of the formula. ESSEN and FROOME, 1952.

1.1.6. In the propagation path the relation

$$(R + H)n \sin z = \text{constant} \tag{1.9}$$

is valid for any point. (In fact the differential relation defining the path can be derived from this relation, which is well known from general refraction theory). From (1.9) it is easy to find the ratio of tangent angular variation to displacement on the path, which defines the curvature. The curvature is

$$-\frac{dn}{dH}\frac{\sin z}{n} \cong -\frac{dn}{dH} \tag{1.10}$$

The simple approximation on the right hand side has an accuracy of better than 2 per cent for $80^0 < z < 100^0$.

The curvature may be related to the curvature of the earth R by the factor k used for trigonometric levelling as

$$-\frac{dn}{dH} = \frac{k}{R}. \tag{1.11}$$

The k used here differs from that used for light. In general $k = 0.25 - 0.30$.

1.1.7. The method used for deriving formulae for trigonometric levelling gives for the height of one terminal H_2 expressed by the height of the other terminal H_1

$$H_2 = H_1 + S\cos z_1 + S^2(1-k)/(2R), \tag{1.12}$$

where S is the length of the station chord, which may be replaced by the path length with an error less than $S\,10^{-6}$.

The error in H_2 may amount to 3 meters for a difference of height of 4000 m, but is below 0.2 m for differences of height less than 1000 m.

From (1.12) the height H of a point P on the propagation path at a distance s from the terminal with height H_1 is given as

$$\begin{aligned} H &= H_1 + s\cos z_1 + s^2(1-k)/(2R) \\ &= [H_1(S-s) + H_2 s]/S + s(s-S)(1-k)/(2R), \end{aligned} \tag{1.13}$$

as $\cos z_1$ can be eliminated by means of (1.12).

1.2. *The Length of the Propagation Path.*

From (1.13) the height needed in (1.3) for expressing n is given. Thus the integration of (1.2) along the propagation path is simple.

$$\begin{aligned} \theta &= \frac{1}{c_v}\left[n_o S + \int\left(-\frac{k}{R}\right)[(H_1(S-s) + H_2 s)/S + s(s-S)(1-k)/(2R)]\,ds\right] \\ &= \frac{1}{c_v}\left[n_o S - \frac{1}{2}\frac{k}{R}(H_1+H_2)S + \frac{1}{12}S^3(1-k)\,'k\,\frac{1}{R^2}\right] \end{aligned} \tag{1.14}$$

If the values of the refractive index at the terminals are n_1 and n_2, (1.3) gives for n_o

$$n_o = \frac{1}{2}(n_1+n_2) - \frac{1}{2}\left(-\frac{k}{R}\right)(H_1+H_2) = n_m + \frac{k}{2R}(H_1+H_2) \tag{1.15}$$

which results in

$$\theta = \frac{1}{c_v}\left[n_m S + \frac{1}{12}S^3(1-k)\,k/R^2\right] \qquad n_m = \frac{1}{2}(n_1+n_2) \tag{1.16}$$

$$S = c_m\theta - \frac{1}{12}S^3(1-k)\,k/R^2 \qquad (c_m = c_v/n_m) \tag{1.17}$$

The second term in (1.17) represents the total effect of the "dip" of the propagation path into lower layers of the atmosphere,*) (and not only the partial effect of the pressure). The derivation rests on the assumption of an average gradient of the refractive index, but it seems better also to include the contributions from the temperature and the humity even if these effect may be varying strongly, than just to put these effects equal to zero and consider only the pressure effect.

1.3. *The Length of the Station Chord.*

The curvature of the propagation path is k/R. Consequently the length of the station chord K becomes

$$K = S - \frac{1}{24}S^3 k^2/R^2 \tag{1.18}$$

$$K = c_m\theta + \frac{1}{24}S^3(k^2 - 2k),$$

where S on the right hand side of course may be replaced by $c_m\,\theta$ or almost any other approximated value.

---

*) The dip correction is the „zweite Geschwindigkeitskorrektion" given by HÖPCKE, 1964.

The method shown by MORITZ, 1961 gives with one step directly the station chord, but here the two steps have been preferred in order to show the effect of the "dip" of the path.

1.4. *The Length of the Ellipsoid Chord.*

The reduction here is pure geometry and not related to refraction. If one should work with three-dimensional geodesy the station chord of course is the reduced observation. However, the reduction from ellipsoid chord to ellipsoidal distance completes the reduction term in a neat way.

1.5. *The Ellipsoidal Distance.*

The correction term from the ellipsoid chord of length E to the ellipsoidal length L is

$$L = E + \frac{1}{24} L^3/R^2 \tag{1.19}$$

With the approximation $L \sim K \sim S \sim c_m \theta$ in the small correction terms, the reduction from observed transit time to ellipsoidal distance becomes

$$L = c_m \theta \left(1 + \frac{L^2}{24}(1 - k)^2/R^2\right) - g\,, \tag{1.20}$$

where g is the reduction from station chord to ellipsoid chord. This expression is basis for the general rule-of-thumb used from the early days of radar propagation theory that all curvature effects, i. e. (1) dip of the path, (2) curvature of the path, and (3) curvature of the earth can be corrected for by assuming the path plane and the earth having a radius of curvature of $R/(1 - k)$, which mostly is $4R/3$.

1.6. *Possible Improvements of the Model of the Atmosphere.*

It follows directly that the value of the gradient — if it remains constant — used in (1.3) only is of importance for the curvature terms. This means that if a reasonable value is selected, a standard value will suffice, at least for small differences of height. For large differences of height it may be necessary to introduce a second order derivative d^2n/dH^2, which will result in a term

$$\frac{1}{12} S (H_1 - H_2)^2 \frac{d^2 n}{d H^2} \tag{1.21}$$

(See PODER, LEHN, and ANDERSON, 1960 or PODER and ANDERSEN, 1963)

As d^2n/dH^2 is most difficult to determine, it seems most sensible to avoid long lines with large difference of altitude, and instead break them up in shorter sections, thereby reducing the term to be negligible.

A constant horizontal gradient along the line will of course not affect the results, if n_0 is found from terminal measurements, (due to the symmetry) and a horizontal gradient perpendicular to the line will give a curvature term of the form (1.18), but as horizontal gradients are magnitudes smaller than vertical gradients, the effect is negligible.

The height used in (1.3) is the height over the ellipsoid, and not the height over the ground. This is most unfortunate, if the observations are made near the ground or if a large part of the line is running near the ground, because the gradients here will deviate strongly from the gradients of the more "free" atmosphere. A better knowledge of these effect might lead to better corrections in general.

1.7 *Practical Modification of the Reduction Formula.*

The reduction formulae shown here all have the term $c_m \theta$, where c_m is found from

$$c_m = c_v/n_m\,, \tag{1.22}$$

where c_v is the vacuum velocity of EM-waves and n_m is the mean of the refractive indices at the terminals (measured directly or indirectly by more or less cunning methods.)

Some instruments give 2θ, others $c_s \theta$, where c_s is some standard velocity. The standard refractive index 1.000.308 6 gives with the accepted vacuum velocity 299 792.5 km/sec the convenient standard velocity

$$c_s = 299\,700 \text{ km/sec} = 300\,000(1 - 1/1000) \text{ km/sec}$$

With this value multiplication becomes so simple that manual calculation is easy. With this value of c_s, $c_m\,\theta$ becomes

$$c_m\,\theta = c_s\,\theta\left(1 + \frac{n_s - n_m}{n_m}\right)$$
$$= c_s\,\theta\,(1 - M\,10^{-6}),$$

where M is given by (1.8) with $n = n_m$.

2. *The Determination of the Refractive Index.*

2.1. *Determination with Refractometers.*

Several reports on refractometers have appeared recently, and practical refractometers have been available even before geodetic EDM equipment existed. The accuracy is sufficient, but it is rather important that the indications are integrated over a reasonable period corresponding to a natural measuring period, e. g. for a set or for a measurement, and the reading of the refractometer must then be in accordance with this rythm in the measurement.

It is evident that such integration considerations are highly important if refractometers are sent on sampling missions in aircrafts during the measurements.

2.2. *Determination with Meteorological Instruments.*

The determination of the refractive index via the elements found in the formula of ESSEN and FROOME has hitherto been used most for geodetic purposes.

A differentiation of (1.8) gives

$$\left.\begin{aligned} \frac{\partial M}{\partial P} &= 0.36 && P = 760 \text{ mm } Hg \\ \frac{\partial M}{\partial T} &= -0.96 - 0.047\,e = -1.4 && T = 288^0\,K \\ \frac{\partial M}{\partial e} &= 5.9 && e = 10 \text{ mm } Hg \end{aligned}\right\} \qquad (2.1)$$

These values show how errors of the three elements P, T, and e affect M. For visible light the corresponding coefficients are respectively 0.36, -1, and approx. 0. Microwaves thus have almost the same dependency of the pressure and 1.4 times higher of the temperature and more than 50 times higher dependency of the humidity. Estimates of errors due to non-representative measurements must be based on these figures. Estimates of errors due to the met. instruments must be based on quite different figures, because in most methods temperature and humidity measurements are correlated.

If the measurement of e is made with a dew-point hygrometer, all three elements are independent. A dew-point hygrometer measures e as

$$e = E(t_d), \qquad (2.2)$$

where E is the saturated vapor pressure at the temperature t_d.

With a crude approximation

$$E(t) = 4\,\exp(t/16), \qquad (2.3)$$

and thus

$$\frac{dE}{dt} = E/16\,. \qquad (2.4)$$

From this

$$\frac{\partial M}{\partial t_d} = 3.6\,. \qquad (\text{At } e = 10 \text{ mm } Hg) \qquad (2.5)$$

No hygrometers of this type for field use and with sufficient accuracy are known to the author. Aspirated hygrometers give e as

$$e = E(v) - c\,P(t - v), \qquad (2.6)$$

where v is the wet-bulb temperature and t is the dry-bulb temperature, $c = 0.00066$ for water and $c = 0.00055$ for ice. E and P have the same meaning as hitherto. The measurement of M now shows a correlation of P, t, and v. The expression (1.8) may be written as

$$M = 103.49\, P/T_p + 4.904\, E(v)/T^2 - 308.6, \tag{2.7}$$

where T_p the "parameter temperature" is given as

$$T_p = T/(1 - 3\,.\,24\, d/T \sim T + (10/3)\, d, \tag{2.8}$$

$$d = t - v. \tag{2.9}$$

For ice 3 . 24 is replaced by 2 . 70. The value 10/3 for 3.25 serves two functions, viz. easy calculation and better general approximation for larger values of d.

The derivatives of M now are

$$\left.\begin{aligned} \frac{\partial M}{\partial P} &= 0.36 \\ \frac{\partial M}{\partial t} &= -0.96\,(1 + 3.25) - 0.047\, e = -4.5 \\ \frac{\partial M}{\partial v} &= -0.97\,(-3.25) + 3.6 = 6.9 \end{aligned}\right\} \quad \begin{aligned} P &= 760 \text{ mm } Hg \\ t &= 15^0 \text{ C} \\ e &= 10 \text{ mm } Hg \end{aligned}$$

These derivatives are used for estimates of the effect of met. instrument errors on M, while (2.1) shows the effect of non-representative measurements of P, t, and e, e. g. by selection of a bad observation site.

The thermometers consequently must be calibrated with an accuracy of $0.1^0 C$ if the general scale error of the network is to be kept below 1 p. p. m.

On the other hand, if the met. observations e. g. are made in a site, where the temperature deviates by $1^0 C$ from that of the line but the humitdity happens to be the same as for the line, then the resulting error will only be -1 . $\dashv$ p. p. m. (from 2 . 1) which shows how M depends on the air temperature). In this case v would differ from a v observed in a more representative site.

Reference is made to BULL, 1946 for a very general discussion of derivatives of M for various types of instruments and several sets of P, t, and e, and to MITTER, 1962 for a discussion of psychrometer formulae and constants.

The concept "parameter temperature" is very useful for pointnomographs for the computation of M. One nomograph can have the arguments P and $t_p (= T_p - 273)$, whilst the other can have the arguments t and v. The sum of the two functions then gives M.

2.3. *Practical Precautions for the Measurement of M.*

The required accuracy of the pressure is so modest, that almost any aneroid barometer may be used. A calibration of the scale "zero" with intervals is necessary, e. g. by means of a mercury barometer or a boiling point hypsometer. The "mean barometer" formed of the barometers used by 3—5 parties may be used over 2—3 months as a standard. In fact, reading errors are much more likely, but this can easily be overcome by using a barometer with dual scale (e. g. in mm and inches) and always reading both scales. As the heights of the terminals are known a check of their pressure differences is possible as well.

The measurement of temperature and humidity should be done with a very careful positioning of the instrument in order to get a good, representative sample of the atmosphere. The instruments should be at the wind-side of the station or better on a pole or in a tower, unless the line really is running very near the ground. Psychrometers of the Assmann type should never be suspended vertically, but rather tilted somewhat with the intakes against the wind, as the air speed in the tubes otherwise might be too low. This air speed may exceed the critical speed (2 m/sec) by more than 5 times without any sensible change of the psychrometer constant, but if it drops below critical speed, the results will be useless.

Regular checks of the air speed in the psychrometer tubes are important. In the field this can done by measuring the time for one revolution of the winding screw, which is given with the certificate of the psychrometer.

The calibration of the thermometers is only required with long intervals and must be done by a laboratory. The thermometers are matched by the manufacturer for a good determination of the humidity, but as calibration errors give a general scale error of the net, it is wise to make every effort to reduce this effect.

The accuracy of the reading of the thermometers is of much less importance, as this error is a random error, a first order side will in general have 16—24 readings of each thermometer, so even a reading to nearest half degree would suffice. In practice reading is made to $0^{0}1C$.

2.4. *The Vertical Gradient of the Refractive Index.*

The vertical gradient may be determined from (1.3) by means of the measurements of n at the terminals. The curvature term, where it is used, will only exceed 1 p. p. m. when the distance exceeds 30 km, and the distance is 50 km before it reaches the magnitude of the random observation error 3. p. p. m. If the difference of height is small, dn/dH (more correctly $\partial n/\partial H$) will be most uncertain due to observation errors and horizontal gradients. Large differences of height may give good values of the gradient, but the second order derivative may be needed if the line is a long one, which thus introduces a fresh unknown. For lines shorter than 30 km a standard value — either constant or calculated from the observed values of P, t, and e assuming a standard atmosphere — is preferable. See BEST, 1946 for suggestions.

Long over-water lines measured under conditions with high curvature require special considerations, but ordinary lines should never be so long that curvature effects become important.

For this reason it is suggested, that a standard value is used for all ordinary lines, $dn/dH = -0.040 \cdot 10^{-6} m^{-1}$.

2.5. *The Use of Intermediate Meteorological Observations.*

It has frequently been suggested, that meteorological observations "in the propagation path" would be useful. It is evident that the possibility of testing the atmosphere model increases by this, especially if the measures are able to check the gradient as well.

But if the intervening ground permits, it would be far more advantageous to devide the line and measure in sections, not least because the curvature effects are reduced considerably, thus requiring very little accuracy of the atmosphere model. The question actually reduces to add an MDM instrument to the met. instruments brought to the intermediate site.

3. *Estimate of Errors.*

3.1. *Errors of the MDM Instrument.*

Measurements on short ranges 200—1000 m, where refractive index errors are less than 1 cm, show that the interval instrument errors have a magnitude of 1—2 cm (such errors as cyclic errors found with some instrument types must be included in the necessary corrections).

Measurements of the modulation frequency under field conditions show that this error has a magnitude of 0.1 — 0.5 p. p. m.

This means that for distances exceeding 20 km, errors exceeding 1 p. p. m. must arise from the propagation. Reflections from the ground is one of the possible sources, but for an individual side, reflections will generally produce the same effect, at least for lines over land.

For these reasons the variations of the measurements of one side must have errors of the refractive index as their source. (The variations of the 10—12 sets forming a measurement have mainly reflections (ground swing) or instrument swing as their main source, and this variation is useless for estimates of the accuracy).

3.2. *Refractive Index Errors.*

From the difference of the refractive index measurements executed before and after each measurement of distance, an estimate of the compound effect of short time (10 minutes) variation of refractive index and indication and reading errors of barometers and psychrometers can be found.

From 150 measurements of distance (600 det. of. refr. index) in the Danish first order network a value of 2 p. p. m. was found. This magnitude may be explained from $0^{0}2C$ of reading and indication error for each thermometer.

900 measurements of 150 sides (the entire first-order network) show, however, 2.6 p. p. m. for one measurement of a side as the internal agreement. The sides have in general been measured 6 times, which will give 1 p. p. m. for the mean sq. error of the mean.

An adjustment of the network jointly with Laplace azimuths and ordinary angular measurement (the latter with a m. sq. e. of 0".2 for a direction-mean of 12—24 sets) gives a m. sq. e. of 0".4 or 2 p. p. m. for an observed direction or side, respectively.

From this it is estimated that the observed mean values of the sides may have errors of 2 p. p. p. m. not randomized by the reiterated measurements. There may even be larger errors hidden, as the measurements of the sides of a triangle have some correlation, because neighbouring sides frequently are measured with short time interval and a general scale error will not be shown by the "comparison" via the angles.

It seems that 6 measurements spread over 3 days with at least one intermediate day between the measurement-days is more than necessary because the interval aggreement is too "optimistic". On the other hand the increase of the m. sq. e. from 0".2 to 0".4 was also found when the angles were adjusted separatly.

The error of the refractive index therefore must exceed 2.6 p. p. m., and 4—5 p. p. m. is a more realistic estimate.

These measurements have been executed in a lowland with a windy, humid climate. The assumption of horizontal stratification therefore is well stratified, but the high humidity is of course a disadvantage.

3.3. *Conclusions.*

MDM can be used for measurements of sides in geodetic networks with an accuracy of 2 p. p. m. provided the sides are not too long, i. e. less than 50 km. For sides exceeding this length, the curvature effects get increasing importance.

Referneces

Appleton, E.: The influence of tropospheric conditions on ultra-shortwave propagation. — Met. Factors in Radio-Wave Propagation, London 1946.

Best, A. C.: A standard radio atmosphere for microwave propagation. — Met. Factors in Radio-Wave Propagation, London 1946.

Bull, G. A.: Note on errors in measurement of the refractive index. — Met. Factors in Radio-Wave Propagation, London 1946.

Höpcke, W.: Über die Bahnkrümmung elektromagnetischer Wellen. — Z. f. V., 1964, 6.

Mitter, J.: Über die Bestimmbarkeit der Ausbreitungsgesch. der Trägerwellen bei el. Entfernungsmessungen. — AVN, 69, 1962, 5.

Moritz, H.: Zur Reduktion elektronisch gemessener Strecken und beobachteter Winkel wegen Refraktion. Z. f. V., 1961, 7.

Poder, K., Chr. Lehn, and Ole Bedsted Andersen: Some Preliminar Results and Considerations of Tellurometer Investigations. — IUGG, Helsinki, 1960.

Poder, K. and Ole Bedsted Andersen: Results and Experiences of Electronic Distance Measurements 1960—1963, København, 1963.

Investigations of Refraction Correction in Tellurometer Measurements

by *Teuvo Parm*, Helsinki

Finnish Geodetic Institute measured with tellurometers the Vihti enlargement net in May—June, 1965. It was intended to calibrate the institute's tellurometers type MRA 3 MK II Serial No. 574 and 726 and simultaneously to investigate refraction correction.

The base-line of the net was measured with tellurometer five times, four other sides four times and the other six two times each. On the base-line the instrument 574 was used three times and the instrument 726 two times as master. The measurements on the other sides were equally divided among the instruments. As a rule the measurements with both instruments were carried out one after the other.

Assman-type psychrometers were used for temperature and humidity measurement and Thommen barometers for the measurement of the atmospheric pressure. The dry and wet bulb temperatures were observed on the endpoints of each side close to the tellurometer i. e. in towers of heights 10—24 m and at 1.5—2 m above the ground at the foot of towers. In addition to this these meteorological observations were made near the middle of the side, where the dry and wet bulb temperatures were observed at the altitudes of 1.5—2 m and 10—17 m above the ground. The air pressure was observed at end stations in towers and in mid-stations on the ground.

Assuming that the surfaces of constant temperature and of constant humitidy are parallel with the earth's surface, the temperatures [1] and the pressure of water vapour [2] were transferred

Results:

No	Side	Master	S m	$(S - S_m)$/1 km mm		$(S - S_i)$/1 km mm	
1	Hky — Rot	574	6 049.814	+ 6		—	
2	Rot — Hky	726			+ 6		—
3	Hky — Rot	574		+ 5		—	
4	Hky — Rot	726			— 4		— 5
5	Rot — Hky	574		— 2		— 2	
6	Rot — Klo	726	6 769.224		+ 9		+ 13
7	Klo — Rot	574		0		— 1	
8	Klo — Rot	574		— 1		— 8	
9	Rot — Klo	726			+ 7		+ 5
10	Klo — Hky	726	8 220.128		+ 1		— 2
11	Hky — Klo	574		— 12		— 15	
12	Hky — Kmk	574	9 435.182	— 1		— 11	
13	Kmk — Hky	726			— 3		— 8
14	Kmk — Hky	574		— 3		— 6	
15	Hky — Kmk	726			— 4		— 8
16	Kmk — Rot	574	9 749.138	— 2		— 8	
17	Rot — Kmk	726			— 2		— 4
18	Kmk — Fa	574	20 293.070	— 3		— 3	
19	Fa — Kmk	726			0		— 5
20	Ro — Fa	574	29 114.137	— 2		— 4	
21	Fa — Ro	726			— 2		— 7
22	Ro — Fa	574		— 3		— 4	
23	Fa — Ro	726			— 2		— 4
24	Klo — Kmk	574	15 913.840	— 4		— 11	
25	Kmk — Klo	726			— 3		— 11
26	Kmk — Ro	574	17 412.094	— 6		— 11	
27	Ro — Kmk	726			— 7		— 13
28	Kmk — Ro	726			— 3		— 6
29	Ro — Kmk	574		— 7		— 16	
30	Ro — Klo	574	19 197.186	— 2		— 2	
31	Klo — Ro	726			+ 1		— 9
32	Klo — Fa	574	10 456.478	— 2		— 6	
33	Fa — Klo	726			— 1		— 5
	Mean value		13 847.0	— 2.3	— 0.4	— 7.2	— 4.6
	Mean error			± 1.0	± 1.1	± 1.2	± 1.7

logarithmically to the altitude of 15 m at both ends and in the middle of the side. It was confirmed that these values were consistent. The mean deviation of the arithmetical mean of the end stations and the mid-station was $\pm 0.3^0 C$ only, which corresponds to $\pm 0.4 \cdot 10^{-6}$ in refraction index. The corresponding values for the water vapour pressure are ± 0.14 mmHg or $\pm 0.9 \cdot 10^{-6}$ in refraction index. The mean value of the all three 15 meter values was transferred correspondingly logarithmically to the different heights. Using so computed values of temperature and water vapour the integrating temperature and the integrating water vapour were determined for each observation. The mean air pressure along the path was computed from the mean pressure of the endpoints and the mid-station and corrected with the additional pressure caused by the earth curvature and by the curvature of the ray. The standard error of one value of the air pressure is on the average ± 0.3 mmHg or $\pm 0.1 \cdot 10^{-6}$ in refraction index.

With the obtained values of T, e and p the refraction indices were computed with the formula [3]

$$(n-1) \cdot 10^6 = \frac{103 \cdot 49}{T}(p-e) + \frac{86 \cdot 26}{T}\left(1 + \frac{5748}{T}\right) \cdot e$$

The results are collected in the table. There is S the side length from the classical triangulation. S_m is the corresponding length, when the refraction correction is computed with arithmetical mean of meteorological values observed directly on the endpoints. S_i is the side lenght, when refraction correction is computed by the numerical integration explained above.

The base-line of Vihti enlargement net, Hky-Rot, has the lenght 6049.8135 $\pm$ 0.0010 m or 1 : 6 000 000 measured with invar wires and the main net side, Fa-Ro, has the lenght 29114.1372 $\pm$ 0.0573 m or 1 : 500 000 according to the triangulation. It is seen in the table that $S - Sm$ is ($-$ 2.3 $\pm$ 1.0)mm/km and ($-$0.4 $\pm$ 1.1)mm/km for the instruments 574 and 726 correspondingly. The results of the integration for these instruments differ more, ($-$ 7.2 $\pm$ 1.2)mm/km and ($-$ 4.6 $\pm$ 1.7)mm/km from side lenght from the classical triangulation, what is just the opposite as it would be expected. The mean deviations of these mean values have increased, too.

References:

[1] *Jordan/Eggert/Kneissl:* Handbuch der Vermessungskunde Band VI p. 255
[2] " " Band VI p. 261
[3] " " Band VI p. 217

The Effect of Meteorological Factors on the Accuracy of Tellurometer Measurements

by *Seppo Härmälä*, Helsinki

1. Observation Technique of Meteorological Data

In order to establish the refractive index of the atmosphere, the temperature and the vapor pressure are measured. Usually the observations are made at both ends of the line, at the beginning and at the end of the distance measurement. Only gross errors in the measuring of the air pressure can have a major effect on the final result, so they will not be taken into regard in this connection.

The temperature and the vapor pressure have generally been measured with a psychrometer by observing the readings of the ventilated thermometers. The readings of the dry thermometer are used as observations of the air temperature as such, whereas the vapor pressure can be derived from the readings of the dry and the wet bulb thermometer applying the Sprung formula

$$e = E' - 0{,}50\,(t - t')\frac{p}{775}$$

In the formula e is the vapor pressure (mm), t the reading of the dry and t' the reading of the wet thermometer (^{0}C) and p the air pressure (mm). The pressure of the saturated vapor in the temperature t' is E'.

It is important that attention be paid on the right observation technique. The sleeve of the thermometer bulb must be absolutely clean and only distilled water may be used to moisten it. The sleeve must not have too much water because in that case the water temperature might affect the readings, but on the other hand, it must not get too dry. It has to be watched there is no bridge of water between the frame and the sleeve. Moreover, the speed of the ventilating air should be right and disturbances such as exhaled air must not affect the psychrometer.

By meteorological observations the fluctuation has to be taken into account and eliminated as well as possible. The readings should be recorded only when the effect of the fluctuation has been eliminated from the readings watched for some minutes.

In order to investigate the accuracy of meteorological data at one station the sample *C* of the table I has been used. The general course of the temperature and the vapor pressure are assumed to be linear between three succesive observations. From the deviations the mean square error of a single observation has been computed with a result $m_t = \pm 0{,}28^0$ C and $m_e = \pm 0{,}25$ mm *Hg*. The mean square error of the average from four observations would be half of these numbers.

Even after careful meteorological observations the data at both ends of the line may differ from each other more than the distribution at one station implies. This is due to two different factors.

The local disturbances and the microclimate produce errors which may be eliminated by setting up more meteorological stations. This source of error may be dominant at stations close to the ground.

On the other hand, the differences between the stations at the ends of the line may be due to the general weather gradient along the line. In this case the mean from the two stations eliminates the most of the difference.

In order to get an idea about the agreement between the ends of a line three different samples have been taken to the table I. The circumstances of the samples differ remarkably from each other. The sample *C* meets best the methods and circumstances of the field works of National Board of Survey. The table I shows the number of sides at the sample, the number of meteorological observations at each end of the line and the stand of the instrument. The elevation of ground stations is about 1,5 m and that of tower stations is 15 m in the average. The method of the ventilation has been mentioned and so has the average temperature and the average vapor pressure and finally the mean square error for the mean from the ends computed from the distribution of differences

Table I

sample	n_1	n_2	stand	whirled	t	e	m_t	m_e
A	62	2	ground	manual	+ 22,2° C	12,6 mm *Hg*	± 1,06	± 0,28
B	30	2	tower	manual	+ 18,9	8,0	± 0,56	± 0,37
C	49	3	tower	motor	+ 13,2	7,1	± 0,37	± 0,25

As the differences from two stations are much greater than the inner accuracy of one station would imply another attempt has been made to find a solution between alternative explanations. The data of the table VI represent a case where two intervening meteorological stations have been established as is shown in figure 1. The mean square errors m_t and m_e for the average of the end-

Table II

Day	m_t	d_t	m_e	d_e
7. — 8. 7.	± 0,32	± 0,30	± 0,26	± 0,19
21. — 22. 7.	0,52	0,08	0,33	0,10
4. — 5. 8.	0,59	0,12	0,91	0,31
18. — 19. 8.	0.19	0,15	0,27	0,20
8. — 9. 9.	0,41	0,11	0,15	0,14
2. — 3. 11.	0,56	0,11	0,36	0,07
1. — 2. 12.	0,52	0,26	0,29	0,13
average	± 0.47	± 0,18	± 0,43	± 0,18

stations have been computed from the differences between them. Then the difference between the average of the end stations and the average from all four stations has been developed to a corresponding mean square error d. If the differences between the end stations were due to random disturbances of stations, d would be equal $m/\sqrt{2}$. In that case the average d_t at the end of the table II would be $d_t = \pm 0{,}33$ and $d_e = \pm 0{,}30$.

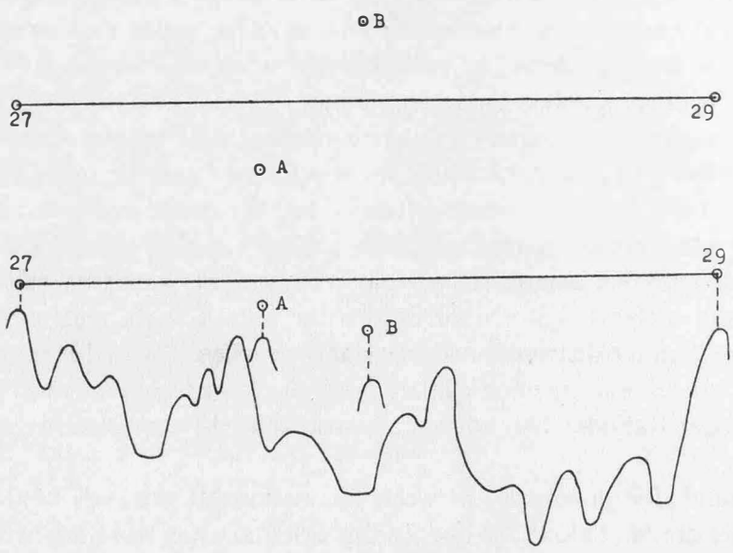

Fig. 1

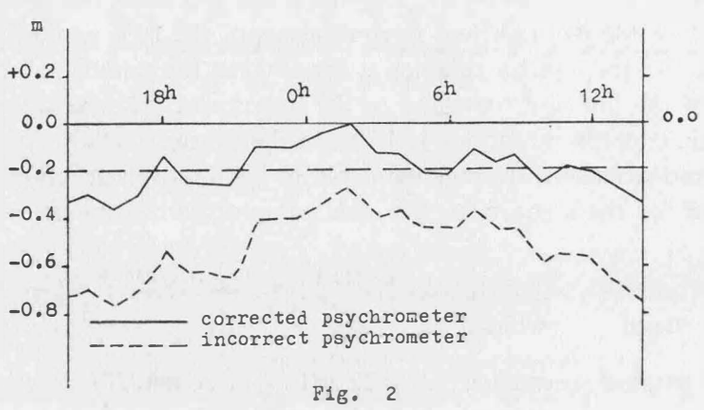

Fig. 2

The data of the table II show that in this material a great deal of the difference between the ends of the line will be eliminated from the mean. Without the intervening stations the mean square errors m_t and m_e would affect the distances by mean square errors of $\pm$ 0,7 mm/km and $\pm$ 2,1 mm/km or combined $\pm$ 2,2 mm/km. The corresponding values from the sample C of the table I are $\pm$ 0,5 mm/km, $\pm$ 1,5 mm/km and combined value $\pm$ 1,6 mm/km. It is difficult to tell how much these results could be improved by using the intervening meteorological stations. In view of the figures of the table II and of the other sources of error the use of intervening stations does not seem to offer any remarkable advantages.

2. The Systematic Errors of the Meteorological Observations

The accuracy of meteorological observations has been dealt with above in view of the distribution of errors between different observations. There may be, however, such systematic errors in the meteorological observations which are included to all observations and do not alarm therefore. There is an example of this in figure 2. A distance of 43 km between first order points 275 and 277 was measured every hour of the clock with the result that a great systematic and a strong periodical error were revealed. The great systematic error occurred in all of the other first order sides which were measured during those days, too. As interesting as it would have been to build up a brand new meteorological theory based on the phenomenon, the simple truth was found out at the calibration of the psychrometer.

The importance of a good care in the meteorological observations was emphasized above already. As a matter of fact, perhaps not so much inner agreement is obtained doing it, but it has a great effect in decreasing the systematic error of the psychrometer. The proper calibration of psychrometers may be added there as a very important point of the procedure.

Other sources of systematic error are the bending of the ray in the atmosphere, the adjoining systematic changes of the refractive index along the path and the influence of the neighbourhood of the ground on the refractive index.

3. The Path of the Ray in the atmosphere.

The path of the ray may be computed by applying variation calculus. The total time of the propagation between the ends of the line is

$$T - \frac{1}{c_o}\int_{-a}^{+a} n(r)\sqrt{1+y'^2}\,dx = \frac{1}{c_o}\int_{-a}^{+a} f(x, y, y')\,dx$$

The equation of the path is an extremal curve representing a solution of the Euler differential equation

$$y'' = \frac{f_y - f_{y'x} - y' f_{y'y}}{f_{y'y'}}$$

Assuming that the ends of the path have the same height and that the refractive index has a geocentric symmetry

$$n(r) = n_o e^{-z(h-h_o)}$$

the solution of the Euler equation will be the function

$$y = \frac{1}{z} ln\left(\frac{\cos z\,x}{\cos z\,a}\right)$$

It can be easily shown that the result can be simplified by substituting the curve with a circle connecting the ends of the path and the vertex. This does not cause any remarkable error. Now the total time of the propagation is obtained.

$$T = \frac{n_o}{c_o}\left[2a - \frac{k^2}{24r^2}(2a)^3 + \frac{k}{12r^2}(2a)^3\right]$$

In this formula 2a means the chord between the ends of the path. Then it is easy to compute the length s of the curve connecting the ends of the path and following the curvature of the ellipsoid. The arc s will be then

$$s = \frac{c_o T}{n_o} + \frac{(1-k)^2}{24r^2}s^3$$

This final formula is exactly the same which was derived by Saastamoinen with less work. The symbols of the formula are

s arc connecting the ends of the line
n_o refractive index at the ends of the line
c_o velocity of the radio waves in vacuo
T total time of the propagation
r radius of curvature of the ellipsoid
r' radius of curvature of the ray

$$k = r/r' = -r\frac{dn}{dh}$$

$$z = 1/r' = -\frac{dn}{dh}$$

The second term of the formula above may be called the curvature correction. It includes the geometric correction to the shape of the ellipsoid and the systematic change of the refractive index along the path of propagation.

Assuming the coefficient $k = 0{,}25$ for the radio waves and the radius of the curvature of the ellipsoid $r = 6390$ km, the value of the curvature correction will be

$$k_r = 0{,}574 \times s^3 \text{ m, where the unit of } s \text{ is 100 km.}$$

The coefficient of k_r varies remarkably. The examination of the different factors will give an idea about the extent of its variation. The gradient of the atmospheric pressure is the main term and fortunately its variations give only slight changes to the value of the curvature correction.

The long term observations made in England are very valuable in estimating the variations of the meteorological factors, especially those made by Best, Knighting, Pedlow and Stormonth. The temperature and the vapor pressure had been registered every hour for three years at the elevations of 1,1, 15,2, 47,2, and 106,7 m. The extremities of the gradients could be used to find out the greatest errors but the average values are still more important for practical observations. The table III shows the average values of the coefficient k during the different months and the table IV the hourly variation of the coefficient k as an average from different months from May to September.

Table III $k = r/r'$

	01^h	02^h	03^h	04^h	05^h	06^h	07^h	08^h
1,1— 15,2 m	+0,330	+0,244	+0,210	+0,169	+0,368	+0,848	+1,352	+1,526
15,2— 47,2	+0,537	+0,481	+0,440	+0,425	+0,426	+0,551	+0,600	+0,466
47,2—106,7	+0,331	+0,320	+0,287	+0,293	+0,282	+0,294	+0,329	+0,276

09^h	10^h	11^h	12^h	13^h	14^h	15^h	16^h	17^h
+1,421	+1,355	+1,337	+1,344	+1,308	+1,349	+1,294	+1,326	+1,305
+0,422	+0,429	+0,436	+0,440	+0,418	+0,375	+0,394	+0,415	+0,459
+0,245	+0,218	+0,236	+0,236	+0,230	+0,250	+0,239	+0,228	+0,250

18^h	19^h	20^h	21^h	22^h	23^h	24^h	mean
+1,318	+1,191	+0,875	+0,662	+0,541	+0,463	+0,354	+0,937
+0,510	+0,553	+0,586	+0,615	+0,604	+0,565	+0,542	+0,487
+0,268	+0,311	+0,313	+0,328	+0,351	+0,348	+0,338	+0,283

Table IV $k = r/r'$

	I	II	III	IV	V	VI
1,1— 15,2 m	—0,314	+0,123	—0,294	+0,251	+0,868	+1,400
15,2— 47,2	+0,371	+0,300	+0,185	+0,184	+0,479	+0,484
47,2—106,7	+0,264	+0,251	+0,224	+0,234	+0,191	+0,209

	VII	VIII	IX	X	XI	XII	mean
1,1— 15,2 m	+0,671	+0,900	+0,400	—0,048	+0,094	—0,017	+0,336
15,2— 47,2	+0,754	+0,479	+0,375	—0,002	+0,015	+0,038	+0,305
47,2—106,7	+0,244	+0,337	+0,343	+0,352	+0,232	+0,213	+0,258

The tables III and IV reveal the instability of the coefficient at the lowest layers of the atmosphere. However, the coefficient gets more stabile at heights more than 15 m above the ground and at height more than 47 m above the ground the influence of temperature and vapor pressure is rather small compared to the influence of the atmospheric pressure.

After all, the total value of the curvature correction never seems to be great, it seldom exceeds 10 cm at a distance of 50 km. In addition, the long distances, where the errors could be great, are

Table VI

Diurnial variation of the tellurometer measurements

The distances have not been reduced. The first line of each day gives the length in addition of 29110 m. The second line gives the temperature and the third line the vapor pressure.

	18h	21	0	3	6	9	12	15	18	Mean
7.– 8. 7.	4,844	4,841	4,848	4,842	4,837	4,862	4,899	4,834	4,868	4,853 m ±0,007
	+18,0	+15,6	+13,1	+11,2	+11,1	+16,0	+18,5	+19,5	+19,4	+15,8° C
	7,8	8,6	8,4	8,5	8,5	8,3	7,9	7,7	7,8	8,2 mm *Hg*
21.–22. 7.	4,832	4,845	4,876	4,860	4,808	4,724	4,809	4,792	4,837	4,820 m ±0,015
	+18,6	+15,8	+13,2	+13,8	+14,7	+16,5	+17,0	+17,5	+17,5	+16,1° C
	11,3	11,5	11,2	11,7	12,3	12,1	13,4	13,4	11,0	12,0 mm *Hg*
4.– 5. 8.	4,823	4,939	4,843	4,871	4,870	4,769	4,988	4,881	4,837	4,869 m ±0,021
	+16,4	+14,2	+12,1	+12,2	+11,9	+14,8	+17,6	+17,9	+15,6	+14,8° C
	7,7	9,2	9,5	10,4	10,0	11,3	8,9	8,1	8,3	9,3 mm *Hg*
18.–19. 8.	4,867	4,874	4,813	4,814	4,813	4,809	4,836	4,810	4,790	4,825 m ±0,021
	+13,6	+12,9	+11,4	+11,0	+11,0	+11,8	+13,6	+14,4	+14,5	+12,7° C
	8,5	8,2	8,4	8,8	9,3	9,4	9,8	9,8	9,6	9,1 mm *Hg*
8.– 9. 9.	4,824	4,884	4,918	4,878	4,892	4,896	4,901	4,829	4,850	4,875 m ±0,009
	+11,2	+ 9,8	+10,1	+10,1	+ 9,9	+10,4	+12,9	+13,0	+11,6	+11,0° C
	9,2	8,3	8,5	8,6	8,4	7,9	7,5	7,4	7,5	8,1
2.– 3. 11.	4,962	4,972	4,954	4,947	4,976	4,908	4,864	4,882	4,915	4,931 m ±0,013
	+ 6,3	+ 6,8	+ 7,4	+ 7,6	+ 8,2	+ 9,0	+ 9,4	+ 9,5	+ 9,3	+ 8,2° C
	7,1	7,4	7,7	7,8	8,2	8,6	8,9	8,9	8,8	8,1 mm *Hg*
1.– 2. 12.	5,063	5,150	5,095	5,113	5,084	5,088	5,045	5,086	5,023	5,083 m ±0,014
	– 3,3	– 1,9	– 0,8	0,0	+ 0,3	– 0,5	– 0,6	– 1,2	– 1,6	– 1,1° C
	3,4	3,8	4,1	4,3	4,3	4,1	3,9	3,7	4,0	4,0 mm *Hg*
Mean	4,888	4,929	4,907	4,904	4,897	4,865	4,906	4,873	4,874	4,894 m
	+11,5	+10,5	+ 9,5	+ 9,4	+ 9,6	+11,1	+12,6	+12,9	+12,3	+11,1° C
	7,9	8,1	8,3	8,6	8,7	8,8	8,6	8,4	8,1	8,5 mm *Hg*

generally measured so high above the ground that the curvature correction is probably not very far from the average value.

4. *The Error Caused by the Vertical Gradient and the Distance from the Ground*

There is another source of error in addition to the curvature correction which is caused by the vertical gradient of the refractive index. The vertical gradient is influenced more or less by the distance from the ground. Actually, some part of the vertical gradient of the refractive index depends on the elevation only, another part follows the shape of the ground. The final result is a combination of these two components.

If the gradient of the index is determined it will have some connection to the measured distance even in case of extrapolating the gradient. The observations of the variation of the gradient and the distance at the same line should reveal the correlation.

A test was established in order to investigate the correlation between the measured distance and the gradient of the temperature and the vapor pressure above the ground. The side between the first order triangulation points 27 and 29 was measured in three hour intervals around the clock. The meteorological observations were made at the ends of the line and at two intervening stations (figure 1). At all the meteorological stations the readings were taken on the top of a triangulation tower (in average 19 m) and at a height of 1,5 from the ground. The readings at the tower and at the ground were arranged symmetrically in order to avoid systematic errors of the measured gradients. The total procedure was repeated on seven different days as described in the table V. The average air pressure, temperature and vapor pressure are included.

Table V

day	p	t	e	wind	weather
7. – 8. 7.	999,4 m bar	+ 15,8° C	8,2 mm Hg	1–2 b	clear
21. – 22. 7.	995,9	+ 16,1	12,0	3–5	mist, rain
4. – 5. 8.	994.1	+ 14,8	9,3	1–3	rainy
18. – 19. 8.	999,3	+ 12,7	9,1	4–5	rainy
2. – 3. 11.	1004,0	+ 8,2	8,2	1–2	mist
1. – 2. 12.	1006,1	– 1,1	4,0	1–3	clear

The results from the measured distances and meteorological data are collected to the table VI. The distances included to the table are means from four successive measurements and the inner accuracy of the mean is ± 0,029 m in average. Unfortunately, the crystals of the instruments gave some trouble and their calibration was somewhat unsatisfactory at that time. Especially this concerns the last day of the table V, and the crystal frequency of that day remained somewhat uncertain.

The measured distances and temperature gradients and vapor pressure gradients were submitted to an orthogonal regression analysis. As a result from this the correlation coefficient between the distance and temperature gradient was 0,8 % and that between the distance and vapor pressure gradient was 0,3 %. The significance criteria showed that the correlation was in both cases far below the significance level. So the result from the test was then that the measured gradients had nothing to do with the variation of the distance.

The derived result does not exclude completely the possibility of a connection between the distance and the gradients. Unfortunately the test did not include a sufficient number of warm, sunny days. Besides the line was somewhat shallow. Figure 2 shows a case where there seems to be a close connection between the gradients and the distance. Anyway, it is not sure that the psychrometer error was completely eliminated and even then the differences from the mean are not great for a distance of 43 km. The circumstances in the test favoured the appearence of the periodical error in every way. Weather was cloudless and warm and the line very high.

The variation of the temperature gradient would appear in the result of a day and night test more easy than the variation of the gradient of the vapor pressure. The former has a diurnal variation of the lapse rate and the inversion whereas the latter has a lapse rate only. Therefore it would be important to investigate the influence still more with long distances which are known up to a very high degree of accuracy.

The tests of the table VI were carried out at a first order triangulation side. In addition, the length of the side was determined by measuring a base line and connecting it to this side with a base extension net. In order to secure the accuracy, the angles of the net were observed again in the next year. So the length of the side 27 — 29 has the following values.

base extension 1961	29 114,085 ± 0,059
base extension 1962	29 114,183 ± 0,081
combined base extension	29 114,137 ± 0,057
from first order net	29 114,256

The same side from the determinations of the table VI and reduced to the same level gives a value

tellurometer	29 114,176 ± 0,035

It is rather difficult to tell now anything about the possible systematic errors of the tellurometer measurements. Moreover, tellurometer seems to give the most plausible result of all. In addition, the deviation of the tellurometer distance from the triangulation side makes — 2,7 mm/km and the average deviation presented at the appendix makes — 2,9 mm/km.

One of the main troubles when investigating tellurometer measurements is the fact, that there are no adequately accurate long reference distances in the world. As they are lacking it is very difficult to come to any really reliable results about the effect of meteorological factors. Until now every investigation on the accuracy seems to have lead to the accuracy of the reference distances.

5. The Agreement of the Practical Measurements

The investigations and tests described above have lead to some rules in the practical tellurometer work of the National Board of Survey.

1) A careful check of crystal frequences has been established. The crystals are calibrated several times a year. In addition, every distance is measured from both ends of the line and so every change of the crystal is noticed immediately.
2) The meteorological observations are made at both ends of the line three times and the distance measured between the meteorological readings. All possible care is given to the observation technique. No additional stations are established.
3) Preference is given to psychrometers which are whirled electrically so that the speed of air is always constant. No psychrometers whirled by hand are accepted.
4) Psychrometers are calibrated under circumstances when the air conditioning allows a large range of temperatures and vapour pressures.

From the results obtained this way the following can be mentioned. The so-called main order nets have been observed among other triangulation work. There the average distance makes about 30 km. The agreement of these nets has been good as described by M. Jaakkola. Residuals exceeding 10 cm are rare. Anyway, it is too early to tell about the systematic error because until now the junctions have been to temporarily adjusted points. In the nearest future will, however, the final adjustement be carried out. The number of the measured main order sides makes nearly 300.

In connection of other observations some first order triangulation sides have been measured. The comparison between tellurometer measurement and the value from first order net may be a good test to the results of the applied methods. A comparison is made at the appendix. There the material includes 116 sides. The material was presented partly previously by P. Heikkilä, but now a new adjustment of first order net has been carried out and there exists a better basis for a comparison.

The comparison is made in regions. A region has been bordered around a base line of the first order net. The general systematic difference has been computed in every region. When the systematic difference has been substracted the mean square difference has been computed in every region. An average systematic error of — 2,89 mm/km has been found. The mean square difference between tellurometer measurement and the first order side is ± 0.077 m in average for a distance of 30,7 km. How the mean square difference should be distributed between the different sources and what the reason for the systematic difference is, are still unanswered. In spite of these open questions

there seems to be enough knowledge to state that the era of base lines is now over and the electronic distance measurement has matured.

References

1. *Best, Knighting, Pedlow, Stormonth:* Temperature and humidity gradients in the first 100 m over south-east England. London 1952.
2. *Heikkilä:* Jämförelse av tellurometeravstånd och triangelsidor av första ordningen. Stockholm 1966.
3. *Hytönen:* Beobachtungsergebnisse der finnischen Triangulationen in den Jahren 1961 – 1962. Helsinki 1963.
4. *Jaakkola:* Die allgemeinen Dreieckmessungen der geodätischen Abteilung des finnischen Landesvermessungsamtes. München 1966.
5. *Jaakkola:* Tekniska metoder för triangulation och trilaterationsarbeten i Finland. Stockholm 1966.
6. *Johnson, Heywood:* An investigation of the lapse rate of temperature in the lowest 100 m of the atmosphere, London 1938.
7. *Saastamoinen:* On the path curvature of electromagnetic waves. Ottawa 1965.

Appendix

Comparison of Tellurometer Distances and First Order Triangulation Sides

The sides have been divided into groups surrounding the base lines of the net.

At the end of each group is the number of sides, their added length and average length, the sum of differences and the average systematic difference between the tellurometer measurement and the known value. Finally there is the mean square random difference between these two distances.

side	tellurometer	triangulation	differ.	residual
II Hanko				
107 – 105	37907,092	37907,272	−0,180	+0,003
106 – 104	28494,936	28494,978	−0,042	+0,096
104 – 105	26686,151	26686,352	−0,201	−0,072
105 – 103	26307,857	26307,932	−0,075	+0,052
104 – 103	26161,726	26161,845	−0,119	+0,007
104 – 102	36060,698	36060,816	−0,118	+0,056
103 – 102	26158,265	26158,444	−0,179	−0,053
103 – 16	30021,743	30022,054	−0,311	−0,166
102 – 16	34235,892	34236,112	−0,220	−0,054
15 – 16	18996,980	18996,969	+0,011	+0,103
15 – 12	30687,486	30687,614	−0,128	+0,020
102 – 21	22831,630	22831,715	−0,085	+0,025
21 – 24	30972,862	30972,964	−0,102	+0,048
22 – 24	27778,313	27778,432	−0,119	+0,015
22 – 25	30860,655	30860,930	−0,275	−0,126
24 – 25	24125,927	24126,008	−0,081	+0,036
27 – 29	29114,129	29114,256	−0,127	+0,014
29 – 194	32238,880	32239,148	−0,268	−0,112
29 – 30	33780,727	33780,880	−0,163	+0,010
30 – 32	32392,712	32392,772	−0,060	+0,097
20 sides	585814,661	585817,493	−2,832	m = ±0,075
	29290,733		−4,83 mm/km	

side	tellurometer	triangulation	differ.	residual
III Lappträsk				
38 — 39	25829,477	25829,481	−0,004	+0,063
38 — 41	24331,844	24331,916	−0,072	−0,009
38 — 42	37478,032	37478,186	−0,154	−0,057
39 — 40	26702,202	26702,433	−0,231	−0,162
39 — 42	27997,972	27998,018	−0,046	+0,026
42 — 43	30165,333	30165,429	−0,096	−0,018
43 — 45	34743,633	34743,588	+0,045	+0,135
45 — 44	28812,828	28812,882	−0,054	+0,020
44 — 41	27417,304	27417,341	−0,037	+0,034
44 — 207	19934,601	19934,740	−0,139	−0,088
41 — 207	26625,515	26625,441	+0,074	+0,143
41 — 208	31327,855	31327,952	−0,097	−0,017
207 — 208	26710,212	26710,351	−0,139	−0,070
13 sides	368076,808	368077,758	−0,950	m = ±0,085
	28313,601		−2,58 mm/km	
V Maaninka				
213 — 215	45881,461	45881,729	−0,268	−0,072
214 — 215	42369,969	42370,215	−0,246	−0,065
214 — 216	39520,745	39520,746	−0,001	+0,167
216 — 72	36885,398	36885,442	−0,044	+0,113
72 — 70	38595,950	38596,008	−0,058	+0,107
70 — 67	30145,804	30145,977	−0,173	−0,044
66 — 68	24021,178	24021,238	−0,060	+0,043
68 — 69	32415,855	32416,099	−0,244	−0,106
69 — 192	34006,895	34007,024	−0,129	+0,016
71 — 193	37474,062	37474,453	−0,391	−0,231
71 — 73	38364,590	38364,798	−0,208	−0,044
73 — 75	26974,478	26974,631	−0,153	−0,038
75 — 231	24325,944	24325,964	−0,020	+0,084
231 — 234	34703,922	34703,926	−0,004	+0,144
234 — 182	35560,809	35561,035	−0,226	−0,074
15 sides	521247,060	521249,285	−2,225	m = ±0,109
	34749,804		−4,27 mm/km	

side	tellurometer	triangulation	differ.	residual
VII Viljakkala				
194—196	26933,414	26933,495	−0,081	−0,073
195—196	32841,808	32841,893	−0,085	−0,075
195—197	23798,086	23798,146	−0,060	−0,053
196—197	26190,760	26190,797	−0,037	−0,029
196—198	31438,035	31438,044	−0,009	+0,001
197—198	38084,170	38084,158	+0,012	+0,024
197—199	24000,190	24000,155	+0,035	+0,042
198—199	24207,291	24207,268	+0,023	+0,031
199—126	22985,422	22985,414	+0,008	+0,015
198—126	30038,024	30037,990	+0,034	+0,043
198—124	23383,696	23383,594	+0,102	+0,109
125—126	24479,340	24479,293	+0,047	+0,055
124—126	28019,597	28019,536	+0,061	+0,070
124—125	33439,067	33438,991	+0,076	+0,086
123—125	35977,420	35977,373	+0,047	+0,058
123—124	29724,532	29724,509	+0,023	+0,032
122—124	35522,466	35522,600	−0,134	−0,123
122—123	32798,582	32798,741	−0,159	−0,149
121—123	31790,448	31790,371	+0,077	+0,087
121—122	31290,869	31290,858	+0,011	+0,021
108—110	26207,172	26207,159	+0,013	+0,021
106—108	34951,418	34951,623	−0,205	−0,194
22 sides	648101,807	648102,008	−0,201	m = ±0,080
	29459,173		−0,31 mm/km	
VIII Otava				
136—137	27917,278	27917,374	−0,096	+0,009
137—139	22637,953	22638,095	−0,142	−0,570
139—141	34867,449	34867,623	−0,174	−0,043
141—143	25053,733	25053,792	−0,059	+0,035
143— 60	32569,856	32569,932	−0,076	+0,046
139—212	38261,772	38261,894	−0,122	+0,022
139—213	37366,613	37366,716	−0,103	+0,037
141—212	20354,516	20354,574	−0,058	+0,018
212—213	28776,619	28776,822	−0,203	−0,095
212—214	26793,044	26793,102	−0,058	+0,043
213—214	31790,431	31790,565	−0,134	−0,015
11 sides	326389,264	326390,489	−1,225	m = ±0,047
	29671,751		−3,75 mm/km	
IX Soanlahti				
60— 62	30758,931	30759,086	−0,155	−0,027
62— 64	36976,376	36976,472	−0,096	+0,058
64— 67	31341,191	31341,222	−0,031	+0,100
65—145	26873,848	26874,060	−0,212	−0,100
65— 66	36580,599	36580,783	−0,184	−0,031
5 sides	162530,945	162531,623	−0,678	m = ±0,079
	32506,189		−4,17 mm/km	

side	tellurometer	triangulation	differ.	residual
XI Kuhmo				
192–191	30549,394	30549,442	−0,048	+0,022
193–190	28563,768	28563,852	−0,084	−0,018
191–189	30590,751	30590,898	−0,147	−0,076
190–188	24555,538	24555,671	−0,133	−0,076
189–187	35392,567	35392,555	+0,012	+0,094
188–186	25703,318	25703,333	−0,015	+0,044
186–184	28652,616	28652,739	−0,123	−0,057
184–182	27688,960	27689,077	−0,117	−0,053
247–248	34314,568	34314,732	−0,164	−0,085
187–248	23625,152	23625,233	−0,081	−0,027
185–248	29387,362	29387,390	−0,028	+0,040
185–247	20737,596	20737,658	−0,062	−0,014
248–246	31620,058	31620,144	−0,086	−0,013
247–245	23547,503	23547,572	−0,069	−0,015
247–246	35430,768	35430,838	−0,070	+0,012
245–246	21730,012	21730,043	−0,031	+0,019
246–244	24719,182	24719,174	+0,008	+0,065
245–244	27112,405	27112,487	−0,082	−0,019
245–243	35936,053	35936,093	−0,040	+0,044
244–243	28603,445	28603,418	+0,027	+0,092
244–242	34309,202	34309,256	−0,054	+0,025
21 sides	602770,215	602771,605	−1,387	m = ±0,053
	28703,344		−2,31 mm/km	
XIV Laanila				
268–275	34897,053	34897,169	−0,116	−0,059
268–274	42307,085	42307,053	+0,032	+0,101
274–275	33916,250	33916,231	+0,019	+0,075
274–276	28950,835	28950,951	−0,116	−0,069
275–276	42569,886	42569,931	−0,045	+0,025
275–277	43249,257	43249,442	−0,185	−0,114
275–278	46970,150	46970,175	−0,025	+0,052
276–277	33649,454	33649,520	−0,066	−0,011
277–278	44027,414	44027,486	−0,072	0,000
9 sides	350537,384	350537,958	−0,574	m = ±0,071
	38948,598		−1,64 mm/km	

Abstract of the Comparison

region	sides	added length	difference systematic		random difference		
				mm/km	m	mm/km	
II	20	585814,661	−2,832	−4,8±0,6	±0,075	±2,6	or 1:390000
III	13	368076,808	−0,950	−2,6±0,2	0,085	±3,0	1:331000
V	15	521247,060	−2,225	−4,3±0,8	0,109	±3,1	1:318000
VII	22	648101,807	−0,201	−0,3±0,6	0,080	±2,7	1:367000
VIII	11	326389,264	−1,225	−3,8±0,5	0,047	±1,6	1:636000
IX	5	162530,945	−0,678	−4,2±1,1	0,079	±2,4	1:410000
XI	21	602770,215	−1,387	−2,3±0,4	0,053	±1,8	1:544000
XIV	9	350537,384	−0,574	−1,6±0,6	0,071	±1,8	1:547000
	116	3565443,388	−10,075	−2,82	±0,077	±2,5	1:399000
		30736,581					

Some Recent Measurements of Atmospheric Limitations to the Precision of Microwave Distance Measuring Equipment*)

by *M. C. Thompson, Jr.*, and *H. B. Janes*, Boulder, Colorado

The inherent internal precision of present electronic distance measuring instruments is quite high. For example, an instrumental noise level equivalent to 1 micron can be obtained for ranges of tens of kilometers. Unfortunately, this instrumental precision is seriously degraded when the equipment operates under field conditions in the real atmosphere.

Basically, all systems (Geodimeter, Tellurometer, Electrotape, etc.) measure the transit time of an electromagnetic signal over the path being studied. Conversion of this time measurement to an equivalent distance depends on some means of approximating the propagation velocity of the wave along the path [Thompson, Janes, and Freethey, 1960]. At present, the overall accuracy of path measurements from 1 to 50-km is essentially the accuracy of this velocity estimate.

In the simplest method, measurements of temperature, humidity, and barometric pressure are made at one or more points located in the vicinity of the line to be studied. From these data, the propagation velocity of the wavelength being used is calculated. This value is then assumed to apply over the entire path, and the transit time observations are converted accordingly. In some cases [Thompson, Janes, and Freethey, 1960; Richards, 1965], additional stations along the path have been used to improve the effectiveness of the process.

Since 1954, the Central Radio Propagation Laboratory of the National Bureau of Standards (now the Institute for Telecommunication Sciences and Aeronomy of Environmental Science Services Administration), performed several experiments and gathered the following data:

1. Variations in transit time for 9.4 GHz radio signals propagated over various paths.
2. Variations in propagation velocity near the path terminals.
3. General meteorological conditions in the area of the path.

The transit time data (obtained by a phase-measuring technique) were taken continuously and were recorded (on magnetic tape) in analog form, with an overall frequency response up to about 10 Hz, with a precision of about 1-mm equivalent distance. The velocity data (described in terms of refractive index) were obtained at each terminal from psychrometer and barometer observations that were made at $^1/_2$-hour intervals, and had precision of a few parts per million.

To illustrate the results, the phase (transit time) records were read at times corresponding to meteorological observations. Variations of the corrected range, R_c, were obtained from variations in the observed range, R_o, and the corresponding refractive index, n_o. If we express the change of R_c in parts per million of R_o, the variations in the corrected value are obtained by subtracting the corresponding changes in refractivity, N_o, where $N_o = (n_o - 1) \times 10^6$. For this purpose, it is sufficient to know R_o only to the order of 1 %, which is easily attained.

The results from three different paths are given. The first path was 15-km long over relatively flat terrain near Boulder, Colorado, a dry climate. Each terminal of the path was located at the edge of a mesa with steep, sloping foreground. The second path was 17-km long and passed over both land and water in a sub-tropical climate near Florida's east coast. This location needed towers to raise the paths above the dense vegetation. The third path was almost entirely over water, with two terminals on Eleuthera Island, British West Indies. In all cases, the paths were nearly horizontal.

Figures 1, 2 and 3 show plots of variations in the observed range, the observed index, and the corrected range, using the end-point index data both separately and averaged.

Figures 4, 5, and 6 show effects of time and space averaging. In these plots, the corrected ranges from Figs. 1, 2, and 3 were averaged in the following combinations:

1. The terminal measurements of index were used both individually and averaged to correct the observed range.
2. The standard deviations of the average values were computed for periods, T, ranging in length from 3 to 96 hours.

---

*) This report is based on a more complete paper by the same title and authors scheduled for publication in the Aug. 1967 Bulletin of the Seismological Society of America.

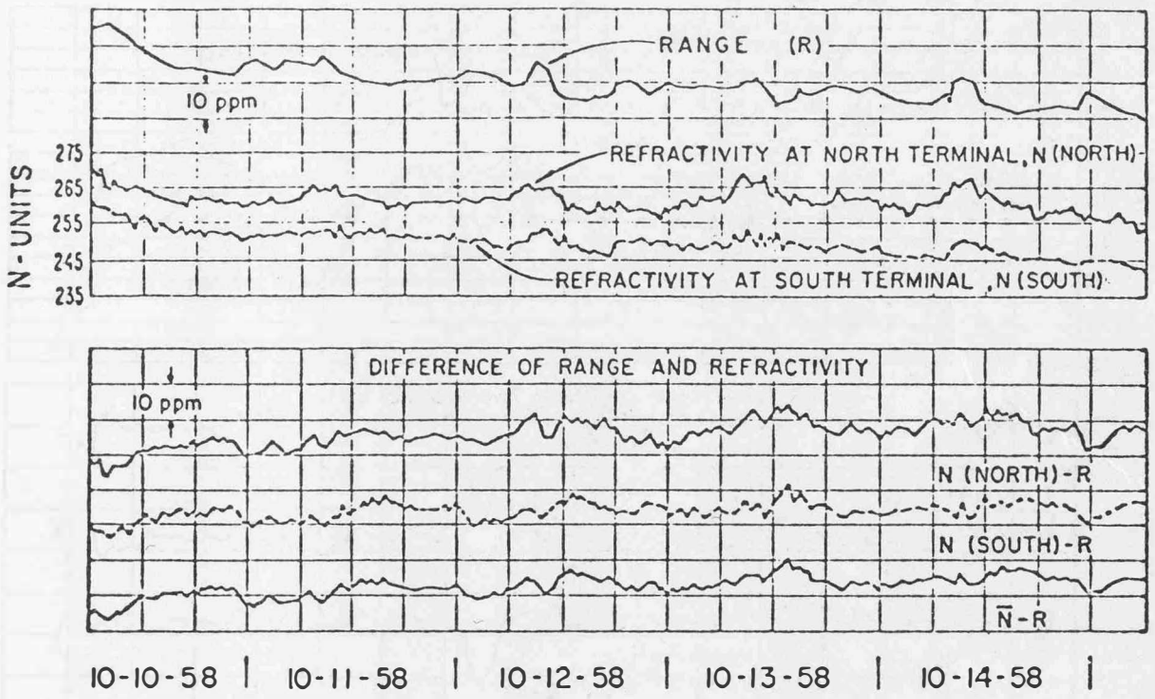
RANGE (R)
10 ppm
REFRACTIVITY AT NORTH TERMINAL, N (NORTH)
REFRACTIVITY AT SOUTH TERMINAL, N (SOUTH)
N - UNITS
275
265
255
245
235
DIFFERENCE OF RANGE AND REFRACTIVITY
10 ppm
N (NORTH) - R
N (SOUTH) - R
N̄ - R
10-10-58
10-11-58
10-12-58
10-13-58
10-14-58

Fig. 1

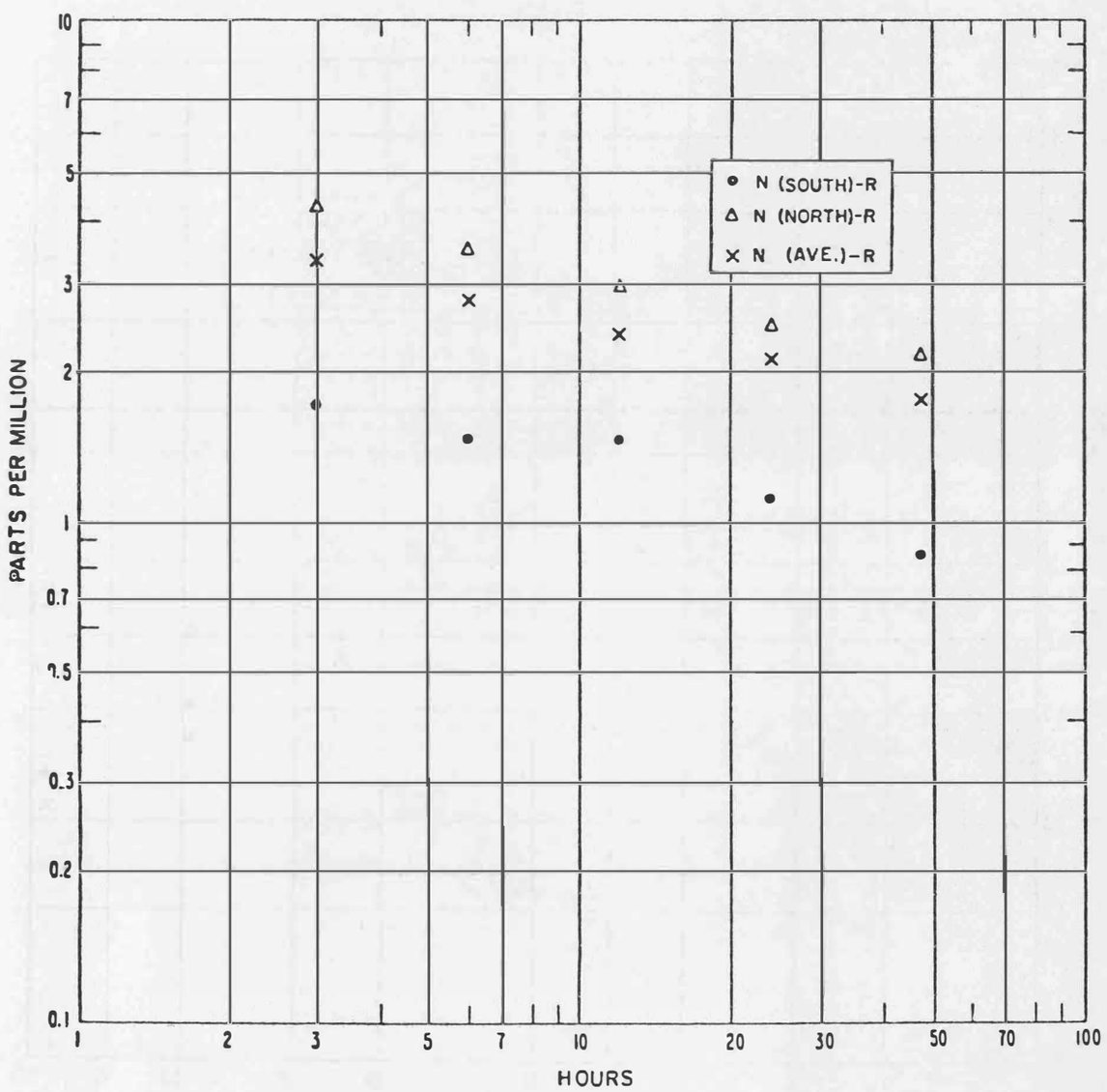
N (SOUTH)-R
N (NORTH)-R
N (AVE.)-R
PARTS PER MILLION
10
7
5
3
2
1
0.7
0.5
0.3
0.2
0.1
1
2
3
5
7
10
20
30
50
70
100
HOURS

Fig. 4

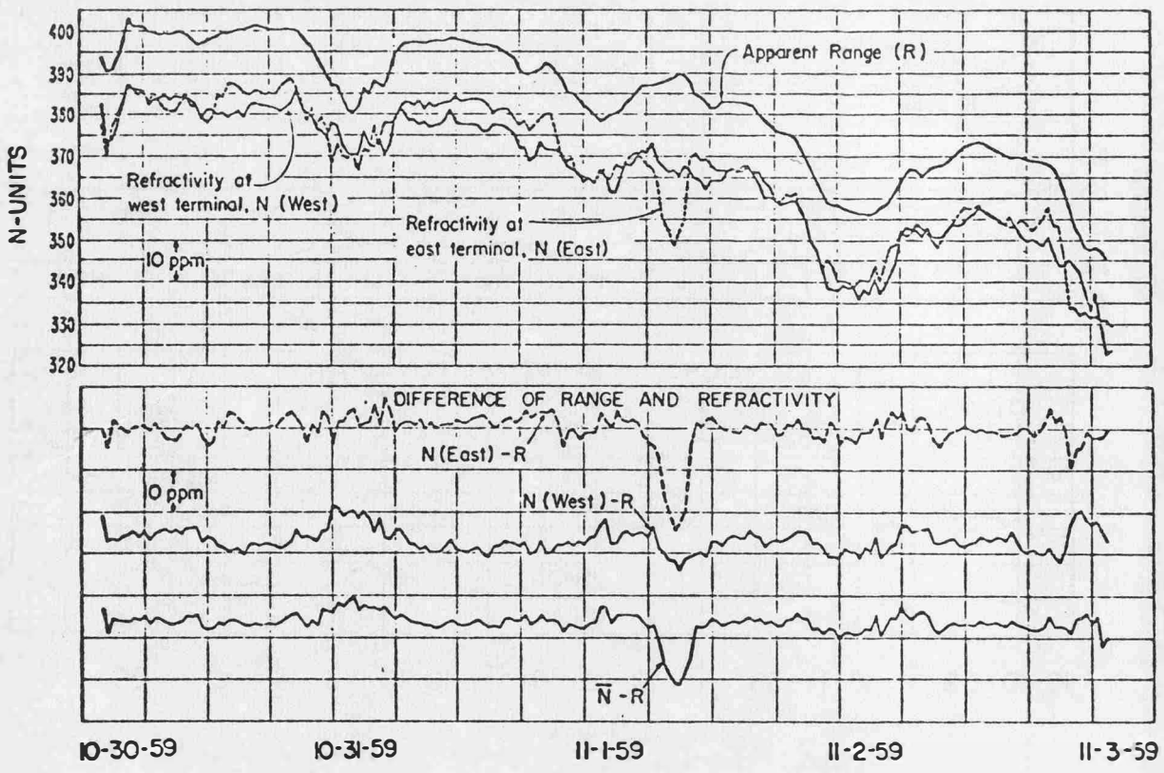
N-UNITS
400
390
380
370
360
350
340
330
320
Apparent Range (R)
Refractivity at west terminal, N (West)
Refractivity at east terminal, N (East)
10 ppm
DIFFERENCE OF RANGE AND REFRACTIVITY
N (East) - R
10 ppm
N (West) - R
$\overline{N}$ - R
10-30-59
10-31-59
11-1-59
11-2-59
11-3-59

Fig. 2

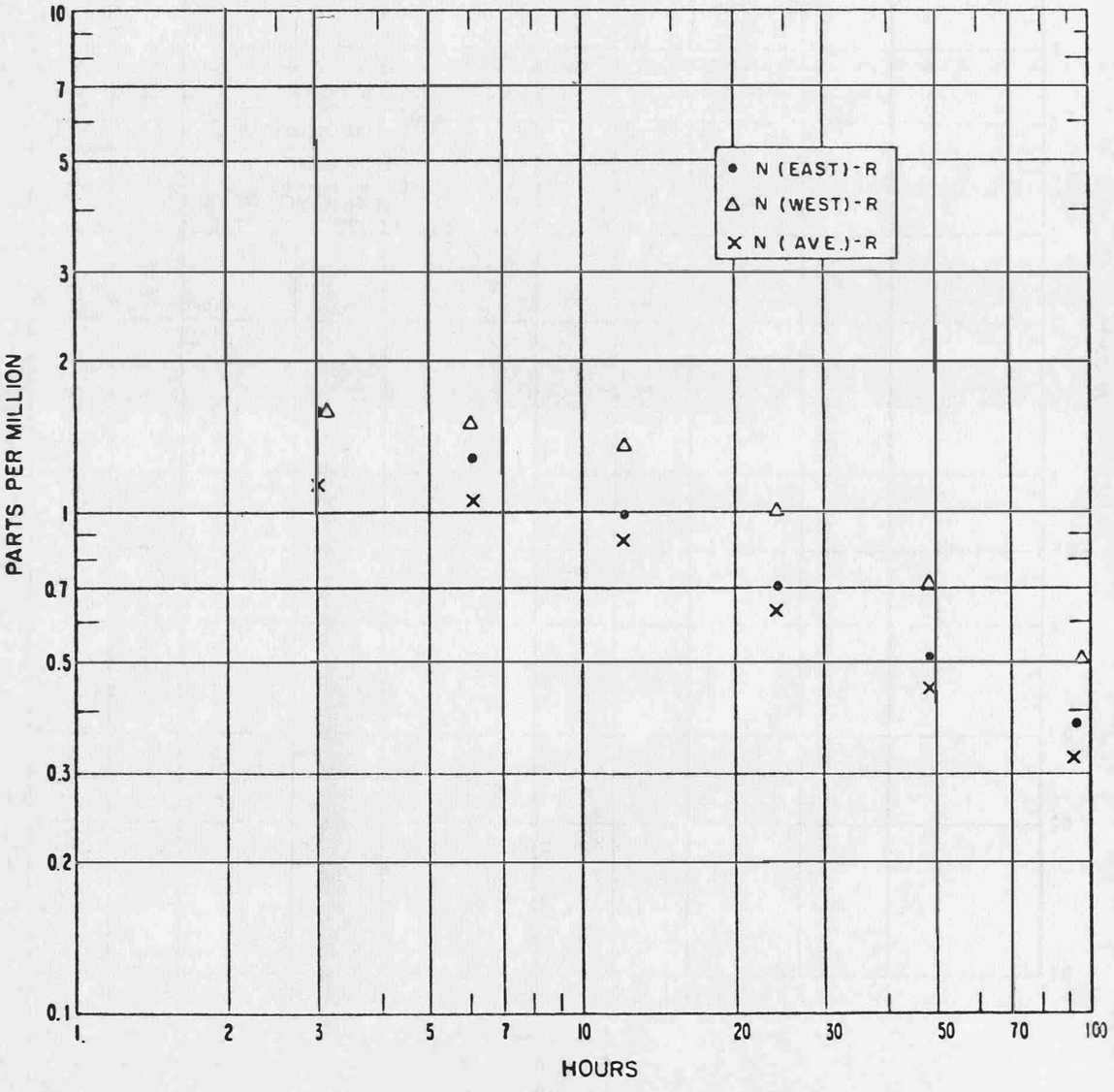
PARTS PER MILLION
10
7
5
3
2
1
0.7
0.5
0.3
0.2
0.1
• N (EAST) - R
Δ N (WEST) - R
× N (AVE.) - R
1
2
3
5
7
10
20
30
50
70
100
HOURS

Fig. 5

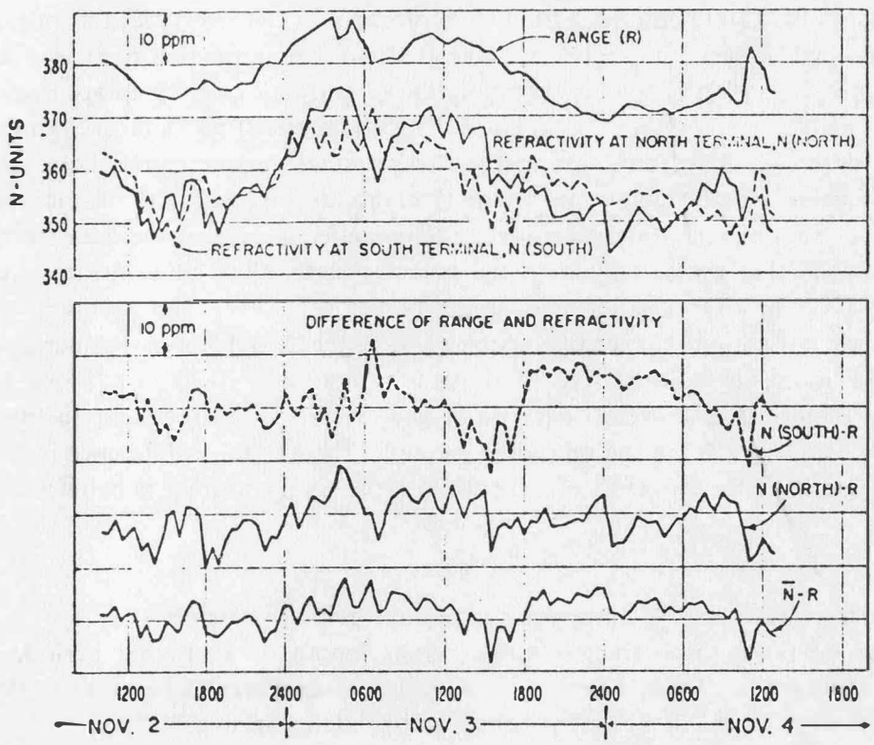
10 ppm
RANGE (R)
380
370
360
350
340
N-UNITS
REFRACTIVITY AT NORTH TERMINAL, N (NORTH)
REFRACTIVITY AT SOUTH TERMINAL, N (SOUTH)
10 ppm
DIFFERENCE OF RANGE AND REFRACTIVITY
N (SOUTH)-R
N (NORTH)-R
N̄-R
1200
1800
2400
0600
1200
1800
2400
0600
1200
1800
NOV. 2
NOV. 3
NOV. 4

Fig. 3

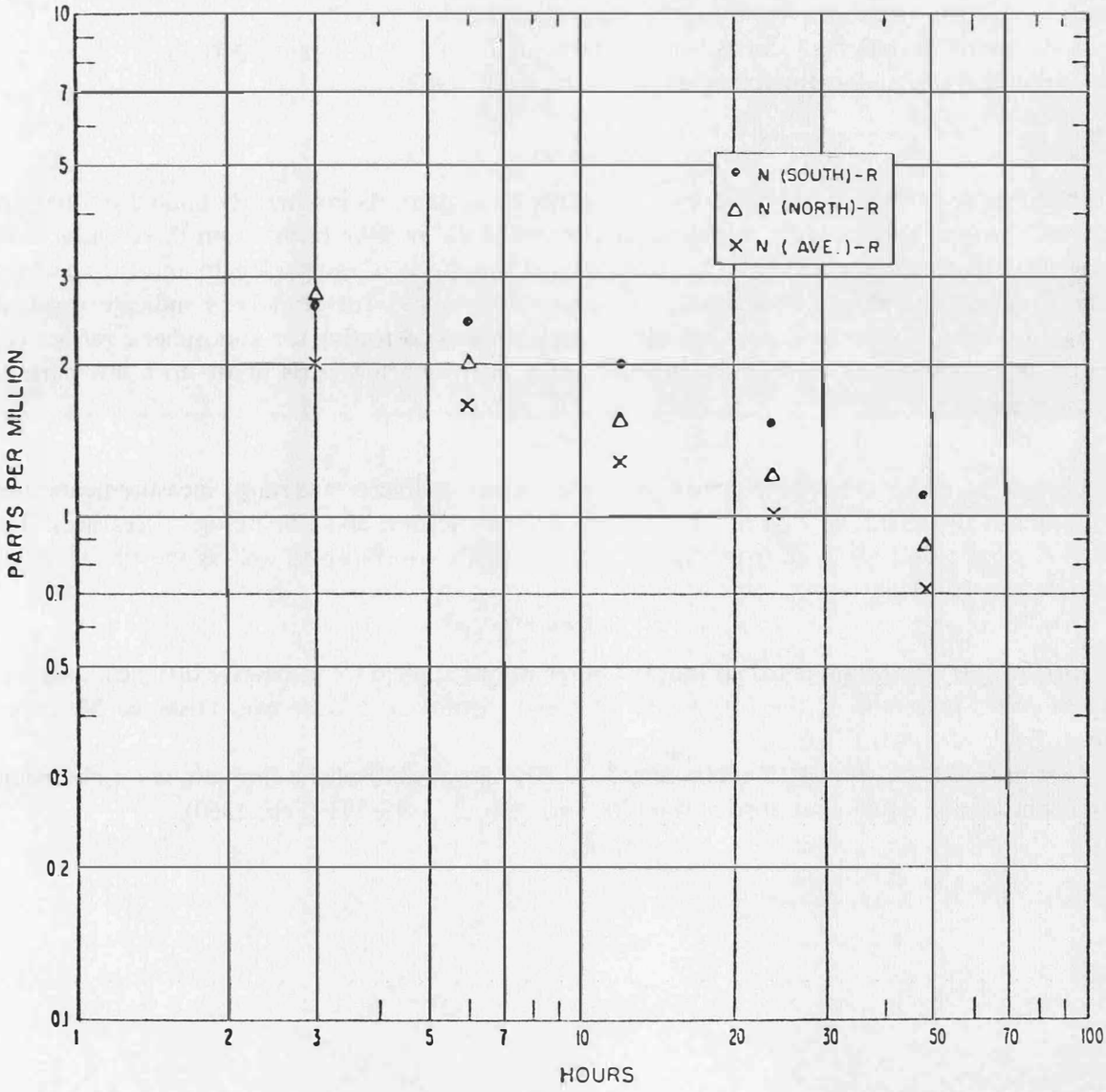
PARTS PER MILLION
10
7
5
3
2
1
0.7
0.5
0.3
0.2
0.1
N (SOUTH)-R
N (NORTH)-R
N (AVE.)-R
1
2
3
5
7
10
20
30
50
70
100
HOURS

Fig. 6

Figure 4 shows the 15-km path near Boulder, Colorado, in October 1958; the index, as measured at the south terminal, appears much better correlated with the measured path length than that at the north terminal. In this case, the best combination of corrections gives an accuracy (of the measured change in path length) of about 0.9 ppm of the path length. If no "a priori" knowledge existed concerning the difference in effectiveness of the two terminal measurements, however, they would probably be weighted equally giving an accuracy of about 2 ppm for the same averaging time.

Figure 5 also shows some difference in the relative effectiveness of the data from the two terminals, but indicates that the equally weighted mean is better than either mean taken separately. On the 17-km path in Florida (during October-November 1959), the accuracy using 48-hour smoothing (the same used in the preceding instance), is better than 0.5 ppm. By increasing the smoothing time to 96 hours, this is improved to about 0.3 ppm.

The 47-km Eleuthera Island path over water gave results (Fig. 6) similar to those in Florida but roughly twice as large. As in the preceding example, there is some difference in effectiveness of the correction data from the two ends of the path, but the simple average is better than either mean alone.

Figures:

Fig. 1 Long-term variations of apparent range and related varibles
Fig. 4 Standard deviation of corrected range versus length of averaging period, Green Montain — Table Mesa path, Boulder, Colorado: 15,2-km, Oct. 1958
Fig. 2 Long-term variations of apparent range and related variables
Fig. 5 Standard deviation of corrected range versus length of averaging period, Cape Kennedy — Cocoa path, Florida: 17,1-km, Oct.—Nov. 1959
Fig. 3 Long-term variations in apparent range and related variables
Fig. 6 Standard deviation of corrected range versus length of averaging period, Eleuthera Island path, Bahamas: 47,3-km, Nov. 1962

Summary

In the field, the precision of microwave distance measurements is currently limited by the propagation effects of the normally turbulent atmosphere. Field measurements from three paths using a 3-cm wavelength system have been analyzed to find the effects of sample length and the spectrum of the propagation-induced fluctuations in measured distance. These analyses indicate residual, propagation-induced fluctuations of measured distance, after correcting for atmospheric refractivity using meteorological data from both path terminals, of from a few parts in 10^7 to a few parts in 10^8 are attainable.

Abstract

The use of end-point meteorological data for correcting microwave range measurements over three paths is discussed. The paths have widely different terrain and climatological features. The effects of using correction data from one or both terminals are shown as well as the effects of observation length.

References

Richards, M. R., Multiple meteorological observations applied to microwave distance measurement (a paper presented at the Int. Assoc. of Geod. Symp. on Electromag. Distance Measure., Oxford, England, 1965).

Thompson, M. C., Jr., H. B. Janes and *F. E. Freethey*, Atmospheric limitations on electronic distance-measuring equipment, *J. Geophys. Res.*, *65*, No. 2, 389—393 (Feb. 1960).

Refractive Effects of Radio Ranging on Artificial Earth Satellites

by *Frank L. Culley, Mark Sherman,* Washington, D. C.

Presented to Special Study Group No. 23, Section I of the
International Association of Geodesy, Vienna, March 1967

The use of electromagnetic waves for direction or distance measurements necessitates corrections for refractive effects of the atmosphere if true values are obtained from observations. Geodesists are familiar with uncertainties of elevations determined by vertical-angle observations. They have blamed these mostly on refraction of the atmosphere, but have also come to suspect that part of these uncertainties is due to differences in deflections of the vertical at different survey points. Horizontal angle measurements over long lines in precise surveys are usually made at night when refraction is at a minimum. The effects of uncertainties due to refractive effects are quite obvious with electromagnetic-wave distance-measuring methods in both the optical and radio portions of the spectrum.

A study of the refractive effect on ranges obtained from use of electromagnetic waves in the radio spectrum is more necessary than one on ranges obtained from the use of light waves. In the optical tracking of satellites, the reflected light from the satellite and the light of the stars pass through the same atmospheric media of the earth. The satellite's direction in space can be determined easily from the known positions of stars in its angular proximity. No range is measured. However, in radio ranging on a satellite (as in the SECOR system), ranges, and not directions, are measured, and there are no known distances with which to compare directly the observed ranges. The radio waves are bent and their velocities are changed much more than the light waves, because refraction increases inversely with frequency. The corrections for humidity and temperature in terrestrial measurements of distances are on the order of 50 times as great for the radio as for the optical spectra.

The electromagnetic waves used for terrestrial distance measurements pass only through the troposphere while those used for satellite geodesy also pass through the ionosphere. In satellite geodesy we have to consider the refractive effects of both the troposphere and the ionosphere.

Tropospheric Refraction Corrections

The refractive effect in the troposphere causes the electronically measured distances to be greater than if the measurements were made in a vacuum due to retardation and to bending of the path of the measuring wave. One can arrive at corrections for conditions of humidity, temperature, and barometric pressure, and then prove them by comparing electronically measured distances (radio ranges) over the same lines measured with invar tapes, assuming that most of the errors from tape measurements (due to tension, temperature, crosswind, etc.) are practically eliminated. Or, they can be compared to long triangulation lines expanded from base lines if the angular errors also can be eliminated.

Neglecting the ionospheric refraction, Figure 1 shows schematically the effect of tropospheric refraction alone. Actually, there is no further effect where the ray is outside of the troposphere.

The measured radio range from ground station to satellite is

$$R_e = c\,\tau \tag{1}$$

where τ is the time of travel between the two points and c = the velocity of an electromagnetic wave in a vacuum.

The index of refraction is

$$n = \frac{c}{v} \tag{2}$$

where v is velocity of the electromagnetic wave in the atmosphere.

$$R_e = \int_o^R n\,d\,R \tag{3}$$

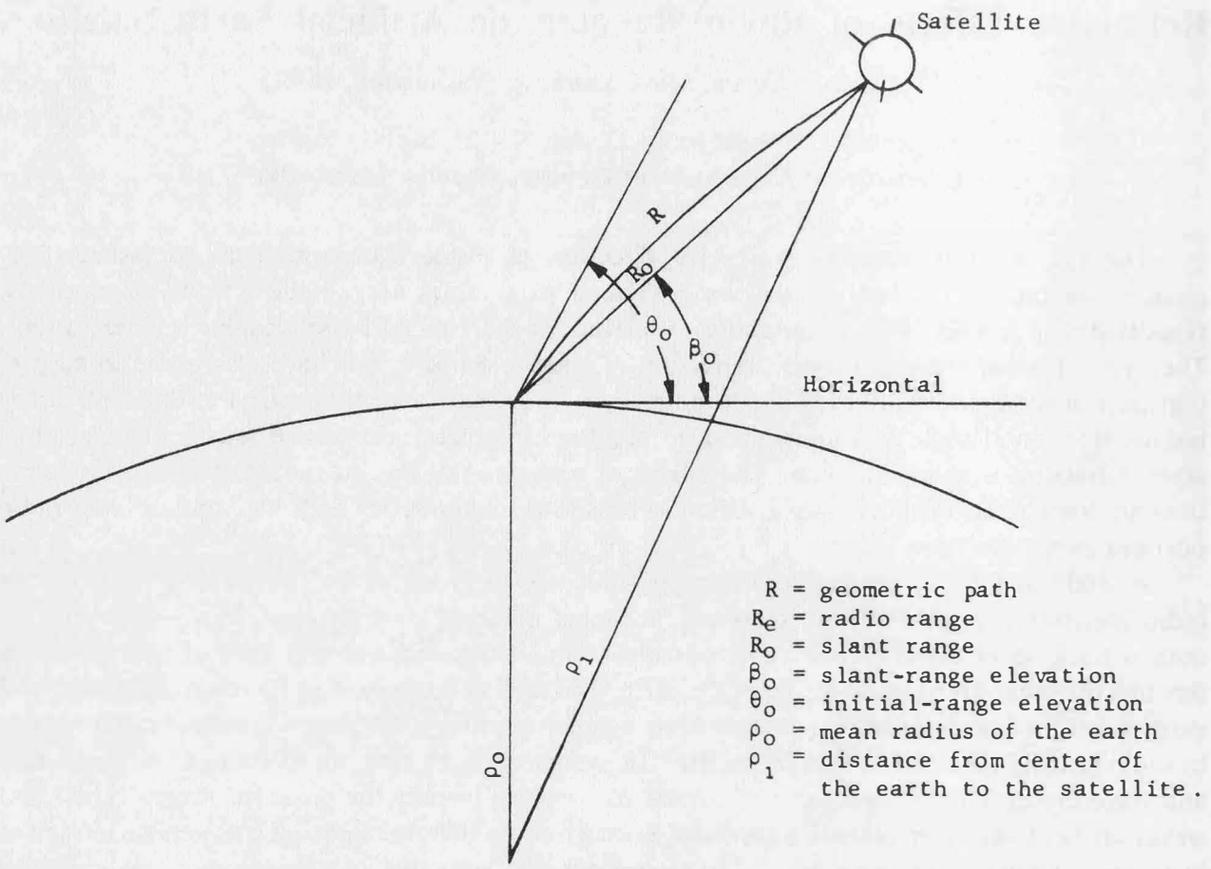

Figure 1. The tropospheric refraction considering the ionospheric refraction to be zero.

The error caused by tropospheric refraction, neglecting all other errors, is

$$\Delta R_t = R_e - R_o = \int_o^R n\, d\, R - R_o \tag{4}$$

The two refractive effects can be seen if we write

$$R_e = \int_o^R n\, d\, R = \int_n^R (1 + n - 1)\, d\, R = R + \int_o^R (n - 1)\, d\, R \tag{5}$$

Then

$$R_e - R_o = R - R_o + \int_o^R (n - 1)\, d\, R \tag{6}$$

where $R - R_0$ is the geometrical effect of ray curvature and $\int_O^R (n - 1)\, dR$ is the retardation effect of decreased velocity.

Several authors, including Bean and Thayer [1], show the curvature effect to be negligible above $\approx 6^0$. No ranges are measured at elevations less than 5^0. The retardation effect must be taken into account. This amounts approximately to 20 meters at 6^0 elevation and 2 meters at 90^0.

Two formulae are used in reduction of SECOR data to find the corrections for tropospheric refraction. The first is the one suggested by the Cubic Corporation [2] and is

$$\Delta R = \frac{T_1(1 - e^{-Z/T_3})}{(T_2 \cos \beta_0) + \sin \beta} \tag{7}$$

where T_1 is the refractive correction in meters at 90° elevation

T_2 is the horizontal-scaling correction = 0.0236

T_3 is a constant (scale height) = 7,000 meters

β_0 is the elevation angle

Z is the height of the satellite (meters).

Since the exponential term is negligible at satellite heights, we have a correction based on the elevation. The Cubic formula gives the following values:

β_0	ΔR (meters)	β_0	ΔR (meters)
0°	114.41	30°	5.19
3	35.62	45	3.77
5	24.41	60	3.08
10	13.71	85	2.71
11.45	12.16		
15	9.64	90	$2.70 = T_1$

The other, more sophisticated, tropospheric model takes into account the changes in temperature, humidity, pressure, and geographic location.

It is

$$\Delta R = \frac{10^{-6} N_s}{C \sin \beta_0} \Psi \tag{8}$$

where N_s is the surface refractivity which is a function of temperature, pressure, and content of water vapor at the surface

C is a parameter varying with location and seasonal and other factors

Ψ is a correction factor used when the elevation is below 10°, but is considered unity above 10°. It is a function of C, range, and β_0.

Using the present values of T_1, T_2, and T_3 of equation (7), there is very little difference between formulae (7) and (8) in the South Pacific area. In desert areas or in extremely humid areas, neglecting atmospheric conditions may result in errors at low elevations amounting to as much as 2.5 meters for 10°.

Wet- and dry-bulb temperatures and pressure are measured at each station before each satellite track. The surface refractivity is computed from

$$N_s = \frac{77.6}{T}\left(P + 4{,}810\,\frac{e}{T}\right) \tag{9}$$

where P is total pressure in millibars

e is partial pressure in millibars of water vapor

T is absolute temperature.

β_0 can be calculated to sufficient accuracy for uncorrected ranges. Without sounding measurements in the atmosphere at a particular location, C can only be approximated and may result in error in ΔR.

Ionospheric Refraction Corrections

The major refraction occurs in the ionosphere. It varies according to the ionization effect of sunlight on the atmosphere and, therefore, varies with time of day, with season of the year, with latitude, and with sunspot activity. Dr. Friedrich Rohde found the maximum ionization to occur at 14,0 hours and the minimum between one and two hours before sunrise (see Figure 2).

In order to determine the effect at the instant of range measurements with the SECOR system, the highest one of four modulating frequencies is returned from the satellite to the ground stations on carrier frequencies of 449 and 224.5 megacycles per second. All modulating frequencies are sent on a 420.9-megacycle carrier from ground station to satellite, and returned on 449 megacycles. This gives the value

$$K = \left(\frac{f_3^2}{f_1^2}\right)\left(\frac{f_2^2 + f_1^2}{f_3^2 - f_2^2}\right) \tag{10}$$

where f_1 = 420.9 megacycles per second

f_2 = 449 megacycles per second

f_3 = 224.5 megacycles per second, which permits calculation of range correction $\Delta R_1 = K(D_1 - IC)$ where IC is the range component of the highest modulating frequency on the 224.5- megacycle carrier.

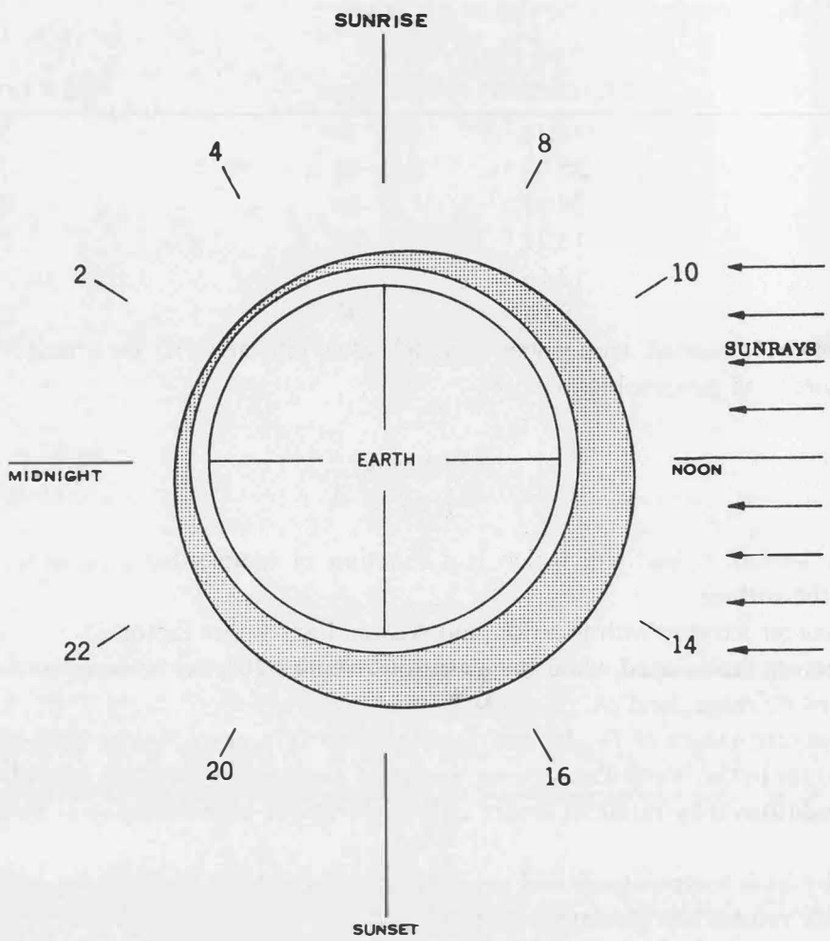

Figure 2. Electron density profile around the earth.

D_1 is the range component of the highest modulating frequency on the 449-megacycle carrier.

Interference on the low-frequency carrier had made it impossible sometimes to get a range measurement on that frequency. Using samples of ionospheric refraction data measured during operations in the Pacific Ocean area, an analytical model was developed. This gives an educated guess at the ionospheric correction. The formula is

$$\Delta R = \frac{40.3}{f^2} S(\Phi) F(X, R^*) \frac{H\left[\tan^{-1}\left(\frac{Z_s - Z_m}{H}\right) + \tan^{-1}\left(\frac{Z_m}{H}\right)\right]}{\left[1 - \frac{\cos^2 E}{\left(1 + \frac{Z_m}{P}\right)^2}\right]} \tag{11}$$

when

H = scale height

Z_s = satellite height

Z_m = height of maximum electron density

P = mean radius of the earth

E = elevation angle of the satellite relative to the horizontal tangent plane

$S(\Phi)$ = function of the earth's magnetic field

Φ = effective magnetic latitude

f = frequency in megacycles per second
$F(X, R^*)$ = sun zenith angle function
X = the effective sun zenith angle
R^* = function of satellite height

All factors except $S(\Phi)$ can be found and put into the program. $S(\Phi)$ is a function of three unknown coefficients.

$S(\Phi) = C_1 \Phi^0 + C_2 \Phi^1 + C_3 \Phi^2$ where Φ is effective magnetic latitude. These parameters are obtained by fitting this linear function to the measured data and to the rest of the model. After the parameters are obtained, they are inserted in the model which can be used to predict measured values in cases where the particular coefficients apply.

When measured ionospheric correction data are not available from all stations, coefficients are fitted to available data. The model is physically significant; therefore, the parameters are constrained and are significant when applied to stations without data.

References

1. *National Bureau of Standards Journal of Research.* May-June 1963. Vol. 67 *D.*
2. "Mathematics of Geodetic SECOR Data Processing," *Final Technical Report FIR/71—2.* San Diego, California: Cubic Corporation. 25 September 1964.

Selected Bibliography

Culley, Frank L.: "Measuring Around the Earth by Electronic Tracking of Satellites." Presented to the Second International Symposium on the Use of Artificial Satellites for Geodesy, Athens Greece. 27 April—1 May 1965.

Culley, Frank L.: "Radio Ranging on an Artificial Satellite; Its Geodetic Application." Presented to the International Association of Geodesy Symposium if Electronic Distance Measurement, Oxford, England. 6—11 September 1965.

"Geodetic SECOR Data Processing System, Army Map Service," *Cubic Corporation Study.* San Diego, California: Cubic Corporation. 15 July 1965.

Henriksen, S. W.: "Range Methods for Geodetic Adjustment," *Army Map Service Geodetic Memorandum No. 1536 A.* Washington: U. S. Army Map Service. October 1964.

"Preliminary Geodetic SECOR Ionospheric Refraction Modeling, Army Map Service," *Cubic Corporation Study.* San Diego, California: Cubic Corporation. Undated.

Prescott, Major N. J. D., RE.: "Experiences with SECOR Planning and Data Reduction." Presented to the International Association of Geodesy Symposium of Electronic Distance Measurement, Oxford, England. 6—11 September 1965.

"Real-time Compensation for Tropospheric Radio Refractive Effects on Range Measurements," *NASA Contractor Report, NASA CR-109.* Silver Spring, Maryland: J. J. Freeman Associates, Inc. October 1964.

Rohde, Friedrich W.: "Propagation Phenomena of Electronic Range Measurements to Satellites." Presented to the 47th Annual Meeting of the American Geophysical Union, Washington, D. C. April 1965.

Rutscheidt, Erich H. and Lowrey, Girard R., Jr.: "SECOR Data Processing and Results." Presented to the 47th Annual Meeting of the American Geophysical Union, Washington, D. C. April 1966.

Addendum

This addendum is provided in response to numerous requests for information dealing with scale height.

The scale height is a parameter that arises in the ionospheric model. It has the effect of changing height units into units of scale height. It is similar to the scale height that arises from the vertical distribution of density or pressure in the atmosphere,

$$\rho = \rho_o \, e^{\left(-\frac{h - h_o}{\text{scale height}}\right)}$$

where

ρ = density or pressure

h = height

o indicates a reference level.

Note that when the height difference is equal to the scale height, ρ has decreased to $\frac{1}{e}$ of its reference value. Thus scale height represents a thickness of the atmosphere over which ρ changes a certain amount.

In our case the scale-height term originates as a parameter in an empirical model of the electron density of the ionosphere. It represents 1/2 the effective thickness of the ionosphere. More precisely, it sets the upper and lower effective bounds at which the electron density has decreased to 1/2 its maximum value.

The empirical formula for the vertical distribution of electron density that we use is

$$N(Z) = \frac{N_{max}}{\left[1 + \left(\frac{Z - Z_m}{H}\right)^2\right]}$$

where

N_{max} = maximum electron density

Z = height

Z_m = height of $N_{\max}$

H = scale height.

When Z is H units above or below the maximum level, $N(Z)$ is 1/2 its maximum value.

Part II

Refraction Effect on the Determination of Directions

A. Use of Relationships Between Different Effects of Refractive Index

The Calculation of Refraction Angles by Means of the Refractive Index and of the Radii of the Curvature of the Refractional Curve.

by C. Sc. Ing. *Pelikán M.*, Praha

1. *Introduction*

The basic member being introduced into the calculation is the refraction coefficient k or any other member aggregately representing the atmospheric properties of the environment in which the measurements are being carried out. The complicated form of the spatial refraction curve is, as a rule, replaced by a simpler plane curve, the equation of which enables an easier numerical assessment of the refraction angle. For the numerical assessment of the values of the refraction angles the meteorological values in the end points of the line of sight are usually known.

Also in this consideration, we start, solving the problems of the vertical refraction, from the following basic assumptions, the definitions or formulation of which is to a certain degree abandoning the conventional procedure, trying at the same time to apply the results obtained in the latest theoretical as well as empirical research work. Moreover it regards the possibilities of utilizing more perfect technical means and methods applicable for measurements.

2. *A new procedure in calculating the refraction angles*

For the numerical assessment of refraction angles are in practical measurements up to now primarily used the refraction coefficient k summarily expressing the meteorological values of the atmosphere according to the line of sight. The calculation of the refraction coefficient k and the numerical assessment of the values of the refraction angles performed in such a way, we can, for instance find, in its whole range in the theory of Jordan-Eggert in the publication /1/.

2.1 *The refractive index of air as the basic element of the calculation*

The explosive development of electronic measuring methods involves also the necessity of expressing as perfectly as possible the refractive properties of the environment for determining the physical reduction. After long years of verification were by the sessions of the UGGI and IAG approved resolutions which recommend the application of certain formulae for assessing the refractive index for diverse geodetic surveying. From these recommended formulae we can make use for the calculation of the refraction angles of Sears-Barrell's formula derived for monochromatic unmodulated light in the form of

$$n_{t,p} - 1 = (n - 1)\frac{273}{T} \cdot \frac{p}{760} - \frac{273}{T} \cdot 5{,}5\, e \cdot 10^{-8}, \qquad (1)$$

where

$$n - 1 = (2876{,}04 + 16{,}288\,\lambda^{-2} + 0{,}136\,\lambda^{-4}) \,.\, 10^{-7} \,.$$

In these equations represents p the air pressure in Torr, T the air temperature in ^0K, e the air humidity in Torr and λ the wave length of visible light in μ. For the mean value of the wave length $\lambda = 0{,}55\mu$ and with regards to the imperfect monochromatics of light we can after the calculation mentioned in the publication /2/ arrange the formula (1) to the form of

$$(n_{t,p} - 1) \,.\, 10^6 = \frac{105{,}62\,p - 15{,}02\,e}{T} \,. \tag{2}$$

By means of the optical refractive index $n_{t,p}$, expressing at present according to the adopted conclusions by the sessions of UGGI and IAG the most perfect condition of the environment and its refractive properties, we are going to try now to express the refraction angle.

2.2 *The derivation of the formulae for the calculation of refraction angles*

The derivation of formulae for the calculation of refraction angles by means of the refractive index n is based on the following assumptions:

The curvature of the refraction curve s is from a certain altitude in the environment of the earth atmosphere incessantly, combinably diminishing and is, with the increasing distance from the earth, converging to zero. The curve of such a quality can be replaced in a limited interval by the simple equation curve which would be meeting the mentioned conditions, i. e. for instance the hyperbola in the simple form of

$$y^2 = A\,x^2 + B\,x \,. \tag{3}$$

The coordinate system for the equation (3) has been selected in such a way, that the tangent of the curve s in the point 1 is the coordinate axis y (Fig. 1.).

Let's assume that we know the radii of the curvature of the curve s in the point 1 (ρ_1) and in the point 2 (ρ_2). The oblique distance D' as well the horizontal distance D is known too. The radii of the curvature in the points 1 and 2 we can calculate according to the law of the geometrical optics defining the radius of the curvature in dependence upon the refractive index n, upon the m. s. l. h and upon the zenith distance z in the differential form of

$$\rho = - \frac{n}{\frac{dn}{dh} \,.\, \sin z} \tag{4}$$

Anticipating we know in the points 1 and 2 the m. s. l. h_1 and h_2, the zenith distance z, the meteorological value and thus also the refractive index n_1 and n_2, we can define then the course $n = f(h)$ between the points 1 and 2 by any equation with two parameters a, b, which we eliminate by calculating from two equations $n = f(h)$ written for the points 1 and 2.

Assuming a linear dependence $n = ah + b$, we should obtain dn/dh constant and thus also ρ = constant. The refraction curve would be the circular line which is merely a special case of the refractional influences and we are not going to employ it furthermore. The dependence $n = f(h)$ in the standard atmosphere (Fig. 2) implies that this dependence could, in a certain final interval h, be defined for instance by the equation

$$n - 1 = b \,.\, e^{a\,h} \,. \tag{5a}$$

By means of the equations (4) and (5a) we are thus able to define the radii ρ_1 and ρ_2 of the curve s in the points 1 and 2

$$\rho_1 = - \frac{n_1}{\sin z_1} \cdot \frac{h_1 - h_2}{(n_1 - 1)\, ln \frac{n_1 - 1}{n_2 - 1}}, \qquad \rho_2 = - \frac{n_2}{\sin z_2} \cdot \frac{h_1 - h_2}{(n_2 - 1)\, ln \frac{n_1 - 1}{n^2 - 1}} \,. \tag{4a}$$

In the further solution we eliminate by means of the equations of the curvature radii written for the curve (3) in the points 1 and 2 the parameters A, B of the curve (3) and after some arrangements and slight simplification (see /2/) we obtain the general formulae for the refraction angles Δ_1 and Δ_2.

$$\Delta_1 = \frac{n_1 - 1}{1 + tgz \,.\, tg\,\varphi/2} \cdot \frac{ln\dfrac{n_1 - 1}{n_2 - 1}}{1 + \left(\dfrac{n_1 - 1}{n_2 - 1}\right)^{1/3}} \,.\, tgz \,, \qquad \left(\varphi = \frac{D}{R}\right) \tag{6a}$$

$$\Delta_2 = \frac{n_2 - 1}{1 + tgz \,.\, tg\,\varphi/2} \cdot \frac{ln\dfrac{n_1 - 1}{n_2 - 1}}{1 + \left(\dfrac{n_2 - 1}{n_1 - 1}\right)^{1/3}} \,.\, tgz \,. \tag{6b}$$

The forms of the equations imply that it is possible to calculate the refraction angles only for the finite value $D' = \widehat{12}$ due to the fact that in the infinite $n_2 - 1 = 0$ and the expressions in the fractions of the equations (6) are becoming thus for this case undefinable.

In the numerical assessment of the refraction angles, while calculating the terrestrical refraction, it is possible to attain a substantial simplification as in the zenith distance $z \doteq 90^0$ and in the equation it is possible without minimizing its accuracy to insert also $\sin z \doteq 1$. The same is valid for the refractive index $n \doteq 1$. By these simplification and assuming moreover the displacement of the refraction curve s in the points 1 and 2 by means of the osculating circular lines K_1 and K_2 of the radii ρ_1 and ρ_2 (see /3/), we are to obtain for the refraction angles in calculating the terrestrical refraction very simple relationships

$$\Delta_1 = \frac{D}{2}\left(\frac{dn}{dh}\right)_1 , \quad \Delta_2 = \frac{D}{2}\left(\frac{dn}{dh}\right)_2 . \tag{7a, 7b}$$

If we work out dn/dh from the equation (5a) eliminating the constants a, b and inserting them into the equation (7a,b), we are to obtain for the refraction angles in the point 1 the formula

$$\Delta_1 = \frac{D}{2\,\Delta\, h}(n_1 - 1)\, ln\frac{n_1 - 1}{n_2 - 1} \tag{8a}$$

and in point 2

$$\Delta_2 = \frac{D}{2\,\Delta\, h} \,.\, (n_2 - 1)\, ln\frac{n_1 - 1}{n_2 - 1} \,. \tag{8b}$$

If we should, instead of the exponential dependence (5a) assume a similar dependence for instance

$$n - 1 = \frac{b}{a + h} \,, \tag{5b}$$

we should obtain the formula for calculating the refraction angles without the function of the natural logarithmus

$$\Delta_1 = \frac{D}{2\,\Delta\, h} \,.\, (n_1 - n_2)\frac{n_1 - 1}{n_2 - 1} \,, \tag{9a}$$

$$\Delta_2 = \frac{D}{2\,\Delta\, h} \,.\, (n_1 - n_2)\frac{n_2 - 1}{n_1 - 1} \,. \tag{9b}$$

Comparative calculation described in the next chapter proved that the formulae (8 a, b) and (9 a, b) yield in the field of the terrestrial refraction virtually the same results. The difference of the refraction angles $\Delta_1 - \Delta_2$ worked out from the equations (9 a, b) is slightly larger than the same difference of the refraction angles derived from the equations (8 a, b).

The values of the optical refractive index n in all equations (6 a,b), (8 a,b) or (9 a,b) we work out from the equation (2).

2.3 *Comparative calculations*

The newly worked out formulae (8 a, b) and (9 a, b) for the calculation of the refraction angles in the terrestrical refraction have been verified by the comparative calculation on larger sets

of measurements performed by foreign authors as well as on a specially selected set of measurements performed by the author of this paper. By comparative calculations were judged the mean values m pertaining to the difference of the refraction angles which had been measured as well as calculated. The results of the comparative calculations are listed in the tables 1. to 4. (The values of the various refraction angles measured and calculated at various times of the day are quoted in full detail in /3/ .)

In the tables 1, 2, 3 the calculations derived from Jordan-Eggert's formula and from the newly worked out formula (8 a, b) are compared. In column A are listed the mean values m_{J-E} of the differences of the refraction angles measured and calculated according to /1/. In column B then are listed similar values $m_{(8)}$ worked out by means of the formulae (8 a, b). In table 1 you can find the calculation applied for the set of measurements published by Bauernfeind /4/, in table 2 for the set of measurements published by Levallois-de Masson /5/ and finally in table 3 for the set of measurements performed by the author himself over a densely built up area /3/. The table 4 comprises a comparative calculation worked out from the formulae Levallois-de Masson /5/ (column A) and from the formulae (8 a, b) (column B). The calculation is being applied for the set of measurements published in /5/ during the period from 28th till 30th June 1950 and further similar values applied for measurements also in /5/ performed during the period from 20th till 27th June 1950 which were not worked out in the quoted publication.

Table 1

Line of sight	m''_{J-E}	$m''_{(8)}$	Distance	Diff. in level
Höhensteig — Irschenberg	12,1	11,0	17,238,46 m	269,63 m
Irschenberg — Höhensteig	9,3	8,8		
Höhensteig — Kampenwand	13,2	10,1	20,445,80 m	1,081,97 m
Kampenwand — Höhensteig	3,3	3,0		
Irschenberg — Kampenwand	11,6	6,7	34,038,22 m	812,34 m
Kampenwand — Irschenberg	6,6	5,7		

Table 2

Line of sight	m''_{J-E}	$m_{(8)}$	Distance	Diff. in level
Goult — Lubéron	20,3	15,8	19,065,4 m	865,57 m
Lubéron — Goult	26,1	25,0		
Goult — Oppède	12,4	10,2	8,138,3 m	454,84 m
Oppède — Goult	16,9	16,8		

Table 3

Line of sight	m''_{J-E}	$m_{(8)}$	Distance	Diff. in level
Strahov — Vidoule	5,2	3,9	3,047,56 m	39,845 m
Vidoule — Strahov	6,1	5,8		

Table 4

Line of sight	28th—30th June 1950		20th—27th June	
	$m''_{/5/}$ A	$m''_{(8)}$ B	$m''_{/5/}$ A	$m''_{(8)}$ B
Goult — Lubéron	7,5	19,5	28,0	20,0
Lubéron — Goult	15,4	24,0	41,3	21,0
Goult — Oppède	3,2	10,4	16,4	8,4
Oppède — Goult	16,6	17,2	30,8	20,4
Goult — Murs	5,0	21,8	17,9	16,5
Murs — Goult	51,2	64,4	49,8	44,0

An analysis of the results listed in the tables 1—4 proves that the newly worked out formula (8 a, b) furnishes as a whole better results than those derived from Jordan-Eggert's formula. In comparing it with the formula of Levallois-de Masson the formula (8 a, b) proved to be more suitable during the period from June 20th till June 27th 1950 when the temperature with regards to the

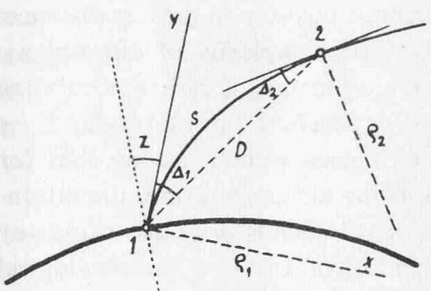

Fig. 1

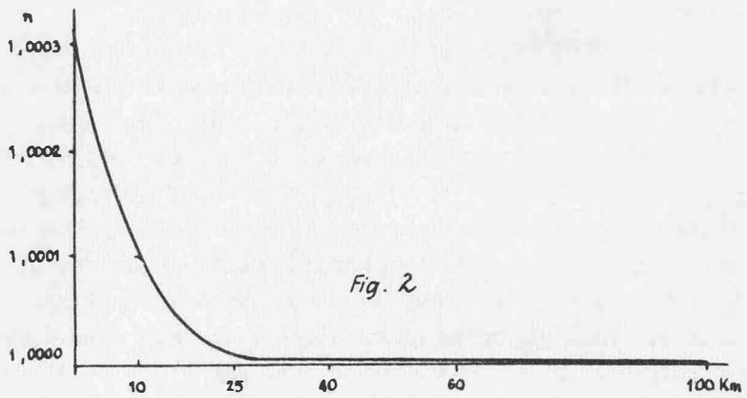

Fig. 2

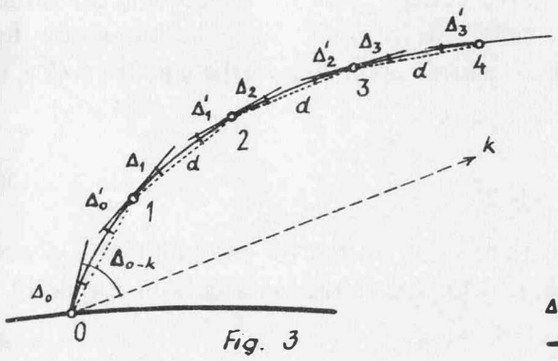

Fig. 3

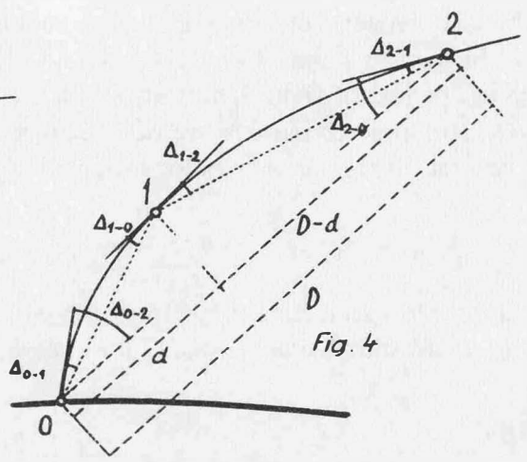

Fig. 4

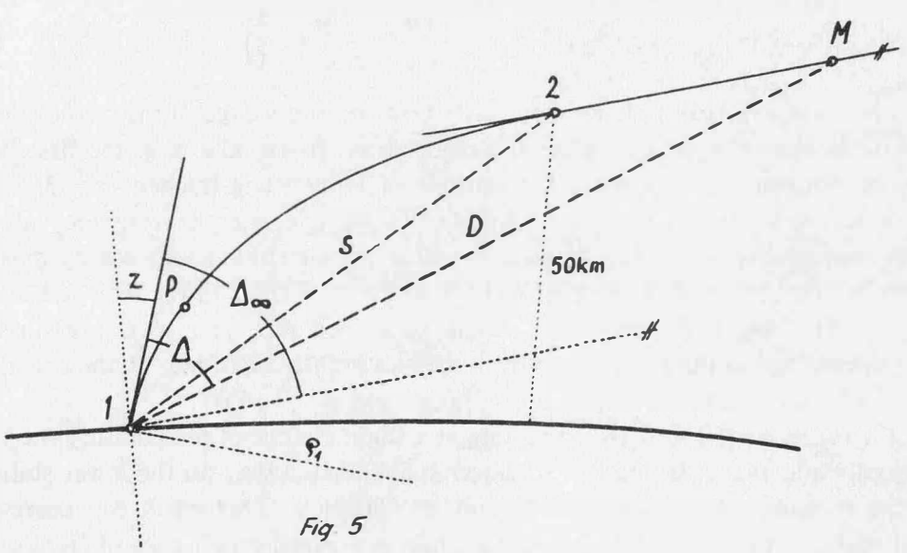

Fig. 5

data relating to wind strength in /5/ was by far more mixed than during the period from June 28th till June 30th 1950. In the latter time period from June 28th till 30th, 1950, when in the forenoon hours occured temperature inversions quite to midday Levallois-de Masson's formula is giving markedly better results.

It was not the aim of this comparison to bring about the preference of a certain formula over another since there may always occur a certain set of measurements in which the proved preference of certain formula is to be overshadowed by another formula. The main aim of the comparison performed was to prove that the formula (8 a, b) comprising the refractive index derived from the formulae recommended by the UGGI and IAG, is in the quoted sets of measurements in the entire range discernibly better matching the refractive properties of milieu, than the formula comprising the refractive coefficient determined according to Jordan-Eggert.

2.4 *Particular cases in calculating refraction angles*

The history of trying to express in a more accurate way the refractive effects shows that not even rather ingeniously compiled symplifying assumptions concerned with the atmospheric conditions or any suitably selected approximations of the refraction curve cannot possibly in greater distances or in greater differences in level of the line of sight fully satisfy the complexity of atmospheric influences of the milieu. Provided we make an effort in order to obtain the most accurate calculation of the refraction angles there seem to be all in all the best means for reaching this aim today if we gain meteorological values in several points of the line of sight. It goes without saying that for the calculation of the refraction angles the most significant value is the air temperature, the attainment of which by means thermistores in loose or fixed meteorological sounds does not cause any difficulties whatever. If we try to evaluate now, how this possibility of knowing meteorological values in several points of the line of sight, would manifest itself in the formulation of the formulae derived in the last chapter. Let's assume for the sake of simplicity that in addition to the meteorological values in the end points 1 and 2 we should also be familiar with the meteorological values in the centre of the line of sight S thus also with the refractive index n_S. Since we know now for the course $n = f(h)$ three conditions, we can analogically choose according to the equations (5 a, b) the dependence with three parameters for instance

$$n - 1 = \frac{1}{a\,h^2 + b\,h + c} \,. \tag{5c}$$

After eliminating the parameters a,b,c from the equations (5 c) written for the points $1,2,S$ and after inserting dn/dh into the equations (7 a,b), we obtain for the refraction angles in the point 1 the formula

$$\Delta_1 = \frac{D}{2\,\Delta\,h}(n_1 - 1)\left(4\,\frac{n_1 - 1}{n_s - 1} - \frac{n_1 - 1}{n_2 - 1} - 3\right) \tag{10a}$$

and in point 2

$$\Delta_2 = \frac{D}{2\,\Delta\,h}(n_2 - 1)\left(3 + \frac{n_2 - 1}{n_1 - 1} - 4\,\frac{n_2 - 1}{n_s - 1}\right) . \tag{10b}$$

By means of a simple numerical example we may verify how the knowledge of the meteorological values in the centre of the line of sight can affect the calculation. If we take e. g. the first line of sight from the series of measurements between the stations of Höhensteig-Irschenberg /3/ we are to obtain refraction angles worked out from the formula (8 a, b), i. e. merely from the values of the temperature in the end points $\Delta_H = 64{,}4''$ and $\Delta_I = 62{,}2''$. If we should find out by measurements the temperature in the centre of the line of sight S to be by $0{,}15^0 C$ lower than the average temperature determined from the end points and should take then the barometric pressure with the humidity into the calculation as the mean value from the end points, we obtain by the calculation from the formulae (10 a, b) the refraction angles $\Delta_H = 60{,}8''$ and $\Delta_I = 66{,}0''$.

We can see that the formulae (10 a, b) are correcting at a slight change of temperature the values of angles rather markedly and that it is possible to determine in such a way on the lower station H the lower value of the refraction angle than on the higher station I. This result can correspond with reality, since for instance on lower stations were actually measured on all lines of sight quoted in the sets of measurements in /4/ as well as in /5/ during the afternoon hours, values of refraction angles which were smaller than those on higher stations.

The increasing number of members in the equations (10 a,b) implies, that while calculating the refraction angles, providing we know the meteorological values in several points, the formula would become relatively complicated. For such cases a formula was worked out in /2/ expressing the resulting refraction angles as the function of the sum of various refraction angles calculated for the parts of the line of sight between the points in which the meteorological values had been known. If we know these values in the points $0,1,2,3,\ldots,k$, being in the same distance from each other, we can read off the resulting refraction angle according to /2/ from the relationship (see Fig. 3)

$$\Delta_{o-k} = \frac{k\,.\,\Delta_o + (k-1)\,\Delta_o' + (k-1)\,\Delta_1 + (k-2)\,\Delta_1' + \ldots + \Delta'_{k-2} + \Delta_{k-1}}{k} \tag{11}$$

We calculate the angles $\Delta_o, \Delta'_o, \Delta_1, \ldots, \Delta_{k-2}, \Delta_{k-1}$ for the different sections from the simple equations (8 a, b) and (9 a, b) respectively ,in which we determine again the values of the refractive index from the formula (2). (Note: the coefficients $k, k-1, k-2, \ldots$ are not inserted as the weights of the various angles, but are resulting from the simple calculation of the geometrical dependences between the various angles Δ_i. See /2/2/.) In case the distance of the points with the known meteorological values is not the same one, it is possible to calculate according to /2/ the refraction angles from the formula derived again from the geometrical dependence one trio of points

$$\Delta_{0-2} = \Delta_{0-1} + \left(1 - \frac{d}{D}\right)(\Delta_{1-0} + \Delta_{1-2}) \ , \tag{12a}$$

$$\Delta_{2-0} = \Delta_{2-1} + \frac{d}{D}(\Delta_{1-0} + \Delta_{1-2}). \tag{12b}$$

The values for the different symbols are being demonstrated in Fig. 4.
The angles $\Delta_{0-1}, \Delta_{1-0}, \Delta_{1-2}$ then we work out from the formulae (8 a, b) or (9 a, b). The calulation of the refraction angles from the formulae (11) or (12 a, b) is very recommendable for those cases in which the line of sight is based over a very unhomogeneous new wood terrain at a terrestrical refraction, or while calculating the satellite refraction when the object observed is at a height $H < 50$ km, i. e. in the region of the atmosphere where the greatest deviations from the standard course are to be expected.

3. *A note relating to the calculation of the satellite refraction*

Analogically as with calculating the satellite refraction, that term is holding top position which comprises the meteorological data gathered on the observation site. These data determine to the largest extent the values of the astronomical and to a considerable extent also those of the satellite refraction. It would be only correct, if in such cases these basic elements of calculation having in the hitherto quoted formulae very differing values, should be replaced by the refractive index derived from the formula recommended by the UGGI and IAG. Provided this formula comports most satisfactorily with the refractive effects of the atmosphere, it would first all conribute to the greater accuracy of the calculation and secondly enable a more correct comparison of the calculation attained under different theoretical assumptions regarding the form and changes of the refraction curve or providing other convergent series and the like.

The significance of the calculation of the satellite refraction is, due to the successful applicability of the optical observation of satellites, getting into the foreground of attention. It is obvious that the importance of the accuracy of the calculation of the satellite refraction is to increase simultaneously with the improvement of photo-registering devices and the like. In context with these increasing claims we have to pay due attention to calculating methods being partly of different character than those applied for the astronomical refraction in which only those meteorological elements prevailing at the observation site figure as the influence of the environment, whereas other factors perhaps even anomalous atmospheric conditions are without any influence on the calculation of astronomical refraction. It is essential to find out how such atmospheric anomalies affect the calculation of the satellite refraction when the object observed is in a finite distance from the observation site. The majority of formulae (Dufour, Baldini and others) anticipate between the observation site and the object observed a standard course in the atmosphere, or there is, in derivating formula a certain defined model of the atmosphere.

For this ascertainment a formula was derived in /6/ for the calculation of the satellite refraction coupled with such a condition that the meteorological elements were to be known even in any further arbitrary point of the line of sight (in addition to the observation site) enabling thus the correction of the calculation by these values, that is to say, not anticipating for instance, the standard state of the atmosphere. The formula for the calculation of the satellite refraction has been worked out in /6/ under the following anticipations:

1. The object of observation M is at the height $H > 50$ km (see Fig. 5).
2. The refraction curve is given by the equation

$$y = a x^4 + b x^3 + c x^2 + d x \ . \tag{13}$$

3. From the height of 50 km on can the refraction curve be replaced by the tangent (in Fig. 5 point 2).
4. We are familiar with the meteorological data in point 1 and even in point P, at the best in the lower layers of the atmosphere.

From these data we work out first the refractive index n_1 and n_P according to (2) and by means of the equation (4a) we determine then the radius of the curvature ρ_1. From the condition, that the curve (13) is passing through point 1 (0,0) through point 2 (S,0) and from the condition that the curvature is zero in point 2 and moreover from the known radius ρ_1 then the equation for the calculation of the satellite refraction was derived in the form of

$$\Delta = \Delta_\infty \left(1 - \frac{S}{2D}\right) + \frac{S^2}{12 D \rho_1} . \tag{14}$$

The values Δ, S, D are being demonstrated in Fig. 5. The angle Δ_∞ represents the angle of the astronomical refraction in point 1 under the zenith distance z. If we replace the real meteorological values in point P by the values of the standard atmosphere defined for instance in /7/, the formula (14) takes the form

$$\Delta = \Delta_\infty \left(1 - \frac{S}{2D}\right) + \frac{0{,}00801 \,.\, S^2 \,.\, \sin z}{D} (n_1 - 1) . \tag{15}$$

In order to find out how in the calculation of the satellite refraction the difference of the real and the standard atmosphere is to manifest itself, were selected lines of sight on objects under the zenith distances $30^0, 45^0, 60^0$ and 85^0 for targets being at a distance from the earth station from 300 km up to 10,000 km, i. e. for targets at the heights ranging from 200 up to 5,000 km. For comparing the absolute values of the calculated quantities the calculation of the satellite refraction according to Dufour's formula quoted in /8/ was added. The results of the calculation are listed in Table 5. In line A are listed the values derived from the equation (15), i. e. for the conditions prevailing in the standard atmosphere. In line B then, are the refraction angles of the atmosphere, in which the temperature at the height of 3 km was differing by -5^0C from the standard course, i. e. a calculation according to the formula (14). In line C there is a calculation according to Dufour's formula. Finally in the last line D is, for the varying zenith distances worked out the astronomical refraction, which is also applied for the calculations in the formulae (14) and (15). This astronomical refraction is calculated according to L. Oterma's formula /9/, in which the basic value $(n - 1)$ is determined from formula (2).

Note: The calculation of the refraction angles providing a temperature difference of $-5^0 C$ was regarded as a really measured case quoted in /7/.

Table 5

Zenith distance	30^0		45^0		60^0			85^0	
D_{km}	300	1,000	300	1,000	300	1,000	10,000	1,000	10,000
A	32,41	32,76	55,78	56,67	95,52	97,79	98,50	583,46	597,24
B	32,23	32,70	55,40	56,56	94,61	97,50	98,47	572,61	596,15
C	31,88	32,63	54,76	56,33	92,98	96,84	98,34	553,81	592,82
D	32,93		57,04		98,58			598,77	

On the ground of these calculation can be drawn the following partial conclusions:

1. If we want to reckon the refraction angles with accuracy of $\pm$ 1″ (0,1″), it is necessary to take into account for the calculation the real atmospheric conditions approximately from the zenith distance $z > 50^0$ ($z > 30^0$).
2. If we want to reckon out the refraction angles with an accuracy of less than $\pm$ 0,5″, it is not necessary for the zenith distance $z > 80^0$ to take into account the real atmospheric conditions provided the object observed at the height $h < 1{,}000$ km.
3. By comparing the astronomical and satellite refraction it becomes evident, that by the lines of sight of objects being at greater heights than $h = 5{,}000$ km it is possible to replace the calculation

of the satellite refraction by that of the astronomical refraction, provided it is $z < 85^0$ and if it is sufficient to work out the refraction angle with an accuracy of $\pm 1''$.

It is needless to elaborate the analysis of the results in the table any further since the accuracy of the photoregistrated position of the satellites is, for the time being, lower than the accuracy enabled by the calculation according to formula (14). The technical character of the photoregistration of the position implies, however, that it will be already possible within a short time to make some practical use of the accuracy resulting from formula (14).

References

/1/: *Jordan W.-Eggert O.:* Handbuch der Vermessungskunde II/2, Stuttgart, 1943.
/2/: *Pelikán, M.:* Ein Beitrag zur Bestimmung der Satelliten- und astronomischen Refraktion, Studia geophysica et geodaetica, 1967, 11, Praha.
/3/: *Pelikán, M.:* Berechnung des Brechungswinkels mittels des Brechungsindexes, Studia geophysica et geodaetica, 1964, 8, Praha.
/4/: *Bauernfeind, C. M.:* Beobachtung der terrestrischen Refraktion, München.
/5/: *Levallois J. J. -de Masson G.:* Étude sur la réfraction géodésique, Paris, 1953.
/6/: *Pelikan, M.:* Problémy vertikální refrakce, (Habilitation), Praha 1966.
/7/: *CIRA* — Committee on space research, Amsterdam, 1961.
/8/: *Dufour, H. M.:* Choix de formule de la réfraction... Bull. géod. 73, 1964.
/9/: *Oterma, L.:* Computing of the refraction... Turku, 1960.

A Mathematical Model for Temperatures in the Lower Atmosphere, and its Application in Refraction Calculations

by *P. V. Angus-Leppan*, Kensington

Abstract

By making use of long-term observations of temperature at various heights in the lowest 100 m of the atmosphere, a mathematical model can be derived for the temperature gradient as a function of height and time of day:

$$G(z, t) = g_o + c_1 e^{-c_2 z} + c_3 e^{-c_4 z} \sin(t + c_5 + c_6 z) + c_7 \sin(2t + c_8)$$

This represents the observations, with a standard deviation between model and observations amounting to less than 4% of the total variation in G. Different values of the ten parameters g_o, the $c's$ are obtained for each month, for each station, but the seasonal variation is fairly regular, and corresponding parameters are of similar magnitudes for all stations except one where the circumstances of observation are exceptional.

The coefficient of refraction calculated from this formula, using the appropriate parameters, shows how large the expected refraction is under field conditions, and the large diurnal variation. As an example, in South East England, in April, on a 20,000 foot line 25 feet above the surface, refraction varies from −1.55 (early afternoon) to 7.33 feet (after midnight). Desert conditions give refraction corrections which are not as different as expected.

Temperature differences also cause considerable errors on lines where the distance is measured electronically.

Introduction

For visible wavelengths of the spectrum, temperature is the chief cause of variations in refractive index, which in turn cause variations in the velocity and direction of light waves passing through the atmosphere. A first approach in dealing with this problem is to assume that the refractive index is constant in the horizontal direction and that there is a constant rate of change in the vertical direction. The assumption of constant gradient of temperature (or refractive index) is implied when in trigonometric levelling we adopt a coefficient of refraction, or in electronic distance measurements we take the mean of temperatures at the ends of a line to represent the average over its length.

Greater precision can be sought by measuring the temperature gradient directly, but this is an observation requiring high precision and it is difficult to obtain sufficiently representative values. Or the refraction effect can be deduced by making the measurement with two different wavelengths. Again this is an operation requiring very sophisticated apparatus.

Between the very simple model of constant gradient of temperature, and the more elaborate measurement of the actual conditions, there is another approach possible, namely to refine the model so that it approximates more closely to the actual conditions. The present paper is the result of an investigation which followed this approach.

Such a model can take into account the major causes of variation in the temperature gradient, giving the average values for the conditions of observation. The gradient is a complex phenomenon affected by a large number of factors working directly, indirectly and in cross-combinations. Height above ground, time of day, season, the various factors of climate and weather, vegetation cover and the surface material, colour and texture all affect the gradient. However by sorting out the most significant causes of variation it is possible to devise a comparatively simple model representing average conditions. In the present instance the temperature gradient is determined as a function of time of day and height above surface. A separate set of constants is calculated to fit the observations at the station for each month of the year, thus taking into account the season. Comparison of results at different stations illustrates the effects of climate, and some generalisation is possible. The limited observations available for clear and overcast days in summer and winter months are analysed to indicate in a gross manner, the effects of weather. Even though the model can reflect only major factors, and not the vagaries of the weather, the particular site and the time of observation, it is worth having such a model even if it is only used as a standard against which to measure the peculiarities. If it is in error there is always a possibility of refining and improving the model, and it may even be found that a simple measurement will give an indication of the divergence between the standard and the actual conditions, thus enabling corrections to be calculated at different points in the model. The detailed analysis and the expression in mathematical terms of the variation of temperature gradient, give a clearer understanding of this phenomenon.

Analysis: Form of Function

Basic data are from those meteorological stations where continuous temperature observations have been made over a period of at least one year at various heights above the surface (generally on towers). Eight such stations are listed in "The Climate near the Ground" (1) and the results from five are suitable for analysis. The geographical distribution is limited, most stations being in England or Germany, but there is one in the desert at Ismailīā, Egypt. Further details are given in Table II. The analysis is restricted to the lowest 100 metres of the atmosphere, and it is in this layer that the largest fluctuations and most rapid changes occur. To minimise the random day to day variations, mean values for one month, taken at each height and each hour of the day, were used in the analysis.

It has previously been shown that the diurnal temperature variation at a particular level is well represented by the first two terms of a Fourier series. (2, 3). This time variation is designated $f(t)$. The amplitude of the daily variation is largest at the ground and decreases to a small amount at high altitudes. This variation with heights is $B(z)$. The average temperature at any height, about which the daily fluctuations occur, is also variable with height and is given by the function $A(z)$. We have then that the temperature T is given in the form

$$T = A(z) + B(z)f(t) \tag{1}$$

In trigonometric levelling it is the temperature gradient, not the temperature, which is required. Similarly in electronic distance measurement a method of interpolating temperatures is necessary, so that the gradient is of more use. The gradient appears to be a better behaved quantity, and it is slightly simpler to determine. Thus the analysis deals with temperature gradients. Curves for these show characteristics almost identical to those of temperature. This suggests immediately an exponential form for $A(z)$ and $B(z)$. However a number of different functions were tried. All except two, the exponential and a form containing a fractional power of the height, were rejected as unsuitable after testing. The remaining forms were fully tested:

$$A(z) = g_o + c_1 z^{-c_2} \tag{2}$$

$$A(z) = g_o + c_1 e^{-c_2 z} \tag{3}$$

$$B(z) = c_3 z^{-c_4} \tag{4}$$

$$B(z) = c_{10} + c_3 z^{-c_4} \tag{5}$$

$$B(z) = c_3 e^{-c_4 z} \tag{6}$$

$$B(z) = c_{10} + c_3 z^{-c_4} \tag{7}$$

The basic form of the temperature gradient function is, as for temperature:

$$\frac{dT}{dz} = G(z, t) = A(z) + B(z) f(t)$$

$$= A(z) + B(z) \quad \sin(t + c_5 + c_6 z) + c_7 \sin(2t + c_8)$$

where T represents the temperature, t the time of day (1 hour = 15°) and z the height above the surface.

Analysis: Least Square Calculations

A set of nine or ten constants was determined for each station by least squares, for each month of the year and for the different functional forms $A(z)$ and $B(z)$. Since there are observations for each hour of the day at each of three or four heights, there are either 72 or 96 observations to determine the unknowns. The results show that the addition of the constant c_{10} does not improve the accuracy. It is not clear whether the exponential or the power form is the most suitable and further investigations, covering a greater height range, will be necessary to give a conclusive answer. However the exponential form provides slightly more favourable results for $A(z)$ (Equation 3) and markedly more favourable results for $B(z)$ (Equation 6). For large z $G(z, t)$ tends to a constant value g_o. In nature the gradient settles to a constant which is not subject to marked daily, annual or irregular changes, and which is known. The analysis showed that this known value of g_o could be inserted as a fixed quantity in the solution, with no loss of accuracy.

Results: Some Examples

It is significant that the same functional form has been successful in all cases, covering the full cycle of seasons, and climates ranging from moist temperate to desert. The fit is imperfect, some of the differences between model and observations being systematic, though a proportion are due to irregularities in the observations which appear to be due to particular idiosyncrasies of weather and site. In some respects the model may be the better representative of the climate, because it smooths out these irregularities.

Differences between the model and the observations, expressed as a standard deviation, average 0.7° C/100 m for all months, for four of the five stations. (All gradients are expressed in degrees Centigrade per 100 metres.) The fifth station, Porton, is exceptional, the lowest measurements being made only 2.5 cms. above the surface. As a result the range of gradients is exceptionally large, from $-100°C$/100 m to $+330°C$/100 m. Under these conditions the irregularities are also large. In addition the analysis at Porton married observations for a higher and lower height range, taken in different years. Expressed as a percentage of the average range of the gradients for all months, the standard deviations are always less than 6% and in the case of Porton only 2.5%, and as a percentage of the highest monthly range always less than 4% and only 1.6% for Porton.

Figures 1 and 2 illustrate the variation of the gradient in the lowest 80 metres for the station Rye, Sussex, England, for the month of April (4). The diurnal variation at the three heights is shown in Figure 1. Here the curves represent the model and the observations are shown by point symbols. Although the characteristics of such observed gradients have been discussed frequently, (5) and formulae fitted to particular characteristics it is believed that this is the first attempt at a comprehensive mathematical model.

There is a wide range of values, from -6 to $+9°C$/100 m, but the range is rapidly damped with increasing height. The curves closely resemble sine waves, though in winter months the amplitude decreases and the second harmonic becomes proportionately larger.

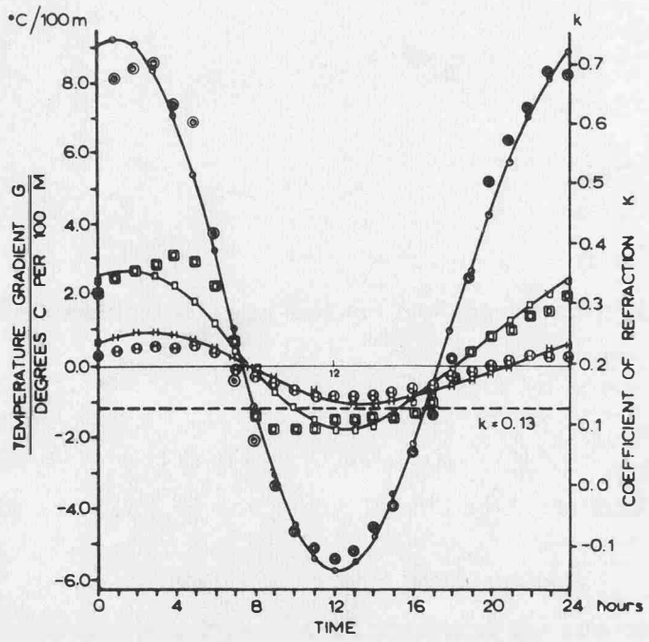

FIGURE 1. DIURNAL VARIATION IN TEMPERATURE GRADIENT AND REFRACTION COEFFICIENT.

STATION: RYE MONTH: APRIL

GRADIENTS OBSERVED

HT.

77 m — ×

31 m — □

8.1 m — ○

GRADIENTS CALCULATED

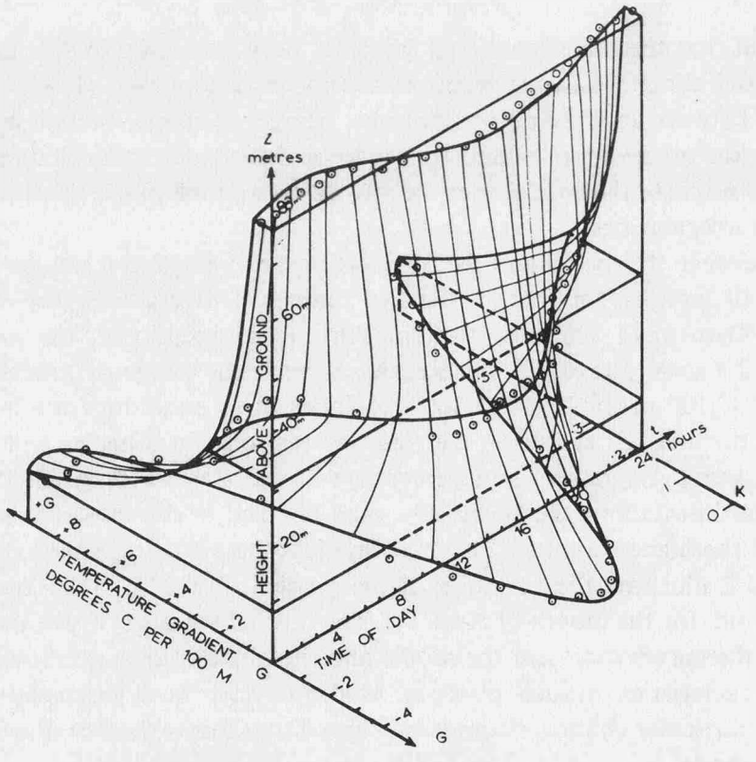

FIG. 2. ISOMETRIC REPRESENTATION OF TEMPERATURE GRADIENT AS A FUNCTION OF HEIGHT AND TIME — OBSERVED AND CALCULATED.

Figure 2 is an isometric projection of the gradient as a function of height and time of day. It shows that the gradient close to the surface is always numerically highest, and decreases with height. There is a maximum positive gradient shortly after midnight. As the sun begins to warm the ground the gradient becomes constant (vertical graph) and soon the negative gradient indicates that the lowest layers are warmest. The negative gradient becomes more marked with time, reaching a minimum soon after noon. With afternoon cooling the gradient returns to zero and at nightfall begins to take up positive values again. The cycle is completed with the maximum gradient occuring after midnight.

Generally the fit between observed and calculated values is close, though errors, both random and systematic, can be distinguished. The standard deviation is $\pm\ 0.6^0 C/100$ m and the errors are small in relation to the variations.

As a further example the model for the gradient at Quickborn, Holstein, W. Germany is, for the month of February:

$$G(z, t) = -0.2 + 1.7e^{-0.067z} + (1.2 + 14.2e^{-0.18z})$$

$$[\sin(t + 5.3 - .060\ z) + 0.52 \sin(2t - 8.4)]$$

with standard deviation $\pm$ 0.6.

For August it is:

$$G(z, t) = 12.3\ e^{-0.19z} + (2.5 + 24.6\ e^{-0.14z})$$

$$[\sin(t + 6.0 - .042\ z) + 0.06 \sin(2t + 6.8)]$$

Standard deviation $\pm$ 1.0

Annual Variation

When the results for all months at a station are compared there are some constants which show a fairly smooth and regular variation from month to month, but others are somewhat irregular. This is partly because of true irregularities, but partly because many of the constants determined are unstable — a considerable change can be made in c_1 and c_2 for example and the accuracy will not be perceptibly changed. This flexibility can be used in constructing the generalised "Year Model" and investigations are now in progress. This model will contain approximately 20 constants and for its station will represent the gradient as a function $G(z, t, y)$ of height, time of day and time of year. There will be some loss of accuracy but it is unlikely to be great.

Comparing values for all months shows some significant characteristics. The constant g_o is small and variations in c_1 and c_2 can compensate for changes imposed on g_o. The quantity c_1 determining the starting point of $A(z)$ is large in winter, diminishing in summer and sometimes, as for Ismailia, dropping to negative values, while its damping coefficient is always close to 0.1. Like g_o the quantity c_{10} does not add any accuracy to the solution. Diurnal range constant c_3 is maximum in spring and minimum in autumn. Its damping constant c_4 has a similar variation. Phase angle c_6 does not vary greatly above and below 6 hours, being larger in winter. The phase change factor c_6 is somewhat irregular. The phase change with height is only linear over a restricted height range. The amplitude of the second harmonic, as a proportion of the first is given by c_7. This is a maximum of approximately 0.5 in winter, decreasing to 0.1 in summer. Finally the phase constant c_8 is approximately eight hours in winter, decreasing in summer and becoming somewhat indeterminate due to the small amplitude c_7.

Clear and Overcast Days

The same functional form was used in the analysis of clear and overcast days. Results for Rye are given in Table I (next page).

In interpreting the results it should be borne in mind that the number of clear or overcast days is very limited thus causing inconsistencies in the results, and that the clear and overcast days are included in the middle values for "all days". The most significant changes illustrated are in the $A(z)$ and $B(z)$ sections. Increasing cloudiness causes c_1 to decrease, with a tendency for the damping coefficient c_2 to decrease too. A more marked change is the decrease in diurnal amplitude c_3 with increasing cloudiness and a smaller decrease in c_4. Quantities c_5 to c_8 vary irregularly, indicating a distortion of the shape and phases of the diurnal curves.

Table I

Effect of cloud cover — Clear and Overcast days

Station	Month	Weather	g_o	c_1	c_2	c_{10}	c_3	No. of days
Rye	June	Clear days	0.4	6.3	0.060	2.1	29.3	19
		All days	−0.6	1.3	0.022	1.4	17.1	74
		Overcast days	−0.2	−3.7	0.032	0.0	7.5	4
Rye	Dec.	Clear days	0	28.0	0.110	1.3	13.5	3
		All days	0.2	7.4	0.057	0.1	5.5	67
		Overcast days	−2.0	6.3	0.050	0.0	1.4	21

Station	Month	Weather	c_4	c_5	c_6	c_7	c_8	No. of day
Rye	June	Clear days	0.059	5.9	−0.026	0.05	−1.1	19
		All days	0.060	4.9	0.011	0.023	3.2	74
		Overcast days	0.041	7.0	−0.042	0.22	−5.4	4
Rye	Dec.	Clear days	0.115	5.2	0.0	0.72	−6.8	3
		All days	0.045	7.5	−0.079	0.49	−8.4	67
		Overcast days	0.038	5.2	−0.032	0.79	−6.7	21

Climate

Some indication of differences of climate and other circumstances such as surface material and vegetation can be gained from a comparison over the limited range of observations available.

Comparing along the lines, the most interesting feature is probably the similarity of the ranges for all cases except Porton. The unusual circumstances at this station have already been mentioned. However, the model should be able to cover a wide range of heights and this is one reason why the power form of $A(z)$ and $B(z)$ cannot be discarded yet, as they fit Porton with less radical changes in parameters. The similarity of parameters is most marked in c_1, c_2, c_3 and c_4 though climate causes differences for Ismailia in c_1 and c_3. A difference between Rye and Leafield shows up in c_1 and c_3. This is attributable to differences in subsoil, moisture content and vegetation.

Coefficient of Refraction

The coefficient of refraction K is related to the temperature gradient G by

$$K = \frac{258\, R\, P\,(.\,010 + G)}{(273 + T)^2}$$

Table II

Values of parameters for different stations — Range over the months of the year

$$A(z) = g_o + c_1 e^{-c_2 z}$$

$$B(z) = c_{10} + c_3 e^{-c_4 z}$$

Station	Rye	Leafield	Quickborn	Ismailia	Porton
Country	England	England	W. Germany	Egypt	England
Latitude N	51°	52°	59°	30½°	51°
Biblio. Ref.	(4)	(6)	(7)	(3)	(2), (8)
Height Range in metres.	8.2—77	6.8—72	7.5—49	8.6—54	0.16—12.1
Range of g_o	—1.4 to 3.0	—3.8 to 0.0	—0.9 to 1.1	—0.9 to 1.8	—2.7 to 5.2
Range of c_1	1.2 to 26.3	—0.1 to 9.2	1.7 to 28.2	—14.8 to 29.0	—740 to 250
Range of c_2	0.02 to 0.10	0.00 to 0.20	0.07 to 0.24	0.00 to 0.2	0.6 to 6.1
Range of c_{10}	—0.1 to 1.5	—1.5 to 1.6	0.5 to 3.6	1.3 to 5.0	4.6 to 15.2
Range of c_3	5.5 to 20.0	4.8 to 32	7.0 to 65.0	27.0 to 40.0	200 to 1360
Range of c_4	0.03 to 0.08	0.10 to 0.15	0.13 to 0.27	0.07 to 0.13	2.9 to 3.9

where G is in ^0C/metre

R is the radius of the earth in millions of metres.

P is the air pressure in millibars.

T is the temperature in ^0C.

If average values are assumed for R, P and T, the relationship between K and G is linear, and the plotted curves of Figures 1 and 2 can be used to indicate variation in K. Graphs of Figure 1, read against the right-hand scale, show the diurnal variation in K, while the vertical variation of K is seen from Figure 2, reading against the lower right-hand scale. Though these graphs only indicate variation for one month of the year, at a single station, they show clearly that the coefficient of refraction is not constant at 0.13, which value is indicated by a plane, dotted, in Figure 2.

In order to assess these effects on trigonometric levelling, Table III below shows the magnitude of the refraction correction based on the temperature model for Rye, in England's moist temperate climate and, as a contrast, at Ismailia, in the harsh desert climate of Egypt. The corrections are quoted for three different months of the year, for lines of three different lengths, 4000, 20,000 and 100,000 feet (. 75, 3.8 and 19 miles) and at heights 5, 25 and 250 feet above the ground. Finally, the daily minimum, which occurs at about noon, and the daily maximum, shortly before dawn, are quoted. A positive entry in the table indicates that refraction lifts the apparent line of sight upwards, and vice versa. Refraction is proportional to the square of the distance.

The first half of the table refers to refraction calculated from temperature gradients at Rye. The most notable feature is again the wide variation particularly at the lowest level, and the large magnitude of the refraction effect. Even for a 4000 foot line, it reaches nearly one foot (April minimum, height 5 ft). At higher levels the magnitude decreases, but at 25 feet above the surface it reaches over seven feet on a line 20,000 feet long. Even at 250 feet above the surface, the effect is over 60 feet on a 100,000 foot line.

The diurnal variation will follow a course similar to gradient in Figure 1. The table gives minimum and maximum values and again these show remarkably large variations. For the lower levels the minimum becomes negative, indicating a line of sight curved convex downwards. It is only at the highest level that values begin to resemble those calculated using a standard value for the coefficient of refraction $K = 0.13$ (right hand column). Even here the daily variation is of the same order of size as the correction using $K = .13$.

It is interesting to note the close similarity between April and August. In December all values are very much reduced, diurnal variation is far smaller, and the standard K values are no longer appropriate at high levels. The coefficient K would have to increase to 0.19 for these conditions.

Although some lines in the table would hardly occur in practice, 100,000 foot line constantly at 5 feet above the surface, for example, the results are nevertheless of pratical interest. Nearly all lines pass close to the ground for a short distance at least. It should be borne in mind that the effect of a particular gradient is of greater importance if it occurs close to the observer's end. To take a simple example: If a certain curvature F were present for the whole length of a line AB, refraction would be R''. If however there were no bending for nine-tenths of the distance, and the curvature F for the remaining one-tenth, adjacent to A, then refraction measured from A would be 20% of R'' whereas from B it would be 1% of R''.

The refraction at Ismailia, a far more harsh climate, is surprisingly similar to that at Rey. In April refraction produces a greater variation at 5 and 25 feet, but at 250 feet it has steadied down to similar values. However August at Ismailia produces far more extreme values. Note the values of over 2000 feet. Even the maximum values, at night, are negative, so that the bending is constantly downwards. Mirages could be expected under these conditions. However the effects dampen quickly with height and at 250 feet the day values are lower than in April. Night values (maxima) are considerably higher than at other seasons. December still shows extremes, and whereas at Rye the level for which the '$K = 0.13$' values are appropriate is below 25 feet, for Ismailia it is above 250 feet.

Generally our coefficient of refraction method is applicable for a line that is the same distance above the surface, over similar surface conditions, for its whole length. The value of 0.13 is suitable for heights of about 250 feet above the surface. Practically all lines are for a short section at least within five feet of the surface. The table shows what extreme conditions are experienced in this layer.

Electronic Distance Measurement

The effect of temperature on electronic distance measurements is approximately 1 part per million for each 1°F.*) In the case of a line extending between two hills on a plain, or across a flat valley, the temperature will be measured close to the surface but the line will be well above the surface of the valley or plain for nearly all of its length. Very close to the ground, the strata of air between isotherms are parallel to the surface, but higher up, the undulations of the topography are followed in a smoothed fashion, until at a considerable altitude they become smooth and horizontal. This means that above a hill the intervals between isotherms will be smaller while over the valley they will tend to be extended. In terms of isotherms the elevation difference between high and low points is decreased. If this effect is taken into account then the diminished depth of the valley can be referred to as the 'equivalent depth'.

Table IV sets out the errors due to the difference between observed temperature (hilltop) and the actual temperature of the line (over the plain or valley) according to the temperature models for Rye and Ismailia. These are given for an equivalent depth of 150 feet. The values quoted are part per 100,000, since the effect is proportional to distance. Alternatively they can be considered as errors, in feet, on a line of 100,000 feet.

Table IV

Temperature Effect on Geodimeter and Tellurometer Lengths in Parts per 100,000

Rye

Height. feet	APRIL		AUGUST		DECEMBER	
	DAY	NIGHT	DAY	NIGHT	DAY	NIGHT
Parts per 100,000 — *or error in feet on line* 100,000 *feet long*						
150	−0.30	+0.46	−0.31	+0.37	−0.03	+0.21
			Ismailia			
150	−0.64	+0.60	−0.79	+0.20	−0.30	+1.12

The table shows that, even for the modest depth of 150 feet, errors of nearly one-half foot can be expected at Rye and over one foot at Ismailia. The greatest errors are experienced during

*) The exact figure varies, depending on whether, as temperature is varied, the relative humidity, the vapour pressure, or the depression of the wet bulb is kept constant.

Table III

Effect of Refraction in Trigonometric Levelling

1. *Station: Rye, Sussex, England*

Month	APRIL		AUGUST		DECEMBER		K = 13
Max. or min. Refraction	Minimum (noon)	Maximum (before dawn)	Minimum	Maximum	Minimum	Maximum	
Length feet	REFRACTION EFFECT IN FEET						
Height above ground: 5 feet							
4,000	− .59	.96	− .48	.77	.01	.42	+ .05
20,000	− 14.8	24.0	− 12.1	19.3	.45	10.6	+ 1.25
100,000	−371.	601.	− 304.	484.	11.	264.	+31.0
Height above ground: 25 feet							
4,000	− .06	.29	− .06	.24	.07	.18	+ .05
20,000	− 1.55	7.33	− 1.72	6.20	1.78	4.63	+ 1.25
100,000	− 39.	183.	− 43.	155.	45.	116.	+31.0
Height above ground: 250 feet							
4,000	.05	.09	.05	.09	.07	.09	+ .05
20,000	1.31	2.39	1.31	2.42	1.76	2.25	+ 1.25
100,000	32.9	60.0	32.8	60.7	44.1	56.4	+31.0

2. *Station: Ismailia, Egypt*

Height above ground: 5 feet							
4,000	1.40	1.16	− 3.44	− .14	.75	3.37	.05
20,000	− 35.1	29.2	− 86.1	− 3.7	18.9	84.3	1.25
100,000	−877.	730.	−2120.	−93.	473.	2110.	31.0
Height above ground: 25 feet							
4,000	− .25	.32	− .26	.19	− .09	.54	.05
20,000	− 6.39	8.11	− 6.67	4.94	− 2.4	13.6	1.25
100,000	−160.	203.	− 167.	124.	−61.	341.	31.0
Height above ground: 250 feet							
4,000	.06	.13	.05	.07	.05	.15	.05
20,000	1.67	3.35	1.25	1.97	1.49	3.77	1.25
100,000	41.9	84.0	31.5	49.5	37.5	94.3	31.0

Supplement to paper of Prof. Angus-Leppan

the day in the summer, and during the night in the colder months. Observing during both day and night will usually improve the results as errors tend to have similar magnitude with opposite sign, but this is by no means certain; note for example the values in December.

These figures are based on a temperature measured at five feet above ground level. If it were measured at two and one-half feet, the effect would generally be to increase the error, by amounts which vary for different times, but which average 0.05 feet for Rye and 0.2 feet for Ismailia. Observing temperature at about ten feet should, in these circumstances, decrease the error by a similar amount.

Further Investigations

Sufficient has been shown of the Lower Atmosphere Temperature Model to indicate that it has applications but that they are at present limited by lack of generality. Investigations will continue in the development of a satisfactory generalised form for the whole year at one station and, as far as possible with the limited geographical spread, a generalisation for climate. Any new data which become available will be incorporated. By studying the errors of the present form it is hoped to improve the accuracy. A detailed statitical study is being made by C. McGilchrist of the individual daily observations and their sequential correlations.

It is also proposed to extend the model upwards and to attempt a similar model for humidity. It should then be possible to apply the results in tellurometer measurements, in photogrammetry and in aerodist measurements.

Acknowledgements

Most of the work described was undertaken during 1966 while the author held a Canadian Commonwealth Research Fellowship at the University of New Brunswick. Grateful acknowledgement is made for the Fellowship and the opportunity which it provided. The author wishes to thank those at the University of New Brunswick, particularly in the Computing Centre, who assisted, and Dr. C. McGilchrist of the Department of Statistics, University of New South Wales.

Bibliography

MOGM – Meteorological Office Geophysical Memoir

1. *Geiger, Rudolf.:* The Climate near the Ground. (tr.from 1961 edition of *Das Klima der bodennahen Luftschicht*). Harvard University Press, 1965. Pages 70, 71.
2. *Best, A. C.:* Transfer of heat and momentum in the lowest layers of the atmosphere. *MOGM* No. 65. HMSO 1935.
3. *Flower. W. D.:* An investigation into the variation of the lapse rate of temperature in the atmosphere near the ground at Ismailia, Egypt. *MOGM* No. 71, HMSO 1937.
4. *Best, A. C. et al.:* Temperature and humidity gradients in the first 100 m over South-East England. *MOGM* No. 89. HMSO 1952, (reprinted 1962).
5. *MOGM* No. 46, 1929; No. 71, 1937; No. 77, 1938. HMSO; also Geiger. op. cit. pages 68–102.
6. *Johnson, N. K. and Heywood, G. S. P.:* An investigation of the lapse rate of temperature in the lowest 100 m of the atmosphere. *MOGM* No. 77. HMSO, 1938.
7. *Frankenberger, E.:* Über vertikale Temperatur-, Feuchte- und Windgradienten in den untersten 7 Dekametern der Atmosphere... bei Quickborn/Holstein. *Berichte des Deutschen Wetterdienstes.* 3, Nr. 20. 1955.
8. *Johnson, N. K.:* A study of the vertical gradient of temperature in the atmosphere near the ground. *MOGM* No. 46. HMSO 1929.
9. *Angus-Leppan, P. V. Surveyor vs. Refraction:* The effects of the atmosphere on surveying observations. *The Australian Surveyor*, vol. 20, No. 3. September 1964.
10. *Angus-Leppan, P. V.:* Diurnal and seasonal variations in the coefficient of refraction. Paper read at *Third S. A. Conference of Surveyors*, Johannesburg, 1967.

Note: Table III erroneously is missing in the author's manuscript, but will be submitted later.

Electrical Measurement of the Temperature Gradient at Astronomical Stations

by *O. Hirsch*, Berlin

Summary:

The problems of considering the effect of refraction on astronomical measurements are pointed out; the influence of errors in the meteorological data is discussed, and the effect of the gradient of the index of refraction on the curvature of the light path is considered.

A review of the methods of measurement of temperature by electrical instruments follows, special attention being given to resistance thermometers using semiconductor sensors. Applications of these techniques are mentioned.

Zusammenfassung:

In einem Überblick wird auf die Problematik der Berücksichtigung des Refraktionseinflusses bei astronomisch-geodätischen Beobachtungen hingewiesen, die Auswirkungen in der Unsicherheit der Erfassung der meteorologischen Daten auf den Brechungsindex aufgezeigt und schließlich der Einfluß von Änderungen des Brechungsindex auf die Lichtstrahlkrümmung angegeben.

Es folgt eine kurze Übersicht über die verschiedenen Möglichkeiten der Temperaturmessung mit elektrischen Thermometern, um anschließend auf die Vorteile der Widerstandsthermometer mit Halbleitermeßfühlern ausführlicher einzugehen. Die Anforderungen, die an das Temperaturmeßgerät zu stellen sind, werden an Hand eines speziellen Gerätes erläutert, abschließend werden einige Anwendungsmöglichkeiten genannt.

The Consideration of the Effect of Refraction

As is well known, a simplified theory of the astronomical refraction is used for evaluation of astronomical measurements. — The earth is considered a globe and spherical stratification of the air is assumed.

Usually, in particular for zenith distances $< 60^0$ as occur in astronomical observations, the effect of refraction is represented (after repeated application of *Snellius'* law of refraction) by the statement

$$\text{refr.} = (n - 1) \,.\, \tan \zeta \tag{1}$$

Here n denotes the refractive index in the immediate vicinity of the observation instrument. In general the refractive index is defined by

$$n = 1 + \frac{n_{gr} - 1}{1 + \alpha \,.\, t} \,.\, \frac{p}{760} - \frac{5{,}5 \,.\, 10^{-8}}{1 + \alpha} \,.\, e \tag{2}$$

with

n_{gr} ... group refractive index (at standard atmospheric conditions),
t ... air temperature in ^0C,
p ... atmospheric pressure in terms of mm of mercury,
α ... gas expansion coefficient $1 : 273 \,.\, 15 = 0{,}003661$
e ... partial pressure of atmospheric water vapor in terms of millimeters of mercury

Among other hypotheses concerning the structure of the atmosphere, several assumptions for the computation of the formulas mentioned have to be set up. Hence it happens that the correction factors so obtained differ slightly, too. If we take the Berliner Astronomisches Jahrbuch for instance, the tables are based on numerical data given by *Bauschinger*; for instance, n_{gr} (formerly μ_o) $= 291{,}6 \,.\, 10^{-6}$ and $e = 6$ mm Hg giving $R'' = (n - 1)/\sin 1'' = 60''.154$ at $0^0\,C$ and 760 mm Hg.

This standard index of refraction is denoted by R_o. In conclusion we have the resultant final formula, after inserting the factors A and B for consideration of deviation of temperature and pressure from standard atmospheric conditions:

$$R = R_o\,(1 + A + B) \tag{3}$$

Other tabular compilations are of the same general type. They always give as a first result a mean (standard) refractive index with the observed (apparent) zenith distance ζ as argument. It has then to be corrected because of the actual meteorological conditions during observation [6], [13].

The uncertainties in considering the influence of meteorological facts upon the index of refraction (2) have been investigated in detail recently, especially with respect to electronically measured distances, i. a., [9, p. 232]. These uncertainties cause the following errors

$$\begin{aligned} \Delta t &= \pm 1^0\,C \quad \rightarrow \Delta n(t) \simeq \pm 1{,}0 \,.\, 10^{-6} \\ \Delta p &= \pm 1\ \text{Torr} \rightarrow \Delta n(p) \simeq \pm 0{,}4 \,.\, 10^{-6} \\ \Delta e &= \pm 1\ \text{Torr} \rightarrow \Delta n(e) \simeq \pm 5{,}3 \,.\, 10^{-8} \end{aligned} \tag{4}$$

Usually, the air temperature at astronomical-geodetic measurements is taken near the telescope by means of a sling thermometer. Furthermore, the barometer reading is noted, while a variation of vapor pressure is not taken into consideration because of its relatively unimportant influence. Thus the data having considerable effect on the refractive index n are determined only at one point.

Indeed several assumption concerning the theory of refraction do not agree with reality; for instance, the stratification of the air by concentric spheres.

As is well known, the atmosphere is divided into a lower stratum near the ground up to the height of some hundred meters, and the free atmosphere lying on top of it. While relatively constant temperature conditions (negative temperature gradient of about $0{,}7^0\,C/100$ m annual average) prevail within the latter, the layer close to the earth is subject to extremely variable influences.

There is a considerable difference between daytime temperature fields and those at night. [4], [5], [8] and [9].

The most important effects acting on the temperature field at night are the reemission of the received thermal radiation during the day and the cooling of the earth' surface. The so-called temperature inversion caused in this way effects a stratification of the air according to the decrease in temperature. The thickness of this inversion layer depends among other things on the general weather character. It may be assumed of about 100 m average, sometimes even up to 300 m altitude. The near-the-ground zone of the inversion layer, which is in intimate contact with the surface, is the so-called lower stratum of inversion. Within this layer, which is of about 20 m annual average at midnight, air temperature foilows the laws of an exponential function; which according to *Brocks*' investigations contains the elevation multiplied by a small coefficient [5].

This lower stratum of inversion represents the intrinsic temperature boundary layer of atmosphere. Reviewing the comprehensive statistical material we can see that the area that exhibits most variations in the temperature curve is one third of the lower stratum of inversion closest to the ground. Therefore systematic variations caused by topographical features may occur within different azimuths at one station. A possibility to dertermine anomalies of that kind for derivation of a gradient $\partial T/\partial z$ is the measurement of temperature in the vertical plane through the light path.

Differences in temperature and pressure along the light path in variable layers of air and height effect variation of the refractive index n. The influence of the gradient $\partial n/\partial z$ has been neglected in (1).

It is, however, of great interest to know the effect of the gradient of the refractive index n on the curvature of the light path $\varkappa$. Since these relations were already analyzed by *Moritz* [12], we only refer to this paper.

The curvature of the light path is

$$\varkappa = \frac{1}{n}\,\frac{\partial n}{\partial z} \tag{5}$$

Because of $n \doteq 1$ we may equate

$$\varkappa = \frac{\partial n}{\partial z}\,, \tag{6}$$

i. e., the gradient of the index of refraction is approximately proportional to the curvature of the light path. In literature $\varkappa$ is often unfortunaltely termed "the local coefficient of refraction".

According to [2] we have

$$\varkappa = \frac{(n_{gr} - 1) \,.\, T_u}{n \,.\, 760} \,.\, r \,.\, \frac{p}{T^2}\left(\frac{g}{R} + \frac{\partial T}{\partial z}\right) \sin \zeta = \varkappa' \sin \zeta \tag{7}$$

with

n_{gr} ... standard group refractive index
n ... refractive index of air for visible light
p ... atmospheric pressure in terms of mm of mercury
r ... radius of curvature in azimuth of ray
g ... gravitational acceleration
$\frac{\partial T}{\partial z}$ ... vertical gradient of air temperature taken in ^{0}C per 100 m, negative with increasing height
T ... absolute temperature in degrees Kelvin ($T = T_u + t = 273{,}15 + t$; t in ^{0}C)
R ... gas constant

Specific assumption and data applicable for Central Europe may now be made, but the exact knowledge of them would yield negligible corrections only. Thus we have as a result a good expression for the influence of meteorological facts on light path curvature [3]

$$\varkappa \doteq 5{,}03 \frac{p}{T^2}\left(3{,}42 + \frac{\partial T}{\partial z}\right) \sin \zeta = \varkappa' \sin \zeta \tag{8}$$

The formulas mentioned above are not to be discussed in detail here. Nevertheless, it is worth noting that in any case average equivalents for the measured meteorological data are to be introduced before they are taken into further consideration or applied for computation. The change ot temperature with elevation involving a negative air-pressure gradient may be neglected only in the lower zone near the ground. [5], [8 p. 37 and 84], [9 p. 236ff].

Possibilities of Temperature Measurement with Electrical Thermometers

The measurement of air temperature near the ground causes difficulties that not should be underestimated. On one hand the temperature feelers of the device are heated by radiation, at the other hand they are in touch with the open air. Finally, an artificial turbulent air current would falsify results, for instance in the case of a gradient measurement with control points of short distances. For a most comprehensive and objective sampling of temperatures the electrical thermometers seem to be most suitable, not necessarily for gaining meteorological reference temperatures as, for example, obtained in the „Wildsche Hütte", but for "laboratory determination of isothermals".

There is a basic distinction drawn between two categories of contact thermometers- the thermocouple elements and the resistance thermometers. The latter ones are classified into those with metallic sensitive elements and those using semiconductor feelers. [1], [7 p. 380ff].

Thermocouple Elements

If the free ends of two electrical conductors of different metals or alloys are connected to form a thermoelectric circuit and differing temperatures are applied to the juncture (soldering point), a e. m. f. (thermoelectric current) will be produced. Because of its relative insignificance very sensitive measurement and test equipment as well as adequate treatment are necessary. Of advantage are the small dimensions of the thermoelements and their wide range of capacity. This lies between $-$ 250^0 and $+$ 2800^{0}C. Thermoelements represent the only electrical thermometers for temperature measurement at 1000^{0}C and more. The main field of application is the measurement of very high and very low temperatures. Further details are not to be explained here, because temperature measurements with thermocouple elements are of no interest for geodetic purposes.

Resistance Thermometers with Metallic Primary Elements

The variation of electric resistance of pure metals with temperature is regular and follows the laws of a power series. The functional temperature dependence of resistance covering the range of 0^0 to 100^0C is represented in most cases precisely enough by the linear term

$$R_t = R_o (1 + \alpha \, . \, t) \tag{9}$$

with

R_t ... resistance at t^0C
R_o ... resistance at 0^0C
α ... temperature coefficient (dimension $\simeq 4 \, . \, 10^{-3}$ degr.$^{-1}$)

Within the stated range temperature can be measured to 10^{-3} degrees. For example the resistance variation of platinum is 39% at that extent. A drawback of this technique is that errors caused by self-heating of the resistance thermometer become effective, so that development of feelers of any required size is impossible. The reason is that resistance windings always are relative bulky, preventing a point-shaped construction of primary elements.

Finally, the feeder line resistance is of no influence on the result of measurement only if a two-wire circuit system is employed an the resistance of the conductor is eliminated by an additional manganin-trimming resistor. In spite of this drawback of restistance thermometers they are accurate enough to be used as reference standards for many purposes:

Resistance Thermometers with Semiconductor Sensors

Similar to pure metals the change in resistance with temperature of semi-conductors can be used for temperature measurements. In this description we only refer to semi-conductors with negative temperature coefficient. Semiconductor resistors of that kind often are termed NTC-resistors, hot conductors (with negative temperature coefficient), or thermistors.

The fundamental distinguishing features in contrary to mercury-in-steel thermometers are the following: the resistance of pure metals increases with temperature with about 0,4% each 1^0C while the temperature coefficient α of thermistors is negative and approximatley ten times that of metals (at indoor temperatures it is about 2 to 6% each 1^0C).

Contrary to pure metals there is no linear relation between temperature and resistance. The functional relationship of temperature and resistance of these thermistors is expressed to a sufficient accuracy by

$$R_T = A \, . \, e^{B/T} \tag{10}$$

for very small temperature intervals.

Here R_T stands for the resistance at absolute temperature (degree Kelvin), and A and B are parameters of a thermistor. The constant factor A denotes resistance at $T = \infty$, but may be eliminated by introducing the resistance R_{T_b} at a standard point T_b (e. g., $t = 25^0$C, hence $T_b = 298^0$ K. Then we have

$$R_T = R_{T_b} \, . \, e^{B\left(\frac{1}{T} - \frac{1}{T_b}\right)} \tag{11}$$

and

$$B = \frac{\log R_T - \log R_{T_b}}{1/T - 1/T_b} \tag{12}$$

and finally

$$\alpha = \frac{d\,R/d\,T}{R} = -\frac{B}{T^2} \tag{13}$$

The resistance R_{T_b} of thermistors at a standard point of 20^0C varies between 0,1 and 10^7 ohms. Generally, however, only thermistors with a basic resistance of some thousand ohms are employed

because the lead resistance may be neglected then. The preferred range of application of thermistors is between $-$ 40°C and + 180°C; application is limited within $-$ 200°C and + 300°C.

Thermistors can be produced in nearly any structural shape desired, even of smallest proportions as to size and weight. They may be disk-shaped, rod-like or even "beads" of 0,1 millimeters in diameter. Thermistors are made from very pure oxides sintered under carefully controlled conditions of high temperature and atmosphere. Normally they vary greatly as to resistance in consequence of the manufacturing process and mixture, so that they cannot be interchanged. The usual tolerances of thermistors commercially available amount to $\pm$ 10 or 20% in R_{T_b} and $\pm$ 5% for factor B of one same type. If they are mass produced they may stay within $\pm$ 0,5% tolerance.

By an individual selection of thermistors this dispersion will be reduced, thus attaining interchangeability. Though thermistors are exposed to an artificial ageing process, they show substantial ageing effects. At measurements over longer periods therefore reproducibility is very doubtful. But over short time periods temperature difference measurements can be carried out very exactly (e. g., 10^{-2} degrees with 10^{-4} degrees accuracy).

If we compile some characteristic data of the resistance thermometers mentioned above, we can see that those working with semiconductor sensors exhibit the highest degree in accuracy and sensitivity for restricted ranges of temperature. On the other hand thermistors with metallic feelers allow highest precision within a comparative wide range. Their drift velocity is near 0,1 % in 5 years, that of thermistors 0,1 to 1,5°C p. a. The reproducible accuracy of resistance thermometers with metallic feelers is 0,02° to 0,05° and that of thermistors is about 0,1° up to 0,5°. So-called precision thermistors will be described later.

Some Aspects on the Selection of a Temperature Meter

The continuous experiments and tests of measuring instruments performed at the Chair of Higher Geodesy and Astronomy of the Technical University of Berlin required the exact determination of the temperature difference between the two ends of a level tube. For this purpose thermistors with disk-shaped sensors had been selected and temperature difference measurements had been registered by means of a moving-coil instrument after previous calibration in a bridge circuit (deflection method). The meter, however, showed some serious deficiencies: it had no zero stability and the balancing range covered only a few degrees.

To find a relation to the thermometric scale, time-consuming reference temperature standards had to be prepared. The smallest temperature differences of some hundredth degrees which occured during the measurements were near the limits of accuracy of the instrument. This seemed to be correct, because there are several hints in literature that the reliability of indicators mostly is not equivalent to accuracy of thermistors. Moreover, in the last two or three years manufacturing methods have been developed to produce precision thermistors whose R_{T_b}- and B-values were so much smoothed that they follow the same temperature-resistance curve. Thus they show the same properties as metallic resistance feelers.

To give an example, the YSI thermistor (SASCO-Stewart Aeronautical Supply Company Ltd.) 32 TD 25 type with a nominal resistance of 2 $k\Omega$ at 25°C deviates from the values provided in the specification sheet only within $\pm$ 0,2 degrees over the range of 0° to 100° C. For this thermistor the drift is 0,005° p. a. and the reproducible accuracy amounts to 0,01°C.

The use of these adjustable thermistors requires a suitable meter with a power dissipation capability so effective that to a first approximation the instrumental errors may be neglected. As is known from experience, there are not only a few commercially available temperature meter of general applicability. An instrument of that kind, which would be most suitable for thermistor measurements within the scope of geodetic laboratory test work too, is utilized in chemical laboratories for the determination of molar weights by means of cryoscopia.

This KNAUER universal temperature meter consists essentially of a modified Wheatstone Bridge arrangement with artificially aged precision manganin resistors and a regulated power supply. It permits the individual measurement with one single primary element and temperature difference measurements with two sensors (resistance between 50 and 100 $k\Omega$; in the first case only up to 12 $k\Omega$).

To intensify the efficiency of the meter the diagonal voltage of the bridge is multiplied by a fully transistorized test amplifier. (linearity better than 99.9 %). Measurements are performed either by deflection method or by the compensating method. Sensitivity is about 0,05°C over the whole scale of the indicator, running from 0 through 100.

The indicating scale is continuously variable from 0,05°C ≙ 100 scale intervals up to 20°C ≙ ≙ 100 intervals. Moreover it is reducible by 8 switch steps alternately with factor 2, i. e., from 1 to 1/2, 1/4, 1/8 and so on down to 1/128. Dissipation capacity comes to 2/10 000°C when using thermistors, and to 2/1000°C applying platinum resistance feelers. The quality features of the apparatus are preset by the temperature coefficient of the 10-turn coiled potentiometer. A recorder

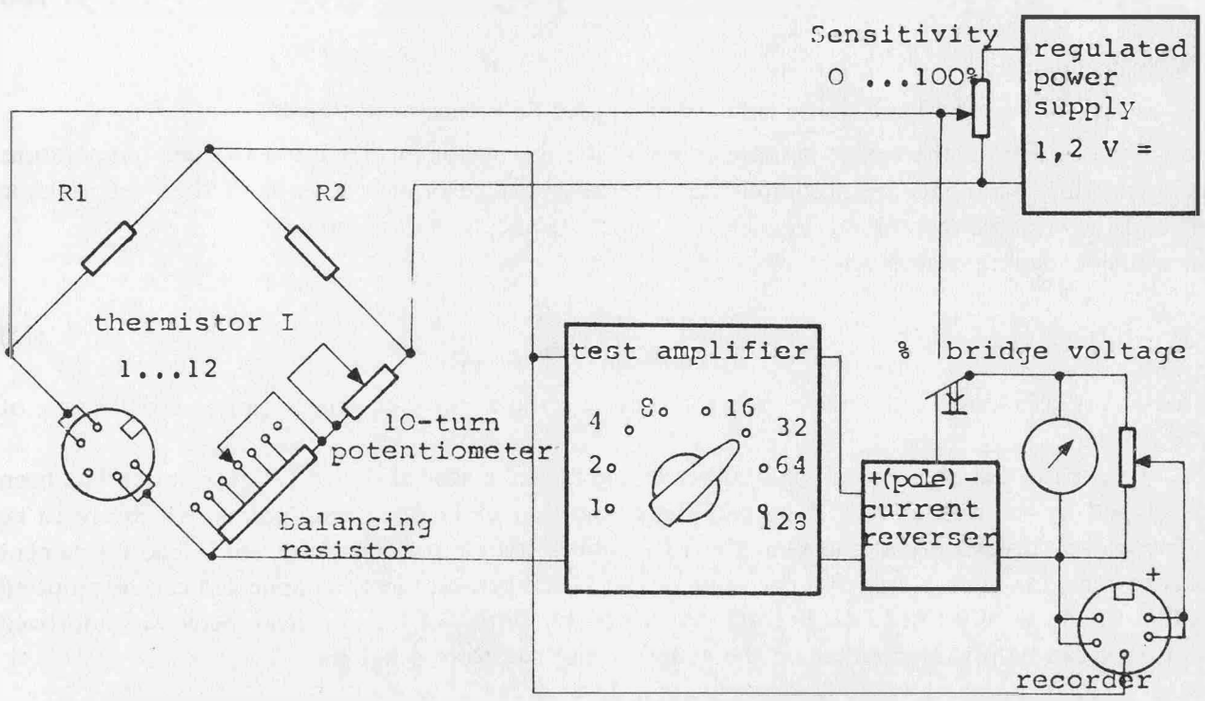

Fig. 1 Basic circuit diagram for individual measurement

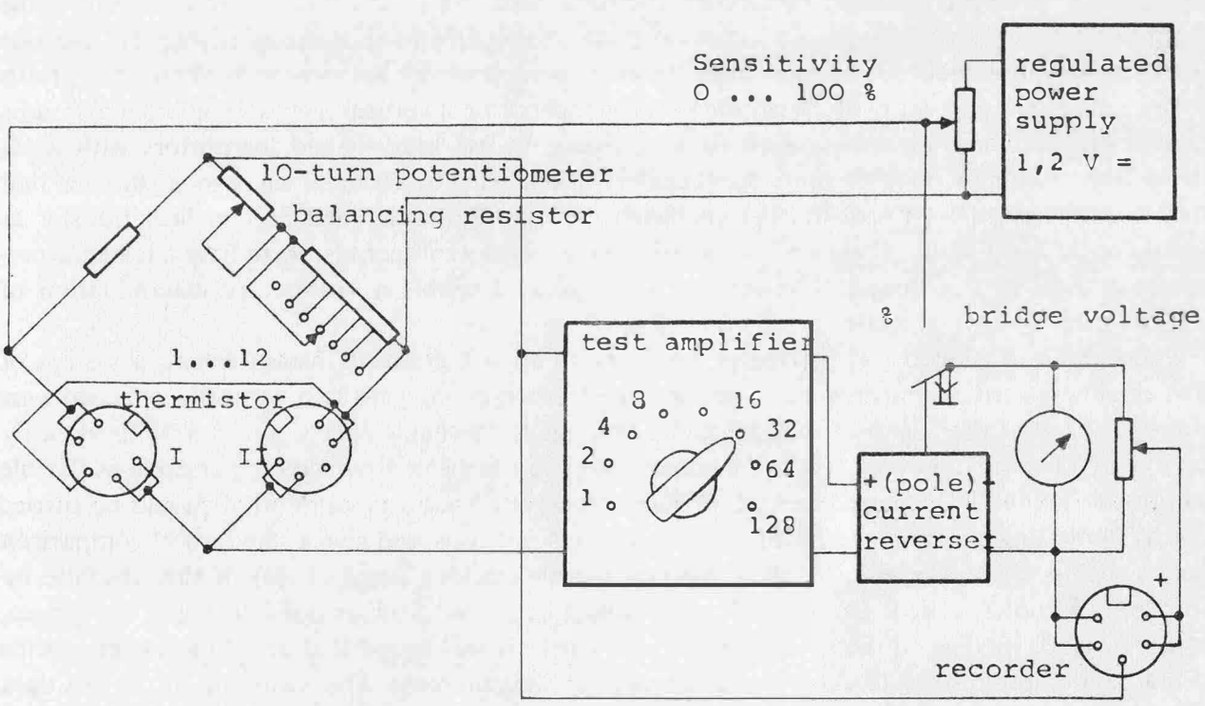

Fig. 2 Basic circuit diagram for difference measurements

output is supplied. Furthermore a changeover switch "current reverser" serves to keep the pointer deflection of the indicator acting in the same direction with temperature rising or falling. Bridge supply voltage is 1,2 V max., and can be continuously and reproducibly decreased. It is also indicated (in %) by the meter.

The method of operation of the device is illustrated by the two figures on page 233 showing the underlying principle [10]:

Fig. 1. Basic circuit diagram for individual measurement

Adjustment of the temperature meter is attained by

$$\frac{R_1}{R_2} = \frac{R_{thermistor}}{R_{balance}} \tag{14}$$

The instrument then gives zero reading.

Fig. 2. Basic circuit diagram for difference measurement

The one arm of the bridge is represented by the thermistor probes I and II when temperature difference measurements are accomplished. The other bridge branch consists of the fixed resistor R_1 and the variable resistor R_2, by means of which balancing is done now.

Instrument reading is zero when

$$\frac{R_{I\,thermistor}}{R_{II\,thermistor}} = \frac{R_1}{R_{balance}} \tag{15}$$

holds. Any temperature difference occuring between the two feeler gauges causes a deflection of the pointer.

To expand the operational possibilities of the meter, a special design selector switch has been developed by the manufactor. It permits the connection of 11 measuring points, which are to be interrogated successively at the switchboard position "differential measurement". The instrument is constructed in such a way that each one of the 11 temperature feelers connected can be adjusted within the range of 0 to 12 $k\Omega$. Beyond that the power supply of the universal meter was improved so that it can be operated either on the mains or else run from a battery.

Some Applications

As we have already mentioned above, the instrument was purchased primarily for examination of instruments and has been employed accordingly till now. Because these investigations are parts of doctor's theses they cannot be further discussed here. As is well known, often considerable scattering will appear in the results of astronomical measurements in different nights. To find out whether such systematic deviations from "normal stratification" are caused by local conditions at the station, the possibility of measuring the air temperature in vertical planes of different azimuths and in different height presents itself. It is advisable to use bead-shaped thermistors with leads fused into a vitreous body of some 5 millimeters in diameter by 60 millimeters long. Besides that they should have a high heat-transfer coefficient to keep the radiational part in heat transfer as small as possible. Finally, attention is to be paid to the selection of thermistors to have a temperature-response time not too low ($\leq$ 5 seconds), which should enable a satisfactory determination of a mean value of air temperature.

To obtain a general view of the performance of such a gradients measurement, a system of five equally spaced thermistors had been mounted experimentally to two vertically attached wire ropes. The "glass thermistors" used are rather immune to mechanic effects and may be fixed easily by some PVC insulating tape. To link the thermistors to the meter stranded copper cable as flexible as possible should be preferred (e. g. LifYY 0,14 $mm^2\varnothing$). Necessary calibration should be carried out by immersing a second thermistor in a Dewar vessel. This would give a standard of comparison and render possible a relation to the temperature scale (melting point of ice). If this absolute information is not required, another normal temperature as constant as possible might be chosen, as for instance by digging the thermistor into the earth. It was found that all of the 11 test points could be monitored some few minutes in a repetition measurement. The scattering of the test data is based but only on temperature variations, in the course of which the amount of the personal reading errors is of secondary importance. Experience has shown that the measured values are

reliable within $\pm 2/10^0$ as the standard deviation of the single measurement, representing the true air temperature.

In geodetic literature usually only measurements with resistance thermometers furnished with metallic feelers are dealt with. Therefore it seemed appropriate to give some informations about measurement possibilities with semiconductor primary elements. The advantages of thermistors are considerable, particularly when it comes to temperature difference measurements, or when even only the difference of differences is to be determined.

The measuring device referred to above is flexible enough and even qualified for field work that it would be quite possible to apply it for measurements for the determination of the refractional effect in leveling in the sense of *Kukkamäki's* papers [11].

References

1. *Birr, H.:* Vorteile und Grenzen der Temperaturmessung mit Halbleiterwiderständen. Zeitschrift Messen Steuern Regeln (Zmsr). No. 5 (pp. 215–221), 1962.
2. *Brocks, K.:* Die terrestrische Refraktion in polytropen Atmosphären. Deutsche Hydrographische Zeitschrift, vol. 2, 1949, pp. 199–211.
3. *Brocks, K.:* Die Lichtstrahlkrümmung in Bodennähe. Deutsche Hydrographische Zeitschrift, vol. 3, No. 3/4, 1950.
4. *Brocks, K.:* Die Lichtstrahlkrümmung in den unteren 500 m der Atmosphäre. Annalen der Meteorologie. No. 1/2, 1950.
5. *Brocks, K.:* Die Höhenabhängigkeit der Lufttemperatur in der nächtlichen Inversion. Meteorologische Rundschau, No. 5/6 (pp. 159–167), 1949.
6. *Coast and Geodetic Survey* Manual of Geodetic Astronomy. Spec. Publication No. 237, U. S. Department of Commerce Government Printing Office, Washington, 1952.
7. *Flügge, S.:* Encyclopedia of physics, Vol. XXIII, Electrical instruments, Springer-Verlag, Berlin 1967.
8. *Geiger, R.:* Das Klima der bodennahen Luftschicht, 4th edition, 1961, Spec. Publ. No. 78 of the series *Die Wissenschaft* Friedr. Vieweg & Sohn, Braunschweig.
9. *Jordan–Eggert–Kneissl:* Handbuch der Vermessungskunde, 10th edition Vol. VI (Die Entfernungsmessung mit elektromagnetischen Wellen und ihre geodätische Anwendung), Stuttgart, 1966.
10. *Knauer, H.:* Wissenschaftlicher Gerätebau, Dr.-Ing. H. Knauer, 1 Berlin/West 33, Breite Str. 10.
11. *Kukkamäki, T. J.:* Über die nivellistische Refraktion. Allgemeine Vermessungs-Nachrichten, (p. 503), 1938.
12. *Moritz, H.:* Zur Geometrie der Refraktion. Österreichische Zeitschrift für Vermessungswesen, (50), 1962, No. 1, pp. 3–13.
13. *Mühlig, F.:* Astronomisch-geodätische Ortsbestimmung. H. Wichmann-Verlag, Berlin 1960.

Contribution to the Vertical Gradient of Refractive Index for Microwaves in the First 100 m of the Atmosphere

by *Hans Pelzer*, Brunswick, W. Germany

1. *The vertical gradient of the refractive index and of its components*

For the determination of the geometric distance between two points from the measured transit time of microwaves it is necessary to know the curvature of the ray path. The curvature $1/\rho$ of the ray path is given by the sine relationship as

$$\frac{1}{\rho} = -\frac{dn}{dh}, \tag{1.1}$$

where the horizontal derivation of the refractive index is neglected. The curvature is the negative vertical gradient of the refractive index of the atmosphere [6].

It is a function of the air temperature t, the vapour pressure e and the air pressure p,

$$n = n(t, e, p), \tag{1.2}$$

and it follows that the vertical gradient can be written as

$$\frac{dn}{dh} = \frac{\partial n}{\partial t}\frac{dt}{dh} + \frac{\partial n}{\partial e}\frac{de}{dh} + \frac{\partial n}{\partial p}\frac{dp}{dh}. \tag{1.3}$$

It is possible to obtain the partial derivations with respect to temperature, vapour pressure and air pressure from the formula by Essen and Froome [5]

$$(n-1) \cdot 10^{-6} = \frac{103.49}{T}(p-e) + \frac{86.26}{T}\left(1 + \frac{5748}{T}\right)e \tag{1.4}$$

T: air temperature [^{0} Kelvin].

These derivations are constant with sufficient accuracy, so that follows from (1 . 3)

$$\frac{dn}{dh} = c_t\frac{dt}{dh} + c_e\frac{de}{dh} + c_p\frac{dp}{dh}, \tag{1.5}$$

and we have to find the vertical gradients of temperature, vapour pressure and air pressure.

We will restrict ourselves to those conditions which the ray path always runs near the surface of the earth. Therefore, we have to investigate the first 100 meters of the atmosphere.

The gradient of temperature in the lowest layer of the atmosphere has been manifold investigated [1] [2] [3] [4]. The result shall be here condensed with reference to the works of Brocks. In the day-time it will be discriminated the unstable lower layer and the adiabatic intermediate layer.

On the average of a year, the unstable lower layer is thick about 21 meters. In summer, it is thicker (30—40 meters) than in winter. It is possible to represent the gradient of temperature in the lower layer by

$$\frac{dt}{dh} = a_t \cdot h^b. \tag{1.6}$$

The factor a_t is dependent on the time of day and the season as well as on the weather conditions. It is negative in the day-time. For the exponent b we have the relation

$$b_t = -1 \pm 0.2. \tag{1.7}$$

The adiabatic intermediate layer has an extension up to several hundred meters. There, the gradient of temperature is weakly overadiabatic and decreases slowly with the height.

At night, the unstable lower layer will be replaced by the lower layer of inversion with a thickness of about 20 meters. The function (1 . 6) will be preserved, only the sign changes. The exponent b_t fluctuates here around a mean value of -0.9. In the layer of inversion situated over that, the gradient of temperature decreases slowly to the isothermic state.

Because of the considerable fluctuation of the coefficient it may be permissible to approximate the gradient of temperature in the first decameters by

$$\frac{dt}{dh} = \frac{a_t}{h}. \tag{1.8}$$

The distribution of vapour pressure in the atmosphere is known worse than the distribution of temperature. However, the observations in hand till now allow the inference, temperature and vapour pressure have similar height functions, i. e. the gradient of vapour pressure can be written likewise in the form

$$\frac{de}{dh} = a_e \cdot h^b \tag{1.9}$$

Although Adlung [1] found no strong correlation between the exponents b_t and b_e in the height-functions of temperature and vapour pressure, his investigations give the result that in a first approximation

$$b_e = -1 \tag{1.10}$$

can be admitted. By this will be

$$\frac{d\,e}{d\,h} = \frac{a_e}{h}\,. \tag{1.11}$$

In comparison with that the height-function of air pressure can be given very easy. The derivation

$$\frac{d\,p}{d\,h} = a_p \tag{1.12}$$

can be taken for a constant. With $p = 755$ Torr and $t = 15^0$C it will be obtained

$$a_p = -0.091\ (\text{Torr/m})\,. \tag{1.13}$$

The derivations of the components of the refractive index are now found and can be substituted into the equation (1 . 5). That leads to

$$\frac{d\,n}{d\,h} = c_t \,.\, \frac{a_t}{h} + c_e \,.\, \frac{a_e}{h} + c_p \,.\, a_p\,, \tag{1.14}$$

or, by use of abbreviations,

$$\frac{d\,n}{d\,h} = \frac{k_1}{h} + k_2\,. \tag{1.15}$$

By the published material [2] [4], for the coefficient k_1 the median value

$$k_{1\,(\text{mean})} = -1.0\,.\,10^{-6}\,, \tag{1.16}$$

and the bounds

$$-4.1\,.\,10^{-6} \leq k_1 \leq +0.2\,.\,10^{-6} \tag{1.17}$$

can be roughly estimated. The material published in [2] [4] consists of monthly mean values. The values in (1 . 16) and (1 . 17) were estimated with the assumption the actual range of variation will be got by multiplication of the published values by the factor 2.

Within wide bounds is furtheron true

$$k_2 = -0.033\,.\,10^{-6}\,(1/\text{m}). \tag{1.18}$$

With (1 . 15) a formula for the vertical gradient of the refractive index is found being certainly a rough approximation to the actual conditions only. However, it is to suppose this approximation will be better than the assumption of a constant gradient of the refractive index.

The inferences for the form of the ray path and the atmospheric corrections shall be investigated in the following.

2. Projection of the normal section of the sphere into the x, z-plane

First of all, the problem shall be simplified by a transformation of coordinates.

If the lateral refraction will be neglected, and with assumption of a sphere as reference surface the ray path is a plane curve running in a normal section of the sphere. In this plane E a system of polar coordinates shall be introduced with the origin in the center of the earth, and with the direction of reference through the terminal point A.

Then a running point along the ray path has the coordinates (r, Φ) and the optical length L between two terminals A and B is given by

$$L = \int_A^B n\,(r, \Phi)\,.\,d\,s \tag{2.1}$$

with

$$d\,s = \sqrt{r^2\,.\,d\,\Phi^2 + d\,r^2}\,. \tag{2.2}$$

By means of the equations of the projection

$$\left.\begin{aligned} x &= r \,.\, \Phi\,, \\ z &= r - R\,, \end{aligned}\right\} \tag{2.3}$$

where R the radius of the earth,

this plane can be projected into a x, z-plane $\overline{E}$, in which the differential of arc is given by

$$\overline{d\,s} = \sqrt{d\,x^2 + d\,z^2}\,. \tag{2.4}$$

With respect to the scale factor of the projection will be

$$d\,s = \sqrt{\frac{(z+R)^2\,\frac{d\,x^2}{R^2} + d\,z^2}{d\,x^2 + d\,z^2}}\;\overline{d\,s}\,. \tag{2.5}$$

from which for the optical length (2 . 1) will be obtained

$$L = \int_A^B n\,(x, z)\,\sqrt{\frac{(z+R)^2\,\frac{d\,x^2}{R^2} + d\,z^2}{d\,x^2 + d\,z^2}}\;\overline{d\,s} = \int_A^B m\,(x, z)\,\overline{d\,s} \tag{2.6}$$

With the relation

$$n = 1 + N\,.\,10^{-6}\,, \tag{2.7}$$

and with restriction to heights < 1000 meters and slope angles $< 1g$, with an accuracy better than 10^{-7} will be

$$m = 1 + N\,.\,10^{-6} + \frac{z}{R} \tag{2.8}$$

or

$$m = 1 + M\,.\,10^{-6} \tag{2.9}$$

with

$$M = N + \frac{z\,(m)}{6\,.\,37}\,. \tag{2.10}$$

The further investigations can be carried out in the x, z-plane with use of the modified refractive index m. Its vertical derivation is

$$\frac{\partial\,m}{\partial\,z} = \frac{\partial\,n}{\partial\,z} + \frac{1}{R}\,, \tag{2.11}$$

from which with (1 . 15) will be

$$\frac{\partial\,m}{\partial\,z} = \frac{k_1}{z} + \left(k_2 + \frac{1}{R}\right). \tag{2.12}$$

3. Shape of the ray path

According to Fermat's principle the ray path must comply with the condition

$$L = \int_A^B m\,(x, z)\,\overline{d\,s} = \int_{x=o}^{S} m\,(x, z)\,\sqrt{1 + z'^2}\;.\;d\,x = \text{min.!}\,. \tag{3.1}$$

This problem of variations leads to the differential equation of Euler

$$\left(\frac{\partial\,n}{\partial\,z} + \frac{1}{R}\right).\,(1 + z'^2) - \frac{\partial\,n}{\partial\,x}\,z' - \left(\frac{\partial\,n}{\partial\,z} + \frac{1}{R}\right)z'^2 - \left(n + \frac{z}{R}\right)\frac{z''}{1 + z'^2} = 0. \tag{3.2}$$

With the same restrictions as in section 2 ($z < 1000$ meter, vertical angles $< 1g$) and by neglecting the horizontal derivation of the refractive index as well as with respect to (1 . 14) it will be

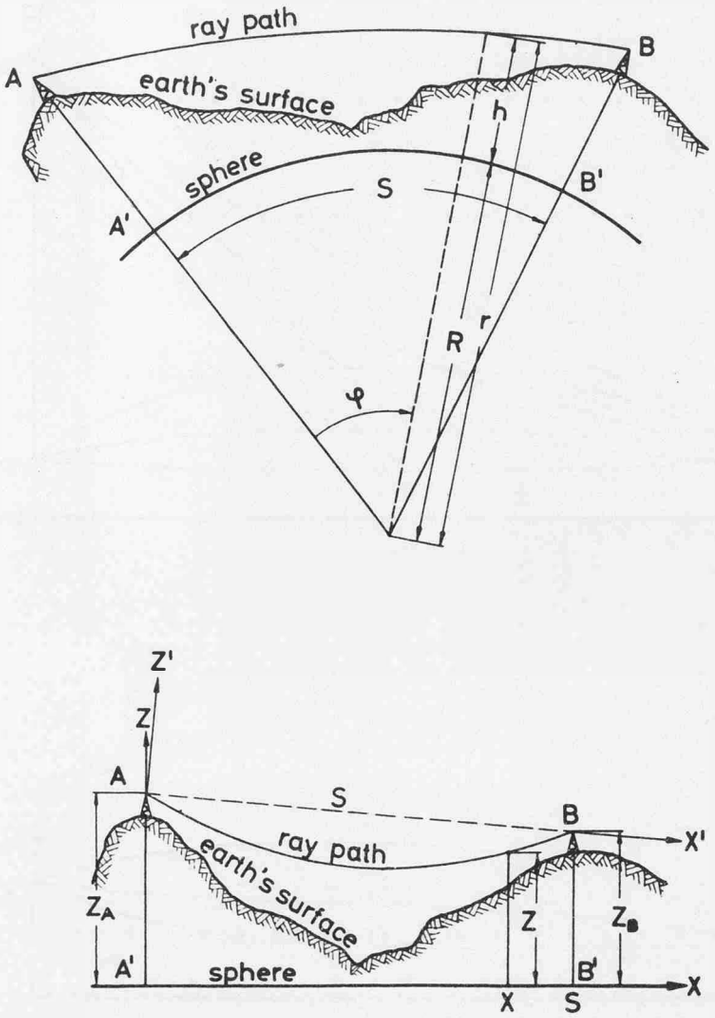

figure 1

Projection of the normal section into the x,z-plane

$$\frac{k_1}{z} + \left(k_2 + \frac{1}{R}\right) - z'' = 0\,. \tag{3.3}$$

The integration of this differential equation can be carried out numerically, e. g. by means of the method of Nyström, carrying on the method of Runge-Kutta. The details shall be omitted here, see [8].

The ray path along a distance of 50 km is plotted in the figures 2 and 3. The following will be evident:

a) The shape of the ray paths is strongly dependent on the heights of the terminals. For example in figure 2 the rays to the terminal B_{80} are convex curved, on the other hand the rays to the other terminals are concave curved on the same conditions. Even along the same ray, the curvature can be strongly variable.

b) The deviations from that circle which corresponds with a uniform refractive coefficient $k = 0.25$ can be considerable. (In figure 2, the curve of $k_1 = 0.00$ corresponds to a refractive coefficient $k = 0.21$).

c) Even in the case of very low terminals it will be often possible to make a distance measurement, if no hindrances to the ray are present. That is in conformity with the experience, that in the flat even longer distances usually could be measured.

4. The optical length

The result of an electronic distance measurement is the optical length L between the terminals of the distance. From that, it is necessary to compute the distance reduced to the reference surface.

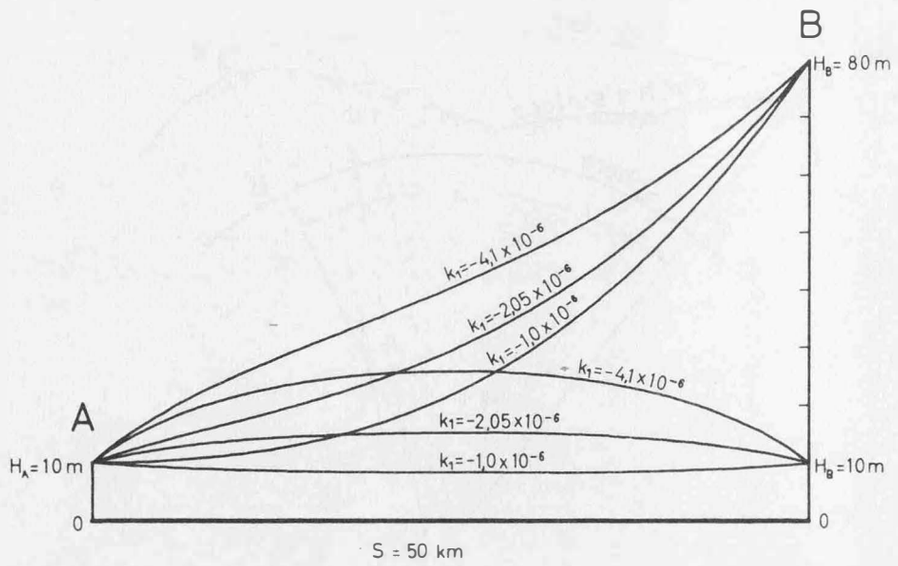

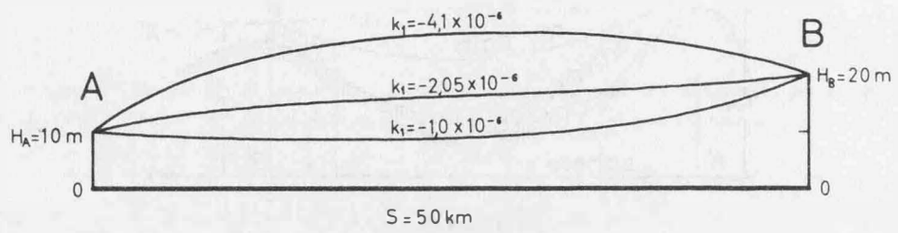

figure 2

ray paths with different gradients of refractive index

For the case of a logarithmic high-function of the refractive index the reduction formulas shall be deduced.

With the denotations (figure 1):

L: optical length between A and B
S: spherical length between A' and B'

can be written:

$$S = L + \Delta s. \tag{4.1}$$

The computation of Δs shall be carried out in the x, z-plane. It is

$$\Delta s = S - L = (S - s) + (s - L) = \Delta s_1 + \Delta s_2 , \tag{4.2}$$

where s is the geometric distance between the points A and B in the x, z-plane.

$$s = \sqrt{(x_B - x_A)^2 + (z_B - z_A)^2} = \sqrt{S^2 + (z_B - z_A)^2} \tag{4.3}$$

Hence it follows with sufficient accuracy

$$s \simeq S + \frac{(z_B - z_A)^2}{2\,S} \simeq S + \frac{(z_B - z_A)^2}{2\,L} , \tag{4.4}$$

as well as

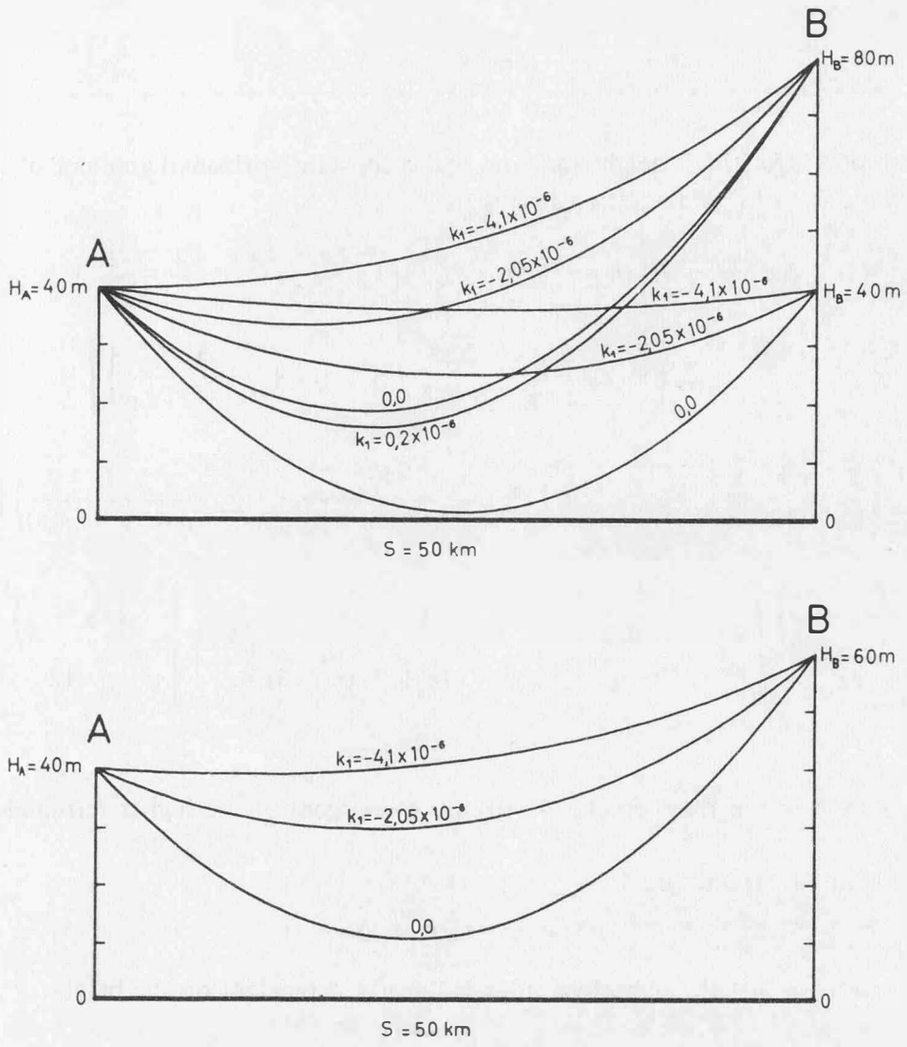

figure 3

ray paths with different gradients of refractive index

$$\Delta s_1 = -\frac{(z_B - z_A)^2}{2L}. \tag{4.5}$$

For the determination of Δs_2 a method given by Moritz can be used. If the refractive index n used by Moritz will be replaced by the modified refractive index m,

$$m = 1 + M \,.\, 10^{-6} \tag{4.6}$$

by substitution in the deduced relations will be found

$$\Delta s_2 = 10^{-6} \int_0^S M(x, z)\, dx' - \frac{10^{-12}}{2} \int_0^S \frac{A_3^2}{x'^2}\, dx'. \tag{4.7}$$

with

$$A_3 = \int_0^{x'} \frac{\partial M}{\partial z'} \xi\, d\xi\,. \tag{4.8}$$

All integrations must be carried out along the straight line between A and B in the projection.

By consideration of

$$\frac{\partial m}{\partial z} = \frac{k_1}{z} + \left(k_2 + \frac{1}{R}\right) \tag{2.12}$$

and by assumption

$$\frac{\partial n}{\partial x} = c, \tag{4.9}$$

i. e. in the case of a logarithmic height function and a constant horizontal gradient of the refractive index the carrying out of the integration results in

$$\Delta s_2 = -L\left[(n_A - 1) + c \cdot \frac{L}{2} + k_2 \frac{z_B - z_A}{2} + \frac{z_A - z_B}{2R} + \right.$$

$$\left. + \frac{k_1}{z_A}\left\{-\Delta z + z_B \frac{\Delta z}{2 z_A} + \frac{\Delta z^2}{3 z_A^2} + \ldots\ldots + \frac{\Delta z^n}{(n+1) z_A^n}\right\}\right] +$$

$$+ \frac{L^3}{2}\left[\frac{k_1^2}{z_A^2}\left\{\frac{1}{12} + \frac{1}{12}\frac{\Delta z}{z_A} + \ldots\ldots + \left(\sum_{p=1}^{n+2} \frac{1}{p(n+3-p)} - \sum_{p=1}^{n+3} \frac{1}{p(n+4-p)}\right)\left(\frac{\Delta z}{z_A}\right)^n\right\} + \right.$$

$$\left. + \frac{k_1\left(k_2 + \frac{1}{R}\right)}{z_A}\left\{\frac{1}{6} + \frac{1}{12}\frac{\Delta z}{z_A} + \ldots\ldots + \frac{1}{(n+2)(n+3)}\left(\frac{\Delta z}{z_A}\right)^n\right\} + \frac{\left(k_2 + \frac{1}{R}\right)^2}{12}\right] \tag{4.10}$$

with $$\Delta z = z_A - z_B .$$

The series involving in the formula (4 . 10) are convergent, if the higher terminal will be designated as A.

It follows from (4 . 1) and (4 . 2)

$$S = L + \Delta s_1 + \Delta s_2 \tag{4.11}$$

In the special case that the refractive index is linearly dependent on the height,

$$\left.\begin{aligned} k_1 &= 0 \\ k_2 &= -\frac{1}{\rho} \end{aligned}\right\} \tag{4.12}$$

becomes from (4 . 11)

$$S = L - \frac{\Delta z^2}{2L} - \left(\frac{n_A + n_B}{2} - 1\right) \cdot L - \frac{z_A + z_B}{2R} \cdot L + \left(1 - \frac{R}{\rho}\right)^2 \frac{L^3}{24 R^2}, \tag{4.13}$$

in coincidence with the reduction formulas deduced in [6].

Finally the reductions for the ray paths plotted in the figures 2 and 3 shall be tabulated.

Because the quantity $\Delta s'$ being the correction of a distance with respect to the curvature of the ray path is only interesting, it shall be formed the expression

$$\Delta s' = \Delta s_2 + L\left[\frac{n_A + n_B}{2} - 1 + \frac{z_A + z_B}{2R} - \frac{L^3}{24 R^2}\right] \tag{4.14}$$

with $$n_B = n_A + k_1 ln \frac{z_B}{z_A} + k_2 (z_B - z_A) + c \cdot L . \tag{4.15}$$

On the other hand it is possible to introduce a mean refractive index by

$$\bar{k} = -R \frac{n_B - n_A}{z_B - z_A} \tag{4.16}$$

resp., if $z_A = z_B$, by

$$k = -R \cdot \left(\frac{k_1}{z_A} + k_2\right). \tag{4.17}$$

With that the curvature correction can be computed by [6] as

$$\Delta s'' = \frac{L^3}{24\,R^2}\,(\overline{k^2} - 2\,\overline{k})\,. \tag{4.18}$$

The values $\Delta s'$ are likewise given. The differences are generally inconsiderable. The dependence of the curvature correction on the height of the terminals is very striking.

$z_{A(m)}$	$z_{B(m)}$	$k_1 \cdot 10^6$	$\Delta s'_{(m)}$	$\overline{k}$	$\Delta s''$
40	80	−4.10	−0.105	+0.54	−0.101
40	80	−2.05	−0.084	+0.37	−0.078
40	80	0.00	−0.048	+0.21	−0.048
40	80	0.20	−0.044	+0.19	−0.045
40	40	−4.10	−0.126	+0.86	−0.126
40	40	−2.05	−0.101	+0.54	−0.101
40	40	0.00	−0.048	+0.21	−0.048
40	60	−4.10	−0.117	+0.64	−0.112
40	60	−2.05	−0.091	+0.43	−0.086
40	60	0.00	−0.048	+0.21	−0.048
10	80	−4.10	−0.058	+0.54	−0.101
10	80	−2.05	−0.069	+0.37	−0.078
10	80	−1.00	−0.063	+0.29	−0.064
10	10	−4.10	+0.298	+2.82	+0.298
10	10	−2.05	−0.094	+1.52	−0.094
10	10	−1.00	−0.125	+0.85	−0.125
10	20	−4.10	+0.009	+1.52	−0.094
10	20	−2.05	−0.123	+0.86	−0.126
10	20	−1.00	−0.111	+0.52	−0.100

References

1. *Adlung, A.:* Über die Ausbreitung von Zentimeter- und Dezimeterwellen in der bodennahen Luftschicht.
   Dissertation Math. Naturw. Fakultät der Universität Leipzig 1962
2. *Best, A. C., Knighting, E., Pedlow, R. H., Stormonth, K.:* Temperature and humidity gradients in the first 100 m over SE-England.
   Geophys. Memoirs Nr. 89. London 1952.
3. *Brocks, K.:* Über den täglichen und jährlichen Gang der Höhenabhängigkeit der Temperatur in den unteren 300 m der Atmosphäre und ihren Zusammenhang mit der Konvektion.
   Bericht des Deutschen Wetterdienstes in der US-Zone, Nr. 5
4. *Frankenberger, E.:* Über vertikale Temperatur-, Feuchte- und Windgradienten in den untersten 7 Dekametern der Atmosphäre, den Vertikalaustausch und den Wärmehaushalt an Wiesenboden bei Quickborn/Holstein 1953/1954.
   Berichte des Deutschen Wetterdienstes Nr. 20 (Band 3).
5. *Höpcke, W.:* Zur Berechnung des Brechungsindexes für Mikrowellen.
   Allgemeine Vermessungsnachrichten, Bd. 69, Jahrgang 1962, S. 162–166.
6. *Höpcke, W.:* Über die Bahnkrümmung elektromagnetischer Wellen und ihren Einfluß auf die Streckenmessungen.
   Zeitschrift für Vermessungswesen, 89. Jahrgang, 1964, S. 183–200.

7. *Moritz, H.:* Zur Reduktion elektronisch gemessener Strecken und beobachteter Winkel wegen Refraction.
Zeitschrift für Vermessungswesen, 86. Jahrgang, 1961, S. 246 – 252.
8. *Netz, N.:* Formeln der Mathematik, herausgeg. von G. Arnold Braunschweig 1965.

Time-Space Structure of Atmospheric Index Especially Obtained by Refractometer Measurements

by *H. Jeske* and *G. Kruspe*, Hamburg

Zusammenfassung

In diesem Artikel werden die wesentlichen Abweichungen von den in der Geodäsie und Radiometeorologie üblicherweise benutzten Modellen der vertikalen Brechungsindexabnahme diskutiert und durch typische Beispiele belegt. Die wichtigsten Einschränkungen sind gegeben durch die extrem starken Gradienten in den untersten Dekametern über der Erdoberfläche (s. § 2), Schichtbildungen in der Troposphäre (s. § 3), horizontale Inhomogenitäten (s. § 4) und durch den turbulenten Charakter der Atmosphäre (s. § 5).

Summary

In this report the essential deviations from the models of the vertical decrease of atmospheric refractive index, which are normally used in geodesy and radiometeorology, are discussed and illustrated by typical examples. The most important restrictions of these models are given by the extremely strong gradients in the lower decameters above the surface (cf. § 2), by layers in the troposphere (cf. § 3), horizontal inhomogeneities (cf. § 4) and the turbulent character of the atmosphere (cf. § 5).

1. *Introduction*

The inhomogeneous distribution of the atmosperic refractive index may cause several mechanisms of electromagnetic wave propagation such as refraction, ducting, reflection or scattering, which determine the radiated field characterized by amplitude, phase, and angle-of-arrival. The random time variations of the medium give rise to fading effects and fluctuations of phase and angle-of-arrival, which are a source of noise in geodetic measuring systems.

The phenomena of refraction (producing errors in transit time and arrival angle) are caused by the variations of the real part of the refractive index within the propagation medium. The insecurity in the determination of the refractive index limits the accuracy of the geodetic measuring equipments and of tracking devices.

The „Meteorologisches Institut der Universität Hamburg" and the „Institut für Radiometeorologie und Maritime Meteorologie an der Universität Hamburg", both under the direction of Prof. Dr. K. Brocks, investigate the influence of meteorological factors on electromagnetic wave propagation with special interest in the amplitude variations of the signal strength. For geodetic purposes this problem is of less importance. Perhaps there is a certain interest in the attenuation factor of propagation A ($A = E/E_o$, E: field-strength received, E_o: free space level of field-strength) to determine the maximum transmission range of electronic range finders acting on 3 cm and 10 cm waves.

The mean variations of the signal strength are very large especially for distances not too far behind the horizon because of the overlapping influence of several propagation mechanisms. As an example the attenuation factor A for wave lengths of 4 cm and 13 cm measured at a distance of 77 km over sea may be given for the whole year of 1962 as well as for a month with good (June 1962) and with poor (January 1962) propagation conditions [1, 2]. The receiving aerials (being like the transmitting aerials about 30 m above sea-level) were about 32 km behind the horizon. Table 1 shows in each case the median value of the attenuation (50% of all cases in "*dB* below free space field-strength") as well as the differences of the levels reached in 10% and 90% and in 1% and 99% of the given time, respectively.

Table 1: Attenuation factor A and its variances of a 4 cm and a 13 cm radio transmission path

	1962								
	$A_{50\%}$	$A_{10\%-90\%}$	$A_{1\%-99\%}$						
	[dB below E_o]	[dB]	[dB]						
4 cm	−41	44	72						
13 cm	−46	27	72						
	January				June				
$A_{50\%}$	$A_{10\%-90\%}$	$A_{1\%-99\%}$		$A_{50\%}$	$A_{10\%-90\%}$	$A_{1\%-99\%}$			
[dB below E_o]	[dB]	[dB]		[dB below E_o]	[dB]	[dB]			
−61	19	30		−24	35	61			
−56	14	32		−35	47	60			

(The months of August or September often show the best propagation conditions with similar variances as they were given for June)

But for all propagation problems the fine-structure of the atmospheric refractive index is required, thus rejoining the various branches of wave propagation.

We want to report on some investigations which have been carried out in the scope of the research programs of the institutes mentioned above, and which may perhaps be useful for the clarification of geodetic questions, too.

By means of the models of the mean vertical refractive index distribution normally used in radiometeorology and in geodesy (approximation by polynomes [3, 4], by exponential height functions [5, 6], by multilayered models [7], where a linear decrease is supposed up to 1 km) the effects of atmospheric refraction are in general but roughly approximated. This paper deals with some restrictions and limits of these mean models in the lower troposphere.

2. *Refractive Index Structure Near the Surface, Especially Over Sea*

The models mentioned fail (already for the description of the *mean* structure) when used near the surface, where strong vertical gradients (dependent on the stability of the atmospheric stratification) develop as a result of turbulent vertical transfer. The deviations from the neutral equilibrium being not too strong, the height dependence of an exchangeable quality may be represented by logarithmic profiles. The potential refractive index N_p (strictly speaking this should be called potential refractivity defined by $[n_p-1] \cdot 10^6$ where n_p is exactly the potential refractive index) may also be regarded as an exchangeable quality. We write (above a rough surface) [8, 2]:

$$\partial N_p/\partial p = \Gamma \, \Delta N_p/z + z_o \tag{1}$$

(Γ: profile coefficient; z_o: roughness parameter = 0,02 cm over sea [8]; ΔN_p: difference of the potential refractive index between the sea surface and the observation height, in our case always 6 m; Np refers to the height $z = o$). As to the profile coefficient Γ a distinct dependence on Richardson's number *) was discovered, derived from more than one thousand 15-min-vertical profiles of water vapour, temperature, and wind velocity. These measurements were carried out by the „Meteorologisches Institut der Universität Hamburg" over the North Sea and the Baltic Sea [9]. For information some values of the profile coefficient (reference level $z_1 = 4$ m) are presented in table 2 [8, 2]:

Table 2: Profile coefficient Γ as a function of the Ri-number

Ri:	$\leq -0{,}5$	−0,1	−0,05	−0,01	0	0,01	0,05	0,1	0,5
Γ:	0,06	0,065	0,07	0,09	0,1	0,105	0,12	0,14	0,18

*) As stability parameter we use the gradient form of the Ri-number, $Ri = \dfrac{g}{T} \dfrac{\partial \theta/\partial z}{(\partial u/\partial z)^2}$. It can be approximated by logarithmic models; with $\Gamma = 0{,}1$ and $z = 6$ m we get $Ri_b \approx 2 \, \Delta T/u^2$.

In the case of larger deviations from the neutral equilibrium the following equations describe the real profiles in a more exact way [8, 2]:

$$\frac{\partial N_p}{\partial z} = \frac{\Delta N_p}{z + z_o} \cdot \left[\frac{f(R\,i)}{\int_o^{z_1} \frac{f(R\,i)}{z + z_o}\, dz} \right] \quad \text{where} \tag{2}$$

$$f(Ri) = \left(1 + \frac{\alpha}{n} Ri\right)^n \tag{3}$$

Different n-values produce different profile models, α is determined experimentally. With $n = 1$ we get a logarithmic-linear model. With $\alpha = 7$ this model under stable conditions ($Ri > o$) gives useful results; under unstable conditions, especially for $Ri < -0{,}05$, the Ellison-Panofsky model ($n = -1/4$, $\alpha = 4, 5$) is to be preferred. This model obviously describes the observations better than that of Monin-Obukhov ($n = -1$, $\alpha = 4, 5$). In stable range the Rossby-Montgomery model ($n = 1/2$, $\alpha = 4{,}5$) may also be applied.

By means of equation (1), which is usually sufficient for describing the stratification of the different meteorological parameters in the German Bight, one may calculate the height profile of the refractive index, its gradient (i. e. the ray curvature) at a certain height and the mean gradient (i. e. mean ray curvature). Moreover, layer widths on the surface may be specified, in which the gradient of the refractive index is stronger than a given value. In radio wave transmission the thickness of the layer, in which the ray curvature is stronger than the curvature of the earth, the so-called duct is of great importance. In this ground duct an energy transmission with low attenuation is possible, equivalent to large transmission ranges. In order to evaluate the thickness of this evaporation duct (the main reason of its origin being the strong water vapour gradients caused by evaporation) the gradient of the potential refractive index corresponding to the earth curvature has to be inserted in equation (1) or (2), to be solved with regard to z. This critical gradient amounts to $\approx -0{,}125$/m for average meteorological conditions near the surface [2].
Thus the (radio-optical) evaporation duct thickness, called z^*, is obtained:

$$z^* = \Gamma\, \Delta N_p / -0{,}125 \tag{4}$$

Corresponding values of the duct thickness result from equation (2) [2]. Layers with such strong gradients are nearly always present over sea due to evaporation and heat transfer processes.

To demonstrate the strength of the gradients the mean coefficient of refraction $\varkappa$ ($\varkappa = 1/\rho : 1/R$, $1/\rho$: ray curvature, $1/R$: earth curvature) between a height of 0,5 m and the respective upper boundary of the duct are given as a function of the duct thickness z^* in table 3. Column 1 represents the values during logarithmic stratification ($Ri = 0$); columns 2 to 5 show the mean $\varkappa$-values evaluated on the basis of the logarithmic-linear model (column 2 applies for stable condition $Ri = 0{,}006$, columns 3 to 5 for unstable conditions, $Ri = -0{,}006$, $-0{,}012$, and $-0{,}06$).

Table 3: Mean coefficients of refraction within the duct *)

	$Ri = 0$	$Ri = +0{,}006$	$Ri = -0{,}006$	$Ri = -0{,}012$	$Ri = -0{,}06$
z^* $\overline{\varkappa}$:					
3 [m]	1,7	1,7	1,7	1,7	1,7
5	2,3	2,3	2,3	2,3	2,6
10	2,7	2,7	2,8	2,9	3,4
20	3,2	3,0	3,5	3,6	5,0
30	3,6	3,1	3,9	4,2	6,1

For equal duct thickness the gradients ($\varkappa$-values resp.) within the duct (obtained from the logarithmic-linear profile, $\alpha = 4{,}5$) are stronger than those obtained from a logarithmic approximation.

*) Also above the duct the refractive index gradient is superstandard, at a height of the triple duct thickness — values of about 0,5 are still reached.

The strong refraction effects over sea have certain consequences in telemetry [10, 11]. With $\varkappa \to 1$ the curvature corrections disappear.

The equations and models given above also apply for the refractive index in the optical range. In this case the refractive index difference $\Delta N_{opt,\,p}$ of the potential optical refractive indices has to be inserted. The difference $\Delta N_{opt,\,p}$ is largely equivalent to the difference of (potential) temperature between air and sea ($\Delta N_{opt,\,p} = -0{,}95\,\Delta\theta - 0{,}04\,\Delta e$, where $T = 15^0$C, $p = 1013$ *mb*, $f = 60\,\%$). Even the radio-optical duct thickness z^* has its equivalent in the optical range. One effect of the "optical duct", occurring when the air is warmer than the water ($\Delta T > \theta$), is the phenomenon of the elevation of the horizon. In this case the upper boundary of the duct (the „Kimmfläche") is seen as the horizon [12].

For the German Bight some statistics are given for the most important parameters, by which the effects of refraction can be approximated. Table 4 illustrates the values of the radio-optical and the optical refractive index (N_1, $N_{1,\,opt}$ resp.) reached or exceeded in 90%, 50% (median). and 10% of time for the lightships P 8, Elbe 1, and Weser. It shows furthermore the difference of the radio-optical or optical refractive index between a height of 6 m and the sea surface, as well as the duct thickness z^* [13]. *Part a* of the table gives the conditions for the whole year of 1958, *part b* those of a month with poor propagation conditions (January 1958), and *part c* those of a month with good propagation conditions (August).

Table 4a:

		N_1			$N_{1,\,opt}$			$-\Delta N_1$			$-\Delta N_{1,\,opt}$			z^* [m]		
		P8	E1	W	P8	E1	W	P8	E1	W	P8	E1	W	P8	E1	W
	90%:	319	320	321	273	274	275	3,1	1,9	1,6	−3,3	−3,8	−3,7	0,3	0,2	0,6
1958	50%:	325	327	327	278	278	278	20,5	7,1	6,8	−0,4	−0,5	−0,6	5,2	4,3	4,1
	10%:	345	344	345	286	288	288	20,5	17,5	16,9	1,8	2,1	1,7	11,6	10,4	9,2

Table 4b:

	90%:	311	310	310	274	276	278	0,6	1,0	0,5	−4,0	−4,5	−4,5	0,3	0,6	0,2
Jan. 1958	50%:	317	315	315	284	286	286	4,5	4,7	4,2	−0,9	−0,8	−0,9	7,6	8,2	6,2
	10%:	328	325	325	289	292	292	10,7	9,9	9,2	1,2	1,1	1,1	5,7	5,5	5,5

Table 4c:

	90%:	333	322	325	268	270	273	1,5	3,1	1,8	−3,2	−3,7	−3,8	1,3	2,3	1,2
Aug. 1958	50%:	343	343	345	267	270	273	11,0	12,1	9,5	−0,4	−0,5	−0,6	7,6	8,2	6,2
	10%:	351	351	354	267	270	273	20,0	22,9	19,9	1,8	2,1	1,7	11,7	13,9	11,3

The conditions of forming a duct ($z^* > 0$) were present in 98% of the time (for the whole year of 1958). A positive temperature difference air - sea (a requirement for the formation of an optical duct) occurred in 38% (1958) of the time.

It should be emphasized once more that the parameters discussed (and the rafraction properties as well) may be derived from simple meteorological routine measurements. Moreover, measurements at one point over sea are in most cases representative for a large area (cf. Chapt. 4. 1.). Thus a very simple method for determining the propagation conditions in the lowest decameters above the sea surface is given.

The turbulence models presented are also generally applicable over land. The corresponding differences may be obtained from measurements on any two levels, different values of the roughness-parameter z_o have to be used [14, 15]. The main difficulty of getting the refractive index field over land, however, is the high degree of inhomogeneity of the earth surface.

3. Vertical Fine-Structure of Refractive Index Obtained by Refractometer Measurements

In the lower layers of the atmosphere there are always more or less strong deviations from the models of the vertical distribution of the refractive index (described in paragraph 1). The measurements of the vertical refractive index, which will be the subject of the following discussion, are characteristic examples. They were obtained from airborne measurements taken by micro-wave

refractometer of the type NBS 3, and 3A respectively over the German Bight and its coast in the years of 1960 and 1962 [16, 17].

We believe it important to point out that the measuring probes are fixed about 1 m in front of the nose of the plane, which again lies about 1 m in front of the motors. The accuracy of the micro-wave refractometer amounts to $\pm$ 0,1 N; the time response the turbulent variations of our instruments amounts up to about 20 c/s. With higher flow velocities through the resonator the limit of space response lies at about 1 m (own disturbing effect of the cavity [18]). At flying speeds between 60 and 70 m/s space structures down to about 3 m are resolved.

3.1. *Mean Vertical Stratification of Refractive Index Above the Sea*
(April/May and August/September 1960, October 1962)

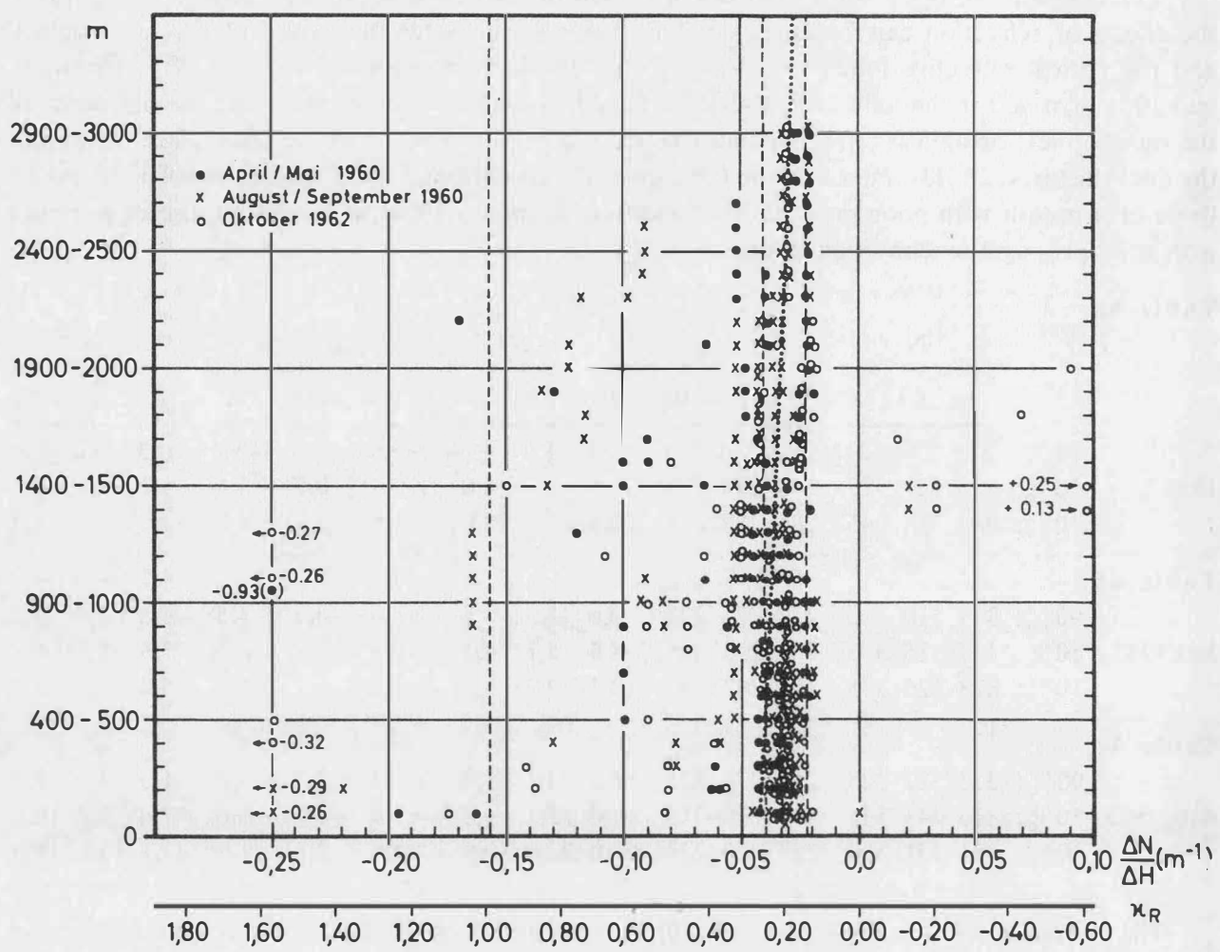

Fig. 1: Height distribution of the mean vertical refractive index gradient near lightship "Elbe I"

$\varkappa_R$ coefficient of refraction for radiowaves
Dashed lines (from left to right):
$\varkappa_R = 1$ critical refraction
$\varkappa_R = 0{,}25$ normal refraction
$\varkappa_R = 0{,}14$ adiabatic decrease of temperature, specific humidity independent of the height, $f = 50\%$, T: 15 to 20° C
Dotted line: changing of $\varkappa$ according to the exponential reference atmosphere
$N = N_s \, exp\,(-z/H)$
$N_s = 310$ in 50 m, $H = 7{,}45$ km
$N = (n - 1) \cdot 10^6$
n: refractive index

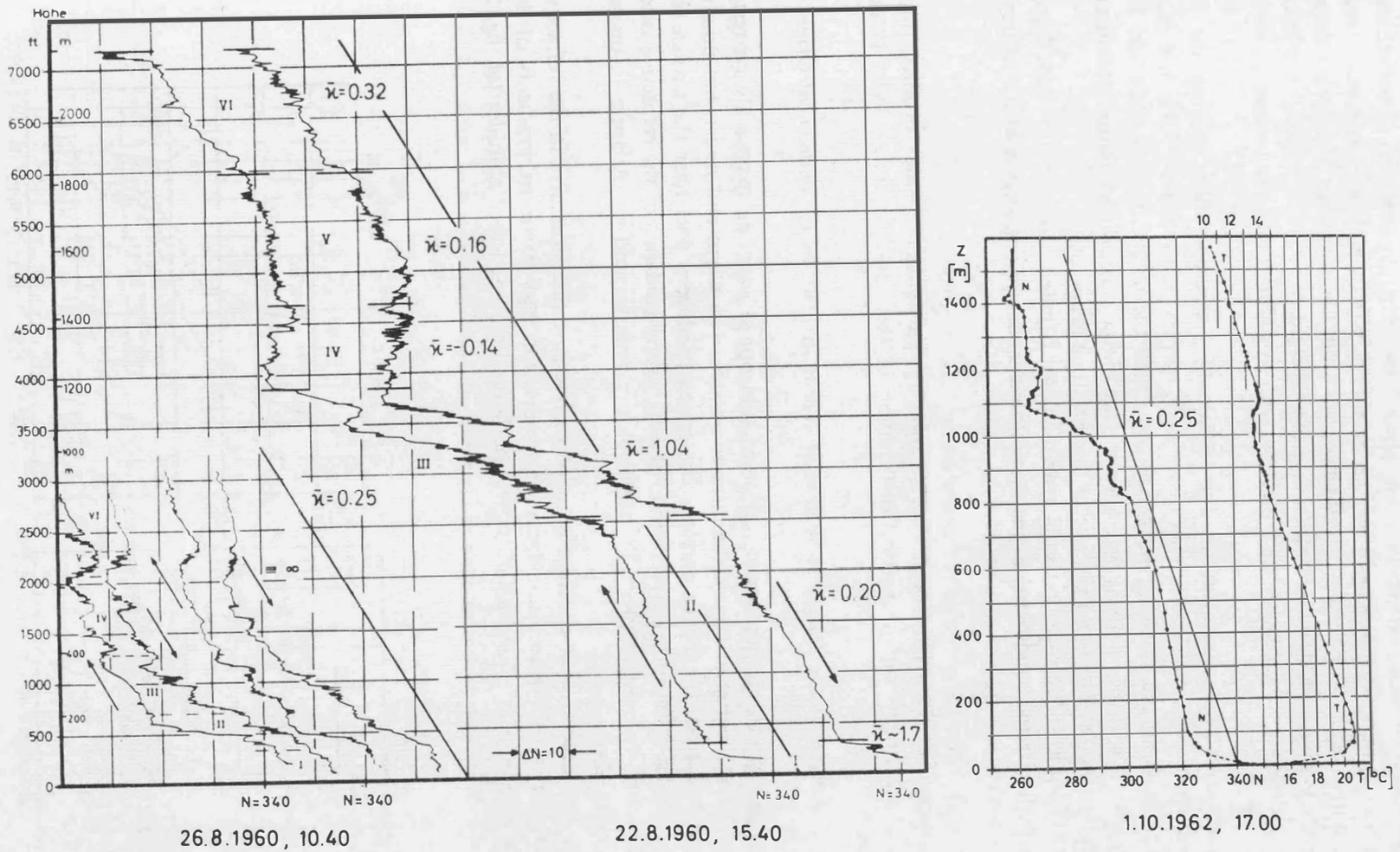

26.8.1960, 10.40

22.8.1960, 15.40

1.10.1962, 17.00

Fig. 2: Refractometer measurements over lightship "Elbe I"

Typical profiles during advection of warm air of subtropical origin

Fig 1. represents results of vertical ascents over lightship Elbe 1 on 23 different measuring days. They provide an insight into the vertical layers of the refractive index appearing mainly in autumn under different weather conditions. The mean gradients refer to intervals of 75 to 100 m.

The strong scattering of the measuring values corresponds to the influence of the different kinds of airmasses and their modifications over sea. The extreme negative gradients of the refractive index (partly with $\varkappa > 1$) have been measured up to a height of 500 m mainly at subsidence-, radiation-, and advection-inversions. Friction-, subsidence-, and upslide-inversions were the meteorological cause for the strong superstandard gradients above a height of 500 m. The positive gradients of the refractive index ($\varkappa < 0$) appeared in connection with upsliding moist air masses as well as with mist layers and clouds.

Apart from these extreme stratifications the remaining measured values, within the first kilometer, accumulate at refraction coefficients of $\varkappa < 0{,}25$, namely at about $\varkappa \approx 0{,}15$. i. e. $\varkappa_{radio} \approx \varkappa_{opt}$, which results from the small humidity variation with the height in well-mixed air. This fact is due to the influence of the relatively warm sea surface on the vertical distribution of temperature and humidity (above the range of influence of the maritime evaporation duct).

The analyses of radio-sonde measurements near the coast (Emden) taken at 12^{00} GMT show (apart from days with extreme conditions) in the first kilometer, due to convection, also coefficients of refraction between 0,1 and 0,2.

3.2 *Typical Cases of Vertical Structure of Refractive Index*

Out of the material at hand have been selected some typical refractive index profiles, which allow some general statements on the vertical distribution of the refractive index under certain weather conditions.

3.2.1. *Profiles of Refractive Index During Advection of Warm Air-Masses of Subtropical Origin in Autumn* (Fig. 2)

Weather situations which account for advection of subtropical warm air-masses always result in layers with distinct vertical gradients of the refractive index. The warm and moist, but unsaturated air-masses flowing from the South over the cooler sea produce a duct near the surface (cf. 22-8-60 and 1-10-62 in fig. 2). Another layer with extremely strong gradients of the refractive index (70 N/400 m on 22-8-60) — consists between the subtropical air-masses and the Atlantic air-masses already upsliding there above.

In addition to the large area layers the formation of intensive fine-structures in the refractive index field is characteristic for these subtropical air-masses. On 26-8-60 strong gradients of the refractive index already appear — under similar weather situation — at lower altitudes (cf. fig. 2, bottom left).

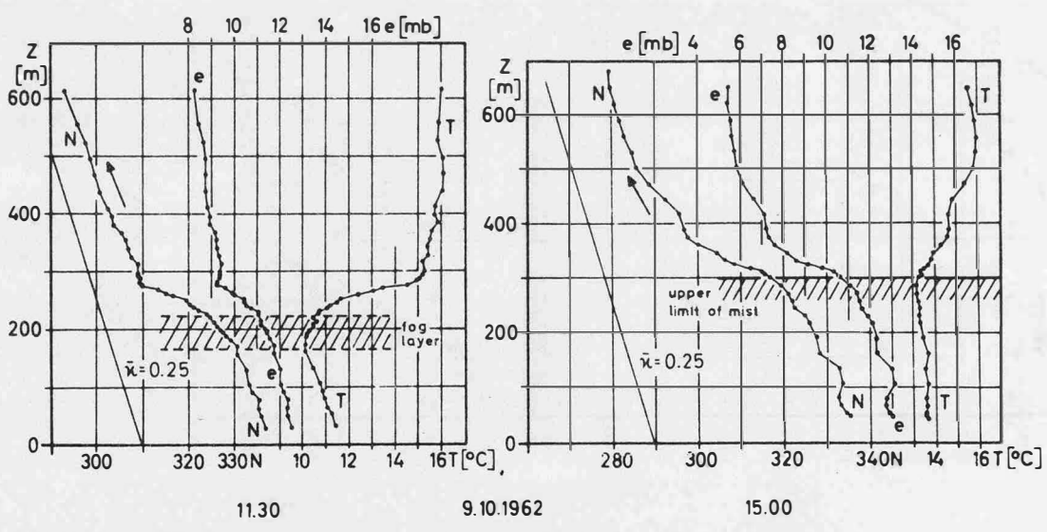

Fig.3: Refractometer measurements over lightship "Elbe I"
Modifications of a radiation and subsidence inversion during a autumnal high pressure situation

3.2.2. *Refractive Index Profiles of High Pressure Areas in Autumn* (Fig. 3)

Characteristic refractive index structures, considerably deviating from the normal atmospheric behaviour, also appear in centres of high pressure (fig. 3). The measurements in the morning (left part of the figure) represent the case of an intense radiation- and subsidence-inversion of a fog-bank at a height of 180 to 220 m. The radiation-inversion causes almost half of the vertical decrease of the refractive index. A coefficient of refraction for radio waves ($\varkappa_{radio}$) of 1,53 and a coefficient of refraction for optical waves ($\varkappa_{opt}$) of 0,69 have been obtained. In the afternoon the distinct inversion weakened by advection of heated continental air (from SE). Above the sea stable conditions developed (contrary to the morning). The decrease of water vapour at the lower limit of the inversion (being at the same time the upper limit of a mist layer) is considerably stronger than in the morning. In this case the following coefficients of refraction observed are $\varkappa_{radio} = 2{,}04$, $\varkappa_{opt} = 0{,}31$.

3.2.3. *Refractive Index Profiles During Advection of Cold Air of Continental Character* (Fig. 4)

Fig. 4 illustrates profile structures of the refractive index developing during the advection of an anticyclonic inflow (from N to NE) of (dry) continental polar air-masses above the warmer sea surface.

Such invasions of cold air-masses promote the forming of the evaporation duct described in paragraph 2. The vertical structures arising above this duct could be devided into two types, which result from the distribution of temperature in the advection layer above the zone of surface friction. The layers discovered are briefly described in the following (fig. 4a).

Type 1: The convective vertical motion exceeds the zone of friction near the ground. The transition from the friction layer to the lower zone of pure convection takes place gradually.

	h (m)	dN/dh	
1.	30 — 685	— 0,025	Surface friction layer. Adiabatic stratification of temperature Tattered clouds.
2.	— 1520	— 0,045	*Moist-unstable* stratification of temperature. Cumuli.
3.	— 1655	— 0,170	Transition into the range of polar air-masses. Temperature inversion. Isotherm temperature distribution.
4.	— 3050	— 0,030	Range of decending dry polar air.
	(top height of the measuring flight)		

Type 2: A moist-stable stratified advection zone limits the friction zone near the ground and blocks the vertical exchange of air-masses. There is a boundary layer, where marked differences of the refractive index are caused by isolated convection cells and parts of clouds, which have penetrated into the dry advection layer. Else the advection layer of polar air-masses appears undisturbed (fig. 4a, right).

	h (m)	dN/dh	
1.	30 — 680	— 0,025	Surface friction layer. Adiabatic stratification of temperature. Tattered clouds.
2.	— 840	— 0,135	Transition into the *moist-stable* advection layer (height of surface friction).
3.	— 1925	— 0,035	Undisturbed advection layer. Cloudless zone.
4.	— 2115	— 0,125	Transition into the range of polar air-masses.
5.	— 3000	— 0,030	Range of descending dry polar air.
	(top height of the measuring light)		

The mean vertical structures obtained under cyclonic influence of maritime polar air-masses (often observed in spring) largely correspond to Type 1 illustrated in fig. 4a. Only in the friction and convection zone near the ground greater space-time variations of the refractive index are observed, especially in the range of moist cloudy air-masses (low fractocumuli). Fig. 4b shows corresponding examples of measurements.

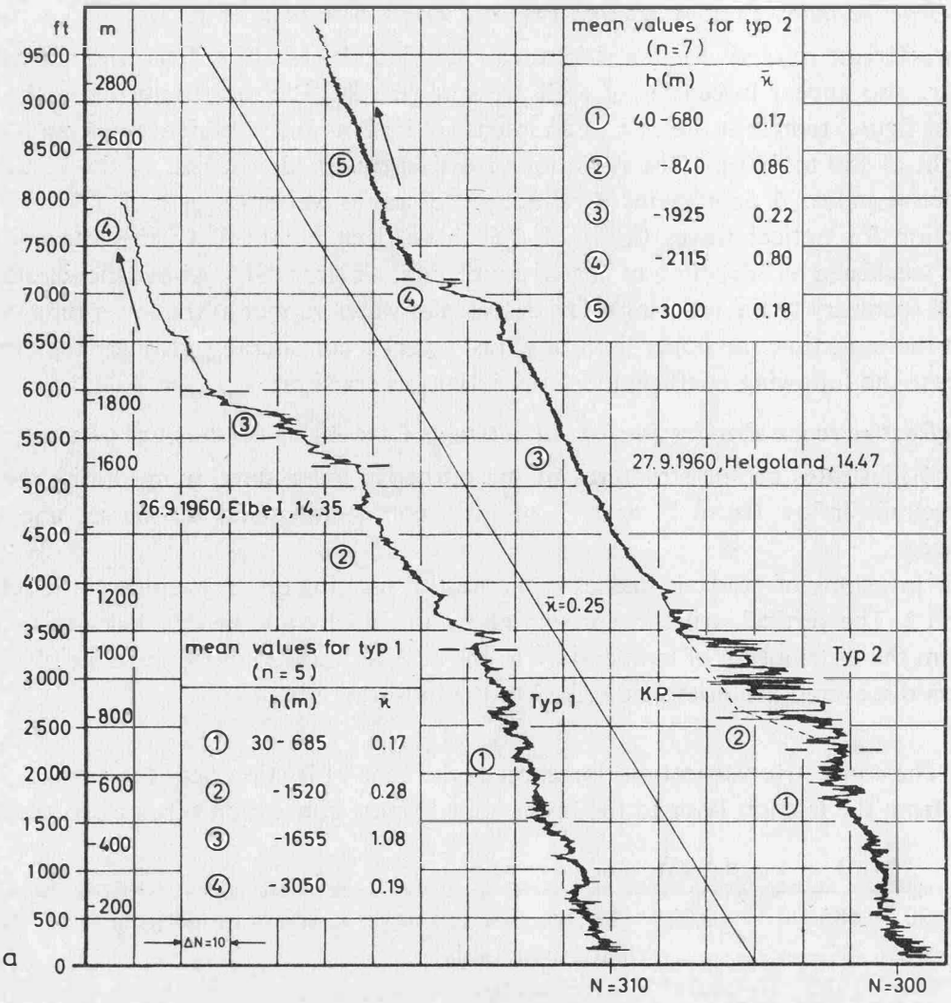

Fig. 4a

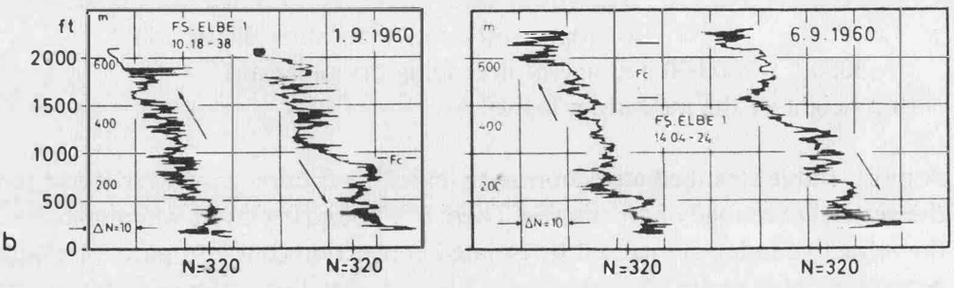

Fig. 4b

Fig. 4a: Two characteristic profiles of refractive index during anticyclonic advection of cold continental air masses

Fig. 4b: Refractive index structures near surface under the influence of cold maritime air masses

4. *Horizontal Inhomogeneities of Refractive Index*

4.1. *Homogeneity of Atmospheric Stratification Above Sea*

The models of refractive index distribution do not account for changes of the refractive index in horizontal direction. Near the surface, however, this assumption is guaranteed only exeptionally. Even above the sea, especially of course near the coast, greater differences can be observed under certain meteorological conditions (even if frontal zones and land-sea breeze effects are not taken into account). This problem, which is of importance also for the practice of geodetical measurements, was investigated by simultaneous meteorological measurements (6 weeks) at several places in the German Bight [19, 9]. The measurements taken at a fixed point of the open sea proved to be representative for an area of about 70 km and near the coast (at least during the period of investigation)

for a range of about 40 km. Particularly the latter statement might only be valid when western winds predominate (long distance over sea covered by the air-masses). Under weather conditions with land winds considerable differences in the meteorological field near the coast may appear. Table 5 gives some statistics of horizontal variations of differences in the refractive index (ΔN_1) between a height of 6 m and the sea surface (important for questions of radio-wave propagation, cf. equations 1,2,4), and of the corresponding differences of air-water temperatures (ΔT) between the lightships Elbe 1 — Weser (distance 25 km), P 8 — Weser (63 km), and P 8 — Elbe 1 (70 km) [13]. For ΔN the median values (50%) of the absolute differences for the two long-distance lightship combinations (P 8 — Elbe 1, P 8 — Weser) amount in January to 1,6 N and in August to 4,3N. The respective values for ΔT are 0,8°C and 0,6°C. It can be seen that there may occur differences for ΔN as well as for ΔT, which are incompatible with the postulation of a horizontal homogeneity. In 10% of the time there are differences, which at distances of about 65 km are greater than 5N (January) or 11N (August) for ΔN and 2,0°C (January) and 1,5°C (August) for ΔT respectively.

Table 5: Absolute horizontal differences of $\Delta N = N_{6m} - N_{om}$ and $\Delta T = T_{6m} - T_{om}$ between the lightships Elbe 1 and Weser (25 km), P8 and Weser (63 km), and P 8 and Elbe 1 (70 km) in January and August 1958
Here are shown the values, which have been reached or exceeded in x% of all observed cases:

Table 5a: $|\Delta N_{(1)} - \Delta N_{(2)}|$:

	(1)	(2)	90%	50%	25%	10%	5%	1%
	Elbe 1	— Weser:	0,3	1,3	2,2	3,4	4,5	6,8 [N_{units}]
January 1958	P8	— Weser:	0,4	1,7	3,2	5,2	6,4	10,3 [N_{units}]
	P8	— Elbe 1:	0,2	1,6	2,9	4,7	6,2	11,4 [N_{units}]
	Elbe 1	— Weser:	0,4	3,4	6,7	10,5	14,0	27,0 [N_{units}]
August 1958	P8	— Weser:	0,4	4,9	8,0	12,0	16,0	23,0 [N_{units}]
	P8	— Elbe 1:	0,4	3,7	7,0	10,5	14,7	20,7 [N_{units}]

Table 5b: $|\Delta T_{(1)} - \Delta T_{(2)}|$:

	(1)	(2)	90%	50%	25%	10%	5%	1%
	Elbe 1	— Weser:	0,1	0,5	1,0	1,4	1,8	2,8 [°C]
January 1958	P8	— Weser:	0,2	0,8	1,3	1,9	2,5	3,6 [°C]
	P8	— Elbe 1:	0,2	0,8	1,3	2,0	2,2	3,1 [°C]
	Elbe 1	— Weser:	0,1	0,5	0,9	1,2	1,5	2,2 [°C]
August 1958	P8	— Weser:	0,1	0,6	1,0	1,5	2,1	2,6 [°C]
	P8	— Elbe 1:	0,2	0,6	1,0	1,5	1,8	2,7 [°C]

The greater spatial differences arise primarily under weather conditions with land winds, especially in summer when there are striking differences of temperature and humidity between sea and land. Fig. 5 may illustrate this fact. It represents the mean diurnal variations of ΔN (summer 1958) at the three lightships mentioned above during a so-called anticyclonic "Südlage" and in a cyclonic "Westlage". Apart from the dependence of the amplitude of the diurnal variation on the distance from the coast (P 8 shows the slightest variations) and apart from the great differences of diurnal variations under the two weather situations the figure illustrates that the horizontal differences in a "Südlage" (land winds) can reach considerable values.

4.2. Horizontal Differences of Refractive Index Obtained by Refractometer Measurements

Over sea, especially in the boundary range of sea and coast, we frequently observed remarkable spatial inhomogeneities of the refractive index and strong variations of its spatial mean value.

In figures 6 and 7 examples of measurements during anticyclonic weather situations with land winds are given.

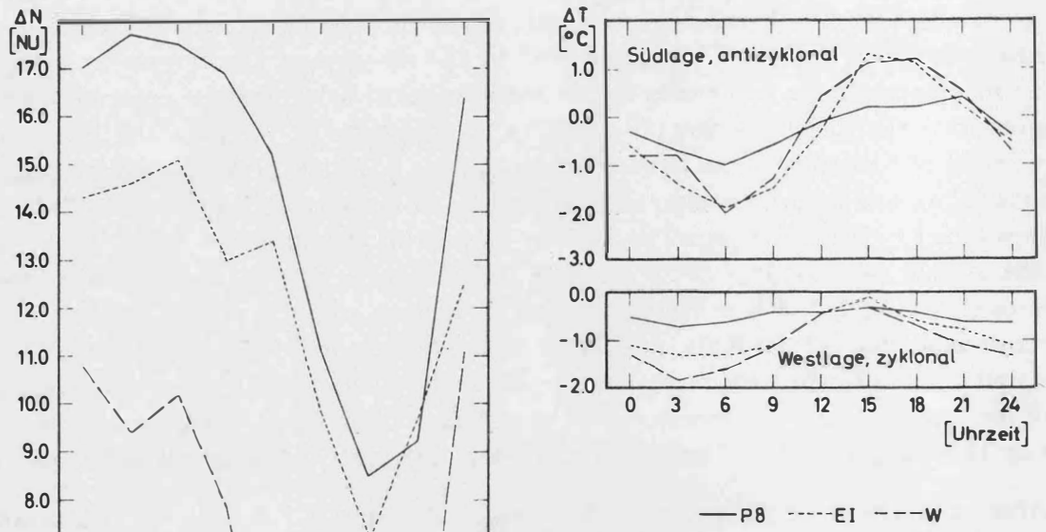

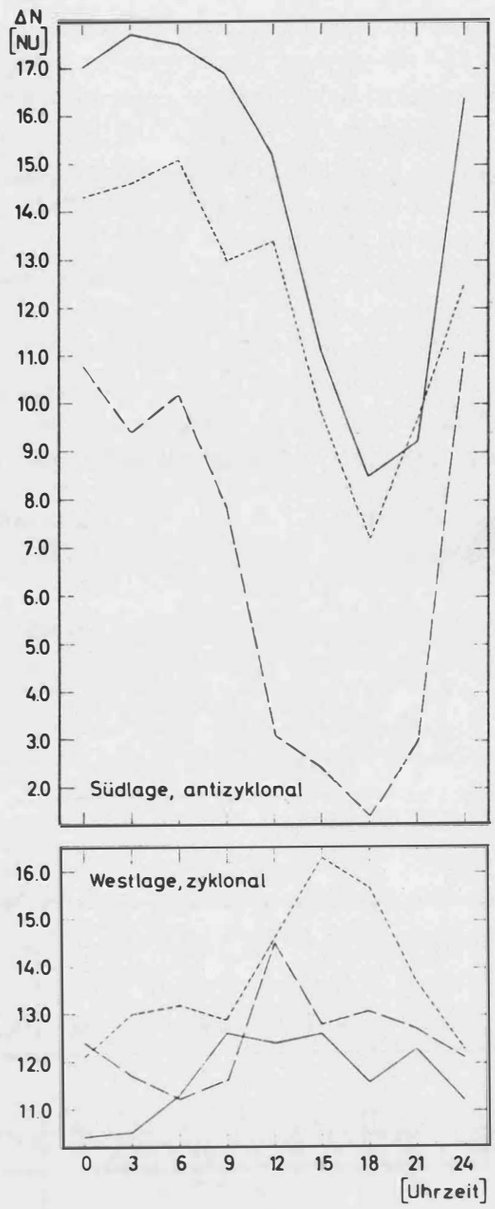

Fig. 5 : Mean diurnal variation of the vertical differences of refractive index during two different weather situations (Summer 1958)

—— P8, ---- EI, — — W.

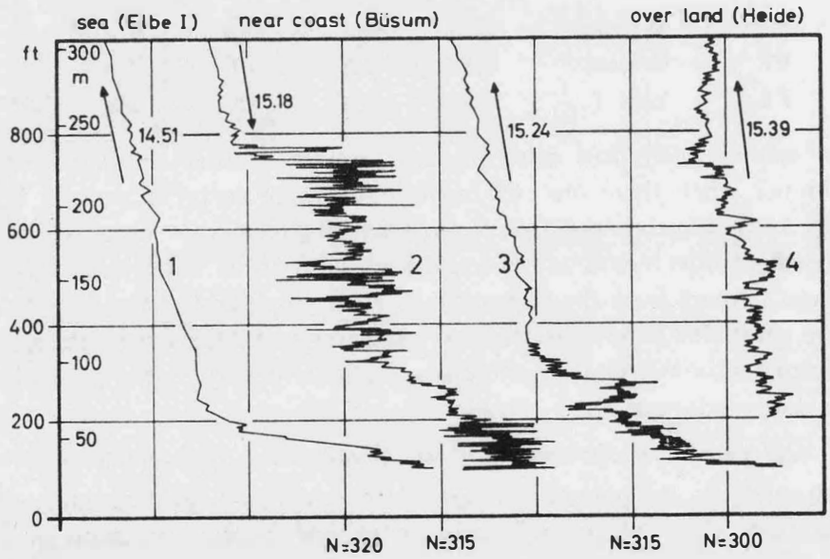

Fig. 7 : Vertical profiles of refractive index on several places 5. 5. 1960

Refractometer measurements

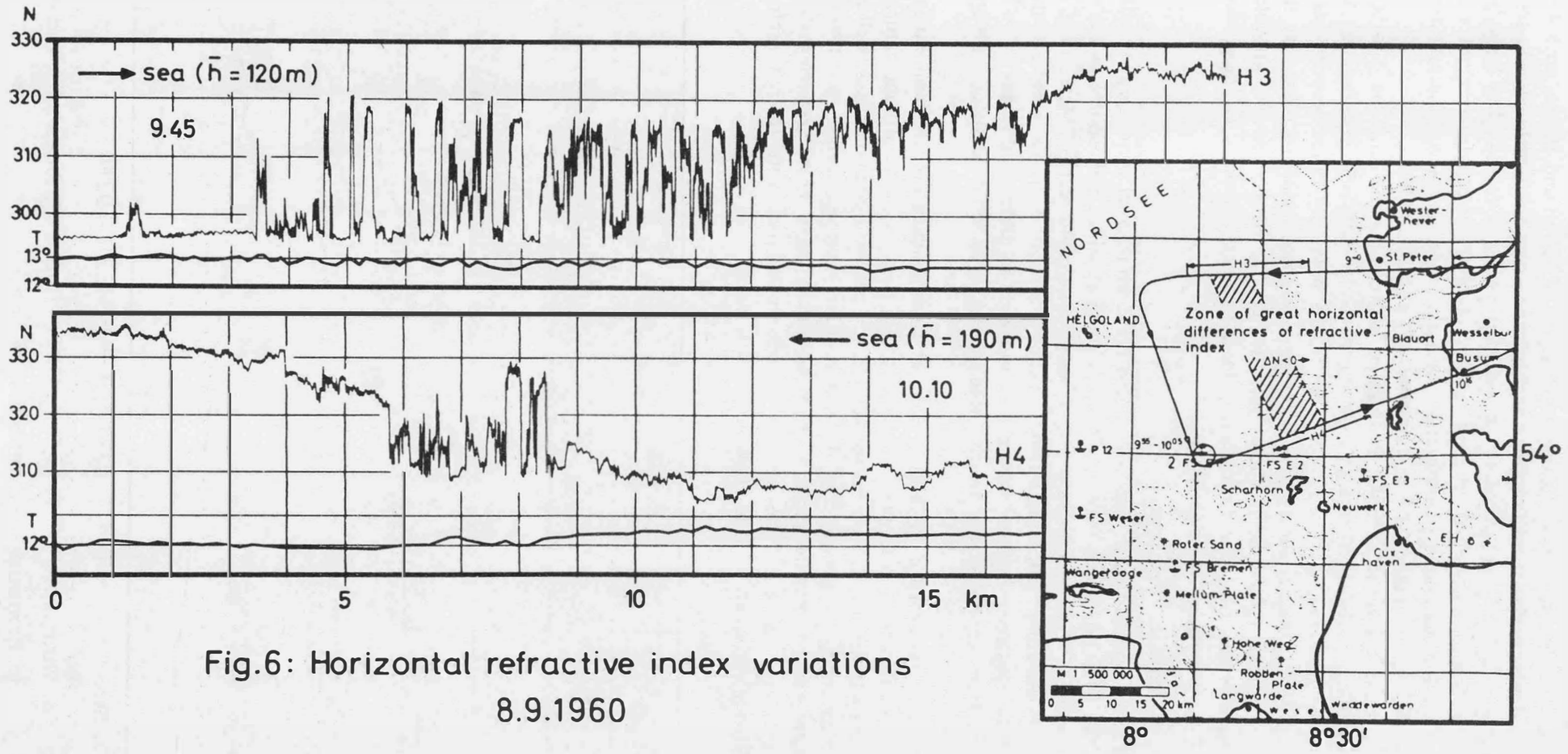

Fig.6: Horizontal refractive index variations
8.9.1960

Course of measuring flight

Figure 6 shows the horizontal flights at the heights of 120 m and 190 m, on 8-9-1960, in the morning. This day there was a small centre of high pressure over the North-Sea. Masses of dry land air (modified polar air) drifted against the moister air-masses over sea. The boundary range is characterized by a mean horizontal difference of the (absolute value) refractive index of about 25 N within a few kilometers only. In connection with this there are horizontal inhomogeneities of the refractive index (due humidity) with comparatively equal amplitudes.

Figure 7 represents vertical profiles in the area between sea and land, on 5-5-1960. It shows measurements during advection of warm air-masses under anticyclonic influence. A stationary surface duct has developed over sea (profile 1). In the boundary range between sea and coast (profile 2 and 3) this duct is superposed by strong time-space variations caused by the influence of flats and by advection from land, where convection during the day appeared (profile 4). Similar conditions were always observed during anticyclonic weather situations. To the geodesist they represent most adverse measuring conditions.

4.3 *Internal Waves in the Atmosphere*

Spatial inhomogeneities also appear in connection with internal waves (gravity waves, 10 min-periods on the average), which may develop in a stable-stratified atmosphere or on an inversion surface, respectively. These problems are also being investigated at the "Meteorologische Institut der Universität Hamburg" [20, 21] and that by means of a net of microbarographs on the one hand, and by simultaneous recordings of temperature and wind in different altitudes up to 250 m on a radio mast in Hamburg-Billwerder or by those of captive balloons equipped with special radiosondes on the other hand.

The examples presented in fig. 8 show the changes of temperature which appear in connection with vertical oscillations in a ground inversion (400 m thick, increase of temperature by 7°C) at different heights (upper part), their horizontal and vertical wind components as well as the micro pressure variations on the ground. The alternation of an isentropic surface ($\theta = 17^0$) derived from the temperature field is equally added to the figure (lower part). There are changes of altitude of about 100 m. Under such conditions also the humidity and consequently the radio refractive index, too, show strong variations (as other measurements reveal).

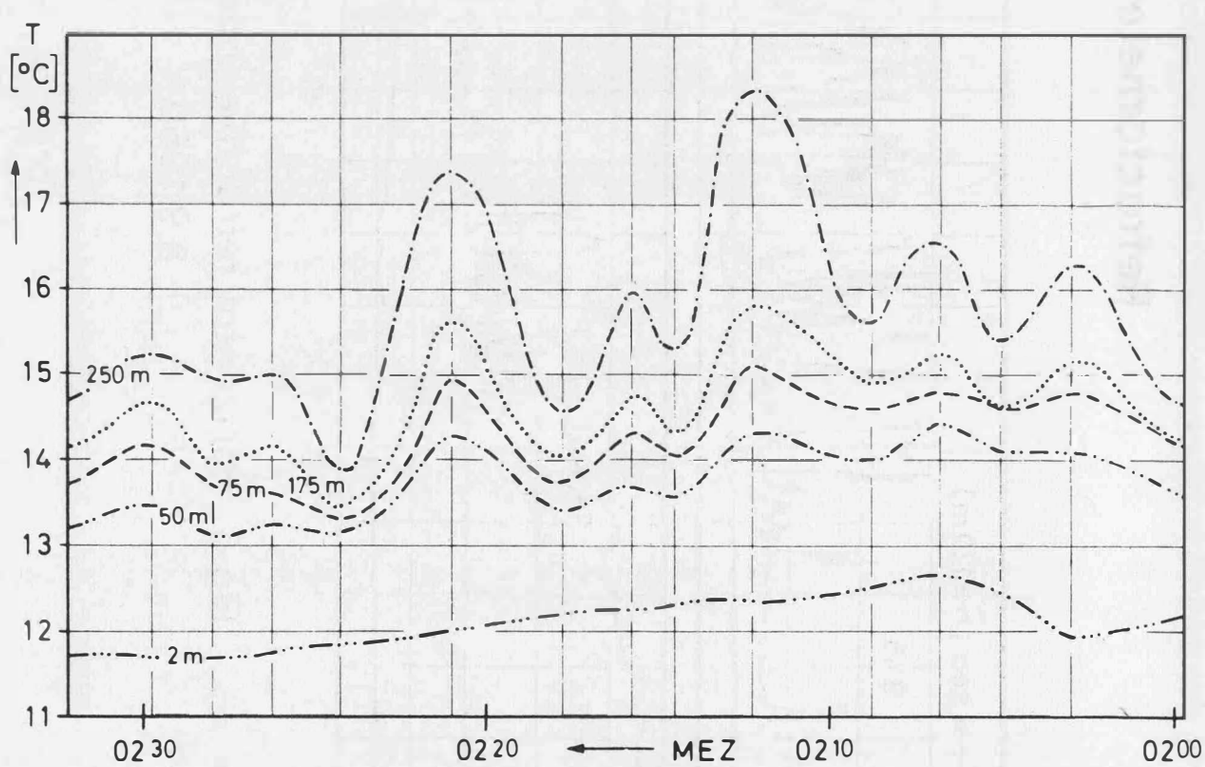

Fig. 8a: Variations of temperature in different altitudes at a radio-mast in Hamburg-Billwerder, 14.5.1966

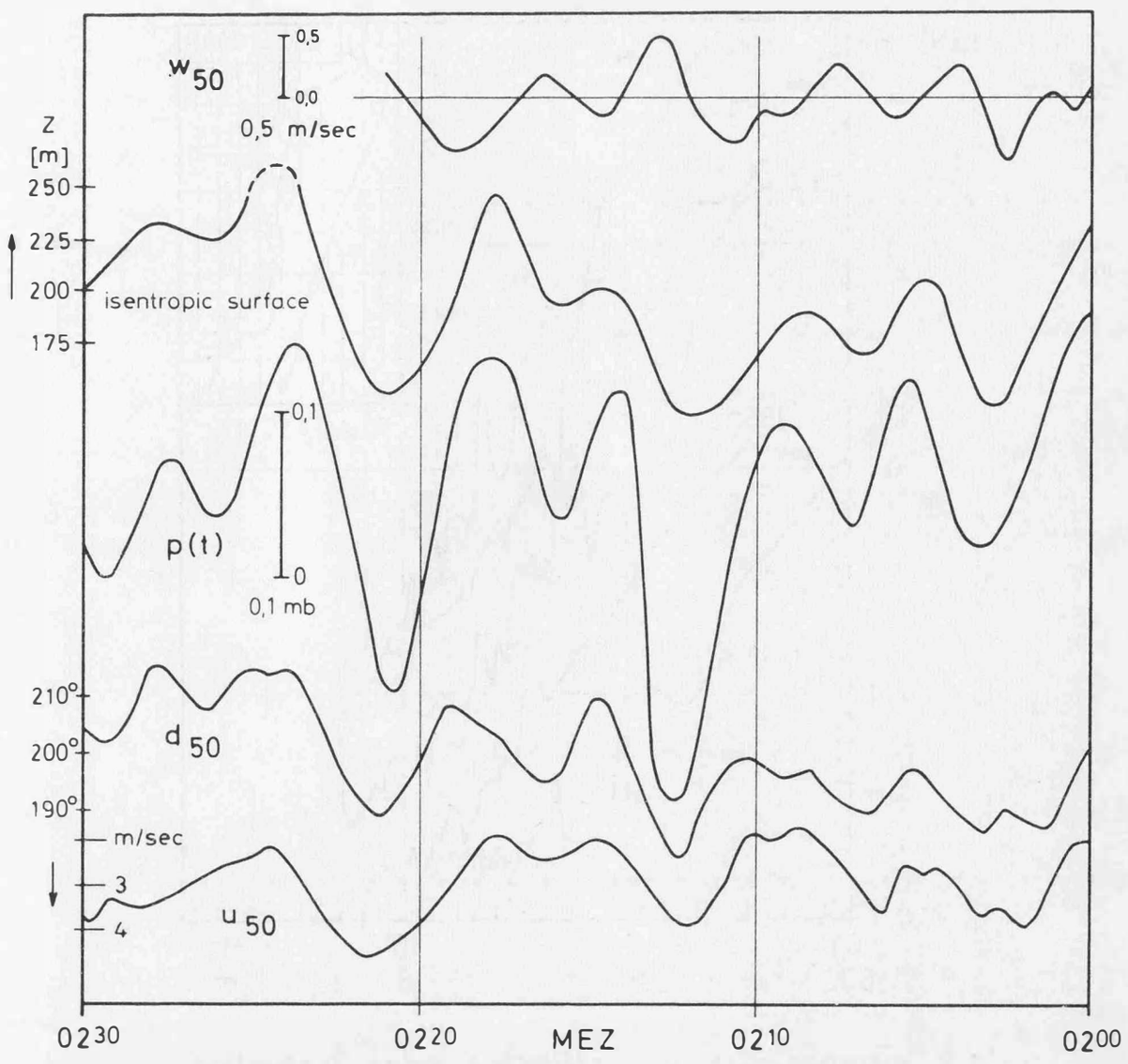

Fig. 8b: Variations of horizontal (u_{50} m) and vertical (w_{50} m) windspeed, winddirection (d_{50} m), micro-pressure at the ground and calculated height variations of an isentropic surface

This is another instructive example for the complexity of the atmosphere illustrating the difficulties arising from it also for the surveyor (as to the most convenient altitude of observation, the order of reading the instruments during the process of meteorological measurements etc.). These wavy layers often are also the cause of so-called radar holes.

5. *Fluctuations of Refractive Index*

The random variations in space and time of refractive index in the always and everywhere turbulent atmosphere are perhaps of not so great interest for geodetic practice. These fluctuations are one of the sources of noise in the measuring system (disturbance of the indicating device etc.), because the N-pulsations are connected with phase fluctuations $\Delta\varnothing$ ($\Delta\varnothing = \{2\pi \,.\, 2d \,.\, \Delta N/\lambda_o\} \,.\, 10^{-6}$, d: distance, λ_o: vacuum wave length). But this problem seems to be no critical point for the geodetic observer. To give an insight into the appearing pulsations of refractive index a typical example of variance-spectra of refractive index fluctuations is shown in fig. 9. These spectra are derived from horizontal refractometer flights (1 min) by means of the autocorrelation method of Blackmann and Tuckey [22].

Measurements taken at a height of 56 and 75 m above the North Sea represent a fairly large total variance ($\overline{\Delta N^2} = 2{,}8$ and 1,4 resp. – always referred to the frequency range from 0,1 to 20 Hz). The fluctuations diminish with increasing height (see also the measurements at the heights of 955 m, $\overline{\Delta N^2} = 0{,}2$, and 1268 m, $\overline{\Delta N^2} = 0{,}1$) unless there are layers. The spectrum of the fluctu-

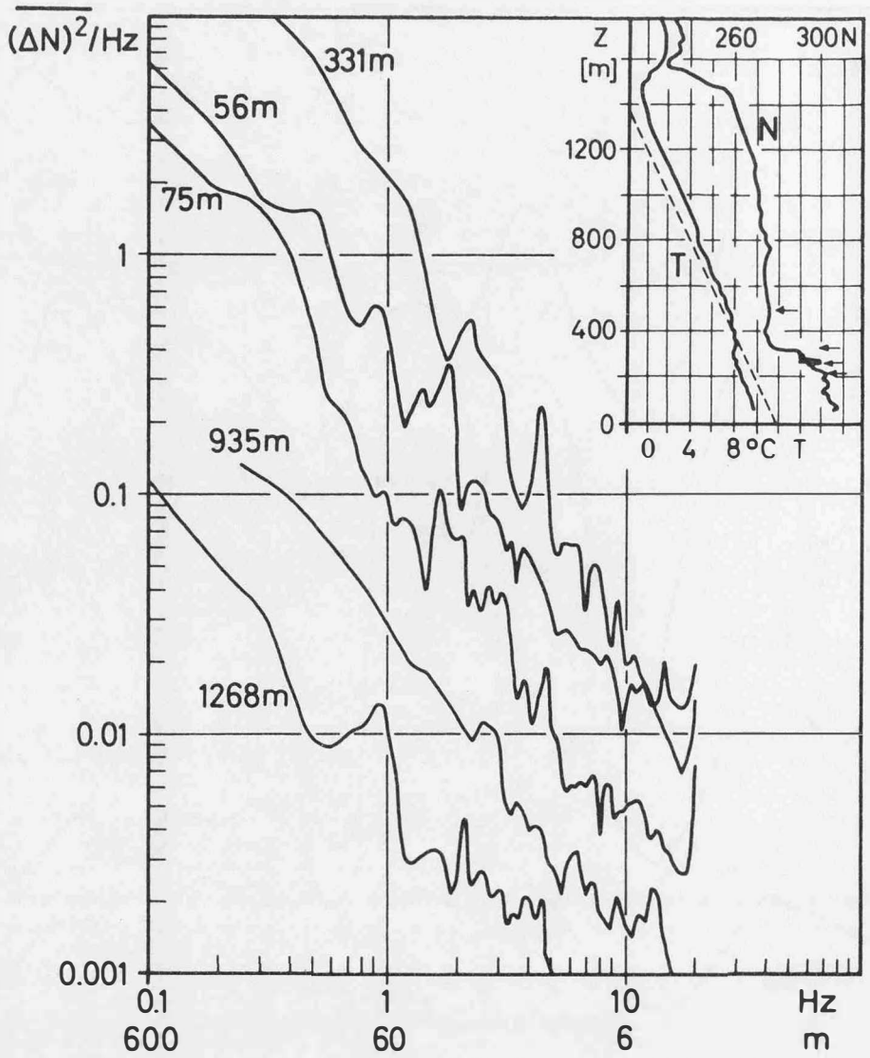

Fig. 9 : Variance-spectra of refractive index fluctuations
German Bight, 15.X.1962 10^{53}-11^{46}

ations near an inversion is illustrated by the horizontal cross-section at a height of 331 m, which was taken directly above the inversion. The total variance $\overline{\Delta N^2}$ amounts to 13. The spectra can be approximated by the relation $\overline{\Delta N^2}/f \sim f^{-n}$. The statistical turbulence theory of Kolmogoroff-Heisenberg gives an exponent of $-5/3$ in the case of isotropic, homogeneous turbulence. The exponents measured all over the world vary between about -1 and -3, but seem to approach $-5/3$ under adiabatic conditions.

The investigations with regard to the comprehension of the atmospheric refractive index field will be continued.

Literature

1. *Brocks, K.* and *H. Jeske:* Analyse gleichzeitiger Feldstärkeregistrierungen über der Nordsee auf den Frequenzen 7; 2; 0, 6; 0,2 und 0,16 GHz
Radiometeorologische Abteilung des Geophysikalischen Instituts der Universität Hamburg, Bericht Nr. 4, 1961
2. *Jeske, H.:* Die Ausbreitung elektromagnetischer Wellen im cm- bis m-Band über dem Meer unter besonderer Berücksichtigung der meteorologischen Bedingungen in der maritimen Grenzschicht
Hamburger Geophysikalische Einzelschriften, Heft 6, Cram, de Gruyter u. Co., Hamburg 1965
3. *Eckart, G. und H. Plendl:* Die Überwindung der Erdkrümmung bei Ultrakurzwellen durch die Strahlenbrechung in der Atmosphäre
Hochfrequenztechnik und Elektroakustik, Bd. 52, Heft 2, 1938

4. *Millman, G. H.:* Atmosperic Effects on VHF and UHF Propagation
Proceedings of the IRE, Vol. 46, No. 8, 1958, p. 1492–1501
5. *Bean, B. R. and G. D. Thayer:* On Models of the Atmospheric Refractive Index
Proceedings of the IRE, Vol. 47, No. 5, 1959, p. 740–755
6. *Bean, B. R.:* Concerning the Bi-Exponential Nature of the Tropospheric Radio Refractive Index.
Zeitschr. Phys. d. Atmosphäre, 34, 1961
7. *Bean, B. R., and E. J. Dutton:* Radio Meteorology
National Bureau of Standards Monograph 92, Boulder, Colorado, 1966, p. 59–65
United States Department of Commerce
8. *Brocks, K.:* Models of the Troposphere Derived from Direct Measurements of the Atmospheric Refractive Index
In: Progress in Radio Science 1960–1963, Vol. II, edited by Du Castel;
Elsevier Publishing Comp., Amsterdam/London/New York, 1965
9. *Brocks, K.:* Probleme der maritimen Grenzschicht der Atmosphäre
Berichte d. Deutschen Wetterdienstes Nr. 91, Offenbach/M., 1964
10. *Höpcke, W.:* Streckenmessung über See
(ZfV, Heft 11, 1964)
11. *Seeger, H.:* Ein Beitrag zur elektromagnetischen Streckenmessung mit 3 cm-Trägerwellen (10 GHz), insbesondere mit dem Elektrotape DM-20
Wissenschaftliche Arbeiten der Institute für Geodäsie und Photogrammetrie der Technischen Hochschule Hannover, 1965
12. *Hasse, L.:* Über den Zusammenhang der Kimmtiefe mit meteorologischen Größen.
Deutsche Hydrogr. Zeitschr., Bd. 13, S. 181, 1960
13. *Pirwitz, K. P.:* Zeitliche Gänge und räumliche Unterschiede der meteorologischen Parameter in der Deutschen Bucht speziell im Hinblick auf die Ausbreitung elektromagnetischer Wellen im maritimen Wellenleiter
Diplomarbeit, Meteorologisches Institut der Universität Hamburg, 1967
14. *Deacon, E. L.:* Vertical Diffusion in the Atmosphere
Quart. J. Roy. Meteorol. Soc. 75, 1949
15. *Priestley, C. H. B.:* Turbulent Transfer in the Lower Atmosphere
University of Chicago Press, Chicago 1959
16. *Kruspe, G.:* Untersuchung von Brechungswertschichtungen über See mit einem im Flugzeug installierten Mikrowellenrefraktometer unter besonderer Berücksichtigung meteorologischer Aspekte
Berichte des Instituts für Radiometeorologie und Maritime Meteorologie an der Universität Hamburg, Nr. 11, Hamburg 1966
17. *Müller, H.:* Messungen vertikaler Brechungsindex- und Temperaturschichtungen in der Troposphäre und ihre Bedeutung für die Radiowellenausbreitung
Berichte des Instituts für Radiometeorologie und Maritime Meteorologie an der Universität Hamburg, Nr. 12, Hamburg 1967 (to be published)
18. *Bean, B. R., R. E. McGavin and R. O. Giher:* The Response of Microwave Refractometer Cavities in Atmosphpric Variations. Proc. 1964 World Conference on Radio Meteorology, Boulder, Colorado, September 1964
19. *Fengler, G.:* Die Homogenität des meteorologischen Feldes über See
Deutsche Hydrogr. Zeitschr., Bd. 19, Heft 3, 1966
20. *Stilke, G.:* On Methods and Results of our Refractive Index Measurements, Carried out with Kytoon-borne Radiosondes and Airborne Refractometers.
1964 World Conference on Radio Meteorology Incorporating the Eleventh Weather Radar Conference, Boulder, Colorado, September 1964, p. 258–263
21. *Stilke, G.:* Meteorologisches Institut der Universität Hamburg,
Persönliche Mitteilung, 1967
22. *Blackman, R. B. and J. W. Tukey:* The Measurement of Power Spectra
Dover Publications, Inc., New York, 1958

B. Errors and Sources of Errors

Investigations on Errors in the Determination of Astronomical Refraction

by *Karl Ramsayer*, Stuttgart

1. *Introduction*

It is well known, that the accuracy of the astronomical determination of latitude, longitude and azimuth is limited by the accuracy of the determination of the astronomical refraction. This is accepted as an inevitable fact, and has led to the general opinion that for precise astronomical measurements it is absolutely necessary to observe during several nights to reduce the influence of refraction anomalies. This opinion means a severe reduction of the efficiency of the celestial geodesy. This efficiency would be increased by several hundred percents, if we could reduce the time of observations at a station to one single night, and if we could get an information that the influence of the refraction errors is within an admissible limit. In the following report it will be shown that this goal seems to be within reach.

The observation methods may be divided in observations of zenith distances and observations of vertical transits. The latter are influenced by the lateral refraction, which is assumed to be zero. The zenith distances are influenced by the vertical refraction, which is so large that it must be determined and taken into account. In the following we will only investigate the errors of the determination of the vertical refraction. These errors we will shortly call refraction errors.

2. *Survey of the refraction errors*

Table 1 gives a brief survey of the essential sources of the refraction errors.

1. Actual atmosphere $\neq$ model atmosphere.
2. Inclination of the optical layers.
3. Deviation of the mean partial pressure of water steam.
4. Deviation of colour.
5. Motions of the air.
6. Errors of measured pressure and temperature.

Table 1

The influence of the error sources No. 3 — No. 6 is not important. The resulting refraction errors on the one hand may be determined with a sufficient accuracy or on the other hand may be compensated by the observation of pairs of stars with equal zenith distances and an azimuth difference of 180^0, or, if the errors have a random or periodical distribution their influence may be reduced by increasing the number of observations.

3. *Computation of the astronomical refraction*

Before we investigate the influence of the error sources No. 1 and No. 2 we will remember how the astronomical refraction is computed. The atmosphere is divided in thin layers with constant refractive index n, Fig. 1. The angle between the beam of light coming from a star and the perpendiculars to the layers shall be i. Then the refraction R is exactly given by the formula

$$R = \rho'' \int_B^O \tan i \cdot \frac{dn}{n}, \quad \rho'' = 206\,265'', \tag{1}$$

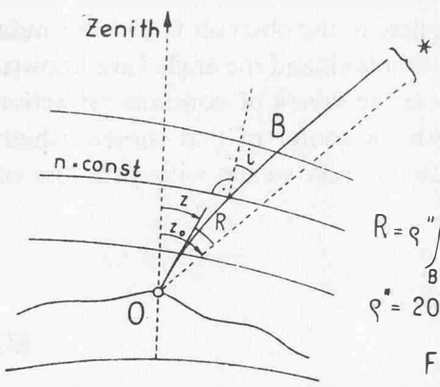

$$R = \varrho'' \int_B^0 \tan i \cdot \frac{dn}{n}$$

$\varrho'' = 206\,265''$

Fig. 1.

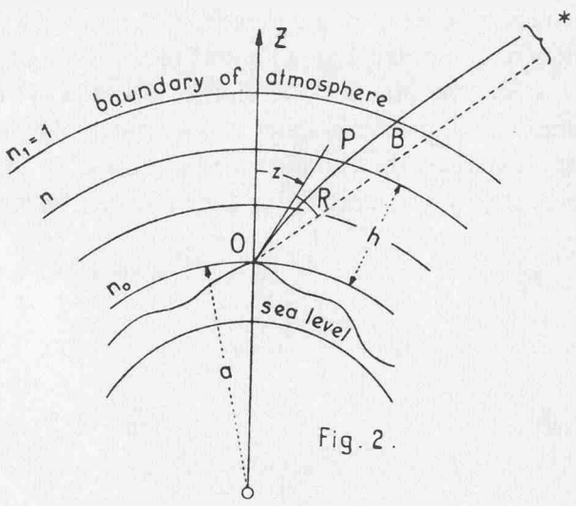

Fig. 2.

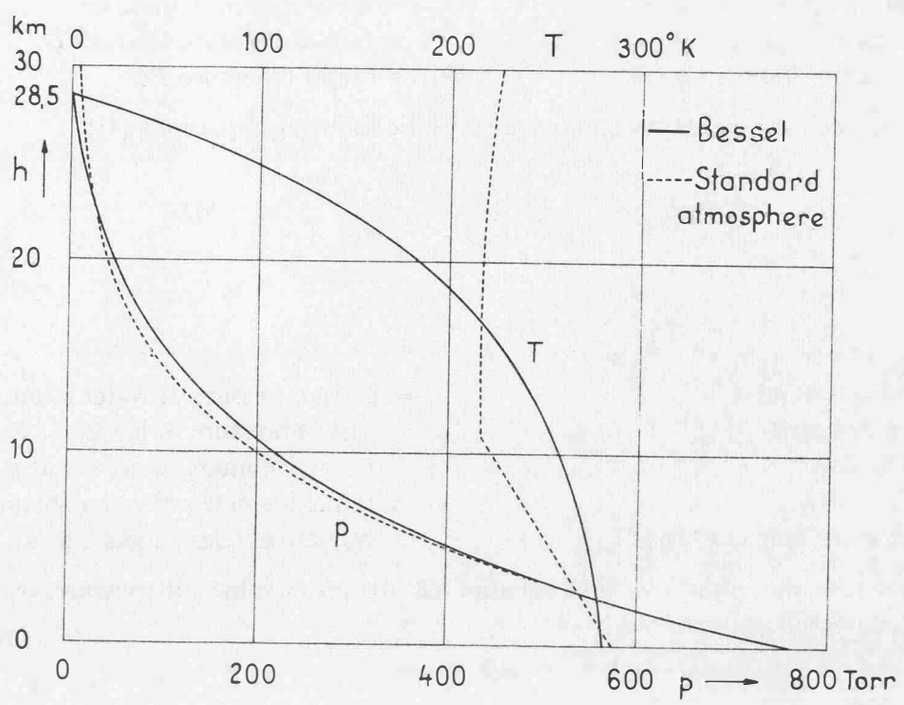

Fig. 4

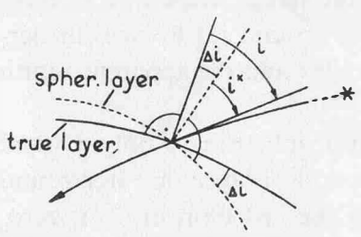

Fig. 5.

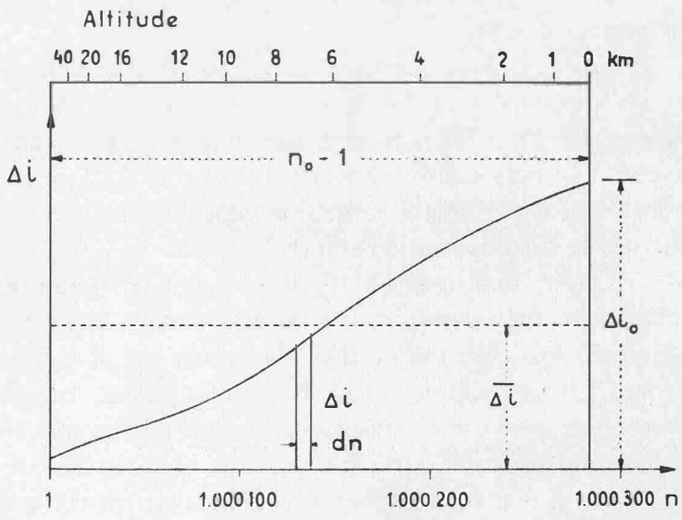

Fig. 6.

whereby we have to integrate from the boundary B of the atmosphere to the observer 0. This formula may be computed, if in all points of the beam of light the refractive index n and the angle i are known.

For the practical solution of formula (1) it is assumed, that the layers of constant refractive index are concentric spheres, the center of which coincides with the center of that sphere, which approximates the equipotential surface in 0, Fig. 2. With this assumption we get without a loss of accuracy worth mentioning the following formula:

$$R = \rho'' (n_o - 1) \tan z + \frac{1}{2} \rho'' (n_o - 1)^2 \cdot \tan^3 z - \tan z (1 + \tan^2 z) \cdot \frac{\rho''}{a} \int_{n_o}^{n_1} h \cdot d\left(\frac{n_o}{n}\right). \tag{2}$$

R = refraction
n_o = refractive index in O
n = refractive index in P
n_1 = refractive index in $B = 1$
ρ'' = 206 265″
z = apparent zenith distance
a = radius of sphere through O
h = height difference PO.

The refractive index n may be computed from the following equations [1]:

Troposphere:
$$n - 1 = \frac{p}{p_o} \cdot \frac{T_o}{T} (\nu_2 - 1) - \frac{e}{p_o} \cdot \frac{T_o}{T} (\nu_2 - \nu_1), \tag{3}$$

Stratosphere:
$$n - 1 = \frac{T}{T_o} \sum \frac{p_\beta}{p_o} (\nu_\beta - 1). \tag{4}$$

n = refractive index
p = air pressure
p_o = 760 Torr
T_o = 273,15 ^0K
T = absolute temperature
e = partial pressure of water steam,
p_β = partial pressure of gas β,
ν_2 = refractive index of dry air at p_o, T_o
ν_1 = refractive index of water steam at p_o, T_o
ν_β = refractive index of gas β at p_o, T_o.

If we compute the refraction from equation (2) for mean values of pressure, temperature etc. we get the normal refraction at sea level

$$R_m = 58'', 282 \cdot \tan z + 0'',0082 \cdot \tan^3 z - 0'',0762 \tan z (1 + \tan^2 z). \tag{5}$$
$$p_o = 760{,}3 \text{ Torr}, \; T_o = 282{,}55^0 K, \; e_o = 4.8 \text{ Torr}.$$

The last term corresponds to the influence of the atmosphere above the observation station for average conditions.

From Fig. 3 we see that for $z < 60^0$ this influence is extremely small. Hence for $z < 60^0$ and always supposed that the optical layers are concentric spheres even large deviations of the actual atmosphere from the standard atmosphere (e. g. by an inversion of the temperature in the lower layers) may only cause refraction errors $< 0'',2$. If we compare formula (2) and (5) we see furthermore that for $z < 70^0$ the refraction depends mainly on the refractive index and the apparent zenith distance in the observation station.

The fact, that changes of pressure and temperature within the atmosphere have only a small influence to the refraction, is seen very clearly, if we assume that the optical layers are horizontal planes. In this case the radii of the layers are of infinite size, so that the last term in (2) is zero. Hence, if the optical layers are horizontal planes, the refraction depends only on z and n_0, and the atmosphere above the observation station has no influence at all. The fact that the atmosphere in reality influences the refraction depends only on the curvature of the optical layers.

Table 2 is a further demonstration, that the refraction is nearly independent from the model atmosphere used for the computation of the normal refraction.

$$R = \varrho''(n_0 - 1)\tan z + \tfrac{1}{2}\varrho''(n_0-1)^2 \cdot \tan^3 z - \Delta R$$

$$\Delta R = \tan z\,(1+\tan^2 z)\cdot \frac{\varrho''}{a}\int_{n_0}^{n_1} h \cdot d\left(\frac{n_0}{n}\right)$$

$$R_m = 58,''282 \cdot \tan z + 0,''0082\ \tan^3 z - \Delta R_m$$

$$\Delta R_m = 0,''0762 \cdot \tan z\,(1+\tan^2 z)$$

$p_0 = 760{,}3$ Torr, $T_0 = 282{,}55°$ K

$e_0 = 4{,}8$ Torr .

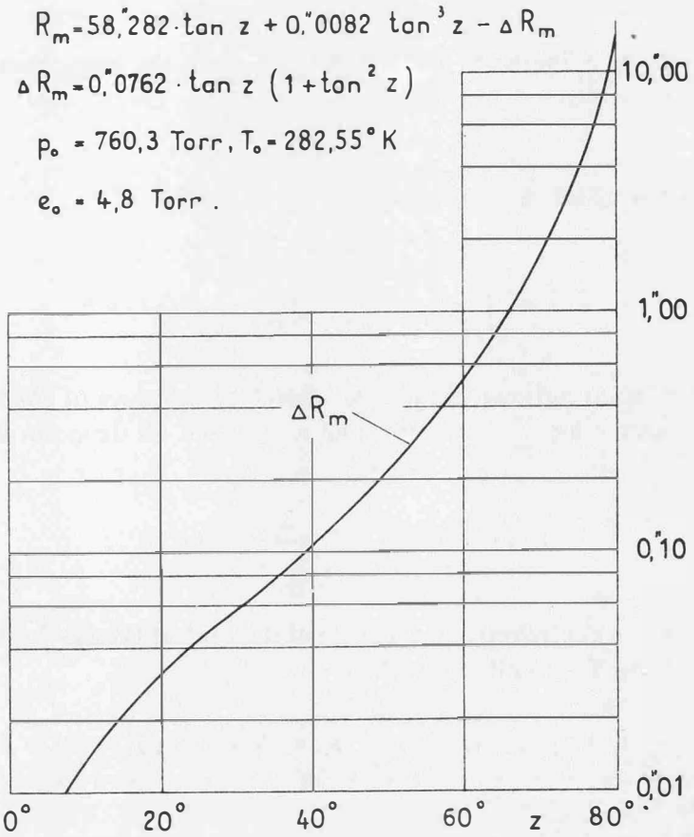

Fig. 3.

Z =	40°	50°	60°	70°	80°
Harzer	48,7″	69,1″	100,2″	158,1″	317,9″
Gyldén	48,6″	69,0″	100,1″	157,9″	317,7″
Radau	48,6″	69,0″	100,1″	157,9″	317,7″
Bessel	48,9″	69,3″	100,6″	158,7″	318,9″

Table 2: Comparison of different refraction tables at 760 Torr, + 10°C and 6 Torr pressure of water steam.

In this table only the values of Harzer are computed from mean values of the true atmosphere. The other values are computed from hypotheses which deviate essentially of the actual atmosphere. Nevertheless the deviations from the values of Harzer are very small. Even the refraction table of Bessel gives good values though the Besselian atmosphere differs extremely of the standard atmosphere, Fig. 4.

4. *Influence of the inclinations of the optical layers*

For the computation of the normal refraction we supposed that the layers with constant refractive index are concentric spheres. In reality this will not be the case. In a point P of the light beam coming from the star the true optical layer will have the inclination Δi against the corresponding spherical layer, Fig. 5. If we set i = angle between the light beam and the perpendicular to the true optical layer and i^* = angle between the light beam and the perpendicular of the spherical layer we get

$$i = i^* + \Delta i\,. \tag{6}$$

Herewith we get from the exact formula (1)

$$R = \rho'' \int_B^O \tan i \frac{dn}{n} \approx \rho'' \int_B^O \tan i^{\times} \cdot \frac{dn}{n} + \rho'' \int_B^O \frac{\Delta i}{\cos^2 i^{\times}} \cdot \frac{dn}{n}. \tag{7}$$

The last term gives the influence of the inclinations Δi of the true optical layers. This term is small. Therefore it is allowed to set

$$i^{\times} \approx z, \quad n \approx 1.$$

Then we get with $n = 1$ in B and $n = n_0$ in 0

$$\Delta R \approx \rho'' \int_B^O \frac{\Delta i}{\cos^2 i^{\times}} \cdot \frac{dn}{n} \approx \frac{\rho''}{\cos^2 z} \int_{n=1}^{n=n_0} \Delta i \, . \, dn. \tag{8}$$

Fig. 6 shows the relation between Δi and n, whereby the values of Δi are chosen arbitrarily. Now we introduce a mean value $\overline{\Delta i}$ of the inclinations, which we define in the following manner:

$$\overline{\Delta i}\,(n_0 - 1) = \int_{n=1}^{n=n_0} \Delta i \, . \, dn. \tag{9}$$

This mean value $\overline{\Delta i}$ we call *effective* inclination of the optical layers. $\overline{\Delta i}$ is changing with zenith distance, azimuth and time. Herewith and with

$$n_0 - 1 \approx 0{,}000\,283 \cdot \frac{p}{p_0} \cdot \frac{T_0}{T}, \; p_0 = 760 \text{ Torr}, \; T_0 = 283^0 K \tag{10}$$

we get from (8)

$$\Delta R \approx \rho'' \cdot \overline{\Delta i}\,(n_0 - 1) \cdot \sec^2 z \approx 1{,}''0 \cdot \frac{\overline{\Delta i^0}}{1^0} \cdot \frac{p}{p_0} \cdot \frac{T_0}{T} \cdot \sec^2 z. \tag{11}$$

ΔR is positiv, if the layers ascend in the direction of the observation.

According to [2] the main cause of the inclination of the optical layers is the horizontal gradient of the temperature in the vertical of the observation. For sea level we get

$$\Delta i_0 \approx 1{,}7^0 \cdot \frac{dT}{ds}\left[\frac{^0C}{Km}\right]. \tag{12}$$

We see, that in the neighbourhood of the ground, Δi_0 may be several degrees. But on the other hand Δi will rapidly decrease with altitude because in higher altitudes the atmosphere will be better balanced. If we suppose a linear decrease, we get for stations near sea level

$$\Delta R \approx 0{,}050'' \cdot \frac{\Delta i_0^o}{1^0} \cdot \frac{h_{Km}}{1\,Km} \cdot \sec^2 z \approx 0{,}085'' \cdot \frac{dT}{ds} \cdot h \cdot \sec^2 z, \tag{13}$$

where h = height above the observation station, where Δi gets zero. We may also assume an exponential decrease of Δi with altitude [3]. But all these hypotheses may only give a rough idea of the influence of the inclinations of the optical layers, which is to be expected.

5. *Empirical values of refraction errors*

A better information about the influence of the inclinations of the optical layers we get from real determinations of refraction errors. In Fig. 7a and 7b we see the standard deviations of the difference between computed and observed zenith distance of a star passing the meridian. These standard deviations are derived of 6700 meridian zenith distances by J. Bauschinger [4] and L. Courvoisier [5]. They may be approximated by the following terms:

Bauschinger: $$m \approx \pm \sqrt{(0{,}''31)^2 + (0{,}''23 \cdot \tan z)^2 + (0{,}''035 \cdot \sec^2 z)^2}, \tag{14a}$$

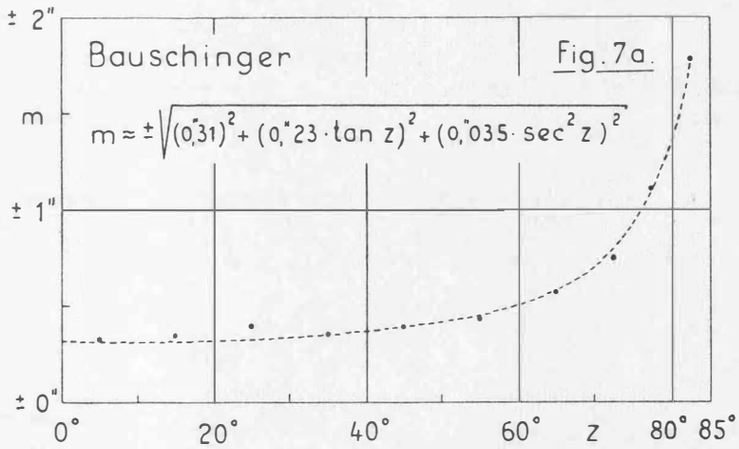

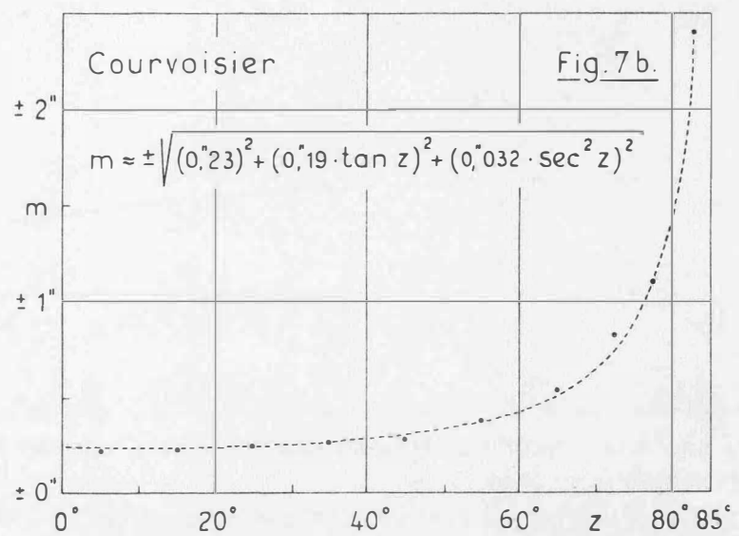

Courvoisier: $$m \approx \pm \sqrt{(0,''23)^2 + (0,''19 \,.\, \tan z)^2 + (0,''032 \,.\, \sec^2 z)^2}\,. \qquad (14b)$$

The first terms in the square roots mainly represent the influence of the errors of the observations and of the declinations of the stars. The second terms are mainly caused by a systematic error of the refraction constant. Both, Bauschinger and Courvoisier, used the Besselian refraction constant 60″44 instead of the better value 60″,10. A part of the second terms is also caused by the systematic difference between the interior and exterior temperature of the observation stations. The last terms represent the influence of the inclinations of the optical layers. The statistical basis of these last terms is not well founded. But it is sure, that the influence of the inclinations of the optical layers is astonishingly small, because the standard deviations are well approximated by the formulae 14a resp. 14b.

As a further proof, that the influence of refraction anomalies is small, the results of latitude determinations with the Astrolab Danjon at Potsdam in the years 1961 and 1962 [6] may serve. Fig. 8 shows the latitude for each series of observations of about 24 stars. The averaging curve represents the true value of the latitude with the influence of the polar motions. We see that the errors are small and have approximately a random distribution. Fig. 9 shows the distribution of the errors according to their size and sign. The maximum errors are −0″,34 and + 0″,27. The mean error of one observation is ± 0″,10. The mean observation error of one determination of latitude is ± 0″,08. Hence the mean influence of refraction anomalies is only ± 0″,06.

6. *Determination of refraction errors by determinations of latitude with the Sterneck method*

In [3] the author made the sugestion to determine latitude and longitude by the combination of small and large zenith distances and to introduce a mean value of the inclination of the optical layers as a further unknown into the adjustment. Meanwhile a student in his diploma work [7] made corresponding investigations with the Sterneck method for the determination of latitude.

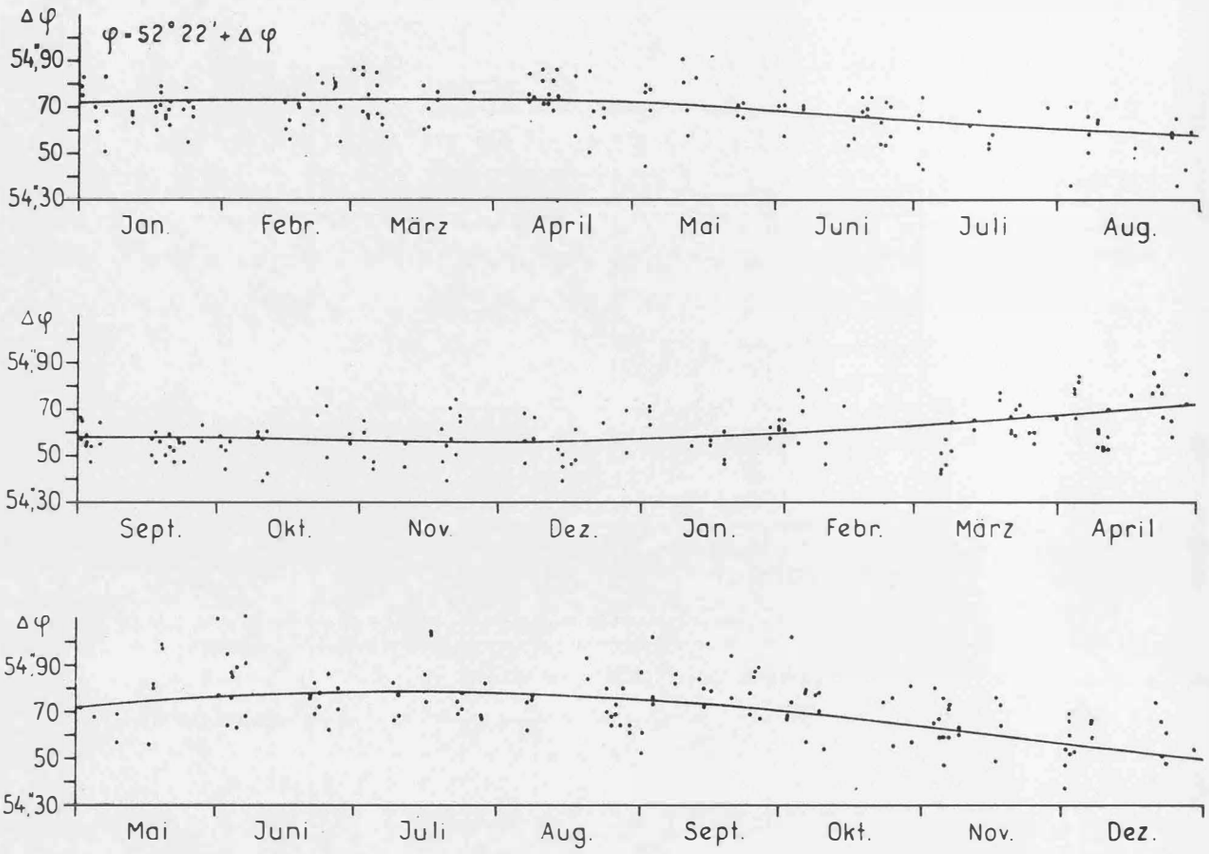

Fig. 8.

He observed pairs of stars with approximately equal zenith distances, whereby the zenith distances of the different pairs changed from 3^0 to 73^0.

From the observation of one pair of stars we get the latitude φ from

$$\varphi = \frac{1}{2}(\delta_S + \delta_N) + \frac{1}{2}(z_S - z_N) + \frac{1}{2}(R_S - R_N), \quad N \text{ star upper culm.} \tag{15}$$

$$\varphi = \frac{1}{2}(\delta_S + 180^0 - \delta_N) + \frac{1}{2}(z_S - z_N) + \frac{1}{2}(R_S - R_N), \quad N \text{ star lower culm} \tag{16}$$

δ = declination, R = refraction.

The results are free of the influence of the flexure of the telescope and of periodical errors of the division of the circle, because the north star and the south star have approximately the same zenith distance. The error of the half difference $1/2\,(R_S - R_N)$ mainly corresponds to the influence of the inclination of the optical layers, hence with (11)

$$\frac{1}{2}\,d\,(R_S - R_N) \approx \frac{1}{2}\,\rho''\,(n_o - 1)\,(\overline{\Delta i_S} - \overline{\Delta i_N})\,.\,\sec z \approx \rho''\,(n_o - 1)\,.\,\overline{\Delta i}\,.\,\sec^2 z\,. \tag{17}$$

Hereby $\overline{\Delta i_S}$ and $\overline{\Delta i_N}$ in general will have different signs.

If we suppose that $\overline{\Delta i}$ is constant within a series of observations and independent of the zenith distance, then it should be possible to determine simultaneously φ and $\overline{\Delta i}$. This procedure failed, because $\overline{\Delta i}$ is changing with zenith distance, azimuth and time. But the results showed again that the refraction errors are small even in large zenith distances.

Fig. 10 shows the squares of $\varepsilon_i = \overline{\varphi} - \varphi_i$

φ_i = latitude from observation i, $\overline{\varphi} = \frac{1}{2}[\varphi_i]$.

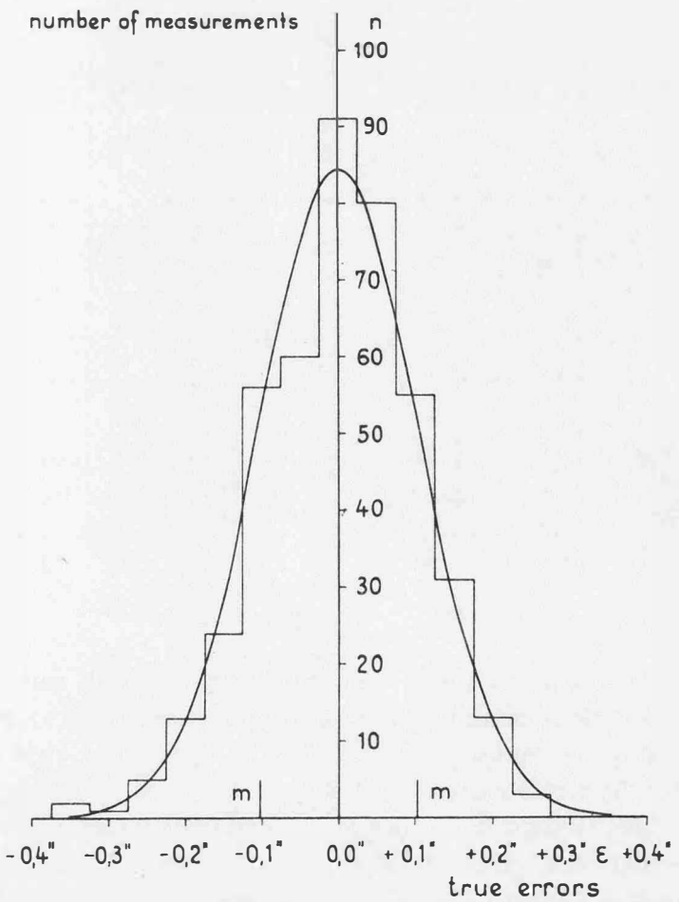
number of measurements
n
100
90
70
60
50
40
30
20
10
m
m
-0,4"
-0,3"
-0,2"
-0,1"
0,0"
+0,1"
+0,2"
+0,3"
ε
+0,4"
true errors

Fig. 9

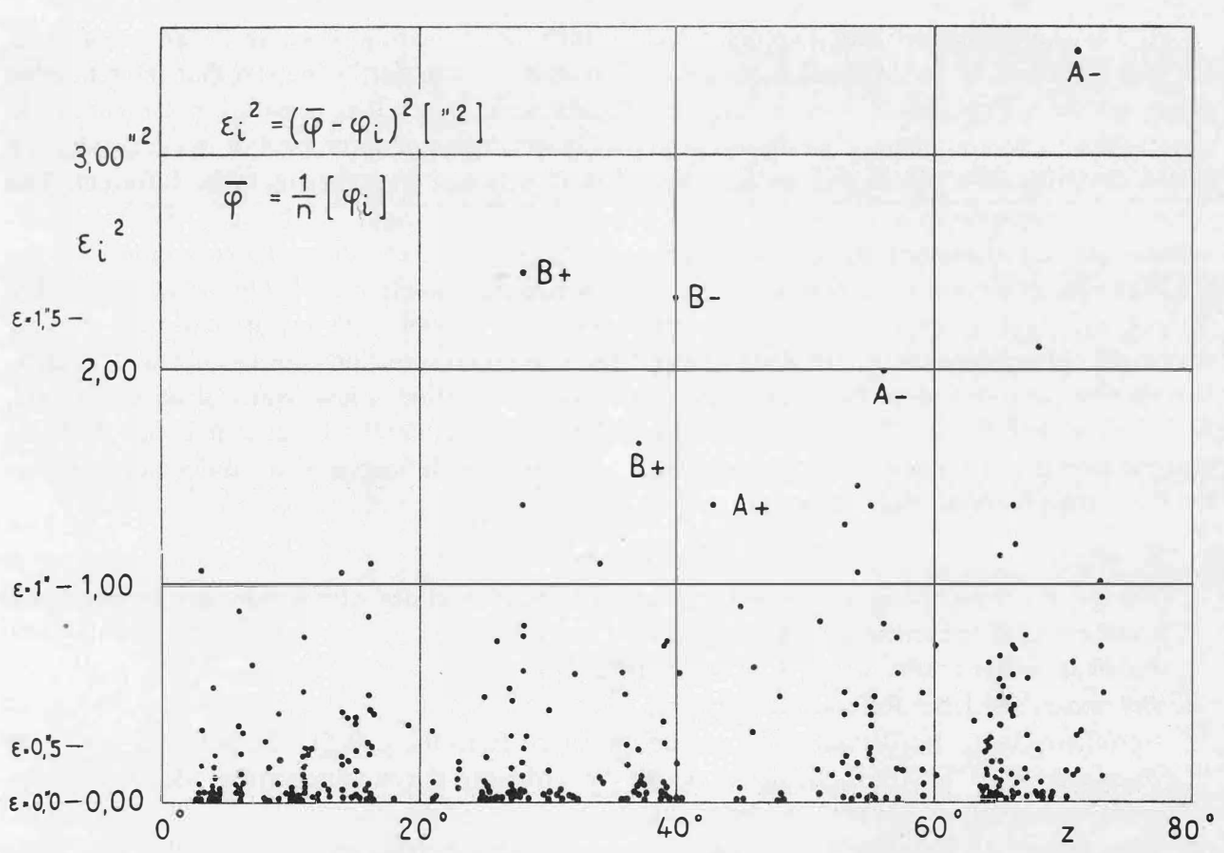
$\varepsilon_i^2 = (\bar{\varphi} - \varphi_i)^2 \,[''^2]$
$\bar{\varphi} = \frac{1}{n}[\varphi_i]$
3,00"2
ε_i^2
ε=1,"5 –
2,00
ε=1" – 1,00
ε=0,"5 –
ε=0,"0 – 0,00
A–
B+
B–
A–
B+
A+
0°
20°
40°
60°
z
80°

Fig. 10.

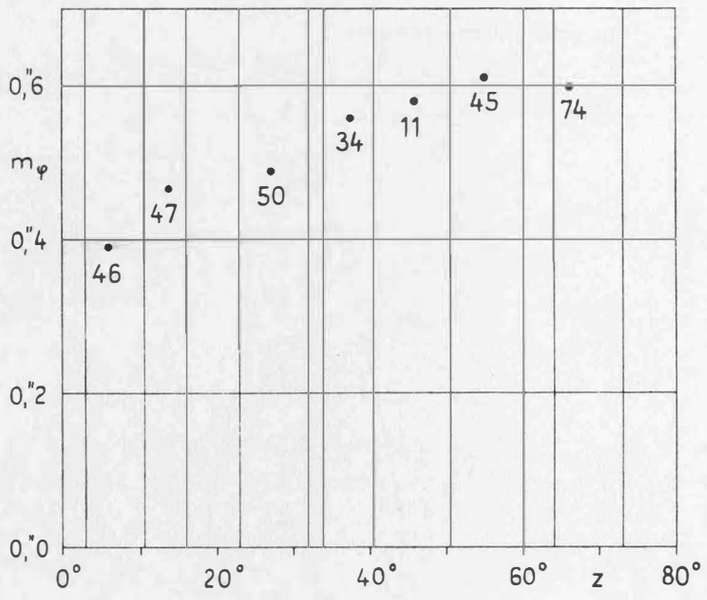

Fig. 11.

We see that the increase of ε_i^2 with the zenith distance is only small. The great values marked with *A* belong to the same programme. They correspond probably to observation errors and not to a large inclination of the optical layers because the signs of the ε-values are not the same ones. This is also valid for the errors marked with *B*.

Fig. 11 shows the standard deviations m_φ of one determination of latitude depending on the zenith distance. The numbers correspond to the number of latitude determinations within the marked zone of *z*. The errors are mainly caused by observation errors. The influence of the inclinations of the optical layers is very small. This is very surprising because the observation station is situated amidst an extended slope where large inclinations of the lower optical layers are to be expected.

7. *Conclusions*

It was shown that refraction errors, which disturb the measuring of zenith distances of stars, are mainly caused by the inclinations of the optical layers. It was further shown that the refraction errors are surprisingly small even at large zenith distances. Hence it is generally not necessary to observe during several nights if we do not need the highest degree of accuracy. For the determination of the deviation of a plumb line an accuracy of $\pm$ 0",3 (mean error) seems to be sufficient. This accuracy is reachable in most cases within a few hours in one neight. To be sure, that the observations are not disturbed by unusual large refraction anomalies, the author recommends the simultaneous observation of zenith distance and horizontal direction of about twenty stars. The simultaneous observation of a star in two directions is easily possible with an automatic star tracking device [8]. Afterwards the zenith distances and the horizontal directions are evaluated separately. If both computations give the same latitude and longitude within a few tenths of an arc second, we are sure that the result is free of an essential refraction anomaly, because it is not probable that the lateral and vertical refraction anomalies have the same influence. If the difference surpasses the limit, the observations must be repeated.

Literature

1. *Harzer, P.:* Berechnung der Ablenkung der Lichtstrahlen in der Atmosphäre der Erde auf rein meteorologisch-physikalischer Grundlage.
   Publikation der Sternwarte in Kiel. XIII (1922–24).
2. *Bohrmann, A.:* Über Refraktionsstörungen.
   Veröffentlichung der Badischen Landessternwarte zu Heidelberg, 8, (1932), No. 9.
3. *Ramsayer, K.:* Über die Genauigkeit der Bestimmung der astronomischen Refraktion.
   Acta Techn. Hung. 52 (1965) S. 361–372.
4. *Bauschinger, J.:* Untersuchungen über die astronomische Refraktion.
   Neue Annalen der K. Sternwarte in München, 3 (1898).

5. *Courvoisier, L.:* Untersuchungen über die astronomische Refraktion.
Veröffentlichung der Sternwarte zu Heidelberg, 3 (1904).
6. *Geodätisches Institut Potsdam:* Astronomische Zeit- und Breitenbestimmungen. Empfangszeiten von Zeitsignalen 1961/1962.
Arbeiten aus dem Geodätischen Institut Potsdam, Nr. 10, 1965.
7. *Henn, R.:* Ermittlung des Einflusses der Schichtneigungen auf die astronomische Refraktion aus Breitenbestimmungen nach der Sterneckmethode.
Diplomarbeit 1965.
8. *Ramsayer, K.:* Automatische Sternnachführung für astronomischen Theodolit.
Veröffentlichung der Deutschen Geotätischen Kommission, Reihe B, Nr. 81, 1962.

Definition of the Refraction and Shimmer Problem Affecting Geodetic Observations of Satellites

by *Darwin G. Abby, Michael S. Tavenner*, Bedford

Abstract

A large amount of apparently good information collected from optical field observations of various light sources is expected to be lost during the data reduction and analysis phase due solely to atmospheric effects. Experience has shown this to be true. The available observational techniques each require individual consideration primarily as a function of time. Observations of satellites equipped with flashing strobe lights are subject to all the long term and short term shimmer effects which compare with the flash duration. The continuous trace technique of letting the satellite image trail across a photographic plate is subject only to the long term shimmer effects, characteristically longer than 0.1 seconds in time. "Chopped" image trails fall between these extremes of observational techniques as the reflected satellite image position is integrated for an exposure period of 10 to 50 milliseconds, thus eliminating the extremely short fluctuation effects. A curve-fitting approach using a least squares analysis can be used to resolve the problem and can be readily applied to the continuous trace and chopped trail techniques where sufficient data is collected. However, this least squares approach is somewhat limited in the case of active light sources as there is an energy and weight versus number and interval of flashes trade off in the design of an active satellite experiment.

Introduction and Background

During the past several years the art of observing artificial earth satellites for the purpose of making precise geodetic measurements has developed into an advanced science. A variety of individual techniques have proven to be feasible as well as there exists a series of new techniques which are currently being analyzed and tested. ([13]) No single technique of observation can be listed as the panacea for the problems of satellite geodesy; rather, each must be carefully applied to those problems whose parameters can best be matched to the available technique which will produce the best and most accurate solution.

The uses of all optical geodetic satellites are similar in nature: the satellite is used as an object-of-reference in space and as such its exact positions in space and time must be obtainable somewhere in the geodetic solution. To insure this, the satellite must be in an orbit which is geometrically favorable to all observing stations, such that a strong and rigid geometry is produced during the time of observation.

In general, it is the geographical area which contains the geodetic problem to be solved that dictates the approach and individual technique that is optimal. For example, simultaneous observations from participating ground stations have been used almost exclusively to date in the solution of moderate size networks (1 to 2000 km). Large reflecting balloons of the ECHO and PAGEOS types have been ideal for simultaneous observations. Yet, they have a limited value when it is necessary to extend observations to a dynamic mode where individual, or small graphs of stations observe the target satellite along an extended orbital arc. In this case, a dense satellite

of a large mass to surface area ratio is necessary to permit the application of precise orbital constraints to determine the satellite position along its orbit as a function of time.

In todays inventory, there are at least four artificial earth satellite techniques available to the geodetic community:

(1) Active satellites such as the ANNA and GEOS series whose optical beacons flash for durations of the order of a millisecond at precisely prescribed times.

(2) Cooperative satellites (those equipped with special directional reflectors) which reflect optical signals of short duration from ground laser sites.

(3) Passive satellites used in a "chopping" mode where sun reflected energy is integrated on film for characteristic periods of 10 to 50 milliseconds.

(4) Passive satellites used in a "continuous trace" mode where the satellite image is trailed across the photographic plate.

In all of the satellite techniques, corrections for refraction must be made in the plate reduction phase. Normally, the gross refraction corrections using a computed value derived from standard refraction equations, such as Garfinkels[3] [7] [12] and station-observed meteorological parameters of pressure and temperature, are straight forward and pose little problem since the referenced astronomical background suffers approximately the same refraction. Additionally the correction for the satellite being at a finite distance rather than the assumed infinite distance of the star background is also straight forward and has been sufficiently discussed by Baldini and Schmid.[2] [12] Normally, these computed corrections are sufficiently accurate and are *not* a limiting factor in obtaining a satisfactory solution. However, the fundamental atmospheric limitation is the minute spatial and temporal fluctuation of the apparent index-of-refraction termed "seeing" which is characterized by the observed shimmer and scintillation effects.

Scintillation, the fluctuation in intensity of the observed source, is not a significant problem as one is interested only in a positional relationship, provided that there is significant energy density such that an image can be recorded during all phases of observation. It is shimmer, the apparent short term angular displacement of an object, which must be recognized as the problem. This is not to say the two effects are independent, but rather they have the same cause. Considerable literature[4] [5] [6] [9] [11] exists on the subject and the magnitude of shimmer has been satisfactorily measured; yet, complete agreement does not exist as to the exact cause, size, or mechanism that produces the apparent fluctuations in the index-of-refraction. The reason for this is obvious, it is still impossible to measure the precise and instantaneous index-of-refraction continuously along the light ray from an extra-terrestrial source through the atmosphere to an observer.

Analysis of the Problem

Since angular displacements of several seconds-of-arc can be expected during optical observations, steps must be taken to minimize the degradations of the final geodetic solution. Recognition of the problem is the first step, selecting the mode of observation is next, and finally comes the minimizing of these degrading atmospheric effects in the reduction and analysis phase.

The criteria for observing are based on the environmental and system conditions in existence at the time of observation:

(1) From a visibility standpoint, in the temperate zones of the earth, the best weather occurs shortly after the passage of frontal systems. Normally the weather will be clearest after a fast moving cold front, yet, this is just the time when shimmer and scintillation will be at a maximum. This is the time of the highest winds both at ground level and high altitudes. As time passes (over the period of days) even though shimmer becomes less, haze and atmospheric extinction increase. Past experience has shown that a significantly large number of observations are made during times when shimmer effects are the greatest. A surprisingly large number of plates with apparently good data (good image, time records, etc.) have been lost in the reduction phase. The bulk of this loss-of-data can be attributed directely to excessive shimmer and camera vibration effects.

(2) The actual source and spectral content of the observed energy source (sun, satellite strobe, or ground based laser) is of no real consequence for obtaining positional information. The criteria that must be met is that sufficient energy must be received by an observing instrument

to be recorded. If the satellite is small and/or the energy leaving the satellite is of low power, the signal must be integrated for a finite length of time. During this time the satellite will move a finite distance. When observing a sun-reflecting satellite each integration period as currently experienced in using geodetic cameras has a time interval of 10 to 50 milliseconds. Range, satellite albedo, satellite size and shape, camera resolution, and angular velocity must all be duly considered. When a strobe light is used, it characteristically has a higher instantaneous output power than the sun reflecting satellite, yet its total duration is considerably less. For example the ANNA satellite had a flash duration of 2.3 milliseconds and the GEOS-A satellite possessed a flash duration of approximately one millisecond. For obtaining angular information in the reduction phase, instantaneous times are computed as a simple mean of the duration of the event, either flash duration or shutter open time.

The problem of refraction in making optical geodetic satellite observations is not one of measuring the gross refraction but rather can be stated as "How does shimmer affect these observations, what is the magnitude of the effect, and how can these effects be minimized?" The actual excursion of the angular position as a result of shimmer is difficult if not impossible to express mathematically. However, an assumption can be made that the movement is periodic in nature and is a superposition of both high and low frequencies. Whit this assumption, the duration-of-event can then be treated as acting as a low band-pass filter which produces a mean of the high frequency excursions.(6)

Experimental Result and Discussion

To obtain representative values of what could be expected during normal operations with the standard Air Force Geodetic Camera, the PC-1000 (*f*/5, 1 meter focal length), a random plate was selected which was exposed with a continuous trace during a pass of the ECHO I satellite (Figure 1). Under magnification, the star and satellite trails showed both scintillation and shimmer. A star close to the satellite trail was selected and measured as well as a portion of the satellite trail, such that the measured section of the trails would coincide in time. The trails were measured on a small Mann Comparator which had a reading and operator error of $\pm$ 1 . 5 microns, determined

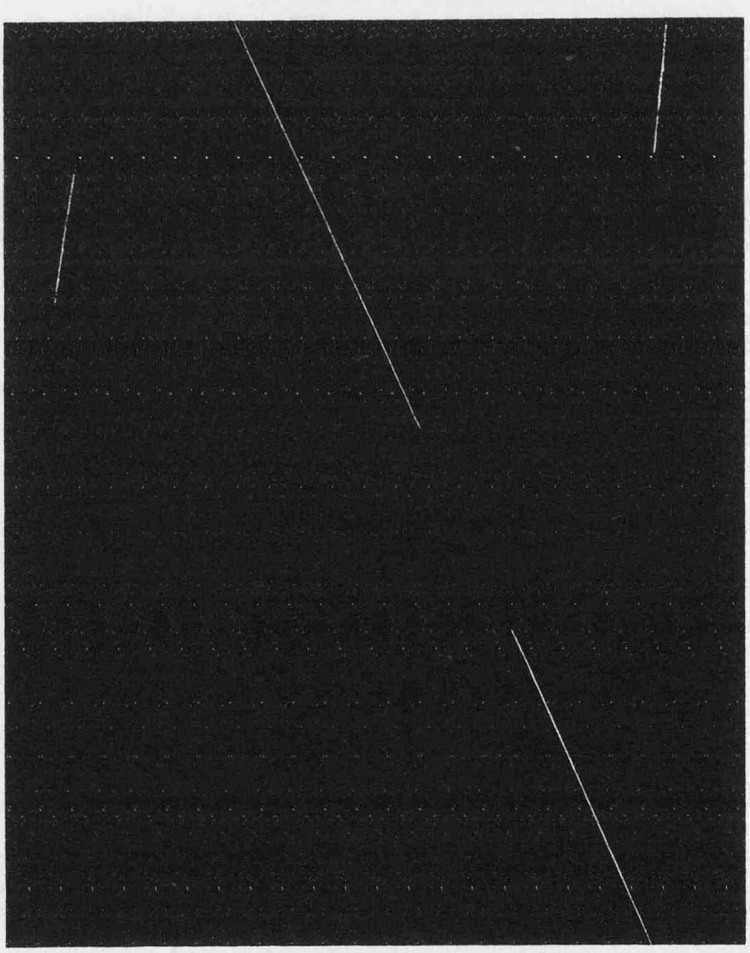

Fig. 1

by repeated measurements on a single point. The x-axis was measured in relation to increments of 20 and 200 microns along the y-axis for the satellite and 25 microns in the y-axis along the star trail.

Since the star background has a slow angular velocity of 15 seconds-of-arc per second of time versus 606 seconds-of-arc per seconds of time for the ECHO I satellite, the high frequency shimmer effects are masked along the star trail but become obvious along the satellite trail. On this particular plate 3 distinct frequencies were observed along the satellite trail of 37, 5 . 9, and 0 . 28 hertz with comparable periods of 27, 170 and 3600 milliseconds. Along the star trail the longer period angular movement was almost identical to the satellite period of 3600 milliseconds while the higher frequency effect was obscured as would be expected. The magnitude of the excursions for this particular plate were of the order of $\pm$ 1 second-of-arc. This seemed to be characteristic of all observed frequencies. These results compared well with what would be expected based on previous studies. (11) (9) (5) (8). (Figures 2 and 3)

Another type of examination has been conducted where simultaneous observations of the active GEOS-A satellite taken from a network of ground stations in the southeastern U. S. and Caribbean area, have been investigated for shimmer effects. The assumption has been made that an observed orbital-segment can be expressed by a polynomial of given degree. The observed right ascension and declination have been used in a least-squares curve fitting technique to form the

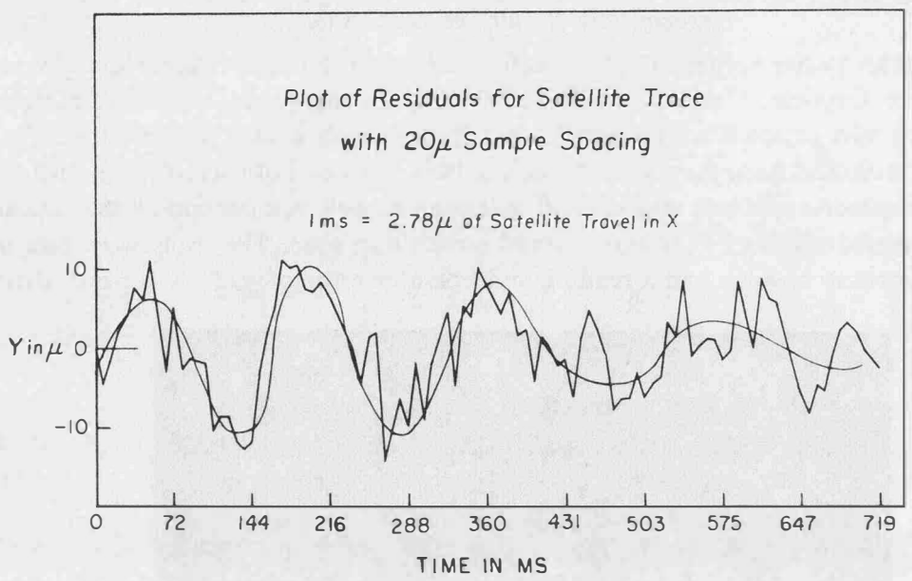

Fig. 2

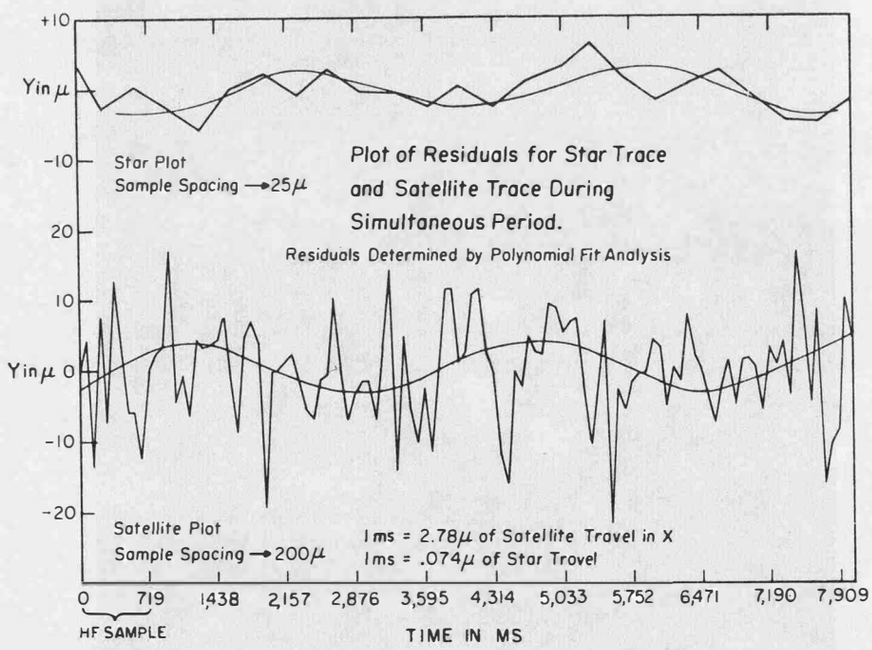

Fig. 3

polynomial, then by comparing the orbit as defined by the polynominal with the observed data, residuals were obtained as an approximation of the total random error remaining after the plate reduction.

The available data for this evaluation was received on IBM computer card format as the output of the plate reductions phase. Previous to this, the raw observations had been made by the 1381st Geodetic Survey Squadron (USAF) in the field and shipped to the Aeronautical Chart and Information Center (USAF) at St. Louis. Here the plate measurements were performed on a Mann Semi-Automatic Stellar Comparator which has a repeatable, reading accuracy of one micron. The plate measurements were then processed through computer programs where the right ascensions and declinations of the stars are adjusted for sidereal time, refraction, lens distortion, camera orientation and focal length, and differential refraction along the satellite orbit. When finally recieved, each flash point is associated in time with a right ascension and declination and referenced to a plate reduction error.

The total error, σ_T, in the combined right ascension and declination can be treated as the square root of the sum of the squares of the individual errors.

$$\sigma_T = \sqrt{\Sigma \sigma_i^2}$$

Table I

Error Sources

1. Emulsion and Image Shifts
2. Comparator Measuring Error
3. Distortion (Tangential, Radial, and Random)
4. Refraction
5. Differential Refraction
6. Star Catalog
7. Flash Event Time
8. Shimmer
9. Camera Vibration

Listed in Table I are the errors which affect an individual measurement. The first six are accounted for in the plate reduction error, σ_{PR}, which has been derived in the plate reduction phase. The remaining possible errors will be Flash Event Time Error, σ_{Time}, which is dependent on the accuracy of the satellite clock and electronics; the shimmer error, σ_S; and camera vibration error, σ_V. Therefore:

$$\sigma_T = \sqrt{\sigma_{PR}^2 + \sigma_{Time}^2 + \sigma_S^2 + \sigma_V^2}$$

The probable error of the GEOS-A clock at all times when the clock rate is reasonably close to nominal has been estimated to be 100 microseconds relative to a WWV test point.(1) The strobe lamp flash intervals will not vary from flash to flash by a value greater than 100 microseconds. Therefore the inaccuracy along the satellite trail due to flash interval inaccuracies will be less than 1 meter (less than 0 . 05 seconds-of-arc at normal ranges.) Therefore it can realistically be stated that σ_{Time} is of no consequence and can be considered as zero.

The errors from shimmer and high frequency camera vibration (a frequency such that could be seen in the satellite trail, yet masked by the filtering effect of the slower moving star image) are found to be very difficult to separate. The low frequency vibrations can be observed by examining each star on a plate and comparing the image trails for an exact similarity of motion since the entire emulsion is undergoing the vibration. This would differ from shimmer in that this exactness of similar motion between separate star trails would not be expectes to occur over the full plate. In examining the vibration problem associated with the active satellite technique, wind velocity would appear to be the primary cause, since in normal operation there are no shutter or camera movements during the actual flash times. The shutter is normally opened several seconds prior to event time and any inherent shutter vibration is dampened out. Additionally, results have not

Listing of GEOS Film Plates Analyzed and the Results

Station #3649 (Jupiter, Florida)

Date 1966	UT	Elev	Az	Temp bulb dry/wet	Press	Wind	Sky Condition	σ_{RA}	σ_{δ}	σ_{T}	σ_{PR}	σ_{S}
01/02	08-17	42.7	265.9					0.63	0.88	1.08	1 09	—
01/13	04-52	33.6	338.6					0.43	0.73	0.85	2.54	—
01/15	05-02	44.7	309.1	63/54	29.85	Calm	Lt haze	1.10	0.17	1.11	2.07	—
01/16	03-01	25.3	17.4	67/64		S-5 kts	Clear	1.84	0.33	1.87	2.10	—
01/16	05-06	37.2	297.4	65/63	29.80	Calm	Clear	0.34	0.09	0.35	1.04	—
01/19	03-14	38.1	358.4	55/51	30.15	SE-3 kts	Clear	0.66	1.57	1.70	0.89	1.4
01/28	01-54	45.1	137.3	47/41	30.25	SE-3 kts	Clear	0.54	1.18	1.30	1.01	0.8
02/05	00-16	31.4	326.1	46/39	30.30	NE-10 kts	Clear	0.73	0.82	1.10	1.05	0.3
02/09	00-37	31.1	259.5	68/57	30.45	NW-10-15 kts	Clear	0.84	0.33	0.90	0.93	—
02/16	10-18	26.7	104.1	67/66	30.05	Calm	Lt haze	0.44	0.69	0.82	0.94	—
02/17	10-18	29.4	136.1	63/62	30.05	Calm	mod. haze	0.57	0.92	1.08	1.10	—

Station #3861 (Homestead, Florida)

01/13	04-52	30.2	341.5					0.67	0.82	1.06	1.03	0.2
01/15	05-02	41.1	316.7	69/65	29.80	Calm	Clear	1.35	0.55	1.46	0.92	1.1
01/16	03-01	22.3	16.6	67/64	29.79	NE-5-10 kts	Clear	0.11	0.69	0.70	0.82	—
01/16	05-06	35.6	304.1	65/63	29.81	NW-0-5 kts	Clear	0.44	0.39	0.59	1.12	—
01/19	03-14	33.9	359.5	57/52	30.08	S-5-10 kts	Broken cum.	0.89	1.23	1.52	1.09	1.1
01/28	01-54	48.4	128.7	49/43	30.22	SE-10-15 kts	Clear	0.95	0.76	1.22	1.02	0.6
02/05	00-16	28.8	329.6	/	30.22	SE-10-15 kts	Clear	0.64	0.30	0.71	1.06	—
02/09	00-37	32.4	263.3	67/64	30.28	W-5-10 kts	Hazy	0.48	0.42	0.64	0.93	—
02/16	10-18	26.8	100.2	72/68	30.06	N-0-5 kts	Broken cum.	1.62	0.46	1.69	0.97	1.4
02/17	10-18	31.2	132.5	63/61	29.95	Calm	Lt haze	0.19	0.13	0.22	0.97	—
04/15	08-36	45.5	86.7					1.18	0.47	1.27	1.11	0.6

Table IIa

Listing of GEOS Film Plates Analyzed and the Results

Station #3106 (Antigua Island)

Date 1966	UT	Elev	Az	Temp	Press	Wind	Sky Condition	σ_{RA}	σ_{δ}	σ_{T}	σ_{PR}	σ_{S}
04/01	01-01	40°.2	34°.6					0.60	0.81	1.00	1.05	—
Station #3401 (Bedford, Mass)												
01/12	04-49	48.0	238.2					1.02	0.89	1.35	0.89	1.0
01/13	04-52	37.7	259.4					0.86	0.97	1.30	0.98	0.8
01/19	03-14	51.6	246.2					0.47	0.62	0.78	0.76	0.2
Station #3402 (Mobile, Alabama)												
01/02	08-17	60.4	201.8					0.23	0.67	0.71	0.74	—
01/12	04-49	45.2	41.6					0.75	0.31	0.81	0.68	0.4
01/28	01-54	23.5	125.1					0.77	1.22	1.44	1.09	0.9
Station #3404 (Swan Island)												
01/28	01-54	40.9	71.9					1.31	1.76	2.19	1.01	1.9
04/15	08-36	30.9	58.7					0.88	2.47	2.62	1.09	2.4
Station #3405 (Grand Turk Island)												
01/29	02-00	47.2	201.1					0.76	4.33	4.40	1.09	4.2
Station #3406 (Curacao Island)												
01/29	02-00	59.1	288.5					0.77	1.11	1.35	1.13	0.7
04/01	01-01	23.6	39.8					0.45	0.71	0.84	0.88	—

Table IIb

Listing of GEOS Film Plates Analyzed and the Results

Date 1966	UT	Elev	Az	Temp	Press	Wind	Sky Condition	σ_{RA}	σ_{δ}	σ_{T}	σ_{PR}	σ_{S}
Station #3407 (Isle of Trinidad)												
01/29	02-00	32.4	285.1					0.63	0.46	0.78	1.02	—
Station #3648 (Savannah, Georgia)												
01/02	08-17	39.9	235.7					0.64	1.40	1.54	0.86	1.3
01/19	03-14	56.2	05.2					0.75	0.13	0.76	0.82	—
01/28	01-54	31.1	148.4					1.13	1.53	1.90	1.02	1.6
02/05	00-16	43.6	314.7					0.67	0.23	0.71	1.08	—
Station #3657 (Aberdeen, Maryland)												
01/12	04-49	68.6	242.2					0.75	0.90	1.17	1.02	0.6
01/15	05-02	35.3	240.2					0.70	0.85	1.10	0.94	0.6
04/01	01-01	25.6	109.5					1.13	1.12	1.59	0.73	1.4
04/15	08-36	34.6	150.8					1.22	1.49	1.93	1.41	1.3

Table IIc

demonstrated that the vibration is a problem in the PC-1000 observations of active satellites. Therefore, for the remainder of this paper the effects of vibration shall be treated as minimal and/or included as shimmer.

The total error for an individual plate or flash point can be obtained by computing a polynomial using a least squares adjustment to obtain the residuals and variance. Since only seven flashes are available per observation in the GEOS-A sequence a third order polynomial was chosen as a best representation of the data. To arrive at this decision, second, third, and fourth-order polynomials were computed and it was found, in general, that the residuals for the third order fit were minimal. Also, it was observed that the third order polynomial produced a changing satellite acceleration representative of the real case.

A total of 43 observations from 11 sites were analyzed and the results can be examined in Table II. All error columns are in seconds-of-arc. (The figures for right ascension have been corrected for convergence of the meridians.) The total plate error, σ_T, was computed by

$$\sigma_T = \sqrt{\sigma_{RA}^2 + \sigma_\delta^2}$$

Since σ_{time} is negligible and σ_V is treated as negligible or a part of the error due to shimmer, σ_S then

$$\sigma_S = \sqrt{\sigma_T^2 - \sigma_{PR}^2}$$

Where σ_{PR} equaled or exceeded σ_T, shimmer is regarded as having no significant affect in degrading the plate data. This occurred in 42% of the plates examined while in the remaining plates σ_S ranged as high as 2 . 4 seconds-of-arc with an average value of 0 . 9 seconds-of-arc.

Two stations, at Jupiter and Homestead, Florida were of particular interest. These stations were separated approximately 150 kilometers and as a result were under the influence of the same general meteorological conditions. Of the data evaluated, these two stations participated in 10 sets

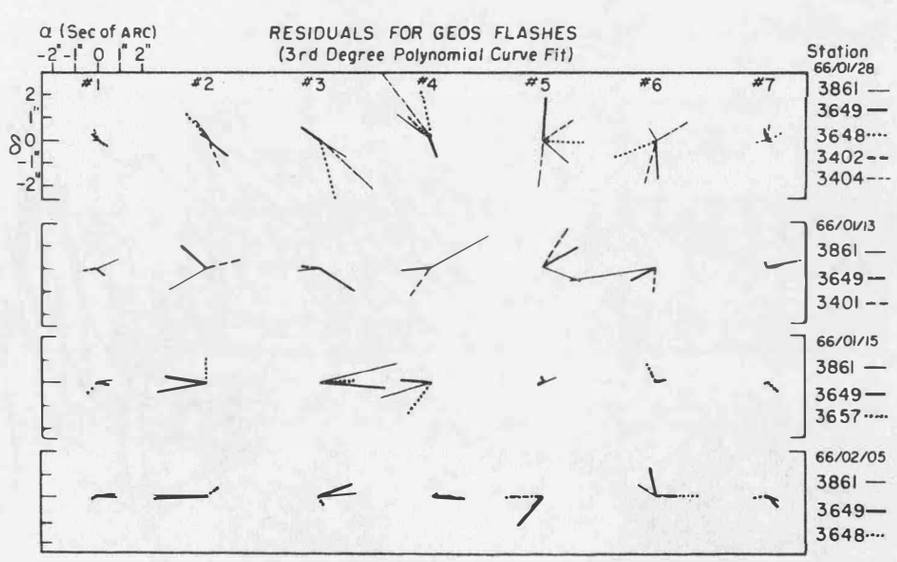

Fig. 4

of simultaneous observations. In three of these sets of simultaneous observations, the plotted residuals of the least-square curve fits to the flash image points compared both in magnitude and direction between the two stations. This can be seen in Figure 4 where four sets of residuals are plotted. The observation of 0154 on 28 Jan 66 is presented as an example of a random distribution. The observation of 0452, 13 Jan 66 show a small effect, while the observations of 0502, 15 Jan 66, and 0016, 5 Feb 66, show a marked degree of similarity.

Weather data for the observations at Jupiter and Homestead was collected from the camera operators log and further compared with meteorological surface charts, the upper air analysis charts from 850 to 100 millibar levels, and the balloon sounding from Miami, Jacksonville, and Tampa, Florida for this period of time. During January and February the seasonal jet stream winds were active over Florida with speeds characteristically as high as 50 to 70 meters per seconds at the 300 millibar level, (approximately 9,400 meters height). Of special interest, on the night of 15 January 1966, both cameras were looking northwest into an approaching cold front (frontal

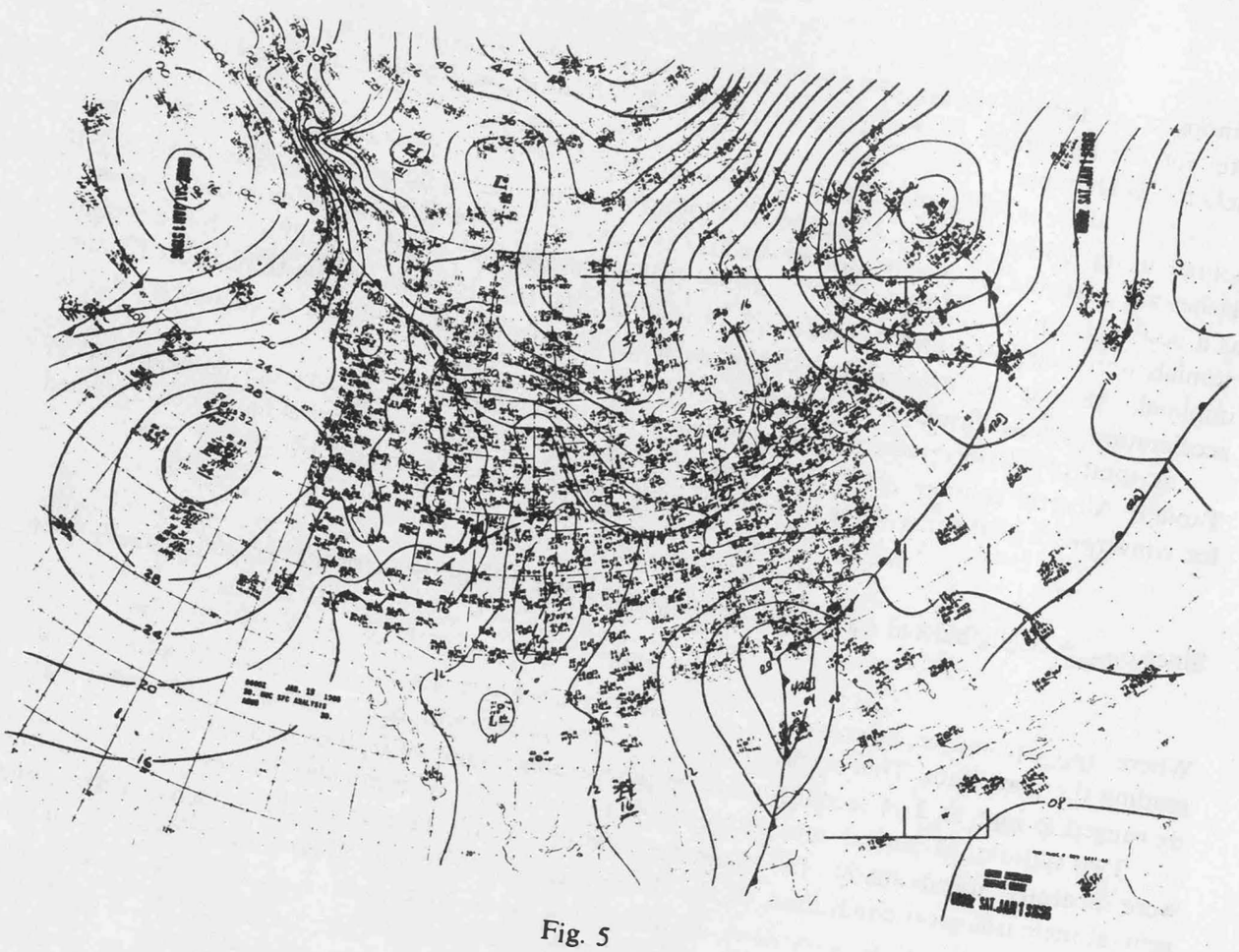

Fig. 5

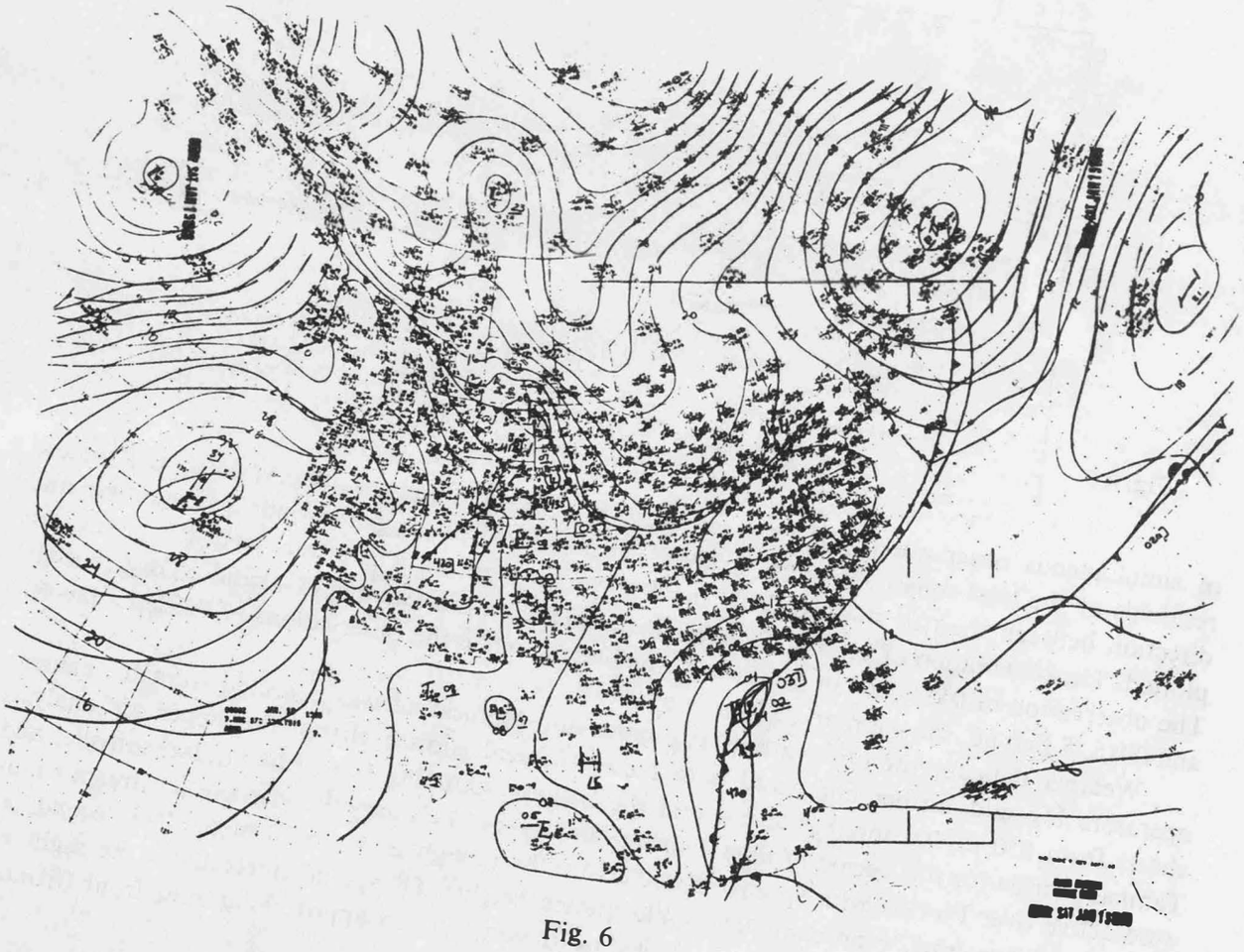

Fig. 6

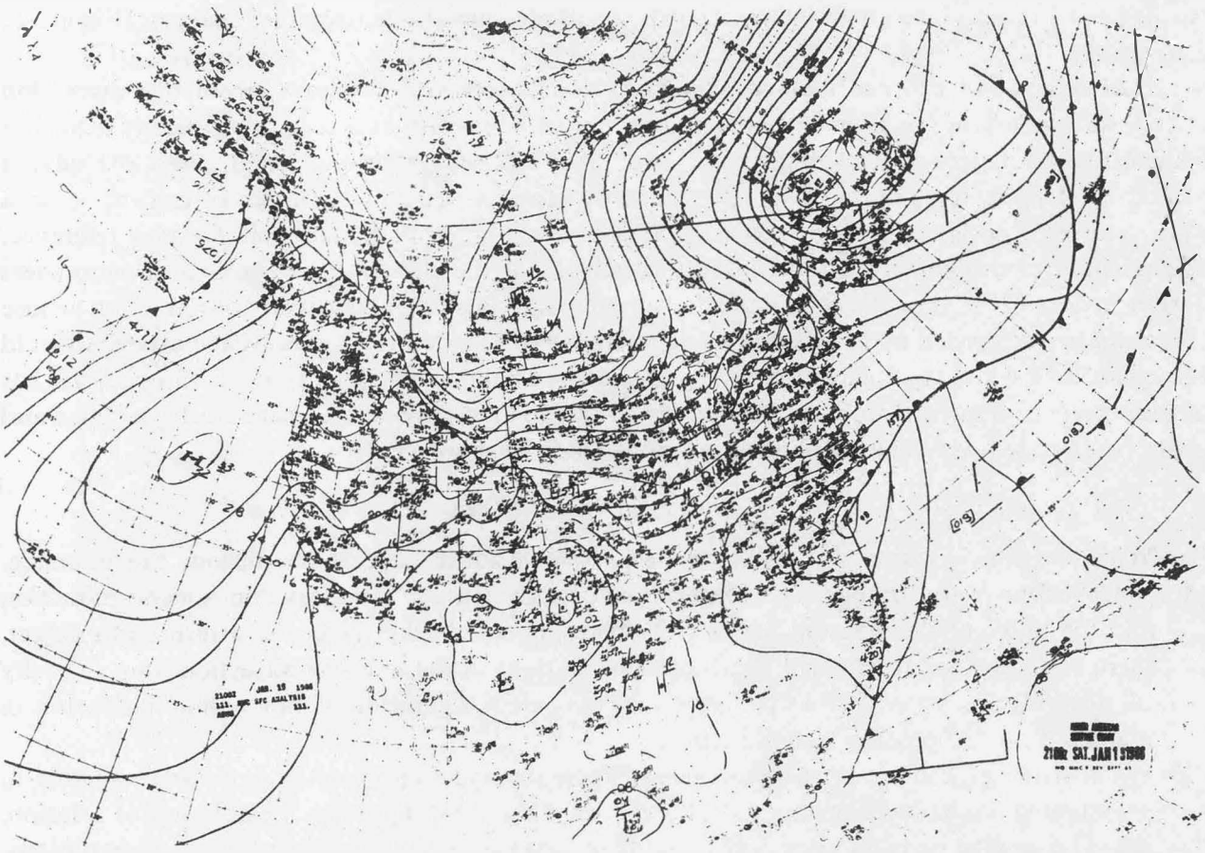

Fig. 7

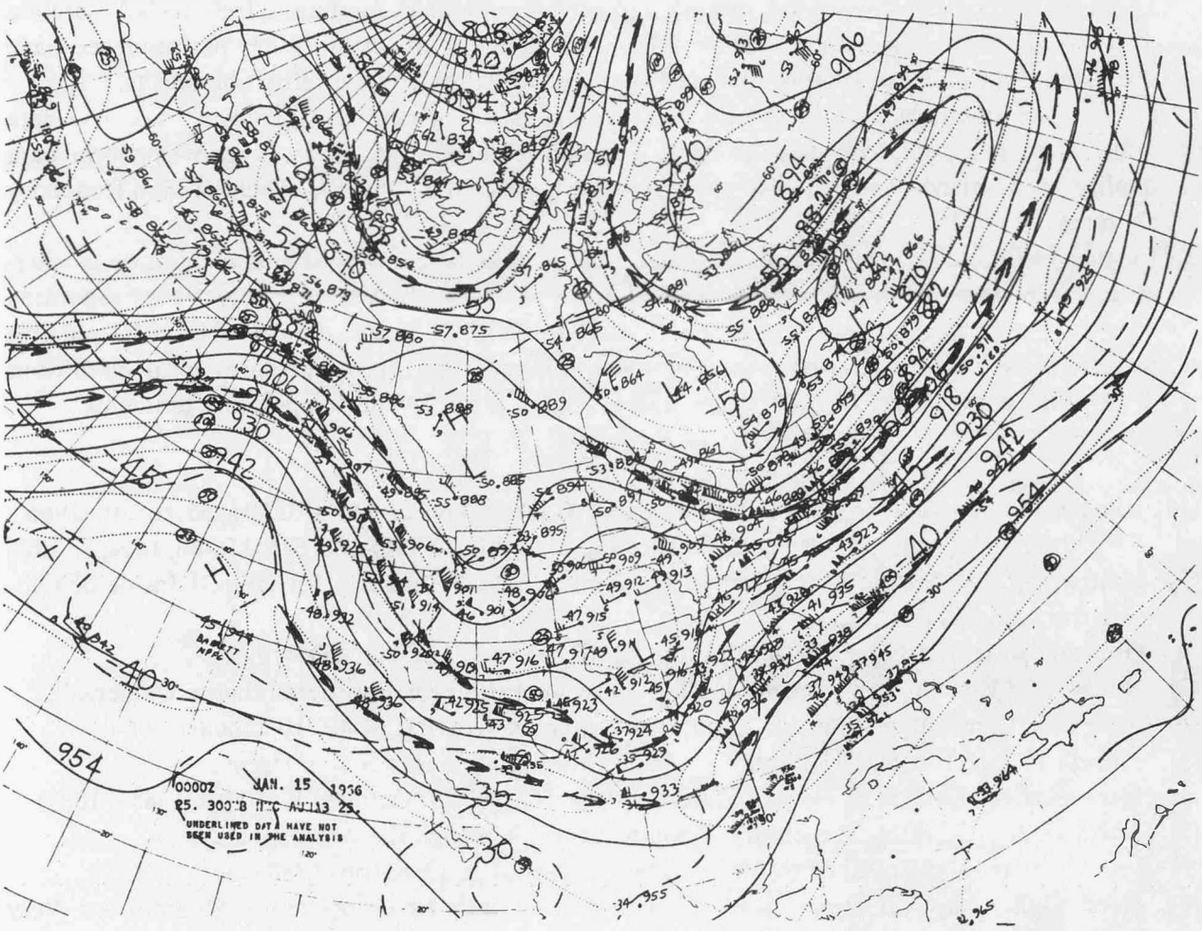
0000Z JAN. 15 1936
UNDERLINED DATA HAVE NOT
BEEN USED IN THE ANALYSIS

Fig. 8

passage was 14 hours later) with the associated frontal pressure and temperature changes. (Figures 5, 6, 7, and 8)

It is recognized at once that no significant conclusions can be drawn from this discussion since insufficient data has been collected and examined. However, as a scientific curiosity a further comparison of meteorological data to observed shimmer would be warranted. With the advent of active satellites, a significant experiment could be performed by a network of cameras over a wide area by observing the satellite flashes that provide a common time and position reference. The purpose of this experiment would be to determine if the changing meteorological parameters over a geographical area do contribute to a systematic, fast-changing, index-of-refraction whose effect can be recognized and measured by separated observing stations. Ideally, the cameras would be separated from a few meters up to several hundred kilometers. This type of observations has already been attempted at Jupiter, Florida by NASA for the purpose of image quality studies and could be extended with slight modification to the study of shimmer. (10)

Summary and Conclusions

With due consideration of the discussion presented above, several conclusions can be made.

1. Independent of the problem of measuring and/or computing the gross atmospheric refraction and the differential refraction between the astronomical background and a near earth object, there exists the apparent small short-term fluctuations in the index-of-refraction. In a majority of observations made, these fluctuations do become a significant if not a limiting factor in making a precise geodetic determination.
2. When making geodetic satellite measurements a statistical approach is extremely valuable in overcoming the limitations imposed by shimmer. As well as improving the accuracy of solution, it can be used an early monitor of the quality of data prior to the lengthy solution computations.
3. For active satellites, in order to reduce shimmer by using a least-squares fit, the number of flash points during a camera observation sequence should be increased to as great a number as possible consistent with the satellite's power capabilities. Certainly the ANNA satellite with five flashes per sequence and the GEOS-A satellite with seven flashes per sequence have not provided an overabundance of data for eliminating atmospheric refraction effects.
4. For passive satellites, collection of sufficient data is not generally a problem since 100 data points can easily be recorded during a single observation. Yet, some improvement in data quality is obtainable when the exposure duration is selected to filter the effects of high frequency shimmer.
5. Further examination of the effect of meteoroligical parameters or systematic shimmer is warranted. One possible step would be to perform an experiment where a network of separated cameras simultaneously observe an active satellite. With sufficient data, it should be possible to determine if a correlation exists between shimmer and gross meteorological conditions of frontal systems, high altitude winds, and changing pressure and temperature gradients.

References

(1) *Applied Physics Laboratory:* "GEOS-A Clock Calibration for Days 321, 1965 to 50, 1966" APL, Johns Hopkins University, Silver Spring, Maryland, TSSD-186, SIP-116-66, 14 April 1966

(2) *Baldini, A. A.:* "Formulas for Computing Atmospheric Refraction for Objects Inside or Outside the Atmosphere",
Gimrada Research Note No. 8, 9 January 1963, Ft. Belvoir, Va. AD 41995

(3) *Brown, P. C.:* "An Advanced Reduction and Calibration for Photogrammetric Cameras",
Air Force Cambridge Research Laboratories Report AFCRL 64-40, 10 January 1964.

(4) *Farrell, E. J.:* "Intrinsic Limitations in Locating Photographic Star Images",
Journal of the Optical Society of America, Vol. 56, No. 10, October 1966 (pp. 1385—1389)

(5) *Fried, D. L.:* "Limiting Resolution Looking.Down Through the Atmosphere",
Journal of the Optical Society, Vol, 56, No. 10, October 1966, (pp. 1380—4)

(6) *Fried, D. L.:* "Optical Resolution Through A Randomly Inhomogeneous Medium for Very Long and Very Short Exposures".
Journal of the Optical Society, Vol. 56, No. 10, October 1966 (pp. 1373—9)

(7) *Garfinkel, B.:* "An Investigation in the Theory of Astronomical Refraction", Astronomical Journal, Vol. 50, No. 8, (pp. 169—179).

(8) *Mancini, A. and L. A. Gambino:* "Results of Space Triangulation Adjustments from Satellite Data",
Gimrada Research Note No. 13, September 1965 (pg. 16).

(9) *Mikesell, A. H.:* "The Scintillation of Starlight",
1955, U. S. Naval Observatory, Washington, D. C.

(10) *Moss, S. J., E. Hyman, R. L. Brooks, and R. C. Mollece:* "Procedures and Analysis for the Determination of Geodetic Camera Sensitivity Coefficients",
Wolf Research and Development Corporation Contract Report, 14 November 1966.
NASA Contract No. NAS 5-9756-6C, —25, —28.

(11) *Reiger, S. H.:* "Starlight Scintillation and Atmospheric Turbulence",
Astronomical Journal Vol. 68, No. 6 August 1963 (pp. 395—406).

(12) *Schmid, H. H.:* "The Influence of Atmospheric Refraction on Directions Measured To and From a Satellite",
Gimrada Research Note No. 10, 7 February 1963, Ft. Belvoir, Va.

(13) *Williams, O. W.:* "Surveying the Earth by Satellite",
Science Journal, January 1967 (pp. 69—73)

C. Refraction in Connection with Spatial Geodesy

Formules essentielles de la refraction d'un rayon lumineux entre 2 points a distance finie ou infinie

par *H. M. Dufour*, Paris

L'exposé ci-après se propose de rappeler les formules de base de la réfraction et donner leur caractéristique d'application dans les divers cas qui se présentent en pratique.

Ces démonstrations se trouvent dans 2 articles précédemment parus [1, 2]

I — *Formules de Base*

On se limite au cas d'un arc $A\,\widehat{B}$ plan.

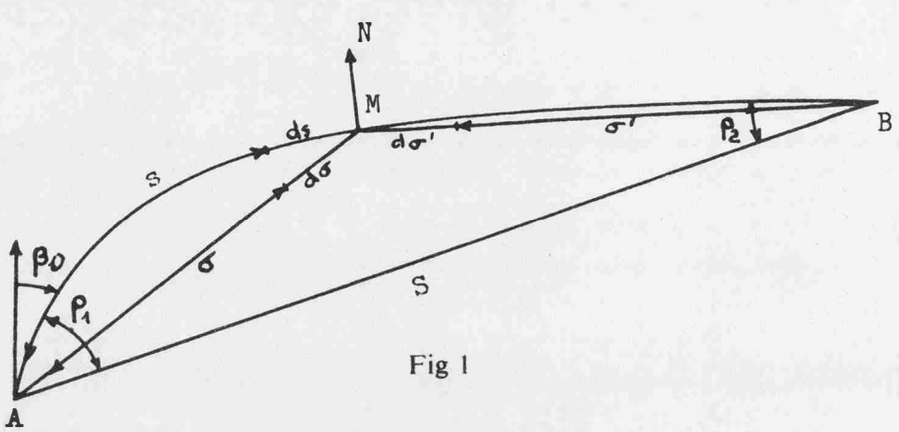

Fig 1

Avec les notations de la figure ci-dessus, on a:

$$\text{Réfraction totale: } \zeta = \rho_1 + \rho_2 = \int_o^s \Gamma(M)\, ds$$

$$\text{Angle } \rho_1 : \rho_1 \# \sin \rho_1 = \frac{1}{S}\int_o^s (S - \sigma')\,\Gamma\, d\sigma'$$

$$\text{Angle } \rho_2 : \rho_2 \# \sin \rho_2 = \frac{1}{S}\int_o^s \sigma\,\Gamma\, d\sigma$$

Γ étant la courbure du rayon lumineux en M.

En pratique, sauf de rares exceptions, s et σ peuvent être remplacés par leurs projections sur $A\,B$.

Remarques

1) La courbure Γ est égale à $\left(-\frac{1}{n}\frac{dn}{N}\right)$, n étant l'indice de l'air, N la normale extérieure à la trajectoire $\left(\vec{AB}, \vec{N} = +\frac{\pi}{2}\right)$.

2) L'application de l'intégration par la formule des 3 niveaux donne les expressions:

$$\begin{cases} \zeta = S\dfrac{\Gamma_1 + \Gamma_2 4\,\Gamma_{1/2}}{6} \\ \rho_1 = \dfrac{S}{6}(\Gamma_1 + 2\,\Gamma_{1/2}) \\ \rho_2 = \dfrac{S}{6}(2\,\Gamma_{1/2} + \Gamma_2) \end{cases}$$

3) Ces formules donnent aussi les corrections pour passer de la transformée d'une ligne géodésique $\overset{\frown}{A\,B}$ à la sécante $\overrightarrow{A\,B}$, en projection conforme. L'indice n est remplacé par l'échelle e de la projection.

4) Elles se généralisent sur la sphère (projection conforme sur la sphère de rayon 1):

$$\begin{cases} \zeta = \displaystyle\int_o^S \Gamma(s)\,ds \\ \sin\rho_1 = \dfrac{1}{\sin S}\displaystyle\int_o^S \sin\sigma'\,\Gamma(M)\,d\sigma' \\ \sin\rho_2 = \dfrac{1}{\sin S}\displaystyle\int_o^S \sin\sigma\,\Gamma(M)\,d\sigma \end{cases}$$

la fonction "longueur" devenant un sinus et la courbure Γ devenant la courbure géodésique.

II

Le problème des couches horizontales planes est une première approximation toujours intéressante. Il permet en particulier de voir apparaître une quantité tres importante, que nous appellerons la *hauteur équivalente d'air*

$$l_M = \int_M^\infty \Delta\,dh$$

Δ étant la densité de l'air.

L'indice n peut en effet s'écrire:

$$n = 1 + \alpha_o\Delta \qquad (\alpha_o = 0{,}000\,292\,55)$$

et l'intégration fait intervenir la seule quantité l_M, qui est une donnée pratiquement équivalente à la *pression*.

$$\begin{cases} \rho_\infty - \rho_1 = \alpha_o\,tg\,\beta_o\dfrac{l_1 - l_2}{H} \\ \rho_\infty = \alpha_o\,tg\,\beta_o\,\Delta_1 \end{cases}$$

[β_o = distance zénithale en A, $l_1 = l_A$, $l_2 = l_B$, Δ_1 = densité en A, H = dénivelée]

Pour un satellite, $l_2 = 0$; on pourra écrire:

$$\frac{\rho_2}{\rho_\infty} = \frac{l_1}{H\,\Delta_1} \# \frac{8^{\text{km}}}{H^{\text{km}}} \frac{T_1}{273} \qquad (T_1 = \text{témperature absolue en } A)$$

formule amplement suffisante jusqu'à $\beta = 80^0$

L probleme des couches horizontales sphériques est un peu plus nuancé. On pourra distinguer 2 cas;

A) $\beta < 80^0$

L'intégrale reste réalisable dans tous les cas; elle fait apparaître les intégrales:

$$I_1(M) = \int_M^\infty \Delta\, dh \qquad \text{avec } h = h'\left(1 + \frac{h'}{2R}\right)$$

(h' = *altitude vraie*)

$$I_2(M) = \int_M^\infty \Delta\, h\, dh \qquad \left(I_3(M) = \int_M^\infty \Delta\, h^2\, dh \ldots \text{etc} \ldots\right)$$

L'intégrale $I_1(M)$ qu'on continuera à appeler *hauteur équivalente d'air* est toujours très voisine d'une pression. Les autres intégrales nécessitent de faire une *hypothèse* sur la loi des températures en altitude, mais l'influence de cette hypothèse sur le résultat est pratiquement minime . . .

Il apparaît aussi une erreur de ligne d'integration, qui peut être non négligeable pour $\beta > 75^0$.

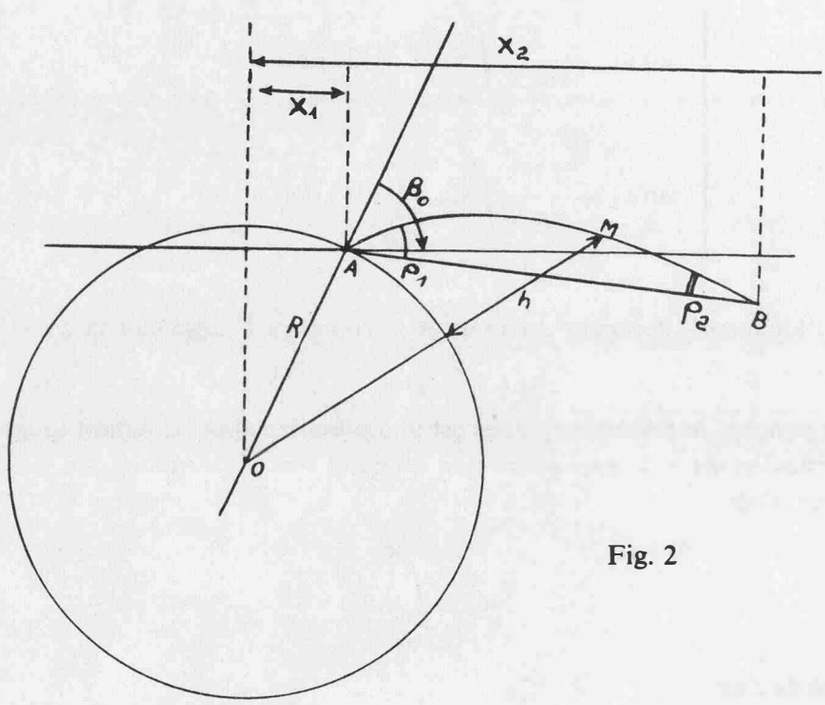

Fig. 2

$$\rho_1 = \alpha_o\, tg\, \beta_o \left[\Delta_1 - \frac{X_2}{R\,S\cos^2\beta_o}(l_1 - l_2)\left(1 - \frac{3\,H_m}{(n+1)\,R\cos^2\beta_o} - \frac{3\,n}{(n+1)}\frac{l_2\,X_2}{R^2\cos^3\beta_o}\right.\right.$$

en prenant pour ligne d'intégration $\beta_o = \beta_1 + \frac{\rho_1}{2}$

avec $X_1 = R\cos\beta_o$, $X_2 = X_1 + S$

en adoptant une loi linéaire de décroissance de la température:

$$T = T_1\left[1 - \frac{h}{H_m}\right] \text{ d' où } \Delta = \Delta_1\left(1 - \frac{h}{H_m}\right)^{n-1},\quad l = l_1\left(1 - \frac{h}{H_m}\right)^n$$

$$\text{et } n = \frac{H_m}{l_1}\Delta_1$$

$$\left| \text{par exemple } T = 288 \left(1 - \frac{h}{48}\right), \; n = 5{,}7 \, , \; \frac{dT}{dh} = -\, 6^0/\text{km} \right|$$

La hauteur l équivalente d'atmosphère est liée à la pression barométrique par la relation:

$$l = \frac{P^{mm}}{760} \times 8{,}010$$

Quand B va à l'infini (cas d'une visée sur étoile):

$$\rho_\infty = \alpha_o \, tg \, \beta_o \left[\Delta_1 - \frac{l_1}{\cos^2 \beta_o} \left(1 - \frac{3 \, H_m}{(n+1) \, R \cos^2 \beta_o}\right)\right]$$

expression équivalente à la formule de Laplace $\left(\text{avec } \beta_o = \beta_1 + \frac{\rho_\infty}{2}\right)$ mais qui peut aussi s'écrire pratiquement:

$$\rho_\infty = \alpha_o \, tg \, \beta_o \left(\Delta_1 - \frac{l_1}{\cos^2 \beta_o}\right) \qquad \text{avec } \beta_o = \beta_1 + \rho_\infty$$

(c'est-à-dire en prenant pour β_o les distances zénithales calculées d'après les éphémérides).

On notera aussi la formule, pour des engins hors de l'atmosphère terrestre:

$$\rho_2 = \alpha_o \, tg \, \beta_o \left[\frac{l_1}{S \cos \beta_o} \left(1 - \frac{3 \, H_m}{(n+1) \, R \cos^2 \beta_o}\right)\right].$$

Remarque importante

Les pressions barométriques étant supposées mesurées, les grandeurs l s'en deduisent facilement: les hypothèses sur l'atmosphère n'interniennent que dans des termes correctifs.

B) $\beta > 80^0$

Il semble que la seule façon de résoudre pratiquement le problème consiste à se définir des lois de l'indice en fonction de l'altitude:

$$h = h' \left(1 + \frac{2 \, h'}{R}\right).$$

On peut songer par exemple à se définir 2 zones:

$$0 < h < H \, , \; \Delta = P + Q \, h + T \, h^2 \, , \quad \nu = \frac{1}{n} = p + q \, h - t \, h^2$$

$$H < h < \infty \, , \; \Delta = P' + Q' \, h + T' \, h^2 \, , \; \nu = \frac{1}{n} = p' + q' \, h - t' \, h^2$$

Les formules générales conduisent alors à des calculs relativement faciles à mener à bien.

A titre d'exemple, quand A et B sont dans la même zone, on aura:

$$\zeta = n_1 \sin \beta_1 \, S \left[q - t \, S \cos \beta_1 - t \, \frac{S^2}{3 \, R} \right]$$

$$\rho_1 - \rho_2 = n_1 \sin \beta_1 \, t \, \frac{S^2}{3} \left[\cos \beta_1 + \frac{S}{2 \, R} \right]$$

$$\rho_1 = \frac{n_1 \sin \beta_1 \, S}{2} \left[q - 2 \, t \, \frac{S}{3} \cos \beta - t \, \frac{S^2}{6 \, R} \right]$$

Les coefficients (p, q, t) qui dérivent des (P, Q, T) pourront être définis par les diverses conditions qu'ils doivent satisfaire:

— Valeur de Δ au point $h = 0$
— Valeur de $\int \Delta dh$ ($\rightarrow$ pression) — Equation barométrique
— Hypothèses sur les températures
— Mesures effectuées. Hypothèses météorologiques . . . etc. . . .

Conclusion

Nous avons surtout voulu insister sur le fait que l'introduction de la pression, quantité mesurable, dont dérive la grandeur *l*, hauteur équivalente d'atmosphère, permet de réaliser des intégrations rigoureuses pour $\beta < 80^0$, avec des hypothèses très générales sur la structure de l'atmosphère; ce phénomène, déjà bien connu pour les calculs sur les étoiles (terme complétentaire de la formule de Laplace), se généralise aux points visés à distance finie.

On notera que c'est aussi la *pression* qui intervient comme terme correctif principal dans les calculs de l'effet de la réfraction atmosphérique sur les *distances* mesurées.

References

(1) *Dufour, H. M.:* Etude générale de la correction angulaire finie (réduction à la corde) pour une courbe quelconque tracée sur le plan ou sur la sphère (Bulletin géodésique 1953)
(2) *Dufour, H. M.:* Choix de formules de la réfraction atmosphérique pour les observations par chambres balistiques (Bulletin géodésiquen^0 73, Septembre 1964).

Determination of Refraction When Adjusting Spatial Triangulation

by *L. Hradilek*, Prague

The problem of refraction was solved by the adjustment of spatial triangulation in the Western Carpathians. Theoretical investigations and practical tests proved that it is possible to estimate the main value of the coefficient of refraction (one or two parameters defining the refraction) without meteorological measurements at every point of the network.

It is necessary to fulfill two conditions:

1. The station points are to be chosen on sharp peaks or at least 10—12 m above the ground.
2. All vertical angles measured at the observation station are to be considered as one observation unit. They must be measured quickly for the changes of refraction not to exceed substantially the limits of the observation errors.

When repeating the measurements of vertical angles at least twice (in two hours' intervals) we can trace the changes of refraction and consider the applicability of each vertival angle for the adjustment.

Fig. 1 represents the changes of vertical angles at the station point Baranec (2 200 m) during the whole day. All these vertical angles are suitable for adjustment.

It sometimes happens that the first measurements are anomalous (Fig. 2). The cause is in the apparatus which must get adapted to the temperature conditions at the station point. On the 3rd picture we can see the anomalous changes before sunset. These last measurements cannot be taken into adjustment.

New condition equations were derived for adjustment of vertical angles, and there was used an approximative solution of normal equations with unknown coefficients of refraction and deflections of the vertical by the adjustments without the possibility of using electronic computers.

For adjustment with high-speed computers there was devised an exact method of combined adjustment of all measured quantities yielding the spatial geodetical coordinates, deflections of the vertical and coefficients of refraction at every point of the network.

In the Western Carpathians the coefficients of refraction varied within the limits of 0,09 — 0,19 at different station points. The mean difference 0,011 between their values was estimated both by the approximative and the exact method.

For an independent check-up of the computation of refraction was used the precise levelling transformed by Molodensky's method to the ellipsoid heights and the computation of height

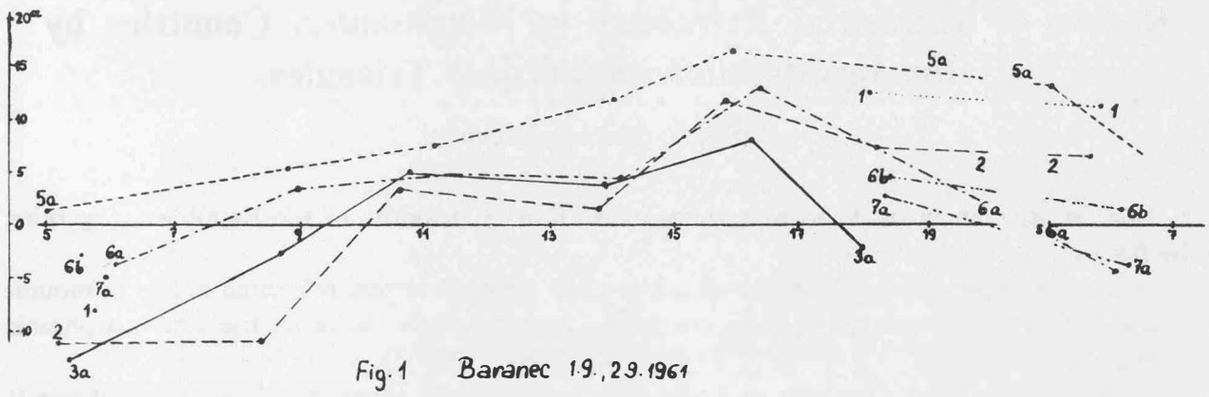

Fig. 1 Baranec 1.9., 2.9. 1961

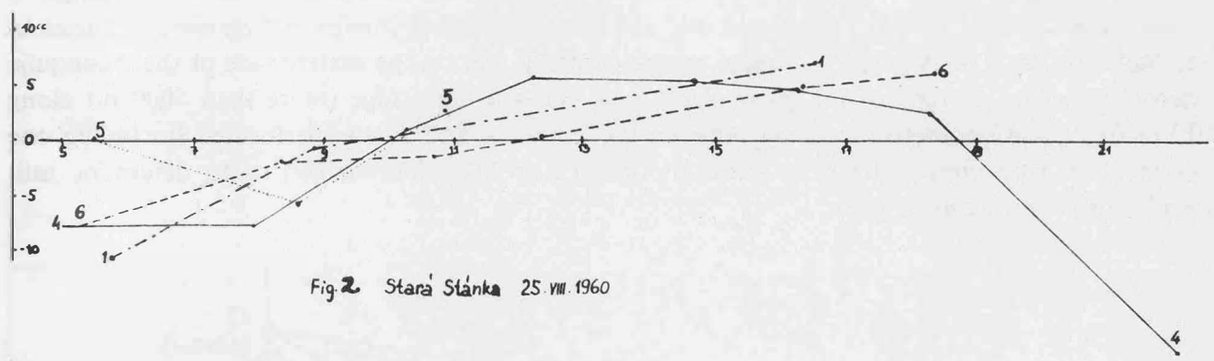

Fig. 2 Stará Stánka 25. VIII. 1960

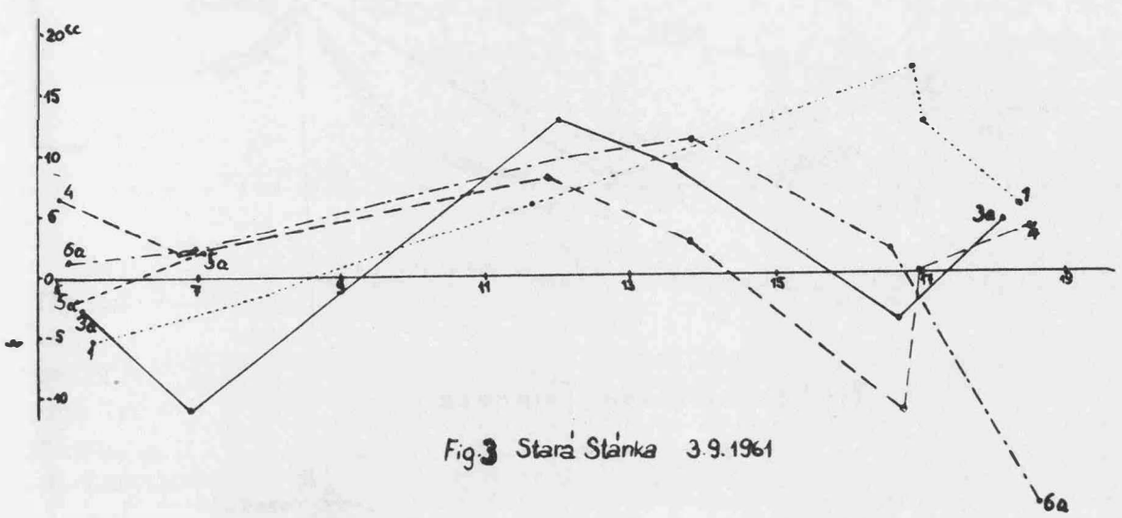

Fig. 3 Stará Stánka 3.9.1961

differences from directly measured lines (as inclined as possible). The difference of 2 — 3 cm at the distance of 10 — 15 km shows that the refraction errors are within the limit of 1".

The following problems and questions were solved together with the refraction problem. There was

1. realized the project "Passo Pordoi" of the Symposium at Cortina d'Ampezzo in 1962.
2. reached nearly the same accuracy in the horizontal and vertical coordinates. (The ratio of the weights of horizontal angles and vertical angles was about 2 : 1).
3. answered the question of the possibility of mapping the quasigeoid by combining geometric methods with the ordinary levelling.
4. there were investigated the conditions and tested the possibility of using classical methods of separated adjustments of horizontal and vertical angles in high mountain regions.

Results of Terrestrial Refraction in Mountainous Countries by the Investigation of Vertical Triangles.

by *Rafael N. Sánchez*, Tucuman

The Consejo Nacional de Investigaciones Cientificas y Técnicas of the Republica Argentina subsidized this research.

1. In a previous paper it has been shown that we can compute vertical refraction angles in mountains without limitation in height by combining zenithal angle, tellurometric and astronomic measurements.

At the University of Tucumán we chose two very different zones: the Tolombón triangle is across the Calchaquí valley, a long and dry one in the argentine provinces Catamarca, Tucumán and Salta (fig. 1). The Alpachiri triangle, on the contrary, lies on the eastern side of the Aconquija "sierra" which is in front of the great plains and shows a high ridge (more than 5000 m) along 50 km (fig. 2). A geometric levelling between the points *A* and *P* was performed (including one intermediate astronomic station to know the geoid's profil). This enabled us to determine univocally the six refraction angles.

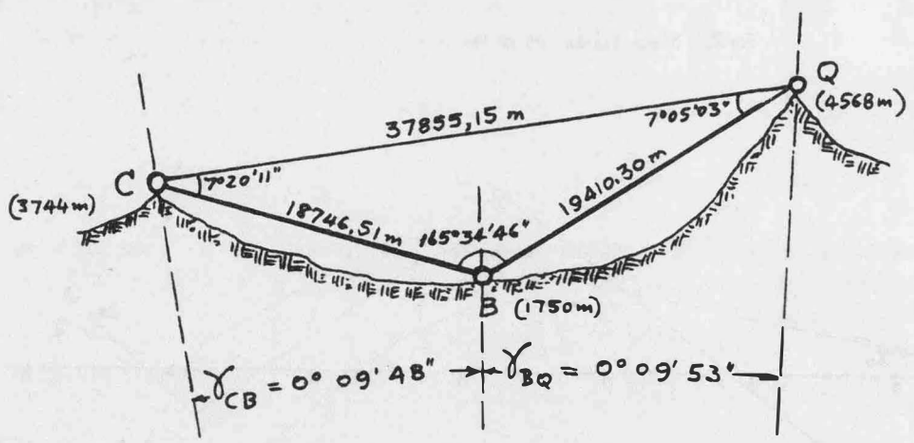

Fig. 1 : Tolombón Triangle

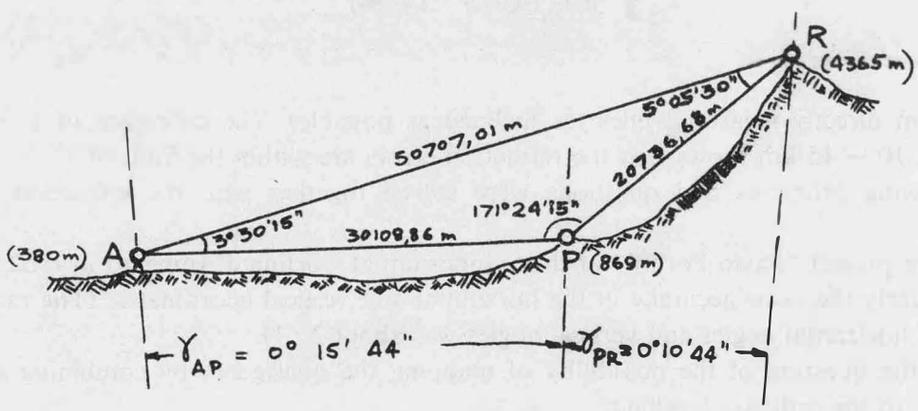

Fig. 2 : Alpachiri Triangle

2. Tellurometric measurements: the distances were computed by averaging the values *N* calculated at the extremities of each side, near the MRA2 units. Measurements were only made if a breeze or wind ran at the terminals, between 8 and 11 in the morning, 16 and 19 in the afternoon, in general during two or more days. Only one side, *PR* (20,7 km with 3400 m in diff. of height) showed a strong correlation between observed retards and computed distances; i. e. variations of mean *N* along the microwave path were not sufficiently represented by the

changes of N computed as above was indicated. (Radio soundings in Córdoba simultaneous with the measurements in Alpachiri – July 64 – showed in average a linear relation between N and h).

The results were:

BQ = 19410,30 m (± 3,5 cm) from 8 measurements
CQ = 37855,15 m (± 5,4 cm) " 10 "
BC = 18746,51 m (± 3,1 cm) " 11 "
PR = 20736,68 m (± 3,0 cm) " 12 "
AR = 50707,01 m (± 7,5 cm) " 10 "
AP = 30108,86 m (± 3,1 cm) " 10 "

3. Zenithal angles: in Tolombón reciprocal and simultaneous measurements were performed during 6 days (April 64) from 10 to 17 hours. The reciprocal z generally showed similar patterns; also maxima values within the period of observation. On the contrary, a definite relation didn't appear between z and the observed temperatures. Sets of six z steady values were taken to deduce vertical refraction angles.

	days July 1964				adopted values
	18	19	20	21	
z_{PA} = 91°02′ . .	41,5″	43,4″	41,5″	43,1″	91°02′42,4″
z_{AP} = 89°10′ . .	40,8″	40,5″	41,2″	57,1″	89°10′44,9″
z_{PR} = 80°21′ . .	01,5″	07,0″	00,1″	01,3″	80°21′02,5″
z_{RP} = 99°48′ . .	17,4″	23,5″	26,5″	22,0″	99°48′22,4″
z_{AR} = 85°40′ . .	08,5″	57,2″	57,0″	04,6″	85°40′01,8″
z_{RA} = 94°42′ . .	24,9″	25,4″	28,8″	22,8″	94°42′25,5′

Table 3: Averages z in the Alpachiri triangle.

In the Alpachiri trilateral reciprocal z were observed from 10 to 16 hours during 6 days (July 64). The side AP (30 km, between 380 and 890 m osl) only showed a definite trend of maxima values with maxima temperature. Strong variations in the z values on the sides AR and PR were observed: tens of seconds were the differences between the observed z_{AR} (AR= 50,7 km, from 380 to 4360 m osl). The z averages of each day, nevertheless are within few seconds (Table 3) and the means of the complete days (18, 19, 20, 21 July) were taken to compute the vertical refraction angles.

4. Latitude and Longitude determinations: 10 to 15 stars at $h = 30^0$ were observed at the 6 stations with 1″ theodolites, radioreceivers and marine clocks. A standard error between ± 2″ and ± 4″ can be assigned to the computed latitudes and longitudes. The resulting angles between the plumb lines, were in Tolombón:

$$\gamma_{CQ} = 0^0\,19'\,41'' \qquad \gamma_{BQ} = 0^0\,09'\,53'' \qquad \gamma_{BC} = 0^0\,09'\,48''$$

in Alpachiri:

$$\gamma_{AR} = 0^0\,26'\,28'' \qquad \gamma_{AB} = 0^0\,15'\,44'' \qquad \gamma_{PR} = 0^0\,10'\,44''$$

5. Geometric and astronomic leveling between A and P: In order to apply the classical method to compute Δz_{AP} and Δz_{PA}, a geometric leveling and an astronomic station were performed between A and P. The former gave Δh = 488,71 m and the later a plumb line deflection of 7″. Thus the zenithal angle of the right side AP at A was

$$\zeta_{AP} = 89^0\,12'\,07''$$

6. Refraction angles at Tolombón: Table 5 shows 9 sets of observed z taken at moments of steady variations. The Δz were calculated with the hypothesis

$$\Delta z_{CQ} = \Delta z_{QC}$$

for the presumable less perturbed side CQ.

As a further step it can be taken the CQ light path as a 3rd degree polynomial:

Table 5. Tolombón triangle: observed z and refraction angles Δz (in the case $\Delta z_{QC} = \Delta z_{CQ}$)

	a	b	c	d	e	f	g	h	i
April 64. Hour	11 11.15	11 11.30	11 14.30	11 15.30	12 11.15	14 14.45	15 15.00	15 16.00	16 14.45
	° ′ ″	° ′ ″	° ′ ″	° ′ ″	° ′ ″	° ′ ″	° ′ ″	° ′ ″	° ′ ″
z_{QC}	91 21 48	91 21 48	91 22 04	91 21 51	91 21 52	91 21 49	91 21 36	91 21 41	91 21 42
z_{CQ}	88 55 47	88 55 47	88 55 57	88 55 55	88 55 58	88 55 51	88 55 50	88 55 48	88 55 54
z_{QB}	98 19 08	98 19 09	98 19 23	98 19 24	98 19 08	98 19 05	98 19 11	98 19 01	98 19 09
z_{BQ}	81 49 41	81 49 41	81 49 47	81 49 55	81 49 49	81 49 48	81 49 49	81 49 50	81 49 51
z_{BC}	84 00 38	84 00 35	84 00 30	84 00 32	84 00 31	84 00 37	84 00 31	84 00 28	84 00 37
z_{CB}	96 08 05	96 08 07	96 08 09	96 08 09	96 08 07	96 08 10	96 08 14	96 08 09	96 08 14
$\Delta z_{QC}=\Delta z_{CQ}$	1 03	1 03	50	57	55	1 00	1 07	1 06	1 02
Δz_{QB}	54	53	42	35	50	55	43	57	46
Δz_{BQ}	10	10	1	−1	6	5	10	5	7
Δz_{BC}	15	18	26	18	18	14	14	21	9
Δz_{CB}	50	48	43	45	52	47	49	50	48

Table 7. Refraction Angles in Tolombón

	a	b	c	d	e	f	g	h	i
day hour	11 11.15	11 11.30	11 14.30	11 15.30	12 11.15	14 14.45	15 15.00	15 16.00	16 14.45
	″	″	″	″	″	″	″	″	″
Δz_{CQ}	65,8	67,2	57,5	61,5	58,5	65,5	66,4	73,2	62,1
Δz_{QC}	60,2	58,8	42,5	53,9	52,5	55,5	68,6	58,8	62,9
Δz_{QB}	51,2	48,8	34,5	31,9	47,5	50,5	44,6	49,8	46,9
Δz_{BQ}	12,8	14,2	08,5	2,1	08,5	09,5	08,4	12,2	06,1
Δz_{CB}	52,8	52,2	50,5	52,1	54,5	51,5	47,4	57,2	47,1
Δz_{BC}	12,2	13,8	18,5	14,9	15,5	09,5	15,6	13,8	09,9
$\zeta_{CQ} =$ 88° 56′ . .	52,8	54,2	54,5	56,5	56,5	56,5	56,4	61,2	56,1

$$y = A_{CQ}x^2 + B_{CQ}x^3$$

(x-axis coinciding with the tangent to the light path at C) and the CB and QB light paths as a 4th degree polynomial:

$$y = A_{CB}x^2 + B_{CB}x^3 + C_{CB}x^4$$

$$y = A_{QB}x^2 + B_{QB}x^3 + C_{QB}x^4$$

with the condition of a common curvature (for the horizontal light path) of the two light paths meeting in one point.

Table 7 shows the solutions for the 9 sets. The last row, zenithal angles ζ_{CQ} corrected by refraction, shows a little dispersion: it could be interpreted as an indication of the goodness of the hypothesis used.

It appears, nevertheless, a strong inverse curvature of the paths CB and QB near B. A proof made on these sides using the Saastamoinen tables (Bulletin Géodésique No. 78, 1965) by integration of temperature gradients in each tenth of the sides didn't verify the temperatures taken at the terminals (diff.: 12°!).

It can be eliminated the inverse curvature if the CB and QB light paths were described by a complete 2nd degree equation. The integration of temperature vertical gradients showed in this case a difference of 10°.

It seems to be impossible to represent by a simple model of atmosphere the strong asymmetry of Δz at the light paths CB and QB.

Finally, it also seems unlikely to attribute that asymmetry to an erroneous estimation of N in the computation of the tellurometric distances CB and QB. The two tables of Saastamoinen were used to verify that atmospheric models approaching such z asymmetry, give mean values of N from 5 to 8 ppm (with several hypothesis about U and dU) smaller than the N averaging the terminals: i. e. the sides would be 5 to 8 ppm greater and the Δz asymmetry would be increased in 8" to 12".

7. Refraction angles at Alpachiri: with the z values of Table 3 could be computed the 6 mean refraction angles:

$$\Delta z_{AP} = 1'22'' \qquad \Delta z_{AR} = 2'21'' \qquad \Delta z_{PR} = 0'49''$$

$$\Delta z_{PA} = 0'55'' \qquad \Delta z_{RA} = 1'39'' \qquad \Delta z_{RP} = 0'30''$$

The light paths AP and AR can be represented by 3rd degree polynomials: curvatures at the common terminal A coinciding within 2,5% and integration of t-gradients along the AR path compatible with the observed t at the terminals. That integration along PR gives a difference of 15°: PR runs near the mountain side from 890 to 4360 m *osl.*

8. Conclusions: First order sides (~20 km) in mountainous countries, with great differences in height (2000 to 3500 m) show strongly different reciprocal refraction angles: the greatest ones are not necessarily at the lower end.

First order sides with moderate differences in height ($CQ = 40$ km with 800 m; $AP = 30$ km with 500 m) seem to adapt to the linear variation of curvature derived from a 3rd degree polynomial, as Jordan-Eggert had traced. Likewise the long side AR (50,7 km with 4000 m diff. height) shows the same pattern: its curvature is compatible with the met. data taken at the terminals.

Part III

Elimination of Refraction from Geodetic Angular Measurments. Nivellitic Refraction. Conformal Theory of Refraction

Elimination of Refraction at Vertical Angle Measurements, Using Lasers of Different Wavelengths

by *Erik Tengström*, Uppsala

Introduction

The knowledge of the influence of the distribution of the scalar n in air is necessary both for optical distance measurements and for optical direction measurements. The same holds true, of course, also for corresponding measurements of microwave propagation, but we shall here deal with the visual spectrum, only. For a) optical *distance measurements* the distribution of group-index n along the path is essential, but also the distribution of phase-index n along the same path is needed. The former can be used to correct the observed optical path-length

$$\int_A^B n_g \, ds = L \quad \text{with}$$

$$\Delta s_1 = -\int_A^B (n_g - 1) \, ds \tag{1}$$

to obtain the length of the curved path in space between A und B. The latter distribution can be used to compute the difference Δs_2 between the Euclidean distance S and the distance $L + \Delta s$, so that

$$S_A^B = L + \Delta s_1 + \Delta s_2 \tag{2}$$

is the correct distance.

Δs_1, is the s.c. *phase-correction*, Δs_2 the *curvature-correction*, and we denote by S_A^B the curved path-length,

$$S_A^B = L + \Delta s_1 \tag{3}$$

Using two different wave-lengths, λ_B and λ_R, it would be possible to determine for a certain λ, Δs_1 in the following way, from measured $L_B - L_R$: In comparison with Δs_1, $S_A^B(B) - S_A^B(R)$ is a quantity of second order, and therefore,

$$\begin{aligned} \delta \Delta s_1 = \Delta s_1 (R) - \Delta s_1 (B) = L_B - L_R = \Delta L_R^B \\ = \int_A^B \{n_g (B) - n_g (R)\} \, ds \, (\lambda) \end{aligned} \tag{4}$$

ΔL_R^B can be measured, and the last integral can be written

$$\int_A^B F(R, B, \lambda)\,[n_g(\lambda) - 1]\,d\,s(\lambda), \text{ where} \tag{5}$$

$$F(R, B, \lambda) = \frac{n_g(B) - n_g(R)}{n_g(\lambda) - 1}$$

This expression is a function of the position along $s(\lambda)$, where the temperature is t^{0}C, total pressure of air p/mm Hg, and absolute humidity pressure e mm Hg. We have

$$n = 1 + \frac{n_o - 1}{1 + \alpha t} \cdot \frac{p}{760} - \frac{5{,}5 \cdot 10^{-8}}{1 + \alpha t} \cdot e \tag{6}$$

where n_0 is the group-index in dry air (0,03% CO_2) with t = 0^{0}C, p = 760 mm Hg. $a = 0{,}003660$; the termal coefficient of expansion of air.
We obtain

$$\begin{aligned} n_g(B) &= 1 + \frac{n_o(B) - 1}{1 + \alpha t} \cdot \frac{p}{760} - \frac{5{,}5 \cdot 10^{-8}}{1 + \alpha t} \cdot e \\ n_g(R) &= 1 + \frac{n_o(R) - 1}{1 + \alpha t} \cdot \frac{p}{760} - \frac{5{,}5 \cdot 10^{-8}}{1 + \alpha t} \cdot e \\ n_g(\lambda) &= 1 + \frac{n_o(\lambda) - 1}{1 + \alpha t} \cdot \frac{p}{760} - \frac{5{,}5 \cdot 10^{-8}}{1 + \alpha t} \cdot e \end{aligned} \tag{7}$$

$$F(R, B, \lambda) = \frac{n_o(B) - n_o(R)}{1 + \alpha t} \cdot \frac{p}{760} \cdot \frac{1}{\dfrac{n_o(\lambda) - 1}{1 + \alpha t} \cdot \dfrac{p}{760} - \dfrac{5{,}5 \cdot 10^{-8}}{1 + \alpha t} \cdot e} \tag{8}$$

$$\text{or, } F(R, B, \lambda) \simeq \frac{n_o(B) - n_o(R)}{n_o(\lambda) - 1}\left(1 + 0{,}14\,\frac{e}{p}\right) \tag{8a}$$

We can now write (4) as

$$\Delta L_R^B \simeq \frac{n_o(B) - n_o(R)}{n_o(\lambda) - 1}\left[1 + 0{,}14\left(\frac{e}{p}\right)_m\right] \cdot \int_A^B [n_G(\lambda) - 1]\,d\,s = -N\,\Delta s_1(\lambda) \tag{9}$$

$\left(\frac{e}{p}\right)_m$ being an estimated mean over the path. If we measure L in monocromatic light (λ), we have

$$S_A^B = L(\lambda) - \frac{\Delta L_R^B}{N},$$

$$\Delta s_1(\lambda) = \frac{\Delta L_R^B}{N} \text{ being the } \textit{path-correction} \tag{10}$$

for the λ-measurement. N may be computed from Barrel and Sears' formula for *group velocity index*

$$n = A + \frac{3\,B}{\lambda^2} + \frac{5\,C}{\lambda^4}, \tag{11}$$

λ being the wavelength in microns, reduced to vacuo and

$$A = 1 + 2876{,}04 \cdot 10^{-7}; \qquad B = 16{,}288 \cdot 10^{-7}; \qquad C = 0{,}136 \cdot 10^{-7}.$$

Experiments of determining path-corrections in aforesaid way, using lasers of different wavelengths, are now going on at ESSA, Boulder, Colorado, USA. The method and observation techni-

que was proposed in 1965 (or earlier) by Owens and Bender [1], who seem to have obtained already very promising results. For determining the *curvature correction* the same theory as used for b) optical *direction measurements* can be applied.

Determination of refraction through dispersion measurements.

For simplicity, we regard the light-beam as a plane curve through the observer A and the light-source *B*.

Let *P* be nearest point from *A*, where the tangent of the lightbeam is parallel to *AB*. Then the refraction angle a_A at *A* (Fig. 1) is

$$\alpha_A = \int_P^A \frac{d\alpha}{ds}\, ds = \int_A^P \sigma\, ds \tag{12}$$

where $-\frac{d\alpha}{ds} = \sigma$ is the variable curvature along *s*.

We know from Heath's formula, that

$$\sigma = \frac{\partial \ln n}{\partial \nu} = \frac{1}{n}\frac{\partial n}{\partial \nu} \tag{13}$$

Here *n* is the *wave refractive index* (*phase index*), being the positive normal of the ray. Applying Gladstone's and Dale's law, this can be written

$$\sigma = \frac{n-1}{n} \cdot \frac{1}{\rho}\frac{\partial \rho}{\partial \nu} \tag{13 a}$$

Writing (6) as

$$n - 1 = M_1 (n_o - 1) + M_2 \tag{6 a}$$

where M_1 and M_2 are atmospherical functions of position along *s*, we have

$$\sigma = \frac{M_1 (n_o - 1) + M_2}{1 + M_1 (n_o - 1) + M_2}\,\frac{1}{\rho}\frac{\partial \rho}{\partial \nu} \tag{13 b}$$

and therefore in radians

$$\alpha_A = (n_o - 1) \cdot \int_A^P \frac{M_1}{\rho}\frac{\partial \rho}{\partial \nu}\,\frac{ds}{1 + M_1 (n_o - 1) + M_2} + \int_A^P \frac{M_2}{\rho}\frac{\partial \rho}{\partial \nu}\,\frac{ds}{1 + M_1 (n_o - 1) + M_2} \tag{14}$$

If we denote the "meteorological integrals" with *R* and *Q*, we have

$$\alpha_A = (n_o - 1)\, R + Q \tag{14 a}$$

where n_o can be computed from *Barrel and Sears' formula* for any λ (reduced to vacuo)

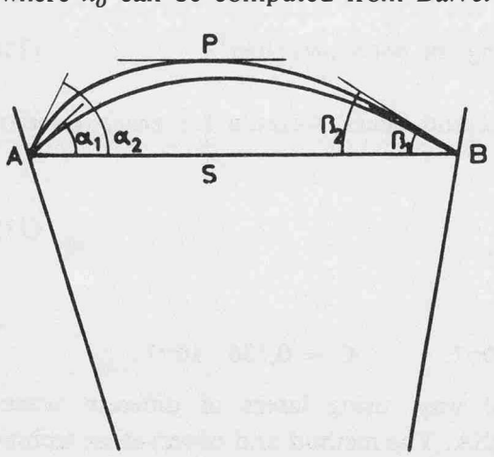

$$r_1 = \alpha_1 + \beta_1\,, \qquad r_2 = \alpha_2 + \beta_2$$
$$\delta_A = \alpha_2 - \alpha_1\,, \qquad \delta_B = \beta_2 - \beta_1$$

Refraction angles and total refraction

Fig. 1

$$n_o = A + \frac{B}{\lambda^2} + \frac{C}{\lambda^4},$$

and valid for *wave-index* (constants, see [11]). Now, using two wavelengths λ_1, and λ_2 ($\lambda_2 > \lambda_1$), we get

$$\begin{aligned} \alpha_A(\lambda_1) &= [n_o(\lambda_1) - 1] \cdot R + Q \\ \alpha_A(\lambda_2) &= [n_o(\lambda_2) - 1] \cdot R + Q \end{aligned} \tag{15}$$

Reasonably presuming R and Q being the same for both beams, we obtain the dispersion between the arriving rays at A equal to

$$\delta_{\lambda_1}^{\lambda_2} = [n_o(\lambda_1) - n_o(\lambda_2)] \cdot R \tag{16}$$

δ can be measured with high accuracy by interferometric methods (see below), so (16) gives R, and the refraction angle at A is

$$\alpha_A(\lambda) = [n_o(\lambda) - 1] \frac{\delta_{\lambda_1}^{\lambda_2}}{n_o(\lambda_1) - n_o(\lambda_2)} + Q = \bar{\alpha}_A(\lambda) + Q \tag{17}$$

for any wavelength λ. Q, which is very small for the visual spectrum, depends mainly on the humidity along s between A and P. It may be estimated accurately enough in the following way:

$$Q = \left(\frac{M_2}{M_1}\right)_m \int_A^B \frac{M_1}{\rho} \cdot \frac{\partial \rho}{\partial \nu} \cdot \frac{ds}{1 + M_1(n_o - 1) + M_2} = \left(\frac{M_2}{M_1}\right)_m \cdot R = -5{,}5 \cdot 10^{-8} \left(\frac{e}{P}\right)_m \cdot 760\, R, \tag{18}$$

where m denotes mean values between A and P.
Obviously the percentage Q of $\bar{\alpha}$ is approximately equal to

$$\frac{100 \cdot 5{,}5 \cdot 10^{-8} \cdot 760}{n_o - 1} \left(\frac{e}{p}\right)_m \%$$

or, with $n_o - 1 \sim 0.0003$ in all visual cases

$$Q = -0.14 \left(\frac{e}{p}\right)_m \alpha$$

E.g., if the relative humidity along s between A and P (approximately half way between A and B) is 70% and the corresponding mean temperature 10°C, we get at $p_m = 700$ mm, $e_m = 0{,}70.9.4 = 6.6$ mm and $\left(\frac{e}{p}\right) \sim 0.0094$, which means

$$Q = -0.0013\, \bar{\alpha}$$

Neglecting Q, we consequently commit an error of only 0.13%. A very rough estimate of $\left(\frac{e}{p}\right)_m$ is sufficient in most cases. If e.g. the refraction angle at A for a beam from B has been found to be 64.″2, when omitting Q, the error from neglecting humidity in abovementioned case is only 0.″08. We may of course also determine the total refraction $r = \alpha + \beta$ (see fig. 1) at a certain moment by means of simultaneous dispersion measurements δ_A and δ_B from A and B. We have, neglecting Q

$$r(\lambda) = [n_o(\lambda) - 1] \frac{\delta_A + \delta_B}{n_o(\lambda_1) - n_o(\lambda_2)} \tag{19}$$

The accuracy of this method for determining α and r is naturally depending on the magnitude of $\Delta\lambda = \lambda_1 - \lambda_2$. The bigger this difference is, the more accurate is the result. We therefore need to use two wavelengths, one in the red, one in the blue region of the spectrum. As the differential dispersion increases with decreasing wavelength (approximately as $1/\lambda^2$), it is especially important to go rather far out into the blue region, when choosing λ_1.

Interferometric method for measuring δ

The method of determining refraction by measuring the dispersion angle between two wavelengths in the arriving spectrum at A from a white lightsource at B is not new. It was proposed by *Näh-bauer* several decades ago, but the use of an interferometric observation technique for measuring δ was practically introduced at first at the Royal Institute of Technology in Stockholm 1948 [2 (Introduction)], when the author of this paper started his experiments with a double-slit interferometer, using conventional white lightsources and narrow filters. The old idea of using filters and of *pointing* at the red and blue images with a theodolite, and measuring with its circle the dispersionangle—or the angle between a red and blue lightsource—can never be accurate enough.

The aim of the author's experiments [3], [4], [5], [6], was originally to determine r accurately enough at the same time as the vertical angle measurements were carried out. With r and the results of the zenitdistances, the difference in the components of deflection of the vertical in the plane of the beams could be derived, enabling the determination of geoidal undulations by a purely geometrical method, avoiding the tedious astronomical position observations. The *msq* error in δ, desirable for achieving same accuracy as obtained from astronomical deflection stations of reasonable density (20--30 km) should be of the order of $\pm 0''.3$. Using phase-velocity and phase-index, which should be the case in this kind of determinations, the refraction angle is approximately $\frac{15}{\Delta\lambda}$ microns times δ. When e.g. $\Delta\lambda = 2000$Å, refraction is about 75 times the dispersion angle. The first experiments were carried out with interferometric filters at A for C and F of the Balmer series ($\Delta\lambda = 1700$Å), using a white filement lightsource at B. Later on a $Hg-Cd$ lamp, containing excited Hg- and Cd-vapour was introduced ($\Delta\lambda = 2088$Å). To obtain the wanted accuracy in α and r in these two cases, δ *must be measured to within at least* $0''.003$.

The first instrument used (see figures 2*a*, . . .), which was adapted to a Wild $T3$ theodolite, and had two double slits with variable slit-distances d, which always satisfied the condition

$$\frac{d_{\lambda,1}}{d_{\lambda,2}} = \frac{\lambda_1}{\lambda_2},$$

gives an internal mean error in δ (or in a small apparent angle between two light sources with different wavelengths) from 10 coincidence-measurements of the fringe-systems with equally spaced fringes (principle: see fig. 2) of about $\pm$ 0."03, which means an error in refraction (or deflection of the vertical difference) of the order of 2—3 seconds of an arc. The red fringe-system was always easy to see, and the accuracy in measuring coincidendes between two such systems often surpassed the one, mentioned above. But the blue fringes were very faint, also at small distances (visibility failed at distances greater than 1000 meters).

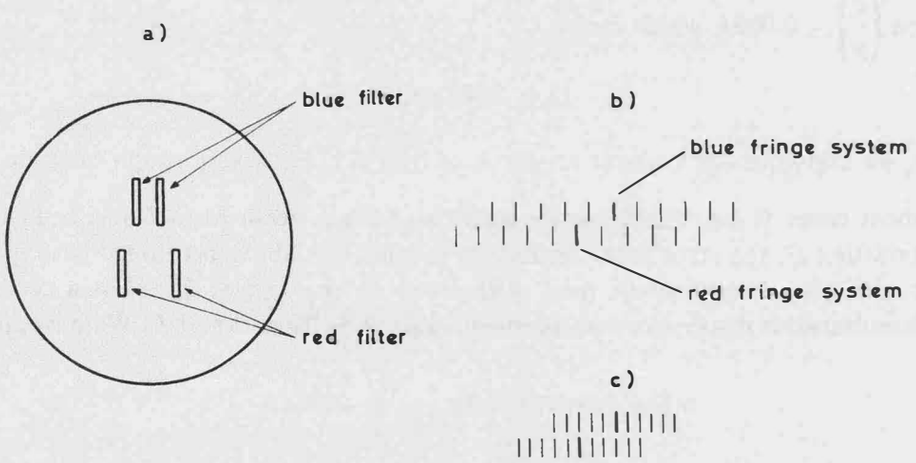

Prinziple of coincidence observation with small interferodispersometer

Fig. 2

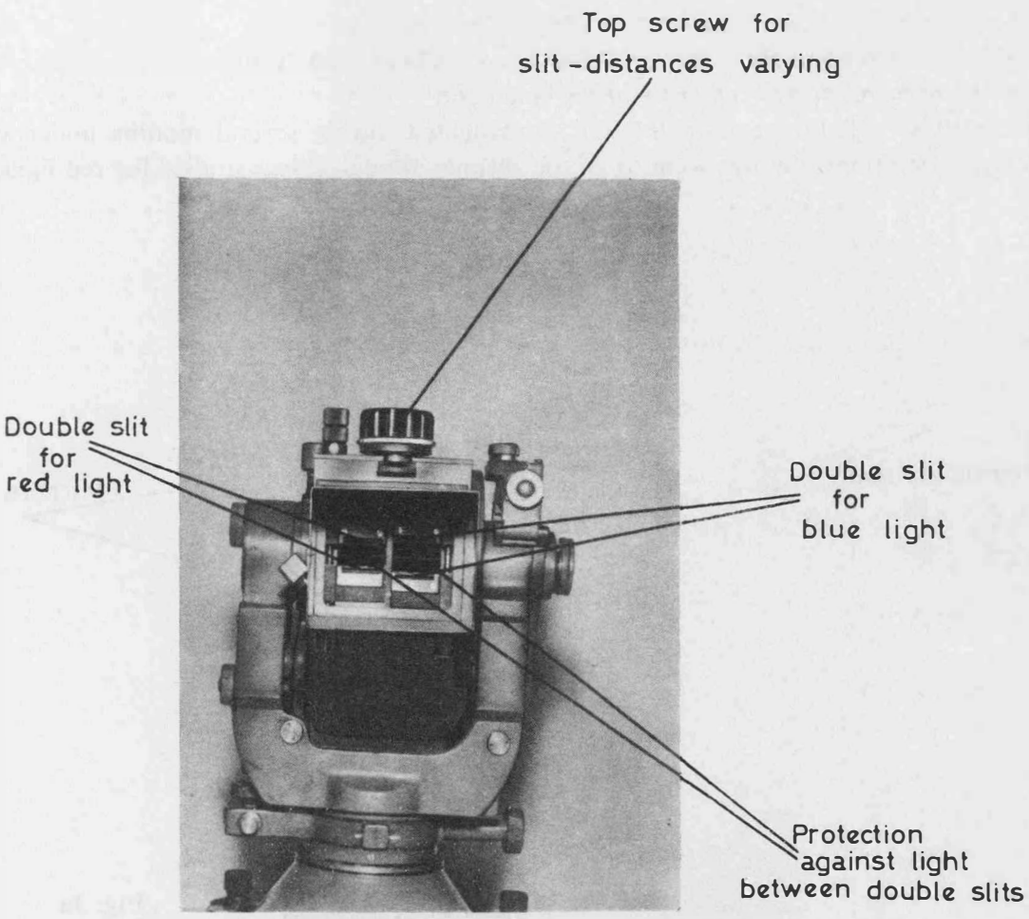

Fig. 2a

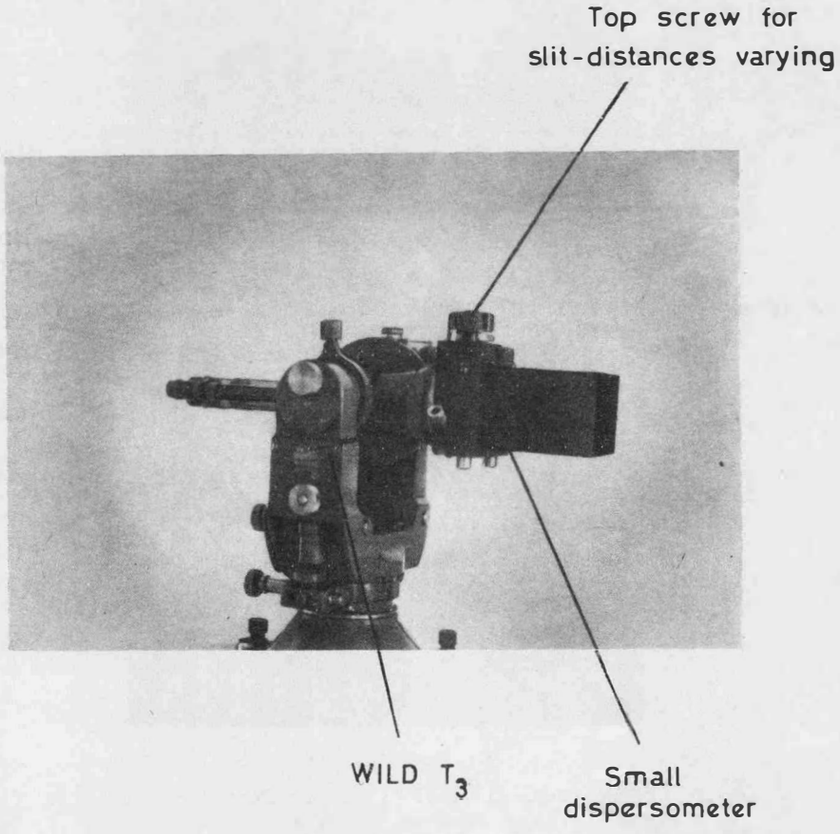

Fig. 2b

Small interferodispersometer with variable slit distances

We therefore had to face at least two problems to be solved:

1) *The problem of increasing the accuracy of δ-measurements at least 10 times*

2) *The problem of increasing the intensity of the blue light.*

The problem of scintillation and undulation, investigated during several months under various meteorological conditions, did not seem to be too serious, though it was studied for red light, only.

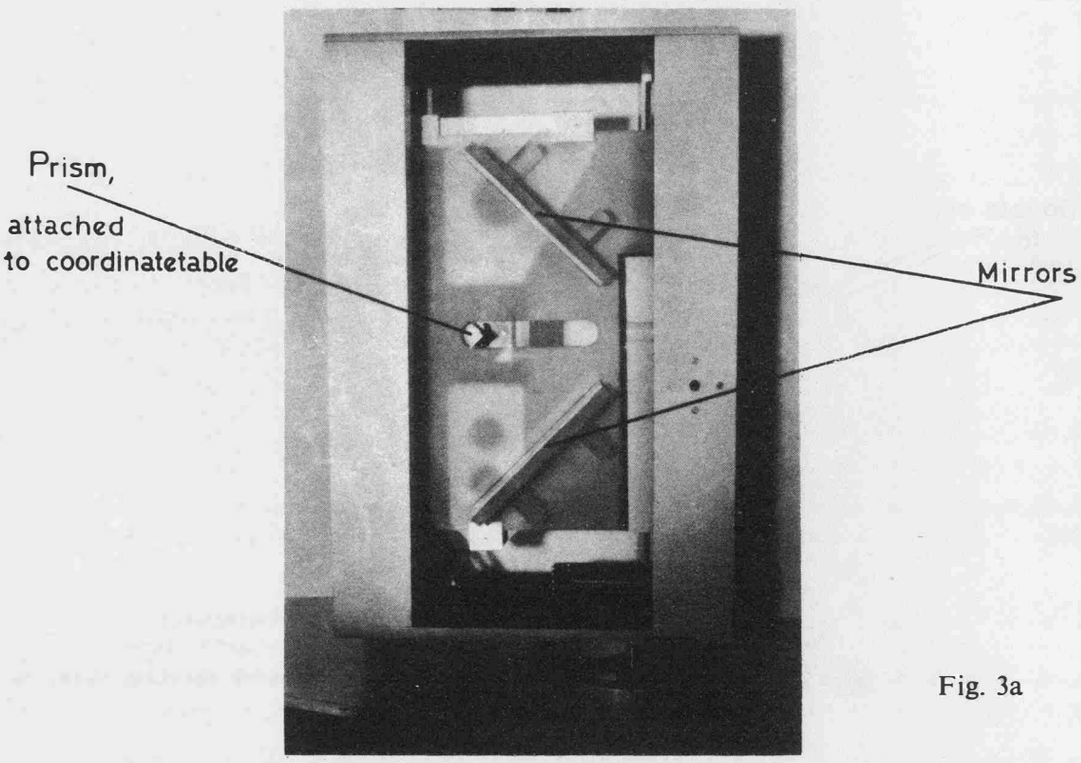

Fig. 3a

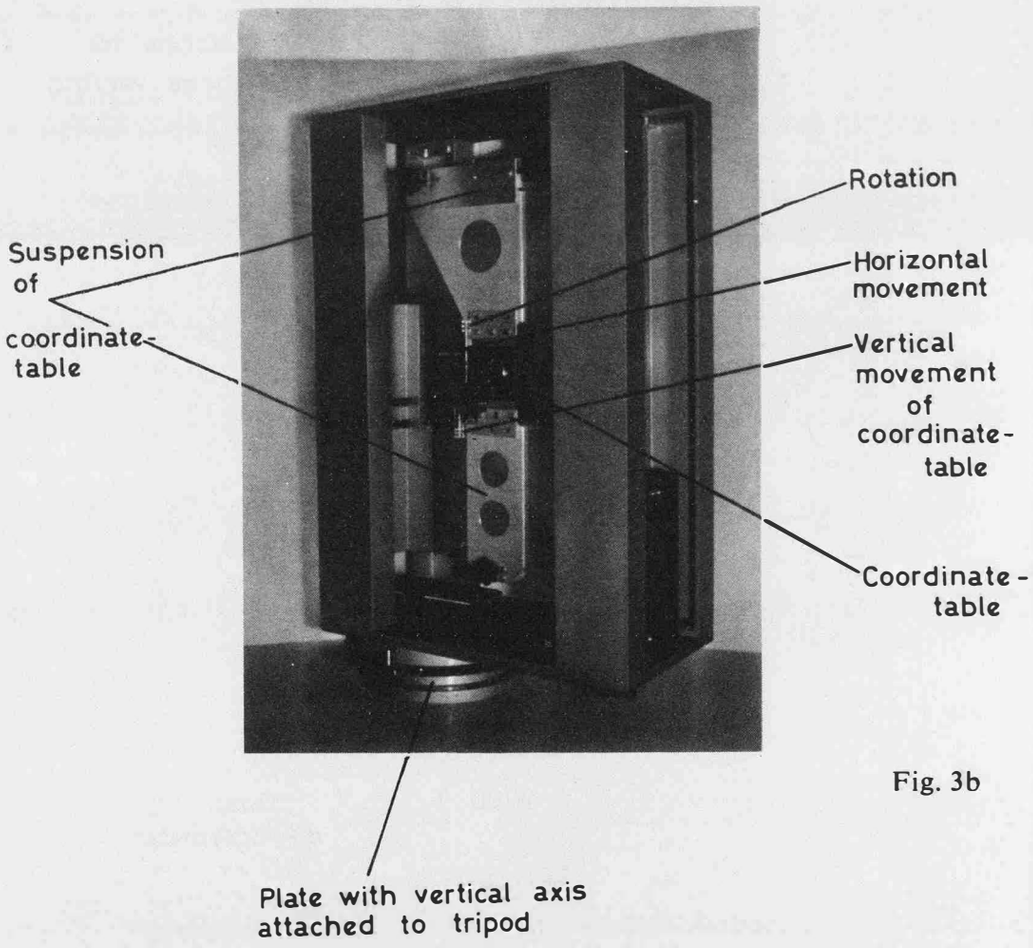

Fig. 3b

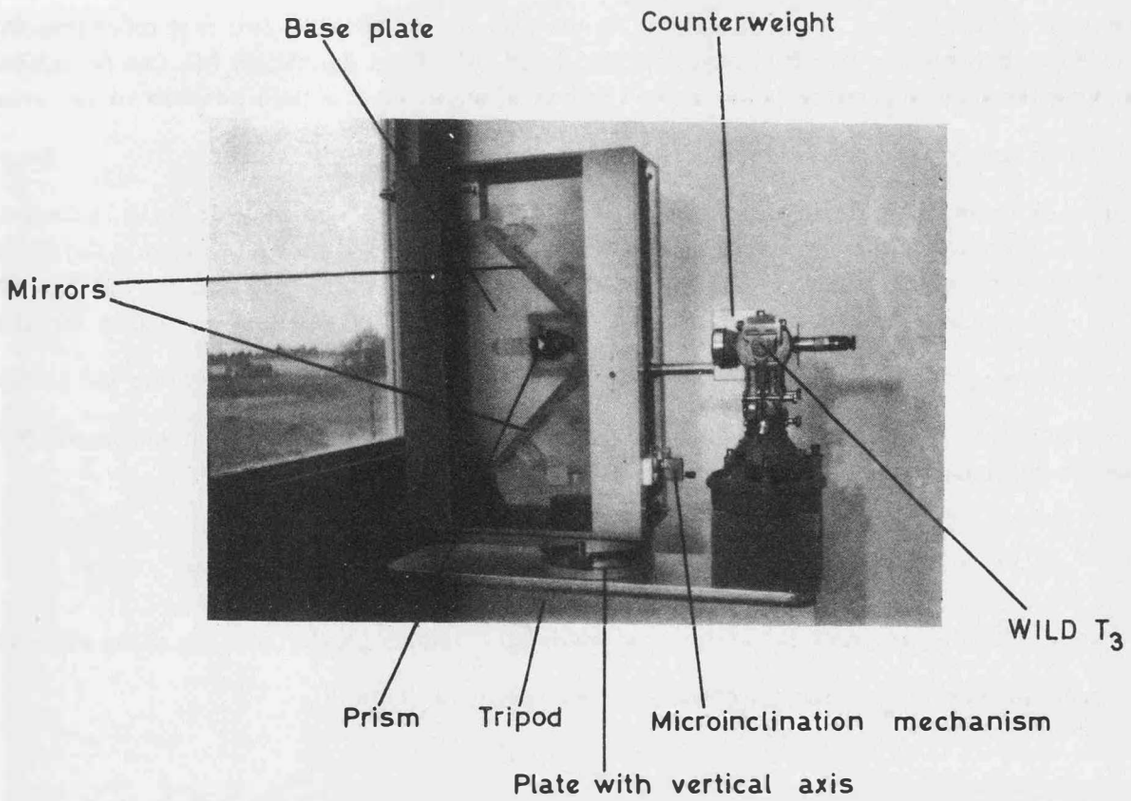

Fig. 3c

First type of big interferodispersometer

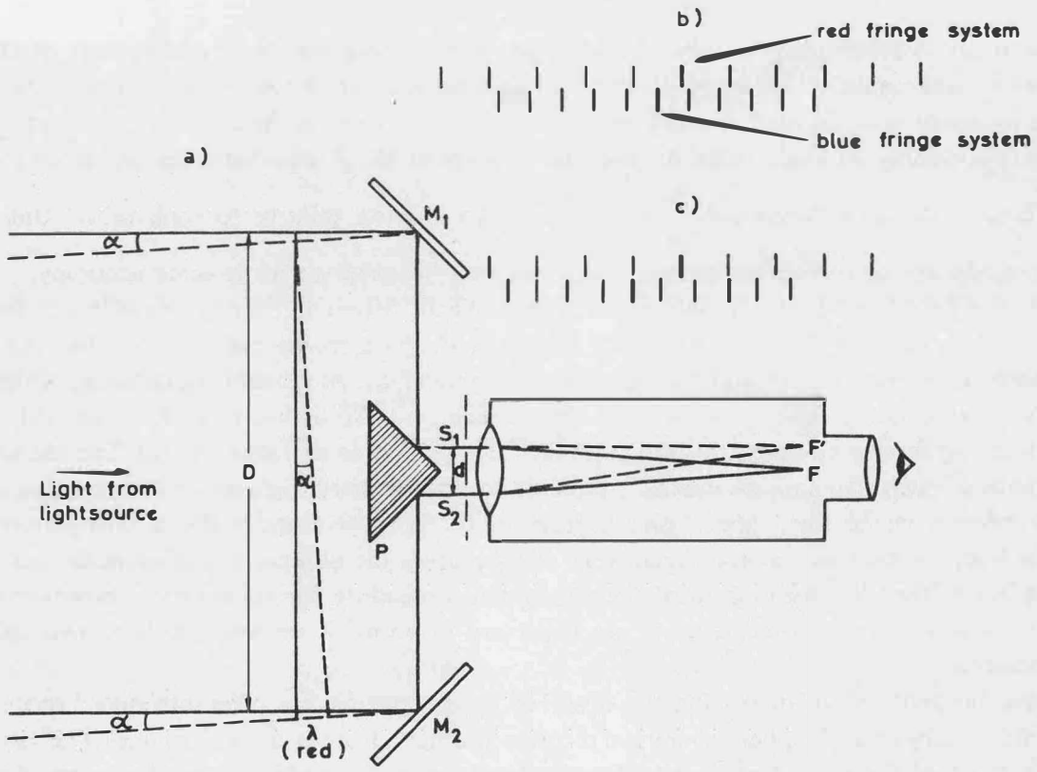

Principle of determining δ with first type of big interferodispersometer

Fig. 3

1) The accuracy might be increased more than 10 times by utilizing Michelson's principle in his big stellar interferometer. To make the system more stable, we built the instrument with fixed mirrors and a centered prism, which could move perpendicularly to the line, connecting the centres

of the mirrors (see fig. 3*a*, ...), thus changing the distance between the two first reflexionpoints. Coincidences between the two fringe-systems, produced by a fixed double slit (d), can be achieved by moving the reflecting centre prism along the line of sight. At a certain position of the prism, the distance between the reflexionpoints (see figure 3) is D_1. If δ is exactly equal to $\frac{\lambda_r}{D_1}$, the red vibrations at M_1 and M_2 differ in phase by one red wavelength. As δ is very small (α in fig 3), there will be enough diffraction at the mirrors, so that we can select a pair of red rays (not obeying the normal law of reflexion) which reach the slits by paths, identical with those traversed by the blue pair of rays. The phase difference between the red vibrations being increased by λ_1 makes the angle between the two zerofringes equal to $\frac{\lambda_r}{d}$, which means, that the red fringe of order one will coincide with the blue zerofringe. The dispersionangle (or a small angle between two monochromatic lightsources) is consequently

$$\delta = \frac{\lambda_r}{D_1} = \frac{\lambda_r}{d} \cdot \frac{d}{D_1},$$

which shows that the accuracy in determining δ will be $\frac{D_1}{d}$ times greater than by using the small instrument. Increasing D, a second coincidence will occur at D_2, and

$$\delta = \frac{2\lambda_r}{D_2} = \frac{2\lambda_r}{d} \frac{d}{D_2}.$$

or in general

$$\delta = \frac{n\lambda}{D}. \tag{20}$$

In the small "interferodispersometer" (first instrument), there will be a contraction of the fringesystems by increasing slitdistances. In order to observe accurately very minute angles, the objective of the telescope and the magnification power of the eye-piece must be increased without decreasing the optical quality of the system. In the big instrument the fringe-distances are always constant. The fringe-systems (with spacings $\frac{\lambda_r}{d}$ and $\frac{\lambda_b}{d}$ are only moving relative to each other, thus producing coincidences of increasing orders, which may all be observed with same accuracy.

As the light from conventional sources is not perfectly coherent, only fringes of low order are possible to observe. It is therefore necessary to adjust the instrument carefully, so that the prism is symmetrical to the mirrors and the mirrors symmetrical to the distant lightsource, which means, that we may observe the region close to the zerofringes. (Adjusting procedure, see [6]).

By using *lasers*, however, this difficulty has been overcome to a great extent. The extremely high coherence of such lightsources makes it possible to observe very high order fringes (also such fringes, produced inside the higher order diffraction patterns). Naturally the intensity falls rapidly, but the high intensity of the laser beam very often enables the observation of coincidences of orders greater than 2000. A speeding up of the adjustment-procedure for symmetry is however obtained, and the number of the coincidence is not necessary to know, if we make at least two coincidence observations.

Another principle of increasing the observed fringe-spacing has been introduced recently at our Institute in Uppsala. A spherical mirror receives the light from a distant source. The two parallel slits in front of the mirror produce diffraction patterns with double-slit fringes in the focal plane of the mirror, which are not possible to observe directly with desirable accuracy. However, by placing a wide angle optical edge of glass inside the focus (see. fig 4) it is possible to increase the apparent fringespacing, so that coincidences may be observed with same accuracy as in the Michelsoninstrument. The image in the focal plane is free from chromatic aberration, which is a great advantage. A careful one time adjustment of the edge solves the difficulty of finding the zerofringe region (low order fringes). Figures 4*a*, *b* . . show the new instrument.

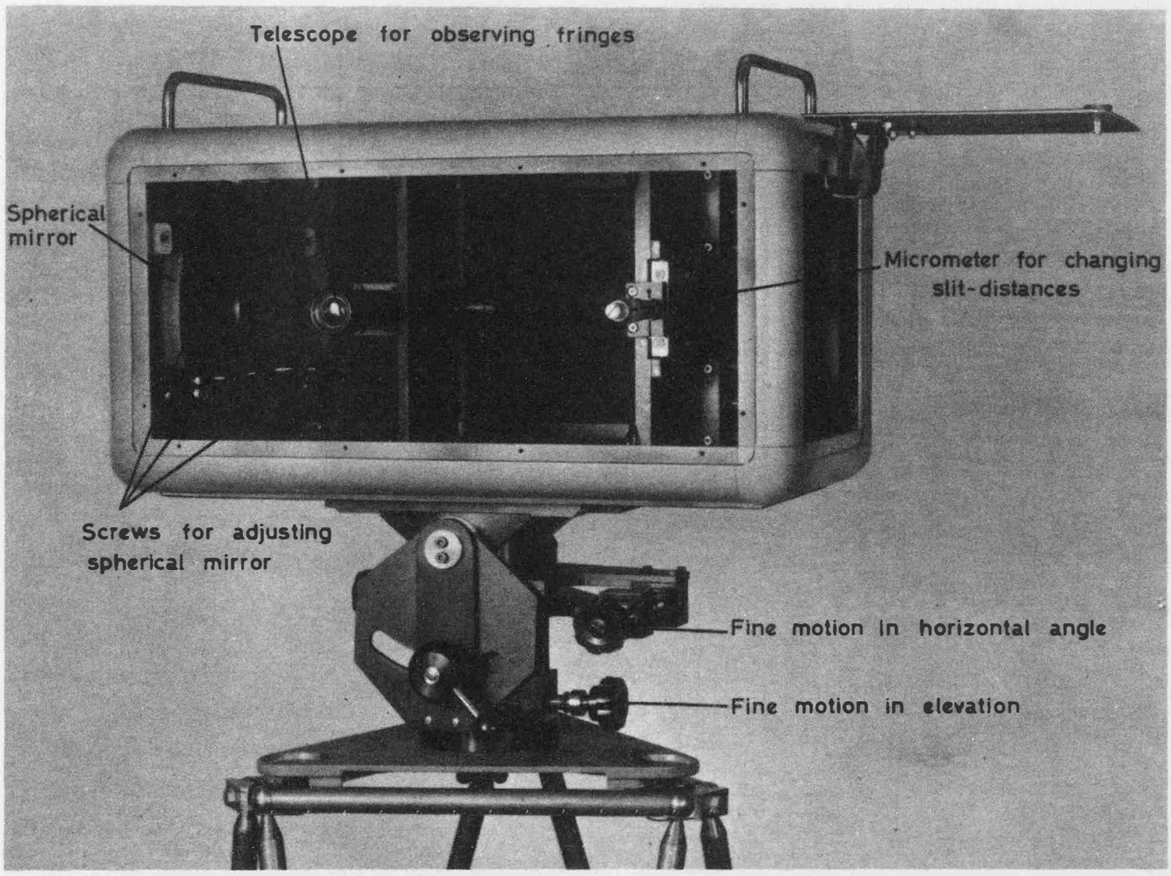

Fig. 4a

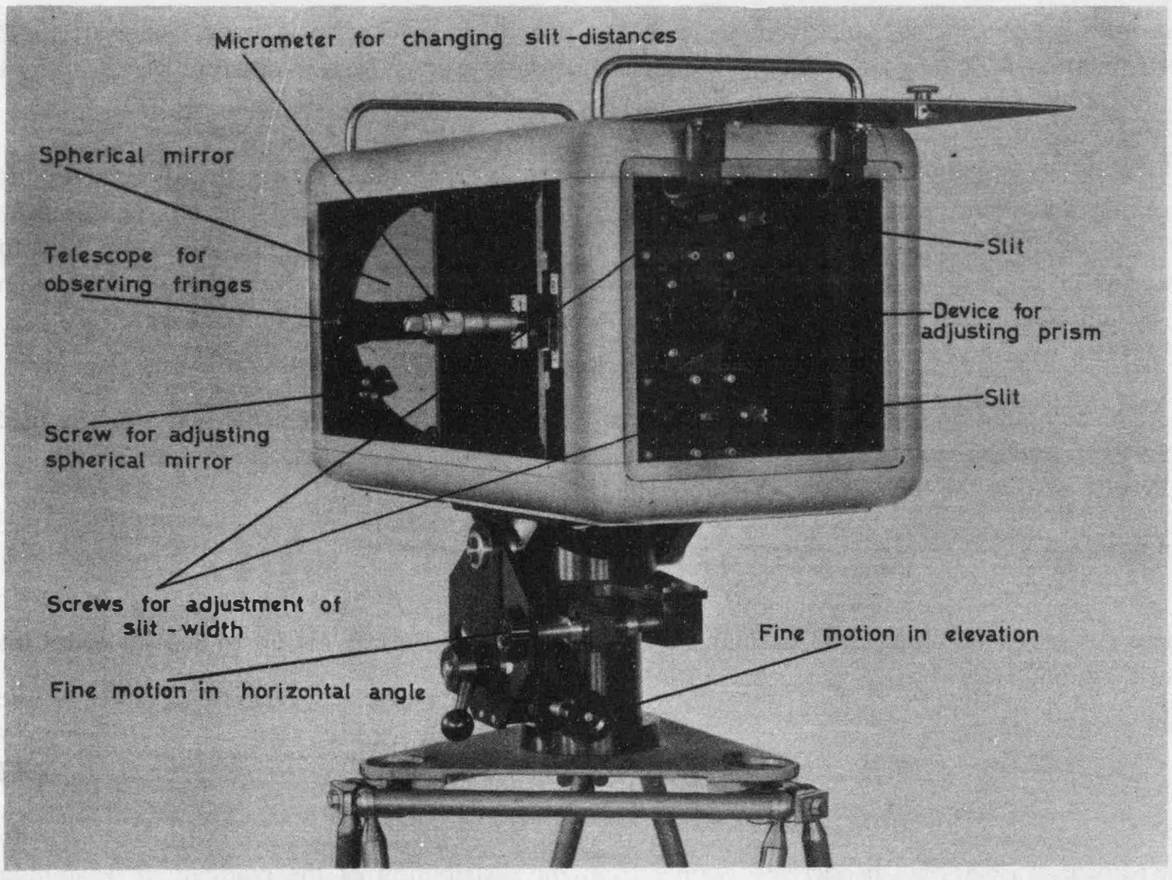

Fig. 4b

Second type of big interferodispersometer

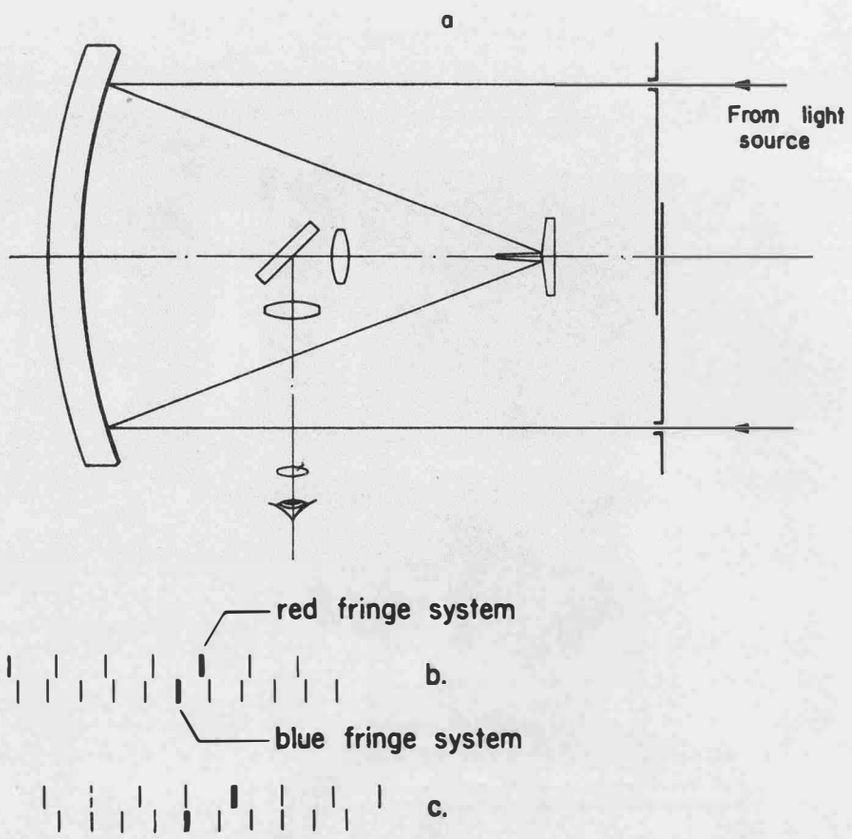

Principle of second type of interferodispersometer

Fig. 4

Laboratory experiments, already made with the two big interferodispersometers show, that the determination of δ may be made from coincidence observations in two different wavelengths to within $\pm$ 0″002, which corresponds to a mean error in α and r of less than $\pm$ 0″2.

The use of lasers will probably solve our second problem:

2) *Increase of intensity* over greater distances. A He-Ne laser (6828 Å) has already been used for checking the intensity of fringes, and it seems as if such lightsources may enable measurements to be made over more than 20 km. The blue source will be either a shortpulse Argon- or Krypton laser, which are now both commercially available. Experiments with two lasers are probably going to be started this fall in Uppsala at two bases, one 7 km long and one 15 km long.

Addendum:

The computation of the curvature-correction Δs_2 at distance-measurements may now be made from the refraction results above in the following way:

We have
$$\Delta s_2 = \int_O^S \cos\left(\alpha_A + \int_O^l \sigma\, dl\right)^2 dl - s\,.$$

where l is reckoned along S. This may be simplified, taking only terms up to second order into consideration. Thus

$$\Delta s_2 = -\frac{1}{2}\int_O^S \left(\alpha_A + \int_O^1 \sigma\, dl\right)^2 dl \qquad (A\,1)$$

The l-function $\int \sigma\, dl$ may be derived mainly from the distribution of the gradient of wave-index $\left(\frac{\partial n}{\partial \nu}\right)$ along S. (Temperaturegradient along S). For constant σ ($\alpha_A = \beta_B$, $r = 2\,\alpha_A$) we get

$$\Delta s_2 = -\frac{\alpha_A{}^2}{6}\, s \text{ or } \Delta s_2\,(\text{mm}) = -\,3{,}9174\,.\,10^{-6}\,\alpha''^2\, s_{\text{km}} \qquad \text{(A 2)}$$

If, e.g., we use the "3-level solution" for α_A, β_B viz $\frac{r}{s} = \frac{\alpha_A + \beta_B}{s} = \sigma_M(\frac{s}{2})$

we obtain $\delta\,(l) = a + b\,l$, where $a = \frac{2\,(3\,\beta_B - r)}{s}$; $b = \frac{6}{s^2}\,(\alpha_A - \beta_B)$

$$\text{and } \Delta s_2 = -\frac{s}{30}\,(17\,\alpha_A{}^2 + 17\,\beta_B{}^2 - 29\,\alpha_A\,\beta_B) \text{ or} \qquad \text{(A 3)}$$

$$\Delta s_2\,(\text{mm}) = -\,0.78348\,(17\,\alpha''_A{}^2 + 17\,\beta''_B{}^2 - 29\,\alpha''_A\,\beta_B'')\,.\,10^{-6}\,s_{\text{km}} =$$

$$= -\,0.78348\,(17\,r''^2 - 63\,\alpha''_A\,.\,\beta''_B)\,.\,10^{-6}\,s_{\text{km}}$$

Numerical example: $r = 500''$; 1) $\alpha_A = \beta_B$; $\Delta S_2 = -\,24$ *mm*

$S = 100$ km; 2) $\alpha_A = 300''$, $\beta_B = 200''$; $\Delta S_2 = -\,37$ mm

3) $\alpha_A = 400''$, $\beta_B = 100''$: $\Delta S_2 = -\,135$ mm

References

1. *Bender, K. and Owens, C.:* "Correction of optical distance-measurements for the fluctuating atmospheric index of refraction". Journal of Geophysical Research No 2461, Washington DC, 1965.
2. *Tengström, E.:* "Outlines of a method of determining the Geoid in Sweden", Geographical Survey Office of Sweden, RAK Meddelande No 22, Stockholm 1954.
3. *Tengström, E.:* "On a method of determining terrestrial refraction by means of double slit interferometers", Proceedings of the Third Meeting of the Nordic Geodetic Commission, Copenhagen 1959.
4. *Tengström, E.:* Same title, Report to Sec I at the IAG-meeting (General Assembly) in Helsinki, 1960.
5. *Tengström, E. and Vogel, A.:* "On the determination of atmospherical refraction by measuring dispersion with interferential methods". Paper, presented at the Second Symposium on Three-dimensional Geodesy, Cortina d'Ampezzo 1962, Review in Bull. Géod. No 67 by P. L. Baetsle.
6. *Tengström, E. and Vogel, A.:* "Research on Methods of Determining Level Surfaces of the Earth's Gravity field", Final report to AFCRL, Contract AF 61(052)-226 pp 1—14. Uppsala 1964.

Refraction in Precise Levelling

by *T. J. Kukkamäki*, Helsinki

The effect of refraction on precise levelling is small owing to the shortness of sights and because of the fact that we can eliminate most of the refraction by using equal sight lengths forwards and backwards. Levelling refraction differs in nature from refraction in the trigonometrical height measurements owing to the nearness of the ground.

Refraction in levelling has been studied for a long time. Names such as Lallemand, Hugershoff, Kohlmüller, de Graaff-Hunter, Cole and Bomford come to mind. Climatological parameters were measured with quite complicated instruments. The purpose of most of these investigations was only to elucidate the phenomenon qualitatively. The knowledge obtained on levelling refraction, however, was the same as it is now.

When we began the Second Levelling of Finland in 1935, we studied the possibility of determining the refraction quantitatively. The results were promising and since 1937 we have measured the vertical temperature gradient in connection with levelling and computed the refraction correction.

Since the second world war more attention has been paid to levelling refraction.

K. Brocks of Hamburg has made an exhaustive study of microclimatics and has calculated the parameters on which levelling refraction and trigonometrical refraction depend.

G. Reissmann of Dresden has compared numerous temperature functions by measuring the vertical gradient with mercury thermometers. R. Eger of Dresden has made observations on a test line.

R. Hase of München has constructed a gradient meter with constantan-copper thermoelements. H. Ellenberg of München has compared several gradient meters of different types.

O. Simonsen of Copenhagen has endeavoured to determine levelling refraction at different heights above ground in order to derive absolute values of refraction. He has also observed the refraction and temperature gradient simultaneously.

Several studies have been performed in Yugoslavia. J. Stevanović has computed the refraction in the levelling net of the country. He has also studied refraction on a special test line.

In Poland H. Strusinsky has made large-scale experiments in test areas.

In Hungary D. Csatkai and E. Hönyi have attempted to determine refraction with the aid of statistical temperature values.

A lot of work has been done, but the results do not seem to be very convincing. M. Kneissl for instance has found that the observation of meteorological parameters takes too much time and thus it is not practical enough to determine the levelling refraction in that way. Other sources of errors are more dominant. I. I. Entin of the Soviet Union has made 3400 observations without discovering any correlation between the levelling refraction and vertical temperature gradient.

Investigations in recent decades have given a fairly clear qualitative picture of the levelling refraction. Quantitative determination has not yet been solved satisfactorily for regular levelling. The following conclusions can be drawn:

The refraction effect in precise levelling depends on the vertical temperature gradient. Other factors are insignificant.

In day light the vertical temperature gradient is negative. The sight bends up and the image vibrates several times a second. Staff readings are dependable provided the vibration is not too strong.

At night the gradient is positive, the sight bends down and slow swaying occurs with a period ranging from seconds to minutes. Staff readings are unreliable because of the swaying.

It makes little difference whether the temperature is expressed as a function of log h, h^2 or h^c of the height h. The exponent c varies with the hour of day and with the weather, but an average value of $c = -0.1$ gives satisfactory accuracy for the computation of levelling refraction.

In precise levelling with equal sight lengths the refraction effect is eliminated on level ground but on slopes refraction causes a systematic error. In regular levelling work in daytime under favourable weather conditions and using a sight length of 50 m, the refraction decreases elevation differences by 0.05 – 0.10 mm per metre.

The temperature gradient can be observed without delaying the work. The refraction correction has little significance in regular levelling but in special levellings, where exceptional accuracy is needed, the correction for refraction may improve the result.

Eliminating the Refraction Error from the Long Optical Sights in the Water-Crossings

by *Juhani Kakkuri*, Helsinki

The Finnish part of the levelling across the Aland archipelago and Aland sea from Finland to Sweden is going on. This levelling can be carried out with the same accuracy as the precise levelling around the Gulf of Bothnia, [1]. The agreement between the different elevation systems in the nordic countries can be made essentially better by closing the levelling line around the Gulf of Bothnia. In addition to this the precise elevations are aquired to Aland. These elevations can be used in order to study the crustal movements in the area of the Aland archipelago.

The Finnish part of this levelling contains the lines running from the little parish Kustavi via the islands of Åva, Enklinge and Vårdö to the mainland of Aland and from Aland to the rocky islet of Märket on the boundary line. The line from Kustavi to Aland was measured during the years 1963–1966, containing the following water-crossings

Length of crossing in meters	Number of crossings
shorter than 300	54
300– 500	19
500–1000	8
1000–1850	6
Total	87

On the basis of the good results of the test measurements made in the year of 1963 these 87 water-crossings were measured optically. The optical measurements were made using the classical levelling instruments Zeiss NiA and the modern automatic instruments Zeiss Ni2 as equipped with their special water-crossing devices.

The most harmful error source of the optical methods is refraction. When using the sight lengths of several hundred meters the refraction causes serious errors, which are difficult to eliminate. The main part of the refraction can be eliminated by carrying out simultaneous observations with two levelling instruments in opposite directions and taking the mean of these observations. The remaining error, the asymmetrical refraction error, can be made smaller either by the Kukkamäki's method in which the refraction correction is computed from the direct measurements of the vertical temperature gradient, or by avoiding measurements in weather conditions causing asymmetrical refraction fields.

The measurements of the levelling line from Kustavi to Aland were made in suitable weather conditions, and in addition to this the refraction corrections were computed.

1. Observing the vertical temperature gradient and computing the refraction correction

Kukkamäki has shown that the main part of the levelling refraction can be determined by measuring the vertical temperature gradient. The other microclimatical factors: humidity, air pressure, and the content of carbonic acid in the air, which have effects on the levelling refraction can be neglected as compared with the vertical temperature gradient, [2].

The application of Kukkamäki's method to the water-crossings is as follows. The crossing, the length of X, is divided into n parts for measuring the vertical temperature gradient. These divisions are $x_1, x_2, \ldots, x_n$. The temperature gradient $\frac{dt}{dz}$, belonging to each division x, is measured along the sight line. The refraction, R, can be computed from the formula

$$R = A \sum_{\nu=1}^{n} x_\nu s_\nu \left(\frac{dt}{dz}\right)_\nu \qquad (1)$$

in which s_ν is the distance between the division x_ν and the levelling staff. The coefficient A depends on the temperature t, air pressure p and humitidy e. It can be computed from the formula, [3],

$$A = -10^{-6}\left[\frac{1.116}{(1+0.00367\,t)^2}\,\frac{p}{760} - \frac{0.0002\,e}{(1+0.00367\,t)^2}\right] \tag{2}$$

When deriving the formula (2) the values 0.556. μm for the wave lenght of white light and 0.03 percent for the content of carbonic acid in the air are used. In normal conditions, $t = +15^0$C, $p = 760$ mmHg, and $e = 7.7$ mmHg (corresponding relative humitidy of 60 percent), the coefficient has the value

$$A = -1.001 \cdot 10^{-6} \tag{3}$$

The accuracy of the refraction R as computed from the formula (1) is determined by the gradient $\frac{dt}{dz}$ while the other quantities A, x, and s can be determined with sufficient accuracy.

1.1 Measuring the vertical temperature gradient

The vertical temperature gradient is measured by the differential thermometer, which has been used by the Finnish Geodetic Institute since 1938, [2], [4]. The operation of the thermometer is based on the principle of the Wheatstone's bridge. There are two electric resistors, D_1 and D_2, made of thin nickel wire, in the thermoneter, and the temperature difference between the resistors is measured. According to Hytönen, this temperature difference Δt can be measured with accuracy $\pm$ 0^0.087, [4].

In addition to the inner error of the differential thermometer the temperature difference between electric resistors D_1 and D_2 is affected mainly by external errors from the measuring altitude of the gradient and from the fluctuation of the gradient field during observation

1.11. Measuring altitude of the gradient

It is presupposed that when computing the refraction R from the formula (1) the vertical temperature gradient is measured from the right altitude which is equal with the altitude of the sight line, Z_0. Supposing that the altitude of the lower resistor is z_1 and that of the higher is $z_2 = z_1 + 2$ meters, and that there exist the temperatures t_1 and t_2 at the altitudes z_1 and z_2 respectively. The altitudes of the resistors have to be determined so that

$$\left(\frac{dt}{dz}\right)_{z=Z_o} = \frac{t_2 - t_1}{z_2 - z_1} = \frac{\Delta t}{2} \tag{4}$$

Thus, the altitudes of the resistors D_1 and D_2 are bound to the altitude of optical sight. The connection between them is determined by the function, expressing the dependence of the temperature on the altitude. This function is above the smooth and uncovered surfaces as follows

$$t = a + b\,z^c \tag{5}$$

in which a, b, and c are the constants. The most important of them is the exponent c, which depends on the elevation angle of the sun and the quality of the surface. In summer in Finland its value alternates daily as follows, [5], [6]:

$$-0.5 \leq c \leq +0.5\,. \tag{6}$$

From the formulae (4) and (5) we have $\frac{\Delta t}{2} = b\,c\,Z_o^{c-1}$, and because of $b = \Delta t/(z_2^c - z_1^c)$ we finally have

$$Z_o^{c-1} = \frac{z_2^c - z_1^c}{2\,c} \text{ when } c \neq 0 \tag{7}$$

and

$$Z_o = \frac{2}{ln\,(z_2/z_1)} \text{ when } c = 0\,. \tag{8}$$

The connection between z_1, z_2, and Z_0 is determined by the formulae (7) and (8). On the basis of these formulae we can show, that in all weather conditions z_1 can be determined approximately from the formula

$$z_1 = Z_o - 0.85 \text{ meters, when } 1.75 \text{ m} \leq Z_o \leq 5.00 \text{ m} \tag{9}$$

without making greater than 10 percent relative error.

1.12. Fluctuation of the gradient field

In practice it is impossible to carry out gradient measurements in all divisions x_v simultaneously. Generally the gradients of the divisions are measured one after another firstly in the direction from the levelling instrument to the staff and then in the opposite direction from the staff to the levelling instrument. Thus we have two gradient measurements for each division, and the average values are used. Simultaneously optical observations are made. If the gradient of the division fluctuates a random error results.

The fluctuation of the gradient field was studied during the summer of 1963. It was found on the basis of about 1500 observations that the larger the fluctuation of the gradient, the stronger the mean gradient of the crossing is. The fluctuation is further most serious when the sun is being covered by a cloud or coming out from a cloud. The wind diminishes the fluctuation. The mean error of one gradient observation measured at the altitude of about 2 meters is the function of the mean gradient of the crossing, g, as follows:

$$m_g = (1.862 \pm 0.215)\, g^2 + (0.031 \pm 0.023)\, g + (0.018 \pm 0.002). \tag{10}$$

On the basis of the interpolation formula (10) the following table is computed

Table 1

g in ^{0}C/m	m_g in ^{0}C/m
− 0.20	± 0.086
− 0.10	0.034
0.00	0.018
+ 0.10	0.040
+ 0.20	0.099
+ 0.30	0.195

The mean error of one gradient given in Table 1 is the result from the following factors: 1) the inner errors of the differential thermometer, 2) the altitude error of the gradient, and 3) the fluctuation error, and thus it expresses the total error of one gradient observation. According to Hytönen the accuracy of the temperature difference Δt is $\pm$ 0^0.087 as measured by the differential thermometer, [4]. In the gradient measurement it causes the error $\pm$ 0.044 ^{0}C/m. This error is, when there exists the zero gradient, $\pm$ 0.018 ^{0}C/m according to table 1, and thus it is smaller than Hytönen's value. When deriving the inner error of the differential thermometer Hytönen estimated that the reading error of the galvanometer is $\pm$ 0.2 scale divisions causing the error of $\pm$ 0^0.082 for the temperature/difference Δt. Estimating that the reading error of the galvanometer is $\pm$ 0.1 scale divisions and taking into account also the other inner errors of the differential thermometer we have the error of $\pm$ 0^0.045 for the temperature difference and $\pm$ 0.023 ^{0}C/m for the temperature gradient which shows a rather good agreement with the errror of $\pm$ 0.018 ^{0}C/m.

The inner error of the differential thermometer is, however, a quite unessential factor when criticizing the accuracy of the measurement of the vertical temperature gradient. The fluctuation of the gradient field is the decisive factor. The accuracy of the gradient measurements is rather good when the prevailing gradient is small, but it quickly gets worse when the gradient becomes stronger and reaches the relative error of 65 percent already at the gradient's value of $\pm$ 0.30 ^{0}C/m. This means that the optical water-crossings are possible only when the vertical temperature gradient is small.

1.2. The accuracy of the refraction correction

The refraction correction can be computed from the formula (1). If all the divisions x_v are equally long, $x_1 = x_2 = \ldots = x_n = x$, the formula (1) can be put in the form

$$R = 0.5\, Ax^2 \sum_{v=1}^{n} [2(n - v) + 1] \left(\frac{dt}{dz}\right)_v$$

The mean error of the refraction correction as computed from the formula (1′) is the following

$$m_R = \pm 0.5\, AX^2 m_g \sqrt{\frac{4n^2 - 1}{3n^3}} \qquad (11)$$

in which $X = nx$ is the length of the crossing, n is the number of the divisions, and m_g the mean error of one gradient observation. The mean error m_R is the function of the length X, the mean error m_g, and the number n. Thus, the accuracy of the refraction correction can be made better by adding the number of the divisions of X, i. e. by making the measuring points of the vertical temperature gradient thicker. The mean error m_g is given in table 1.

The following example of how to compute the refraction and its mean error is given. On the 27th of May 1963 the following gradients were observed at the measurement of the 413 m long water-crossing: $\pm$ 0.18, + 0.12, + 0.20, +0.15, + 0.20, + 0.12, + 0.08 and 0.00 ^{0}C/m. Thus, the mean gradient of the crossing was $g = + 0.13\,^0$C/m. The mean error m_g is according to table 1 the following $\pm$ 0.053 ^{0}C/m. Because the lenght of the crossing is 413 m, and the number of the divisions is 8, the division x has the following value 51.6 m. From the formulae (1′), (3) and (11) we have

$$R = - 13.29 \text{ mm}$$

$$m_R = \pm\ 1.85 \text{ mm}.$$

Thus, the relative error of the refraction R is 13.9 percent, which is a quite satisfactory result.

1.3. Practical experiments

In the spring of 1963 some test measurements over water-crossing were carried out on the islands of Suomenlinna off Helsinki in order to study the possibility of also eliminating the asymmetric refraction error from the water-crossings by using Kukkamäki's method. Two bench marks A and B were fastenend on the cliffs along each of the shores of the 413 meters long water-crossing. The elevation difference between these bench marks was measured by ordinary precise levelling, which was carried out many times along the shore line. The levelling instrument, a Zeiss NiA, was set up at the other end of the crossing, and the collimation error of the spirit level of NiA was eliminated as exactly as possible. The elevation difference between the bench marks A and B was then observed onesidedly in the course of several days. The effect of the curvature of the earth and the elevation difference between A and B as determined by the ordinary levelling were subtracted from these elevation differences. The absolute refraction values belonging to each one-sided observation were thus observed. Simultaneously with the optical observations, the vertical temperature gradient was measured at 8 points, equally distriuted along the sight line. The refraction values were computed from these gradients by using the formula (1). The refraction values, computed on the basis of gradients observed were consistent with the absloute refraction values from $-$ 25 mm to + 2 mm. The statistical calculations showed a strong correlation

$$r = 0.86 \pm 0.05$$

which shows that the computed refraction agrees well with the real refraction.

The elimination of the asymmetric refraction error was studied as follows. The above-mentioned 413 m long water-crossing was measured during asymmetric conditions in order to study large asymmetric errors. By using the levelling instrument Zeiss NiA, two one-sided water-crossings were measured. The first onesided crossing was observed on the 27th of May, when the weather was warm, and the vertical temperature gradient was strongly positive. The levelling instrument was set up on the shore B of the crossing. The elevation difference between the bench marks A and B was then measured in the direction from B to A. The second one-sided crossing was measured on the 30th of May in the evening, when the vertical temperature gradient was nearly zero. The levelling instrument Zeiss NiA was set up on the shore A. The elevation difference was on that day measured one-sidedly in the direction from A to B, consequently in the opposite direction on the 27th of May. The collimation error of the levelling instrument was eliminated on both days as exactly as possible. The refraction correction belonging to the optical observaton of both days was computed in the above mentioned way. The results were the following:

Table 2

1.	2.	3.	4.	5.	6.	7.
− 534.54	+ 7.99	− 527.30	+ 0.20	− 530.92	+ 4.10	− 526.82
− 532.54	+ 8.63	− 526.70	+ 3.26	− 529.62	+ 5.94	− 523.68
− 532.68	+ 5.78	− 525.38	+ 0.13	− 529.03	+ 2.96	− 526.07
− 535.08	+ 7.00	− 526.44	+ 2.84	− 530.76	+ 4.92	− 525.84
− 537.43	+ 11.69	− 524.71	+ 0.64	− 531.07	+ 6.16	− 524.91
− 534.94	+ 9.01	− 525.50	+ 1.44	− 530.22	+ 5.22	− 525.00
− 538.72	+ 10.42	− 525.17	+ 0.83	− 531.94	+ 5.62	− 526.32
− 537.62	+ 5.91	− 525.08	+ 0.83	− 531.35	+ 3.37	− 527.98
− 534.83	+ 7.32	− 525.00	+ 0.64	− 529.92	+ 3.98	− 525.94
− 528.46	+ 0.48	− 526.54	0.00	− 527.50	+ 0.24	− 527.26
− 528.84	+ 0.64	− 524.56	+ 1.37	− 526.70	+ 1.00	− 525.70
− 528.52	− 2.11	− 524.72	+ 0.77	− 526.62	− 0.67	− 527.29
	Mean			− 529.64	+ 3.57	− 526.07
	Mean error			± 0.53		± 0.35

Explanation of columns in Table 2.

Column 1. The elevation differences from *A* to *B* observed on the 27th of May in mm.

Column 2. Refraction corrections to the values of the column 1. in mm.

Column 3. The elevation differences from *A* to *B* observed on the 30th of May in mm.

Column 4. Refraction corrections to the values of columns 3. in mm.

Column 5. The uncorrected means of the elevation differences from *A* to *B* in mm. Computed from the values of columns 1. and 3.

Column 6. Final refraction corrections to the values of column 5. in mm. Computed from the values of columns 2. and 4.

Column 7. The final refraction corrected elevation differences from *A* to *B* in mm. Computed from the values of the columns 5. and 6.

The direct measurements over water surface have given the following values to the elevation difference between the bench marks *A* and *B*. Without the refraction correction the value is -529.64 ± 0.53 mm and with the refraction correction -526.07 ± 0.35 mm. The comparison of these values with the real elevation difference -526.16 ± 0.22 mm as determined by the ordinary precise levelling along the shores shows that the computation of refraction correction on the basis of vertical temperature gradient has improved the result by eliminating the asymmetric refraction error and also made the mean error smaller.

1.4. Measurements in the Aland archipelago

Several water-crossings in the Aland archipelago have been measured in two different days. The difference between the mean of the first day observations and the mean of the second day observations is marked with $\Delta H'$ if the refraction correction is not computed and with ΔH if the refraction correction is computed. The results were as follows:

Table 3

Length of crossing (m)	$\Delta H'$ (mm)	ΔH (mm)
480	+ 0.11	+ 0.11
325	+ 0.78	+ 0.38
436	− 0.74	− 0.43
444	− 0.31	− 0.16
680	− 0.91	+ 0.07
342	− 1.98	− 1.50
482	+ 0.05	− 0.12
330	− 0.81	− 0.61
635	− 3.25	− 2.15
313	+ 0.05	+ 0.13

The mean error per $\sqrt{\text{km}}$ of the average of one observation day can be computed on the basis of the values given in table 3. by using the formula

$$m = \sqrt{\frac{1}{2n} \sum \frac{(\Delta H)^2}{X}} \tag{12}$$

in which X is the length of the water-crossing. The following mean errors are obtained

without the refraction correction $\pm$ 1.32 mm/ $\sqrt{\text{km}}$

with the refraction correction $\pm$ 0.90 mm/ $\sqrt{\text{km}}$.

It is found on the basis of the above mentioned mean errors that the refraction corrections have improved the mutual agreement of the averages of the different observation days. The achieved mean error of $\pm$ 0.90 $\sqrt{0.45}$ mm = $\pm$ 0.60 mm for levellings over the water-crossings on the average 450 m long is smaller than was expected.

All the observations for table 3. have been made in side wind conditions. This circumstance is important as we shall see later.

2. The asymmetry of the refraction field

The asymmetry of the refraction fields has been studied on the optical water-crossings in the Aland archipelago in the summers of 1963—1965, and in addition to this the special investigations concerning the refraction at the shore line were made during the summer of 1966.

The quality of the surface has great influence in the causing of asymmetric refraction conditions due to the fact that different kinds of surfaces, ground and water, have different capacities of absorbing radiation energy from the sun.

The dry ground gets warm rapidly during sunny summer days. The surface temperature in Finland can even reach a temperature value of + 70 °C. The heat energy coming from the sun is stored in only a thin surface layer of the ground, which has a small heat capacity. The daily temperature variations of the ground are great as compared with the daily temperature variations of the air. For that reason the vertical temperature gradient, prevailing above the dry ground, is negative in the day time and positive at night.

A part of the radiation of the sun, coming to the surface of the sea, is reflected back, another part is absorbed by the water. The heat energy, remaining in the water, is mixed into a considerably thick layer. The surface of the sea warms up slowly, and its daily temperature variations are small as compared with those of the air. For that reason the vertical temperature gradient, prevailing above the sea, is positive in the day time and negative at night.

Thus, the values of the vertical temperature gradient, prevailing above the dry ground, are essentially different as those above the surface of the sea. The gradient above the ground changes sharply at the shore line to the sea gradient. The width of the area of change is only a few meters, according to the observations.

If the levelling instrument at both shores are set up at the shore lines or at the same distance from the shore lines, the sights of both instruments go over the same kinds of surfaces, and in these circumstances the arithmetical mean of the simultaneous observations of both instruments does not contain the asymmetric refraction error. The wind, however, can cause a change in this circumstance by transferring the changing area of the vertical temperature gradient with regard to the shore line.

2.1. The influence of the wind

Some of the water-crossings in the Aland archipelago were measured in two different days. These were divided in two groups:

group 1. The observations of only one day or those of both days were carried out with a land wind, i. e. with the wind blowing from the land to the sea.

group 2. The observations of both days were carried out with a side wind, i. e. with the wind blowing in the direction of the shore line.

By using the formula (12) the following mean errors for the average value of one observation day were computed:

with a side wind without the refraction corrections ± 1.32 mm/ $\sqrt{\text{km}}$

with a land wind without the refraction corrections ± 2.14 mm/ $\sqrt{\text{km}}$

which shows that the agreement of the observations carried out on different days is, in side wind conditions, better than with a land wind. The symmetry of the refraction fields is obviously better in side wind conditions. The temperature measurements carried out during the summer 1966 have strengthened this view.

2.11. The termistor thermometer

The purpose of the temperature measurements, which were carried out at the shore, was to make clear the course of the isotherms in the area of the shore in different wind conditions. The special thermometer was constructed for this purpose.

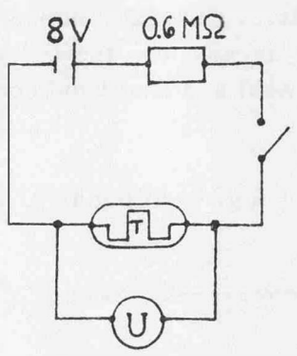

Fig. 1.

The standard miniature N. T. C. resistors, type Philips E 205CE/P/6k8, were used as the sensitive elements for the temperature. The coupling shema of this termistor thermometer is given in figure 1. The other components of the thermometer are the power supply Klein TSRG for the constant voltage of 8 volts, the carbon resistor of about 600000 ohms, and the digital voltmeter Solartron L 1420. Because the resistance of the digital voltmeter is very great (greater than 500 M) as compared with the other resistances of the circuit, the digital voltmeter does not load the circuit but measures the voltages between the terminals of the termistor. In the temperature area of − 10°C, + 30°C the resistance of the termistor, R_T, can be computed from the formula

$$R_T = \alpha e^{\beta/T} \tag{13}$$

in which T is the absolute temperature, α and β are the specific constants of the termistors, and e is the base of the natural logarithm.

If R_V is the resistance of the carbon resistor, V the voltage of the power supply, and U the reading of the digital voltmeter, the absolute temperature can be computed with sufficient accuracy from the formula

$$\frac{1}{T} = k_1 \log\left(\frac{U}{V-U}\right) + k_2 \tag{14}$$

in which k_1 and k_2 are constants depending on the values of R_v, α, and β as

$$k_1 = \frac{1}{0.43429\,\beta} \text{ and } k_2 = \frac{\log R_v - \log \alpha}{0.43429\,\beta} \tag{15}$$

The reading accuracy of the thermometer described above is better than ± 0.04 °C.

The main disadvantage of the thermometer is its sensitivity to contact errors resulting from the uncleanliness, for instance from the moisture in the thermometer.

The advantages are the great reaction ability and the stability of the calibration. The influence of the radiation error of the sun is smaller because of the small size of the termistor.

2.12. The temperature measurements at the shore

The termistor was fixed to the end of a long rod in order to place it in different measuring points. The calibration was made before and after the measurements every day.

The situations of 33 measuring points are given in Figure 2. The temperatures at these points were measured as follows: firstly from the sea to the land and from the lowest point to the highest, then from the land to the sea and from the highest point to the lowest. One observation series included two of this kind of measurements, and it took 20–50 minutes depending on the violence of the turbulent fluctuation of the air. In addition to this the surface temperature of the sea and the temperature prevailing a few centimeters above the ground at a distance of 10 meters from the

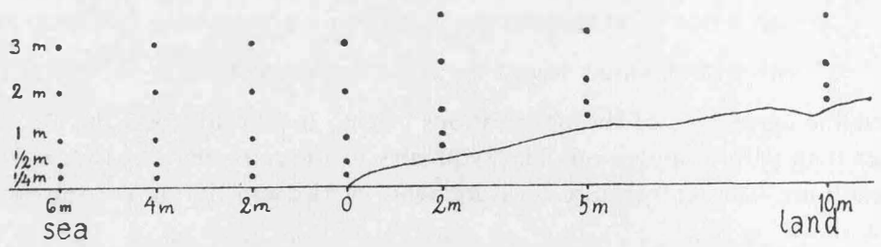

Fig. 2. The measuring points of the temperature.

shore line were measured. Also the cloudiness and the wind direction with regard to the direction of the shore line were recorded.

The measurements were carried out in May, August, and October in 1966. The measuring place was chosen from the island of Suomenlinna. It was an uncovered cliff gently sloping to the sea.

The observation material is still under treatment, but already now the following provisory results from the structures of the isothermal surfaces in sea wind and land wind conditions can be given.

2.13. The profile with a land wind

An example of the typical profile in land wind conditions is given in Figure 3.

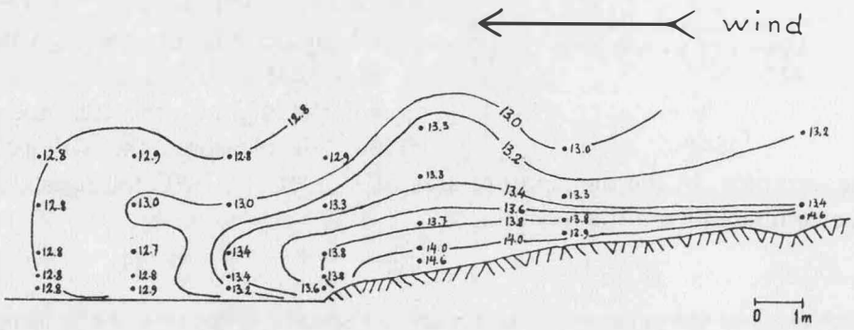

Fig. 3. The isothermal surfaces with a land wind.

The surface temperature of the sea is + 7.8 °C in this example. The temperature of + 21.0 °C is prevailing 2.5 cm above the dry ground at a distance of 10 m from the shore line. A gusty wind of 2 beauforts is blowing from the land to the sea. The cloudiness is 20 percent. The sun is shining.

The wind is bringing warm air from the land to the sea. The isotherms are parallel to the surface above the dry ground as far as the shore line whereas they are rising in a vertical direction above the sea and form curved surfaces there.

2.14. The profile with a sea wind.

An example of the typical profile in sea wind conditions is given in Figure 4.

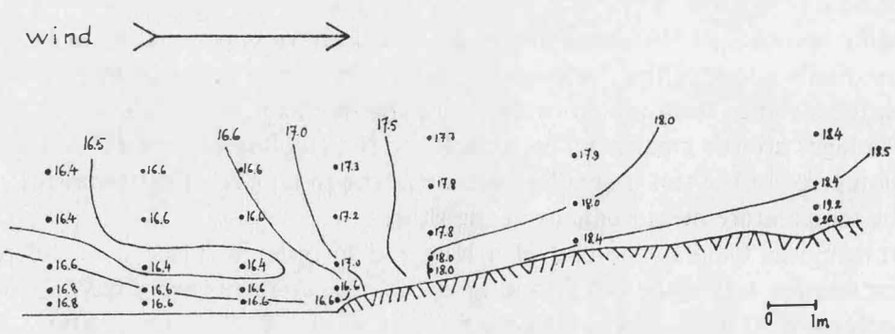

Fig. 4. The isothermal surfaces with a sea wind.

The surface temperature of the sea is + 19.1 °C in this example. A temperature of + 25.5 °C is prevailing 1 cm above the dry ground at a distance of 10 m from the shore line. A wind of 1 beaufort is blowing from the sea to the land. The cloudiness is 20 percent.

The wind brings cold air from the sea to the land. Cold air penetrates at the shore line below the warmer air masses by forming there a bag of cold air.

Above the sea nearest to the shore line the isotherms are curved. Above the ground in a zone of about 5 m beginning from the shore line the isotherms rise in a vertical direction, and then they are overturned and become again parallel to the surface.

2.15. The profile with a side wind

An example of the profile in side wind conditions is not given in this paper because of its less stable form. It seems, however, to resemble that of the sea wind.

2.16. The vertical temperature gradient at the shore line

The refraction, which has an influence on the levelling results, depends on the magnitude of the vertical temperature gradient at the sight line. It is found on the basis of the temperature profiles given above that the gradient, while being the same outside the area of the shore, is in the immediate vicinity of the shore line essentially different in different wind conditions, Tables 4. and 5.

Table 4.

Dat. 1966		Time	1.	2.	3.
V	27.	13.19	+ 0.13	− 0.20	− 0.18
		13.46	+ 0.10	− 0.10	− 0.06
		14.44	0.00	− 0.10	− 0.17
	30.	13.50	+ 0.30	− 0.50	− 0.29
		14.56	− 0.10	− 0.50	− 0.53
VIII	2.	13.00	+ 0.05	− 0.10	− 0.19
		15.00	− 0.10	− 0.04	− 0.31
		16.16	+ 0.05	0.00	− 0.10
		mean	+ 0.05	− 0.19	− 0.23

The vertical temperature gradient at the altitude of 1.5 m above the surface in the land wind conditions. The columns are

1. The vertical temperature gradient above the sea at the distance of 4 meters from the shore line in $^0C/m$.
2. The vertical temperature gradient above the shore line in $^0C/m$.
3. The vertical temperature gradient above the dry ground at the distance of 4 meters from the shore line in $^0C/m$.

Table 5.

Dat. 1966		Time	1.	2.	3.
V	31.	13.05	− 0.09	+ 0.02	− 0.24
		16.21	− 0.09	+ 0.04	− 0.13
VI	1.	13.16	− 0.05	− 0.14	− 0.06
		14.14	+ 0.01	− 0.06	− 0.10
VIII	4.	11.45	− 0.15	+ 0.25	0.00
		12.55	0.00	+ 0.15	− 0.12
		14.16	− 0.05	+ 0.05	− 0.12
		14.40	+ 0.10	− 0.25	− 0.18
		mean	− 0.04	+ 0.01	− 0.12

The vertical temperature gradient at the altitude of 1.5 m above the surface in the sea wind conditions. The columns are the same as in table 4.

In land wind conditions the vertical temperature gradient continues the same as far as the shore line. After that the isotherms turn to oblique and vertical positions, and therefore the vertical temperature gradient diminishes to values close to zero.

With a sea wind the isotherms are already rising to a vertical position before the shore line, and after that overturn even to an inverse position.

When the wind is blowing in the direction of the measuring line, one shore of the water-crossing is under the influence of the land wind and the other shore under the influence of the sea wind. Because the levelling instrument cannot generally be set up outside the strong temperature gradient area on that shore, where the land wind is prevailing, a clear difference exists between the conditions of the different shores. This asymmetry causes refraction error.

With a side wind there are the same wind conditions on both shores of the water-crossing. Thus, in that case the refraction field is symmetrical.

3. Conclusion

The optical measurements carried out in Suomenlinna and in the Aland archipelago have shown that the asymmetric refraction error, which remains in the arithmetical mean of the simultaneous observations in opposite directions, can be reduced by measuring the vertical temperature gradient.

The asymmetric refraction error exists in such kinds of optical measurements over water-crossings, in which the sight line has gone over the heterogeneous surface or when the measurements have been carried out in land wind conditions. If, however, the measurements have taken place with a side wind and at the same time the vertical temperature gradient has been measured along the sight line in order to determine the refraction correction, the accuracy of the measurements over the water-crossings has been essentially greater. The mean errors are $\pm$ 1.43 mm in land wind conditions without the refraction correction, $\pm$ 0.89 mm in side wind conditions without the refraction correction, and $\pm$ 0.60 mm in side wind conditions with the refraction correction for the levellings over the water-crossings of an average length of 450 meters.

References

1. *Kukkamäki, T. J.:* Levelling over Turku and Aland archipelago. Det Tredie Nordiske Geodaetmøde i København 25.—30. Maj 1959.
2. *Kukkamäki, T. J.:* Über die nivellitische Refraktion. Veröff. Finn. Geod. Inst. n:o 25, Helsinki 1938.
3. *Jordan/Eggert/Kneissl:* Handbuch der Vermessungskunde, Band VI, S. 215.
4. *Hytönen, Erkki:* Measuring of the refraction in the Second Levelling of Finland. Presented at the Symposium on "Recent research on atmospherical refraction for geodetic purposes" in Vienna, March 16—17, 1967.
5. *Franssila, M.:* Mikroklimatische Untersuchungen des Wärmehaushalts. Mitteilungen der Meteorologischen Zentralanstalt No. 20, Helsinki 1936.
6. *Kukkamäki, T. J.:* Formeln und Tabellen zur Berechnung der nivellitischen Refraktion. Veröff. Finn. Geod. Inst. n:o 27, Helsinki 1939.
7. *Honkasalo, Tauno:* A differential thermometer for the Väisälä comparator. Annales Academiae Scientiarum Fennicae Series A, III Geologica-Geographica, 61.
8. *Huovila, Seppo:* On the measurement of temperature, humidity and wind velocity very near the ground. Geophysica, Vol. 6, No. 3—4, 243—274.

Measuring of the Refraction in the Second Levelling of Finland

by *Erkki Hytönen*, Helsinki

1. *Introduction*

Owing to different density of air layers a line of sight is refracted towards a layer where the density is greater. The error caused by this phenomenon, appearing e. g. in precise levelling, tends to diminish the measured height differences. The effect is of such order that it ought to be eliminated. In the following a method is explained, which is used in Finland.

2. *Formulae for refraction*

The levelling refraction has been determined by a method developed by Kukkamäki (cf. Kukkamäki 1938, 1939). The computing formulae have been derived from the interpolation formula

$$t_z = a + bz^c \qquad (a, b \text{ and } c \text{ const.}) \tag{1}$$

where t_z (°C) is a temperature at the height z (≤ 300 cm) above the ground. From this formula (1) the following equation is derived

$$R = d \cdot \frac{s^2}{(Z_o - Z_1)^2} \frac{\vartheta}{z_2^c - z_1^c} \left[\frac{1}{c+1} (Z_1^{c+1} - Z_2^{c+1}) - Z_o^c (Z_1 - Z_2) \right] \tag{2}$$

Following symbols have been used

R = refraction error for one instrument station (in mm),

$d = -10^{-6} [0.933 - 0.0064 (t - 20)] \cdot \frac{B}{760}$, where t (°C) is a temperature and B barometric reading (in mmHg) [1],

ϑ = temperature difference $t_{z_2} - t_{z_1}$,

s = length of sight,

Z_o = height of instrument (in m),

Z_1 and Z_2 = height of line of sight respectively on the fore and the back staves.

Assuming that the refraction is directly proportional to the levelled height difference D the equation (2) gives the refraction error

$$R = 10^{-5} \cdot \gamma \cdot \left(\frac{s}{50} \right)^2 \cdot \vartheta \cdot D \tag{3}$$

in mm, when s is given in m and D in "staff-unit" ($= SU = 5$ mm). The coefficient γ means a tabulated (Kukkamäki 1939, pp. 11 . . . 18) quantity

$$\gamma = \frac{5.95}{250^c - 50^c} \left[\frac{1}{c+1} (50^{c+1} - 250^{c+1}) + 150^c \cdot 200 \right] \tag{4}$$

In addition to the quantities s and D, observed in connection with the levelling, the temperature difference ϑ is measured.

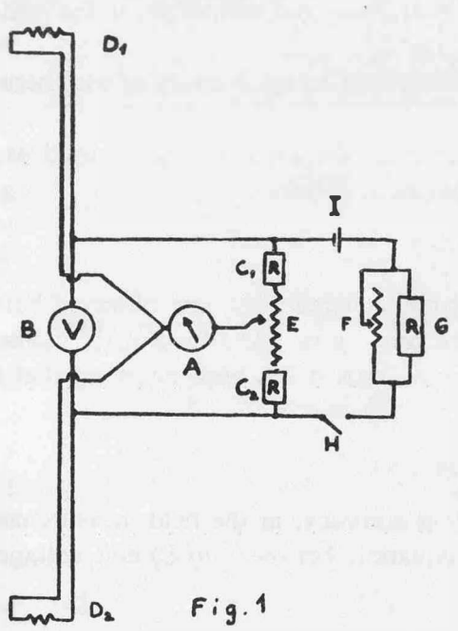

Fig. 1

3. *Differential thermometer*

In order to determine the value of ϑ a so-called differential thermometer has been used in Finland since 1938. In the preliminary experiments the thermometers were devices based on thermocouples, later on resistors and on the principle of Wheatstone bridge (Kukkamäki 1938, p. 15). The writer constructed the thermometers used nowadays making some alterations in the earlier model. It has been tried to improve the accuracy by adding a voltmeter and by replacing a resistance wire made of platinum by a nickel wire. The galvanometer is not used as a null-instrument but the current, which flows through it and which is caused by temperature difference of the resistances, is measured.

3.1. Parts and coupling scheme of instrument. In Fig. 1 the coupling scheme is illustrated with following notations:

[1]) The above formula has been used for d in this paper. The new formula has been accepted by IUGG Assembly Berkeley 1963 (Resolution No. 9). This means a change of 3.6 per cent in the refraction correction, which is, however, insignificant concerning the results presented in this paper.

A: Moving-coil galvanometer (model Siemens KMP 66, D1 20) with scale (500-0-500), one scale division of which corresponds to about 33 μA. Because one division is 1.2 mm wide, the reading accuracy is about 0.2 mm. The internal resistance is 10 Ω.

B: Moving-coil voltmeter (model Siemens KMP 66). The scale is divided into 20 parts (each being 1.8 mm wide) with a reading accuracy of 0.02 V. The internal resistance is 2000 Ω .

C_1 and C_2: The known resistances (model Vitrohm 1W) each of 10 Ω, which are inside a thick insulating cover, made of constantan wire.

D_1 and D_2: Resistances (each of 10 Ω) of nickel wire, made artificially older. The temperature difference existing between these is exactly that to be measured. Each consists of a spiral of 90 cm-long wire (in diameter 0.1 mm), wound around a cross-shaped 8 cm long frame made of insulating material. The temperature coefficient of the nickel resistance wire is 0.005. The wire is coated with enamel.

E: Potential divider of constantan wire with pre-set adjustment (model Vitrohm GLA, total resistance 1 Ω), by which the bridge can be "balanced".

F: Variable resistance (model Bulgin IVC4) of constantan wire, range of regulation 5 . . . 30 Ω.

G: Shunt resistance of 33 Ω (Vitrohm 1 *W*), made of constantan wire.

H: Circuit switch.

I: Flashlight battery of 1.5 V being a source of energy. In field work the battery lasts 1.5 months. By a voltage of 0.7 V the total current in the circuit is 70 mA and that going through D_1 and D_2 35 mA.

All parts are placed in a plywood box (total weight 2.5 kg, size 23 × 8 × 27 cm), which is carried on the shoulder by a leather belt. D_1 and D_2 are during the measurement fastened on a 3 m long rod, at 0.5 m distance from its end. In order to reduce the radiation error, the frames of the resistance wires D_1 and D_2 are inside a hollow aluminium cylinder (10 cm long and dia. 4 cm), the surface of which is reflective.

3.2 Procedure of measurement. The differential thermometer is calibrated against a known temperature difference in order to determine a value of the scale division. The procedure of an actual field measurement is as follows: the record keeper reads at each instrument station the galvanometer three times, closing the circuit between readings. In order to eliminate any possible change of the zero point he changes the places of the resistances (i. e. turns the rod) and reads the galvanometer again three times. The temperature difference ϑ to be measured is a difference of the means of the observed readings. The measurement is carried out near the instrument and temporally in the middle of the levelling observations.

3.3 On errors of differential thermometer. In the following only internal errors of the thermometer will be examined.

3.31 Error of calibration. By calibration of the thermometer the same voltage is used as in the field, ordinary of 0.7 V. For the present thermometers has been obtained

$$1 \text{ scale division of galvanometer } p \sim 0^0.5.$$

The value of p has been defined as a difference of two galvanometer readings, one observed before and another after turning of the rod. The internal standard error of p is $\pm\, 0^0.015$. But the calibrations made at different times differ from each other much more, thus it has been observed that the final standard error caused by the calibration is

$$m_p{}^c = \pm\, 0^0,035 .$$

The voltage is regulated, within the limits of the reading accuracy, in the field measurements to be the same as at calibration. There is theoretically an equation between $p(^0\text{C})$ and voltage V (in volts)

$$p = \frac{0.38}{V} .$$

So the accidental error of the voltage brings on p the error

$$m_p^V = \pm\, 0^0.016 .$$

The error of the temperature difference ϑ to be measured arising from the whole calibration error $\sqrt{(m_p{}^c)^2 + (m_p{}^V)^2} = \pm 0^0.038$ depends on the value ϑ itself. Because the average temperature difference $t_{250} - t_{50} = 0^0.3$, i. e. 0.6 scale divisions in galvanometer, is the final error of the calibration

$$m_p = \pm 0^0.023.$$

3.32 Reading error of galvanometer. The galvanometer can be observed, as said, with a reading accuracy of about $\pm$ 0.2 scale division. Because the final temperature difference is a mean of three observations, the effect of the reading error on the quantity ϑ is accidentally

$$m_g = \pm 0^0.082.$$

3.33 Ventilation error. Theoretically, the temperature of the nickel wire rises during the reading of the galvanometer by $0^0.9$, without radiation and transmission of heat. It has been experimentally proved, that the maximal value of the ventilation error, caused by a different ventilation of the resistances D_1 and D_2, is $\pm 0^0.05$. Therefore the accidental error of the temperature difference ϑ, arising from the ventilation error, is

$$m_\vartheta = \pm 0^0.02.$$

The internal accuracy of the temperature difference ϑ, measured by the differential thermometer in a manner before-mentioned, is consequently given by

$$m_\vartheta = \sqrt{m_p{}^2 + m_g{}^2 + m_v{}^2} = \pm 0^0.087 .$$

According to the equation (3) the influence of m_ϑ upon the result of R is in average circumstances ($\gamma = 70$, $\left(\frac{s}{50}\right)^2$, $D = 150\ SU$)

$$m'_R = \pm 0.009 \text{ mm}. \tag{5}$$

4. Errors due to methods of measuring and computing

There is, in addition to the internal errors of the thermometer appearing in the determination of ϑ, a lot of errors, which have an effect on the computing of R. These errors decide, in fact, the accuracy of the correction for the levelling refraction.

4.1 Statistical exponent c'. The exponent c is not determined in connection with the levelling, but for it statistical values recorded by Best in England are used (Kukkamäki 1938, p. 14). However, these values have been reduced to different latitudes, the differences in the time of sunrise and sunset having been taken into consideration. In order to estimate the error arising from the introduction of the statistical exponent, which will be denoted by c' in following, the procedure is as follows: Starting with the test measurements, carried out by Kukkamäki and Behrendt, a standard error m_c given by the test measurements and a standard error $m_{c'-c}$ of the difference $c' - c$ will be computed. Consequently, the standard error $m_{c'}$ of the statistical exponent is equal to $\sqrt{m^2_{c'-c} - m^2_c}$.

4.11 Formulae of errors. The expression for the standard error of the exponent c is obtained starting with the equation for the determinations of c

$$\frac{\vartheta_1}{\vartheta_2} = \frac{t_2 - t_1}{t_3 - t_2} = \frac{z_2{}^c - z_1{}^c}{z_3{}^c - z_2{}^c}, \quad (t_{z_\vartheta} = t_\vartheta), \tag{6}$$

z_1, z_2, z_3 ($z_1 < z_2 < z_3$) mean three temperature measurement points, ϑ_1 and ϑ_2 the measured temperature differences corresponding to the interpolation formula (1)

$$\vartheta_1 = b\,(z_2{}^c - z_1{}^c), \qquad \vartheta_2 = b\,(z_3{}^c - z_2{}^c).$$

In the next the following symbols are used:

m_θ = standard error of $\frac{\vartheta_1}{\vartheta_2} = \theta$,

m_t = standard error of a single temperature observation,

m_ϑ = standard error of a single observation of temperature difference.

No.	Local time 1936		ϑ_1	ϑ_2	c	c′	c′ − c
1	VI 29	8h8	−0°47	−0°34	−0.29	−0.35	−0.06
2		9.9	−0.34	−0.86	+0.84	−0.30	−1.14
3		11.4	−0.45	−0.74	+0.45	−0.26	−0.71
4		12.1	−0.60	−0.94	+0.41	−0.24	−0.65
5		14.9	−0.51	−0.76	+0.36	−0.13	−0.49
6		15.8	−0.46	−0.53	+0.13	−0.11	−0.24
7		16.5	−0.44	−0.53	+0.17	−0.10	−0.27
8		17.1	−0.31	−0.29	−0.06	−0.08	−0.02
9	VI 30	13.4	−0.94	−0.75	−0.21	−0.19	+0.02
10		14.2	−0.82	−1.03	+0.21	−0.18	−0.39
11		14.9	−0.68	−0.84	+0.19	−0.18	−0.37
12		15.7	−0.78	−0.83	+0.06	−0.12	−0.18
13		16.4	−0.62	−0.76	+0.19	−0.10	−0.29
14		17.5	−0.38	−0.34	−0.10	−0.07	+0.03
15		18.4	−0.43	−0.24	−0.53	−0.04	+0.49
16		19.1	−0.15	−0.36	+0.80	−0.02	−0.82
17		19.9	−0.01	−0.09	(0.00)	0.00	(0.00)
18		20.6	+0.15	+0.22	+0.35	+0.02	−0.33
19		21.1	+0.38	+0.29	−0.25	+0.05	+0.30
20	VII 1	2.4	+0.20	+0.17	−0.15	+0.39	+0.54
21		3.1	+0.31	+0.03	(0.00)	+0.39	(+0.39)
22		4.1	+0.04	+0.15	(0.00)	+0.11	(+0.11)
23		4.9	−0.01	−0.07	(0.00)	−0.24	(−0.24)
24		5.9	−0.01	−0.20	(0.00)	−0.39	(−0.39)
25		6.6	−0.46	−0.49	+0.06	−0.39	−0.45
26		7.4	−0.16	−0.38	+0.79	−0.37	−1.16
27		8.1	−0.46	−0.64	+0.30	−0.37	−0.67
28		9.1	−0.58	−0.49	−0.15	−0.32	−0.17
29	VII 2	9.4	−0.66	−0.67	+0.01	−0.32	−0.33
30		10.3	−0.43	−0.65	+0.38	−0.29	−0.67
31		11.3	−0.64	−0.83	+0.24	−0.26	−0.50
32		11.8	−0.71	−0.70	−0.01	−0.24	−0.23
33		12.6	−0.71	−0.74	+0.04	−0.21	−0.25
34		13.6	−0.72	−0.73	+0.01	−0.19	−0.20
35		14.4	−0.78	−0.93	+0.16	−0.15	−0.31
36		15.2	−0.68	−0.99	+0.34	−0.14	−0.48
37		15.9	−0.64	−1.04	+0.44	−0.11	−0.55
38	VII 3	16.3	−0.65	−0.83	+0.22	−0.09	−0.31
39		17.1	−0.52	−0.59	+0.11	−0.07	−0.18
40		17.9	−0.35	−0.28	−0.20	−0.06	+0.14
41		18.4	−0.24	−0.27	+0.11	−0.04	−0.15
42		19.1	−0.15	−0.14	−0.06	−0.02	+0.04
43		20.1	−0.10	−0.06	−0.46	+0.02	+0.48
44		20.9	−0.08	−0.01	(0.00)	+0.04	(+0.04)
45		21.5	−0.02	−0.01	(0.00)	+0.09	(+0.09)
46	VII 4	3.0	+0.21	+0.22	+0.04	+0.40	+0.36
47		3.6	+0.34	+0.18	−0.58	+0.26	+0.84
48		4.4	+0.27	+0.10	−0.90	0.00	+0.90
49		5.1	−0.01	−0.20	(0.00)	−0.26	(−0.26)

No.	Local time 1936		ϑ_1	ϑ_2	c	c′	c′ − c
50	VII 4	6.1	−0.23	−0.48	+0.67	−0.39	−1.06
51		6.9	−0.50	−0.38	−0.25	−0.37	−0.12
52		7.6	−0.28	−0.78	+0.93	−0.37	−1.30
53		8.3	−0.37	−0.80	+0.70	−0.35	−1.05
54		9.1	−0.65	−0.93	+0.33	−0.32	−0.65
Mean values			−0°.34	−0°.45	+0.13		

Since

$$\frac{\partial\theta}{\partial t_1} = \frac{\vartheta_2}{\vartheta_2^2}, \quad \frac{\partial\theta}{\partial t_2} = \frac{\vartheta_1 + \vartheta_2}{\vartheta_2^2}, \quad \frac{\partial\theta}{\partial t_3} = \frac{\vartheta_1}{\vartheta_2^2}, \quad m_t = \frac{m_\vartheta}{\sqrt{2}}, \quad (t_{z_\vartheta} = t_\vartheta),$$

it follows that

$$m_\theta = \frac{1}{\vartheta_2}\sqrt{1 + \theta + \theta^2}\, m_\vartheta . \tag{7}$$

By the expression (6)

$$m_\theta = \frac{\partial}{\partial_c}\left(\frac{z_2^c - z_1^c}{z_3^c - z_2^c}\right) m_c$$

or

$$m_c = \frac{(z_3^c - z_2^c)^2}{(z_3^c - z_2^c)(z_2^c \ln z_2 - z_1^c \ln z_1) - (z_2^c - z_1^c)(z_3^c \ln z_3 - z_2^c \ln z_2)}\, m_\theta . \tag{8}$$

4.12 Observations by Kukkamäki. Kukkamäki has used in the test measurements the values $z_1 = 33.3$ cm, $z_2 = \sqrt{z_1 z_2}$, $z_3 = 9z_1$. Then the equations (6) and (8) give

$$c = -\frac{\ln\theta}{\ln 3} \tag{9}$$

and

$$m_c = \frac{2}{\left(\frac{z_1}{z_3}\right)^{\frac{c}{2}} \ln\frac{z_1}{z_3}}\, m_\theta . \tag{10}$$

In the above table the observed quantities ϑ_1 and ϑ_2 (Kukkamäki 1938, p. 30) and the computed values c, c' and $c' - c$ have been collected. The value of c has been computed by using the equation (9). If $|\vartheta_1|$ or $|\vartheta_2| \leq 0°.05$, the corresponding c has been marked = 0 and has been not taken into consideration by computing the means mentioned in the table. A constant γ corresponding to the local time of the observation has been obtained from the tables by Kukkamäki (Kukkamäki 1939, pp. 15 . . . 16, $\varphi = 60°.25$). The corresponding value of the statistical exponent is taken from the curve for $\gamma = \gamma(c)$ (Fig. 2), drawn on the basis of the equation (4). During observations, the quantities ϑ_1, ϑ_2 and c have had the average values of

$$\vartheta_1^0 = -0°.34, \quad \vartheta_2^0 = -0°.45, \quad c^0 = +0.13 .$$

Using these values the equations (7) and (10) give

$$m_\theta = \pm 3.39\, m_\vartheta, \quad m_c = \pm 1.05\, m_\theta, \quad m_c = \pm 3.56\, m_\vartheta .$$

The temperature differences ϑ_1 and ϑ_2 observed by Kukkamäki are the means of 6 . . . 12 measurements, in which besides the thermometer errors the external errors are also included. The accuracy of the mean computed from the observations is 0°.1, hence

$$m_c = \pm 0.36.$$

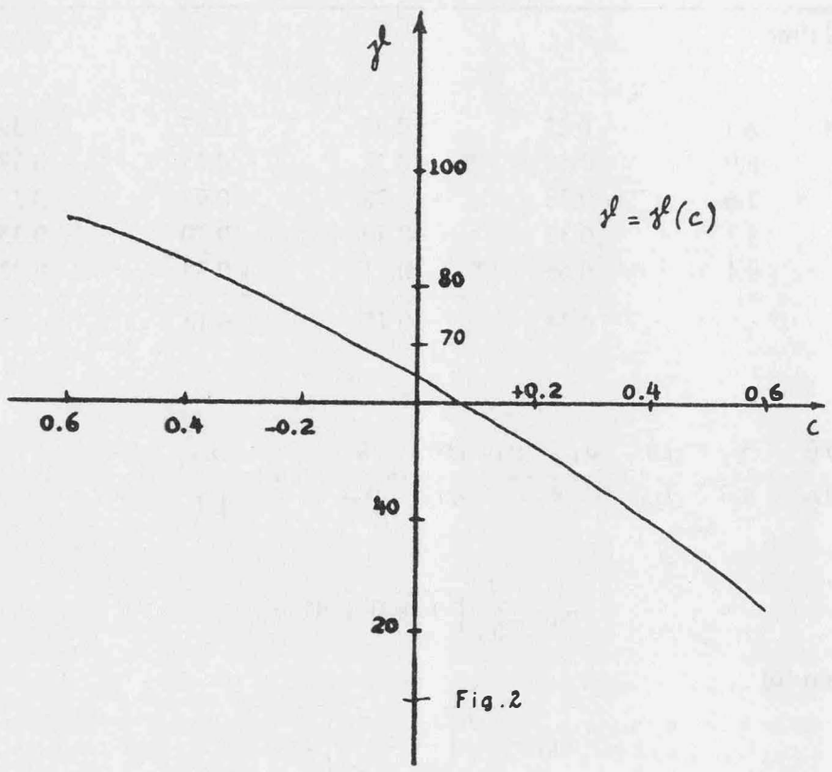

Fig. 2

The quadratic mean of the difference $c' - c$

$$m_{c'-c} = \pm 0.56.$$

Hence

$$m_{c'} = \pm 0.43. \tag{11}$$

4.13 Observations by Behrendt. Behrendt determines the exponent c by two groups of heights (cf. Behrendt p. 14)

1. group $\begin{cases} z_1 = 5\text{ cm} \\ z_2 = 50\text{ cm} \\ z_3 = 150\text{ cm} \end{cases}$ 2. group $\begin{cases} z_1 = 50\text{ cm} \\ z_2 = 150\text{ cm} \\ z_3 = 250\text{ cm} \end{cases}$

The means being observed by him being computed separately from each group are respectively (Behrendt, table 1)

$$c_1{}^0 = -0.47, \qquad c_2{}^0 = +0.78.$$

The means of the measured temperatures are

$$\vartheta_1{}^0 = t_{50} - t_5 = -1^\circ.80,$$
$$\vartheta_2{}^0 = t_{150} - t_{50} = -0^\circ.39,$$
$$\vartheta_3{}^0 = t_{250} - t_{150} = -0^\circ.35.$$

By using the equation (7) is

$$m_{\theta_1} = \pm 13.3\, m_\vartheta, \quad m_{\theta_2} = \pm 5.23\, m_\vartheta \left(\theta_1 = \frac{\vartheta_1}{\vartheta_2},\ \theta_2 = \frac{\vartheta_2}{\vartheta_3}\right).$$

According to the expression (8) for the standard error of c is

$$m_{c_1} = \pm 0.11\, m_{\theta_1}, \quad m_{c_2} = \pm 1.14\, m_{\theta_2}$$

The statistical exponent c' (Behrendt's symbol c_3) has been computed by the method of Kukkamäki from Best's observations. The quadratic differences of the statistical exponent and of the exponent computed from the observations are respectively

$$m_{c'-c_1} = \pm 0.43 \ , \quad m_{c'-c_2} = \pm 1.62. \tag{12}$$

Appearing from the values of $c_2{}^0$, $m_{c'-c_2}$ and m_{c_2} the values of the exponents being computed from the group 2 are too great, and the weight of m_{c_2} compared with that of m_{c_1} is very small. Therefore we use only a value resulted from 1. group

$$m_{c_1} = \pm 1.46\, m_\vartheta \tag{13}$$

Behrendt's values of ϑ are the means with a standard error of $\pm$ 0.13 noticed by him. Hence the equations (12) and (13) give results

$$m_{c_1} = \pm 0.19$$

and

$$m_{c'} = \pm 0.39. \tag{14}$$

4.14 The results observed by Kukkamäki and Behrendt can be considered as of equal weight. Concluding from this we get from the equations (11) and (14) the standard error of the exponent c'

$$m_{c'} = \pm 0.41.$$

This brings on the coefficient γ the standard error of $\pm$ 22. Under average circumstances

$$Z_o = 150 \text{ cm}, \ z_1 = 50 \text{ cm}, \ z_2 = 250 \text{ cm}, \ \gamma = 70, \ |\vartheta| = 0.3 \left(\frac{s}{50}\right)^2 . \ |D| = 150\, SU \ , \tag{15}$$

the error of γ causes according to the equation (3) on a height difference at one instrument station the error of

$$m' = \pm 0.010 \text{ mm}.$$

4.2 Uneveness of the ground level. By deriving the refraction formula some assumptions have been made. So the ground level between the staffs is supposed to be a plane and the isothermal surfaces parallel to this. The height of the instrument (Z_o = 150 cm) is considered equal to the distance above this plane. If we suppose a real height measured from the ground to differ from the afore-mentioned height by $\pm$ 20 cm that influences on γ an error about equal to one caused by c' Consequently its effect on the refraction is

$$m_\gamma = \pm 0.010 \text{ mm}.$$

4.3 Air humidity. When computing the refraction error, the effect of air humidity and the ones of pressure and content of carbonic acid is neglected. The total effect of these, mainly caused by the humidity, is at the most 0.025 mm. We can suppose an average effect to be one third of the former or

$$m_n = \pm 0.008 \text{ mm}.$$

4.4 Influence of assumption $R = k\,D$ (k = const.). By deriving the formula (3) it has been supposed, that the quantities R and D are directly proportional. Provided that the line of sight goes at least 30 cm above a ground level, the error caused by the before-mentioned assumption is on an average about 5 per cent or

$$m_r = \pm 0.002 \text{ mm}.$$

4.5 Other sources of errors. Since the gradient is a locally and temporally quickly changing quantity, the temperature difference ϑ ought to be known right at the moment of the reading of the staffs. In fact, the value of the gradient should be known at every point along the line of sight. The measured value of ϑ has therefore an accidental character. It is, however, difficult to estimate the error caused by this at one instrument station.

The means of the differences $c' - c$ and $c' - c_2$ being computed from the observations by Kukkamäki and Behrendt are resp.

$$[c' - c]^0 = -0.27, \qquad [c' - c_2]^0 = -1.11.$$

Concluding from this, the values of c', computed from the temperature observations by Best, seem to be too small. At a height of 0 . . . 3 m above the ground level the exponent c may be dependent upon height. The material is, however, too small to estimate an eventual error.

s, z_1 and z_2 are the measured quantities. Provided that s has been measured with an accuracy of 0.5 m and z_1 and z_2 with ones of 5 cm the errors caused by the measuring inaccuracy are negligible in R.

The influence of the before-computed errors on the refraction correction at one instrument station under the normal circumstances (15) is

$$m_R'' = \sqrt{m'^2 + m_\gamma^2 + m_n^2 + m_r^2} = \pm 0.016 \text{ mm}. \tag{16}$$

5. *Conclusions*

The accomplished estimation of the errors and partly the following conclusions are valid in respect to the ordinary precise levelling work, which is carried out in daytime along the railway or highway when the weather conditions are suitable for levelling, but not aplicable to a water crossing observations by night etc.

5.1 Computing of coefficient γ. On the basis of what has been presented above, an inaccuracy is included in the determination of γ. This results mainly from the error of the statistical exponent. It is not, however, possible to determine c itself in the field in connection with the levelling not even with an accuracy of c', because it is tried to carry out the levelling during the time, when the gradient is near zero (cf. (7) and (8)). Therefore we can always use, when computing results, an average value for γ or the value 70 without reducing an accuracy.

5.2 Effect of the refraction on levelling net. According to the formula (3) the refraction for a bench mark interval is calculated as a sum

$$\rho = 10^{-5} \cdot \gamma \sum \left(\frac{s}{50}\right)^2 \vartheta D .$$

The error of the measured temperature difference ϑ may be great at any instrument station arising from the noticeable changing of ϑ. In spite of that, an average gradient of the whole bench mark interval is obtained accurately enough, because ϑ is measured with intervals of about 100 m. The reality of the refraction correction $-\rho$ appears clearly from the test measurements carried out by Kukkamäki on the bench mark interval with length of 1958 m (Kukkamäki 1938, pp. 38 . . . 39). Similarly, by adding statistically the refraction correction to the First Levelling, the systematical error of the net has diminished by one third. On the contrary, the quadratic mean of the closing errors of the levelling loops diminished much less, only by 10 per cent. It was to be expected, because the effect of the systematical changes of the refraction do not appear in the closing error of the loops, only the effect of its accidental changes do.

The whole error of the determination of the refraction for one kilometer (about ten instrument stations) of the forward and backward levelling is according to the equation (5) and (6)

$$m_{1\text{ km}} = \sqrt{5\,(m_R'^2 + m_R''^2)} = \pm 0.04 \text{ mm}.$$

Accordingly the inclusion of the refraction correction to the result of the levelling does not increase essentially the accidental error of the levelling (0.3mm / $\sqrt{\text{km}}$) not although m_R, in consequence of the accidental changes of ϑ, should increase doubly.

5.3 Adaptability of different thermometer. The internal error of the thermometer has influence on the standard error of the refraction correction $\sqrt{m_R'^2 + m_R''^2} = \pm 0.018$ mm only by about 12 per cent. Hence the internal accuracy of the thermometer is enough. More significant than any increasing of the accuracy is a correct performing of the measurement. Thus the current is not allowed to be coupled longer than a few seconds. Wind must be permitted to produce freely an effect upon both resistances, i. e. the axes of the cylinders serving as radiation shelters must always be turned in the direction of the wind. The rod with the resistances has to be placed so, that the resistances are exactly in similar conditions as a line of sight between the staffs. When measuring along the railway it should be avoided to place the lower resistance too near a rail, which radiates

heat. Though the wire resistances are protected, the results given by the thermometer in the rain are hardly real.

5.4 Necessity of determination of the refraction. The systematical influence of the refraction is on the average 0.06 mm per one metre rise. When the greatest possible accuracy is required, it must be tried to eliminate this systematical error. It is statistically possible, by using the beforementioned thermometer and formulae. In addition to the proper refraction determination, the thermometer can be used to establish the magnitude of the refraction. Thus the observation time may be applied to such circumstances, when the influence of the refraction is as slight as possible. As further the determination of the levelling refraction neither needs extra person nor retards the levelling, the presented method for the determination of the refraction correction may be recommended in the ordinary precise levelling work.

References

Kukkamäki, T. J.: Einwirkung der bodennahen Refraktion auf das Präzisionsnivellement. (Verh. d. 9. Tagung d. Balt. Geod. Komm. in Helsinki 1936, Helsinki 1937.)

Kukkamäki, T. J.: Über die nivellitische Refraktion. (Veröff. Finn. Geod. Inst. Nr. 25, Helsinki 1938.)

Kukkamäki, T. J.: Formeln und Tabellen zur Berechnung der nivellitischen Refraktion. (Veröff. Finn. Geod. Inst. Nr. 27, Helsinki 1939.)

Kukkamäki, T. J.: Die nivellitische Refraktion in dem finnischen Landesnivellement. (Schw. Zeitschrift für Verm. u. Kulturtechnik XLVIII, Nr. 3 und 4, 1950.)

Kääriäinen, Erkki: The Second Levelling of Finland in 1935–1955. (Veröff. Finn. Geod. Inst. Nr. 61, Helsinki 1966.)

Behrendt, Wolfgang: Ein Beitrag zur Refraktion im Nivellement. (Veröff. d. DGK, Reihe C, Heft Nr. 28, München 1958.)

Franssila, Matti: Mikroilmasto-oppi, Helsinki 1949.

Huovila, Seppo: On the measurement of temperature, humidity and wind velocity very near the ground (Geophysica Vol. 6, Helsinki 1958.)

Hase, R.: Bestimmung der Refraktion bodennaher Luftschichten. (Optik 14, Heft 10, 1957.)

Ellenberger, H.: Die Temperaturgradientenmessung beim Feinnivellement. (Zeitschrift für Vermessungswesen Nr. 4, 1954.)

Brocks, K.: Die Lichtstrahlkrümmung in Bodennähe. (Deutsche Hydrographische Zeitschrift, Band 3, Heft 3/4, 1950.)

Application of the Conformal Theory of Refraction

by *Helmut Moritz*, Berlin

Abstract

A unified theory of geodetic refraction, covering horizontal and vertical angles and electronically measured distances, is provided by treating the light ray as a geodesic in a curved three-dimensional space which is conformally related to ordinary Euclidean space. The principles of this wellknown three-dimensional conformal mapping are pointed out; then explicit practical formulas for refractional correction of distances and angles are derived on the basis of a solution of the eiconal equation by means of a series.

Zusammenfassung

Eine einheitliche Theorie der Refraktion in ihrer Auswirkung auf Horizontal- und Höhenwinkel und auf elektronisch gemessene Entfernungen ist möglich, indem man den Lichtstrahl als eine geodätische Linie in einem gekrümmten drei-dimensionalen Raum auffaßt, der mit dem gewöhnlichen euklidischen Raum durch eine konforme Abbildung verbunden ist. Die Grundlagen dieser bekannten dreidimensionalen konformen Abbildung werden erläutert. Hierauf werden praktisch

verwendbare Ausdrücke für die Refraktionskorrektion von Strecken und Winkeln abgeleitet, wobei eine Reihenlösung der Eikonalgleichung die Grundlage bildet.

Introduction

A light ray or an electromagnetic wave of high frequency describes a slightly curved path in the atmosphere, rather than a straight line. In electronic distance measurement the straight distance $s = AB$ between two points A and B is to be computed from the measured travel time T. This is usually done in two steps:

1. Computation of the length S of the curved light path between A and B from the travel time T.
2. Computation of the chord $s = AB$ from the curved arc S.

It is, however, possible to give a method of directly obtaining the straight distance s from the travel time T, without needing the curved arc S. By an extension of this method vertical and lateral refraction affecting measured directions can be treated as well; we thus obtain a unified theory of all geodetically important phenomena of refraction.

A convenient geometrical visualization of this method is furnished by the theory of conformal mapping in space. Conformal mapping between two surfaces being familiar to geodesists, it is gratifying that the reduction of electronically measured distances and observed directions for atmospheric refraction is the precise three-dimensional analogue of the reduction of distances and directions in the conformal mapping of a surface such as an ellipsoid onto a plane.

2. Refraction and Conformal Mapping

Essentially the same laws hold for the propagation of light and of radio waves of high frequency. Henceforth we shall speak only of light, implying high-frequency radio waves as well.

According to the well-known Fermat principle, light traveling from point A to point B describes the shortest path; the travel time

$$T = \int_A^B dt = \int_A^B \frac{ds}{v} \tag{1}$$

is a minimum. The instantaneous light velocity v is related to the constant light velocity in vacuum c by

$$v = \frac{c}{n},$$

where n is the index of refraction. Hence (1) becomes

$$T = \frac{1}{c}\int_A^B n\,ds,$$

where

$$ds = \sqrt{ds^2 + dy^2 + dz^2},$$

is the ordinary line element. If we define the element of "optical length" $\bar{s}$ by

$$d\bar{s} = n\,ds = n\sqrt{dx^2 + dy^2 + dz^2}, \tag{2}$$

then

$$T = \frac{1}{c}\int_A^B d\bar{s} = \frac{\bar{s}}{c}. \tag{3}$$

Since c is a constant, Fermat's principle is equivalent to

$$\bar{s} = \text{minimum}. \tag{4}$$

The optical length has indeed the dimension of a length. It is obtained from the measured travel time T by simple multiplication by c according to

$$\bar{s} = c\,T \ ;$$

hence *the optical length* $\bar{s}$ *can be considered the direct result of electronic distance measurement.*

For the moment, assume for simplicity that the light is propagated along the xy-plane, which we shall denote by S. Then $z = 0$, and we have by (2)

$$d\bar{s}^2 = n^2\,(dx^2 + dy^2) \ , \tag{5}$$

whereas the ordinary line element is given by

$$ds^2 = dx^2 + dy^2 \ . \tag{6}$$

Obviously $d\bar{s}$ in (5) may be considered the line element in isothermic coordinates *of a certain curved surface* $\bar{S}$. The condition (4), $\bar{s}$ = minimum, defines *geodesic lines* on this surface $\bar{S}$.

The length of such a geodesic on $\bar{S}$, the geodesic distance, is identical with the optical length and can therefore be considered the direct result of measurement. The reduction for refraction consists in computing the straight distance AB in the plane,

$$s = \sqrt{(x_B - x_A)^2 + (y_B - y_A)^2} \ ,$$

from the measured optical length $\bar{s}$. The plane S is related to the surface $\bar{S}$ by a *conformal mapping*, since the line elements (5) and (6) have the form corresponding to such a mapping; hence the relation between the geodesic distance $\bar{s}$ and the straight distance s is given by the conventional reduction of distances in conformal mapping,

$$\Delta\bar{s} = \bar{s} - s,$$

which, physically, is precisely the reduction of the measured optical lenght $\bar{s}$ for refraction.

Consider now the measurement of directions, again in the plane, disregarding the third dimension. The direct result of our measurement is the angle between light rays in the plane S. These light rays are geodesics in our auxiliary surface $\bar{S}$; in the plane S they are consequently the image curves of these geodesics. The angle between image curve and chord is well-known as the arc-to-chord or angle correction of conformal mapping (Bomford, 1962, p. 169); it is thus identical with the angle between light path and straight line which is needed for the reduction of measured angles for refraction.

Hence we see that the introduction of our auxiliary surface $\bar{S}$ helps to reduce the problem of refraction to the theory of conformal mapping familiar to geodesists. In this way we achieve two purposes: first, we obtain a uniform treatment of the influence of refraction on observed angles and electronically measured distances; and second, there results a conceptual simplification: the relatively complicated light paths are represented by the simplest curves, the geodesics, in the auxiliary surface, and the travel time of the light waves gets a simple geometrical interpretation as geodesic distance.

Clearly the light ray moves in three-dimensional space and not in a plane. This means that we must restore the z-coordinate, which we have omitted for simplicity. The essential relations, however, which we have just found, remain intact. The plane S is replaced by three-dimensional ordinary space R, and the auxiliary surface $\bar{S}$ is replaced by an auxiliary space $\bar{R}$. Since $\bar{S}$ is a curved surface, $\bar{R}$ will in general be a curved "Riemannian" space (it is no longer Euclidean). Hence the light rays are geodesics in this auxiliary space $\bar{R}$, and the measured optical length (proportional to the travel time of light) is the geodesic distance in $\bar{R}$. We may thus say that there is a certain (fictitious) curved space $\bar{R}$ in which we measure directly by means of its geodesics, both when observing angles and measuring distances electronically.

The transition from this "refraction space" with linear element given by

$$d\bar{s}^2 = n^2\,(dx^2 + dy^2 + dz^2) \tag{7}$$

to ordinary Euclidean space with

$$d s^2 = d x^2 + d y^2 + d z^2 \tag{8}$$

is effected through a three-dimensional conformal mapping; the reduction of observed horizontal and vertical angles and electronically measured distances is identical with angle and distance correction of this conformal mapping.

The mathematical properties of three-dimensional conformal mappings and their application to the problem of refraction have been studied extensively; we mention (Marussi, 1953), (Moritz, 1962), and (Hotine, 1965). Hence we need not go into the details here. We shall instead use the principles just explained to give explicit, practically applicable formulas for the reduction of angles and distances for refraction.

3. The Eiconal Equation

The geodesics in Riemannian space are described by two differential equations:

1. the ordinary differential equation for the geodesic curve; and
2. the partial differential equation for the geodesic distance.

These two equations occur in many different contexts. (In mechanics, for instance, we have Newtons equation of motion, which is a system of ordinary differential equations corresponding to 1., and the Hamilton-Jacobi equation, which is a partial differential equation corresponding to 2.) They therefore deserve closer attention.

Let the square of the linear element of a three-dimensional space in curvilinear coordinates x_1, x_2, x_3 be

$$d s^2 = \sum_{i,j=1}^{3} a_{ij}\, d x_i\, d x_j \tag{9}$$

Then the ordinary differential equation for the geodesic line is

$$\frac{d^2 x_i}{d s^2} + \frac{1}{2} \sum_{k,l,r=1}^{3} a^{ir} \left[\frac{\partial a_{rk}}{\partial x_l} + \frac{\partial a_{rl}}{\partial x_k} - \frac{\partial a_{kl}}{\partial x_r} \right] \frac{d x_k}{d s} \frac{d x_l}{d s} = 0 \qquad (i = 1, 2, 3)\,, \tag{10}$$

and the partial differential equation for the geodesic distance s is

$$\sum_{i,j=1}^{3} a^{ij} \frac{\partial s}{\partial x_i} \frac{\partial s}{\partial x_j} = 1\,. \tag{11}$$

Here the matrix (a^{ij}) is simply the inverse to the matrix (a_{ij}).

The reader familiar with Ricci calculus will notice that the formulas (9) through (11) could be simplified by the use of certain notational conventions peculiar to this calculus. We have purposely dispensed with these conventions here in order to be more generally intelligible.

It should be mentioned that the formulas (9) through (11) are as well valid for a surface if all subscripts are assumed to take the values 1,2 only and if consequently the summation goes from 1 to 2 instead of from 1 to 3. To get the familiar form, substitute

$$\begin{gathered} x_1 = u\,, \quad x_2 = v\,; \\ a_{11} = E, \quad a_{12} = a_{21} = F, \quad a_{22} = G\,. \end{gathered} \tag{12}$$

Then (9) becomes

$$d s^2 = E\, d u^2 + 2 F\, d u\, d v + G\, d v^2. \tag{13}$$

Furthermore, assume that the coordinates u, v are orthogonal; then $F \equiv 0$. In this case it is readily shown that

$$a^{11} = \frac{1}{E}, \quad a^{12} = 0\,, \quad a^{22} = \frac{1}{G}\,.$$

Then (10) becomes the system

$$u'' + \frac{1}{2E}(E_u u'^2 + 2 E_v u' v' - G_u v' v'^2) = 0 ,$$

$$v'' + \frac{1}{2G}(- E_v u'^2 + 2 G_u u' v' + G_v v'^2) = 0 , \tag{14}$$

where

$$u' = \frac{du}{ds} ; \; E_u = \frac{\partial E}{\partial u}, \text{ etc.}$$

The distance equation (11) takes the form

$$\frac{1}{E}\left(\frac{\partial s}{\partial u}\right)^2 + \frac{1}{G}\left(\frac{\partial s}{\partial v}\right)^2 = 1 . \tag{15}$$

These equations are important in geometrical geodesy, for computations on the reference ellipsoid on which u and v are orthogonal coordinates (usually, geographical coordinates φ and λ). The system (14), in a somewhat modified form, is the usual starting point for solving the "direct geodetic problem", the computation of coordinates from distance and azimuth.

Similarly, (15) is the best starting point for the solution of the "inverse geodetic problem", the computation of geodesic distance s and azimuth α from coordinates. Curiously enough, this simple equation seems to have never been used for this purposes, except by Gauss (1828). He needed the quantities $s \cos\alpha$ and $s \sin\alpha$ for obtaining his well-known formulas for small geodesic triangles on an arbitrary surface. Although Gauss' work belongs to general differential geometry, it may be properly quoted in connection with geodesy since the problem of geodesic triangles has important geodetic applications and since Gauss was inspired by his practical experience with triangulation. [1])

After Gauss, the partial differential equation for the geodesic distance, (11) or (15), was neglected in geodesy as well as in differential geometry and its most important physical application, the General Theory of Relativity. This is the more surprising as the Hamilton-Jacobi equation (Bergmann, 1949, sec. 2.4) and its equivalent in optics, the "eiconal equation" (Bergmann, 1949, sec. 10.3), have had very successful physical applications. Only recently Synge (1964) has made extensive use of the distance equation (11) in General Relativity and has obtained important results in this way.

After this digression, intended to point out related problems, we shall return to atmospherical refraction.

Here we have by (7)

$$d\bar{s}^2 = n^2 (dx^2 + dy^2 + dz^2) .$$

The comparison with (9) shows that

$$x_1 = x, \quad x_2 = y, \quad x_3 = z$$

and

$$a_{11} = a_{22} = a_{33} = n^2, \; a_{12} = a_{13} = a_{23} = 0;$$

hence we have

$$a^{11} = a^{22} = a^{33} = \frac{1}{n^2} , \; a^{12} = a^{13} = a^{23} = 0,$$

because the matrix (a^{ij}) is inverse to the matrix (a_{ij}).

Thus (11) becomes

$$\left(\frac{\partial \bar{s}}{\partial x}\right)^2 + \left(\frac{\partial \bar{s}}{\partial y}\right)^2 + \left(\frac{\partial \bar{s}}{\partial z}\right)^2 = n^2 . \tag{16}$$

---

[1]) The spirit of his work on differential geometry is shown by the concluding sentence of (Gauss, 1828): "Si eadem formula triangulis in superficie curva non sphaerica applicatur, error generaliter loquendo erit quinti ordinis, sed insensibilis in omnibus triangulis, qualia in superficie telluris dimetiri licet."

This is the *eiconal equation* already mentioned. It is a first-order partial differential equation for the optical distance $\bar{s}$. The following developments will be based on the eiconal equation.

4. *Solution of the Eiconal Equation*

We shall now solve the eiconal equation (16) by a suitable series expansion. Since for the atmosphere the index of refraction, n, is very nearly 1 (it is approximately 1.0003) we may put

$$n^2 = 1 + \varepsilon\mu\,, \tag{17}$$

where ε is a small constant parameter (e. g., $\varepsilon = 0.0006$) and $\mu = \mu\,(x, y, z)$ is a function of position. Hence the measured optical length $\bar{s}$ (see sec. 2) will deviate little from the ordinary straight distance s, so that we may expand $\bar{s}$ as a power series with respect to the small parameter ε:

$$\bar{s} = s + \varepsilon\, s' + \varepsilon^2 s'' + \ldots\,. \tag{18}$$

Here

$$s = \sqrt{(x - x_1)^2 + (y - y_1)^2 + (z - z_1)^2} = s\,(x, y, z) \tag{19}$$

is the straight distance of a variable point $P(x, y, z)$ from a fixed point $P_1(x_1, y_1, z_1)$ as a function of the coordinates of P. The functions $s', s'', \ldots$ will be obtained from the eiconal equation (16); we may safely neglect terms of order ε^3 and higher. We keep in mind that (18) is the desired *direct relation between measured optical length* $\bar{s}$ *and straight distance* s mentioned at the beginning.

The straight distance (19) satisfies the partial differential equation

$$\left(\frac{\partial s}{\partial x}\right)^2 + \left(\frac{\partial s}{\partial y}\right)^2 + \left(\frac{\partial s}{\partial z}\right)^2 = 1\,, \tag{20}$$

which is obtained from (16) by replacing $\bar{s}$ by s and n by 1. This is readily verified by substituting (19) into (20).

By introducing the vector

$$\operatorname{grad}\bar{s} = \left(\frac{\partial \bar{s}}{\partial x}, \frac{\partial \bar{s}}{\partial y}, \frac{\partial \bar{s}}{\partial z}\right) \tag{21}$$

we may abbreviate the eiconal equation as

$$(\operatorname{grad}\bar{s})^2 = n^2\,. \tag{22}$$

We substitute (17) and (18) into this equation, obtaining

$$(\operatorname{grad} s + \varepsilon \operatorname{grad} s' + \varepsilon^2 \operatorname{grad} s'')^2 = 1 + \varepsilon\mu\,.$$

Working out the square and comparing the terms independent on ε, those multiplied by ε, and those multiplied by ε^2 we find

$$(\operatorname{grad} s)^2 = 1\,, \tag{23a}$$

$$2 \operatorname{grad} s' \,.\, \operatorname{grad} s = \mu\,, \tag{23b}$$

$$2 \operatorname{grad} s'' \,.\, \operatorname{grad} s + (\operatorname{grad} s')^2 = 0\,. \tag{23c}$$

With (23a) we have recovered (20), whose solution (19) may be abbreviated as

$$s = \sqrt{\left(\vec{x} - \vec{x_1}\right)^2} \quad \text{mit } \vec{x} = (x, y, z)\,. \tag{24}$$

For later application we evaluate

$$\operatorname{grad} s = \left(\frac{\partial s}{\partial x}, \frac{\partial s}{\partial y}, \frac{\partial s}{\partial z}\right) = \frac{\vec{x} - \vec{x_1}}{s} = \vec{e}\,, \tag{25}$$

where $\vec{e}$ denotes the unit vector of the direction $P_1 P$; see Fig. 1. In agreement with this figure we

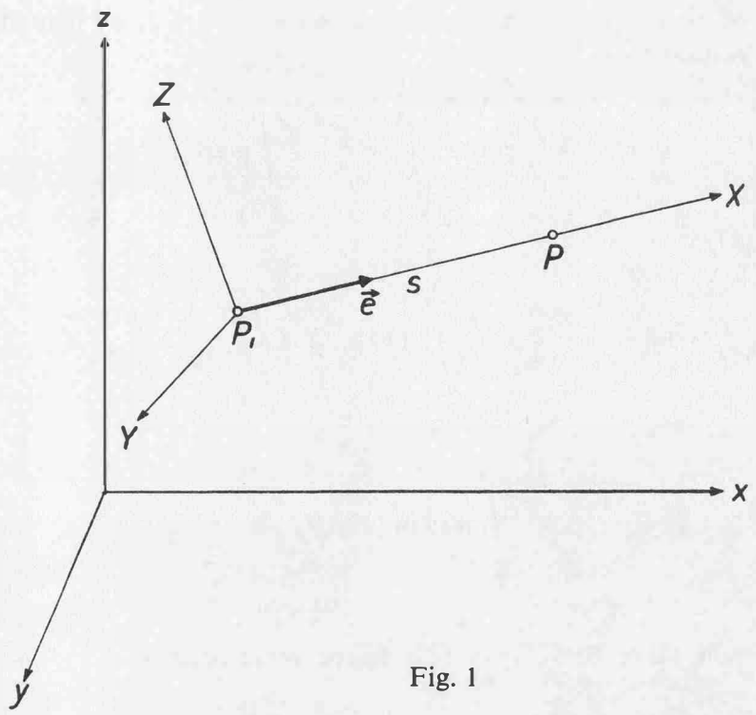

Fig. 1

introduce an additional rectangular coordinate system XYZ with origin at P_1, whose X-axis contains P and whose Y-axis is parallel to the original xy-plane.

Now we consider (23b). In view of (25) it may be written as

$$2\vec{e} \,.\, \operatorname{grad} s' = \mu .$$

Here $\vec{e} \,.\, \operatorname{grad} s'$ is the projection of grad s' onto the direction of $\vec{e}$; it is therefore identical with the derivative of s' along the direction of X, $\partial s'/\partial X$.
Hence we obtain

$$2\frac{\partial s'}{\partial X} = \mu ,$$

$$s' = \frac{1}{2}\int_0^s \mu \, dX . \tag{26}$$

This integral is extended over the straight line $P_1 P$.

To evaluate s'' by (23c), we need grad s'. For this purpe we must express (26) as an explicit function of the coordinates x, y, z of P. This is simply achieved by introducing a parameter

$$t = \frac{X}{s} \tag{27}$$

which runs from 0 to 1 as the current point of integration moves along the straight line from P_1 to P. Since the coordinates of this current point are given by

$$\vec{x}_1 + t(\vec{x} - \vec{x}_1) ,$$

we have along $P_1 P$ explicitly

$$\mu = \mu\left[\vec{x}_1 + t\left(\vec{x} - \vec{x}_1\right)\right] .$$

Substituting this into (26), taking (27) into account ($dX = s\,dt$), we find

$$s' = \frac{s}{2}\int_0^1 \mu\left[\vec{x}_1 + t\left(\vec{x} - \vec{x}_1\right)\right] dt .$$

Having thus obtained an explicit expression of s' as a function of $\vec{x}$, we may at once perform the differentiation with respect to x, y, z to get

$$\operatorname{grad} s' = \frac{1}{2} \operatorname{grad} s \cdot \int_0^1 \mu \, dt + \frac{s}{2} \int_0^1 \operatorname{grad} \mu \cdot t \, dt$$

Returning to X by (27) we have

$$\operatorname{grad} s' = \frac{s'}{s} \vec{e} + \frac{1}{2s} \int_0^1 \operatorname{grad} \mu \cdot X \, dX = \frac{s'}{s} \vec{e} + \frac{1}{2s} \vec{a} \tag{28}$$

as the desired result; we shall find the abbreviation

$$\int_0^1 \operatorname{grad} \mu \cdot X \, dX = \vec{a} \tag{29}$$

quite useful.

Now we can attack (23c). By (25) and (29) this equation becomes

$$2 \vec{e} \cdot \operatorname{grad} s'' + \left(\frac{s'}{s} \vec{e} + \frac{\vec{a}}{2s} \right)^2 = 0$$

or

$$2 \vec{e} \cdot \operatorname{grad} s'' + \left(\frac{s'}{s} \right)^2 + \frac{s}{s^2} \vec{a} \cdot \vec{e} + \frac{a^2}{4 s^2} = 0 . \tag{30}$$

This equation is considerably simplified by using the system XYZ. The components of the vectors $\vec{e}$ and $\vec{a}$ in this system are denoted by capital letters. Thus

$$\vec{e} = (E_1, E_2, E_3) = (1, 0, 0) .$$

$$\vec{a} = (A_1, A_2, A_3)$$

in the system XYZ. Then we have

$$\vec{a} \cdot \vec{e} = A_1, \quad \vec{a}^2 = A_1^2 + A_2^2 + A_3^2 .$$

For A we obtain the simple expression

$$A_1 = \int_0^s \frac{\partial \mu}{\partial X} X \, dX = \mu s' - \int_0^s \mu \, dX = \mu s - 2 s' \tag{31}$$

by partial integration; A_2 and A_3 are obviously given by

$$A_2 = \int_0^s \frac{\partial \mu}{\partial Y} X \, dX , \quad A_3 = \int_0^s \frac{\partial \mu}{\partial Z} X \, dX . \tag{32}$$

Thus (30) reduces to

$$2 \frac{\partial s''}{\partial X} + \frac{\mu^2}{4} + \frac{A_2^2 + A_3^2}{4 s^2} = 0 \tag{33}$$

for the end point P. To integrate this equation we write it for a current point along the straight line $P_1 P$ by replacing s by X and (32) by

$$A_2 = \int_0^X \frac{\partial \mu}{\partial Y} \xi \, d\xi, \quad A_3 = \int_0^X \frac{\partial \mu}{\partial Z} \xi \, d\xi \tag{32'}$$

(we have now denoted the integration variable by ξ to avoid confusion with the upper limit X). We thus obtain

$$2 \frac{\partial s''}{\partial X} + \frac{\mu^2}{4} + \frac{A_2^2 + A_3^2}{4 X^2} = 0 \tag{33'}$$

with the solution

$$s'' = -\frac{1}{8} \int_0^s \mu^2 \, dX - \frac{1}{8} \int_0^s \frac{A_2^2 + A_3^2}{X^2} \, dX, \tag{34}$$

A_2 and A_3 being given by (32').

By (24), (26), and (34) we have expressed $\bar{s} = s + \varepsilon s' + \varepsilon^2 s''$ as a function of the index of refraction and its partial derivatives in a practically exact way. If these quantities have been determined by suitable measurements, we can evaluate

$$\Delta s = \bar{s} - s = \varepsilon s' + \varepsilon^2 s'' \tag{35}$$

using (26) and (34) and computing these integrals by numerical or graphical integration. It may be pointed out again that these integrals are taken along the straight line $P_1 P$ and not along the light path.

The quantity Δs defined by (35) represents the desired reduction of the measured optical length for refraction. According to sec. 2, it corresponds to the distance reduction in three-dimensional conformal mapping.

Estimates show that the first integral of (34) is of the order of $5 \times 10^{-8} s$ and is consequently negligible. We may also neglect A_2, which is caused by lateral refraction, so that there remains as a practical approximation

$$\Delta s = \frac{\varepsilon}{2} \int_0^s \mu \, dX - \frac{\varepsilon^2}{8} \int_0^s \frac{A_3^2}{X^2} \, dX. \tag{36}$$

The term with ε^2 reaches the order of some 10 meters for $s = 1000$ km.

5. *Effect on Horizontal and Vertical Angles*

This method also furnishes the effect of vertical and lateral refraction on measured angles. The principle is as follows; see Fig. 2.

We consider the two unit vectors $\vec{e}$ and $\vec{\bar{e}}$, the first directed along the chord $P_1 P$, the second tangent to the light path at P. It may be shown that this tangent has the direction of grad $\bar{s}$ which is not, however, a unit vector. Hence

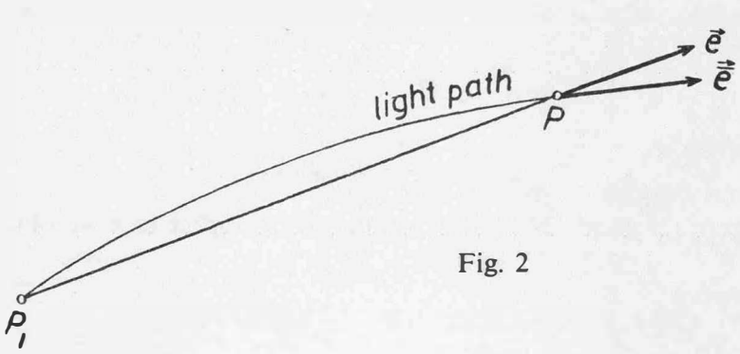

Fig. 2

$$\vec{\bar{e}} = \frac{\operatorname{grad} \bar{s}}{|\operatorname{grad} \bar{s}|} = \frac{\operatorname{grad} \bar{s}}{n} = \frac{\operatorname{grad} \bar{s}}{\sqrt{1 + \varepsilon \mu}} . \tag{37}$$

Here we have used (22) and (17). We again use an expansion with respect to:

$$\vec{\bar{e}} = \vec{e} + \varepsilon \vec{e'} + \varepsilon^2 \vec{e''} + \ldots \tag{38}$$

with

$$\vec{e} = \operatorname{grad} s, \; \vec{e'} = -\frac{1}{2} \mu \vec{e} + \operatorname{grad} s', \; \vec{e''} = \frac{3}{8} \mu^2 \vec{e} - \frac{1}{2} \mu \operatorname{grad} s' + \operatorname{grad} s'' . \tag{39}$$

Thus we know $\vec{\bar{e}}$; it is obvious that all refractional changes of directions or angles can be obtained through $\vec{\bar{e}}$. We shall outline the derivation. Consider the vector $\bar{e}$ according to Fig. 3. Its components in the system xyz (z-axis being parallel to the vertical of P) are $\bar{e}_1, \bar{e}_2, \bar{e}_3$. By Fig. 3 we have

$$tg\, \bar{\alpha}_1 = \frac{\bar{e}_2}{\bar{e}_1}, \quad \sin \bar{\beta}_1 = \bar{e}_3 .$$

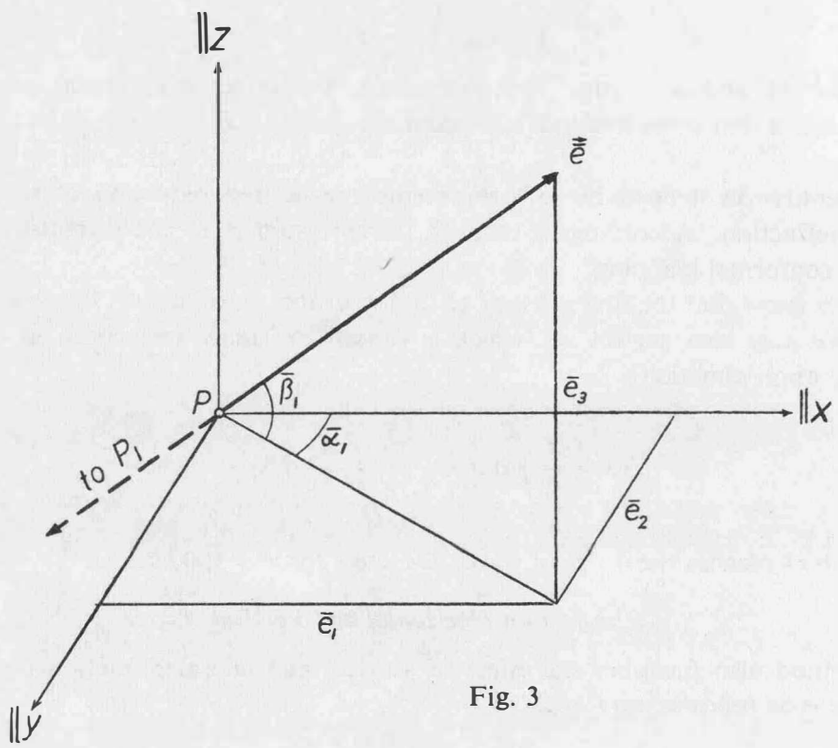

Fig. 3

Here $\bar{\alpha}_1$ and $\bar{\beta}_1$ are taken in the direction $P_1 P$, whereas our angles are measured at P, thus referring to the opposite direction $P P_1$. Hence the measured horizontal angle is $\bar{\alpha} = \bar{\alpha}_1 \pm 180^0$, and the vertical angle is $\bar{\beta} = -\bar{\beta}_1$, so that

$$\bar{\alpha} = \operatorname{arc} tg \frac{\bar{e}_2}{\bar{e}_1}, \qquad \bar{\beta} = -\operatorname{arc} \sin \bar{e}_3 . \tag{40}$$

Inserting $\bar{e}_1, \bar{e}_2, \bar{e}_3$ from (38) and (39) and expanding with respect to ε we obtain after some calculations

$$\bar{\alpha} = \alpha + \varepsilon \alpha' + \ldots, \quad \bar{\beta} = \beta + \varepsilon \beta' + \varepsilon^2 \beta'' + \ldots \tag{41}$$

with

$$\alpha' = \frac{A^2}{2\,s\cos\beta} = \frac{1}{2\,s\cos\beta}\int_0^s \frac{\partial\,\mu}{\partial\,Y}\,X\,d\,X,$$

$$\beta' = -\frac{A_3}{2s} = -\frac{1}{2\,s}\int_0^s \frac{\partial\,\mu}{\partial\,Z}\,X\,d\,X,$$

$$\beta'' = -\frac{A_2^2}{8\,s^2}\,tg\,\beta + \frac{\mu}{4\,s}\,A_3 + \frac{1}{8\,s}\int_0^s \frac{\partial\,\mu^2}{\partial\,Z}\,X\,d\,X + \tag{42}$$

$$+\frac{1}{4\,s}\int_{X=0}^{s}\frac{A_2}{X_2}\left[\int_{\xi=0}^{X}\frac{\partial^2\,\mu}{\partial\,Y\,\partial\,Z}\,\xi^2\,d\,\xi\right]d\,X + \frac{1}{4\,s}\int_{X=0}^{s}\frac{A_3}{X_2}\left[\int_{\xi=0}^{X}\frac{\partial^2\,\mu}{\partial Z^2}\,\xi^2\,d\,\xi\right]d\,X.$$

The notations are those of the preceding section. The angles α and β refer to the straight line PP_1. We have omitted α'' because the effect of lateral refraction is small as compared to the vertical effect.

Estimates indicate that $\varepsilon^2\beta''$ is usually only of the order of a few tenths of a second of arc even for $s = 50$ km. Consequently it may often be neglected. In this case we have with $\varepsilon\mu \doteq 2\,(n-1)$ simply

$$\Delta\,\alpha = \bar{\alpha} - \alpha = \frac{1}{s\cos\beta}\int_0^s \frac{\partial\,n}{\partial\,Y}\,X\,d\,X,$$

$$\Delta\,\beta = \bar{\beta} - \beta = -\frac{1}{s}\int_0^s \frac{\partial\,n}{\partial\,Z}\,X\,d\,X. \tag{43}$$

These equations have been derived in an elementary geometric way in (Moritz, 1962), using the theory of conformal mapping. We remind the reader that $\Delta\alpha$ and $\Delta\beta$ correspond to the angle corrections of three-dimensional conformal mapping; see sec. 2. As a matter of fact, a formula such as the second of (43) can also be used for evaluating the angle correction in the conformal mapping of a surface such as the ellipsoid onto a plane.

Inspecting our results such as (36) for Δs and (42) or (43) for $\Delta\alpha$ and $\Delta\beta$ we see that these formulas require the index of refraction n and certain of its partial derivatives to be known along the straight line P_1P. These values may be obtained by performing measurements in the neighborhood of this line. Formulas for practical computation and a numerical example will be found in (Jordan-Eggert-Kneissl, 1966, p. 527–531).

References

Bergmann, P. G.: (1949) Basic theories of physics-mechanics and electrodynamics. New York, Prentice-Hall (reprinted by Dover Publications, New York, 1962).

Bomford, G.: (1962) Geodesy, 2nd. ed. Oxford University Press.

Gauss, C. F.: (1828) Disquisitiones generales circa superficies curvas. Comm. soc. reg. sci. Gottingensis rec., vol. VI.

Hotine, M.: (1965) Geodetic applications of conformal transformations in three dimensions. Second Symposium on Mathematical Geodesy, Turin, April 1965.

Jordan-Eggert-Kneissl: (1966) Handbuch der Vermessungskunde,
10th ed., vol. VI by K. Rinner and F. Benz. Stuttgart, J. B. Metzler.

Marussi, A.: (1953) Un'analogia fra le leggi della propagazione della luce in mezzi rifrangenti continui isotropi, e la rappresentazioni conformi.
Pubbl. dell'istituto nazionale di ottica, Arcetri-Firenze, Ser. no. 142.

Moritz, H.: (1961) Zur Reduktion elektronisch gemessener Strecken und beobachteter Winkel wegen Refraktion.
Zeitschrift f. Vermessungswesen, v. 86, pp. 246–252.

Moritz, H.: (1962) Zur Geometrie der Refraktion.
Österr. Zeitschrift f. Vermessungswesen, v. 50, pp. 3–13.

Synge, J. L.: (1964) Relativity — The General Theory.
Amsterdam, North-Holland Publishing Co.

Extract from the Symposium Report

by *Dr. E. Tengström*

(to be published in Bull. géod.)

These two conferences were originally planned to be inofficial working sessions for members of the study groups 16 and 23 as part of their running work during the period between the two general assemblies in Berkeley and Lucerne. The number of participants was estimated to about 25 for each conference. Due to the great interest also from many scientists, who are not officially members of aforesaid groups, and thanks to generous pecuniary help from the Austrian government and IAG, it became possible to organize a more official symposium on "Figure of the Earth and Refraction".

The first part of the Symposium was devoted to the subjects "The Normal Spheroid and the Figure of the Earth", and following contributions to these questions were presented during three sessions:

Tuesday March 14, $14^h - 17^h30$, Chairman Prof. U. Uotila

K. Ledersteger:

a) Equilibrium Figure of the Earth and Normal Spheroid
b) Critical Notes on the Equipotential Ellipsoid
c) The Mass-functions $J_2 - J_6$, Derived from Orbital Perturbations of Artificial Satellites
d) The Definition of Topography and Isostasy

A contribution by Dr. J. A. O'Keefe was not presented because of the author's absence, but it was printed in these Proceedings. Prof. Ledersteger's explanation of his opinion about suitable equilibrium figures and non-equilibrium figures to be used as possible physical models for the Boundary Value Problem of Physical Geodesy, and for an improved study of the internal constitution of the real earth was clear and convincing. The discussion, which followed his presentations, and in which Moritz, Fischer, Levallois, Pick, Tengström and others participated did not contain critical remarks but merely reflected some needs for further clarifications of some of Ledersteger's statements. A paper of Ząbek: "New Conception of the Equilibrium Condition of One-parametric Spheroid and the Normal Spheroid of the Earth" was presented too late and therefore could not be discussed, but Ledersteger published his Critical Remarks in this book.

Wednesday March 15, $9^h - 12^h$, Chairman Prof. Moritz

The first paper, presented by Mrs. Fischer dealt with a problem, intimately connected to the questions of Tuesday-session, namely: "Deviations of the Geoid from an Equilibrium Figure",

Mrs. Fischer described her opinion about the difference between Ledersteger's and O'Keefe's way of reasoning and demonstrated a new geoidal chart, giving the geoidal heights, referred to Jeffreys' hydrostatical model (C maintained) with flattening 1/299, 67 and a = 6378133 m. She also took into account the spheroidal shape of Jeffreys' figure, having a maximum depression with respect to the ellipsoid with same axis of 3.2 m. According to Ledersteger's theory this depression would be about twice as much $\left(\frac{a}{4} f_4\right)$. A discussion between Ledersteger and Mrs Fischer cleared up a misunderstanding concerning the effect on geoidal heights from the difference between mean radius of the actual geoid and the mean radius of Ledersteger's spheroid, which is 234 m greater, defined from equality of volume for spheroid and real earth-body, and used by Ledersteger in his regularization procedure. The undulations will be the same, because the mass of the Earth is same as mass of the spheroid.

The subsequent papers during this session dealt with various questions on the Boundary Value Problem and its solution. The contributions read were:

M. Pick: "On the solvability of Molodenskij's Integral Equation."

H. Moritz: "Lineare Lösungen des Problems von Molodenskij."

L. Bragard: "Sur un systéme d'èquations integrales pour la determination de la figure de la terre".

Pick's contribution tried to answer the question of an appropriate numerical treatment of the integral equation, which avoided the use of divergent series for topographical slopes, greater than 45°. Moritz' treatment of the linear solution postulated the possibility of computing à priori, e.g. from surface-anomalies, the quantity $\frac{\partial \Delta g}{\partial h}$. Bragard referred to his most recent investigations of solving the Boundary Value Problem by means of two integral equations.

The discussion, in which, except the authors, also Levallois, Tengström and others participated, dealt with other practical forms of G_1 (Moritz) and with the non-proved existence of a unique and correct solution of Molodenskij's problem, given only surface-anomalies and shape of telluroid (Tengström). The approach of Bragard was appreciated by Moritz, some doubt about its correctness were expressed by Pick.

The importance of using satellite information for the determination of the figure of the Earth was stressed by *K. Arnold* in a paper with title: "Analytische Integration der durch die Schwereanomalien hervorgerufenen Satellitenbahnstörungen", which was presented by Dr. Stange. It was explained, how unknown mean anomalies over big squares could be deduced from satellite observations, utilizing already known mean surface-anomalies as additional information. In the following discussion, the question of independence between the mean anomalies used in computation was dealt by several participants (Moritz and others).

About the difficulty to avoid systematical errors, when using satellite observations to determine geocentric coordinates *Milan Burša* was talking. His paper: "On the Deviation of the Earth's Ellipsoid on the Basis of Satellite Observations" was discussed by Veis, Tengström and others, who presented different opinions about the danger of getting systematically disturbed results.

An interesting paper about different types of coordinate-systems, used in the problems of the Figure of the Earth was presented by *G. J. Bruins.* Its title was: "Some Remarks about Parameters, Used by Hirvonen, Molodenskij and Jordan". Other contributions during the same session were

I. Pola: "Mass Sources as a Representative of Surface Gravity Values and their Use for Solving Integral Equations", and

J. Kaspar: "Beitrag zur Bestimmung des Geoides".

A manuscript by *L. Egyed*: "Some Consequences of the Expansion on the Figure and Rotation of the Earth" and a paper of *G. Barta*: "The Asymmetric Structure of the Earth and its Secular Processes" were presented by Dr. Biró, but were not discussed.

The third session, same day, $14^h - 17^h30$, Chairman Dr. Burša

treated miscellaneous questions about Gravity Anomalies, Deviations of the Vertical, Observations and Interpolations. The following papers were presented:

B. Szabo: "Aerial Gravimetry for Direct Observation of the External Gravity Anomalies",
V. Vyskočil: "Some Remarks on the Accuracy of Interpolation of Gravity Anomalies".
P. Biró: "Über die Genauigkeit der auf gravimetrischem Wege interpolierten Lotabweichungen"
M. Pick—J. Pola: "Some Experiences with the Determination of the Figure of the Earth in Test Areas"
The discussion in connection with these papers mainly dealt with questions of hereto achieved and expected accuracy in the future.
K. Rinner presented a very interesting paper entitled "Zur Maßbestimmung im PAGEOS-Weltnetz" and *P. V. Angus-Leppan* presented a paper by *M. R. S. Mather:* "The Extension of the Gravity Field in South Australia". Rinner's contribution has a special interest to all scientists, dealing with the problem of optimum configurations and their accuracies in geodesy, a problem which may be practically solved also in very complicated cases with highspeed computers, as Rinner shows. A contribution by *A. Bjerhammar* and *B. G. Reit* was distributed but not presented; an extract is published here. A paper by *Killian* about Marine Geodesy and its importance for the study of the Figure of the Earth, and a paper by *Kobold* about "Lotabweichungen and Niveauflächenundulationen in der Schweiz" could unfortunately not be presented during the meeting because of lack of time, but the first one is printed in the Proceedings.

The conference on "The Normal Spheroid and the Figure of the Earth" was closed by the president of the SSG 16, Dr. Tengström, who expressed his great satisfaction with the result of the meeting, which had shown all participants important new aspects on many problems in the field, which are now worth while to become familiar with. He stressed especially on the necessity of carefully studying the problem of selecting a suitable physical model of the Earth, to be used by geodesists, as well as by geophysicists. He anticipated further discussions to be held on this subject during the meetings of Sec V in Lucerne.

Dr. Tengström explained also on behalf of the participants, his gratitude to the Austrian hosts for the good organization of the conference and for all hospitality shown to the guests, who will certainly always remember this meeting as scientifically inspiring, and: "We shall never forget the atmosphere of friendship and pleasure, which is typical for Vienna, and has once more been demonstrated to us", he ended.

The second part of the Symposium had the title "*Recent Research on Atmospherical Refraction for Geodetic Purposes*".This conference contained four sessions, two on Thursday, March 16, and two on Friday, March 17.
Thursday, March 16, 9^h-12^h, Chairman Prof. L. Asplund, president of Sec I of IAG.
Professor Asplund opened the conference with a short review of existing methods for determining the influence of the refractive power of the atmospere upon various kinds of geodetic measurements. He ended his opening speech: "I am confident, that very much of new and promising results will be reported, and I am sure the discussions will be fruitful, and that many new ideas for the future will be born."

Thursday-sessions were devoted to *problems of atmospherical refractive index and its influence upon electro-optical distance measurements.*

After a report from SSG 19 by its president *Brig E. W. Denison:* "Report on refraction-investigations in connection with the work of SSG 19 until end of 1965," the following papers were read on the subject "*Refraction-Effect on Optical Distance-Measurements*".
C. Owens: "Recent Progress in Optical Distance-Measurements: Lasers and Atmospherical Dispersion."
G. B. Lesley: "Preliminary Measurements with a Laser Geodimeter". Ref. ESSA, Technical Memorandum No 1, CGS 1966.
M. C. Thompson: "A Radio Optical Dispersion Technique for Higher Order Correction of Optical Distance Measurements."
C. G. Lehr: "Satellite Ranging with Laser, and the Correction for Atmospherical Refraction."
K. Bretterbauer: "The Effect of the Atmosphere on Precise Satellite Ranges with Laser."
The papers by Owens, Thompson and Lehr reported about the most recent practical investigations in the field. Bretterbauer's contribution was more theoretical, and the discussion seemed to indi-

cate a general opinion, that the accuracy obtainable as expected by the author was a little too optimistic. It was obvious that for all optical ranging the laser has completely distanced the conventional lightsources.

Second session same day, 13.30—17^h treated the subject "*Refraction effect on Distance Measurements, using Radio Wave Propagation*". *Chairman Brig E. W. Denison*

Presented papers:

K. Poder: "Atmospherical Corrections at Tellurometer Measurements."

T. Parm: "Investigations of Refraction Correction in Tellurometer Measurements."

S. Härmälä: "The Effect of Meteorological Factors on the Accuracy of Tellurometer Measurements."

These papers dealt with the same problem, but the theoretical and practical approaches were different. It was, however, extremely interesting to see, that the results of the investigations almost completely agreed.

Further *M. C. Thompson's* paper: "Recent Measurements of Atmospheric Limitations on Precision of Microwave Distance Measuring Equipment" treated the question of accuracy obtainable at present and in the future, when accounting for atmospheric refraction-effect. The paper by *F. Culley:* "Refractive Effects of Radio Ranging on Artificial Earth Satellites" explained the procedure used in the SECOR-system (and similar systems). Some questions of definition of the total effect were touched during the following discussion. It should be pointed out, that both the actual speed of propagation *and* the curvature have to be taken into account in deriving the correction for atmospherical refraction.

See also *Pelzer's* paper on Friday morning!

Unfortunately, *W. Höpcke's* announced paper: "Increased Pathcurvatures in Radio-Distance Measurements" could not be presented at the meeting because of Prof Höpcke's absence. The very interesting paper will, however, probably be presented in Lucerne.

Friday, 17 March, 9^h*—13*^{h}*, Chairman Prof. P. L. Baetsle.*

This third meeting on refraction dealt with *the effect on direction measurements.*

After a short introduction by the chairman, who also presented his work on an extensive bibliography list concerning the refraction problem, as it shows up in Geodesy, and which list will appear in complete shape at Lucerne, Prof Baetsle announced the following topics to be treated during the session:

A. Use of Relationships between Different Effects of Refractive Index.

B. Errors and Sources of Errors.

C. Refraction in Connection with Spatial Geodesy.

Under A, the following papers were presented:

M. Pelikán: "Berechnung des Brechungswinkels mit Hilfe des Brechungsindexes und der Krümmungsradien der Brechungskurve." This paper contained a purely mathematical deduction of the refractionangle and a comparison with already existing formulas. In principle, it has already been printed. Ref. Studia geoph. et geod. 8 (1964).

A very interesting investigation on *temperature-models* for the lower atmosphere with title: "A Mathematical Model for Temperature Models in the Lower Atmosphere and its Application in Refraction Calculations" was presented by *P. V. Angus-Leppan.* The discussion, in which, among others, Levallois, Owens and Poder participated, showed the great appreciation of this work but also pointed out the danger of treating models as relevant under actual atmospheric conditions (Levallois). Accuracy-questions and the needs for further information were touched by Owens and Poder.

About some measurements of temperature-gradient distribution for computing astronomical refraction, made by the Institute of Geodesy, Technical University, Berlin, was reported by *O. Hirsch:* "Elektrische Messung des Temperaturgradienten auf astronomischen Beobachtungsstationen". The formulas utilized in the measurements seem to be correct, if we use wave-index for n_{Gr}, *not* group-index. In the discussion Poder asked for a nearer explanation of the actual goal of such measurements.

Questions of the *distribution of the vertical gradient of refractive index* near the ground were treated in the paper by *H. Pelzer:* "Beitrag zum Vertikalgradienten des Brechungsindexes für Mikrowellen in den unteren 100 m der Atmosphäre." This investigation, which should have been presented during the Thursday afternoon session, dealt especially with the curvature influence on distance measurements with micro-waves but is of course also interesting from the point of view of direction-measurements with radio-waves. The paper by *H. Jeske* and *G. Kruspe* (presented by H. Jeske), "Time-Space Structure of Atmospheric Refractive Index, Especially Obtained by Refractometer Measurements" reported about very interesting investigations of the refractive index distribution at low heights over sea, which clarify how dangerous it is to assume simple vertical and horizontal distribution of the index near water level, valid for a certain time of observation. The fast-changing turbulent effect seems not to be too critical for observations towards a fixed object, but the actual "noise-free" distribution is the more important to know for a correct computation of atmospherical corrections. In the discussion Poder and others took part.

Under B, the following papers were presented: About "Investigations on Errors in the Determination of Astronomical Refraction", *Prof. K. Ramsayer* was talking. This interesting study showed that the error in zenit-distance measurements of stars mainly depended on the actual inclination of the optical layers and that the error is surprisingly small, even for rather large zenit-distances. No discussion followed, thus indicating that the participants agreed with these statements. It could be questioned, however, if astronomical determinations (e.g. with almucantarat-methods) are not more seriously effected by local refraction at deflection-stations, situated in forest areas of other certain types of groundvegetation (opinion by author of this review, justified by his own experience in Sweden).

In the highly instructive and important paper by *G. Abby* and *M. S. Tavenner*: "Definition of the Refraction and Shimmer Problem Affecting Geodetic Observations of Satellites" presented by the latter, the s.c. undulation or shimmer (short period fluctuation in refractive index), was given most of the responsability for the relatively low upper limit of accuracy in direction determinations of satellites (reflecting or flashing). Further studies of means for minimizing the influence of this effect at stellar triangulation, were anticipated by the authors.

About investigations of the shimmer-problem, also *Lambeck* reported. His paper was not announced, and is not published here.

Under C, the following papers appeared:

H. M. Dufour: "Choix des formules de la réfraction atmosphérique pour les observations par chambres ballistiques."

L. Hradilek: "Determination of Refraction, when adjusting Spatial Triangulations."

R. N. Sanchez: "Results of Refraction at Vertical Angle Measurements in Mountainous Countries."

Dufour's important work on the subject was again recognized in the discussion. *Hradilek's* extremely interesting paper was recognized by Levallois as the first attempt of a spatial triangulation, taking all sources of errors into account. Mr. Levallois also stressed upon the necessity to encourage this type of work in the future. In the discussion Gale asked for more precise information of m.sq. errors in the determination of refractive effect. *Sanchez'* paper, presented by Prof Baetsle, in the author's absence, showed once more, after the Symposium on Three Dimensional Geodesy in Cortina d'Ampezzo 1962, the importance of the work, being done by Sanchez in Argentina to solve the problem of refraction-correction at vertical angle measurement in mountainous areas.

The fourth (and last) meeting on the refraction problem was held at the same day between 15- and 17^{30}, *Chairman Dr. E. Tengström*, and began with the following paper:

E. Tengström: "Elimination of Refraction at Vertical Angle Measurements, Using Lasers of Different Wave Lengths." This paper, which actually belonged to the previous session, explained a dispersion-method at terrestrial vertical angle measurements, introduced already 1948, which corresponds to Owens' and Bender's approach at optical distance measurements but has to use wave-propagation index instead of group-index. Three types of instruments, constructed by the auther were described, and the obtained (resp. obtainable) accuracy in determining the refraction angle at the observation-site, was stated. The discussion, in which Poder, Asplund, Dufour and others participated, showed that this method probably could solve the problem of instantaneous refrac-

tion determination also in the case of astronomical (and "rocket-") refraction and in case of lateral refraction.

The Nivellitic Refraction was treated by *T. J. Kukkamäki*, who, after a short review of the problem, read two recent papers on the subject, one by *J. G. Kakkuri:* "Refraction in the Long Distance Water-cross Levelling", and one by *E. Hytönen:* "Measuring of the Refraction in the Second Levelling of Finland." The experience, demonstrated in these investigation, which may be used by all levelling-observers, was highly appreciated by the audience. *Dr. Tengström* congratulated the Finnish scientists to their fruitful research in a very important area of refraction-studies and thanked Prof. Kukkamäki for his most interesting contribution.

Dr. Tengström then asked Prof *H. Moritz* to explain his opinion of the best way of mathematically treating the problem of refraction. Moritz' paper was entitled: "Applications of the Conformal Theory of Refraction", and showed that using Fermat's principle a clear understanding of the effect of refractive-index distribution could be obtained by treating the grad n as a space function. Suitable practical formulas for the refraction effect were deduced and might be applied to all kinds of geodetic measurements. In the following discussion, especially Dufour stressed upon the necessity of treating mathematically grad n also as a function of time.

Before closing the session and the conference on refraction, the chairman asked the audience about further remarks, at the same time announcing, that the conference, and also the whole Symposium did not expect recommendations or proposals of resolutions to be made. Such recommendations and resolutions should be discussed during the General Assembly in Lucerne. After the chairman's question, Brig. Denison read a letter from Brig. Hotine, asking for the best up to date definition of a model atmosphere. The letter from Hotine caused a rather lively discussion, in which Levallois and Moritz denied the necessity of defining such an atmosphere. The chairman pointed out, however, that if Brig. Hotine for some reason needed such an up to date model atmosphere, we should try to give it to him, not discussing whether it is necessary or not. The whole question was postponed until Lucerne-meeting. Dr. Tengström finally closed the conference on "Recent Research on Atmospherical Refraction for Geodetic Purposes", thanking all authors and participants for their valuable contributions. He expressed his sincere hope that this conference had been a good preparation for the special session on refraction problems, which will be organized by the president of Sec I in Lucerne.

He also asked the audience to excuse him for forcing the participants to work so hard, without giving them coffee-breaks enough. But he was confident, that their scientific interest was greater than their interest in drinking coffee. He repeated his thanks to the Austrian hosts, who had made this conference such a success. He felt sad to leave this country, where Scientific Power and Human Understanding always had worked hand by hand. After a warm "Good Bye" from Prof. Ledersteger, containing also his appreciation of the scientifically high standard of all contributions during the whole Symposium, he anticipated further interesting discussions in Lucerne.

Finally Dr. Tengström worded as follows: "As representative of Sec. V, SSG 16 and SSG 23, I would like, myself, to explain my deep gratitude to our Austrian hosts for their giving us such a wonderful time in Vienna, March 1967, making us scientifically inspired, and also helping us to enjoy life in the very best way. The fine social program organized by Prof. Hauer, was highly appreciated. The Smoker at the "Rathauskeller", the receptions by the Minister and by the Mayor of Vienna, the "Heurigenabend" in Deutsch-Wagram, and the wonderful excursion to Wachau-Dürnstein, all these events were parts of an unforgettable time in Vienna".

Contents

Second Conference (SSG 23): Recent Research on Atmospherical Refraction for Geodetic Purposes

Part I: Problems of Atmospherical Refractive Index and its Influence upon Electro-optical Distance Measurements

A: Refraction Effect on Optical Distance-Measurements

B: Refraction Effect on Distance Measurements, Using Radio Wave Propagation

Part II: Refraction Effect on the Determination of Directions

A: Use of Relationships Between Different Effects of Refractive Index

B: Errors and Sources of Errors

C: Refraction in Connection with Spatial Geodesy

Part III: Elimination of Refraction from Geodetic Angular Measurements. Nivellitic Refraction. Conformal Theory of Refraction